THE UNIVERSITY
of EDINBURGH

Ethanol-induced formation of colorectal tumours and precursors in a mouse model of Lynch Syndrome

THE UNIVERSITY *of* EDINBURGH

Guia Cerretelli

Doctor of Philosophy

The University of Edinburgh

2021

Declaration

I declare that this thesis was composed entirely by myself and that all research presented is my own except for where clearly indicated. No part of this work has been submitted for any other degree or qualification.

Guia Cerretelli

Acknowledgements

First and foremost I am extremely grateful to my supervisor Professor Mark J. Arends for givimg me the opportunity to undertake my PhD at the University of Edinburgh. I want to thank him for his enthusiasm and assistance all the way through the research project, for his support, help, patience and belief in me. It has been a pleasure to be your student. I would also like to extend my gratitude to my second supervisor Susan Farrington for all her help and advice.

I would like to thank all those at the IGMM who have helped me during these 3.5 years; my fellow PhD student Marion Bacou for her help at the bay, for listening and sharing with me the high and lows of a PhD, for our coffee breaks and who have become a precious friend; Vidya Rajasekaran for her advice on my experiments and for sharing with me her protocols, reagents and lab experience; Alessandro Brombin for all his help and advice. I would like to thank the Division of Pathology, especially Helen Caldwell and Elaine Mclay; and all those in the S1.02 lab and ECRC-Ground floor office (Ying Zhou, Carrie Cunningham, Monika Sobol, Sarah Taylor, Alison Munro, Kenneth Macleod, John Dawson, Becka Hughes and Karen Taylor) for making it a wonderful environment to work in and, especially Mark Grey, James Meehan, Carlos Martinez Perez, Arran Turnbull and Charlene Kay for treating me like part of their group. I would like to thank the staff in the BRF, particularly Kyle Davies, Kostas Gournopanos, Gary Waugh, John Tomlins and Linda Clark; IGMM Technical Services and Stores; the IGMM Advanced Imaging Resource. A special thanks to Jennifer Lawrie for her assistance and support, thanks for all the laughs, coffees, chats and to be a great friend.

Certo non posso non ringraziare i miei gnari che mi hanno accompagnato in questo percorso; a Lorenzo il miglior coinquilino di sempre, insieme abbiamo iniziato quest'avventura ed abbiamo condiviso momenti indimenticabili; a Michele un genio che non smette mai di sorprendermi e che si e' rivelato un vero amico; alla mia scatenata rossa, Veronica, la mia spalla, il mio braccio destro, abbiamo iniziato con "Maracaibo" in mezzo a Cowgate e abbiamo continuato con mille altre avventure. A Nicoló, grazie per esserci sempre stato nei momenti belli e brutti, per aver saputo leggere i miei silenzi e le mie espressioni meglio di chiunque altro, ho scoperto in un riccio introverso veronese il milgior amico che io abbia mai avuto. Grazie ragazzi per essere diventati la mia famiglia in Edinburgh, grazie per tutte le risate, le serate folli e tutti i memorabili momenti che mi avete regalato, grazie a voi non mi sono mai sentita persa o sola. Thanks to Aggeliki who has become a great friend. A special thanks to Stephen whose love, patience and support have helped me during the completion of this thesis. Grazie al mio babbo, alla mia mamma e a mio fratello per avermi sostenuto e incoraggiato in ogni scelta che mi ha permesso di raggiungere questo traguardo (tranquilli che dopo questa non saro' piu' una studentessa). Grazie per il vostro infinito amore che e' forte, intenso e va oltre i confini.

Abstract

Lynch Syndrome (LS) confers an inherited cancer predisposition, particularly for colorectal cancer, due to germline mutations in one of the DNA mismatch repair (MMR) genes, such as *MSH2*. MMR is a DNA damage repair pathway involved in the removal of base mismatches and insertion/deletion loops, caused by several endogenous and exogenous factors. Loss of MMR through somatic alteration of the wild-type MMR allele in LS results in defective MMR (dMMR). Lifestyle factors can modify cancer risk for LS and sporadic patients. Ethanol and its metabolite acetaldehyde, are classified as group one carcinogens by the International Agency for Research on Cancer, and are risk factors for sporadic cancers of the upper aerodigestive tract, liver, breast and colorectum. Acetaldehyde is metabolised to acetate by the Aldh family of enzymes, particularly Aldh1b1 in the intestines. Acetaldehyde is very reactive and may cause a range of DNA lesions. However, DNA repair pathways responsible for correcting such lesions remain unknown. It was hypothesized that MMR plays a role in protecting intestinal cells from ethanol/acetaldehyde-induced DNA damage. This study aimed to determine if there is a gene/environment interaction between dMMR and ethanol/acetaldehyde that accelerates colorectal tumour development and progression.

A conditional *Msh2* knockout ("Msh2-LS") mouse model with one deleted and one conditional knockout *Msh2* allele was used, as it mimics the LS patients' pattern of MMR gene inactivation. The Msh2-LS model mice were fed either with 20% ethanol in drinking water or normal drinking water. Long-term ethanol consumption led to large intestinal mucosal epithelial hyperproliferation and adenoma formation in 65% (15/23) mice and, in some cases, invasive adenocarcinoma (5/23 mice, 21.7%) within 6 months (mostly in the proximal and mid-colon), compared with 0% (0/23 mice) at 6 months and only one colonic tumour after 15 months in the water-treated mice ($p<0.0001$). No small intestinal tumours were observed. Additionally, a conditional *Aldh1b1* knockout (*Aldh1b1*$^{flox/flox}$) Msh2-LS mouse model and a constitutive *Aldh1b1* knockout (*Aldh1b1*$^{-/-}$) Msh2-LS mouse model were generated, in which the lack of Aldh1b1 enzyme caused increased acetaldehyde levels and acetaldehyde-induced DNA damage. In these Aldh1b1-deficient mice, long-term ethanol consumption led to increased numbers of colorectal adenomas per mouse (4.2, 21 neoplasms in 5 tumour-bearing conditional *Aldh1b1*$^{fl/fl}$ Msh2-LS mice; and 4.8, 35 neoplasms in 8 tumour-bearing constitutive

Aldh1b1$^{-/-}$ Msh2-LS mice) compared with 2.4 (36 neoplasms in 15 tumour-bearing mice) colorectal adenomas per mouse observed in the Msh2-LS mouse model with wild-type Aldh1b1 (p=0.0319 and p=0.0103) , but no colonic tumours were observed in water-treated controls.

Precursor lesions were observed as dMMR crypts in the murine colon in all of these mouse models, and their quantification showed increased numbers of dMMR crypt foci in ethanol-treated mice compared with water-treated controls (p=0.0029 in *Aldh1b1*^{wt} Msh2-LS mice, p=0.0006 in *Aldh1b1*$^{fl/fl}$ Msh2-LS mice and p<0.0001 in *Aldh1b1*$^{-/-}$ Msh2-LS mice). A significant increase in DNA damage was detected in the large intestinal epithelium of ethanol-treated mice of all genotypes compared with the respective water-treated controls (p=0.0009 in *Aldh1b1*^{wt} Msh2-LS mice, p<0.0001 in *Aldh1b1*$^{fl/fl}$ Msh2-LS mice and in *Aldh1b1*$^{-/-}$ Msh2-LS mice), along with increased plasma acetaldehyde levels in ethanol-treated mice and acetaldehyde levels were higher in the plasma of *Aldh1b1*$^{flox/flox}$ Msh2-LS mice and *Aldh1b1*$^{-/-}$ Msh2-LS mice than in the plasma of Msh2-LS mice.

In this study, evidence was provided for a role for Msh2 in protecting the MMR-proficient colonic epithelial cells against ethanol/acetaldehyde-induced DNA damage by activating DNA mismatch repair, triggering cell cycle arrest or cell death by apoptosis. A key role for Aldh1b1 was confirmed for protecting the large intestines from acetaldehyde-induced DNA damage and tumour formation. Long-term ethanol/acetaldehyde exposure was shown to accelerate dMMR-driven intestinal tumour formation and this is proposed to act via promoting proliferation (mucosal epithelial hyperproliferation) and suppressing apoptosis, thus enhancing survival of aberrant dMMR intestinal epithelial cells/crypts relative to MMR-proficient intestinal epithelial cells/crypts, leading to adenoma development (with microsatellite instability) with some progressing to adenocarcinomas. In conclusion, there is strong evidence for a gene/environment interaction between acetaldehyde/dMMR, causing the acceleration of dMMR-driven intestinal tumour formation upon ethanol exposure.

Lay Summary

Lynch Syndrome (LS) is an inherited genetic disease that increases a person's risk of developing a range of cancers, especially colorectal cancer. Developing tumours are known to acquire mutations occurring within the DNA of cells. To combat the accumulation of DNA mutations, cells have several DNA repair pathways that can accurately identify and repair DNA damage. One such pathway is termed the DNA mismatch repair (MMR) pathway and it is this pathway which is defective in LS patients. Alcohol consumption, specifically ethanol (and its toxic breakdown intermediate acetaldehyde), is a known risk factor for cancer development, as it can induce various types of DNA damage. However, as yet the specific DNA repair pathways responsible for correcting such DNA damage remain unknown. It was hypothesized that MMR plays a role in protecting cells from alcohol-induced DNA damage. This study aimed to determine if there is an interaction between defective MMR and alcohol that accelerates colorectal tumour development and progression.

To investigate this hypothesis, a mouse model of LS was used that was previously developed, which allows controllable inactivation of one of the MMR genes (called *Msh2*) similar to that known to occur in human LS patients. Long-term alcohol consumption by these mice led to increased cell proliferation in the large intestine, with benign and malignant intestinal tumour formation within 6 months, compared with no tumours in the same time period (and only one intestinal tumour after 15 months) in the same mice given normal drinking water instead of alcohol.

New mouse models were made that had both controllable inactivation of one of the MMR genes and abnormal metabolism of alcohol with accumulation of one of its toxic breakdown products (acetaldehyde). These mice were fed alcohol to allow study of the effects of alcohol and its toxic breakdown product on the mechanism of alcohol-induced intestinal tumours. Abnormal alcohol metabolism led to increased DNA damage. Long-term consumption of alcohol by these model mice caused increased numbers of large intestinal tumours, compared with those found in the first mouse model of LS over the same time period. No tumour formation was seen in the model mice given normal water.

The results showed that large intestinal tumours arose from those cells unable to activate MMR. In all the mouse models used in this study, a significant increase in DNA

damage was observed in the mice that received alcohol compared with the mice that received water. A significant increase of the toxic breakdown product (acetaldehyde) of alcohol was detected in the blood of alcohol-treated mice compared with water-treated mice, in the mouse models unable to normally metabolise alcohol and unable to activate MMR compared with the mouse model only unable to activate MMR but able to metabolise alcohol normally. The results obtained revealed the importance of DNA MMR in protecting intestinal cells from alcohol-induced DNA damage and also the importance of normal metabolism of alcohol to help reduce DNA damage. This demonstrated that there is an interaction between alcohol and inactive MMR that contributes to accelerated formation of intestinal tumours after exposure to alcohol.

List of Abbreviations

4-NHE	4-hydroxynonenal
AcAld	Acetaldehyde
Acetyl-CoA	Acetyl-coenzyme A
ADH	Alcohol Dehydrogenase
AICR	American Institute for Cancer Research
ALDH	Aldehyde Dehydrogenase
AODS	Anti-oxidative Defence System
APC	Adenomatous polyposis coli
ATM	Ataxia-telangiectasia mutated
ATR	ATM and Rad3-Related
B2M	Beta-2-Microglobulin
BMI	Body Mass Index
BW	Body-Weight
CBCs	Crypt Base Columnar stem cells
cCas-3	cleaved Caspase-3
CCFR	Colon Cancer Family Registry
CD	Crohn's disease
CGAIGC	Collaborative Group of the Americas on Inherited Gastrointestinal Cancer
CIMP	CpG island Methylator Phenotype
CIN	Chromosomal Instability
CK1	Casein Kinase 1
CoA	Coenzyme A
CRC	Colorectal cancer
CrPdG	R- and S-α-CH_3-γ-OH-1,N^2-propano-2'-deoxyguanosine
CTLs	Cytotoxic T Lymphocytes
CYP2E1	Cytochrome P450
DAB	3,3'-Diaminobenzine
DM	Diabetes Mellitus
dMMR	MMR-deficient or defective Mismatch Repair

DNA	Deoxyribonucleic acid
DNA-PKcs	DNA protein kinase catalytic subunit
DNMTs	DNA Methyltransferases
Dst	Distal colon
EtOH	Ethanol
EXO1	Exonuclease 1
FA	Fanconi Anaemia
FACS	Fluorescent-Activated Cell Sorting
FAE	Follicle Associated Epithelium
FFPE	Formalin-Fixed Paraffin-Embedded
FSPs	Frameshift Peptides
GALT	Gut-Associated Lymphoid Tissue
GFP	Green Fluorescent Protein
GSK3	Glycogen Synthase Kinase 3
H&E	Haematoxylin and Eosin
HEVs	High Endothelial Venules
HNPCC	Hereditary Nonpolyposis Colorectal Cancer
HPRT1	Hypoxanthine Phosphoribosyltransferase 1
i.p.	Intraperitoneal
IBD	Inflammatory Bowel Diseases
ICLs	Inter-strand Crosslinks
IGF	Insulin-like Growth Factor
IHC	Immunohistochemistry
ILFs	Isolated Lymphoid Follicles
IMRC	International Mismatch Repair Consortium
InDel	insertion/deletion
InSiGHT	International Society for Gastrointestinal Hereditary Tumours
IVCs	Individually ventilated cages
JNK	c-Jun N-terminal kinase
K_m	Michaelis-Menten constant
Lgr5	Leucine-rich-repeat-containing G-protein-coupled Receptor 5

LI	Large Intestine
LOVDs	Leiden Open Variation Databases
LS	Lynch Syndrome
MAP	MUTYH Associated Polyposis
MAPK	Mitogen-Activated Protein Kinase
MAT 1	Methyl Adenosine Transferase 1
MDA	Malondialdehyde
mG	membrane-targeted modified Green Fluorescent Protein or GFP
MGMT	Methylguanine-methyltransferase
MMR	Mismatch Repair
MSI	Microsatellite instability
mT	membrane-targeted modified Tomato red fluorescent protein
N^2-EtdG	N^2-ethyl-2′-deoxyguanosine
N^2-EtidG	N^2-ethylidene-2′-deoxyguanosine .
NAD	Nicotinamide Adenine Dinucleotide
NBF	Neutral Buffered Formalin
NER	Nucleotide Excision Repair
NICE	National Institute for Health and Care Excellence
NSAID	Nonsteroidal Anti-Inflammatory Drug
o.g.	oral gavage
PCNA	Proliferating Cell Nuclear Antigen
PGA	Percentage Green Areas
PLSD	Prospective Lynch Syndrome database
pMMR	MMR-proficient
PPAP	Proofreading Polymerase-associated Polyposis
Prx	Proximal colon
RFC	Replication Factor C
RFP	Red Fluorescent Protein
RNS	Reactive Nitrogen Species
ROS	Reactive oxygen species
RPA	Replication Protein A

RT	Room Temperature
SAMe	S-adenosyl-L-methionine
SCNAs	Somatic Copy Number Alterations
SD	Standard Deviation
SI	Small Intestine
SNPs	Single Nucleotide Polymorphisms
TGF	Transforming Growth Factor
TIL	Tumour Infiltrating Lymphocyte
TLS	Tertiary Lymphoid Structures
TMZ	Temozolomide
TNF-α	Tumour Necrosis Factor-α
UC	Ulcerative Colitis
VOC	Volatile Organic Compound
VUS	Variants of Uncertain Significance
WCRF	World Cancer Research Fund
WHO	World Health Organization
WT	Wildtype
γ-H2AX	gamma-H2AX phosphorylation
εdA	1,N^6-ethenodeoxyadenosine
εdC	3,N^4-ethenodeoxycytidine

Table of Contents

Chapter 1: Introduction

1.1 Lynch Syndrome

1.1.1 Lynch Syndrome, mismatch repair genes and susceptibility to cancer

Lynch syndrome (LS), previously called hereditary nonpolyposis colorectal cancer (HNPCC), is probably the most common major cause of inherited susceptibility to cancer, with an estimated prevalence in the general population of between 1/100 and 1/180 (Frankel et al., 2019). LS is characterised by predisposition to a range of cancers, involving most frequently the colorectum and endometrium, and also many other organ sites including ovary, stomach, small intestine, hepatobiliary tract, pancreas, urinary tract, prostate, brain, and sebaceous skin tumours (Møller et al., 2017, 2018). LS is caused by constitutional (germline) pathogenic variants affecting one of four genes encoding the DNA Mismatch Repair (MMR) system components: MLH1, MSH2, MSH6, and PMS2, and hence the current commonly accepted diagnostic definition of LS is carrying such a variant (Thompson et al., 2014; Vasen et al., 2010, 2014, 2013; Frankel et al., 2019; Frayling et al., 2016). However, although it is acknowledged that (there is an opinion that) LS can only be diagnosed in such individuals once cancer has been diagnosed, this is contrary to the hereditary polyposes, which are characterised by the macroscopic syndromic feature of multiple pre-malignant tumours (Vasen et al., 2008). Allied to this, a major purpose of diagnosis of a cancer predisposing condition is to identify those who would benefit from surveillance and prophylactic surgery to prevent cancer (Vasen et al., 2010). Hence, the emerging current view is that it is inconsistent to discriminate against LS by expecting such individuals to develop cancer in order to be diagnosed with the condition, especially as cancer does not always occur (Dominguez-Valentin et al., 2020; Møller et al., 2017, 2018). Hence, it has been proposed that the definition of LS should incorporate recently identified specific microscopic and molecular pre-malignant syndromic features (Cerretelli et al., 2020; Seth et al., 2018). The DNA MMR pathway recognises and repairs both mismatched bases (e.g. C opposite T) and insertions or deletions in repetitive sequences. In LS patients, an inherited MMR gene constitutional variant/mutation, when combined with an acquired second pathogenic variant/mutation due to somatic mutation in the wildtype allele of the same MMR gene, results in the complete loss of MMR pathway function in the affected cells. Deficiency of MMR (dMMR) leads to hypermutability, resulting in an increase in the mutation rate by 100-

to 1000-fold due to uncorrected base mismatches, and to microsatellite instability (MSI) due to variation in the lengths of repetitive sequences (e.g. AAAAAAA… or CACACACA…. or similar, known as microsatellites) due to uncorrected insertion/deletion loops that are prone to occur as DNA replication errors in repetitive sequences (Poulogiannis et al., 2010). However, crucially, dMMR does not simply fail to repair mismatches, it elicits a reduced susceptibility to apoptosis or cell cycle arrest induced by DNA damage recognised by the MMR pathway (Poulogiannis et al., 2010; Toft et al., 1999; Tomlinson & Bodmer, 1999; Zhang et al., 1999).

The International Society for Gastrointestinal Hereditary Cancer (InSiGHT) was the first expert group to define pathogenicity of gene variants according to an agreed set of criteria based upon Bayesian probability, using the five-tier classification system of Plon et al. (Plon et al., 2008; Thompson et al., 2014) . In this system, Class 5 variants are pathogenic and Class 4 likely pathogenic, with Class 3 being variants of uncertain significance (VUS), and Classes 2 and 1 being likely benign and benign respectively. InSiGHT maintains the world reference database of variants observed in MMR genes, as Leiden Open Variation Databases (LOVDs), which are now linked to ClinVar as part of the ClinVar-ClinGen partnership. Interestingly, 82% of the Class 4 and 5 variants of MMR genes listed affect MLH1 and MSH2, with 13% affecting MSH6 and 5% PMS2 (Landrum & Kattman, 2018; Rehm et al., 2015). It should be noted that these pathogenic variants are mostly from cases ascertained by family history. As more cases of LS are ascertained from systematic testing of cancer cases and from gene panel testing, more patients may be identified with pathogenic variants in MSH6 and PMS2, and thus the proportions due to the different MMR genes may alter (Vasen et al., 2013). All types of variants can be pathogenic: nonsense, frameshift, splice-site, missense, insertion–deletion, and large deletions/rearrangements, the largest so far being a 10 Mb inversion affecting MSH2 and which is visible cytogenetically (Li et al., 2006; Taylor et al., 2003; Wagner et al., 2002). Approximately 60% of all putative pathogenic missense mutations causing LS actually disrupt splicing and are thus, in effect, truncating (Thompson et al., 2015). Up to 3% of LS cases are due to variants involving the 3’ end of the EPCAM gene (immediately upstream to MSH2), that result in hypermethylation of the MSH2 promoter or partial deletion of MSH2 (Kempers et al., 2011; Niessen et al., 2009). Another infrequent cause of LS is constitutional methylation of the MLH1 promoter, which occurs in 1–2% of cases (Hitchins et al., 2005; Hitchins & Ward, 2009; Morak et al., 2018). Hypermethylation of the MLH1 promoter is usually sporadic in nature, so it is neither inherited nor heritable, and relatives are therefore

not at risk. However, in a small number of patients, the hypermethylation may be secondary to a large deletion involving LRRFIP2, the gene upstream of MLH1, and it is the deletion that is the heritable pathogenic variant, the methylation is secondary (Morak et al., 2018). Given the risks to relatives it is therefore important to distinguish such cases, and this is achieved by testing both the tumour and constitutional DNA, and finding MLH1 promoter methylation in both, perhaps in the context of an LS family history. It has to be borne in mind that approximately 15% of sporadic colonic cancers are also dMMR due to somatic, so acquired, epimutation of both MLH1 alleles by promoter hypermethylation (Sinicrope & Sargent, 2009). This is a function of such tumours arising from right-sided serrated lesions (Noffsinger, 2009). A higher proportion (25-30%) of sporadic endometrial cancers also have bi-allelic hypermethylation of MLH1, and as with colonic cancers a small proportion are due to constitutional methylation plus a somatic mutation in the normal MLH1 allele (Esteller et al., 1998; Hitchins et al., 2005; Hitchins & Ward, 2009; Simpkins et al., 1999).

1.1.2 DNA mismatch repair mechanisms

The MMR pathway is a highly evolutionarily conserved mechanism responsible for the correction of base mismatches (e.g. C or G opposite T or A) and insertion/deletion loops (occurring in repetitive sequences such as AAAAAA … or CACACACA … due to insertion or deletion of a repeat unit during stalled DNA replication of these repetitive sequences). Such stalling is probably mostly due to replication-associated errors, but is also caused by DNA damage due to oxidative stress, lipid peroxidation, base deamination, methylation, and alkylation (Modrich & Lahue, 1996). A base mismatch or single nucleotide insertion/deletion error is recognised by the MutSα complex, which is composed of MSH2 and MSH6 proteins. Insertion/deletion loops of 2–8 nucleotides are recognised by the alternative complex MutSβ, composed of MSH2 and MSH3 proteins. MutSα complex activation is characterized by ATPase activity, which is important for the interaction with the mismatched DNA and initiation of repair. The binding of MutSα stimulates ATP hydrolysis, leading to a conformational change that subsequently triggers the recruitment of a second complex MutLα, composed of MLH1 and PMS2 proteins (although there is redundancy with PMS1 and MLH3 in this complex). The tetrameric complex, by sliding on the DNA, searches for the single strand DNA mismatch on the new strand (daughter strand). This in turn activates proliferating cell nuclear antigen (PCNA) and replication factor C (RFC). MutLα possesses an intrinsic ATP-stimulated endonuclease activity that requires activation by PCNA in order to create an incision in the recently synthesised daughter strand (containing the error). The incision step is followed by the recruitment of exonuclease 1 (EXO1) that removes the newly synthesised DNA strand up to and beyond the mismatch or loop. DNA polymerase δ resynthesises the DNA, whereas ligase 1 seals the remaining nick (Figure 1.1) (Hsieh & Yamane, 2008).

The MMR pathway is involved in a signalling cascade that leads to either cell cycle arrest and/or apoptosis, if DNA damage has occurred (Stojic et al., 2004). It has been observed that MMR-deficient cells fail to recruit ataxia-telangiectasia mutated (ATM) and ATM and Rad3-related (ATR) proteins; and this prevents p53 phosphorylation in response to DNA damage (Brown et al., 2003; Toft et al., 1999). The underlying mechanisms by which MMR proteins promote DNA damage–induced cell cycle arrest and apoptosis have not been fully elucidated. Two models have been hypothesised: the futile cycling model and the direct damage signalling model. In the futile cycling model, MMR recognises the mismatch

triggering the excision of the newly synthesized strand, although the persistent offending damage on the template strand cannot be excised. MMR initiates futile repair cycles, eventually resulting in the formation of DNA double-strand breaks and thus activating the ATM/ATR/p53 signalling pathway to activate cell cycle arrest and/or apoptosis (Stojic et al., 2004). In the direct damage signalling model, MutSα and MutLα directly recruit ATM/ATR and causes cell cycle arrest and/or apoptosis (Yoshioka et al., 2006). A crucial consequence of this is that the low background level of DNA damage in normal cells may stimulate MMR and thus inhibit the cell cycle, or if severe may stimulate apoptosis, and so net cell turnover does not reach its theoretical maximum. However, if MMR deficiency should occur in such cells, there is no such limitation by stalling of the cell cycle or activation of apoptosis and net cell division increases in an uncontrollable fashion, allied to which as a secondary phenomenon the mutation rate increases, which is manifest as MSI and/or abnormal MMR immunohistochemistry (IHC). This is very useful diagnostically, but it is important to appreciate that it is not the increased mutation rate per se that is driving the carcinogenic process, and neither does it make adenomas progress any quicker than usual (Tomlinson & Bodmer, 1999). However, because mutations are strongly biased towards repetitive DNA sequences in dMMR cells, this has profound consequences for the biology of such tumours and patients with LS due to the strong immunological responses this elicits (Llosa et al., 2015; Pfuderer et al., 2019) and the critical consequences of this are manifest in how LS tumours develop and potentially evade the immune system (see later, section 1.1.7) (Seth et al., 2018).

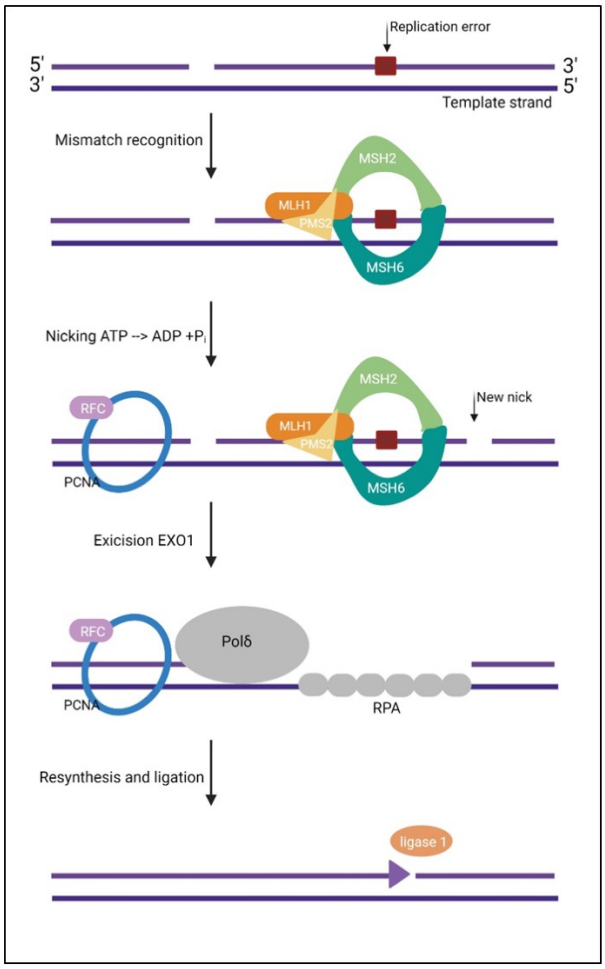

Figure 1.1: Schematic diagram of the DNA Mismatch repair pathway, which is strand-specific (adapted and modified from Hsieh & Yamane, 2008). During DNA synthesis the newly synthesised (daughter) strand (which transiently includes nicks before they are sealed by ligases) may include errors, including base mismatches, insertions or deletions. The base mismatch or single nucleotide insertion/deletion (red square) error is recognized by the complex MutSα composed of MSH2 and MSH6 (whereas insertion/deletion loops of 2-8 nucleotides are recognized by the complex MutSβ composed of MSH2 and MSH3, not shown). The binding of MutSα stimulates ATP-hydrolysis leading to a conformational change triggering the recruitment of a second complex MutLα. MutLα, composed of MLH1 and PMS2, induces ATP hydrolysis causing the translocation of MutSα along the DNA and generation of a new nick of the affected strand. Excision and repair are performed by other factors, including exonuclease 1 (EXO1) which excises the affected strand between the two nicks, whereas proliferating cell nuclear antigen (PCNA), replication factor C (RFC) and DNA polymerase delta (POLδ) repair the strand and this is religated by DNA ligase 1. Replication protein A (RPA) binds to single-stranded DNA, preventing it from winding back on itself or forming secondary structures, keeping the DNA unwound for the polymerase to replicate it. (Image created with BioRender.com).

1.1.3 Lynch syndrome databases and cancer risks

In addition to the MMR gene variant database maintained by InSiGHT (https://www.insight-group.org/), there are other phenotypic databases aimed at understanding the precise risks that LS patients face. Initial estimates were liable to ascertainment bias and thus tended to overestimate by being necessarily retrospective. The penetrance and expressivity of MMR pathogenic variants differs in LS patients according to the MMR gene, age, sex and environmental/lifestyle factors (Diergaarde et al., 2007). Several lifestyle factors, such as smoking, alcohol, and obesity, are associated with an increased risk of sporadic cancer and have been suggested to have similar effects in LS patients. Therefore, as it is fundamental to quantify accurately the risks of developing cancer for LS patients, in order to provide adequate data for surveillance and care, as well as understand the underlying biology, the Prospective Lynch Syndrome Database (PLSD) was established in 2012 by the Mallorca Group of InSiGHT (Dominguez-Valentin, 2020; Møller et al., 2017). The PLSD collects data on LS patients from expert centres and registries worldwide; these patients are thus undergoing colonoscopic surveillance with polypectomy and may also be having therapeutic or prophylactic surgery. It therefore provides information on the natural history of the disease course and the effects of interventions and lifestyle risk factors. The PLSD is linked to the InSiGHT MMR LOVD: all patients on the PLSD must have a Class 4 or 5 MMR variant, so pathogenic or likely pathogenic, according to the InSiGHT classification (InSiGHT, 2020e; Thompson et al., 2014). The PLSD includes basic information on pathogenic genetic variants, sex, and age, plus information such as cancers or pre-cancers diagnosed, age at diagnoses, age at prophylactic surgical removal of organs, and information on pre-cancers. Every patient is followed as an individual, as the family history is ignored so as not to introduce bias, and the database now has >50,000 patient-years of observations (Dominguez-Valentin et al., 2020). The PLSD website (http://lscarisk.org/) is public and allows anyone to determine the risks to an individual of an LS-associated cancer in an interactive graphical form according to their affected gene, age, sex, and whether previously affected by cancer (Dominguez-Valentin, 2020). Important parallel efforts have been made in defining risks in Lynch syndrome by the Colon Cancer Family Registry (CCFR) and the International Mismatch Repair Consortium (IMRC) (Jenkins et al., 2018; Jenkins et al., 2018). The CCFR is an international consortium of six institutes in the United States, Canada, and Australasia formed as a resource to support studies on the aetiology, prevention, and clinical management of colorectal cancer, and utilises a form of modified segregation analysis to minimise

retrospective ascertainment bias (Dowty et al., 2013; Jenkins et al., 2018). It currently has data on >42,500 individuals from >15,000 families on its records and has made significant advances in demonstrating how environmental and lifestyle factors affect cancer risks in LS, such as smoking, increased body mass index, and alcohol consumption (Pande et al., 2010; Win et al., 2011). By contrast, reduced cancer risk is seen with, for example, hormone replacement therapy, vitamin and mineral supplements, nonsteroidal anti-inflammatory drug (NSAID) use, and parity, but there is no change in risk associated with oral contraceptive use (Ait Ouakrim et al., 2015; Chau et al., 2016). The IMRC is a worldwide collaboration of more than 115 investigators from 59 centres, with 20,000 individuals with LS from 8800 families, facilitated by InSiGHT and the Collaborative Group of the Americas on Inherited Gastrointestinal Cancer (CGAIGC) (Jenkins et al., 2018). Reduced cancer risk has been observed in a series of clinical trials using aspirin (Burn et al., 2011, 2012; Liljegren et al., 2008).

1.1.4 Pathology of Lynch syndrome cancers

Typical histological features of LS tumours are best exemplified by colorectal cancer (CRC), which often shows a combination of the presence of prominent tumour-infiltrating lymphocytes, Crohn-like peritumoural lymphoid aggregates, poor differentiation, frequently with areas of mucinous and/or signet-ring cell patterns, sometimes with a medullary growth pattern (Alexander et al., 2001; Truta et al., 2008). These characteristics can be seen in both Lynch syndrome CRC and sporadic dMMR bowel cancers, but are not sufficiently specific to distinguish them from MMR-proficient (pMMR) cancers. Fewer data have been published about non-colorectal LS-associated cancers. LS associated gastric carcinomas are mostly of the intestinal-type with fewer diffuse-type, and rarely of mucinous type, and an associated immune gastritis is reported (Aarnio et al., 1997; Adar et al., 2019; Capelle et al., 2010; Gylling et al., 2007). LS-associated small intestinal adenocarcinomas often display mucinous, signet-ring cell, or medullary differentiation, with tumour-infiltrating lymphocytes and Crohn-like reactions, as do ampullary adenocarcinomas (Jun et al., 2017).

1.1.5 Testing for Lynch syndrome cancers

Testing of (usually selected) patients with CRC, endometrial cancer, and/or other types of LS-associated cancer is recommended by many guidelines and organisations, generally starting with testing the tumours for either the presence of MSI or the absence (or abnormal expression) of mismatch repair proteins. There is no consensus regarding whether MMR immunohistochemistry or MSI testing is the better first test in CRCs as they have similar test performance characteristics in detecting LS: sensitivity of MSI testing is 88 - 100% and MMR IHC is 73 - 100%, with specificity of MSI testing is 68 - 84% versus MMR IHC specificity of 78 - 98% (Snowsill et al., 2014, 2017). They may be used serially, or in combination (National Institute for Health and Care Excellence, 2017; Sie et al., 2014; Wedden et al., 2019). However, evidence is now emerging that IHC may be the preferred option when testing endometrial cancers (systematic testing of which has recently been approved by the UK National Institute for Health and Care Excellence (NICE), as a recent UK study has shown that while MSI and MMR IHC have similar specificity (83.7 versus 81%), MSI has only 56.3% sensitivity compared with 100% for MMR IHC in endometrial cancers (Crosbie et al., 2019; Ryan et al., 2020). MMR IHC is the better option for small biopsies, cancers with a low tumour

cell proportion, or an intense inflammatory reaction. Subsequent testing for MLH1 promoter hypermethylation and somatic (rather than constitutional/germline) mutations can be used to clarify the risk of inherited pathogenic variants in suspected LS patients. MLH1 promoter hypermethylation testing may be used as an alternative to BRAF V600E mutation analysis in colonic cancers (Adar et al., 2017; Bläker et al., 2019; Marks & West, 2020). The use of larger targeted gene mutation panels (or whole exome/genome sequencing) that includes MMR gene testing with mutation analyses is becoming more widespread (Taylor et al., 2018).

Immunohistochemical staining for the four major DNA mismatch repair proteins (MLH1, MSH2, MSH6, and PMS2) is probably the most common UK test to screen CRCs and other tumours for dMMR (Sie et al., 2014; Snowsill et al., 2017; Wedden et al., 2019). The nuclear expression of all four MMR proteins suggests mismatch repair proficiency with microsatellite stability (Arends et al., 2008; Frayling & Arends, 2015; Mensenkamp et al., 2014). Loss or abnormality of nuclear staining for any of the proteins indicates dMMR and suggests the most likely MMR gene involved (Frayling & Arends, 2015; Mensenkamp et al., 2014). Loss of MSH2 alone, or loss of both MSH2 and MSH6, suggests that a mutation or abnormality in MSH2 is most likely. Similarly, loss of MLH1 alone, or loss of both MLH1 and PMS2, suggests an underlying mutation, abnormality, or promoter methylation in MLH1. Combined loss of both MSH2 and MSH6 (or of both MLH1 and PMS2) reflects the heterodimeric binding of MSH2 with MSH6 (or of MLH1 with PMS2) in the mismatch repair complex MutSα (or of MutLα), such that loss of the first protein partner generates instability and loss of the second (South et al., 2008). Usually, there is nuclear staining in the nuclei of both tumour cells and adjacent normal epithelial cells, stromal cells, and lymphocytes. In a dMMR tumour due to MSH2 mutation, there is loss of nuclear MSH2 and MSH6 and intact staining for MLH1 and PMS2. In a dMMR tumour due to MLH1 mutation, there is loss of nuclear MLH1 and PMS2 and intact staining for MSH2 and MSH6. This pattern of combined MLH1 and PMS2 loss could be seen either in a sporadic tumour (most commonly due to MLH1 promoter methylation) or in LS due to constitutional MLH1 mutation. Correct MMR IHC interpretation requires adequate internal control staining of the adjacent stromal and lymphoid cells to confirm good fixation of the tissue region (Arends et al., 2008; Frayling & Arends, 2015). Patchy intact nuclear staining may occur due to variable fixation, tissue hypoxia, or unequal antibody diffusion (Chang et al., 2002; Mihaylova et al., 2003). Cytoplasmic staining may occur, but if nuclear staining is lost, this is considered abnormal, indicating dMMR (Sekine et al., 2017). Weak, patchy nucleolar staining, or sometimes absence of MSH6 has been described in rectal

tumours following neoadjuvant treatment without MSI or a mutation confirmed by molecular testing (Bao et al., 2010; Radu et al., 2011). Notably, heterogeneous staining or loss of MSH6 can be due to secondary (non-germline) acquired somatic mutations in the MSH6 coding repetitive mononucleotide tract (Graham et al., 2015; Shia et al., 2013). Approximately 3–10% of LS associated dMMR tumours show no abnormality on IHC testing (presumably because of variants that disrupt normal MMR protein function but nonetheless enable protein detection by IHC) (Bartley et al., 2012).

Testing DNA extracted from tumours for MSI involves investigating the presence of extra alleles (longer or shorter) at a microsatellite locus compared with normal tissue or blood from the same individual (Frayling, 1999). Microsatellites vary in their propensity to show instability, and thus the frequency with which the same microsatellite is altered varies in different tumour types. Instability is more likely to be observed at mononucleotide repeats (e.g. AAAAA …) than at dinucleotide repeats (e.g. CACACA …). Microsatellite loci or markers used in colonic cancer MSI testing are known to have reduced sensitivity at detecting MSI in non-colonic cancers, including endometrial, small intestinal, or gastric cancers; in tumours from LS patients with MSH6 or PMS2 mutations; and in colonic adenomas (Hause et al., 2016). Therefore, a proportion of LS-associated tumours may not appear to have MSI using the standard test but might be identified by abnormal MMR immunohistochemistry. The efficacy of MMR IHC and MSI testing may be significantly enhanced by testing more than one tumour from the same individual or family, particularly if there are tumours that are multiple or rarely seen in LS (e.g. colorectal adenomas, small intestinal cancers, hepatobiliary, upper urinary tract, and cutaneous sebaceous tumours) (InSiGHT, 2020e; Ju et al., 2018). Consistent IHC abnormality of one mismatch repair protein in more than one tumour from an individual or family represents very good evidence for variant pathogenicity (InSiGHT, 2020e; Loukola et al., 1999). Some CRCs due to MUTYH associated polyposis (MAP) or proofreading polymerase-associated polyposis (PPAP) may exhibit MSI and/or abnormal IHC due to somatically acquired MMR gene mutations. Approximately 13–15% of sporadic colonic cancers have dMMR, usually due to epigenetic silencing of both alleles of MLH1 by promoter hypermethylation. Hence, although overall unselected dMMR colonic cancers have a relatively poor positive predictive value for LS, because the proportion of colonic cancers with MSI due to LS varies with age this can be exploited clinically. In individuals younger than the age of 57, more than half of all dMMR colonic cancers will be due to LS, whereas over this age less than half will be, although even at age 70 approximately 25% dMMR colonic

cancers will be due to LS (Frayling et al., 2016; Mensenkamp et al., 2014; van Lier et al., 2012). In contrast, proficient mismatch repair (pMMR) tumours have a good negative predictive value for LS. Further tests (BRAF mutation and MLH1 methylation tests) are required for MLH1-negative cancers to distinguish between LS and sporadic origin (National Institute for Health and Care Excellence, 2017; Snowsill et al., 2014, 2017). Another important practice point is that rectal cancers are distinct from colonic cancers in the diagnosis of LS. Because sporadic colonic cancers with dMMR arise largely from right-sided serrated lesions, sporadic rectal cancers with dMMR are correspondingly rare, if they occur at all, and hence a rectal cancer with dMMR at any age are considered to be due to LS until proven otherwise (de Rosa et al., 2016; Nilbert et al., 1999). The activating missense variant BRAF p.V600E occurs in sporadic colonic cancers with dMMR, but not in those due to LS; therefore, BRAF p.V600E is highly predictive of the tumour being of sporadic origin rather than LS (National Institute for Health and Care Excellence, 2017; Noffsinger, 2009; Snowsill et al., 2014, 2017; Thiel et al., 2013). However, sporadic tumours may occasionally occur in patients with LS, so the absence of BRAF p.V600E does not definitively diagnose LS but does indicate that LS is more likely. Alternatively, detection of MLH1 promoter hypermethylation in a colonic cancer provides good, although not unequivocal, evidence that the tumour is sporadic in origin, as occasional sporadic tumours do occur in LS and constitutional MLH1 promoter methylation can be found in a small proportion of patients with LS (Hitchins & Ward, 2009; Morak et al., 2018). Patients with digenic LS, who have inherited pathogenic variants in more than one MMR gene, are occasionally seen, but it is unclear if their risks are increased over those patients with a pathogenic variant in one MMR gene. It is often useful to have samples from more than one individual in the family, because case segregation studies may be required to determine pathogenicity or whether an individual is a phenocopy (InSiGHT, 2020e; Thompson et al., 2014). If the family shows evidence of hereditary transmission of LS but no point mutation is found, tests for large-scale mutations, such as deletion of a whole exon (or more), can be performed; 12–40% of pathogenic variants are of this type (InSiGHT, 2020b, 2020a, 2020c, 2020d; Ligtenberg et al., 2009; Smith et al., 2016; Taylor et al., 2003; Wagner et al., 2002). LS-related tumour types that are rare in the general population and thus have a high predictive value for LS, such as small intestinal and hepatobiliary cancer, upper urinary tract and bladder (under age 60) transitional cell carcinoma, or skin sebaceous adenoma/carcinomas, are therefore worth testing (Jessup et al., 2016). Synchronous or

metachronous bowel cancers are also significant, as is the development of any two LS-related tumours (e.g. CRC and endometrial cancer), and all such cases warrant testing for LS.

1.1.6 Precursors of cancers in Lynch syndrome

When LS was being defined in the early 1990s, the only known pathway to CRC was based on the work of Dukes, Bussey, and Morson on FAP. First was Dukes' concept of 'simple tumours and cancer' described in 1925, as part of his system for the staging of rectal cancer in FAP, followed by the adenoma to carcinoma pathway published in 1958 (Dukes & Bussey, 1958; Dukes, 1926; Dukes, 1932). Naturally, the reasonable assumption was that the same pathway applied in LS and colonoscopic surveillance to remove premalignant adenomas would thus be beneficial in LS. When early data on the efficacy of surveillance in LS showed a large number of interval cancers, and, moreover, these cancers occurred despite the interval between colonoscopies being steadily reduced to less than 3 years and sometimes even less than 1 year, it appeared that LS CRCs may develop much more rapidly than sporadic ones, assuming they all arose from adenomas (Vasen et al., 2010, 1995). In addition, because of the increased mutation rate observed in LS cancers, allied with the prevailing concept that genomic instability characterised all cancer, it was further assumed that this must be what was driving a faster adenoma-carcinoma progression (Poulogiannis et al., 2010; Tomlinson & Bodmer, 1999; Tomlinson et al., 1996). Furthermore, although dMMR adenomas could be found in LS patients, further doubts were raised when aspirin treatment failed to reduce the incidence of adenomas (although it later reduced that of CRCs), and results from the PLSD became available (Burn et al., 2011; Loukola et al., 1999; Møller et al., 2017; Seppälä et al., 2017; Seppälä et al., 2019). LS patients on colonoscopic surveillance at various intervals could finally be compared (Seppälä et al., 2017). Remarkably, within the limits measurable, colonoscopy did not appear to reduce the rate at which CRCs were arising in LS patients, despite it being associated with a significant reduction in mortality and, in addition, stage was not related to the interval since last colonoscopy—completely the opposite of population screening programmes, which are based primarily on adenoma removal (Engel et al., 2018; Møller et al., 2017; Seppälä et al., 2017; Seppälä et al., 2019).

LS patient survival was shown to be improved by colonoscopic surveillance, enabling earlier diagnosis and a degree of downstaging, together this mass of evidence led to the conclusion that a pathway independent of adenomas must be occurring, and moreover, a pathway in which precursors were less obvious on colonoscopy (Snowsill et al., 2014). At about the same time, it was discovered that LS patients harbour an enormous number of dMMR crypts in the colorectum (~1/cm2 mucosa, so ~10 000 crypts/ patient), which are not dysplastic, and yet LS patients only go on to eventually develop between zero, one, two, or three cancers (Kloor et al., 2012; Staffa et al., 2015). It was suggested that these dMMR crypts might lead to cancers, perhaps by a route that was not readily visible on colonoscopy and this was supported by the finding of flat intramucosal cancers, in which the Wnt pathway was activated by mutations not in *Adenomatous polyposis coli* (*APC)* as in classical adenomas, but via mutations in repetitive coding sequences in the beta-catenin gene, as predicted from dMMR (Ahadova et al., 2016). It is intriguing that subsequent work to sequence LS cancers has shown that some 61% of *APC* mutations are predicted to occur after MMR deficiency occurs, as they are found in repetitive sequences, exactly as would be expected in dMMR tumours. Hence, a proportion of these beta-catenin–mutant flat lesions acquire secondary *APC* mutations, thence to become polypoid adenomas and subsequently cancers (Ahadova et al., 2018; Binder et al., 2017).

The current model describes at least three pathways to CRCs in LS, not including sporadic colonic cancer due to a right-sided sessile lesion, which are occasionally observed (Figure 1.2). The first pathway is via sporadic adenomas that acquire secondary dMMR. The third pathway is via flat cancers within the mucosa that arise directly from dMMR crypts, and the second pathway is LS-specific polypoid adenomas that arise from flat dysplastic lesions due to secondary *APC* mutations (Ahadova et al., 2018). Hence, a proportion of LS CRCs arise from flat dysplastic / adenomatous lesions, which are inherently more difficult to detect endoscopically, let alone remove on colonoscopy, explaining at least in part the apparent high rate of interval cancers and the previous suggestion (now regarded as incorrect) of a faster progression rate in LS. Building on this, it has been shown that the cancers in patients with LS due to PMS2 mutations arise largely along pathway 1 (from sporadic adenomas), further explaining why patients with pathogenic PMS2 variants have only a small increased risk of CRC (Ten Broeke et al., 2018). It is interesting that very recently it has been found that pathway 3 (dMMR crypts evolving into flat cancers) predominates over pathway 2 (polypoid adenomas arising from flat dysplastic lesions) in patients with pathogenic MLH1 variants, but

pathway 2 predominates over pathway 3 in those with MSH2 pathogenic variants (Engel et al., 2020). These fascinating findings have clear implications for future surveillance strategies, which may soon also include modalities such as prophylactic aspirin and vaccines, to address the inherently limited efficacy of colonoscopy and increased risks of cancers in LS at sites other than the large bowel, which are becoming the predominant cause of mortality in LS patients under surveillance (Møller et al., 2017, 2018). Observers have recently found dMMR glands in morphologically normal endometrium from LS patients, which in turn has implications for the understanding of LS carcinogenesis in that tissue (Crosbie et al., 2019).

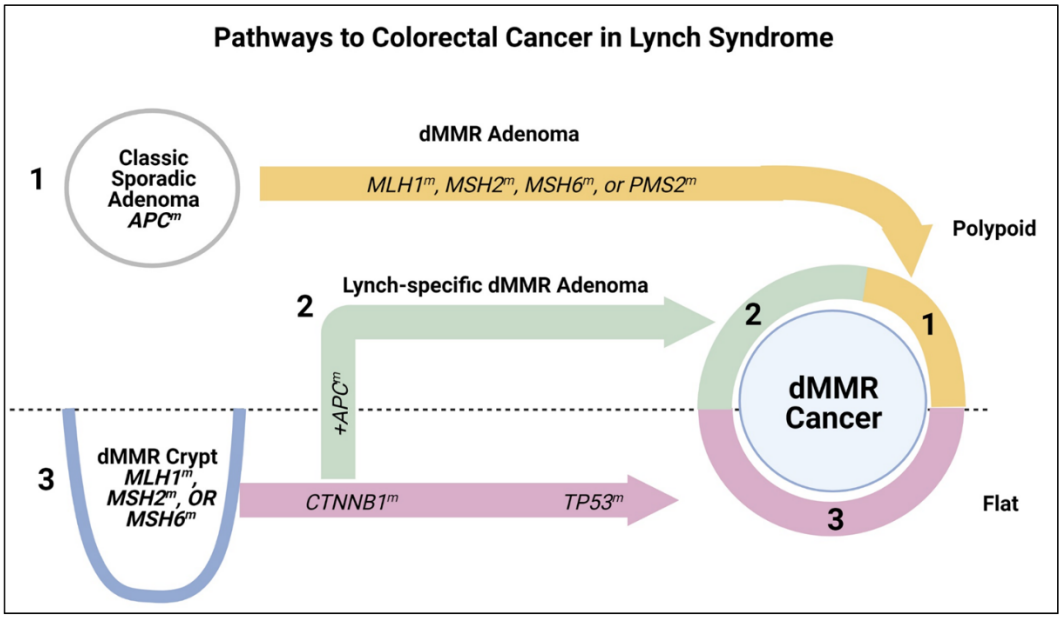

Figure 1.2: Pathways to CRC in Lynch syndrome (adapted and modified from Ahadova et al., 2018, 2016). There are three pathways to dMMR CRCs in LS. Pathway 1: Classic sporadic polypoid adenomas, initiated by Wnt pathway activation due to mutations in APC (APC^m), acquire dMMR through somatic mutation of the remaining normal MMR allele ($MLH1^m$, $MSH2^m$, $MSH6^m$, or $PMS2^m$). This can occur at any stage of adenoma progression, from early adenoma through to adenoma-carcinoma transition. Pathway 3: Crypts that have acquired dMMR due to somatic mutation of the normal MMR allele are not dysplastic, but if they undergo somatic mutation of beta-catenin ($CTNNB1^m$), which activates the Wnt pathway, they become flat adenomas/adenocarcinomas that later acquire mutations in TP53 ($TP53^m$), an otherwise rare event in dMMR CRCs. Pathway 2: A proportion of Pathway 3 lesions acquire secondary APC mutations and thus become polypoid adenomas. Because of this unique combination of somatic events, these Pathway 2 adenomas are, as far as is known, specific to LS (hence 'Lynch-specific dMMR adenomas'). Regarding pathways 2 and 3 in their original proposal, Ahadova and colleagues remark: 'For better visibility, pre-malignant lesions that do not develop into cancer are not included in the diagram, because their number greatly exceeds the number of carcinomas'. Pathway 1 predominates in patients with LS due to PMS2 pathogenic variants, whereas CTNNB1-mutant tumours are more likely in MLH1 patients and APC-mutant tumours are more likely in MSH2 and MSH6 patients. Note that sporadic colonic cancers that arise from serrated lesions with MLH1 deficiency due to somatic biallelic hypermethylation of the MLH1 promoter may occur in LS, albeit perhaps less often due to the enhanced immunity in LS patients against dMMR cells because of chronic autoimmunisation from the novel frameshift peptides generated from dMMR crypts. (Image created with BioRender.com)

1.1.7 Immune escape by Lynch Syndrome neoplasms

The early general observations of large local tumours and a lower rate of metastasis, together with a strong immune reaction to LS cancers, such as increased tumour infiltrating lymphocytes (TIL) and tertiary lymphoid structures (TLS; also termed Crohn-like peritumoural lymphoid aggregates or follicles), later backed up by gene expression signatures characteristic of immune cell activation, all indicate an important role for the immune system in LS (Aaltonen et al., 1994; Llosa et al., 2015; Smyrk et al., 2001). However, in the context of the normal immune architecture in the bowel, gut-associated lymphoid tissue (GALT) comprises both isolated and aggregated lymphoid follicles in both the small and large intestines. Humans have approximately 30,000 isolated lymphoid follicles (ILFs) scattered throughout the large and small intestines, but especially in the colon (Sipos & Muezes, 2011). ILFs vary in their distribution within the large and small intestines, may be mucosal or sub-mucosal, and at their simplest may consist of a single follicle, with or without some T cells (Agace & McCoy, 2017; Mowat & Agace, 2014). They are considered to be the main source of immune priming in the colon and from where Crohn's disease originates, and they have specialised follicle associated epithelium (FAE), which overlies a subepithelial dome containing numerous macrophages, dendritic cells, T and B lymphocytes, and special antigen sampling microfold/M cells (Colbeck et al., 2017; Stranford & Ruddle, 2012). The FAE has a crucial role in the initiation of the mucosal and systemic immune responses (Lorenz & Newberry, 2004). However, the relationship between Crohn-like follicles in LS and ILFs in normal colon is not completely clear. In LS, the follicles are generally peritumoural and not located inside cancers, and although they do not have FAE, they do have T cells, B cells, and germinal centres (Bento et al., 2015; Pfuderer et al., 2019). Whether they are induced de novo, as in chronic inflammation, or develop from submucosal ILFs remains to be determined (Drayton et al., 2006). Crohn-like follicles/TLS are found in CRCs apart from LS; however, the frequency/number is highest in LS cancers compared with sporadic dMMR and pMMR CRCs, which is not simply related to age (Pfuderer et al., 2019).

In recent years, there has been a growing interest in TLSs in a variety of cancers including CRC, in particular as prognostic indicators of cancer progression and response predictors to immunotherapy (Colbeck et al., 2017; Sautès-Fridman et al., 2019). In hepatocellular carcinoma, intra-tumoural TLSs correlated with a lower risk of early relapse after surgery (Calderaro et al., 2019). In sarcoma, melanoma, and renal cell carcinoma, both intra-

tumoural location and the presence of B cells (but not T cells), and particularly germinal centres, correlate with improved outcomes to checkpoint blockade immunotherapy (Cabrita et al., 2020; Helmink et al., 2020; Petitprez et al., 2020). Further studies of the location, cellular composition, and presence of germinal centres in TLS in hereditary dMMR may therefore shed light on their role in LS.

In dMMR cells, predictable mutations can and do occur in repetitive protein coding sequences and result in frameshift peptides (FSPs) (Saeterdal et al., 2001; Schwitalle et al., 2004; Woerner et al., 2001). Such FSPs are novel antigenic epitopes and elicit both humoral and cellular immune responses, which are seen as TILs around the dMMR crypts in LS patients as well as in dMMR cancers, both sporadic and due to LS (Kloor et al., 2012; Linnebacher et al., 2001; Reuschenbach et al., 2010; Schwitalle et al., 2004). In the face of such responses, how is it possible for tumours, let alone cancers, to develop in LS? The answer lies in the proposed three step process of elimination, equilibrium, and escape (Figure 1.3) (Dunn et al., 2004; Seth et al., 2018). Cells generating FSPs, present the FSPs on their surface by MHC-I, and are subjected to attack by cytotoxic T lymphocytes (CTLs), resulting in elimination. However, cells that acquire activating mutations in PDL1 before they are eliminated can hold the immune system to a local standstill (activating the PD-1 – PD-L1 immune checkpoint)—the process of equilibrium. Subsequently, if before being eliminated these cells manage to acquire inactivating mutations in MHC-I or MHC-II (HLA classes I & II) and related genes, that abrogate presentation of FSPs on their surface, they are then able to escape the immune system, at least locally.

Given the huge number of dMMR crypts in an LS patient, but that the average LS patient manifests between zero, one, two, or three CRCs, it is clear that the process of elimination must be highly efficient, giving a different perspective on cancer biology (Ahadova et al., 2018; Møller et al., 2017). A number of different escape mechanisms have been observed. The most common, seen in approximately 30% of dMMR CRCs, is mutation of beta-2-microglobulin (B2M), which prevents MHC-I presentation of FSPs. This was an early observation, the full significance of which is only now apparent (Bicknell et al., 1996; Bodmer et al., 1993; Clendenning et al., 2018; Kloor et al., 2007, 2010). The outgrowth of such B2M mutant clones is a prime example of cancer immunoediting, which has been further related to variation in host immune function, for example, mucosal density of FOXP3-positive regulatory T cells, indicating that such factors may be additional modifiers of LS (Echterdiek

et al., 2016). It is notable that B2M mutations in dMMR cancers are significantly associated with an almost zero rate of metastasis and thus indicate highly favourable prognosis (Koelzer et al., 2012; Tikidzhieva et al., 2012). In addition to mutations in B2M, mutations of CIITA or RFX5 are seen in approximately 20% of dMMR CRCs and prevent MHC-II antigen presentation, whereas approximately 10% of dMMR CRCs have mutations of TAP1 or TAP2, which are antigenic peptide transporters contributing to the process of antigen presentation, thus also preventing antigen presentation on the cell surface (Kasajima et al., 2010; Michel et al., 2010).

In such ways, tumour cells escape the attention of the host's immune system, both locally and in the circulation, but are in turn liable to attack with help from immunotherapy, such as anti-PD-1 or PD-L1 immune checkpoint blockade (Le et al., 2015; Steinert et al., 2014). The full variety of mechanisms by which tumours, and dMMR tumours in particular, manage to evade the immune system has yet to be determined. Undoubtedly, the colorectal microbiome plays an important part in the process of CRC development in LS as well as sporadically (Sears & Pardoll, 2018). Intriguingly, the immune response to dMMR CRCs in the form of the development of high endothelial venules (HEVs) responsible for trafficking lymphocytes into lymphoid follicles/TLS is stronger in LS patients than in sporadic dMMR colonic cancers, and especially high HEV densities in B2M mutant tumours support the concept of immunoediting during tumour evolution (Pfuderer et al., 2019). Such higher HEV densities in B2M-mutant tumours imply that under strong immunoselective pressure created by immune cells recruited via HEVs, tumour cells that have lost MHC class I antigens gain growth advantage due to immunoediting, thus revealing a major role of HEVs in enhancing the immunoselective pressure on highly immunogenic cancers. Taken together with the high numbers of dMMR crypts in LS and the low numbers of CRCs that actually manifest, these findings all point toward a longer process of immunoediting in LS CRCs, possibly due to the pre-existing dMMR crypts immunising LS patients against their own propensity to cancer, and explaining the higher proportion of B2M mutations in LS compared to sporadic CRCs (Kloor et al., 2012; Pfuderer et al., 2019; Staffa et al., 2015). However, HEVs generally recruit naïve lymphocytes from the blood into tissues and HEV-containing Crohn-like aggregates are generally seen in a peritumoural location in both pMMR and dMMR cancers, so our understanding of HEV and TLS in LS is as yet incomplete (Ager & May, 2015; Bento et al., 2015; Pfuderer et al., 2019).

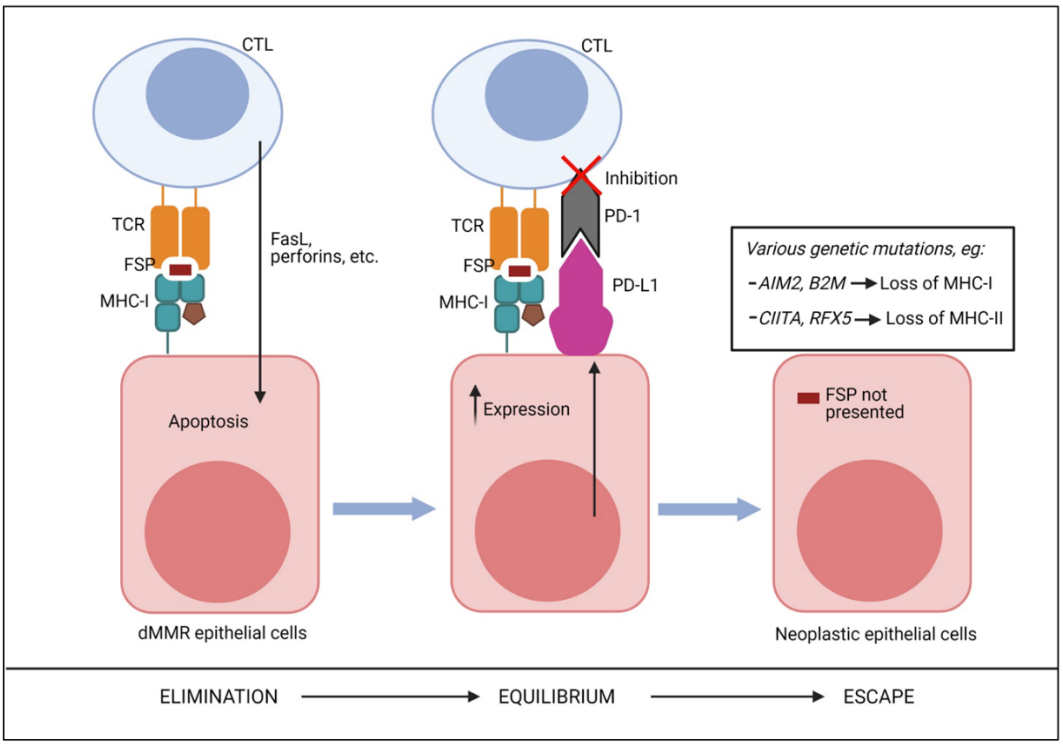

Figure 1.3: Schematic diagram of the three-step process of elimination, equilibrium, and escape in MMR-deficient colorectal neoplasms (adapted and modified from Seth et al., 2018). CRCs in both LS and sporadic MSI CRCs elicit a strong immune response and undergo significant immunoediting. Cytotoxic T-lymphocytes (CTLs) are able to recognise immunogenic frameshift peptides (FSPs, red rectangle) that are synthesised in MMR-deficient cells as a result of unrepaired insertion/deletion loops in repetitive coding DNA sequences. CTLs can induce apoptosis of such dMMR cells (Elimination). However, tumour cells may evolve mechanisms to prevent immune destruction, including inhibition of CTLs by up-regulating expression of immune checkpoint proteins, such as PD-L1 (Equilibrium), or through various genetic mutations leading to loss of FSP antigen presentation (mutations to *AIM2* or *B2M* for loss of MHC class I antigen presentation; mutations in *CIITA* or *RFX5* for loss of MHC class II antigen presentation) (Escape). (Image created with BioRender.com).

1.1.8 Lynch Syndrome mouse models

Mouse models have long been used as an essential tool to study and understand tumorigenesis and its mechanisms in a physiological system (Jahid & Lipkin, 2010). The use of tumour cell lines to modulate a gene's expression has the advantage of being a simple and easy way of performing experiments; however, cell culture does not model the complexity of the tumour microenvironment *in vivo* (McIntyre et al., 2015). The genetic composition of the mouse and human genomes has been mostly maintained through evolution, considering their developmental gap, and most cancer pathways are operative in both organisms. The genomic and transcriptomic landscapes and sequences of inbred laboratory mouse strains are well established and mice have been shown to be good models of a variety of diseases due to their ease of genetic manipulation, allowing experimental testing of genetic mutations in a cost-effective way (McIntyre et al., 2015).

90% of all LS cases with cancer are caused by mutations in *MLH1* and *MSH2*, whereas mutations in other MMR genes are less deleterious (de la Chapelle, 2005). The earliest murine models with potential to represent LS were *Mlh1* knockout (*Mlh1*$^{-/-}$) mice and *Msh2* knockout (*Msh2*$^{-/-}$) mice; *Msh2*$^{-/-}$ mice showed complete loss of MMR pathway function in all cells resulting in high mutation rate (small insertions/deletions in mononucleotide and dinucleotide repeats) leading to high predisposition to cancer development with the MSI phenotype (de Wind et al., 1995; Jahid & Lipkin, 2010). Unfortunately, *Msh2*$^{-/-}$ mice had a short life span caused by the early development of lymphomas (mainly thymic T-cell lymphomas) with only a few mice surviving long enough to develop small numbers of intestinal adenomas (de Wind et al., 1995; McIntyre et al., 2015; Reitmair et al., 1995). Closely similar phenotypes were observed in *Mlh1*$^{-/-}$ deficient mice (Edelmann & Edelmann, 2004; Edelmann et al., 1999; Jahid & Lipkin, 2010). Thus, the possible use of these constitutive knockout mouse models for the study of LS colorectal tumourigenesis and progression is very limited by their early development of lymphoma in around 80% of mice (Toft et al, 1999).

LS mouse models deficient in other MMR genes have also been studied. *Msh6*$^{-/-}$ and *Msh3*$^{-/-}$ deficient mice showed a mild cancer predisposition characterized by late onset of cancer, with *Msh6*$^{-/-}$ mice developing mostly lymphomas with some epithelial tumours originating from the skin and uterus but only rarely from the intestines, whereas *Msh3*$^{-/-}$ mice either did not cause cancer predisposition or did so at a very late age, although combined *Msh6*$^{-/-}$ and

Msh3$^{-/-}$ did produce some late onset intestinal tumours similar to either *Msh2*$^{-/-}$ or *Mlh1*$^{-/-}$ mice (de Wind et al., 1999; Edelmann et al., 1997, 2000) . *Pms2*$^{-/-}$ deficient mice showed only late onset of lymphomas and sarcomas (Baker et al., 1995; Prolla et al., 1998).

To restrict gene modifications to a specific tissue or organ of interest, tissue-specific Cre-recombinase transgenic approaches can be used. Cre is a site-specific recombinase derived from the P1 bacteriophage that catalyses recombination between two loxP sites flanking the critical region of the gene of interest, resulting in excision of this region (flanking loxP sites are commonly termed flox sites) (Nagy, 2000). Tamoxifen-inducible forms of Cre recombinase (CreERT2) were developed that are only active in the presence of Tamoxifen, and expression of Cre or CreERT2 can be targeted to the intestinal epithelium by driving its expression by tissue-specific gene promoters such as either the *Villin* promoter or the *Lgr5* promoter (both are large and small intestinal specific genes) (Barker et al., 2007; Kucherlapati et al., 2010). A *Villin-Cre;Msh2*$^{loxP/loxP}$ mouse model was generated; these *Villin-Cre;Msh2*$^{loxP/loxP}$ mice showed intestinal tumorigenesis (adenomas and adenocarcinomas), but develop few lymphomas (Mcilhatton et al., 2016; McIntyre et al., 2015).

Recently, Wojciechowicz et al (2014) generated a LS mouse model using the *Lgr5* promoter to drive Tamoxifen-inducible Cre recombinase, in which loss of Msh2 expression is induced only in the murine small and large intestinal crypt base columnar stem cells (CBCs) (Wojciechowicz et al., 2014). Wojciechowicz et al generated the *Lgr5CreERT2; Msh2*$^{flox/-}$ mice by intercrossing the *Lgr5CreERT2* mouse line (created by Barker et al. (2007) with the *Msh2*-null (*Msh2*$^{-}$) and *Msh2*-floxed (*Msh2*^{flox}) lines (Barker et al., 2007; Claij & te Riele, 2004; de Wind et al., 1995). This mouse model is described in detail in Chapter 3. In *Lgr5CreERT2; Msh2*$^{flox/-}$ mice, tumorigenesis can be initiated by somatic loss of the second *Msh2* allele in scattered foci along the intestines via Tamoxifen-induced activation of Cre expressed from the *Lgr5CreERT2* transgene, mimicking the situation in LS patients. In Wojciechowicz et al. (2014), *Lgr5CreERT2; Msh2*$^{flox/-}$ mice developed intestinal tumours (adenomas and adenocarcinomas) after 19 months (Wojciechowicz et al., 2014). In this project, the *Lgr5CreERT2; Msh2*$^{flox/-}$ (Msh2-LS) mouse model was used to investigate intestinal tumour formation and progression with and without ethanol exposure.

1.2 Colorectal cancer

1.2.1 Epidemiology of sporadic colorectal cancer

CRC is the third most commonly diagnosed cancer worldwide in males and the second in females, with more than 1.9 million new cases and approximately 935,000 deaths in 2020 according to the World Health Organization (*Global Cancer Observatory*, 2020). In the UK, CRC is the 4th most common cancer, accounting for 11% of all new cancer cases in 2017, with around 42,300 new CRC cases in the UK every year (2015-2017), and approximately 16,600 CRC deaths in the UK every year (2016-2018) (Cancer Research UK, 2016b). In the UK, 44% of CRC cases are in females, and 56% are in males (Cancer Research UK, 2016a). Overall, left-sided (descending colon, sigmoid colon, and rectum) CRCs are more common than right-sided (caecum, ascending colon, and transverse colon) cancers (Hsu et al., 2019). Incidence rates vary geographically, with the highest rates in developed countries, such as North America, Europe and Australia (*Global Cancer Observatory*, 2020), although CRC incidence rates are increasing in developing countries (Arnold et al., 2017).

1.2.2 Pathogenesis and pathology of sporadic colorectal cancer

CRCs are malignant neoplasms of the lining mucosal epithelium of the large intestine, anywhere from the ileocaecal valve to the rectum. The large intestine can be divided into anatomic right and left sides. The right colon consists of the caecum, ascending colon, hepatic flexure and the transverse colon, whereas the left colon includes the descending colon, sigmoid colon, recto-sigmoid junction, and rectum (Figure 1.4). During embryogenesis, the right side derives from the midgut, whereas the left derives from the hindgut and the junction between the two is usually just proximal to the splenic flexure (Glebov et al., 2003). The colorectal wall is composed of four layers: serosa, muscularis propria, submucosa and mucosa that are very similar in mice and in humans (Treuting et al., 2017a, 2017b). The serosa is the outermost layer and has connective tissue and covering mesothelium for those parts of the bowel surface in contact with the peritoneal cavity. The muscularis propria is a double layer of smooth muscle (inner circular and outer longitudinal muscle fibres), which provide peristaltic movement that pushes the contents along the intestines. The connective tissue of the submucosa contains adipose cells, fibroblasts, nerves, blood vessels and lymphatic vessels. The mucosa is the innermost layer that can be further subdivided into

lining columnar epithelium, organised into test-tube shaped crypts, involved in water absorption and mucus secretion, lamina propria (connective tissue supporting the crypts) and muscularis mucosae (thin strip of smooth muscle at the base of the mucosa) (Treuting et al., 2017b).

The mucosal crypts contain a variety of specialized differentiated epithelial cells: colonic enterocytes that are involved in the absorption of water and some nutrients, enteroendocrine cells that produce hormones, goblet cells that secrete mucus and Paneth-like cells that provide the stem cell niche at the base of the crypts to support the estimated 2-4 stem cells in each crypt (although the number of stem cells per crypt may fluctuate) (Barker et al., 2008; Snippert et al., 2010). Barker et al (2007) identified leucine-rich-repeat-containing G-protein-coupled receptor 5 *(Lgr5*), also known as *Gpr49*, as a characteristic epithelial stem cell marker in both the colon and the small intestine in mice and humans, although other stem cell markers have been described (Barker et al., 2007; Barker & Clevers, 2010). These stem cells divide to produce one daughter stem cell that remains in the stem cell niche and one daughter cell that enters the transit-amplifying pathway to expand into more cells to help populate the crypt and eventually differentiate into the different specialized cells described above (Barker & Clevers, 2010). Stem cells play a key role in maintaining cellular homeostasis of the crypt and table surface epithelium of the large intestines which is replaced by new cells every 3 to 5 days (Copstead-Kirkhorn & Banasik, 2014).

There is evidence for mutated stem cells being able to replace other stem cells and fill the crypt with their daughter cells in a process known as monoclonal crypt conversion, and that the life cycle of crypts is linked to stem cell dynamics with crypts able to expand in number by the process of crypt fission (Loeffler et al., 1993, 1997; Reizel et al., 2011). Stem cells often exhibit the highest levels of Wnt signalling as demonstrated by nuclear B-catenin immunstaining; usually there is neutral competition between stem cells in crypts (Lopez-Garcia et al., 2010; Snippert et al., 2010), however if a stem cell has a selective growth advantage, such as that conferred by mutated *Apc* or *Kras,* that stem cell can increase in number, more rapidly undergo monoclonal crypt conversion with crypt expansion by crypt fission, and increase the likelihood of adenoma formation (Huels et al., 2018; Snippert et al., 2014)

Adenocarcinomas are the most common type of CRC (>90%) (Cancer Research UK, 2016b). They are epithelial neoplasms derived from glandular epithelial cells that invade through the muscularis mucosae into the submucosa (and into or though the muscularis propia in most cases). Precursor lesions are thought to include dysplastic crypt foci that can develop into benign adenomas, some of which may subsequently evolve into malignant adenocarcinomas (Figure 1.5) (Cheng & Lai, 2003; Dukes, 1934; Dukes, 1956; Fearon & Vogelstein, 1990; Fleming et al., 2012). This neoplastic process involves loss of the normal regulation of growth control with sustained proliferative signalling and cumulative acquisition of the hallmarks of cancer (Hanahan & Weinberg, 2000; Hanahan & Weinberg, 2011). Underlying these neoplastic hallmarks are genome instability, which generates the genetic diversity that expedites their acquisition (Hanahan & Weinberg, 2011).

The stage of advancement of a CRC is most commonly described using the TNM system (tumour, node and metastasis) with tumours described according to their degree of penetration and spread. T1 cancers are confined to the submucosa, T2 cancers have invaded into (but not through) the muscularis propria, T3 cancers have penetrated the outer limit of the muscularis propria, whereas T4 cancers have infiltrated through the serosal surface and/or grow into other organs and tissues. N0 indicates no metastasis to lymph nodes. Cancers that have spread to lymph nodes are further classified as N1 or N2 according to the number of involved nodes. M0/M1 describes the absence or presence of metastatic spread to distant organs, most commonly the liver (Cancer Research UK, 2019; Loughrey et al., 2020).

The Dukes' staging system is another commonly used system for describing CRC stage, in which Dukes' A cancers have invaded into the submucosa or the muscularis propria, Dukes' B cancers have penetrated through the outer edge of the muscularis propria and invade into the serosa, or beyond, but have not spread to lymph nodes or to other organs, and Dukes' C cancers have involved lymph nodes (although a later addition was Dukes' stage D cancers that have metastasised to distant organs such as the liver) (Cancer Research UK, 2019; Dukes & Bussey, 1958). Histological grading of CRCs may provide further prognostically useful information (Dukes, 1937; Loughrey et al., 2020).

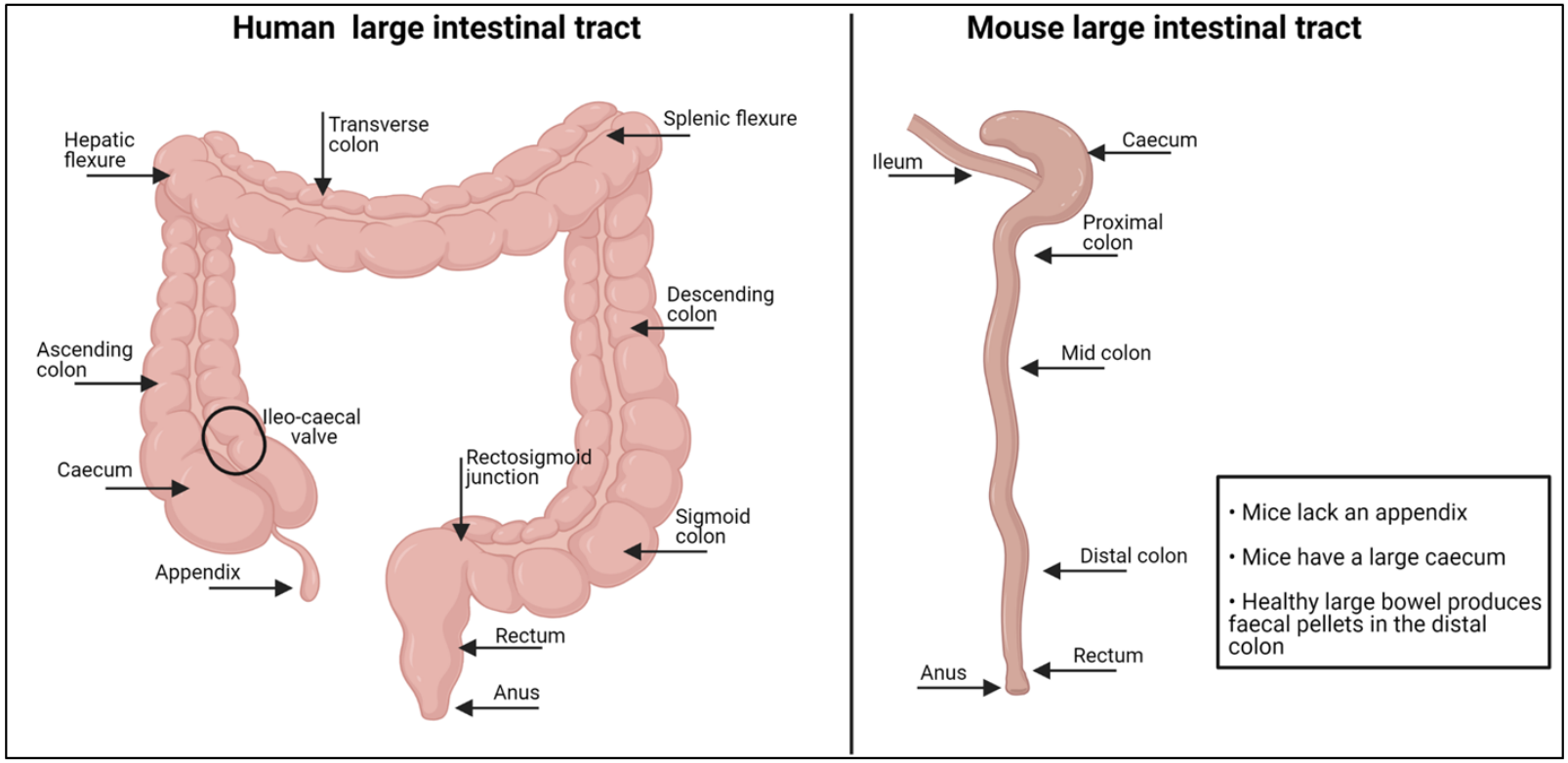

Figure 1.4: Comparison between human and mouse large intestinal tract (adapted and modified from Treuting et al., 2017). In the left panel, the anatomic divisions of the human colorectum are based on its configuration and location. The right colon is composed of the appendix, caecum, ascending colon, and transverse colon. The left colon includes the descending colon, sigmoid colon, and rectum. The outer longitudinal layer of the muscularis propria proximal to the rectum forms three distinct longitudinal bands called taenia coli. The colon becomes sacculated between the taenia, forming the haustra. In the right panel, the mouse large intestinal tract is shown. The cecum is a large J-shaped blind sac. The proximal colon exits near the ileocaecal junction. Faecal pellets are formed by consolidation and dehydration in the mid and distal colon. (Image created with BioRender.com).

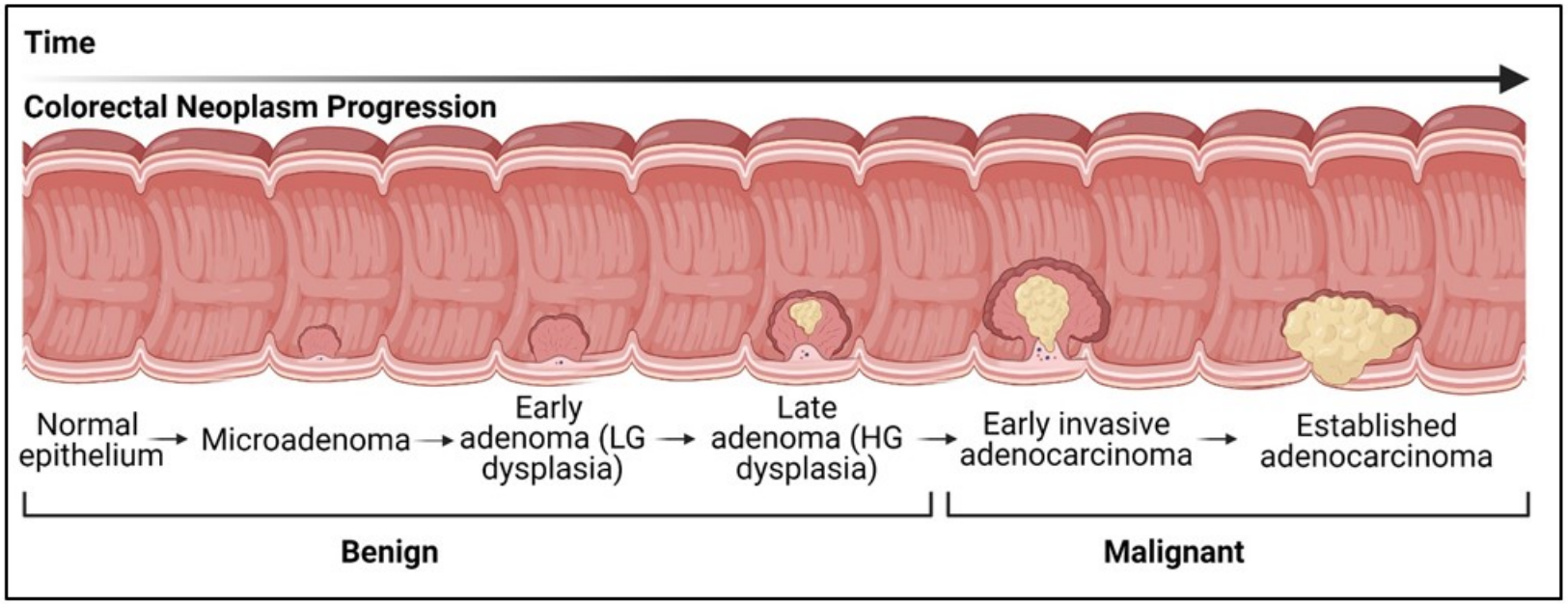

Figure 1.5: Representation of large intestinal tumour progression (adapted and modified from Thrumurthy et al., 2016; Vogelstein et al., 2010, and others). The adenoma-carcinoma progression sequence has transitions from normal through the earliest stage of microadenoma formation (monocryptal adenoma or oligocryptal adenoma) followed by small early adenomas usually with low-grade (LG) dysplasia, then larger late adenomas often with high-grade (HG) dysplasia (yellow clone of cells), a proportion of which may progress to form a malignant clone that shows early invasion into the submucosa of the bowel wall, later becoming an established adenocarcinoma invading deeper into the muscularis propria and/or serosa. The murine sequence may show mucosal crypt hyperproliferation as a very early change before dysplasia is observed, but zones of hyperproliferation are infrequently or rarely seen in human colon. Progression over time is indicated by the horizontal black arrow. (Image created with BioRender.com).

1.2.3 Genetic and epigenetic changes in sporadic colorectal cancer

Molecular analysis of CRCs reveals underlying modifications related to three major mechanisms of genomic/genetic/epigenetic instability: chromosomal instability (CIN), microsatellite instability (MSI), and CpG island methylator phenotype (CIMP). CIN is observed in 65-85% of sporadic CRCs, resulting in high levels of DNA somatic copy number alterations (SCNAs), with DNA gains/amplifications and DNA losses/deletions that may affect small chromosome regions or whole chromosomes, causing aneuploidy and loss of heterozygosity that can affect tumour suppressor gene loci (Arends, 2013; Poulogiannis et al., 2010). MSI is detected in around 12-15% of sporadic CRC cases and is due to defective DNA mismatch repair, with a high mutation rate (hypermutant) affecting a large number of genes. CIMP is observed in around 20% of sporadic CRCs and it is characterised by hypermethylation of promoter CpG islands of susceptible genes, sometimes resulting in the inactivation of multiple tumour suppressor genes (Müller et al., 2016).

One of the most frequent molecular genetic changes in sporadic CRCs is the disruption of the WNT signalling pathway, which occurs in over 90% of sporadic CRCs, (Cancer Genome Atlas, 2012), mostly due to biallelic inactivation of the *APC* gene. *APC* mutations are found in around 80-85% of both adenomas and carcinomas that occur very early in the pathogenetic sequence and appear to initiate adenomagenesis (Arends, 2013). APC is a WNT signalling pathway negative regulator and acts as part of the β-CATENIN degradation complex together with AXIN, Glycogen synthase kinase 3 (GSK3), and Casein kinase 1 (CK1). These *APC* mutations usually lead to truncation of the APC protein with reduced ability to degrade B-CATENIN, leading to its accumulation and nuclear translocation, causing abnormal signalling through the WNT signalling pathway (Morin et al., 1997; Schatoff et al., 2017). Mutations in the β-CATENIN encoding gene *CTNNB1*, upregulation of the Wnt Frizzled (FZD) receptor, and inactivation of *DKK-1* also contribute to deregulation of WNT signalling and are observed in sporadic CRCs (González-Sancho et al., 2005; Morin et al., 1997; Terasaki et al., 2002).

Around 40-45% of sporadic CRCs show mutations in the RAS/MAPK pathway. The majority of the mutations involve *KRAS*, with a small proportion affecting *NRAS* or *BRAF,* resulting in the activation of this pathway. Mutation in any one of these genes, usually at specific sites (such as codons 12, 13 or 61 in the *RAS* gene or codon 600 for the *BRAF* proto-oncogene) cause the constitutive activation of the RAS-RAF-MEK-ERK (MAPkinase) proliferative signalling pathway (Müller et al., 2016; Naguib et al., 2010).

Mutations in the *TP53* tumour suppressor gene are found in around 60% of CRCs and this occurs late in sporadic colorectal tumorigenesis (around the transition of adenoma to adenocarcinoma) (Vogelstein et al., 2010). The p53 protein has been called the "guardian of the genome" as activation of the p53 pathway upon DNA damage detected by DNA damage response pathways (or other cellular stresses), leads to cell cycle arrest to allow opportunity for DNA repair, although in case of severe DNA damage it induces cell death via apoptosis (Kastenhuber & Lowe, 2017).

Mutations in *TGFBR1*, *ACVR2A*, *SMAD3* and *SMAD4* are also common in sporadic CRCs. These genes encode for proteins involved in the transforming growth factor (TGF) β pathway that has growth suppressive roles in modulating proliferation, apoptosis, stem cell renewal, differentiation and adult tissue homeostasis (Weiss & Attisano, 2013).

Some sporadic CRCs may evolve from serrated precursors such as hyperplastic polyps, sessile serrated lesions, and traditional serrated adenomas and these represent around 10-15% of all CRCs. These lesions follow an alternative neoplastic development pathway different to conventional adenomas. They are often characterized by more frequent activating mutations of *BRAF* and less frequent *KRAS* mutations, with greater involvement of the CIMP, in which a range of susceptible genes develop epigenetic promoter hypermethylation that silences their expression, frequently including MLH1 leading to dMMR and MSI (Kedrin & Gala, 2015; Yamane et al., 2014). Although most of the 12-15% dMMR sporadic CRC with hypermethylated MLH1 promoters appear to evolve from polypoid adenomas, and these are strongly associated with *BRAF* mutations.

1.2.4 Lifestyle and other risk factors for sporadic colorectal cancer

Several lifestyle factors, such as tobacco smoking, alcohol consumption, diet (with increased red and processed meat or insufficient fibre) and increased body mass index (BMI) (overweight and obesity) are associated with increased risk of sporadic CRC (Cancer Research UK, 2020; IARC, 2010).

More than 40% of CRC cases are diagnosed in people aged 75 or over in the UK. CRC risk increases from 50 years of age reaching the highest incidence after 75 years of age, higher in men than in women (Bénard et al., 2018).

7% of CRCs are linked to smoking in the UK, more for rectal cancer than colonic cancer (Brown et al., 2018). However, the relation of smoking with CRC is controversial, some, but not all studies include smoking as a risk factor (Lee et al., 2016). The risk of CRC is high in current and former smokers (17%-25%) with increasing risk in those who began smoking at a young age and the risk increases with the number of cigarettes smoked per day (Hannan et al., 2009; Liang et al., 2009).

6% of CRCs are linked to alcohol consumption in the UK (Brown et al., 2018). In 2010, ethanol and its metabolite acetaldehyde were classified as group 1 carcinogens (carcinogenic to humans) by the International Agency for Research on Cancer for the locations: upper aerodigestive tract, liver, breast and colorectum (IARC, 2010). Moderate and heavy drinking (≥50g/day) has been associated with increased risk of CRC of 33% compared with light to non-drinkers, with a stronger association in men than in women (Bagnardi et al., 2015).

13% of CRCs are linked to processed meat consumption in the UK (Brown et al., 2018). In 2015, processed meat was classified as group 1 carcinogen and red meat was classified as group 2A carcinogen (probably carcinogenic to humans) by the World Health Organization (WHO) (Bouvard et al., 2015). Several meta-analyses studies, showed that 100g/day of red meat and 50g/day of processed meat increases CRC risk by 17-18% (Aune et al., 2013; Chan et al., 2011). This is mainly related to the genotoxic compounds generated during the meat metabolism that can cause DNA damage (H-nitroso-compounds, heterocyclic aromatic amines and polycyclic aromatic hydrocarbons) (Bouvard et al., 2015).

11% of CRCs are linked to overweight and obesity in the UK (Brown et al., 2018). Meta-analysis studies showed that a high BMI value can increase CRC risk. In overweight men (BMI=25-29), the risk of CRC is 18% higher, while obese men (BMI≥30) have 48% higher risk of CRC. In obese women, the risk of CRC is 12% higher (Chen et al., 2015; Xue et al., 2017).

The relationship between CRC and increased BMI has been suggested to relate to endocrine abnormalities and metabolic changes linked to obesity, such as insulin resistance, chronic inflammation and altered adipokine secretion (Martinez-Useros & Garcia-Foncillas, 2016; van Kruijsdijk et al., 2009). Meta-analysis studies have observed an increased CRC risk of 22-30% in diabetes mellitus (DM) type 2 (Jiang et al., 2011; Luo et al., 2012). This is linked to the alteration of insulin levels and insulin-like growth factor (IGF) signalling pathway activity, which promotes cell growth and inhibits apoptosis (Schoen et al., 2005).

Inflammatory bowel diseases (IBD) are an established risk factor for CRC, mainly ulcerative colitis (UC) and Crohn's disease (CD) (Lutgens et al., 2008). The severity and duration of the inflammation is associated with the increase in CRC risk. The CRC risk is 70% higher in the IBD patients than in non-IBD patients, making IBD one of the highest non-hereditary risk factors for CRC (Canavan et al., 2006; Castaño-Milla et al., 2014; Kulaylat & Dayton, 2010).

1.3 Ethanol

1.3.1 Ethanol metabolism

Alcohol is one of the most used recreational drugs, with 2.3 billion current drinkers in 2018 (World Health Organization (WHO), 2018). Alcohol consumption is responsible for around 1.8 million deaths per year (3.2% of all death); worldwide, a total of approximately 389,000 cancers representing 3.9% of all cancers derive from chronic alcohol consumption (5.2% in men and 1.7% in women) (World Health Organization (WHO), 2018)]. Chronic alcohol consumption has been associated with cancer development in the upper aerodigestive tract (including oesophageal, pharyngeal, head and neck cancers), liver, breast and colorectum (IARC, 2010).

Carcinogenic effects of ethanol are related to its metabolism. Ingested ethanol is readily absorbed from the gastrointestinal tract, and about 90% is metabolized by oxidative pathways mainly in the liver (Brooks & Zakhari, 2014). Ethanol is oxidized mostly by the cytosolic class I alcohol dehydrogenase (ADH) isoenzymes (ADH1A, ADH1B and ADH1C), that use nicotinamide adenine dinucleotide (NAD^+) to produce acetaldehyde and the reduced form of nicotinamide adenine dinucleotide (NADH). The cytochrome P450 (CYP2E1) is also involved in the oxidation of ethanol to acetaldehyde in the liver, mostly at elevated alcohol concentrations (Figure x), resulting also in the generation of reactive oxygen species (ROS) and reactive nitrogen species (RNS) (Pöschl et al., 2004; Seitz & Stickel, 2007).

Acetaldehyde is considered the important cancer-causing agent in the upper and lower gastrointestinal tract, as acetaldehyde concentrations in saliva and the large intestine are high enough to enable it to act as carcinogen. Acetaldehyde is a highly reactive small molecule able to induce a wide range of DNA damage resulting in tumour development (*vide infra*). Acetaldehyde is metabolized by a large family of mitochondrial aldehyde dehydrogenases (ALDHs), with different isoforms expressed in different cell types that use NAD^+ to convert acetaldehyde to non-toxic acetate, water and NADH (Figure 1.6). Acetaldehyde is the major substrate for the mitochondrial ALDH2 (K_m=3.2µM) and ALDH1B1 enzymes (K_m= 55µM) (Stagos et al., 2010). ALDH2 is the predominant isoform for acetaldehyde detoxification in the liver, whereas ALDH1B1 is highly expressed in the gastrointestinal epithelium, particularly in the epithelial stem cells and transit-amplifying cells, and studies have shown ALDH1B1 to be involved in acetaldehyde detoxification in the intestines (*vide infra*). Polymorphisms in ADH and ALDH genes cause the levels of production

and/or oxidation of acetaldehyde to vary between individuals, leading to an increased cancer risk (*vide infra*) (Marchitti et al., 2008). In the mitochondria, the non-toxic acetate is ligated to coenzyme A (CoA) by acetyl-CoA synthetase and acyl-CoA synthetase 2, to form acetyl-coenzyme A (acetyl-CoA). Acetyl-CoA plays a key role in many metabolic reactions (Pietrocola et al., 2015; Shi & Tu, 2015).

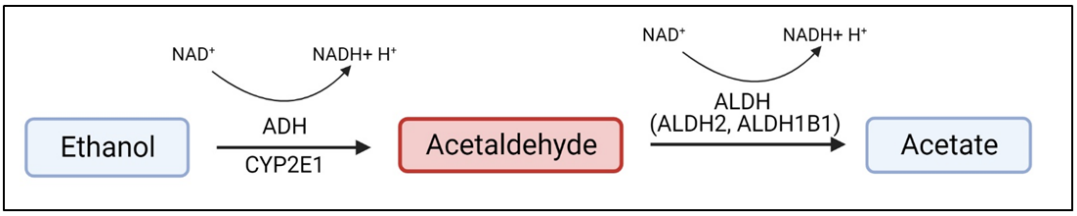

Figure 1.6: Schematic diagram of ethanol metabolism. Ethanol is oxidized to acetaldehyde in a reversible reaction catalyzed by the class I ADH isoenzymes and CYP2E1 in the liver. Ethanol oxidation is coupled to reduction of the cofactor NAD^+. ALDH enzymes (isozymes ALDH2, ALDH1B1) catalyse irreversible oxidation of the acetaldehyde carbonyl to its respective carboxylic acid, acetic acid/acetate. Oxidation of acetaldehyde to acetate by both ALDH2 and ALDH1B1 is coupled to reduction of the cofactor NAD^+. (Image created with BioRender.com).

1.3.2 ALDH1B1 function, genetics and polymorphisms

ALDHs are involved in cell protection against the effects of a wide range of exogenous and endogenous aldehydes (Marchitti et al., 2008). The mitochondrial matrix protein ALDH2 is the main enzyme involved in acetaldehyde oxidization in the liver during ethanol metabolism, showing the lowest Michaelis-Menten constant (K_m) for acetaldehyde (K_m=3.2μM) of all the ALDH isoforms (Stagos et al., 2010). The key role of ALDH2 in acetaldehyde detoxification is exemplified by the study of human single nucleotide polymorphisms (SNPs) in the *ALDH2* gene. 40%-50% of Asians are ALDH2*2 carriers, an inactive variant of the normal allele ALDH2*1, due to a SNP (single base pair change G/C→A/T) in the coding region of the *ALDH2* gene. People heterozygous for ALDH2*2 have reduced metabolism of acetaldehyde, showing a 6-fold increase of blood acetaldehyde levels compared with wild-type individuals, whereas individuals homozygous for ALDH2*2 have very poor metabolism of acetaldehyde, causing a 20-fold increase of blood acetaldehyde levels compared with wild-type individuals. This results in the alcohol flushing syndrome (Seitz & Stickel, 2010; Yokoyama et al., 1998). This SNP has been associated with increased cancer risk for various cancers, including those of the upper aerodigestive tract and colorectum, and increased neoplasms have been observed in *Aldh2*-null mice that show markedly increased incidence of leukaemias and other cancers (Langevin et al., 2011; Yu et al., 2009).

The mitochondrial ALDH1B1 (also known as ALDH5 and ALDHX) exhibits a K_m= 55μM for acetaldehyde, representing the ALDH with the second lowest Michaelis-Menten constant involved in acetaldehyde oxidization. The human *ALDH1B1* gene is located on chromosome 9 (in a 5957-base pair region) and it is characterized by an intronless coding region. The expressed ALDH1B1 protein shares 75% homology in peptide sequence with ALDH2, it contains 517 amino acids with an N-terminal 19-residue mitochondrial lead signal and it functions as homotetrameric enzyme (Hsu & Chang, 1991; Stagos et al., 2010). Immunohistochemical analyses revealed that human ALDH1B1 is expressed at high levels in the small intestine, colon, liver, and pancreas, with the highest protein expression levels in colonic epithelial stem cells. This was also observed in mouse tissues (Stagos et al., 2010).

High expression levels of ALDH1B1 are observed in human colonic adenocarcinomas, probably due to the ALDH1B1-positive normal colonic stem cells that act as progenitors for progression to malignancy during tumourigenesis, and become cancer stem cells. ALDH1B1 is considered a potential CRC biomarker (Chen et al., 2011).

The human ALDH enzymes share the same protein structure that contains three domains: a cofactor-binding domain, a linker domain and a catalytic domain. At the interface of the domains lies a hydrophobic tunnel at the base of which resides the enzyme active site, opposite the cofactor-binding site. The specificity of the ALDHs towards their substrate is determined by the residues from the three domains that line the hydrophobic tunnel of each ALDH subunit. NAD^+ is the cofactor for ALDH1B1, not $NADP^+$ (Marchitti et al., 2008; Steinmetz et al., 1997). The ability of ALDH1B1 (but also ALDH2) to catalyse oxidation is provided by the cysteine at position 302 (Cys302), a highly conserved residue in all catalytically active members of the ALDH family. The Cys302 is essential for the nucleophilic attack on acetaldehyde (Farres et al., 1995; Marchitti et al., 2008).

ALDH1B1 major substrates are short-chain aldehydes, such as acetaldehyde and propionaldehyde. The increasing interest in ALDH1B1 and its role in acetaldehyde detoxification emerged following the identification of *ALDH1B1* polymorphisms that are associated with drinking-behaviour (A69V) and alcohol hypersensitivity (A86V) in Caucasians (Husemoen et al., 2008; Linneberg et al., 2009). Jackson et al., 2015, confirmed that ALDH1B1*2 (A86V) variant/polymorphism is catalytically inactive due to inability to bind NAD^+ (Jackson et al., 2015). In a recent study, our research group provided evidence for a role of Aldh1b1 in protection of the murine intestines from ethanol-induced DNA damage and intestinal tumour formation using Aldh1b1-depleted mice compared with wild-type mice under long-term ethanol treatment for up to 12 months (Müller et al., 2016). Ethanol-treated Aldh1b1-depleted mice showed increased plasma acetaldehyde levels and increased ethanol-induced large intestinal adenomas with occasional adenocarcinomas (Müller et al., 2016). Our research group also described a role of Aldh1b1 in protection from ethanol-induced hepatocellular hyperproliferation and liver tumour development in these Aldh1b1-depleted mice (Müller et al., 2018). However, Aldh1b1 is still a relatively under-investigated member of the Aldh family.

1.3.3 Ethanol & Acetaldehyde induced DNA damage

1.3.3.1 Ethanol, CYP2E1 induction and DNA damage

Chronic alcohol consumption induces CYP2E1 expression by liver cells, resulting in decrease of retinol and retinoic acid tissue levels. Retinoic acid has a key role in cellular growth and differentiation, activating a signalling cascade through its nuclear retinoic acid receptors, resulting in the gene transcription of cell proliferation and migration regulators. The decrease in retinoic acid has consequences for cell proliferation, differentiation and malignant transformation (Liu et al., 2001). Chronic ethanol treatment in rats showed decreased retinoic acid in association with a decrease in mitogen-activated protein kinase (MAPK) and an increase phosphorylation of c-Jun N-terminal kinase (JNK), resulting in hepatic cell hyperproliferation and reduced apoptosis (Wang et al., 1998). Increased CYP2E1 activity results in the activation of the metabolism of certain pro-carcinogens, including nitrosamines, polycyclic hydrocarbons and aflatoxins, by alcohol-induced CYP2E1 (Seitz & Stickel, 2007).

Most importantly, ethanol oxidation by CYP2E1 results in the generation of ROS, such as superoxide anion and hydrogen peroxide that causes oxidative damages contributing to various diseases such as cancer. The CYP2E1-produced ROS can cause the generation of lipid peroxidation products such as 4-hydroxynonenal (4-NHE) and malondialdehyde (MDA). 4-NHE reacts with DNA to form highly mutagenic exocyclic DNA etheno-adducts 1,N^6-ethenodeoxyadenosine (εdA) and 3,N^4-ethenodeoxycytidine (εdC) (Figure 1.7) (Vasiliou et al., 2015). These DNA adducts can cause mutations in TP53 at codon 249, resulting in proliferative advantage and reduced apoptosis (Hu et al., 2002). ROS are usually neutralized by the anti-oxidative defence system (AODS), endogenous mechanisms (glutathione peroxidase and superoxide dismutase) and exogenous mechanisms (antioxidant nutrients) (Seitz & Stickel, 2007).

1.3.3.2 Acetaldehyde and DNA damage

Acetaldehyde can also indirectly induce ROS generation by injuring the mitochondria (Seitz & Stickel, 2007). Following increased alcohol intake, ethanol is oxidized in acetaldehyde generating large quantities of NADH that is reoxidized to NAD^+ in the mitochondria. Furthermore, ROS can also be generated by increased electron leakage from the mitochondrial respiratory chain associated with the stimulation of NADH in the mitochondria (Bailey & Cunningham, 2002). The increased mitochondrial ROS production may also be caused by activation of N-acetylsphingosine by tumour necrosis factor-α (TNF-α) that increases the levels of ceramide, a mitochondrial electron-transport inhibitor (García-Ruiz et al., 2000). The ROS generated indirectly by acetaldehyde may result in lipid peroxidation products that, as explained before, form highly mutagenic exocyclic DNA etheno-adducts (Figure 1.7).

The electrophilic nature of acetaldehyde contributes to its high reactivity and it is provided by its carbonyl group (R-CHO) that reacts with nucleophilic sites in DNA and protein generating adducts. Acetaldehyde can induce DNA adducts by reacting directly with deoxyguanosine (dG) most frequently, followed by deoxyadenosine (dA) and then deoxycytosine (dC) (Vasiliou et al., 2015).

One molecule of acetaldehyde can bind to DNA forming N^2-ethylidene-2'-deoxyguanosine (N^2-EtidG). N^2-EtidG requires chemical reduction to become a stable adduct, N^2-ethyl-2'-deoxyguanosine (N^2-EtdG). High levels of this DNA adduct were observed in Swedish drinkers compared with non-drinkers, and this was observed in ethanol-treated mice (with 10% ethanol in drinking water); these N^2-EtdG adducts were abundant but not highly mutagenic (Brooks & Zakhari, 2014). Two molecules of acetaldehyde can react with DNA to form R- and S-α-CH_3-γ-OH-1,N^2-propano-2'-deoxyguanosine(PdG) adducts, called Cr-PdG because they were first observed in DNA treated with crotonaldehyde. The Cr-PdG adducts are less abundant compared with EtdG adducts, but more mutagenic. Choudhury et al. (2004) showed that nucleotide excision repair (NER) may possibly be involved in the repair of the PdG adducts (Choudhury et al., 2004). The Cr-PdG adducts can exist a ring-opened form when located in double-stranded DNA, in this way it can react with deoxyguanosine of the opposite strand of the DNA forming an interstrand crosslinks (ICLs), but it can also bind proteins forming DNA-protein crosslinks. DNA-protein crosslinks are precursor lesions to altered sister chromatid exchanges, DNA ICLs and DNA-protein crosslinks, that may lead to the generation of chromosomal aberrations (Figure 1.7) (Brooks & Zakhari, 2014; Vasiliou et al., 2015).

Chronic alcohol consumption causes hyperproliferation of the upper aerodigestive tract mucosa and large intestinal mucosa, due to an acetaldehyde toxic effect. Acetaldehyde is highly concentrated in the saliva and colon, where the acetaldehyde generated by the mucosal ADHs combines with acetaldehyde generated by the oral or large intestinal microbiota. High concentrations of acetaldehyde can promote hyperproliferation and generation of Cr-PdG and other DNA adducts in these tissues (Seitz & Stickel, 2007, 2010).

These reactions are possible thanks to the reactive aldehyde group exposed in the open-ring form. Cr-PdG can induce G→T transversions, as well as base deletion and insertion mutations. Furthermore, acetaldehyde can cause point mutations in the hypoxanthine phosphoribosyltransferase 1 (HPRT1) locus in human lymphocytes, and induce sister chromatid exchanges and gross chromosomal aberrations (Seitz & Stickel, 2007). Langevin et al (2011) demonstrated that the Fanconi Anaemia (FA) DNA repair pathway plays a crucial role in counteracting acetaldehyde induced genotoxicity in mice (Langevin et al., 2011), as the FA DNA repair pathway is essential for the repair of DNA ICLs (Kim & D'Andrea, 2012).

Chronic alcohol consumption can cause deficiencies of folate, vitamin B6 and certain lipotropes that are essential cofactors of methyl group transfer. Acetaldehyde seems to alter DNA methylation via inhibition of methyl adenosine transferase 1 (MAT 1) causing reduced production of S-adenosyl-L-methionine (SAMe, the universal methyl group donor and enzyme activator). Acetaldehyde also inhibits DNA methyltransferases (DNMTs) that are involved in the methylation of 1% of the DNA, replacing the hydrogen atom attached at the C5 of cytosine with a methyl group. So far, this has only been observed in rodent studies (Garro et al., 1991; Santamaría et al., 2006). The acetaldehyde hypomethylation effect may contribute to epigenetic alterations of genes involved in carcinogenesis (Seitz & Stickel, 2007; Vasiliou et al., 2015). Acetaldehyde is also able to bind glutathione preventing glutathione-S-transferase activity, a key component of the AODS, which is responsible for the detoxification of ROS and RNS (Vasiliou et al., 2015). In 1988, Espina et al. reported acetaldehyde as a possible inhibitor of O^6-methylguanine methyltransferase (MGMT) activity in rat liver extracts (Espina et al., 1988). However, according to other studies, acetaldehyde is unable to react with MGMT (Brooks & Zakhari, 2014; Worrall & Thiele, 2001). Furthermore, acetaldehyde seems to inhibit DNA repair systems through inhibition of MGMT and 8-oxo-guanine-DNA glycosylase (Seitz & Stickel, 2007). However, much remains to be investigated about ethanol/acetaldehyde-induce DNA damage.

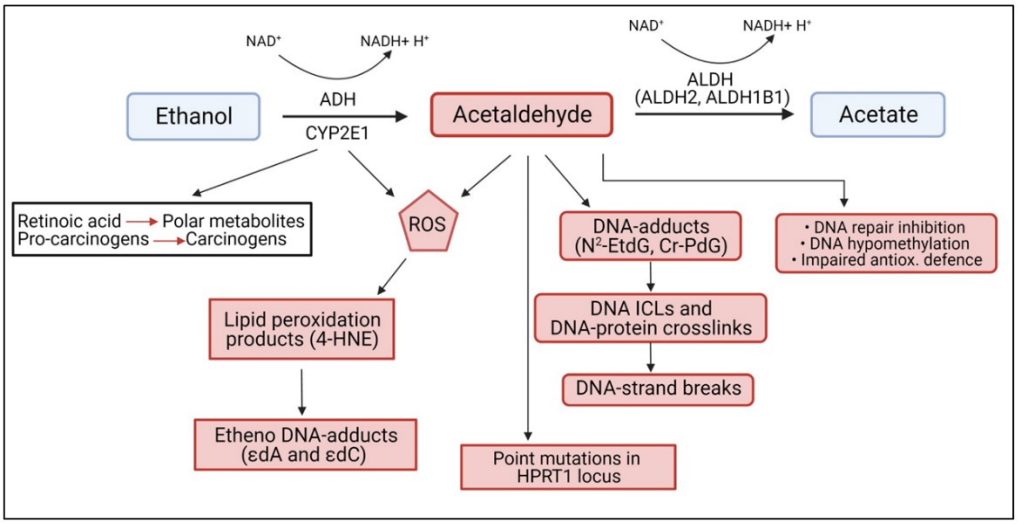

Figure 1.7: CYP2E1, acetaldehyde and DNA damage (adapted and modified from Seitz & Stickel, 2007). Active CYP2E1 decreases tissue levels of retinol and retinoic acid and increases activation of environmental pro-carcinogens. Chronic alcohol consumption induces CYP2E1 leading to reactive oxygen species (ROS) generation that mediate lipid peroxidation producing lipid peroxidation products such as 4-hydroxynonenal (4-HNE). Lipid peroxidation products can form etheno-DNA adducts, such as 1,N^6-ethenodeoxyadenosine (εdA) and 3,N^4-ethenodeoxycytidine (εdC). Acetaldehyde can also increase ROS formation indirectly by injuring mitochondria. Acetaldehyde reacts with DNA directly creating DNA-adducts, such as N^2-ethyl-2'-deoxyguanosine (N^2-EtdG) and R- and S-α-CH_3-γ-OH-1,N^2-propano-2'-deoxyguanosine (Cr-PdG), leading to DNA-protein crosslinks and/or DNA interstrand crosslinks (ICLs) that are precursor lesions for DNA strand breaks, sister chromatid exchanges and chromosomal aberrations. Acetaldehyde can also cause point mutations in the hypoxanthine phosphoribosyltransferase 1 (HPRT1) locus in human lymphocytes, and induce sister chromatid exchanges and gross chromosomal aberrations. Furthermore, acetaldehyde seems to play a role in DNA hypomethylation, inhibition of DNA repair and impairment of anti-oxidative defence systems.

1.4 Aim and Objectives

Lynch Syndrome patients carry an MMR pathogenic mutation that predisposes them to increased lifetime risks for several cancers that develop as a result of defective MMR following inactivation of the wild-type MMR allele during tumour formation. The variable expression of the cancer phenotypes amongst LS patients suggests important effects of allelic variation, genetic modifiers, environmental and/or lifestyle factors, together with complex genetic and environmental interactions. Therefore, it is important to investigate relevant environmental risk factors for developing cancer in LS patients, in order to provide appropriate cancer prevention advice, surveillance and care.

Given the evidence for ethanol consumption being a risk factor for sporadic CRC development, it was decided to investigate whether ethanol is a key environmental/lifestyle risk factor for CRC in LS patients using a genetically altered animal model that can be exposed to ethanol consumption. The overall aim was to determine whether there is a gene/environment interaction between defective MMR and ethanol that accelerates colorectal tumour development and progression. To investigate this, an appropriate experimental mouse model was established, using a modified version of the LS-mouse model based around one inherited mutant allele and one inducible mutation of the murine *Msh2* gene that was recently created by Wojeciechowicz et al (2014) (*Lgr5CreERT2; Msh2*$^{flox/-}$*; mTmG*). The specific objectives of this project included the following.

1. To determine whether ethanol and / or its major metabolite acetaldehyde can cause acceleration of defective MMR-driven intestinal tumour formation.

2. To elucidate whether ethanol and / or acetaldehyde can increase the number and size of intestinal precursor lesions and their progression to intestinal adenoma or invasive cancer.

3. To investigate the role of the DNA mismatch repair system in protecting intestinal cells from ethanol/acetaldehyde-induced DNA damage.

Chapter 2: Materials and Methods

2.1 Animal work

2.1.1 Introduction

In this study, all murine experiments were performed under Professor Mark J Arends' Home Office project licence issued under the United Kingdom Home Office Animals (Scientific Procedures) Act 1986, and my Home Office personal licence in accordance with the Animals (Scientific Procedures) Act 1986. All experiments received approval by the Named Veterinary Surgeons of the University of Edinburgh. Experiments were carried out at the Western General Hospital-BRF (University of Edinburgh) animal facility.

In this study, mice were housed in individually ventilated cages (IVCs) with group sizes and enrichment according to Home Office regulations. Cages were one-time use and recyclable. Light was provided as 12 hours of light and 12 hours of dark every 24 hour period. The room air humidity was kept at 35% and temperature at 21-22°C. The unit had a pathogen health status rating of 4, however the mice were kept in IVCs in a clean room to limit the contact with animal gastrointestinal and other pathogens that could have altered significantly the results in the experiments. Mice were given the RM3 diet (Special Diets Services) in pellet form, a high nutrient diet containing fatty acids, with ad libitum access to food and water. Cages, bedding, cage enrichment, food and bottled water were autoclaved or irradiated before use.

2.1.2 Mouse models

Mouse models used in this project are shown in table 2.1. Mouse model generation is further described in the results chapters (Chapter 3, Figures 3.1-3.3; Chapter 6, Figure 6.1).

Mouse model	Strains crossed	Background strains	Source	Genotype
Msh2-LS	*Msh2*$^{flox/-}$	FVB	Prof. Hein te Riele, Netherlands Cancer Institute	*Msh2*$^{flox/-}$; *Lgr5CreERT2*$^{+/-}$; *mTmG*$^{+/-}$
	mTmG	C57Bl6J	Prof. Ian Jackson, University of Edinburgh	
Aldh1b1$^{flox/flox}$ *Msh2-LS*	Aldh1b1tm1a(EUCOMM)Wtsi	C57Bl6	EUCOMM project	*Msh2*$^{flox/-}$; *Lgr5CreERT2*$^{+/-}$; *mTmG*$^{+/-}$; *Aldh1b1*$^{flox/flox}$
	Flpe	C57Bl6J, B6SJLF1/J	Prof. Ian Jackson, University of Edinburgh	
	Msh2-LS			
Aldh1b1$^{-/-}$ *Msh2-LS*	*Aldh1b1*$^{flox/flox}$ TAT-Cre treatment	C57Bl6	Bioresearch & Veterinary Services, University of Edinburgh	*Msh2*$^{flox/-}$; *Lgr5CreERT2*$^{+/-}$; *mTmG*$^{+/-}$; *Aldh1b1*$^{-/-}$
	Msh2-LS			

Table2.1: Mouse models used in this study and how they were created by crossing the described strains, including the source of the strains and the relevant genotypes of the models investigated (Barker et al., 2007; Claij & te Riele, 2004; de Wind et al., 1995; Muzumdar et al., 2007; Skarnes et al., 2011).

2.1.3 Tamoxifen, Temozolomide and ethanol treatments

Experimental mice of 7-9 weeks age, received treatments with Tamoxifen, Temozolomide and/or ethanol. Tamoxifen (Sigma-Aldrich, T5648) was dissolved in 10ml of molecular grade ethanol and 90ml of sterile corn oil (Sigma-Aldrich, C8267), at a concentration of 10mg/ml. Aliquots were prepared and stored at -20°C. Prior to injection, Tamoxifen was incubated for 10min in a 40°C water bath. Mice were weighed and the correct Tamoxifen dose calculated at either 0.15mg/g body-weight (bw) or 0.1mg/g bw (according to the day of treatment). Tamoxifen was collected with a sterile syringe and intraperitoneal injections were performed with the assistance of an animal technician.

Temozolomide (TMZ, Cayman, 14163) was dissolved in absolute ethanol and sterile water (ratio 1/9) at a concentration of 10mg/mL, sonicated (water bath sonicator; 5 minutes), centrifuged (4000g; 5 minutes; room temperature) and the supernatant was filtered through a 22um filter. Aliquots were prepared and stored at -80°C. Prior to administration, mice were weighed and the correct TMZ dose calculated at 0.1mg/g bw. TMZ was given to animals by oral gavage (o.g.) with the assistance of an animal technician.

Ethanol molecular grade (Sigma Aldrich, E7023) at 20% concentration (v/v) was given in drinking water.

2.1.4 Mouse models acronyms

Specific acronyms were created for each mouse model and the relevant treatments they underwent during this study (Table 2.2).

Acronyms	Treatment	Cre Activation	Mouse model
H_2O_*Msh2*$^{fl\ KO}$	water-treated, 4 i.p. Tamoxifen injections	Induced	Msh2-LS
EtOH_*Msh2*$^{fl\ KO}$	ethanol-treated, 4 i.p. Tamoxifen injections	Induced	Msh2-LS
H_2O_*Msh2*^{fl}	water-treated, 4 i.p. corn oil injections	Non-induced	Msh2-LS
EtOH_*Msh2*^{fl}	ethanol-treated, 4 i.p. corn oil injections	Non-induced	Msh2-LS
5TMZ_H_2O_*Msh2*$^{fl\ KO}$	water-treated, 5 o.g. of Temozolomide and 2 i.p. Tamoxifen injections	Induced	Msh2-LS
5TMZ_EtOH_*Msh2*$^{fl\ KO}$	ethanol-treated, 5 o.g. of Temozolomide and 2 i.p. Tamoxifen injections	Induced	Msh2-LS
10TMZ_H_2O_*Msh2*$^{fl\ KO}$	water-treated, 10 o.g. of Temozolomide and 2 i.p. Tamoxifen injections	Induced	Msh2-LS
10TMZ_EtOH_*Msh2*$^{fl\ KO}$	ethanol-treated, 10 o.g. of Temozolomide and 2 i.p. Tamoxifen injections	Induced	Msh2-LS
H_2O_*Aldh1b1*$^{fl/fl}$_*Msh2*$^{fl\ KO}$	water-treated, 4 i.p. Tamoxifen injections	Induced	*Aldh1b1*$^{flox/flox}$ Msh2-LS
EtOH_*Aldh1b1*$^{fl/fl}$_*Msh2*$^{fl\ KO}$	ethanol-treated, 4 i.p. Tamoxifen injections	Induced	*Aldh1b1*$^{flox/flox}$ Msh2-LS
H_2O_*Aldh1b1*$^{fl/fl}$_*Msh2*^{fl}	water-treated, 4 i.p. corn oil injections	Non-induced	*Aldh1b1*$^{flox/flox}$ Msh2-LS
EtOH_*Aldh1b1*$^{fl/fl}$_*Msh2*^{fl}	ethanol-treated, 4 i.p. corn oil injections	Non-induced	*Aldh1b1*$^{flox/flox}$ Msh2-LS
H_2O_*Aldh1b1*$^{-/-}$_*Msh2*$^{fl\ KO}$	water-treated, 4 i.p. Tamoxifen injections	Induced	*Aldh1b1*$^{-/-}$ Msh2-LS
EtOH_*Aldh1b1*$^{-/-}$_*Msh2*$^{fl\ KO}$	ethanol-treated, 4 i.p. Tamoxifen injections	Induced	*Aldh1b1*$^{-/-}$ Msh2-LS
H_2O_*Aldh1b1*$^{-/-}$_*Msh2*^{fl}	water-treated, 4 i.p. corn oil injections	Non-induced	*Aldh1b1*$^{-/-}$ Msh2-LS
EtOH_*Aldh1b1*$^{-/-}$_*Msh2*^{fl}	ethanol-treated, 4 i.p. corn oil injections	Non-induced	*Aldh1b1*$^{-/-}$ Msh2-LS

Table 2.2: Mouse models acronyms according to the relevant set of treatments received.

2.1.5 Collection of tissues and blood with subsequent processing

At the end of each individual murine experiment, mice were sacrificed by CO_2 asphyxiation and cervical dislocation. Blood was collected via cardiac puncture through the diaphragm under the rib cage, using a 25 gauge pre-heparinised needle (Sterican, 612-0153) and a 1ml syringe. Blood was dispensed in 1.3ml Lithium Heparin Paediatric tubes (Greiner Bio-One Inc, 459084). Blood was fractionated by centrifugation at 3000 x g per 15 minutes at 4°C. Plasma was collected in a 2ml cryo-tube and immediately snap-frozen in liquid nitrogen and stored at -80°C.

Necropsy was performed on the entire cadaver focusing on the gastrointestinal tract, from the oesophagus to the anal canal, and other abdominal organs. The small intestines (SI) and large intestines (LI) were prepared separately. Stomach, caecum, liver, spleen, thymus and any macroscopically abnormal tissues or organs were removed and rinsed with cold PBS prior to incubation in 10% neutral buffered formalin (NBF) (Sigma, HT501128) for 24h at RT. After NBF incubation, tissues were washed in PBS at RT and stored in 70% ethanol at 4°C.

The small intestines (SI) and large intestines (LI) were removed and analysed for the presence of tumours, as whole mount specimens. The SI and LI were flushed twice in PBS and PBS containing Protease Inhibitor (PI, Calbiochem). All possible abnormalities were excised for histopathological analysis. The remaining small and large intestines were inverted using a 30cm long and 3mm diameter bamboo skewer and pre-fixed in 10% NBF: the small intestines were fixed for 4 hours at RT and large intestines were fixed for 1 hour at RT.

After this short-term fixation in NBF, both small and large intestines were opened longitudinally along the antimesenteric border and flattened out as whole mount specimens on a petri-dish (145x20mm, Greiner Bio-One, 639102) containing cold PBS on ice, to allow observation of mucosal surfaces and fluorescent microscopic analysis.

After microscopic analysis, intestines were rolled-up as Swiss rolls around a toothpick for further fixation in 10% NBF over-night. The next day, intestines were washed in PBS at RT and stored in 70% ethanol at 4°C. All tissues collected were processed and paraffin-embedded to generate formalin-fixed paraffin-embedded (FFPE) blocks using standard histological methods by the Pathology laboratory technicians of IGMM, at the University of Edinburgh. Sections were cut from these FFPE blocks for histological and immunohistochemical analysis.

2.2 Molecular Biology techniques

2.2.1 Genotyping

2.2.1.1 DNA extraction from murine tissue

Ear-notches were taken from mice (for identification of individuals) at 14 days of age by animal technicians and stored at -20°C until DNA extraction for genotyping, using the GeneElute kit (Sigma, G1N70), following the kit instructions. DNA samples were stored at -20°C.

2.2.1.2 Genotyping PCR Assays

Genotyping PCR assays were performed for $Msh2^{-}$, $Msh2^{flox}$, Cre, mTmG, $Aldh1b1^{wt}$ $Aldh1b1^{flox}$ and $Aldh1b1^{-}$ alleles. Genotyping primer sequences were taken from the relevant published manuscripts describing these alleles and are shown in Table 2.3 (Barker et al., 2007; Claij & te Riele, 2004; de Wind et al., 1995; Muzumdar et al., 2007; Skarnes et al., 2011). Genotyping PCR reactions were performed using the GoTaq G2 Hot Start Taq Polymerase Mix kit (Promega, M7405) and PCR Nucleotide mix (Promega, C1141) for $Msh2^{wt}$, $Msh2^{-}$, $Msh2^{flox}$, mTmG, $Aldh1b1^{wt}$, $Aldh1b1^{flox}$ and $Aldh1b1^{-}$. Whereas the REDExtract-N-Amp PCR Ready Mix (Sigma-Aldrich, R4775) was used for Cre genotyping, as shown in Table 2.4. DNA was amplified using PCR thermocycler programmes detailed in Table 2.5.

Primer Name		Sequence 5'-3'	Reference
Msh2KO1	fwd	CGGCCTTGAGCTAAGTCTATTATAAGG	de Wind et al., 1995
Msh2KO2	rev	GGTGGGATTAGATAATGCCTGCTCT	
Msh2KO3	rev	CCAAGATGACTGGTCGTACATAAG	
Msh2flox1	fwd	GCATCCTTGCTCGAGTCG	Claij & te Riele, 2004
Msh2flox2	rev	GAGATAGGGTCTGTCTTTGCGG	
Cre A	fwd	TGACCGTACACCAAAATTTG	Barker et al., 2007
Cre B	rev	ATTGCCCCTGTTTCACTATC	
mTmG (Rosa10)	fwd	CTCTGCTGCCTCCTGGCTTCT	Muzumdar et al., 2007
mTmG (Rosa11)	rev wt	CGAGGCGGATCACAAGCAATA	
mTmG (Rosa4)	rev mut	TCAATGGGCGGGGGTCGTT	
Aldh1b1 (FL065)	fwd	TTTCACGGTGTGGGCTTTTCCTCAAAT	Skarnes et al., 2011
Aldh1b1 (FL066)	rev	TGACTTCATCCAGATCCAAGACAT	
Aldh1b1 (En2A)	rev	GCTTCACTGAGTCTCTGGCATCTC	
Aldh1b1-/- (Floxed LR)	rev	ACTGATGGCGAGCTCAGACC	
Aldh1b1 flox/flox (Tm1c)	fwd	AAGGCGCATAACGATACCAC	
Aldh1b1 flox/flox (Tm1c)	rev	CCGCCTACTGCGACTATAGAGA	

Table 2.3: Genotyping primer sequences.

Msh2 -	c final	volume (µl)
water		12.0
Primer Msh2KO1 (20µM)	0.3µM	0.3
Primer Msh2KO2 (20µM)	0.3µM	0.3
Primer Msh2KO3 (20µM)	0.3µM	0.3
dNTPs (10mM each)	0.2mM	0.4
MgCl (25mM)	2mM	1.6
5x GoTaq green buffer	1x	4
GoTaq Hot Start Pol (5U/µl)	0.025U/µl	0.1
DNA tamplate		1.0
Total volume		20
Msh2 flox	c final	volume (µl)
water		12.3
Mshflox1 (20µM)	0.3µM	0.3
Mshflox2 (20µM)	0.3µM	0.3
dNTPs (10mM each)	0.2mM	0.4
MgCl (25mM)	2mM	1.6
5x GoTaq green buffer	1x	4
GoTaq Hot Start Pol (5U/µl)	0.025U/µl	0.1
DNA tamplate		1.0
Total volume		20
mTmG	c final	volume (µl)
water		9.9
Rosa10 (20µM)	1µM	1
Rosa11 (20µM)	1µM	1
Rosa4 (20µM)	1µM	1
dNTPs (10mM each)	0.2mM	0.4
MgCl (25mM)	2mM	1.6
5x GoTaq green buffer	1x	4
GoTaq Hot Start Pol (5U/µl)	0.025U/µl	0.1
DNA tamplate		1.0
Total volume		20
Cre	c final	volume (µl)
water		5.2
Blk buffer mix		3
Primer CreA (20µM)	0.4µM	0.4
Primer CreB (20µM)	0.4µM	0.4
RedAmp 2x mix		10
DNA tamplate		1.0
Total volume		20

Aldh1b1 wt	c final	volume (µl)
water		6.9
Primer FL065 (20µM)	0.5µM	0.5
Primer En2A (20µM)	0.5µM	0.5
Primer FL066 (20µM)	5µM	5
dNTPs (10mM each)	0.2mM	0.4
MgCl (25mM)	2mM	1.6
5x GoTaq green buffer	1x	4
GoTaq Hot Start Pol (5U/µl)	0.025U/µl	0.1
DNA tamplate		1.0
Total volume		20
Aldh1b1-	c final	volume (µl)
water		12.5
tm1c fwd (20µM)	0.2µM	0.2
Floxed LR (20µM)	0.2µM	0.2
dNTPs (10mM each)	0.2mM	0.4
MgCl (25mM)	2mM	1.6
5x GoTaq green buffer	1x	4
GoTaq Hot Start Pol (5U/µl)	0.025U/µl	0.1
DNA tamplate		1.0
Total volume		20
Aldh1b1 flox	c final	volume (µl)
water		12.5
tm1c fwd (20µM)	0.2µM	0.2
tm1c rev (20µM)	0.2µM	0.2
dNTPs (10mM each)	0.2mM	0.4
MgCl (25mM)	2mM	1.6
5x GoTaq green buffer	1x	4
GoTaq Hot Start Pol (5U/µl)	0.025U/µl	0.1
DNA tamplate		1.0
Total volume		20

Table 2.4: Genotyping PCR reaction compositions. (c final= final concentration).

PCR steps	T(°C)	Time	N° of cycles
Msh2 -			
Pre-heat	95°C	2min	1
Denaturation	95°C	30 sec	32
Annealing	60°C	60 sec	1
Extension	72°C	60 sec	1
Termination	72°C	10min	1
	4°C	∞	
Msh2 flox			
Pre-heat	95°C	2min	1
Denaturation	95°C	30 sec	34
Annealing	55°C	60 sec	1
Extension	72°C	60 sec	1
Termination	23°C	60 sec	1
	4°C	∞	
Cre			
Pre-heat	94°C	3min	1
Denaturation	94°C	30 sec	30
Annealing	55°C	30 sec	1
Extension	72°C	90 sec	1
Termination	72°C	10min	1
	4°C	∞	
mTmG			
Pre-heat	95°C	2min	1
Denaturation	95°C	30 sec	32
Annealing	61°C	30 sec	1
Extension	72°C	45 sec	1
Termination	72°C	5min	1
	4°C	∞	

PCR steps	T(°C)	Time	N° of cycles
Aldh1b1 wt			
Pre-heat	95°C	2min	1
Denaturation	95°C	30 sec	32
Annealing	58°C	30 sec	1
Extension	72°C	90 sec	1
Termination	72°C	5min	1
	4°C	∞	
Aldh1b1 -			
Pre-heat	95°C	2min	1
Denaturation	95°C	30 sec	35
Annealing	58°C	30 sec	1
Extension	72°C	180 sec	1
Termination	72°C	5min	1
	4°C	∞	
Aldh1b1 flox			
Pre-heat	95°C	2min	1
Denaturation	95°C	30 sec	32
Annealing	52°C	30 sec	1
Extension	72°C	60 sec	1
Termination	72°C	5min	1
	4°C	∞	

Table 2.5: Thermocycler programmes for genotyping PCR assays. (T=temperature; N°=numbers; ∞= infinite).

2.2.1.3 Genotyping PCR products using gel electrophoresis

Amplified PCR products were separated on gels prepared with agarose (Sigma-Aldrich, A9539) in 1XTris/Borate/EDTA (TBE) buffer. PCR products of genotyping assays for Msh2wt, Msh2flox, Msh2-, mTmG, Aldh1b1wt and Aldh1b1- alleles were separated on 2%(w/v) agarose gels (Sigma-Aldrich, A9539) and the PCR products of genotyping assays for Cre and Aldh1b1flox alleles were separated on 1.5% (w/v) agarose gels. The Sub-cell GT (Bio-Rad, 1704404) buffer tank was filled with 1XTBE and the solidified agarose gel was placed inside this tank. Five microlitres of DNA ladder (100bp / 1 kb, New England Biolabs, N3231L) were loaded into flanking wells at the edges of the gel. Eight microliters for each genotyping PCR product were loaded directly into wells before electrophoretic separation at 140 V in 1XTBE buffer for 1 hour. After electrophoretic separation, the gel was washed with distilled water and incubated with GelRed Nucleic Acid Gel Stain (Biotium INC., 41003) for 30 min to enable DNA visualisation under Ultraviolet (UV) light. The DNA bands within the gel were visualised and photographed under UV light using the UVP GelDoc-It (Analytik Jena).

Representative images of the gel results are shown in Appendix 1 (Supplementary Figure 2.1-2.4).

2.2.2 Microsatellite instability detection

2.2.2.1 DNA extraction from FFPE

DNA was extracted from FFPE sections using the DNAstorm™ Kit, (Cambridge Biosciences, CD502), following the manufacturer's instructions. Four or five FFPE sections of 8µm thick per sample (e.g. from a colonic adenoma), according to the size of the tissue. DNA quality and quantity were tested using the Nanodrop system (Thermo Fisher Scientific, 2000C).

2.2.2.2 Microsatellite instability markers and PCR assays

Microsatellite instability (MSI) detection PCR assays, using PCR primers on either side of selected repetitive microsatellite loci, were performed for a specific panel of 5 MSI markers (A27, A33, mBat26, mBat37 and mBat59), previously established for use in murine DNA (Bacher et al., 2005; Kabbarah et al., 2003), for which primer sequences are shown in Table 2.6. MSI detection PCR reactions were performed using GoTaq G2 Hot Start Taq Polymerase Mix kit (Promega, M7405) and PCR Nucleotide mix (Promega, C1141), as shown in Table 2.7. DNA was amplified using the PCR thermocycler programmes detailed in Table 2.8.

Primer Name		Sequence 5'-3'	Reference
A27	fwd	TCCCTGTATAACCCTGGCTGACT	Kabbarah et al., 2003
A27	rev	GCAACCAGTTGTCCTGGCGTGGA	
A33	fwd	TACAGAGGATTGTCCTCTTGGAG	Kabbarah et al., 2003
A33	rev	GCTGCTTCACTTGGACATTGGCT	
mBat 26	fwd	TCACCATCCATTGCACAGTT	Bacher et al., 2005
mBat 26	rev	CTGCGAGAAGGTACTCACCC	
mBat 37	fwd	TCTGCCCAAACGTGCTTAAT	Bacher et al., 2005
mBat 37	rev	CCTGCCTGGGCTAAAATAGA	
mBat 59	fwd	GTAATCCCTTTATTCCATTTAGCA	Bacher et al., 2005
mBat 59	rev	GGCTCACAACCATCCGTAACAAGA	

Table 2.6: Microsatellite instability marker primer sequences and relevant papers. (fwd=forward, rev=reverse).

A27	c final	volume (µl)
water		to reach 20ul
A27 fwd (20µM)	0.4µM	0.4
A27 rev (20µM)	0.4µM	0.4
dNTPs (10mM each)	0.2mM	0.4
MgCl (25mM)	2mM	1.6
5x GoTaq green buffer	1x	4
GoTaq Hot Start Pol (5U/µl)	0.025U/µl	0.1
DNA tamplate	200ng	variable
Total volume		20
A33	c final	volume (µl)
water		to reach 20ul
A33 fwd (20µM)	0.2µM	0.2
A33 rev (20µM)	0.2µM	0.2
dNTPs (10mM each)	0.2mM	0.4
MgCl (25mM)	2mM	1.6
5x GoTaq green buffer	1x	4
GoTaq Hot Start Pol (5U/µl)	0.025U/µl	0.1
DNA tamplate	200ng	variable
Total volume		20
mBat26	c final	volume (µl)
water		to reach 20ul
mBat26 fwd (20µM)	0.2µM	0.2
mBat26 (20µM)	0.2µM	0.2
dNTPs (10mM each)	0.2mM	0.4
MgCl (25mM)	2mM	1.6
5x GoTaq green buffer	1x	4
GoTaq Hot Start Pol (5U/µl)	0.025U/µl	0.1
DNA tamplate	200ng	variable
Total volume		20

mBat37	c final	volume (µl)
water		to reach 20ul
mBat37 fwd (20µM)	0.2µM	0.2
mBat37 (20µM)	0.2µM	0.2
dNTPs (10mM each)	0.2mM	0.4
MgCl (25mM)	2mM	1.6
5x GoTaq green buffer	1x	4
GoTaq Hot Start Pol (5U/µl)	0.025U/µl	0.1
DNA tamplate	200ng	variable
Total volume		20
mBat39	c final	volume (µl)
water		to reach 20ul
mBat39 fwd (20µM)	0.2µM	0.2
mBat39 (20µM)	0.2µM	0.2
dNTPs (10mM each)	0.2mM	0.4
MgCl (25mM)	2mM	1.6
5x GoTaq green buffer	1x	4
GoTaq Hot Start Pol (5U/µl)	0.025U/µl	0.1
DNA tamplate	200ng	variable
Total volume		20

Table 2.7: Microsatellite instability detection PCR reaction compositions. (c final= final concentration).

PCR steps	T(°C)	Time	N° of cycles
A27			
Pre-heat	95°C	3min	1
Denaturation	95°C	30 sec	1
Annealing	59°C	60 sec	32
Extension	72°C	60 sec	1
Termination	72°C	5min	1
	4°C	∞	
A33			
Pre-heat	95°C	3min	1
Denaturation	95°C	30 sec	1
Annealing	59°C	60 sec	32
Extension	72°C	60 sec	1
Termination	72°C	5min	1
	4°C	∞	
mBat26			
Pre-heat	95°C	3min	1
Denaturation	95°C	30 sec	1
Annealing	60°C	30 sec	32
Extension	72°C	90 sec	1
Termination	72°C	10min	1
	4°C	∞	
mBat37			
Pre-heat	95°C	3min	1
Denaturation	95°C	30 sec	1
Annealing	62°C	60 sec	32
Extension	72°C	90 sec	1
Termination	72°C	10min	1
	4°C	∞	
mBat39			
Pre-heat	95°C	3min	1
Denaturation	95°C	30 sec	1
Annealing	55°C	60 sec	32
Extension	72°C	90 sec	1
Termination	72°C	10min	1
	4°C	∞	

Table 2.8: Thermocycler programmes for MSI detection PCR assays. (T=temperature; N°=numbers; ∞= infinite).

2.2.2.3 Microsatellite instability detection PCR assay products were analysed by polyacrylamide gel electrophoresis

Amplified MSI detection PCR products were separated on 15% polyacrylamide gels. All of the solutions used for making the polyacrylamide gels (both stacking and separating components of the gels) and the various buffers used for this gel electrophoretic analysis are shown in Table 2.9. Eight microlitres of DNA ladder (100bp /1 kb) were loaded into the first well of each gel. Twelve microliters of each PCR product were loaded directly into wells (the loading buffer is included in the PCR reagent kit) before electrophoretic separation at 80V for 30 min, then run 150V for 1.5hours at room temperature (RT). After electrophoretic separation, the gel was washed with distilled water (dH_2O) and incubated with GelRed Nucleic Acid Gel Stain (Biotium INC., 41003) for 30 min to enable DNA visualisation under Ultraviolet (UV) light. Gels were visualised and photographed under UV light using the UVP GelDoc-It (Analytik Jena).

Separating Buffer (1.5M Tris Base, 0.5% (w/v) SDS, pH 8.8.)
90.75g Tris base (Sigma-Aldrich, T1503)
2.5g SDS
Adjust to pH 8.8
Add dH_2O to total volume 500ml. Store at RT
Stacking Buffer (0.5M Tris Base, 0.5% (w/v) SDS, pH 6.8)
30.25g Tris base (Sigma-Aldrich, T1503)
2.5g SDS
Adjust to pH 6.8
Add dH_2O to total volume 500ml. Store at RT
10x Running buffer.
15g Tris base (Sigma-Aldrich, T1503)
72g Glycine (Sigma-Aldrich, G8898)
5g SDS
Add dH_2O to total volume 500ml. Store at 4°C.
4% Stacking gel preparation
6.5ml dH_2O
2.5ml Stacking Buffer
1ml Acrylamide/Bis 40% (Sigma-Aldrich, A7168)
50µl 10% ammonium persulphate (Sigma-Aldrich, A3678)
10µl TEMED (Thermo Fisher Scientific, 17919)
15% Separating gel preparation
7.5ml dH_2O
5.0ml Separating Buffer
7.5ml Acrylamide/Bis 40% (Sigma-Aldrich, A7168)
100µl 10% ammonium persulphate (Sigma-Aldrich, A3678)
10µl TEMED (Thermo Fisher Scientific, 17919)

Table 2.9: List of buffers used for the separation of MSI detection PCR products separated by polyacrylamide gel electrophoresis.

2.2.3 Immunohistochemical and histochemical staining of FFPE tissue sections

The details of the antibodies used for immunohistochemistry (IHC) are shown in Table 2.10 and buffers used for IHC are shown in Table 2.11. Slides were rehydrated by incubation in xylene for 15 minutes, followed by decreasing concentrations of ethanol (99%, 90%, 70%) for 10 minutes each at RT. Slides were dipped in dH_2O for 5min and blocked using 3% H_2O_2 (30% H_2O_2, Honeywell Fluka, 31642) solution for 20 minutes at RT. Slides were washed with 1XTBS-Tween for 5 minutes at RT.

Antigen retrieval was performed with either Tris-EDTA buffer or citrate buffer depending on the antibody (Table 2.10). A pressure cooker was filled with 1L of antigen retrieval buffer and heated to boiling point before slides were added. Slides were boiled in solution for 10, 12 or 15 minutes depending on the antibody (Table 2.10). The pressure cooker containing the slides was filled with dH_2O and the slides were cooled to RT for 1h. Slides were washed for 10min in dH_2O. Slides were permeabilised with 0.5% Triton-X100 (Sigma-Aldrich, X100-500ML) in 1XTBS-Tween for 20 minutes at RT. Slides were washed in 1XTBS-Tween twice for 5 minutes and rinsed in 1XTBS. Slides were blocked with 5% goat serum in 1XTBS-Tween for 1 hour at RT. Primary antibodies at the dilutions shown (Table 2.10) were added to slides in blocking buffer and incubated overnight at 4°C. The following day, slides were washed in 1XTBS-Tween twice for 10 minutes at RT and rinsed in 1XTBS. N-Histofine simple stain mouse MAX PO (2B Scientific, 414341F) was used as secondary antibody, a single drop per slide was added and incubated for 30min at RT. Slides were washed in 1XTBS-Tween twice for 10 minutes at RT and rinsed in 1XTBS.

IHC signal was detected by incubation of the slide with 3,3'-diaminobenzine (DAB) (Liquid DAB+, K346811) for 1 or 2 minutes at RT. Slides were washed in dH_2O for 10 minutes at RT and counterstained in Harris' haematoxylin (Sigma-Aldrich, HHS32) for 30 seconds. Slides were washed under tap water for 5 minutes. Slides were dehydrated in increasing concentrations of ethanol (70%, 90% and 100%) for 10 minutes each, followed by xylene for 15 minutes at RT. Coverslips were applied with mounting medium. The technical controls for the antibodies and immunohistochemical staining can be found in the Appendix (Supplementary Figure 2.5).

Immunohistochemistry for infiltrating immune cells was performed by Dr Seth Coffelt's research group from the Beatson Cancer Institute in Glasgow. The panel of immune cell antibodies and their IHC details are shown in Table 2.12.

Haematoxylin and eosin (H&E) staining was performed by the Pathology laboratory of IGMM, the University of Edinburgh.

Antibody	Source	Manufacturer	Antigen retrieval	Dilution
Anti-Msh2	rabbit, polyclonal	Abcam, ab70270	Tris-EDTA, 12min	1:4000
Anti-Msh6	mouse, monoclonal	Abcam, ab92471	Tris-EDTA, 12min	1:500
Anti-Mlh1	rabbit, monoclonal	Abcam, ab92312	Citrate Buffer, 15 min	1:250
Anti-Pms2	rabbit, monoclonal	Abcam, ab110638	vmt	vmt
Anti-Ki67	rabbit, monoclonal	Abcam, ab16667	Tris-EDTA, 12min	1:500
Anti-β-Catenin	mouse, monoclonal	BD Transduction laboratories, 610154	Citrate buffer, 10min	1:100
Anti-Aldh1b1	rabbit, polyclonal	Proteintech, 15560-a-AP	Citrate buffer, 10min	1:500
Anti-cCas3	rabbit, polyclonal	Cell Signaling, 9664	Tris-EDTA, 12min	1:50
Anti-p53	CM5, rabbit	Phil Coates's lab	Citrate buffer, 15min	1:100
Anti-GFP	rabbit, polyclonal	Life technologies, A11122	Citrate buffer, 10min	1:4000
Anti-γH2AX	rabbit, polyclonal	Cell Signaling,2577	Citrate buffer, 15min	1:100

Table2.10: List of antibodies used for immunohistochemistry (vmt=various methods tried).

Citrate Buffer (10mM, pH6)
18ml Citric acid
82ml Socdium citrate
Add dH_2O to total volume 1L. Store at RT.
Citric acid (0.1M)
10.5g Citric acid (Sigma-Aldrich,C1909)
Add dH_2O to total volume 500ml. Store at RT.
Sodium Citrate (0.1M)
14.7g Sodium citrate (Sigma-Aldrich,S1804)
Add dH_2O to total volume 500ml. Store at RT.
Tris-EDTA Buffer (pH9)
1.21g Tris base (Sigma-Aldrich,T1503)
0.37g EDTA (Sigma-Aldrich, E5134)
Add dH_2O to a total volume of 1L.
Add 0.05% of Tween20 (Sigma-Aldrich, P1379)
10X TBS
60.6g Tris base (Sigma-Aldrich,T1503)
87.6g Sodium Chloride (Fisher Scientific, 10478283)
Adjust to pH 7.6
Add dH_2O to total volume 1000ml. Store at RT
1X TBS
500ml of 10XTBS
Add dH_2O to total volume 5L. Store at RT
1X TBS-Tween
1L of 1XTBS
Add 0.1% of Tween20 (Sigma-Aldrich, P1379)

Table 2.11: List of buffers used for immunohistochemistry.

Antibody	Source	Manufacturer	Autostainer	Antigen retrieval	Dilution	Secondary Ab	Chromogen
CD4	rat, monoclonal	eBioscience, 14-9766-82	Leica Bond Rx	ER2 20 mins	1:500	Rat ImmPRESS	Liquid DAB
CD8	mouse, monoclonal	eBioscience, 14-0808-82	Leica Bond Rx	ER2 20 mins	1:500	Rat ImmPRESS	Liquid DAB
CD45R/B220	rat, monoclonal	Abcam, ab64100	Leica Bond Rx	ER2 20 mins	1:200	Rat ImmPRESS	Liquid DAB
F4/80	rat, monoclonal	Abcam, ab6640	Leica Bond Rx	Enz1 10min	1:100	Rat ImmPRESS	Liquid DAB
Ly6G	rat, monoclonal	BioXcell, BE0075-1	Leica Bond Rx	ER2 20 mins	1:60,000	Rat ImmPRESS	Liquid DAB

Table 2.12: Panel of immune cell antibodies used for IHC with relevant IHC details.

2.2.4 Acetaldehyde assay

Plasma acetaldehyde concentrations were determined using an acetaldehyde assay kit (Megazyme, K-ACHYD). Samples were assayed and analysed according to the manufacturer's instructions. Plasma samples were analysed in experimental batches on the same day to ensure standardised recovery and measurement of acetaldehyde in all samples and to avoid unnecessary experimental variations. 50µl of plasma was used for each analysis and these were performed in triplicate.

2.2.5 RNA extraction from small and large intestinal cells isolated and sorted from the Msh2-LS mouse model

2.2.5.1 Small and large intestinal epithelial cell isolation from tissues

Fresh (unfixed) SI and LI were flushed twice in cold PBS and inverted using the 30cm long and 3mm diameter bamboo skewer to expose the inner mucosal lining. SI and LI were cut in segments of 5-10mm long and placed in separate 50ml Falcon tubes containing cold PBS. These tissue fragments were washed two times with cold PBS. Samples were incubated with 25mM EDTA (in 25ml cold PBS) for 30 min on a tube roller at 4°C. The cold PBS-EDTA buffer was discarded and the tissue fragments were washed with cold Advanced DMEM/F12 medium (Thermofisher, 12634028). Cold PBS was added to the tubes containing the samples and each tube was strongly shaken to detach the intestinal epithelial cells. The supernatant was collected in a clean 50ml Falcon tube and kept on ice. This step was repeated until 30ml of supernatant was collected for each sample. Tubes were filled up to 50ml with Advanced DMEM/F12 medium and centrifuged at 500 x g for 5 minutes. The resulting pellets were re-suspended with 1ml of TrypLE Express Enzyme (1X) (Thermofisher, 12604013) each and incubated in a waterbath for 15 minutes at 37°C. Advanced DMEM/F12 medium was added and samples were filtered using a 70µm strainer (Corning, 15370801) into 50ml Falcon tubes and centrifuged at 500x g for 5 minutes. Supernatant was discarded and the pellet was re-suspended in 5ml of 0.1% BSA in PBS and centrifuged at 500 x g for 5 minutes. Supernatant was discarded and the pellet was incubated with EpCAM antibody (or IgG2a isotype control) diluted to 1:200 (Table 2.13) in 200-500µl of 0.1% BSA in PBS for 30 minutes at 4°C. Two millilitres of 0.1% BSA in PBS were added and transferred to the FACS tubes (Falcon, 352054).

Samples were centrifuged at 500 x g for 5 minutes and re-suspended in 500-1000µl of 0.1% BSA in PBS.

Antobody	Source	Manufacturer
EpCAM Anti-mouse	rat, monoclonal	BioLegend, 118213
IgG2a Isotype control	rat, monoclonal	BioLegend, 400511

Table2.13: FACS antibodies.

2.2.5.2 Fluorescent-Activated Cell Sorting (FACS) of small and large intestinal epithelial cells

The FACS was performed by the flow cytometry facility of the IGMM, University of Edinburgh. Lasers were set up to identify EpCAM positive intestinal epithelial cells and FACS was used to divide them in 4 sub-populations according to their fluorescence signals (RFP+ only, GFP+ only, both RFP+ and GFP+, or no red or green fluorescence).

2.2.5.3 RNA extraction

Immediately after FACS, RNA was extracted from each of the sorted samples. 1ml TRIZOL Reagent (Thermo Fisher Scientific, 15596026) was added to each sample and it was repetitively pipetted and left for 5 minutes at RT. 0.2ml chloroform was added and samples shaken for 15 seconds and left at RT for 10 minutes. Samples were centrifuged at 12000g for 15 minutes at RT. The samples showed a gradient separation in three phases. The colourless upper aqueous phase was removed and added to a new tube, the white solid and red lower aqueous phases were discarded. 0.5ml isopropanol was added and left for 10 minutes at RT. Samples were centrifuged at 12000g for 10 minutes at 4°C and the supernatant discarded.

1ml 75% ethanol was added and samples were mixed by vortexing. Samples were centrifuged at 7500g for 5 minutes at 4°C, the supernatant discarded and the pellet air-dried. RNA was re-suspended in 30µl dH_2O at 57°C, quantified using the Nanodrop system (Thermo Fischer Scientific, 2000C), and stored at -80°C.

2.3 Image analysis

Histopathological examination was performed by Prof. Mark J Arends using a Leica DMR HC microscope (Leica DMR HC 0.7H.21.TL.-.E.16C, 213860) and images were taken from selected fields and acquired using a Leica DFC 450-C camera.

Immunohistochemically stained and histochemically stained FFPE tissue sections were scanned using a Nanozoomer (Hamamatsu) slidescanner and analysed with the Hamamatsu NDP Viewer software (NDP.view2) at the Pathology laboratory of IGMM, the University of Edinburgh. Image analysis software QuPATH v0.2.0 was used to analyse immunohistochemically detected Msh2, Ki67, y-H2AX and p53 protein expression.

Expression of the red and green fluorescent proteins encoded by the *mTmG* transgene were evaluated in whole mount specimens of the small and large intestines using a Leica MZFLIII fluorescence stereo microscope with 1x objective and a Nikon A1R point scanning confocal microscope (IGMM imaging facility, University of Edinburgh). The obtained images were analysed using Fiji (ImageJ)-Trainable WEKA Segmentation software, through which the proportion of green areas divided by the total green + red areas (termed the % green area) were measured.

2.4 Statistical analysis

Data were analysed using GraphPad Prism version v7.0 software, which was used for all statistical analyses and these are mostly shown as mean with standard deviation (SD) error bars. Group data were compared using unpaired, two-tailed Student's t-test (for normally distributed data) or Mann–Whitney U test (for non-parametric data) as appropriate, or two-way ANOVA with Bonferroni's multiple comparisons correction test. Association between two categories was assessed by two-sided Fisher's test. Percentage of survival was analysed by the Log-rank (Mantel-Cox) test. Differences between groups were considered statistically significant if $p \leq 0.05$.

Chapter 3: Establishment of an Msh2-Lynch Syndrome mouse model colony and its characterization

3.1 Introduction

In the past, Lynch syndrome mouse models have been important for the study and understanding of the disease mechanisms and the roles of the MMR genes. However, none of these models fully represented human LS, as described in Chapter 1.1.8. Recently, Wojciechowicz et al (2014) generated a novel Msh2-Lynch Syndrome (Msh2-LS) mouse model that closely mimics key components of the large intestinal disease characteristics in LS patients.

The Msh2-LS mouse model has one constitutive knockout *Msh2* allele (*Msh2*$^{-}$) and one (floxed) conditional knockout *Msh2* allele (*Msh2*^{flox}). The *Msh2*$^{-}$ allele was generated by the incorporation of a *hygromycin (hyg)* resistance gene between codons 588 and 589 in exon 12 of *Msh2* (Claij & te Riele, 2004), completely preventing Msh2 protein expression (de Wind et al., 1995). The *Msh2*^{flox} allele was constructed by insertion of a loxP site 53 bp downstream of exon 13 and another loxP site 2 kb upstream of exon 12 in the opposite orientation (Figure 3.1). Cre-mediated recombination between these two loxP sites results in inversion of exons 12 and 13 (Figure 3.1), abrogating gene activity (Claij & te Riele, 2004).

To target Msh2 loss of activity to only a limited number of self-renewing intestinal epithelial stem cells, the *Lgr5CreERT2* transgene was used. The Cre recombinase protein is fused to the modified oestrogen receptor ERT2. Only in the presence of tamoxifen metabolites, does the CreERT2 protein translocate to the nucleus and become active, where it can execute recombination between the loxP sites leading to inactivation of the conditional *Msh2* allele. As CreERT2 is expressed from the Lgr5 locus, this occurs in Lgr5-expressing intestinal epithelial stem cells (Barker et al., 2007) (Figure 3.2). In this Msh2-LS mouse model, scattered dMMR stem cells are induced among surrounding MMR-proficient cells in the large and small intestinal epithelium (as observed in LS patients). Wojciechowicz et al (2014) demonstrated an increased risk of intestinal tumour development in the Msh2-LS model mice.

In order to visualize those cells that underwent Cre activation, and thus *Msh2* inactivation, the *mTmG* transgene was crossed into the mouse model. The *mTmG* transgene was originally generated by Dr. Lou, Stanford University (Muzumdar et al., 2007). This Cre reporter construct confers a red fluorescence to cells of all tissues without Cre activation,

due to whole body expression of membrane-targeted modified Tomato red fluorescent protein (mT). Upon Cre activation, Cre recombines the two LoxP sites surrounding the floxed mT allele and the adjacent polyadenylation site, thus excising this section of DNA, allowing expression of a membrane-targeted modified Green Fluorescent Protein or GFP (mG) (Figure 3.3).

In this chapter, the aim is to establish an Msh2-LS mouse model colony, provided by Dr Hein te Riele (Wojciechowicz et al., 2014), and upgrade it by introducing the *mTmG* transgene. In this chapter, the modification and characterization of the Msh2-LS mouse model are described.

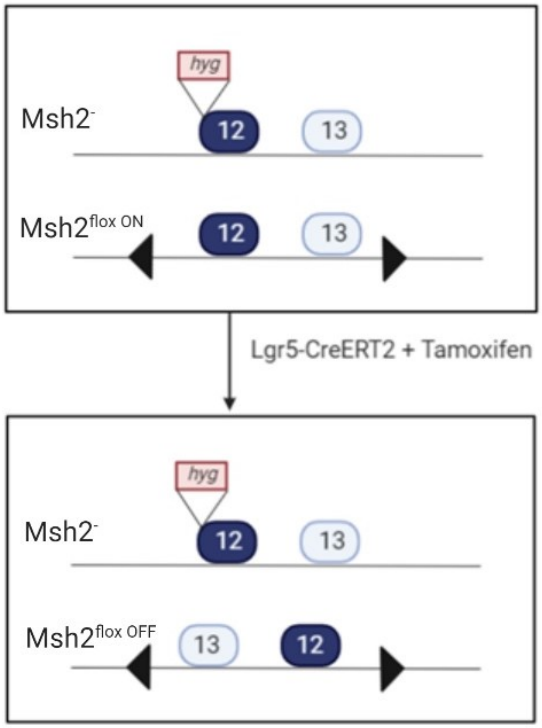

Figure 3.1: Schematic diagram of the *Msh2*$^{fl/-}$ alleles before and after Cre activation. Constitutive (Msh2^{-}) and conditional (Msh2$^{flox\ ON}$) knockout alleles of Msh2 are shown (adapted and modified from Wojciechowicz et al., 2014). Cre activation results in inversion of exons 12 and 13 of the conditional *Msh2* allele (Msh2$^{flox\ OFF}$), thus inactivating it. (Image created with BioRender.com).

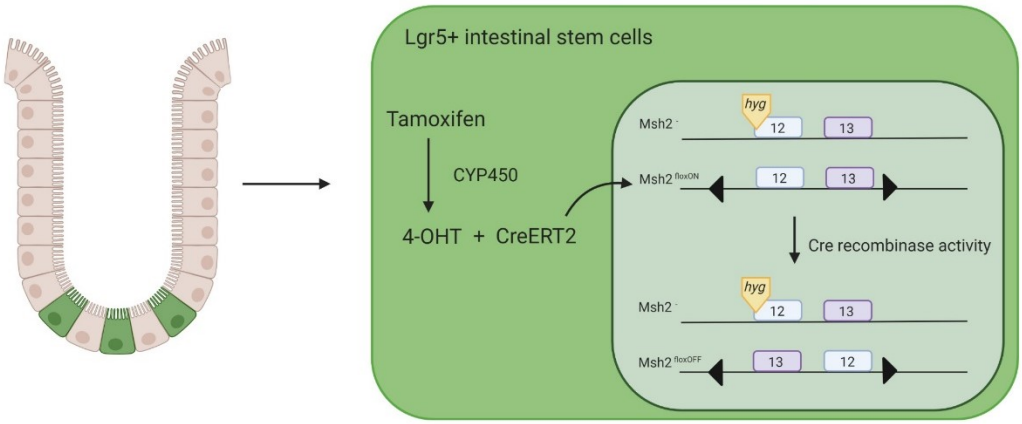

Figure 3.2: Schematic diagram of Tamoxifen metabolite-mediated Cre activation in Lgr5 expressing intestinal epithelial stem cells. The *Lgr5CreERT2* transgene was inserted into the murine Lgr5 locus, ensuring that the CreERT2 protein is only expressed in Lgr5+ intestinal stem cells (green cells at the base of the crypt shown on the left). Tamoxifen is converted by cytochrome p450 enzymes into the active metabolite 4-Hydroxy-Tamoxifen (4-OHT) that binds to the ERT2 ligand-binding domain of the CreERT2 protein, allowing its translocation from the cytoplasm into the nucleus, where the active Cre enzymatic function leads to recombination of *loxP* sites flanking *Msh2* exons 12 and 13 ($Msh2^{floxON}$), resulting in the inversion of exons 12 and 13 sequences, thus inducing inactivation of the second *Msh2* allele ($Msh2^{floxOFF}$) (the first *Msh2* allele has been inactivated by insertion of a hygromycin-resistance gene (*hyg*) into exon 12). This abrogates DNA mismatch repair function in that stem cell and in any daughter cells formed by that stem cell. (Image created with BioRender.com).

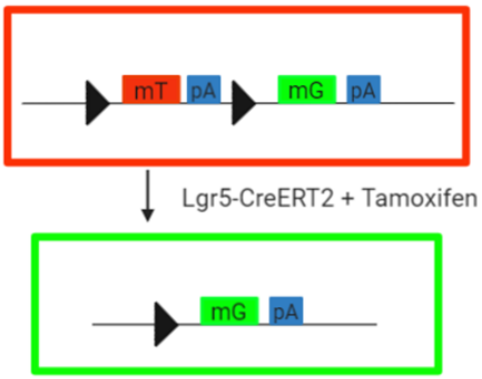

Figure 3.3. Schematic diagram of the mTmG coloured fluorescent protein reporter construct before (cell expresses mT and appears red) and after (cell expresses mG and appears green). Cre-mediated recombination of loxP sites (black triangles) flanking the mT and pA sequences (adapted and modified from Muzumdar et al., 2007). (Image created with BioRender.com).

3.2 Mouse Model Colony Breeding, Maintenance and Husbandry

3.2.1 Methods

Mice were housed in IVCs with group sizes and enrichment according to Home Office regulations. Further details on the mice housing conditions and maintenance can be found in Chapter 2 (2.1.1).

3.2.2 Results

3.2.2.1 Establishment of the colony of Msh2-LS mice and cross-breeding with mTmG transgene bearing mice

Msh2-LS mouse model founder mice were received from Professor Hein te Riele's research group at the Netherlands Cancer Institute (Wojciechowicz et al., 2014). 2 male and 2 female *Msh2$^{flox/flox}$* mice were received, along with 1 male and 2 female *Msh2$^{+/-}$; Lgr5CreERT2$^{+/-}$* mice (*Lgr5CreERT2^{-}* indicates a normal wild-type *Lgr5* allele, whereas *Lgr5CreERT2^{+}* indicates insertion of the *CreERT2* transgene into a modified *Lgr5* locus). All animals were of breeding age. The *Msh2 $^{flox/flox}$* mice were bred with the *Msh2$^{+/-}$; Lgr5CreERT2 $^{+/-}$* mice to obtain the Msh2-LS mouse model experimental subjects (*Msh2$^{flox/-}$; Lgr5CreERT2$^{+/-}$*). Homozygous *Lgr5CreERT2$^{+/+}$* mice are not viable (due to loss of normal *Lgr5* alleles that are required for normal development), so only heterozygous *Lgr5CreERT2$^{+/-}$* mice were used for breeding with *Lgr5* wild-type mice *(Lgr5CreERT2$^{+/-}$ X Lgr5CreERT2$^{-/-}$*), to generate viable and fertile progeny. The genotype frequencies that resulted from this breeding almost perfectly reflected the expected Mendelian ratios with around 25% of the progeny having the correct genotype for Msh2-LS experimental subject mice (*Msh2$^{flox/-}$; Lgr5CreERT2$^{+/-}$*) (Figure 3.4A). Mice with the genotype *Msh2$^{flox/-}$; Lgr5CreERT2$^{+/-}$* were also bred with *Msh2$^{flox/-}$; Lgr5CreERT2$^{-/-}$* mice, in order to obtain a higher number of Msh2-LS experimental subject mice from each litter. The mice resulting from these matings showed 25% progeny with *Msh2$^{flox/-}$; Lgr5CreERT2$^{+/-}$* genotypes and 12.5% progeny with *Msh2$^{flox/flox}$; Lgr5CreERT2$^{+/-}$* genotypes (Figure 3.4B). Mice with these genotypes were used as experimental subject mice or breeders. Tabular representation of the inter-cross to generate the Msh2-LS mouse model experimental subjects is shown in the Appendix (Supplementary Table 3.1). Another 25% (12.5% of *Msh2$^{-/-}$; Lgr5CreERT2$^{-/-}$* and 12.5% of *Msh2$^{-/-}$; Lgr5CreERT2$^{+/-}$)* of the mice resulting from this breeding showed complete *Msh2* deletion (*Msh2$^{-/-}$*). *Msh2$^{-/-}$* mice have been

reported to develop tumours (mostly early thymic and other lymphomas, with some intestinal adenomas in a few surviving mice) that required termination of most of these mice starting from around 10 weeks of age (de Wind et al., 1995). Therefore, *Msh2*$^{-/-}$ pups were culled immediately after genotyping.

In the stage prior to the administration of Tamoxifen, Msh2-LS experimental mice did not present altered or harmful phenotypes. Nor did they show increased tumour predisposition (without Cre activation) compared with wild-type mice (see data below in Chapters 4.3).

To introduce the *mTmG* transgene (Muzumdar et al., 2007), the *Msh2*$^{flox/-}$*; Lgr5CreERT2*$^{+/-}$ mice were cross-bred with *mTmG*$^{+/+}$ mice, generating *Msh2*$^{+/-}$*; Lgr5CreERT2*$^{+/-}$*; mTmG*$^{+/-}$ and *Msh2*$^{flox/+}$*; Lgr5CreERT2*$^{+/-}$*; mTmG*$^{+/-}$ mice (*mTmG*$^{-/-}$ indicates a normal wildtype genotype without the *mTmG* construct, whereas *mTmG*$^{+/+}$ or *mTmG*$^{+/-}$ indicates presence of two copies or one copy, respectively, of the *mTmG* construct) (Figure 3.5A). These mice were interbred to generate *Msh2*$^{flox/-}$*; Lgr5CreERT2*$^{+/-}$*; mTmG*$^{+/-}$ mice and after further breeding *Msh2*$^{flox/-}$*; Lgr5CreERT2*$^{+/-}$*; mTmG*$^{+/+}$ mice, which were used as experimental subject mice or breeders (Figure 3.5B). Tabular representation of the inter-cross to introduce the *mTmG* transgene into the Msh2-LS mouse model is shown in the Appendix (Supplementary Table 3.2).

A

Genotype	Probability
Msh2fl/+, Lgr5Cre+/-	25%
Msh2fl/+, Lgr5Cre-/-	25%
Msh2fl/-, Lgr5Cre-/-	25%
Msh2fl/-, Lgr5Cre+/-	25%

B

Genotype	Probability
Msh2fl/fl, Lgr5Cre+/-	12.50%
Msh2fl/-, Lgr5Cre-/-	25%
Msh2-/-, Lgr5Cre-/-	12.50%
Msh2fl/fl, Lgr5Cre-/-	12.50%
Msh2-/-, Lgr5Cre+/-	12.50%
Msh2fl/-, Lgr5Cre+/-	25%

Figure 3.4: A) Percentage of resulting genotypes from the breeding between *Msh2* $^{flox/flox}$ and the *Msh2*$^{+/-}$*; Lgr5CreERT2* $^{+/-}$ mice. B) Percentage of resulting genotypes from the breeding between *Msh2*$^{flox/-}$*; Lgr5CreERT2*$^{+/-}$ and *Msh2*$^{flox/-}$*; Lgr5CreERT2*$^{-/-}$ mice.

A

Genotype	Probability
Msh2 fl/+, Lgr5Cre+/-, mTmG +/-	25%
Msh2 fl/+, Lgr5Cre-/-, mTmG +/-	25%
Msh2 -/+, Lgr5Cre+/-, mTmG +/-	25%
Msh2 -/+ Lgr5Cre-/- mTmG +/-	25%

B

Genotype	Probability
Msh2fl/-, Lgr5Cre+/-, mTmG+/-	6.25%
Msh2fl/-, Lgr5Cre+/-, mTmG+/+	3.13%
Msh2fl/-, Lgr5Cre+/-, mTmG-/-	3.13%
Msh2fl/-, Lgr5Cre-/-, mTmG+/+	3.13%
Msh2fl/-, Lgr5Cre-/-, mTmG+/-	6.25%
Msh2fl/-, Lgr5Cre-/-, mTmG-/-	3.13%
Msh2fl/+, Lgr5Cre+/-, mTmG+/-	6.25%
Msh2fl/+, Lgr5Cre+/-, mTmG-/-	3.13%
Msh2fl/+, Lgr5Cre+/-, mTmG+/+	3.13%
Msh2fl/+, Lgr5Cre-/-, mTmG+/-	6.25%
Msh2fl/+, Lgr5Cre-/-, mTmG+/+	3.13%
Msh2fl/+, Lgr5Cre-/-, mTmG-/-	3.13%
Msh2+/-, Lgr5Cre+/-, mTmG+/-	6.25%
Msh2+/-, Lgr5Cre+/-, mTmG+/+	3.13%
Msh2+/-, Lgr5Cre+/-, mTmG-/-	3.13%
Msh2+/-, Lgr5Cre-/-, mTmG+/-	6.25%
Msh2+/-, Lgr5Cre-/-, mTmG+/+	3.13%
Msh2+/-, Lgr5Cre-/-, mTmG-/-	3.13%
Msh2+/+, Lgr5Cre+/-, mTmG+/-	6.25%
Msh2+/+, Lgr5Cre+/-, mTmG+/+	3.13%
Msh2+/+, Lgr5Cre+/-, mTmG-/-	3.13%
Msh2+/+, Lgr5Cre-/-, mTmG+/-	6.25%
Msh2+/+, Lgr5Cre-/-, mTmG+/+	3.13%
Msh2+/-, Lgr5Cre-/-, mTmG-/-	3.13%

Figure 3.5: A) Percentage of resulting genotypes from the cross-breeding between *Msh2*$^{flox/-}$*; Lgr5CreERT2*$^{+/-}$ and *mTmG*$^{+/+}$ mice. B) Percentage of resulting genotypes from the cross-breeding between *Msh2*$^{+/-}$*; Lgr5CreERT2*$^{+/-}$*; mTmG*$^{+/-}$ and *Msh2*$^{flox/+}$*; Lgr5CreERT2*$^{+/-}$*; mTmG*$^{+/-}$ mice.

3.2.2.2 Comparison of Tamoxifen treatments for Cre recombinase activation

To verify the efficacy of the *mTmG* transgene and identify the optimal concentration and dosage regime of Tamoxifen for the most appropriate level and pattern of Cre induction using the *LgrCreERT2* construct, different Tamoxifen treatments were tested using *Lgr5CreERT2$^{+/-}$; mTmG$^{+/-}$* mice. The most commonly published Tamoxifen treatment regimens for Cre induction were compared in this strain. Mice were treated with either one i.p. injection of 3 mg Tamoxifen (0.15mg/g bw) on one single day (Group-A) (Barker et al., 2007; Zhang et al., 2014), or one i.p. injection of 3 mg Tamoxifen (0.15 mg/g bw) on day 1 and 2mg Tamoxifen (0.1mg/g bw) on days 2, 3 and 4 (Group-B) (Nandan et al., 2016; Veniaminova et al., 2012). Furthermore, a control group (Group-C) received one i.p. injection of corn oil (the vehicle for dissolved Tamoxifen) without Tamoxifen per day for 4 consecutive days (without i.p. Tamoxifen treatment, Cre recombinase is not activated) (Figure 3.6). Two animals were used for each condition. Mice were culled and the small and large intestines collected on day 8 (after the start of Tamoxifen or corn oil treatment), allowing time for the activated Cre to recombine loxP sites in the stem cells at the bases of the crypts, converting mT expression to mG expression. These mG+ intestinal stem cells form daughter cells that move up the crypts and on to the villi in the small intestine, or up the crypts in the colonic mucosa, thus appearing as green foci surrounded by red background epithelium (when viewed by fluorescence stereomicroscopy). The efficiency of the different Tamoxifen treatments was evaluated through the detection and quantification of these green foci (mG expression), analysing whole mount intestinal tissues (as described in Materials and Methods).

In Group-C, the whole mount intestinal specimens showed only mT protein expression conferring red fluorescence to the tissues with no mG expression, as expected. In Group-A (only one i.p injection of Tamoxifen), mice showed ~25% foci of positive mG crypts/villi in the small intestine and ~10% mG+ crypt foci in the large intestine (Figure 3.7-3.8). In Group-B (4 i.p. Tamoxifen injections over 4 days), mice showed ~35% foci of positive mG crypts/villi in the small intestine and ~15% mG+ crypt foci in the large intestine (Figure 3.7-3.8). No major differences were observed between Group-A and Group-B. However, the Group-B Tamoxifen protocol appeared to be mildly more efficient, showing a more widely scattered distribution of the mG positive crypt foci along both of the small and large intestines, similar to the pattern seen in human LS patients with widely scattered dMMR crypt foci in the colon (Kloor et al., 2012). Hence, the 4 day Tamoxifen treatment protocol was adopted for all

further experiments involving Tamoxifen-induced activation of Cre in this Msh2-LS mouse model.

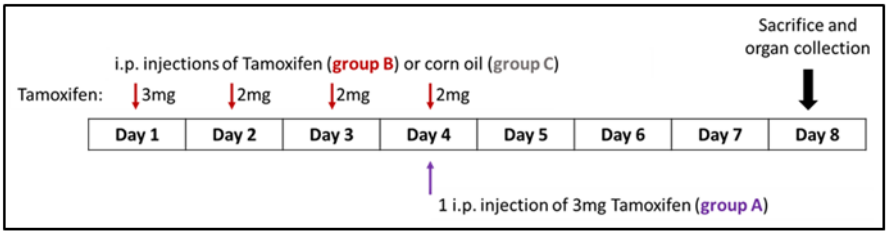

Figure 3.6: Comparison of experimental Tamoxifen treatment protocols for Group-A (one i.p. injection of 3 mg Tamoxifen (0.15mg/g) on one single day), Group-B (one i.p. injection of 3 mg Tamoxifen per mouse (0.15 mg/g) on day 1 and 2mg Tamoxifen (0.1mg/g) on days 2, 3 and 4); and Group–C (one i.p. injection of 3 mg corn oil per mouse on day 1 and 2mg corn oil on days 2, 3 and 4). (i.p. = intraperitoneal).

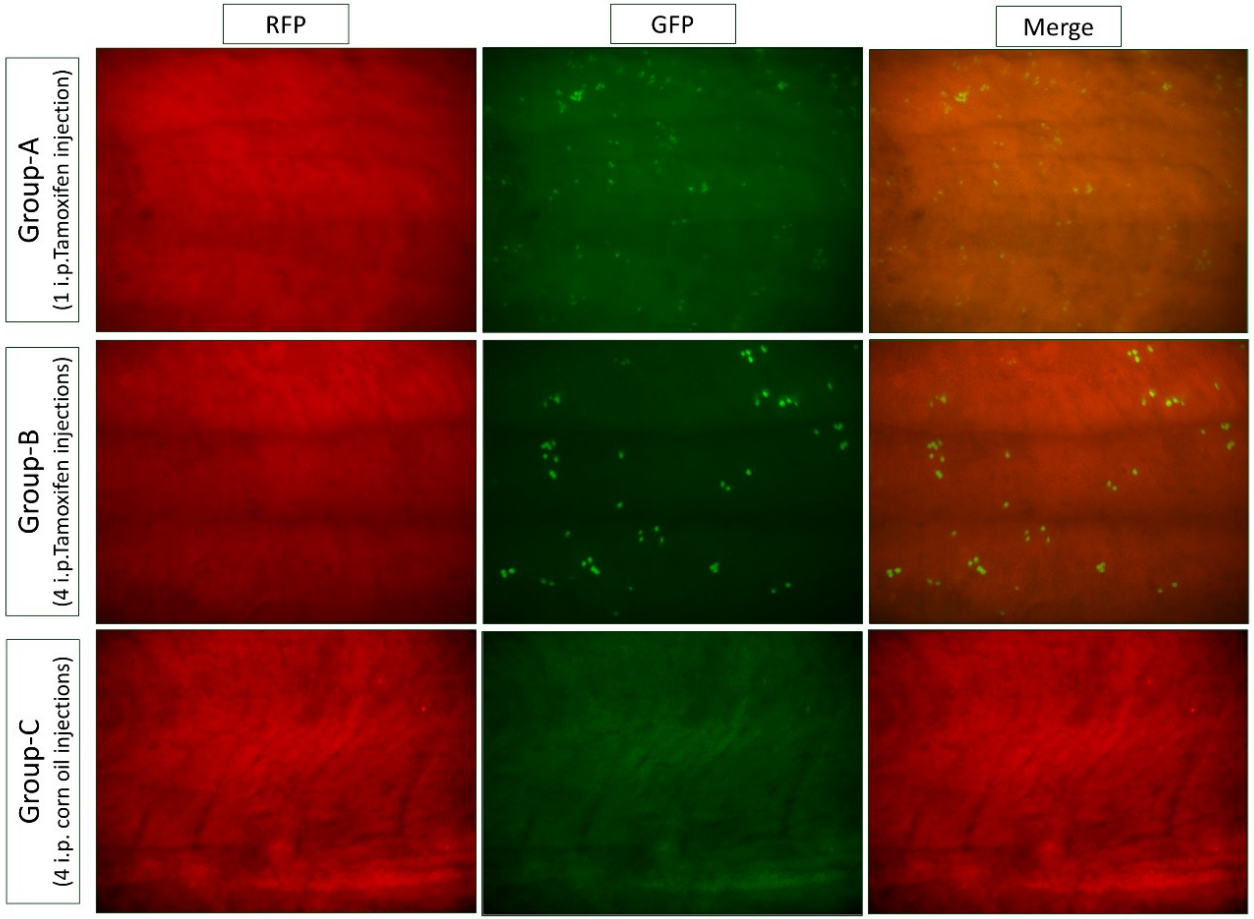

Figure 3.7: Representative fluorescent images of the mT & mG/GFP detection in the colon using the fluorescence stereomicroscope. Pictures acquired from Group-A (1 i.p. Tamoxifen injection) (top row), Group-B (4 i.p. Tamoxifen injections) (middle row), and Group-C (4 i.p. corn oil injections, control cohort) (bottom row) mice, shown as RFP, GFP and merge (left, middle and right columns respectively). Images taken using the Leica (FLIII) stereomicroscope at 2X magnification/1X objective.

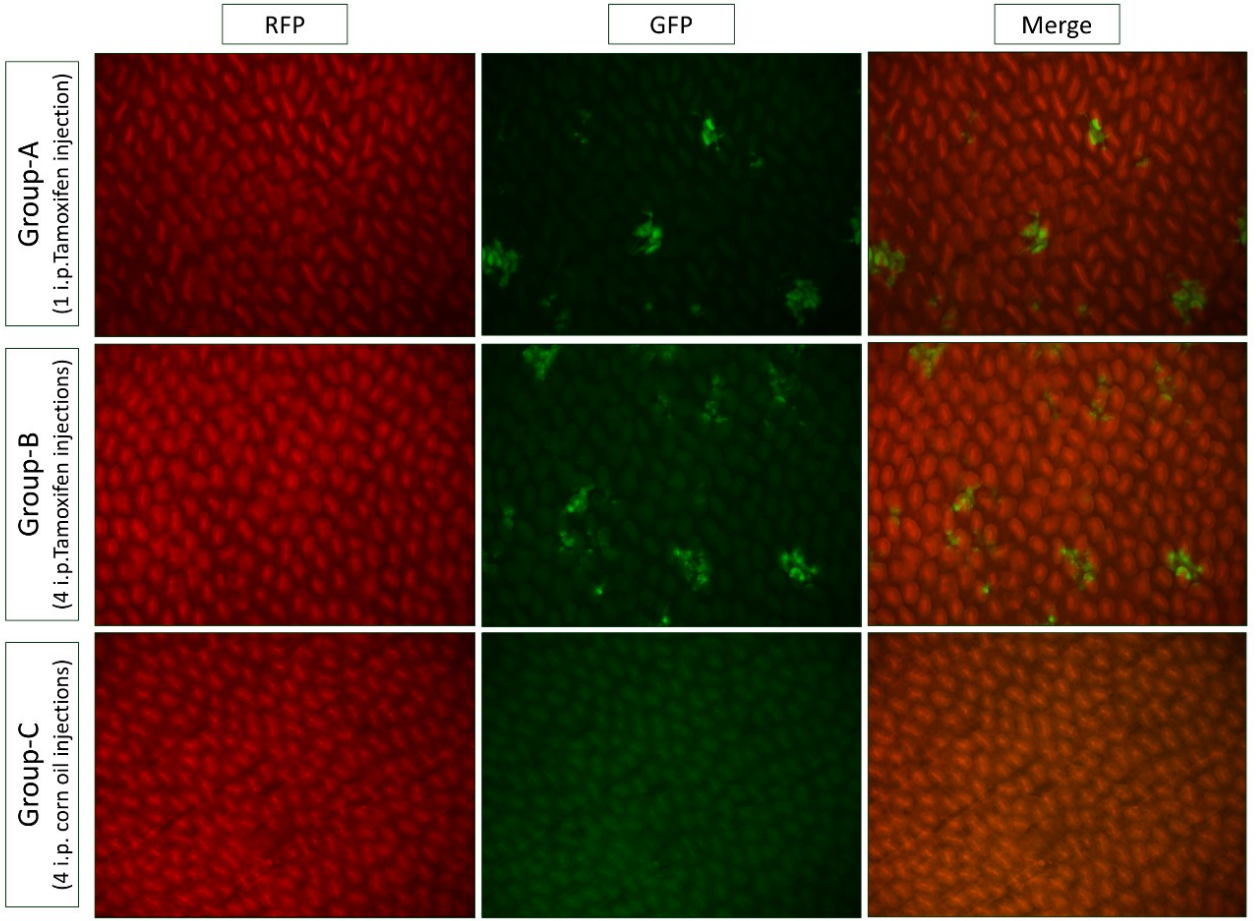

Figure 3.8: Representative fluorescent images of the mT & mG/GFP detection in the distal small intestine using the fluorescence stereomicroscope. Pictures acquired from Group-A (1 i.p. Tamoxifen injection) (top row), Group-B (4 i.p. Tamoxifen injections) (middle row) and Group-C (4 i.p. corn oil injections, control cohort) (bottom row) mice, shown as RFP, GFP and merge (left, middle, and right columns respectively). Images taken using the Leica (FLIII) stereomicroscopeat 5X magnification/1X objective.

3.2.2.3 Immunohistochemical characterization of positive mG-expressing intestinal crypt foci

To test whether the expression of mG/GFP observed by fluorescence microscopic detection, following Cre activation, correlated with the loss of Msh2 expression, immunohistochemical (IHC) analyses were performed using anti-Msh2 antibody and anti-GFP antibody on intestinal tissue serial sections. Small intestine, caecum and colon serial sections were cut from Tamoxifen-induced *Msh2$^{flox/-}$; Lgr5CreERT2$^{+/-}$; mTmG$^{+/-}$* (Msh2-LS) mice and stained for both mG/GFP and Msh2 proteins.

We used small intestinal tissue samples of *Msh2$^{-/-}$* mice as Msh2-null controls and GFP-negative expression controls; and small intestinal (SI) tissue samples of Tamoxifen-induced *mTmG$^{+/+}$* mice as Msh2-positive and GFP-positive expression controls (Figure 3.9). The lack of DAB-brown staining for both anti-Msh2 and anti-GFP IHC in the *Msh2$^{-/-}$* SI tissues confirmed complete loss of Msh2 expression and lack of GFP expression (Figure 3.9 A-B) in the Msh2-null negative control tissues. The presence of DAB-brown staining in the *mTmG$^{+/+}$* SI tissues confirmed presence of Msh2 expression in all tissue and GFP expression in some Cre-activated crypts (Figure 3.9 C-D) in the *mTmG$^{+/+}$* positive control tissues.

The immunohistochemical analysis of Msh2 in *Msh2$^{flox/-}$; Lgr5CreERT2$^{+/-}$; mTmG$^{+/-}$* mouse intestinal tissue showed lack of DAB-brown staining in some crypts scattered along the length of both small intestinal mucosa and large intestinal mucosa (Figure 3.10 A-C). The exact same crypts appeared DAB-brown stained after immunohistochemical analysis of GFP on the adjacent serial section of the same *Msh2$^{flox/-}$; Lgr5CreERT2$^{+/-}$; mTmG$^{+/-}$* mouse intestinal tissue (Figure 3.10 B-D), confirming that the same small and large intestinal crypts had lost Msh2 protein expression and gained GFP expression.

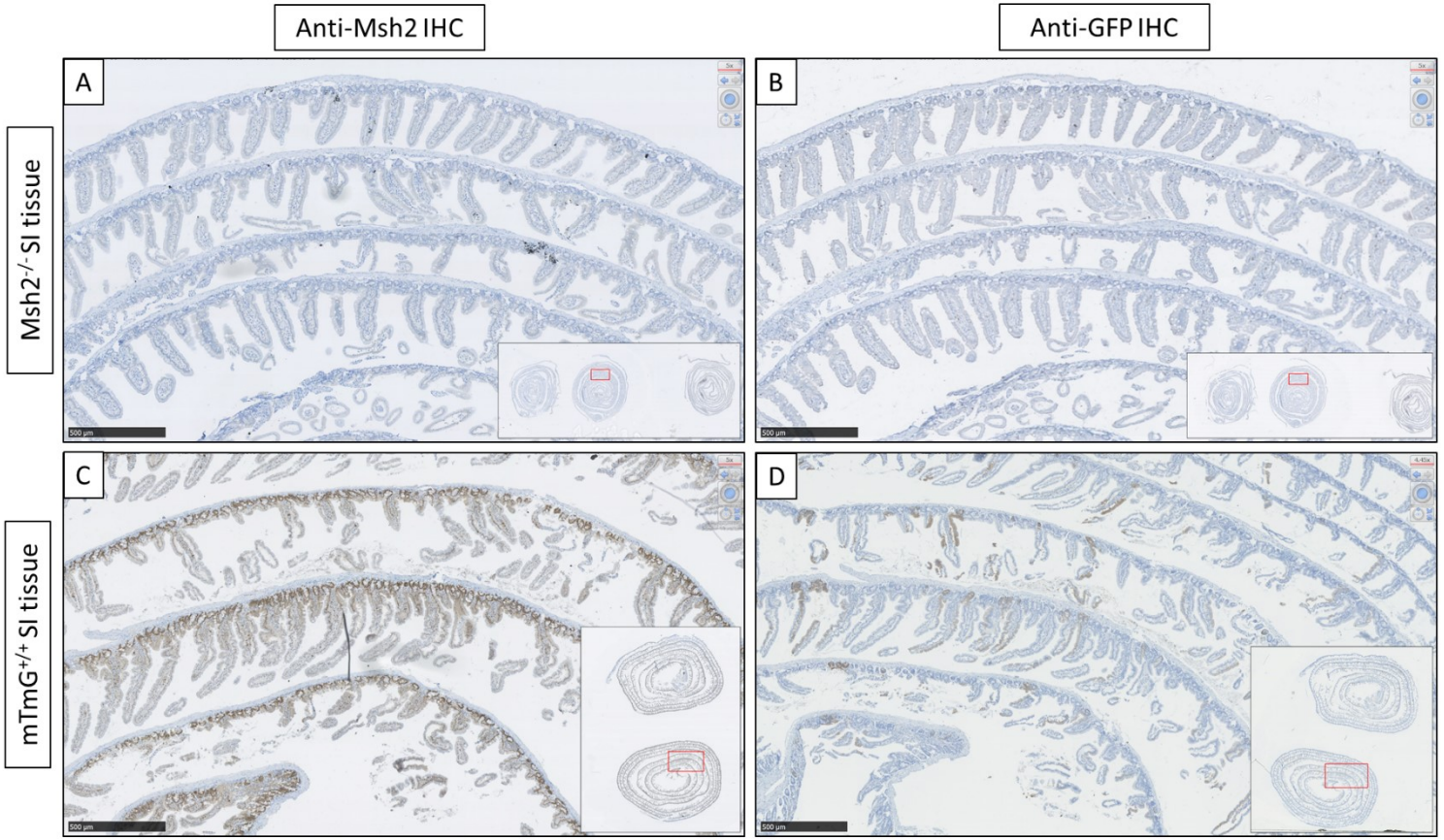

Figure 3.9: Immunohistochemical analysis of Msh2 and GFP protein expression in small intestinal mucosal epithelium from a negative-control *Msh2*$^{-/-}$ mouse (upper row), in which the lack of brown staining confirms the absence of Msh2 (A) and GFP (B) expression in the intestinal mucosal epithelium; and from a positive-control *mTmG*$^{+/+}$ mouse (lower row), in which the brown staining indicates positive Msh2 expression in all crypts (C) and positive GFP expression in some scattered Cre-activated crypts (D). Images taken using the Hamamatsu Nanozoomer and analysed with the Hamamatsu NDP Viewer software at 5X magnification (bar at lower left indicates 500um).

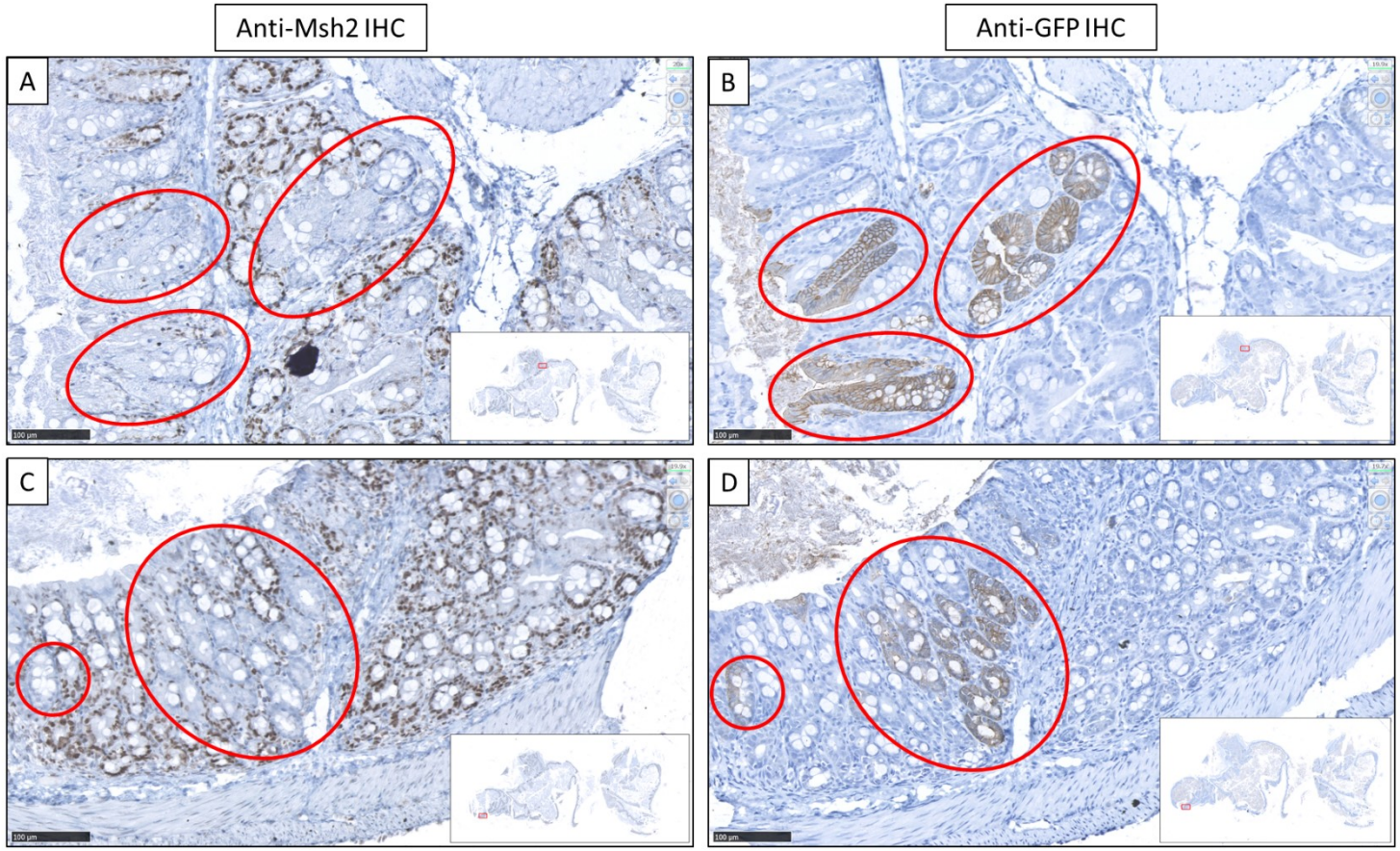

Figure 3.10: Representative comparison between Msh2 and mG/GFP immunostaining of adjacent serial sections of caecum of *Msh2$^{flox/-}$; Lgr5CreERT2$^{+/-}$; mTmG$^{+/-}$* mice treated with Tamoxifen to activate Cre in scattered crypts. The same dMMR crypt foci (A and C) are negative for Msh2 and positive for mG/GFP (B and D) (red ovals). Images taken using the Hamamatsu Nanozoomer and analysed with the Hamamatsu NDP Viewer software at 20X magnification (bar at lower left indicates 100um).

3.3 Discussion

In this chapter, the mouse breeding programme was described to illustrate the generation of the appropriate murine progeny to be used in experiments and for further breeding. The mice obtained from Professor Hein te Riele's research group were acquired to start the Msh2-Ls mouse model colony. The matings between the starting mice produced: 25% *Msh2$^{flox/+}$; Lgr5CreERT2$^{+/-}$* mice*, 25% Msh2$^{flox/+}$; Lgr5CreERT2$^{-/-}$* mice, *25% Msh2$^{flox/-}$; Lgr5CreERT2$^{-/-}$* mice and *25%* of the desired *Msh2$^{flox/-}$; Lgr5CreERT2$^{+/-}$* mice (for use as experimental subjects). To establish a bigger Msh2-LS mouse model colony we bred the *Msh2$^{flox/-}$; Lgr5CreERT2$^{+/-}$* with *Msh2$^{flox/-}$; Lgr5CreERT2$^{-/-}$*. As explained previously, heterozygous *Lgr5CreERT2$^{+/-}$* mice can only be bred with *Lgr5* wild-type mice *(Lgr5CreERT2$^{+/-}$ X Lgr5CreERT2$^{-/-}$*) because homozygous *Lgr5CreERT2$^{+/+}$* mice are not viable (due to loss of wildtype *Lgr5* alleles that are required for normal development), influencing the percentage of mice with the correct genotype per litter (only 25% of the progeny).

The introduction of the *mTmG* transgene into the Msh2-LS mouse model further decreased the percentage of mice with the desired genotype for experimental subjects per litter.

The introduction of the *mTmG* transgene was performed through cross-breeding between Msh2-LS mice and homozygous *mTmG* mice (*mTmG$^{+/+}$*). The progeny obtained from the first breeding showed the following genotypes: 25% *Msh2$^{fl/+}$; Lgr5CreERT2$^{+/-}$; mTmG$^{+/-}$, 25% Msh2$^{fl/+}$; Lgr5CreERT2$^{-/-}$; mTmG$^{+/-}$, 25% Msh2$^{-/+}$; Lgr5CreERT2$^{+/-}$; mTmG$^{+/-}$ and 25% Msh2$^{-/+}$; Lgr5CreERT2$^{-/-}$; mTmG$^{+/-}$.* To obtain mice with the correct genotypes for use as experimental subjects, we used these mice as breeders. The resulting progeny showed only 6.25% of *Msh2$^{fl/-}$; Lgr5CreERT2$^{+/-}$*mice*; mTmG$^{+/-}$* and 3.13% of *Msh2$^{fl/-}$; Lgr5CreERT2$^{+/-}$; mTmG$^{+/+}$* mice.

We cross-bred the progeny to obtain an appropriate number of *Msh2$^{fl/-}$; Lgr5CreERT2$^{+/-}$; mTmG$^{+/-}$* to use as experimental subjects, which required a high number of breeding rounds and time.

Once the Msh2-LS mouse colony was established, we proceeded with the characterisation of the mouse model and identification of the optimal concentration and dosage regime of Tamoxifen for the most appropriate level and pattern of Cre induction using the *LgrCreERT2* construct. We divided the mice into three groups which received either 1 i.p Tamoxifen injection, or 4 i.p. Tamoxifen injections, or 4 i.p. corn oil injections. The introduction of the *mTmG* transgene was used to identify the best treatment by analysing the numbers and patterns of crypts expressing mG/GFP in both the small and large intestines, viewed as

whole-mount specimens using a fluorescent stereomicroscope and counting the numbers of mG-expressing foci. This fluorescent reporter transgene enabled visual monitoring of the effects of Tamoxifen-induced activation of Cre recombinase to convert expression of red fluorescent mT to expression of green fluorescent mG protein in intestinal epithelial Lgr5-expressing stem cells and the crypts that they form.

The whole mount intestinal specimens of corn oil-treated control mice appeared completely red under the microscope, and no mG expression was observed. This confirmed the lack of Cre activation due to the absence of Tamoxifen treatment. By contrast, in both Tamoxifen-treated groups, positive mG/GFP expressing foci were observed scattered along the whole small and large intestines. Mice treated with 1 i.p Tamoxifen injection showed ~25% foci of mG+ crypt/villi in the small intestine and ~10% mG+ crypt foci in the large intestine, whereas mice treated with 4 i.p. Tamoxifen injections showed ~35% foci of mG+ crypt/villi in the small intestine and ~15% mG+ crypt foci in the large intestine. These groups of mice did not show major differences in mG+ expression, however we decided to adopt the 4 day Tamoxifen treatment protocol for Cre induction on *LgrCreERT2* construct. The mice treated with 4 i.p. Tamoxifen injections showed a more widely scattered distribution of the mG+ crypt foci along both the small and large intestine, similar to the pattern seen in human LS patients' colons with widely scattered dMMR crypt foci. Hence, in this experiment, we identified the correct Tamoxifen protocol and we validated the efficacy of the *mTmG* transgene.

In the modified version of the Msh2-LS mouse model, explained in this chapter (*Msh2*$^{flox/-}$*; Lgr5CreERT2*$^{+/-}$*; mTmG*$^{+/-}$ mouse model), the activation of Cre recombinase by Tamoxifen-treatment induced recombination between two inverted *loxP* sites flanking Msh2 exons 12 and 13 and the *loxP* sites flanking the mT allele, generating a *Msh2* knockout allele (*Msh2*$^{flox/OFF}$) and converting the same intestinal stem cells to mG expression, generating dMMR intestinal stem cells that subsequently form dMMR crypts, which are marked by green fluorescent mG expression. We confirmed this by performing IHC for both Msh2 and GFP expression on adjacent serial sections of small intestine, caecum and colon. The results showed the colocalization in the same crypts of mG expression and the loss of Msh2 expression. The detection and quantification of mG+ crypt foci allow evaluation of any subsequent changes of dMMR crypts marked in this way, such as changes in crypt focus size or number or distribution along the intestinal tract.

In conclusion, we generated a modified version of the Msh2-LS mouse model and established a colony of this *Msh2$^{flox/-}$; Lgr5CreERT2$^{+/-}$; mTmG$^{+/-}$* mouse model. The *mTmG* Cre reporter system was validated and the most appropriate Tamoxifen treatment protocol (daily i.p. injection over 4 days) was identified and shown to be sufficient to activate Cre recombinase. We verified that Cre induced loss of Msh2 and expression of mG/GFP were observed in the same crypt foci.

Chapter 4: Investigation of long-term ethanol consumption effects on the Msh2-LS mouse model

4.1 Introduction

LS is caused by a constitutional (often germline) pathogenic mutation in one of the MMR genes (MSH2, MLH1, MSH6, and PMS2). LS patients have a higher lifetime risk for several cancer types, mainly in the large bowel and the endometrium, but also in small intestine, stomach, and several other organs (Bellizzi & Frankel, 2009; Poulogiannis et al., 2010), as previously described in the main introduction, Chapter 1.1.

Several lifestyle-related factors are associated with an increased risk of certain sporadic cancers; these may have similar or enhanced effects in LS patients. Several systematic reviews and cohort studies showed evidence that smoking is linked with an increased risk of CRC (Hannan et al., 2009; Leufkens et al., 2011). In 2011, the World Cancer Research Fund (WCRF)/American Institute for Cancer Research (AICR) published a review providing evidence that body fatness or obesity (expressed as BMI of greater than 30 kg/m2), abdominal fatness (waist circumference and waist-hip ratio), nutrition and physical activity can influence the risk of CRC (Dai, 2007; Ning et al., 2010; van Duijnhoven et al., 2013). Worldwide, a total of approximately 389,000 cancers representing 3.9% of all cancers have been calculated to derive from chronic alcohol consumption (Rehm et al., 2003). However, there are limited studies investigating the effects of alcohol consumption on increased risk of CRC in LS patients. Carcinogenic effects of ethanol are related to its metabolism and mainly to its metabolite acetaldehyde. Acetaldehyde is a highly reactive molecule able to induce a wide range of DNA damage, as described in Chapter 1.3. However, the DNA repair pathways responsible for repairing many of these lesions remain unknown.

The MMR pathway plays an important role in maintaining genomic stability and cellular homeostasis. In addition to its post-replicative DNA error repair, MMR is involved in cellular responses to DNA damage induced by endogenous chemical carcinogens (Stojic et al., 2004). Furthermore, MMR plays a role in the cell's response to DNA damage through cell cycle arrest and/or apoptosis.

In this chapter, the aim is to test the hypothesis that the DNA MMR system plays a role in protecting cells from some types of ethanol/acetaldehyde-induced DNA damage and that

there is a gene-environment interaction between ethanol/acetaldehyde and dMMR pathway that accelerates colorectal tumour development and progression. Here, using the Msh2-LS mouse model, the effects of long-term ethanol treatment on intestinal tumour formation and progression are investigated.

4.2 Long-term ethanol effects on intestinal tumourigenesis in the Msh2-LS mouse model

4.2.1 Methods

Groups of 7-9 weeks old *Msh2$^{flox/-}$; Lgr5CreERT2$^{+/-}$* and *Msh2$^{flox/-}$; Lgr5CreERT2$^{+/-}$; mTmG$^{+/-}$* (Msh2-LS) experimental mice were divided into two groups. Group-A mice received intraperitoneal (i.p.) injections of 0.15mg Tamoxifen/g bw on day 1 and 0.1mg Tamoxifen/g bw on day 2, 3 and 4; on day 5 mice were provided with normal drinking water. By contrast, Group-B received i.p. injections of 0.15mg Tamoxifen/g bw on day 1 and 0.1mg Tamoxifen/g bw on day 2, 3 and 4; but on day 5 the Group-B mice were provided with 20% ethanol in drinking water (as previously validated by our group; (Müller et al., 2016)) (Figure 4.1). Animals were culled and tissues collected when either clinical signs of distress were visible or they displayed >20% body weight loss compared with the initial weight. The small and large intestines, caecum, stomach, liver, spleen, thymus, lymph nodes (if visible) and any other organ or tissue showing abnormalities, were collected following schedule 1 culling and necropsy dissection. Tissues were fixed in 10% NBF, processed using standard tissue processing protocols and were paraffin embedded in preparation for section cutting and staining. The acronyms used for the Msh2-LS model mice and their relevant treatments are shown in Table 2.2.

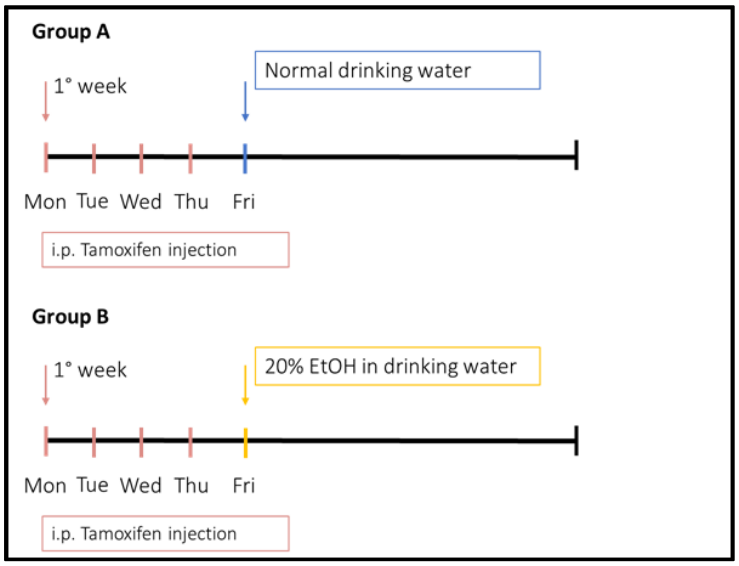

Figure 4.1: Experimental treatment protocols and timelines for Group-A (water-treated) and -B (ethanol-treated) mice, showing 4 days of i.p. injections of Tamoxifen, followed by either standard/normal drinking water (Group-A) or drinking or water containing 20% ethanol (Group-B). (EtOH = Ethanol).

4.2.2 Results

4.2.2.1 Experimental group organization and observations

Previous work using Aldh1b1 depleted mice and control mice treated with 20% ethanol showed intestinal tumour formation within 1 year in both groups (Müller et al., 2016). Long-term ethanol-treatment of Msh2-LS mice followed two different approaches. First, in this tumour watch experiment, the murine subjects included 20 mice in total (12 females and 8 males) were divided into two groups: Group-A (10 mice: 8 females and 2 males; water-treated control group) and Group-B (10 mice: 4 females and 6 males; ethanol-treated test group). Animals from both groups were culled when either clinical signs of distress indicative of intestinal tumour formation were visible or they displayed >20% body weight loss compared with the initial weight.

Second, in this matched control and test subject experiment, 26 mice (10 females and 16 males) in total were divided into two groups of 13 mice, with 5 females and 8 males in each group, and they underwent treatments in drinking water as control Group-A (water) and test Group-B (ethanol). In this experiment, a matching control mouse was culled at the same time point that an ethanol-treated mouse had to be culled for signs of distress due to intestinal tumour formation or >20% loss of body weight.

During Tamoxifen treatment (daily Tamoxifen i.p injections for 4 consecutive days), body weights and health status were recorded. Body weights of the female and male mice didn't significantly differ during the Tamoxifen treatment (Figure 4.2), showing successful drug administration and acceptance of the experimental procedures by the mice. Body weights of Msh2-LS males (~28.34g) were significantly higher than body weights of Msh2-LS females (~21.38g) both before and during the Tamoxifen treatments. After Tamoxifen treatment mice received either 20% ethanol in drinking water or normal drinking water regimes and the body weights and health status of the mice were recorded twice a week (Figure 4.3). Female and male ethanol-treated Msh2-LS mice did not show abnormal behaviour or reduced weight indicating good acceptance of the ethanol regime. EtOH_*Msh2*$^{fl\ KO}$ mice weighed on average 34.3g for the males and 31g for the females, whereas H_2O_*Msh2*$^{fl\ KO}$ weighed on average 36.5g for the males and 29.6g for the females. Significant differences were not observed between the body weights of EtOH_*Msh2*$^{fl\ KO}$ versus H_2O_*Msh2*$^{fl\ KO}$ males or females.

Drinking bottles were changed and bottle weights were recorded once a week. Liquid consumption per mouse was estimated by analysing the weights of the drinking bottles (per cage) and calculating the average weight of consumed liquid per mouse per day (Figure 4.4). An average H_2O_*Msh2*$^{fl\ KO}$ male mouse consumed around 13.85ml of drinking water per day, whereas an average EtOH_*Msh2*$^{fl\ KO}$ male mouse consumed around 11.65ml of 20% ethanol in drinking water. An average H_2O_*Msh2*$^{fl\ KO}$ female mouse consumed around 10.33ml of water per day, whereas an average EtOH_*Msh2*$^{fl\ KO}$ female mouse consumed around 9.65ml of 20% ethanol in drinking water per day. No significant differences were observed between ethanol- and water-consumption for males or females.

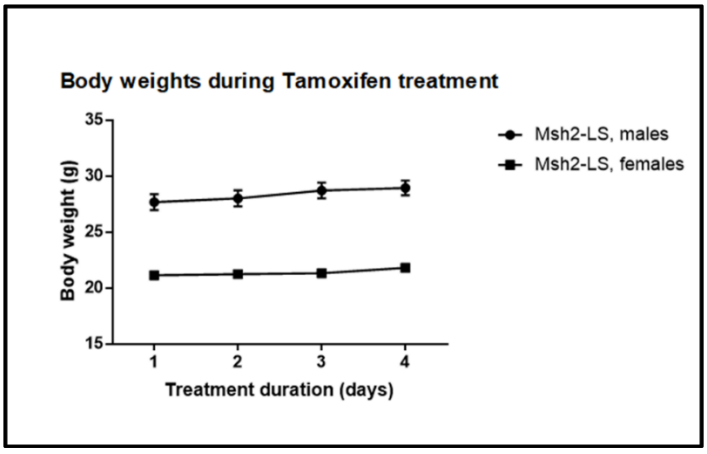

Figure 4.2: Body weights during Tamoxifen treatment. Body weights of Msh2-LS males were significantly higher than body weights of Msh2-LS females, before and during Tamoxifen treatments. 2-way-ANOVA test with Bonferroni post-test correction, $p<0.0001$ on day 1-4 (data shown as mean ± SD, n=20 mice in each group, SD too small to show as bars extending beyond square points for females).

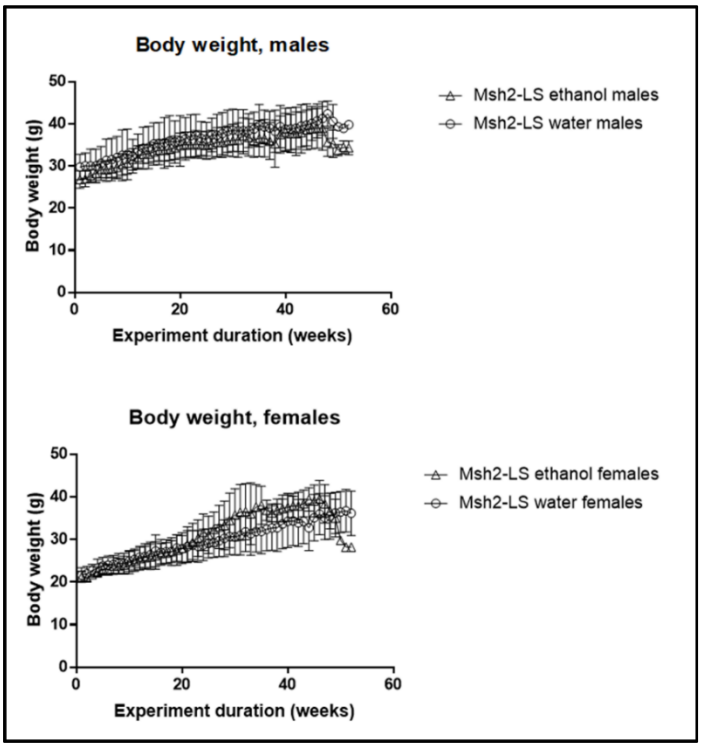

Figure 4.3: Body weights for males and females during 20% ethanol or standard/normal drinking water regimes. There were no significant differences between the body weights of ethanol-treated Msh2-LS (EtOH_*Msh2*$^{fl\ KO}$) versus water-treated Msh2-LS (H_2O_*Msh2*$^{fl\ KO}$) males or females. 2-way-ANOVA with Bonferroni post-test correction analysis (data shown as mean±SD).

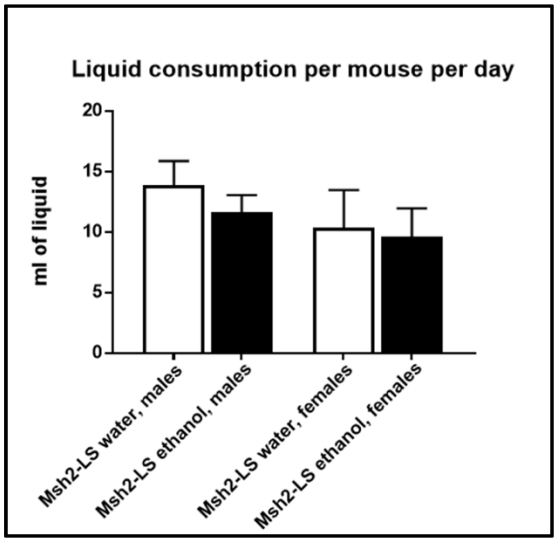

Figure 4.4: Liquid consumption of either 20% ethanol containing drinking water or standard/normal water per mouse per day. 2-way-ANOVA with Bonferroni post-test correction analysis (data shown as mean±SD). No significant differences were observed for any of the comparisons of ethanol versus water treatment or males versus females.

4.2.2.2 Tumour development in Msh2-LS mice under long-term ethanol treatment

The results from both approaches were collected and are presented together. The two cohorts of Msh2-LS model mice, Group-A (water-treated, H_2O_*Msh2*$^{fl\ KO}$) and Group-B (ethanol-treated, EtOH_*Msh2*$^{fl\ KO}$), were monitored for signs of intestinal tumour development or other pathological abnormalities, using a clinical scoring system that included known clinical signs of distress seen in mice that develop intestinal neoplasms (Foltz & Ullman-Cullere, 1999; Burkholder et al., 2012), to determine when the mice should be culled for necropsy dissection and tumour analysis (*Table 4.1*). Most of the mice in Group-B (ethanol experimental group) displayed either anal prolapse or >20% reduction in body weight as common clinical signs of distress, at varying lengths of time from the start of the experimental protocol and were then culled for necropsy dissection. During necropsy dissection, naked eye inspection revealed that the majority of the EtOH_*Msh2*$^{fl\ KO}$ mice showed a thicker colonic wall compared with the colons of the H_2O_*Msh2*$^{fl\ KO}$ mice, but no gross differences were observed in the small intestines. The lengths of the small intestines and colons were measured and recorded, but no significant differences in length were observed (Figure 4.5). The histopathological analyses of Msh2-LS large intestines and small intestines confirmed the macroscopic observations of no significant morphological differences between the two groups in the small intestines, but increased colonic wall thickness in EtOH_*Msh2*$^{fl\ KO}$ mice, due to a widespread increase in the colon crypt length as a result of extended zones of crypt epithelial hyperproliferation that were not observed in H_2O_*Msh2*$^{fl\ KO}$ murine colons (Figure 4.6). These extended zones of colonic crypt hyperproliferation were seen to affect 50% – 90% of the whole colonic length, usually involving parts of the proximal colon and mid colon, in most of the EtOH_*Msh2*$^{fl\ KO}$ mice (65%) who survived more than 1 month of the ethanol treatment protocol. By contrast, histopathological analyses of the small intestines did not show any significant morphological differences between the two groups of animals using H&E-stained Swiss rolls of the intestines (Figure 4.7).

In total, 15 out of 23 (65%) EtOH_*Msh2*$^{fl\ KO}$ mice demonstrated zones of large intestinal crypt epithelial hyperproliferation, with adenoma formation and, in 5 cases, invasive adenocarcinoma was present, all within an average of 6 months (minimum 4 weeks and maximum 48 weeks) of the start of the experimental protocol compared with only 1 case of large intestinal adenoma formation, out of 23 H_2O_*Msh2*$^{fl\ KO}$ control mice, after 15 months (Figure 4.8).

All 15 EtOH_*Msh2*$^{fl\ KO}$ tumour-bearing mice showed both colonic crypt hyperproliferative changes (Figure 4.9) with the adenoma formation mainly in either the proximal colon or the mid colon (Figure 4.10). No Msh2-LS mouse showed only colonic hyperproliferation without tumour formation, all mice with colonic hyperproliferation also showed adenoma formation. Two out of 15 were diagnosed with invasive adenocarcinoma in the proximal colon and 3 out of 15 had invasive adenocarcinoma in the mid colon (Figure 4.11-4.12). Colonic invasive adenocarcinoma was observed in 21.7% of EtOH_*Msh2*$^{fl\ KO}$ mice. In addition, in 6 out of 15 mice, we found caecal adenomas and in one case there was a caecal invasive adenocarcinoma (Figure 4.13). Among these 15 mice only 2 were diagnosed with distal colonic adenoma or rectal adenoma respectively. In total, we observed 36 neoplasms distributed between both the caecum (19.5%), colon (77.8) and the rectum (2.7%) (Figure 4.14). Additionally, 2 out of these 15 mice developed cutaneous sebaceous adenoma (a type of skin tumour that occurs in LS patients) (Figure 4.15).

Eight out of 23 EtOH_*Msh2*$^{fl\ KO}$ mice did not show any intestinal adenoma formation, but in one of these cases there was a uterine endometrial adenocarcinoma (after 12 months of ethanol treatment). The Msh2-LS mouse models have one deleted *Msh2* allele and one functioning *Msh2* allele, the same as in human LS patients who have inherited one mutant *MSH2* allele and one normal *MSH2* allele, and thus are susceptible to LS-associated cancers due to inactivation of the normal or functioning *MSH2* allele, including endometrial adenocarcinoma, which is a common cancer in women with LS.

In Group-A (water-treated control cohort, H_2O_*Msh2*$^{fl\ KO}$), only 1 out of 23 mice showed intestinal tumour formation in the proximal colon (one adenoma with evolution to an invasive adenocarcinoma) and in the caecum (one adenoma) after 15 months. We didn't find any other intestinal abnormality in any of the other 22 H_2O_*Msh2*$^{fl\ KO}$ mice, however we observed uterine endometrial invasive adenocarcinomas in 2 mice (after 12 and 15 months of treatment, respectively; Figure 4.16).

No morphological abnormalities or tumours were observed following necropsy and histopathological analysis of the H&E-stained sections of the small intestines, stomach, liver, spleen, lymph nodes and thymus, of any of the 23 EtOH_*Msh2*$^{fl\ KO}$ or 23 H_2O_*Msh2*$^{fl\ KO}$ mice.

Code	Clinical evaluation
A	no signs of ill health
B	moderate dehydration, scruff test indicates dehydration (when picking up the skin over the shoulders, it does not return to its original shape quickly)
C	severe dehydration, symptoms include: mice are weak or appear paralysed in their hind legs, eyes appear recessed in the head, facial fur appears fuzzier (piloerection), mice might have difficulties gripping the cage bars with their forefeet
D	Blood in cage or on faecal pellets.
E	Prolapse of rectum visible at perianal area
F	Visible tumours at perianal area or elsewhere
G	Pale paw pads (significant anaemia)
H	Clear signs of pain or distress or other signs of ill health. Lost >20% bodyweight in >48 hours.

Table 4.1: Clinical scoring system for monitoring mice for signs of intestinal tumour development.

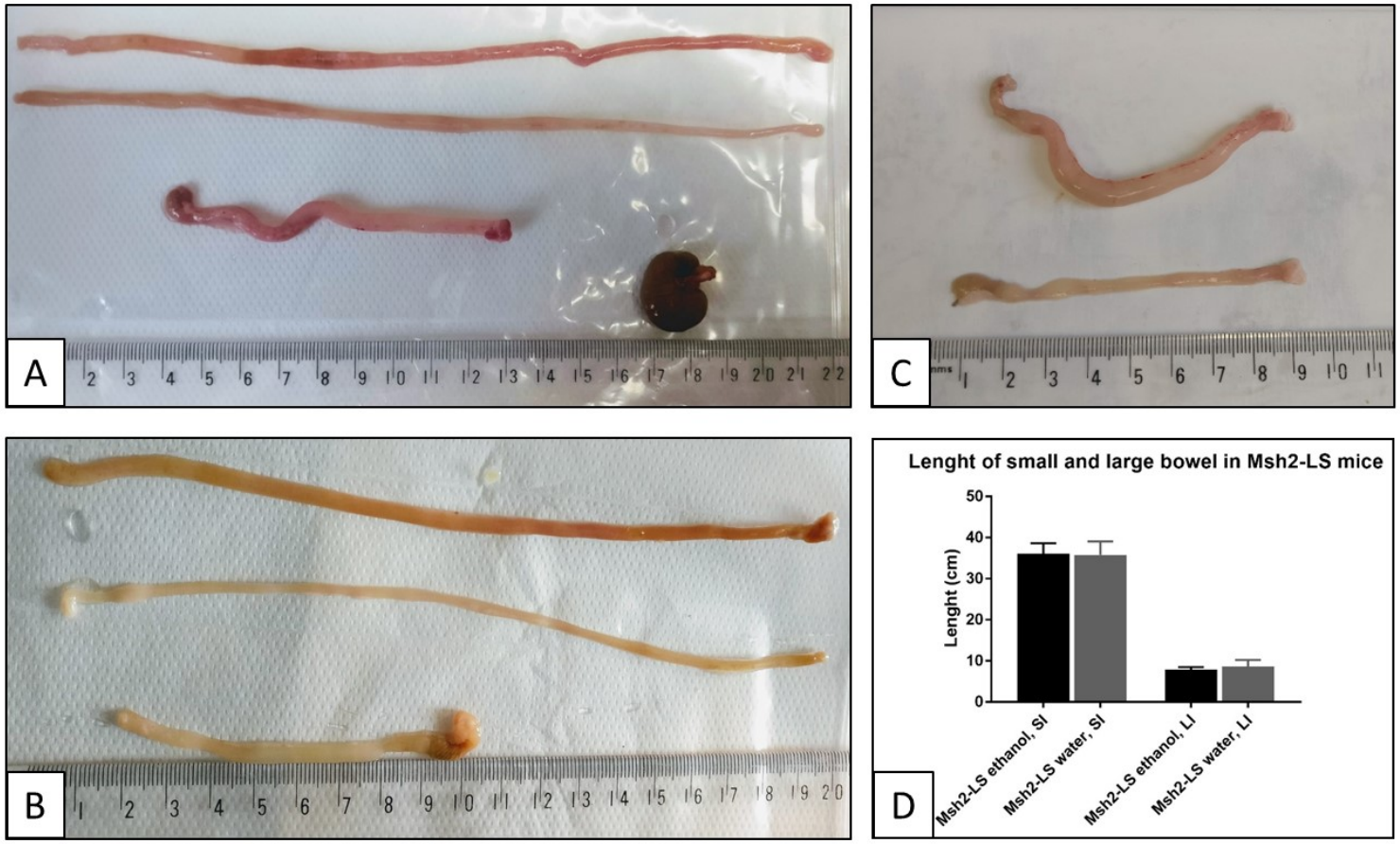

Figure 4.5: Representative macroscopic photographs of the Small Intestine and Large Intestine from an ethanol-treated Msh2-LS mouse (EtOH_*Msh2*$^{fl\ KO}$) (with caecum) (A), and a water-treated Msh2-LS mouse (H_2O_*Msh2*$^{fl\ KO}$) (without caecum) (B). (C) Photograph of two specimens of colons, one from an EtOH_Msh2$^{fl\ KO}$ mouse (upper colon specimen) compared with one from an H_2O_Msh2$^{fl\ KO}$ mouse (lower colon specimen, and showing that the upper ethanol-treated colon has a thicker wall. (D) Quantification of the Small Intestinal lengths and Large Intestinal lengths. Data shown as mean ± SD, Student's t-test analysis. No significant differences in length were observed. LI: Large Intestine; SI: Small Intestine; LS: Lynch Syndrome.

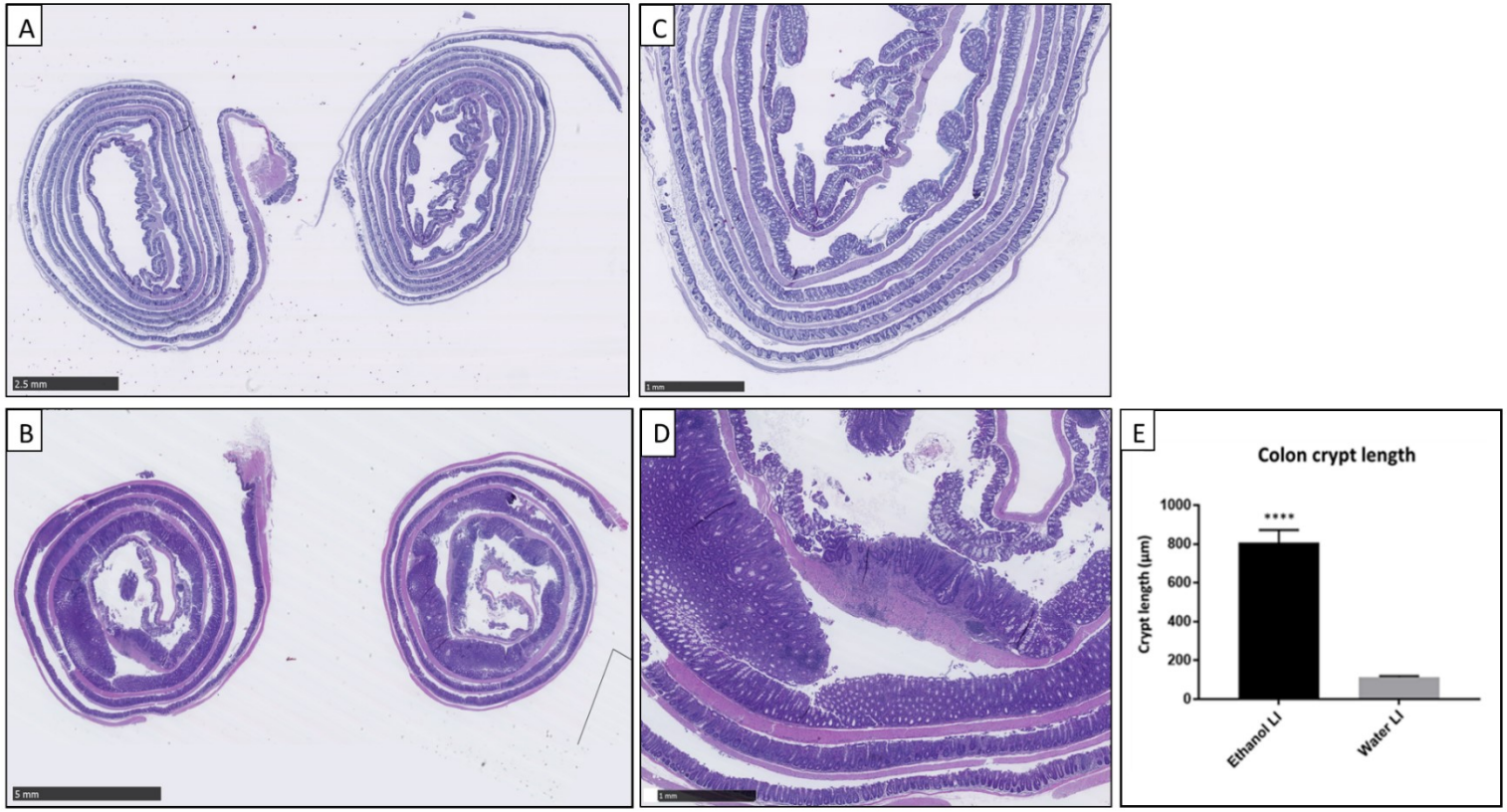

Figure 4.6: Representative H&E stained images of colon Swiss rolls. A) Images of H&E stained LI Swiss rolls from water-treated Msh2-LS (H_2O_*Msh2*$^{fl\ KO}$) mice, further magnified in image (C). Images taken from scanned slide files with the Hamamatsu Nanozoomer NDP Viewer software at 0.8X and 2.5X objective magnification respectively (bar at lower left indicates 2.5mm and 1mm). B) Images of H&E stained LI Swiss rolls from ethanol-treated Msh2-LS (EtOH_*Msh2*$^{fl\ KO}$) mice, further magnified in image (D). Images taken from scanned slide files with the Hamamatsu Nanozoomer NDP Viewer software at 0.5X, and 2.5X objective magnification respectively (bar at lower left indicates 2.5mm and 1mm). E) Quantification of the colon crypt lengths (in µm) comparing colons from EtOH_*Msh2*$^{fl\ KO}$ versus *H_2O_Msh2*$^{fl\ KO}$ mice. Mann-Whitney U test analysis, ****p<0.0001 (data shown as mean ± SD). LI: Large Intestine

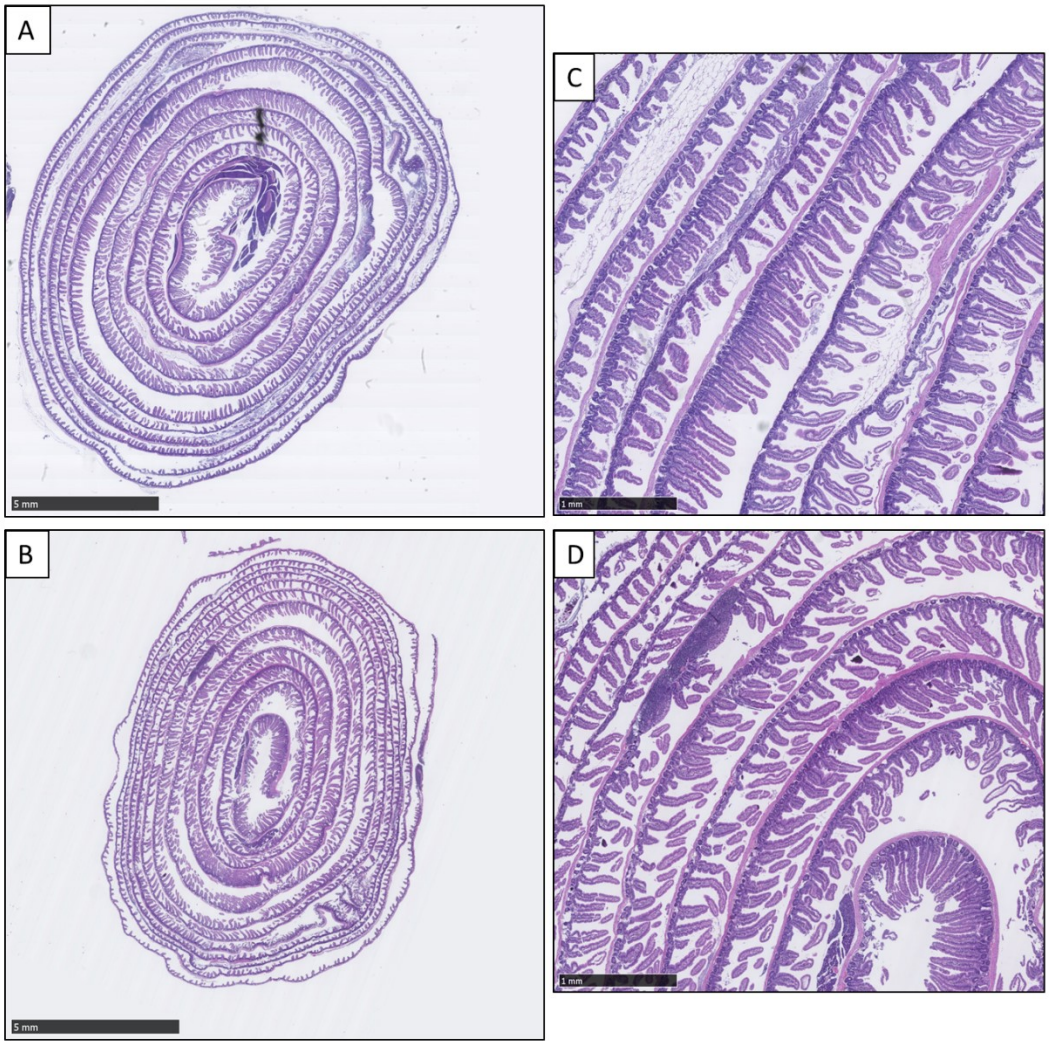

Figure 4.7: Representative H&E stained images of SI Swiss rolls. A) Image of H&E stained SI Swiss roll from a water-treated Msh2-LS (H_2O_*Msh2*$^{fl\ KO}$) mouse, further magnified in image (C). Images taken from scanned slide files with the Hamamatsu Nanozoomer NDP Viewer software at 0.5X and 2.5X magnification respectively (bar at lower left indicates 5mm and 1mm). B) Image of H&E stained SI Swiss roll from an ethanol-treated Msh2-LS (EtOH_*Msh2*$^{fl\ KO}$) mouse, further magnified in image (D). Images taken from scanned slide files with the Hamamatsu Nanozoomer NDP Viewer software at 0.5X and 2.5X magnification respectively (bar at lower left indicates 5mm and 1mm).

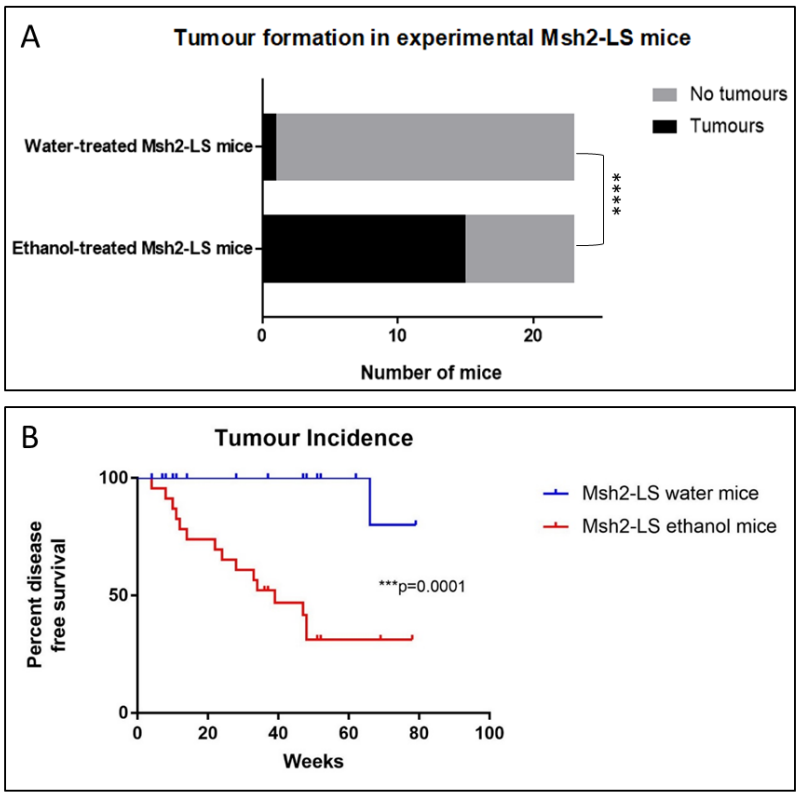

Figure 4.8: A) Bar chart of the number of Msh2-LS mice that developed intestinal tumours (both adenomas and adenocarcinomas) after receiving either 20% ethanol in drinking water or regular drinking water. 15/23 (65%) ethanol-treated Msh2-LS (EtOH_*Msh2fl KO*) mice developed large intestinal tumours compared with 1/23 (4%) water-treated Msh2-LS (H_2O_$Msh2^{fl\ KO}$) mice. Fisher's exact test, **** p<0.0001. B) Tumour incidence in Msh2-LS mice treated with either 20% ethanol or water. The survival plot shows the significantly earlier development of tumours (both adenomas and adenocarcinomas) in the ethanol-treated Msh2-LS (EtOH_$Msh2^{fl\ KO}$) group (red) compared with the water-treated Msh2-LS (H_2O_$Msh2^{fl\ KO}$) group (blue). Log-rank (Mantel-Cox) test, ***p=0.0001.

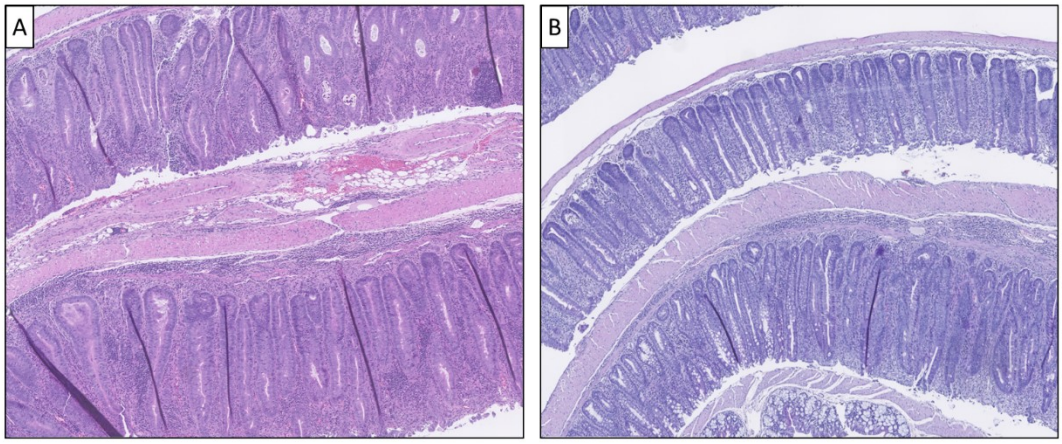

Figure 4.9: A and B show representative images of colonic crypt epithelial hyperproliferative changes in ethanol-treated Msh2-LS (EtOH_*Msh2*$^{fl\ KO}$) mice, demonstrating the increase in length of the affected crypts. Images taken from scanned slide files with the Hamamatsu Nanozoomer NDP Viewer software at 5X magnification.

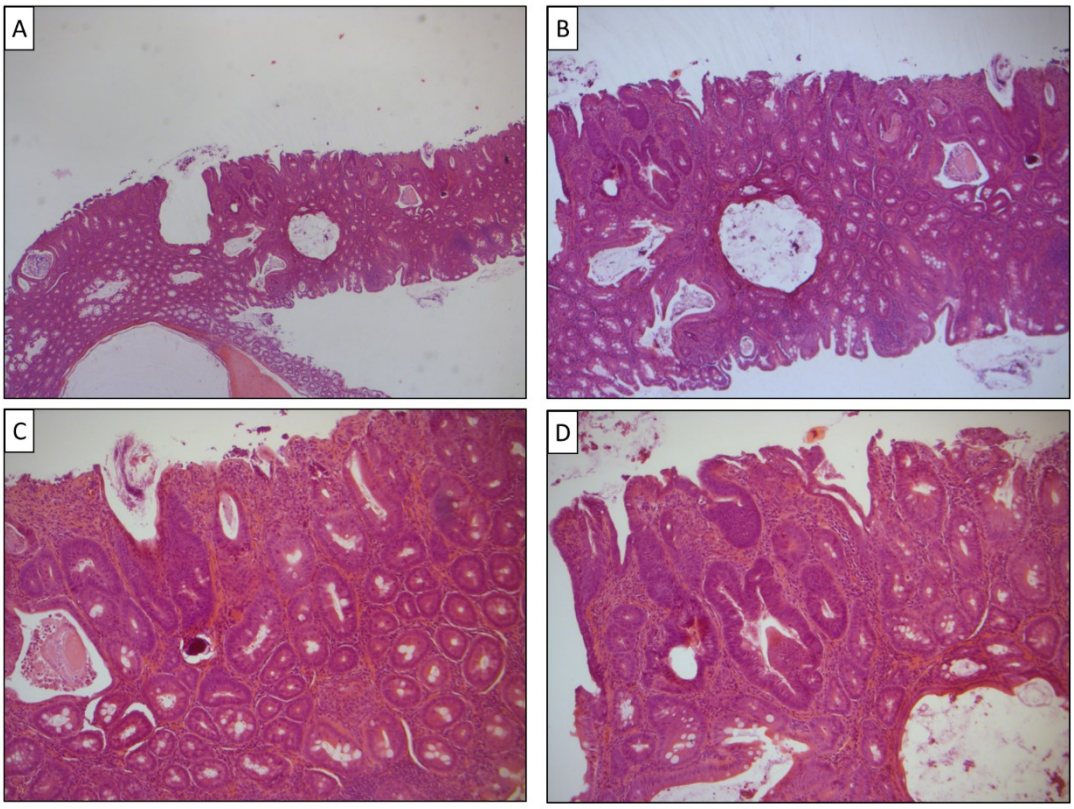

Figure 4.10: Representative images of a proximal colon adenoma in ethanol-treated Msh2-LS (EtOH_*Msh2*$^{fl\ KO}$) mice. Images taken at 25X (A), 50X (B) and 100X (C and D) magnification taken with a Leica DMR HC microscope and Leica DFC 450-C camera.

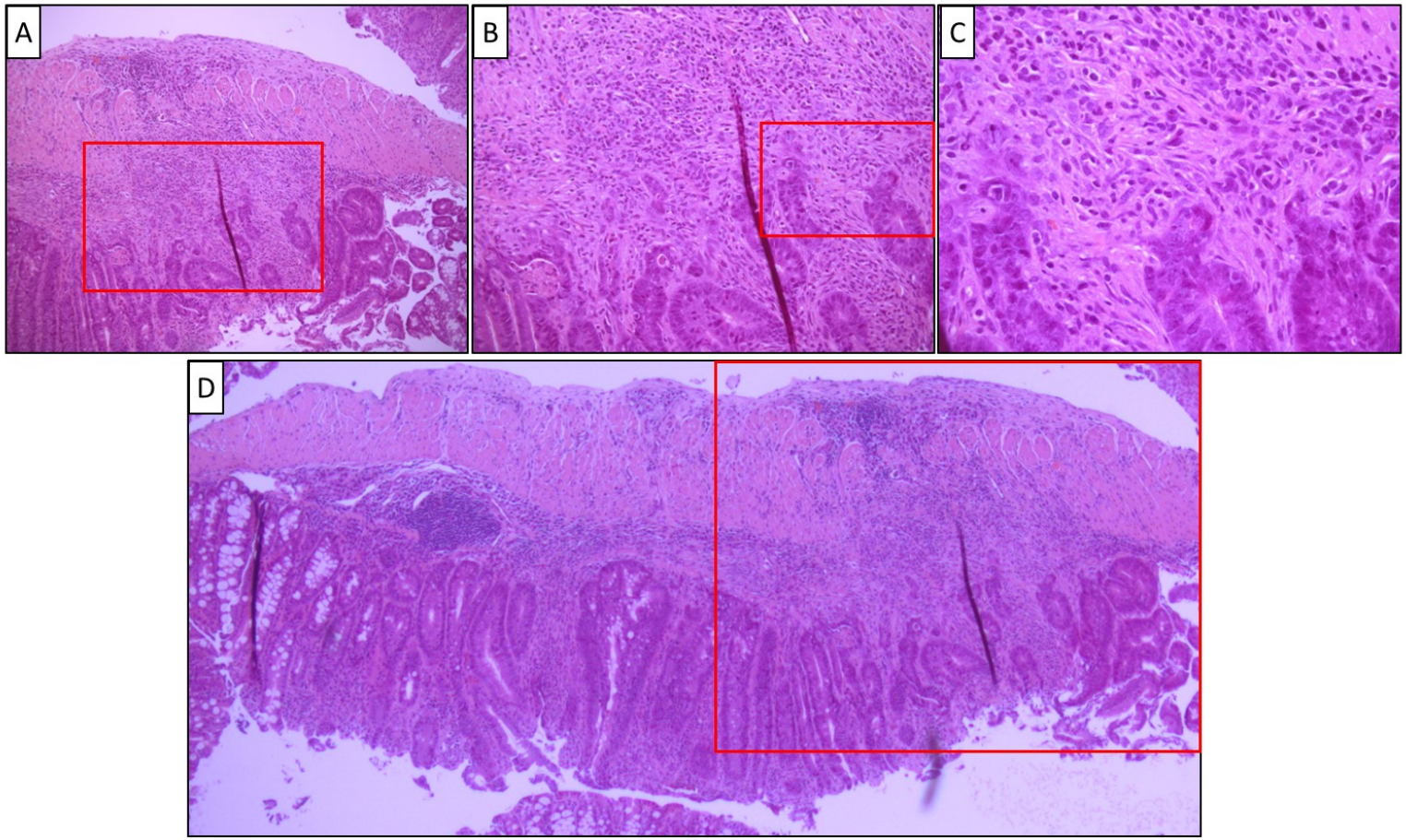

Figure 4.11: Representative images of colon invasive adenocarcinoma in ethanol-treated Msh2-LS (EtOH_*Msh2*$^{fl\ KO}$) mice. Images taken at 100X (A), 200X (B), 400X (C) and 50X (D) magnification taken with a Leica DMR HC microscope and Leica DFC 450-C camera Further magnified areas are indicated by the red rectangles showing regions of invasion .

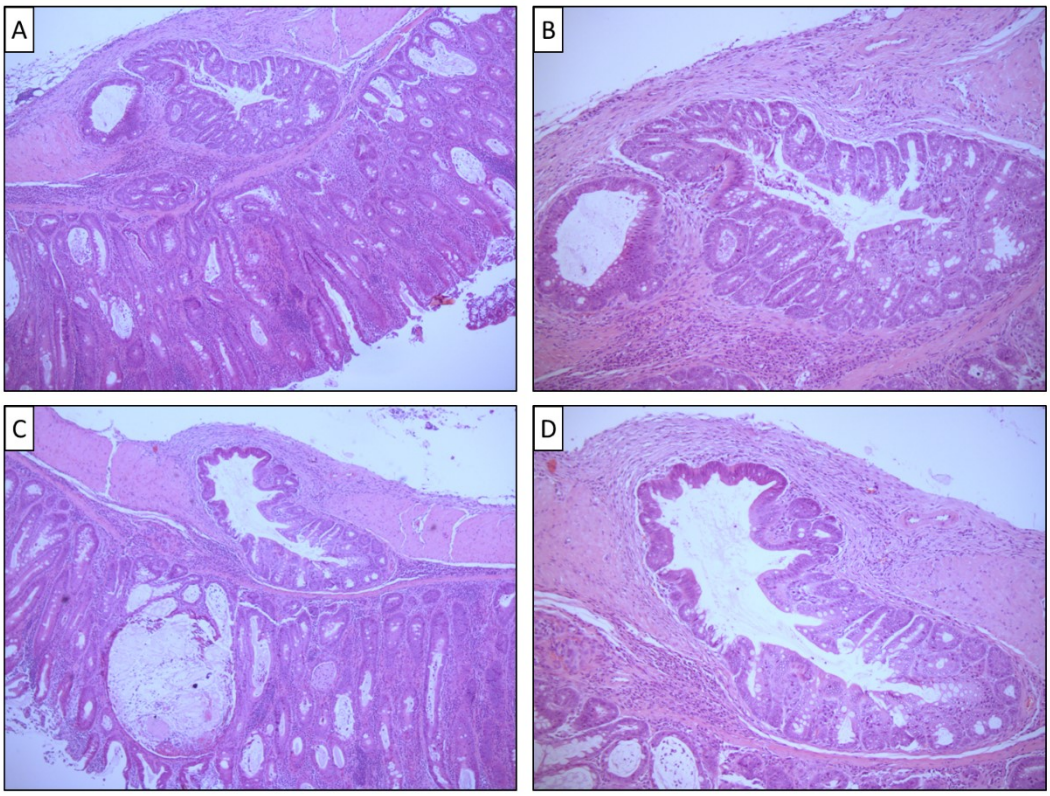

Figure 4.12: Representative images of 2 colon invasive adenocarcinomas in ethanol-treated Msh2-LS (EtOH_*Msh2*$^{fl\ KO}$) mice. Images taken at 50X (left column A and C) and 100X (right column B and D) magnification taken with a Leica DMR HC microscope and Leica DFC 450-C camera.

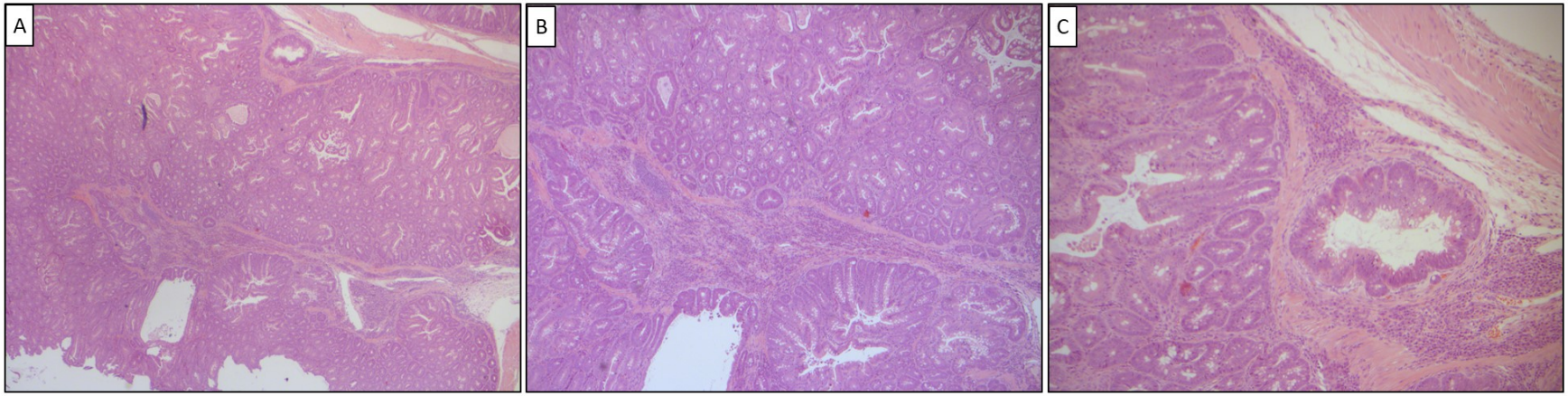

Figure 4.13: Representative images of caecal invasive adenocarcinoma in ethanol-treated Msh2-LS (EtOH_*Msh2*$^{fl\ KO}$) mice. Images taken at 25X (A), 50X (B) and 100X (C) magnification taken with a Leica DMR HC microscope and Leica DFC 450-C camera.

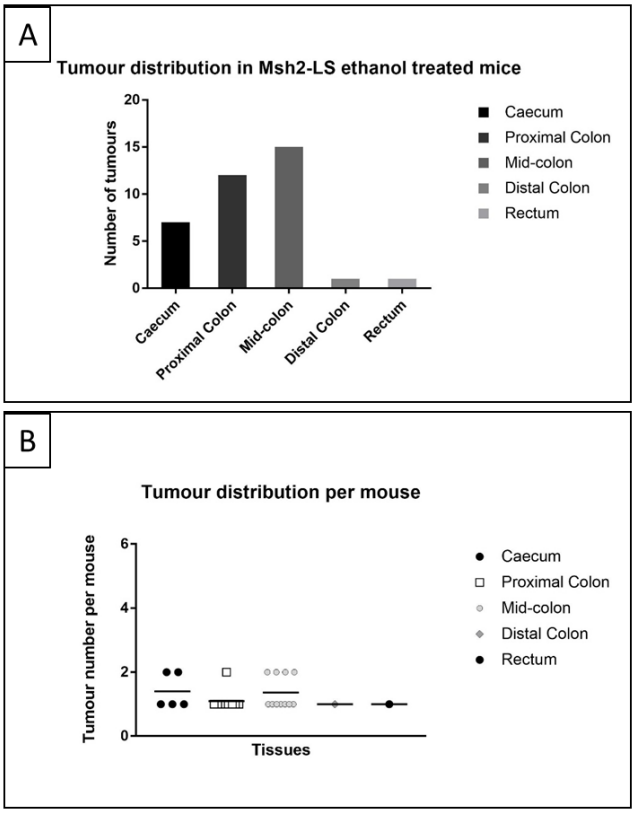

Figure 4.14: Tumour distribution in ethanol-treated Msh2-LS (EtOH_*Msh2*$^{fl\ KO}$) tumour-bearing mice. A) Numbers of adenomas and adenocarcinomas found and their locations. In total, 36 neoplasms were observed, 7 in the caecum (1/7 was an invasive adenocarcinoma), 12 in the proximal colon (2/12 were invasive adenocarcinomas), 15 in the mid-colon (3/15 were invasive adenocarcinomas), 1 adenoma in the distal colon and 1 adenoma in the rectum. B) Tumour distribution and number per EtOH_*Msh2*$^{fl\ KO}$ tumour-bearing mouse. 3/15 tumour-bearing mice showed one caecal adenoma and 2/15 mice showed two adenomas in the caecum. 10/15 tumour-bearing mice showed one proximal colonic adenoma and 1/15 showed two adenomas in the proximal colon. 7/15 tumour-bearing mice showed one mid-colonic adenoma and 4/15 showed 2 adenomas in the mid colon. The remaining two tumour-bearing mice showed respectively one adenoma in the distal colon and one adenoma in the rectum.

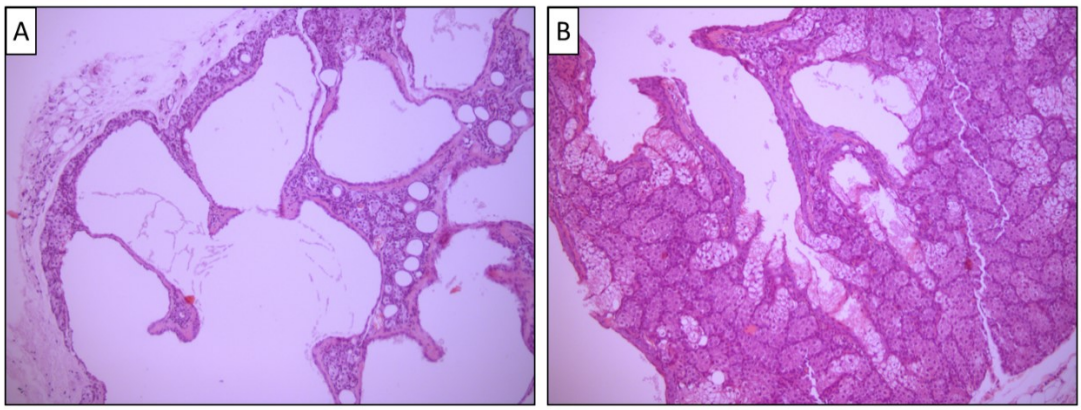

Figure 4.15: A and B show images of the two skin sebaceous adenomas in ethanol-treated Msh2-LS (EtOH_*Msh2*$^{fl\ KO}$) mice (a partially cystic skin sebaceous adenoma on the left in A). Images taken at 100X magnification with a Leica DMR HC microscope and Leica DFC 450-C camera.

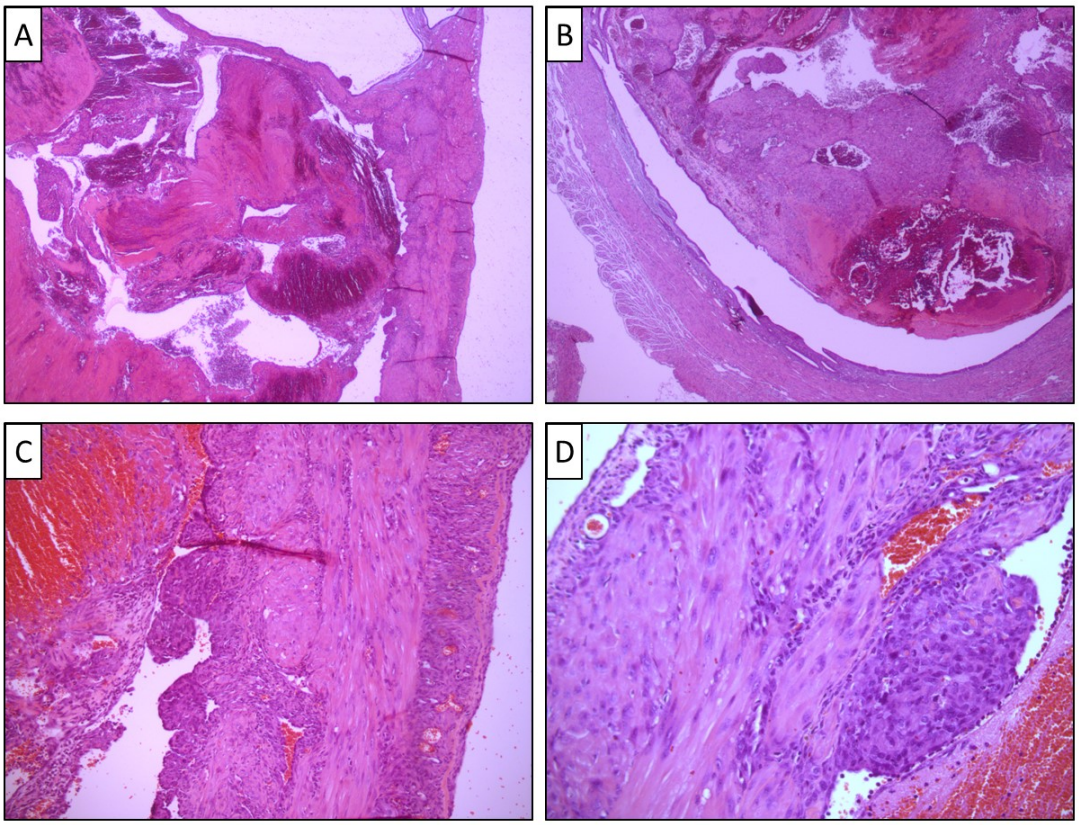

Figure 4.16: Representative images of uterine endometrial invasive adenocarcinoma. Images taken at 25X (A and B), 100X (C) and 200X (D) magnification with a Leica DMR HC microscope and Leica DFC 450-C camera.

4.3 Long-term ethanol effects in Msh2-LS model control mice and wild-type mice

4.3.1 Methods

Groups of 7-9 weeks old Msh2-LS control mice (*Msh2$^{flox/-}$; Lgr5CreERT2$^{+/-}$* and *Msh2$^{flox/-}$; Lgr5CreERT2$^{+/-}$; mTmG$^{+/-}$*) were divided into two groups (A and B) prior to corn oil (without Tamoxifen) treatment.

Both Group-A and Group-B mice received i.p. injections of corn oil on days 1, 2, 3, and 4 (equivalent volume of corn oil as previously used). On day 5 Group-A mice were provided with normal drinking water and Group-B mice with 20% ethanol in drinking water (Figure 4.17).

These control animals were monitored and culled when they reached the same end-time point as the matched experimental Tamoxifen-induced mice (following tumour development or clinical distress in these experimental subjects), or when the control mice showed either clinical signs of distress or they displayed >20% body weight loss compared with the initial weight. The small and large intestines, caecum, stomach, liver, spleen, thymus, lymph nodes (if visible) and any other organ or tissue showing abnormalities, were collected following schedule 1 culling and necropsy dissection. Following standard tissue processing protocols, the tissue blocks were paraffin-embedded in preparation for section cutting and staining.

In previous work, *Aldh1b1* depleted mice were used as experimental subjects, along with wild-type control mice, under long-term (>1 year) treatment with 20% ethanol in drinking water or normal/standard drinking water (Müller et al., 2016). Data related to wild-type mice have been collected by Mike Müeller. The data on the ethanol/acetaldehyde effects in intestinal tumourigenesis were compared for Tamoxifen-induced Msh2-LS mice, non-induced Msh2-LS mice and wild-type mice. The acronyms used for the mouse models and their relevant treatments are shown in Table 2.2.

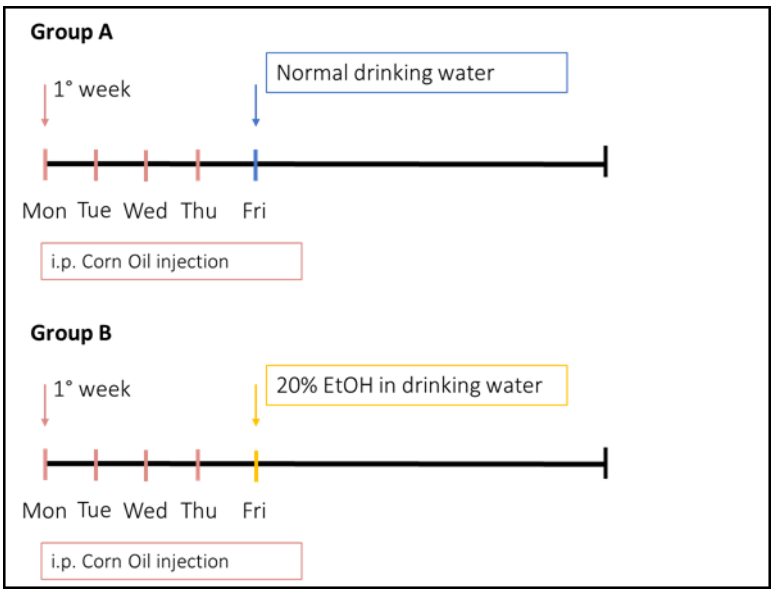

Figure 4.17: Experimental treatment protocols and timelines for Group-A (water-treated) and Group-B (ethanol-treated) mice, showing 4 days of intraperitoneal (i.p.) injections of corn oil, followed by either standard/normal drinking water (Group-A) or drinking water containing 20% ethanol (Group-B). (EtOH = Ethanol).

4.3.2 Results

4.3.2.1 Control group organization and observations

In previous work, 14 WT mice (7 females and 7 males) were provided with 20% ethanol in drinking water and 15 WT mice (8 females and 7 males, control group) with standard/normal drinking water ad libitum for 1 year (Müller et al., 2016).

Twenty-four non-induced Msh2-LS control mice were divided into two groups: 12 mice in Group-A (6 females and 6 males, water-treated control group) and 12 mice in Group-B (6 females and 6 males, ethanol-treated group). Non-induced Msh2-LS animals were culled, necropsy dissected and tissues were collected when they reached the same end-time point as the experimental EtOH_*Msh2*$^{fl\ KO}$ mice (Chapter 4.2.2)

During corn oil administration (daily corn oil i.p injections for 4 consecutive days), body weights and health status were recorded. Body weights of the female and male mice did not significantly differ during the corn oil treatment (Figure 4.18). The average non-induced Msh2-LS male body weight (approx. 33.57g) was significantly higher than the non-induced Msh2-LS female average body weight (approx. 24.2g) both before and during the corn oil treatment.

After corn oil treatment, mice received either 20% ethanol in drinking water regime or standard/normal drinking water regime and the body weights and health status of the mice were monitored and recorded twice a week (Figure 4.19B). The average weight of EtOH_*Msh2*^{fl} mice was 43g for males and 31g for females, and the average weight of H_2O_*Msh2*^{fl} mice was 44.3g for males and 37.3g for females. Significant differences were not observed between the body weights of EtOH_*Msh2*^{fl} versus H_2O_*Msh2*^{fl} mice, regardless of the sex. The body weights of Tamoxifen-induced Msh2-LS mice, non-induced Msh2-LS mice, and WT mice were compared, during either 20% ethanol treatment or normal drinking water treatment (Figure 4.19A, B, C). In every study group, both female and male ethanol-treated Msh2-LS mice did not show significant differences in body weight, or abnormal behaviour, indicating good acceptance of the 20% ethanol treatment regime.

Drinking bottles were changed and bottle weights were recorded once a week. Liquid consumption per mouse was estimated by analysing the weights of the drinking bottles (per cage) and calculating the average weight of consumed liquid per mouse per day (Figure 4.20). H_2O_*Msh2*^{fl} male mice consumed on average 12.17ml of drinking water per day, compared

with 7.2ml of 20% ethanol in drinking water consumed by EtOH_*Msh2*^{fl} male mice. The difference in liquid consumption between EtOH_*Msh2*^{fl} and H_2O_*Msh2*^{fl} males is statically significant (p= 0.0053). Note that, this difference was not observed in the EtOH_*Msh2*^{fl} and H_2O_*Msh2*^{fl} female mice, with both groups consuming (on average) 9.2ml of water per day, with no significant differences observed.

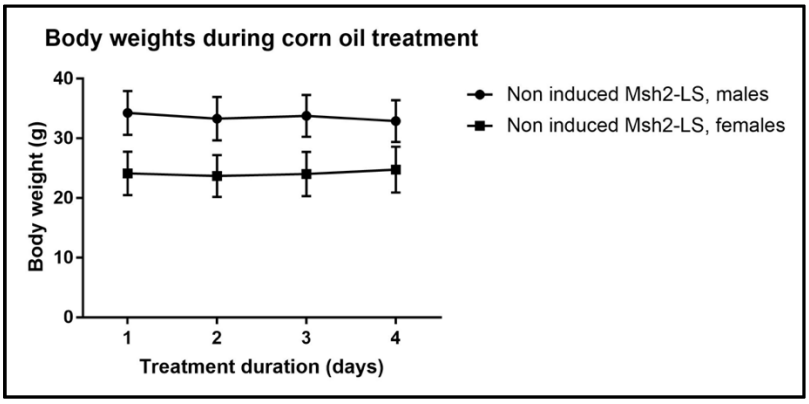

Figure 4.18: Body weights during corn oil treatment. Body weights of non-induced (no Tamoxifen) Msh2-LS males were significantly higher than body weights of non-induced Msh2-LS females, before and during corn oil treatments. 2-way-ANOVA test with Bonferroni post-test correction, p<0.0001 on day 1, p=0.0002 on day 2, p=0.0001 on day 3 and p=0.0015 on day 4 (data shown as mean ± SD, n=10 mice in each group).

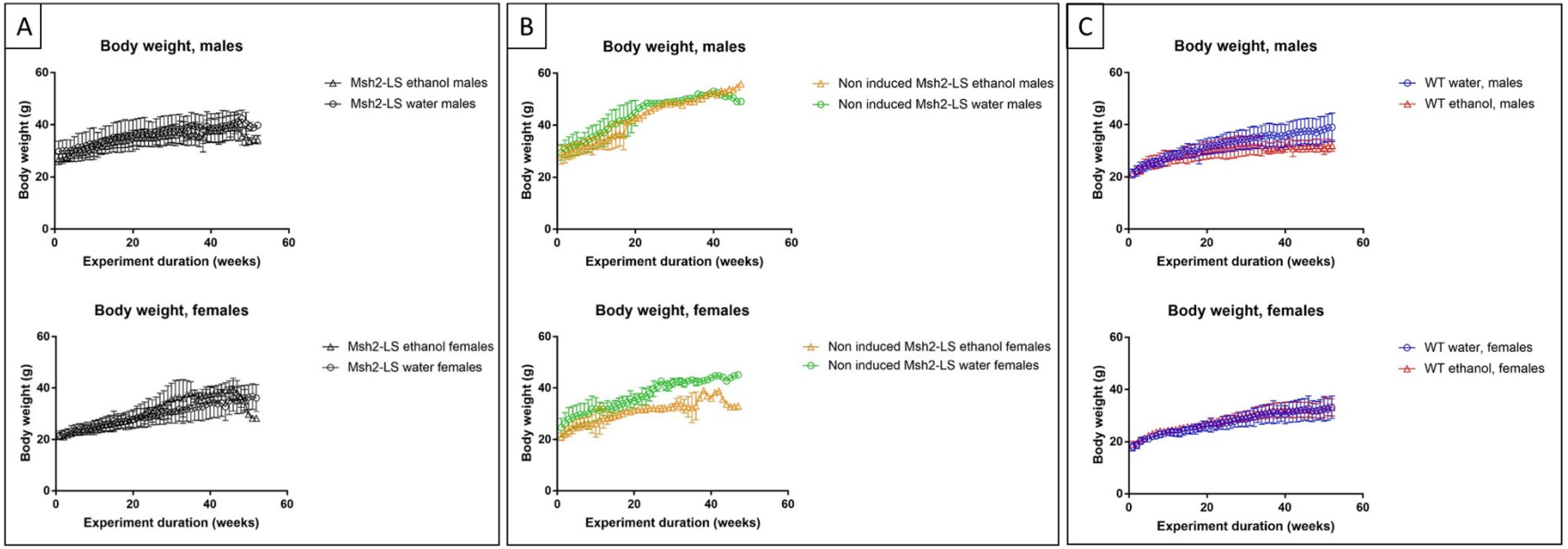

Figure 4.19: Body weights for males and females during 20% ethanol or standard/normal drinking water regimes. Body weight graphs of non-induced Msh2-LS control mice (A), Tamoxifen-induced Msh2-LS experimental subject mice (B), and WT mice (C) during 20% ethanol or standard/normal drinking water regimes. In each group, there were no significant differences between the body weights of ethanol-treated versus water-treated groups of mice for either males or females. 2-way-ANOVA test with Bonferroni post-test correction analysis (data shown as mean±SD, n= 26, n=14, n=14, SD too small to show as bars in some experiments, particularly towards the end of experiments when several mice had been culled leaving too few mice for meaningful calculation of the SD).

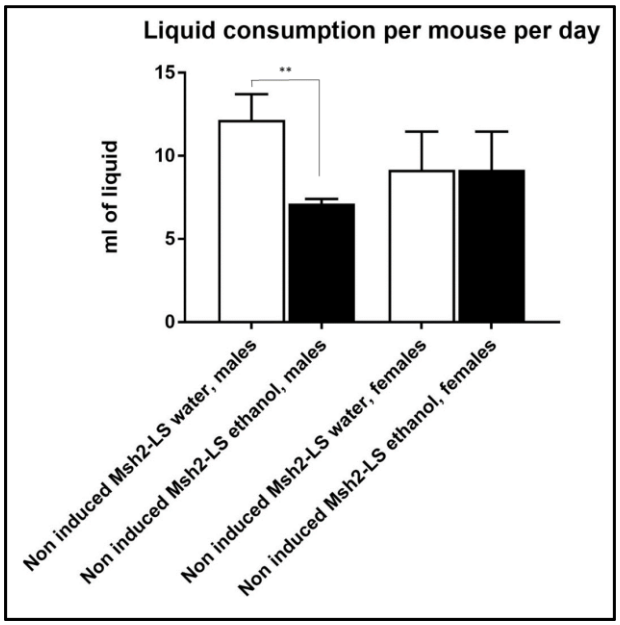

Figure 4.20: Liquid consumption of either 20% ethanol containing drinking water or standard/normal water per mouse per day. 2-way-ANOVA with Bonferroni post-test correction analysis, **p=0.0053 (data shown as mean±SD).

4.3.2.2 Tumour development in control mice exposed to long-term ethanol treatment

The intestines of these mice were analysed and compared to age- and sex-matched induced mice in Chapter 4 (4.2). These control mice underwent necropsy dissection and organ/tissue collection in the same way as the experimental mice. The histopathological analyses of the LI and SI of non-induced Msh2-LS control mice were performed using H&E-stained Swiss rolls. In Group-B (ethanol-treated cohort, EtOH_*Msh2*^{fl}), 3 out of 12 (25%) EtOH_*Msh2*^{fl} mice showed zones of crypt epithelial hyperproliferation involving only the mid colon (after 8, 10 and 22 weeks of 20% ethanol in drinking water regime, respectively) and 1 (8.4%) showed a proximal colon invasive adenocarcinoma (after 28 weeks). Eight out of 12 (66.6%) EtOH_*Msh2*^{fl} mice did not show any abnormality or intestinal adenoma formation. In Group-A (water-treated cohort, H_2O_*Msh2*^{fl}), only 1 out of 12 (8.4%) H_2O_*Msh2*^{fl} mice showed intestinal adenoma formation in the proximal colon (after 22 weeks of treatment). Msh2 expression by this adenoma was tested by IHC, but no loss of Msh2 expression was observed. This tumour was regarded as a sporadic adenoma, with no further tests being performed on it. No intestinal abnormality was observed in any of the other 11 (91.6%) H_2O_*Msh2*^{fl} control mice (Figure 4.21). The tumour incidence was then compared between Tamoxifen-induced Msh2-LS experimental cohort mice and non-induced Msh2-LS control mice (Figure 4.22).

No morphological abnormalities or tumours were observed following necropsy dissection and histopathological analysis of the H&E-stained sections of the caecum, small intestines, stomach, anal canal, liver, spleen, lymph nodes and thymus, of any of the 12 EtOH_*Msh2*^{fl} control mice or the 12 H_2O_*Msh2*^{fl} control mice.

In previous work, 4 out of 14 (28.6%) ethanol-treated WT mice showed proximal colon adenoma formation and in one case also formation of one small intestinal adenoma after over a year of exposure to the 20% ethanol in drinking water regime. No other intestinal abnormality or tumour formation were observed in any of the other 10 out of 14 (71.4%) ethanol-treated WT mice. In this current investigation, no abnormalities or tumours were observed in either LI or SI in the 15 water-treated WT control mice during the same time period. No morphological abnormalities or tumours were observed following necropsy dissection and histopathological analysis of the H&E-stained sections of the caecum, stomach, liver, spleen, lymph nodes and thymus, of any of the 14 WT ethanol-treated or 15 WT water-treated mice.

We next compared the intestinal tumour formation in the 6 groups of Tamoxifen-induced Msh2-LS experimental mice, non-induced Msh2-LS control mice and WT control mice, treated with either 20% ethanol in drinking water or normal/standard drinking water (Figure 4.23).

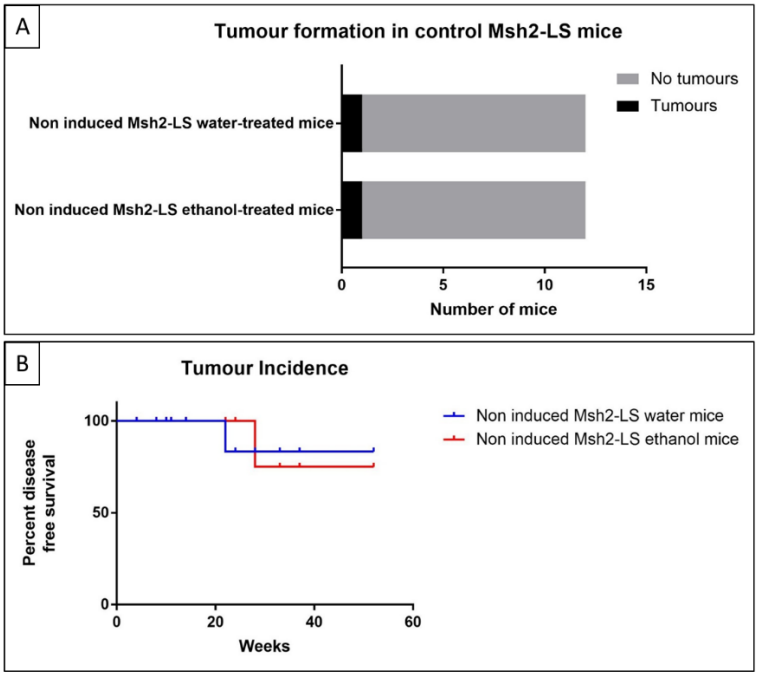

Figure 4.21: A) Bar chart of the number of non-induced Msh2-LS control mice that developed intestinal tumours after receiving either 20% ethanol in drinking water or normal/standard drinking water. In both groups (water-treated cohort and ethanol-treated cohort) 1/12 (8.4%) non-induced Msh2-LS control mice developed large intestinal adenomas (no adenocarcinomas were observed). Fisher's exact test, no significant differences observed. B) Tumour (adenoma) incidence shown as a survival plot in non-induced Msh2-LS control mice treated with either 20% ethanol (red) or water (blue). Log-rank (Mantel-Cox) test, no significant differences observed.

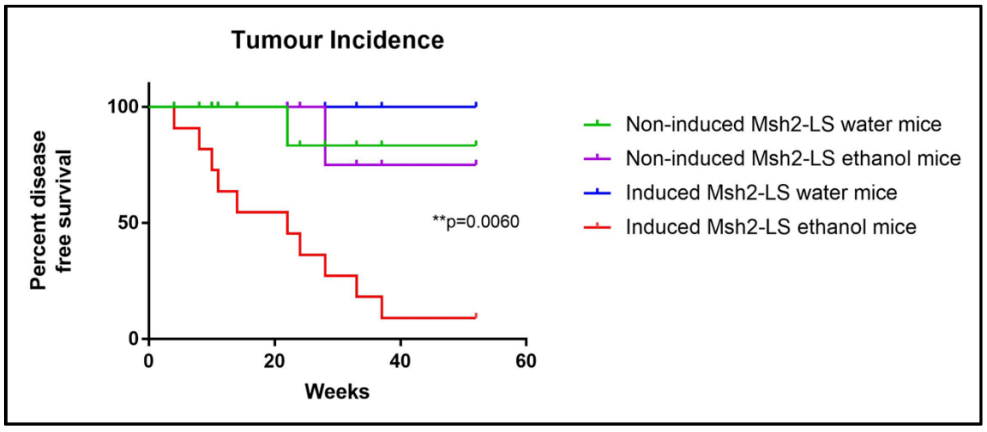

Figure 4.22: Tumour incidence, shown as survival plots, in non-induced Msh2-LS control mice both water-treated (H_2O_*Msh2*^{fl}) (green) and ethanol-treated (EtOH_*Msh2*^{fl}) (violet), compared with Tamoxifen-induced Msh2-LS experimental mice, both water-treated (H_2O_*Msh2*$^{fl\ KO}$) (blue) and 20% ethanol-treated (EtOH_*Msh2*$^{fl\ KO}$) (red). Log-rank (Mantel-Cox) test, **p = 0.0060 indicating significant differences observed between the EtOH_*Msh2*$^{fl\ KO}$ experimental mice and each of the three control cohorts.

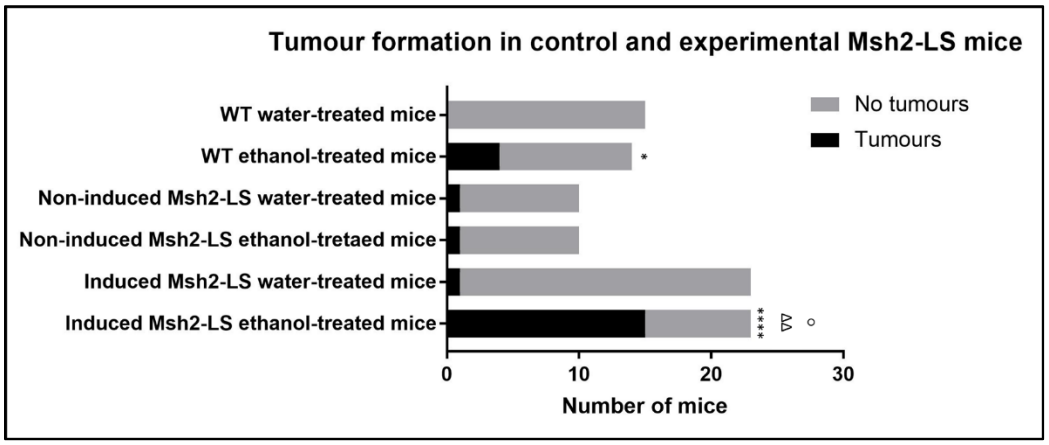

Figure 4.23: Bar chart of the numbers of WT control mice, non-induced Msh2-LS control mice, and Tamoxifen-induced Msh2-LS experimental mice that developed intestinal tumours after receiving either 20% ethanol in drinking water or normal/standard drinking water. Fisher's exact test was carried out to compare the effects of ethanol in the three different pairs of cohorts: 4/14 (28.6%) ethanol-treated WT control mice developed large intestinal tumours compared with 0/14 (0%) in water-treated WT control mice (*p≤0.05); 1/12 (8.4%) ethanol-treated non-induced Msh2-LS (EtOH_*Msh2*^{fl}) control mice and 1/12 (8.4%) water-treated non-induced Msh2-LS (H_2O_*Msh2*^{fl}) control mice each developed a single large intestinal adenoma (no significant differences observed between these two groups); and 15/23 (65%) ethanol-treated Msh2-LS (EtOH_*Msh2*$^{fl\ KO}$) experimental mice developed large intestinal tumours compared with 1/23 (4%) water-treated Msh2-LS (H_2O_*Msh2*$^{fl\ KO}$) experimental mice that developed large intestinal tumours, ****p<0.0001. Fisher's exact test was carried out to compare the tumour incidence between ethanol-treated WT control mice and ethanol-treated non-induced Msh2-LS (EtOH_*Msh2*^{fl}) control mice (no significant differences observed between these two groups); ethanol-treated WT control mice and ethanol treated Msh2-LS (EtOH_*Msh2*$^{fl\ KO}$) experimental mice (°p≤0.0448) and ethanol-treated Msh2-LS experimental mice and ethanol-treated non-induced Msh2-LS control mice ($^{\Delta\Delta}$p≤0.0066).

4.4 Immunohistochemical characterization of tumours and tissues from the Msh2-LS mouse model with and without ethanol treatment

4.4.1 Methods

We performed IHC analyses in FFPE colonic and small intestinal tissues from induced *Lgr5CreERT2; Msh2$^{flox/-;}$ mTmG* mice and non-induced control *Lgr5CreERT2; Msh2$^{flox/-}$; mTmG* mice to verify the expression of various proteins of interest. We performed the same analysis on the colonic and SI tissues comparing ethanol-treated mice with water-treated mice. Small and large intestinal tissues were harvested, prepared as Swiss-rolls and fixed in 10% NBF (as described in Materials and Methods). They were processed using standard tissue processing protocols for paraffin wax embedding and microtome sectioning.

IHC was performed to confirm changes to Msh2 expression (target protein) and other MMR proteins (Msh6, Mlh1 and Pms2), the proliferation marker Ki-67, the Wnt pathway marker β-Catenin, the DNA damage marker γ-H2AX and DNA damage / tumour suppressor marker p53, and cCas-3 a critical executioner of apoptosis. IHC for infiltrating immune cells was performed by Dr Seth Coffelt's research group from the Beatson Cancer Institute in Glasgow (the panel of immune cell antibodies is displayed in Materials and Methods, Table 2.12) Immunohistochemical staining was performed using the protocols described in Materials and Methods (2.2.3). Staining and quantification was performed either by manually scoring or using the bioimage analysis software for digital pathology images, QuPath.

4.4.2 Results

4.4.2.1 Mismatch Repair proteins immunostaining of Msh2-LS murine small intestinal and colonic tissues

Normally, Msh2 is highly expressed in crypt stem cells and transit amplifying cells in the small intestinal crypts, but fades in the non-dividing differentiated SI villus cells, and similarly fades in the differentiated cells of the upper third of the colonic crypts (Tomé et al., 2013).

Tamoxifen treatment induced the loss of Msh2 expression in Lgr5+ expressing crypt epithelial stem cells scattered along the entire small and large intestines. The Lgr5+ expressing stem cells, located at the bottom of the crypts, generate daughter cells that can expand to fill the entire crypt-villus epithelium in SI or entire crypt in the colon (Barker et al., 2007; Wojciechowicz et al., 2014). We used colonic tissue samples of *Msh2*$^{-/-}$ and WT mice as Msh2-negative and -positive expression controls respectively (Figure 4.24). The lack of IHC DAB-brown staining in all of the SI crypts and villi and in all of the colonic crypts of the *Msh2*$^{-/-}$ mice confirmed complete loss of Msh2 expression in the Msh2-null control tissues. In contrast, scattered crypts, in both SI and colon, showed Msh2 expression loss in the Msh2-LS model mice.

The number of Msh2-negative crypts was higher in the SI than in the colon in Msh2-LS model mice, however no tumours were observed in the small intestine. The number of Msh2-negative crypts in the SI was statistically significantly higher in the EtOH_*Msh2*$^{fl\ KO}$ mice compared with the H_2O_*Msh2*$^{fl\ KO}$ mice (Figure 4.25). In EtOH_*Msh2*$^{fl\ KO}$ mice, 43% Msh2-negative small intestinal crypts were observed compared with 25.8% Msh2-negative small intestinal crypts found in H_2O_*Msh2*$^{fl\ KO}$ mice (Figure 4.26).

IHC analysis of Msh2 expression in the intestinal tissue samples from EtOH_*Msh2*^{fl} mice and H_2O_*Msh2*^{fl} mice showed no Msh2-negative crypts in either small or large intestinal mucosal epithelium (Figure 4.27-4.28), consistent with lack of induction of Cre activity with continued expression of protein from the floxed Msh2 allele.

In the colon, the number of Msh2-negative crypts was statistically significantly higher in the EtOH_*Msh2*$^{fl\ KO}$ mice compared with the H_2O_*Msh2*$^{fl\ KO}$ mice (Figure 4.29). In EtOH_*Msh2*$^{fl\ KO}$ mice 11.2% Msh2-negative colonic crypts were observed compared with 5% Msh2-negative colonic crypts found in H_2O_*Msh2*$^{fl\ KO}$ controls (Figure 4.30). EtOH_*Msh2*$^{fl\ KO}$ mice formed

some large intestinal adenomas that were characterized by Msh2-negative dysplastic glands often surrounded by or admixed with Msh2-positive crypts showing reactive or hyperproliferative changes (Figure 4.31).

Furthermore, we performed IHC for Msh6, Mlh1 and Pms2 to investigate expression changes in other MMR proteins in the Msh2-LS mouse model.

In the MMR repair pathway, a base mismatch or single nucleotide insertion/deletion (InDel) error is recognised by the MutSα complex, which is composed of Msh2 and Msh6 heterodimeric proteins. In the absence of Msh2, the heterodimeric MutSα complex cannot be formed and Msh6 is rapidly degraded (Poulogiannis et al., 2010). We used colonic tissue samples of *Msh2*$^{-/-}$ and WT mice as Msh6-negative and -positive normal expression controls respectively (Figure 4.32). As previously observed for Msh2 IHC results (Figure 4.24), the lack of IHC DAB-brown staining in all of the colonic crypts of the *Msh2*$^{-/-}$ mice confirmed complete loss of Msh6 expression, whereas wild-type murine colonic epithelium showed DAB-brown staining in all of the colonic crypts, with the typical MMR protein expression gradient of staining, with strong MMR staining at the crypt base, with decreased staining towards the lumen of the intestine. IHC analysis of Msh6 was performed on large and small intestinal tissue from both Tamoxifen-induced Msh2-LS mice and non-induced (no Tamoxifen treatment) Msh2-LS mice. These samples showed Msh6-negative crypts scattered along both SI and colon of Tamoxifen-induced Msh2-LS mice (Figure 4.33). IHC analysis of Msh6 expression in the intestinal tissue samples from non-induced Msh2-LS mice showed no Msh6-negative crypts in either small or large intestinal mucosal epithelium (Figure 4.33).

The MutLα complex, composed of Mlh1 and Pms2, is recruited by the binding of MutSα (composed by Msh2 and Msh6) to the mismatched or InDel DNA lesion. The absence of Msh2 does not inhibit or modify the expression of Mlh1 or Pms2 (Poulogiannis et al., 2010). Colonic tissue samples of *Msh2*$^{-/-}$ and WT mice were used as expression controls for Mlh1 (Figure 4.34). The DAB-brown staining was observed in the typical MMR protein expression pattern in all of the colonic crypts of both *Msh2*$^{-/-}$ and WT murine colonic tissue. We verified Mlh1 expression in large and small intestinal tissue from both Tamoxifen-induced Msh2-LS mice and non-induced Msh2-LS mice. These samples showed normal Mlh1 expression in both colonic and small intestinal crypts of Tamoxifen-induced Msh2-LS mice and non-induced Msh2-LS mice (Figure 4.35). The immunostaining for Pms2 proved to be technically

problematic due to antibody failure and it was not possible to determine the staining pattern for Pms2 (Supplementary Figure 4.10).

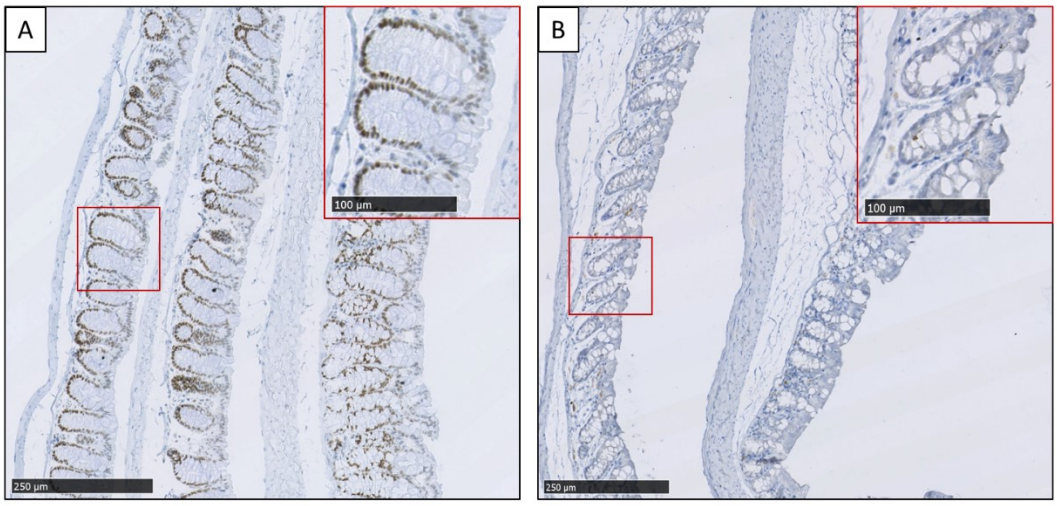

Figure 4.24: Immunohistochemical analysis of Msh2 protein expression in large intestinal mucosal epithelium from a positive-control WT mouse (A), in which the brown staining indicates positive Msh2 expression in all crypts (further magnified in the upper right inset red rectangle); and from a negative-control *Msh2*$^{-/-}$ mouse (B), in which the lack of brown staining confirms the absence of Msh2 expression in large intestinal mucosal epithelium (further magnified in the upper right inset red rectangle). Images taken from anti-Msh2 IHC stained sections scanned using the Hamamatsu Nanozoomer and analysed with the Hamamatsu NDP Viewer software at 10X and 20X magnification (bar at lower left indicates 250µm, bar in red rectangle indicates 100µm).

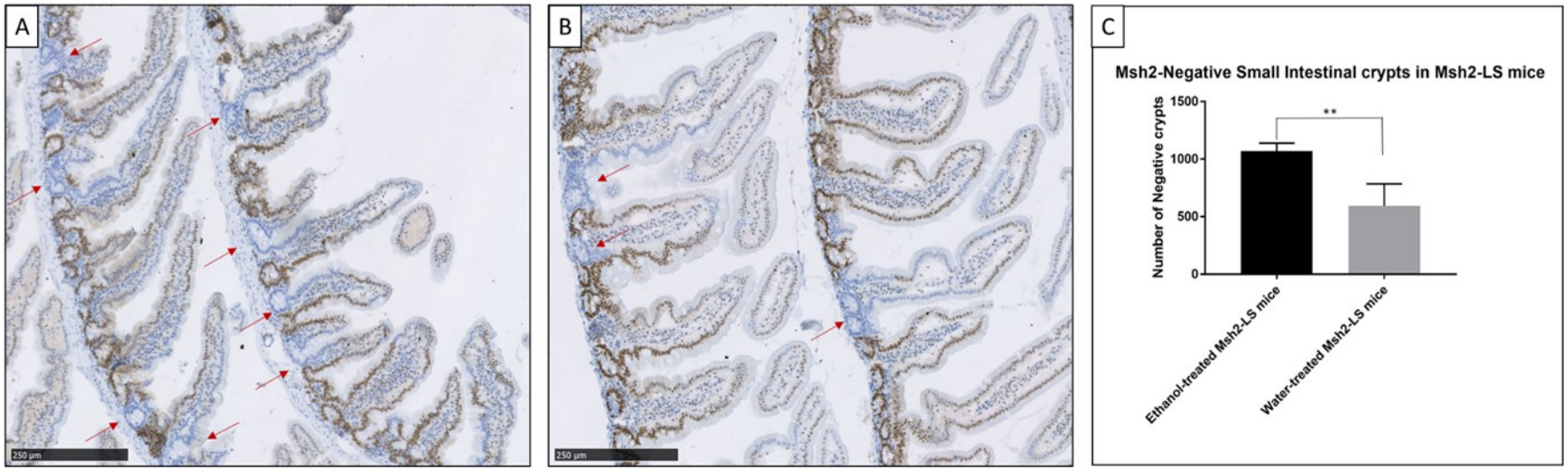

Figure 4.25: Immunohistochemical analysis of Msh2 protein expression in small intestinal mucosal epithelium of *Msh2$^{flox/-}$; Lgr5CreERT2$^{+/-}$; mTmG$^{+/-}$* mice treated with either 20% ethanol in drinking water (A) or normal / standard drinking water (B). Msh2-negative crypts (indicated by the red arrows) were manually counted along the entire small intestine of treated Msh2-LS mice (C). Paired Students t Test, **p= 0.0044 vs. water (data shown as mean±SD, n=6 mice in each group). Images taken from sections scanned using the Hamamatsu Nanozoomer and analysed with the Hamamatsu NDP Viewer software at 10X magnification (bar at lower left indicates 250µm).

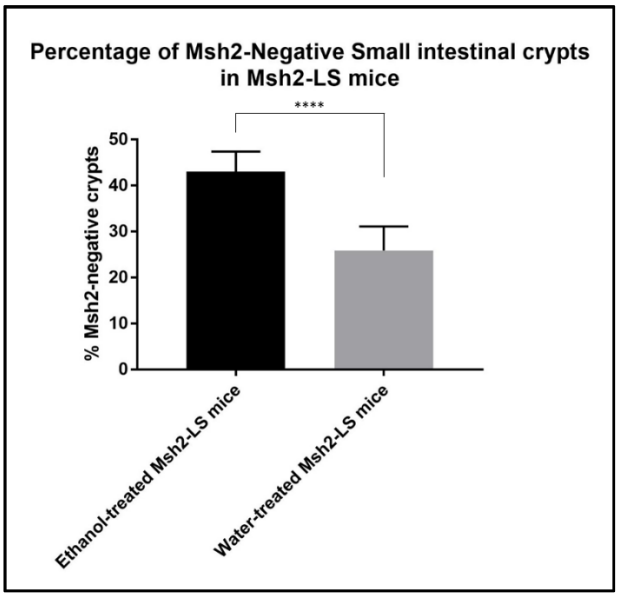

Figure 4.26: Percentage of Msh2 protein-non-expressing crypts in small intestinal mucosa of *Msh2$^{flox/-}$; Lgr5CreERT2$^{+/-}$; mTmG$^{+/-}$* mice treated with either 20% ethanol in drinking water or normal water. Paired Students t Test, ****p<0.0001 vs. water (data shown as mean±SD, 300 crypts counted were analysed, n=6 mice from each group).

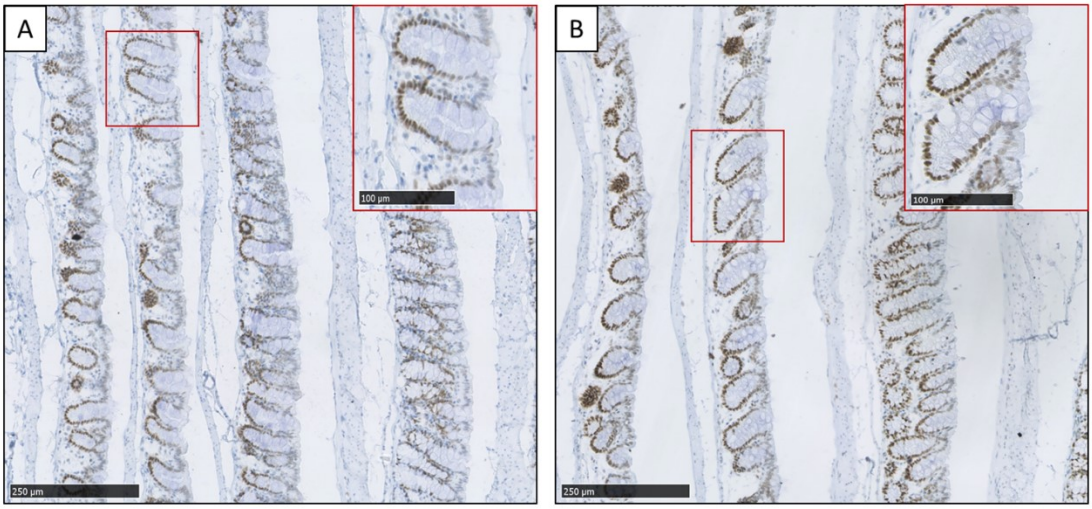

Figure 4.27: Immunohistochemical analysis of Msh2 protein expression in large intestinal mucosal epithelium of non-induced Msh2-LS control mice treated with either 20% of ethanol in drinking water (A) or normal / standard water (B). No Msh2-negative crypts were observed along the entire colon of non-induced Msh2-LS mice (n=6 mice in each group). Images taken from sections scanned using the Hamamatsu Nanozoomer and analysed with the Hamamatsu NDP Viewer software at 10X and 20X magnification (bar at lower left indicates 250µm, bar in red rectangle indicates 100µm).

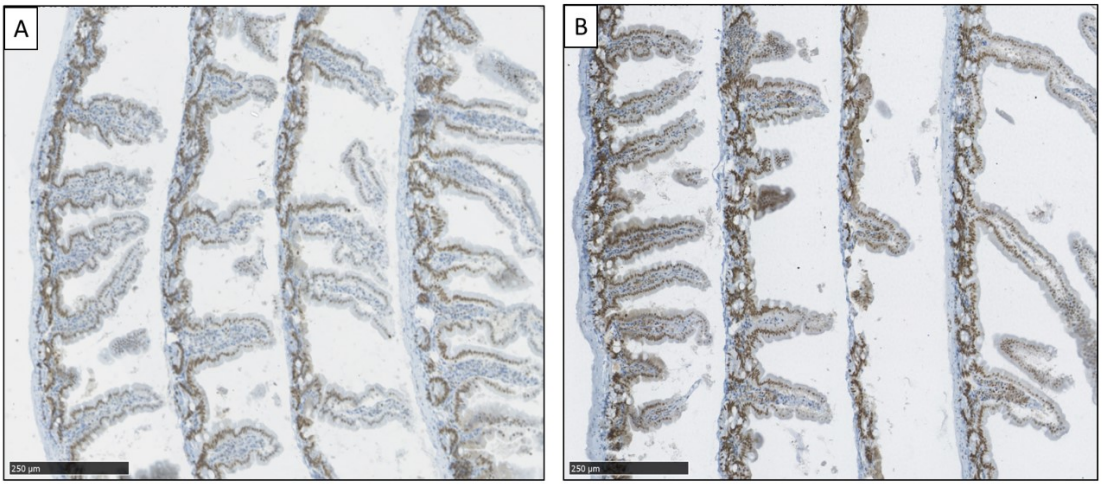

Figure 4.28: Immunohistochemical analysis of Msh2 protein expression in small intestinal mucosal epithelium of non-induced Msh2-LS control mice treated with either 20% ethanol in drinking water (A) or normal / standard drinking water (B). No Msh2-negative crypts were observed along the entire small intestine of non-induced Msh2-LS mice (n=6 mice in each group). Images taken from sections scanned using the Hamamatsu Nanozoomer and analysed with the Hamamatsu NDP Viewer software at 10X magnification (bar at lower left indicates 250µm).

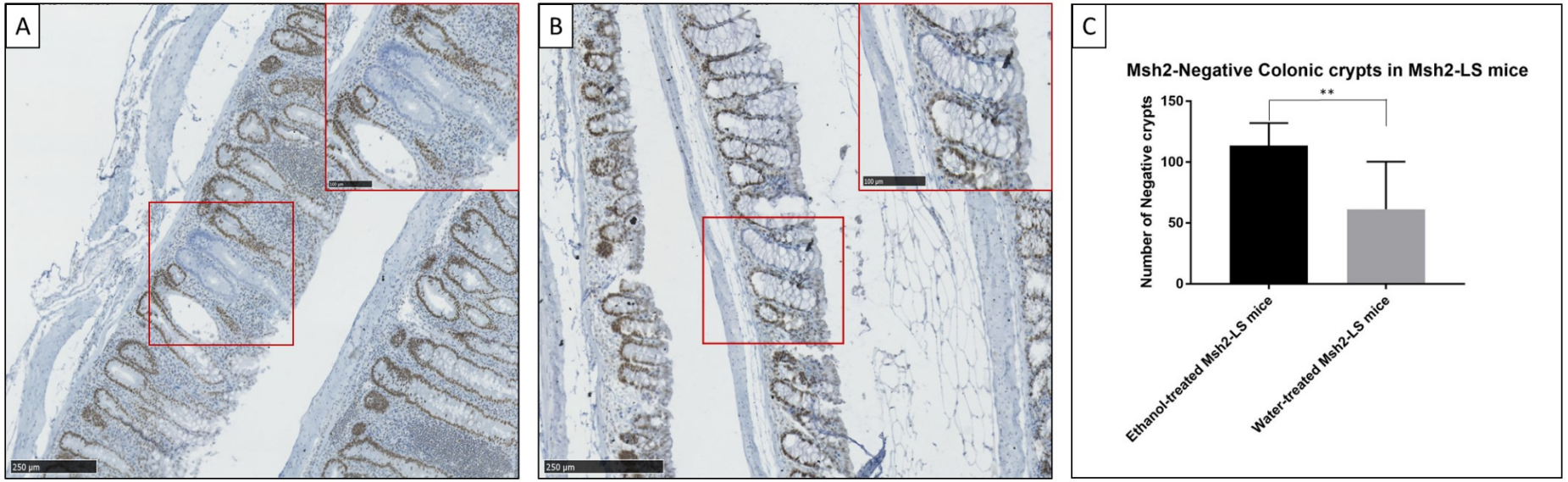

Figure 4.29: Immunohistochemical analysis of Msh2 protein expression in large intestinal mucosal epithelium of *Msh2$^{flox/-}$; Lgr5CreERT2$^{+/-}$; mTmG$^{+/-}$* mice treated with either 20% ethanol in drinking water (A) or normal/standard water (B). Msh2-negative crypts (indicated by the red square and further magnified in the upper right inset red rectangle in Figure panels A and B) were manually counted along the entire colon of treated Msh2-LS mice (C). Mann-Whitney U Test, **p=0.0097 vs. water (data shown as mean±SD, n=6 mice each group). Images taken from sections scanned using the Hamamatsu Nanozoomer and analysed with the Hamamatsu NDP Viewer software at 10X and 20X magnification (bar at lower left indicates 250um, bar in red rectangle indicates 100µm)

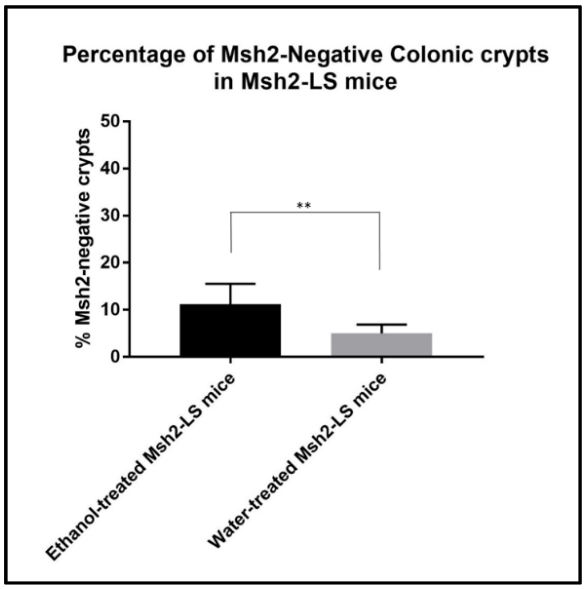

Figure 4.30: Percentage of Msh2 protein-non-expressing crypts in large intestinal mucosa of *Msh2$^{flox/-}$; Lgr5CreERT2$^{+/-}$; mTmG$^{+/-}$* mice treated with either 20% ethanol in drinking water or normal/standard water. Paired Students t Test, **p=0.0029 vs. water (data shown as mean±SD, 300 crypts counted in n=6 mice from each group).

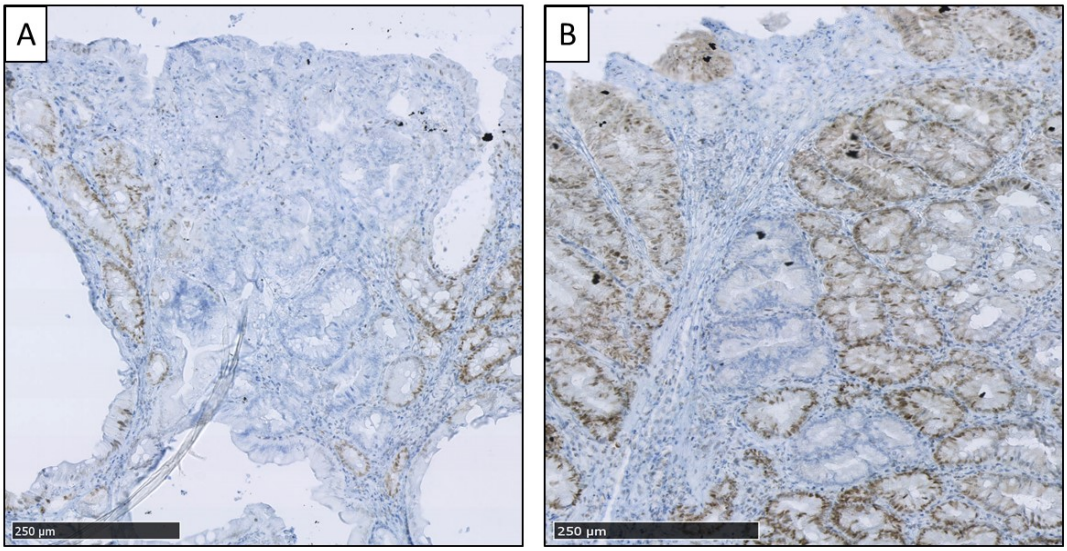

Figure 4.31: Representative images of Msh2 immunohistochemical staining in two large intestinal adenomas from 2 ethanol-treated *Msh2$^{flox/-}$; Lgr5CreERT2$^{+/-}$; mTmG$^{+/-}$* (EtOH_*Msh2$^{fl\ KO}$*) mice (A & B). In both examples, there are Msh2-negative dysplastic or adenomatous glands, either surrounded by or admixed with reactive crypts or hyperproliferative crypts that are staining positively for Msh2. Images taken from sections scanned using the Hamamatsu Nanozoomer and analysed with the Hamamatsu NDP Viewer software at 10X magnification (bar at lower left indicates 250µm).

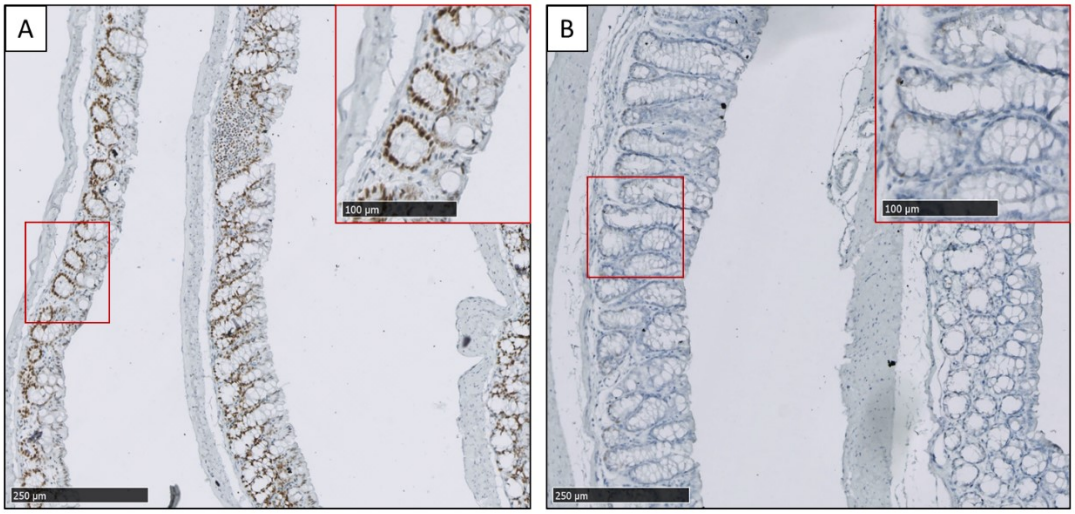

Figure 4.32: Immunohistochemical analysis of Msh6 protein expression in large intestinal mucosal epithelium from a positive-control WT mouse (A), in which the brown staining indicates positive Msh6 expression in all crypts (further magnified in the upper right inset red rectangle); and from a negative-control *Msh2*$^{-/-}$ mouse (B), in which the lack of brown staining confirms the absence of Msh6 expression in large intestinal mucosal epithelium (further magnified in the upper right inset red rectangle). Images taken from anti-Msh6 IHC stained sections scanned using the Hamamatsu Nanozoomer and analysed with the Hamamatsu NDP Viewer software at 10X and 20X magnification (bar at lower left indicates 250µm, bar in red rectangle indicates 100µm).

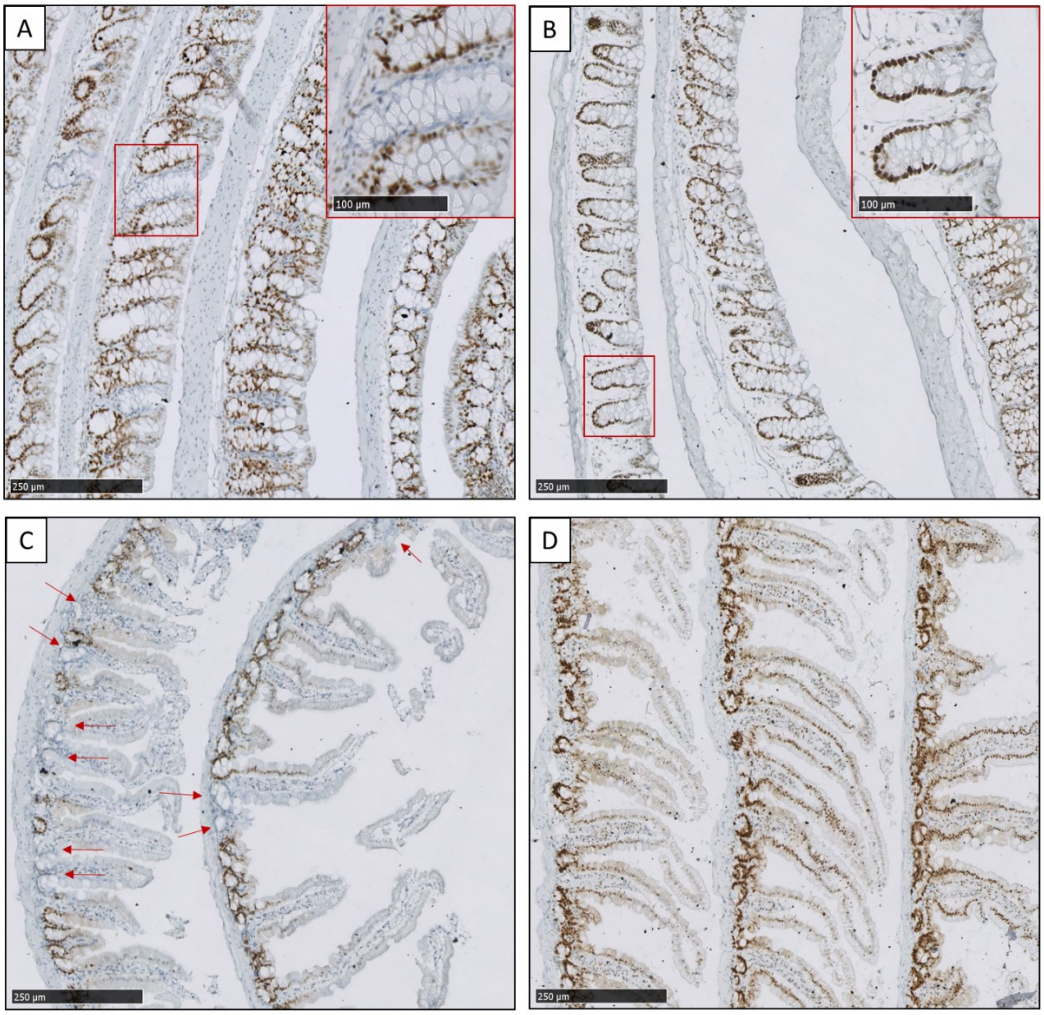

Figure 4.33: Immunohistochemical analysis of Msh6 protein expression in large and small intestinal mucosal epithelium of Tamoxifen-induced *Msh2$^{flox/-}$; Lgr5CreERT2$^{+/-}$; mTmG$^{+/-}$* mice (A and C) and non-induced *Msh2$^{flox/-}$; Lgr5CreERT2$^{+/-}$; mTmG$^{+/-}$* (B and D). Tamoxifen-induced Msh2-LS mice showed Msh6-negative crypts in colonic intestinal mucosal epithelium (indicated by the red square and further magnified in the upper right inset red rectangle in figure panel A) and small intestinal mucosal epithelium (indicated by the red arrows in figure panel C). No Msh6-negative crypts were observed in both large and small intestinal mucosal epithelium (B and D respectively) of non-induced Msh2-LS mice. Images taken from sections scanned using the Hamamatsu Nanozoomer and analysed with the Hamamatsu NDP Viewer software at 10X and 20X magnification (bar at lower left indicates 250µm, bar in red rectangle indicates 100µm).

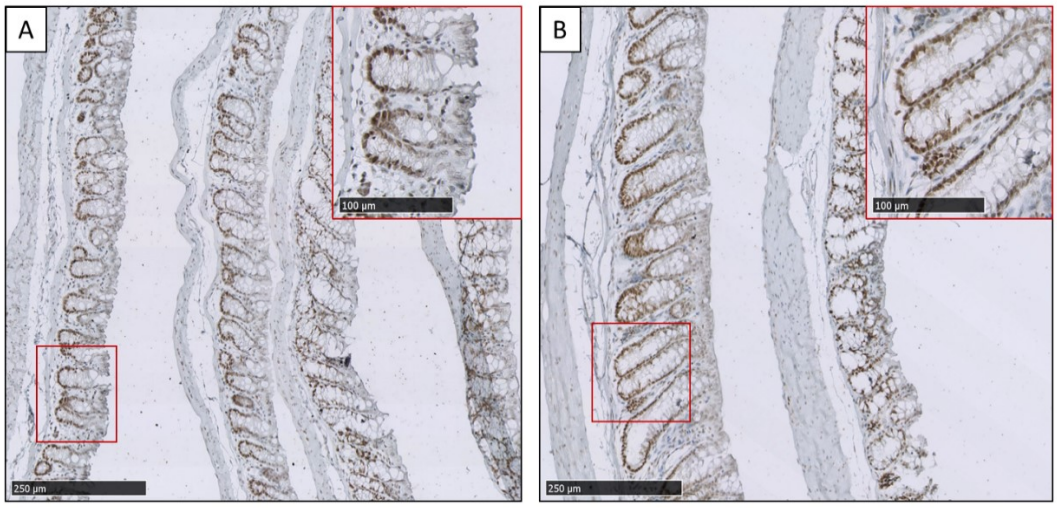

Figure 4.34: Immunohistochemical analysis of Mlh1 protein expression in large intestinal mucosal epithelium from WT mouse (A) and from *Msh2*$^{-/-}$ mouse (B), in which the brown staining indicates positive Mlh1 expression in all crypts (further magnified in the upper right inset red rectangle in figure panels A and B). Images taken sections scanned using the Hamamatsu Nanozoomer and analysed with the Hamamatsu NDP Viewer software at 10X and 20X magnification (bar at lower left indicates 250µm, bar in red rectangle indicates 100µm).

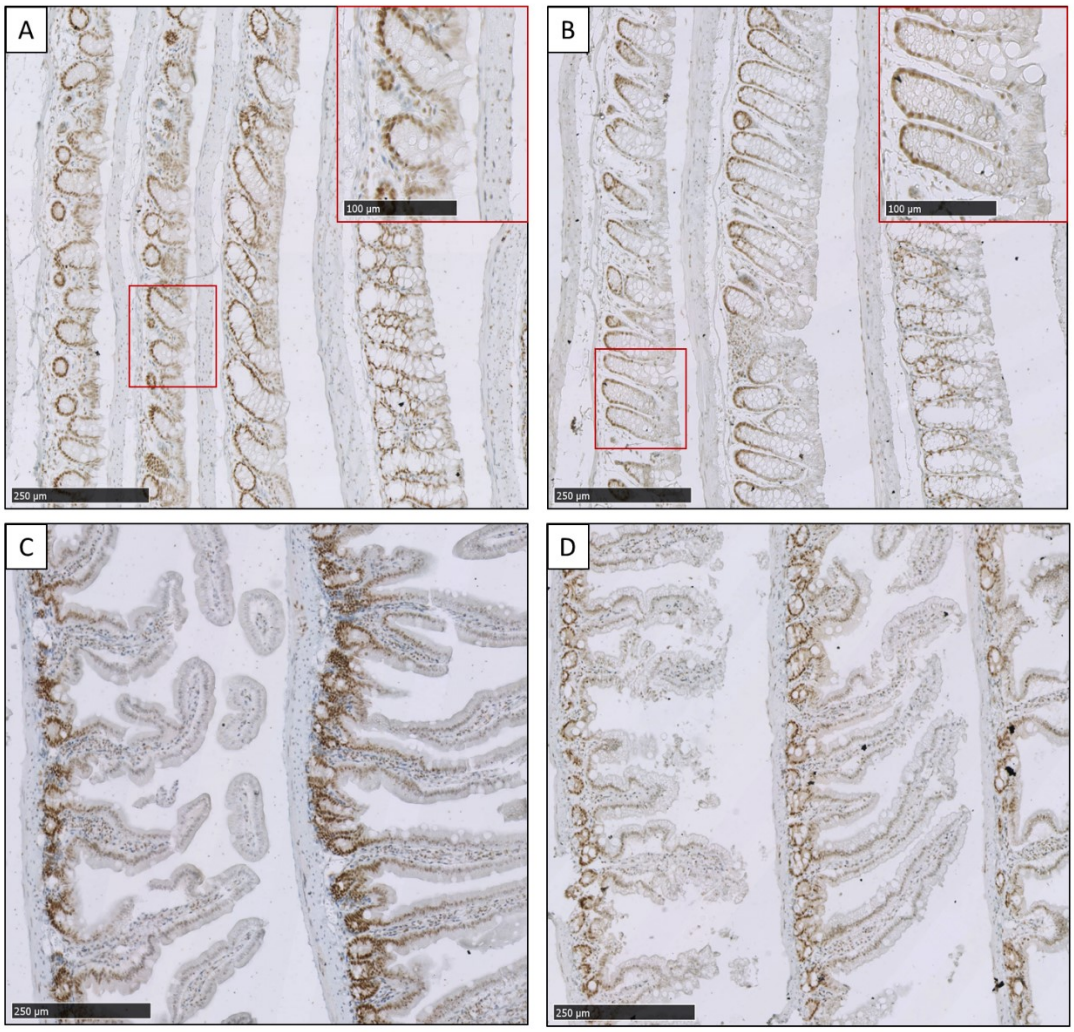

Figure 4.35: Immunohistochemical analysis of Mlh1 protein expression in large and small intestinal mucosal epithelium of Tamoxifen-induced *Msh2$^{flox/-}$; Lgr5CreERT2$^{+/-}$; mTmG$^{+/-}$* mice (A and C) and non-induced *Msh2$^{flox/-}$; Lgr5CreERT2$^{+/-}$; mTmG$^{+/-}$* (B and D). Normal Mh1 expression was observed in both colonic mucosal epithelium (indicated by the red square and further magnified in the upper right inset red rectangle in figure panels A and B) and small intestinal mucosal epithelium (C and D) of both Tamoxifen-induced Msh2-LS mice and non-induced Msh2-LS mice. Images taken from sections scanned using the Hamamatsu Nanozoomer and analysed with the Hamamatsu NDP Viewer software at 10X and 20X magnification (bar at lower left indicates 250µm, bar in red rectangle indicates 100µm).

4.4.2.2 Ki-67 immunostaining of Msh2-LS murine small intestinal and colonic tissues

The Ki-67 protein is a cellular marker for proliferation. During active phases of the cell cycle (part of G1, S, and G2 phases), the Ki-67 antigen can be detected within the cell nucleus, whereas in mitosis (M phase) most of the protein is relocated to the surface of the condensed chromosomes (and the nuclear membrane disappears during most of M phase). Previous studies have shown that Ki-67 is present in proliferating cells, but it is absent in quiescent cells (Gerdes et al., 1984). Detection of Ki-67 by IHC may be performed to determine proliferative activity that may be predictive of some tumour behaviour. In normal large and small intestinal tissue, Ki-67 is expressed only in the proliferating cells at the base of crypts (Johnston et al., 1989).

IHC analysis of Ki-67 showed large and significant differences in the number of intestinal Ki67-positive cells between the EtOH_*Msh2*$^{fl\ KO}$ murine colon and the H_2O_*Msh2*$^{fl\ KO}$ murine colon (Figure 4.36). The percentage of Ki-67-positive cells per crypt was significantly higher in EtOH_*Msh2*$^{fl\ KO}$ mice (75.76%) compared with H_2O_*Msh2*$^{fl\ KO}$ mice (19.64%) (Figure 4.37). This is due to the large regions of mucosal crypt hyperproliferation found in ethanol-treated murine colons (Figure 4.6).

The comparative analysis of SI Ki-67 expression between EtOH_*Msh2*$^{fl\ KO}$ and H_2O_*Msh2*$^{fl\ KO}$ mice didn't show the same large differences. EtOH_*Msh2*$^{fl\ KO}$ murine SI showed similar numbers of Ki-67-positive cells per crypt when compared with H_2O_*Msh2*$^{fl\ KO}$ mice SI, with no significant differences observed between the two groups (Figure 4.38). The percentage of Ki-67-positive cells per crypt was significantly higher in SI of EtOH_*Msh2*$^{fl\ KO}$ mice (12.21%) compared with H_2O_*Msh2*$^{fl\ KO}$ mice (8.7%), but with only a small difference between the two groups (Figure 4.39).

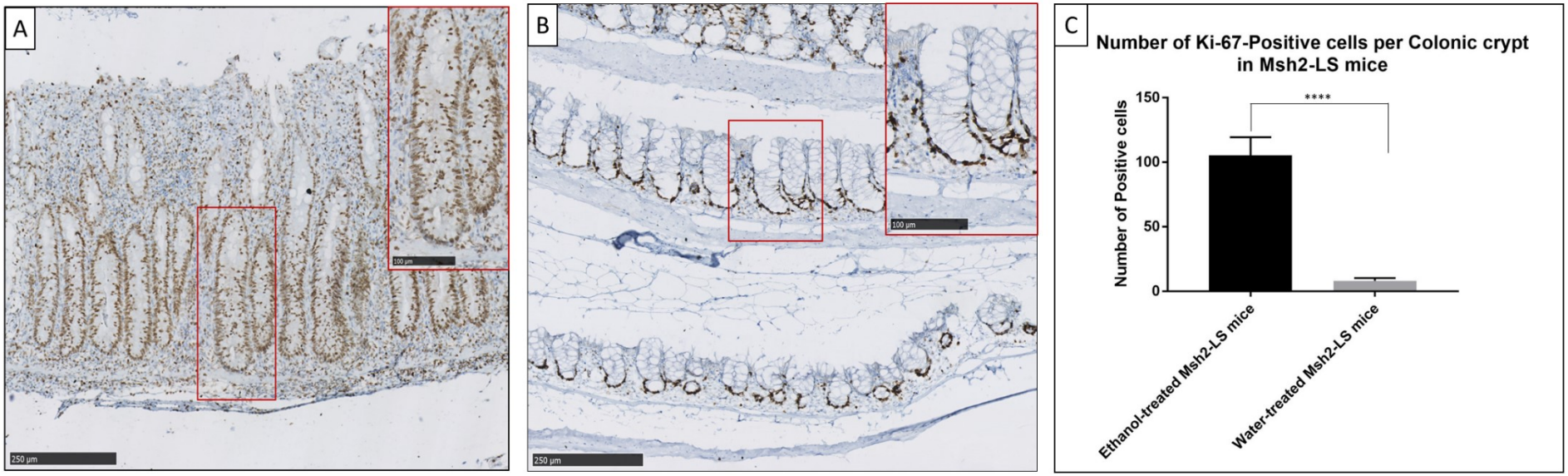

Figure 4.36: Immunohistochemical analysis of Ki-67 protein expression in large intestinal mucosal epithelium of *Msh2$^{flox/-}$; Lgr5CreERT2$^{+/-}$; mTmG$^{+/-}$* mice treated with either 20% of ethanol in drinking water (A) or normal/standard water (B). Numbers of Ki-67-positive cells per colonic crypt (further magnified in the upper right inset red rectangle in figure panels A and B) were counted using QuPath (C). Paired Students t Test, ****$p<0.0001$ vs. water (data shown as mean±SD, 30 crypts per mouse were analysed, n=6 mice in each group). Images taken from sections scanned using the Hamamatsu Nanozoomer and analysed with the Hamamatsu NDP Viewer software at 10X and 20X magnification (bar at lower left indicates 250µm, bar in red rectangle indicates 100µm).

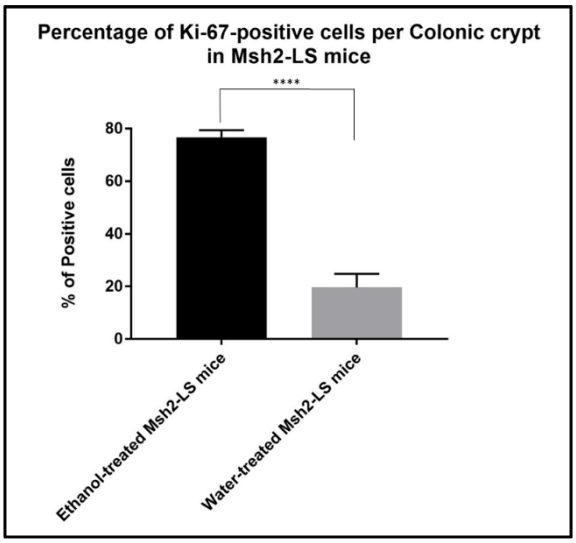

Figure 4.37: Percentage of Ki-67 protein expressing cells in large intestinal mucosal crypts of *Msh2$^{flox/-}$; Lgr5CreERT2$^{+/-}$; mTmG$^{+/-}$*mice treated with either 20% ethanol in drinking water or normal / standard water. Paired Students t Test, ****p<0.0001 vs. water (data shown as mean±SD, 30 crypts per mouse counted, n=6 mice from each group).

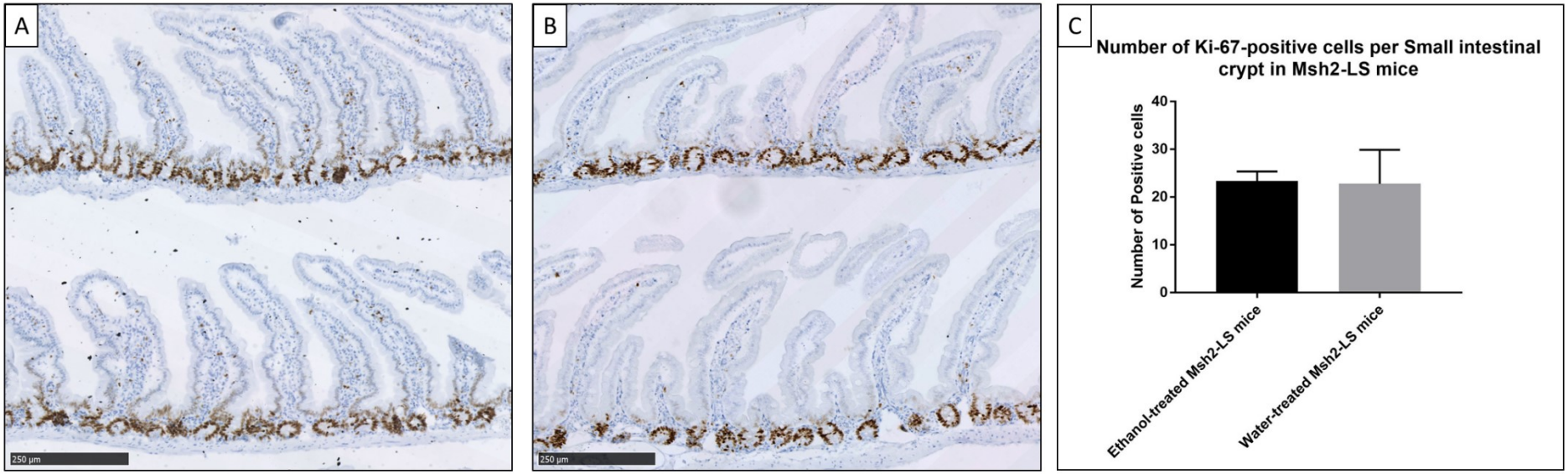

Figure 4.38: Immunohistochemical analysis of Ki-67 protein expression in small intestinal mucosa of *Msh2$^{flox/-}$; Lgr5CreERT2$^{+/-}$; mTmG$^{+/-}$* mice treated with either 20% ethanol in drinking water (A) or normal / standard drinking water (B). Ki-67-positive cells per colonic crypt/villus were counted using QuPath (C). Paired Students t Test, (data shown as mean±SD, 30 crypts/villi per mouse were analysed, n=6 mice in each group).No statistical differences were observed. Images taken from sections scanned using the Hamamatsu Nanozoomer and analysed with the Hamamatsu NDP Viewer software at 10X magnification (bar at lower left indicates 250µm).

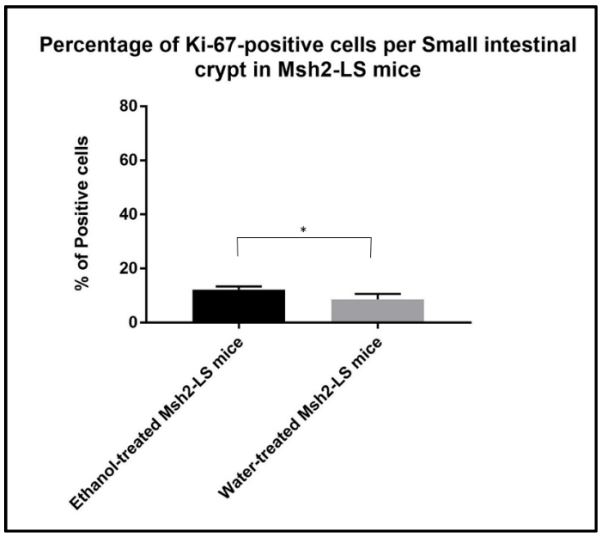

Figure 4.39: Percentage of Ki-67 protein expressing cells in small intestinal mucosa of *Msh2$^{flox/-}$; Lgr5CreERT2$^{+/-}$; mTmG$^{+/-}$* mice treated with either 20% ethanol in drinking water or normal / standard water. Paired Students t Test, *p=0.0172 vs. water (data shown as mean±SD, 30 crypts per mouse counted, n=6 mice from each group).

4.4.2.3 Beta-Catenin immunostaining of Msh2-LS murine small intestinal and colonic tissues

β-catenin is the key effector in the intracellular signal transduction of the Wnt signalling pathway (Cong et al., 2003). Normal colorectal tissue exhibits membranous and cytoplasmic localisation of β-catenin, whereas colorectal adenoma/adenocarcinoma shows nuclear β-catenin localization and thus β-catenin is regarded as a useful CRC biomarker (Lugli et al., 2007).

β-catenin IHC was performed with assistance from Marion Bacou using large intestinal samples from *Apc Min* mice that contained large intestinal adenomas (provided by Vidya Rajasekaran), and WT mice as β-catenin-positive and β-catenin-normal expression controls respectively (Figure 4.40). Whereas wildtype murine colonic epithelium showed membranous and cytoplasmic β-catenin light immunostaining, indicating absent activation of the Wnt signalling pathway, the *Apc-Min* murine adenomas showed increased brown nuclear β-catenin immunostaining in variable numbers of adenoma cells in a heterogeneous pattern, confirming dysregulation of Wnt signalling in this neoplastic intestinal epithelium.

The IHC analysis of β-catenin was performed on large intestinal adenomas and caecal adenomas from *Msh2$^{flox/-}$; Lgr5CreERT2$^{+/-}$; mTmG$^{+/-}$*mice. Analysed samples showed a heterogeneous pattern with variable numbers of adenoma cells showing positive β-catenin nuclear immunostaining due to accumulation and translocation of β-catenin in the nuclei (Figure 4.41).

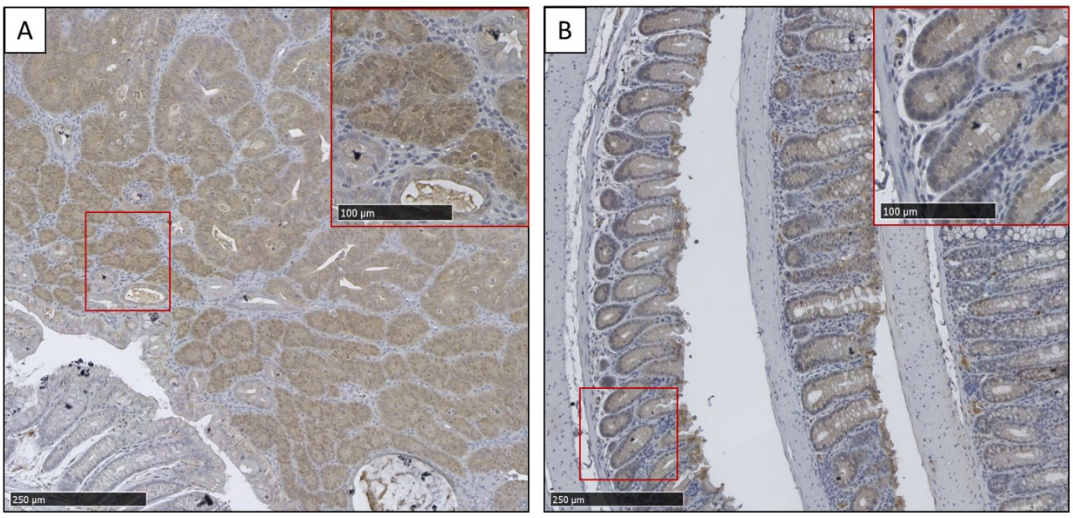

Figure 4.40: Immunohistochemical analysis of β-catenin protein expression and localisation in large intestinal mucosal adenoma and adjacent normal epithelium from a positive-control *Apc Min* mouse (A), in which the increased brown nuclear β-catenin staining in variable numbers of adenoma cells in a heterogeneous pattern confirms dysregulation of Wnt signalling in this neoplastic intestinal epithelium (further magnified in the red rectangle); and from a normal control *WT* mouse (B), in which the membranous and cytoplasmic β-catenin light staining indicates normal large intestinal mucosal epithelium without activation of the Wnt signalling pathway (further magnified in the red rectangle). Images taken from sections scanned using the Hamamatsu Nanozoomer and analysed with the Hamamatsu NDP Viewer software at 10X and 20X magnification (bar at lower left indicates 250µm, bar in red rectangle indicates 100µm).

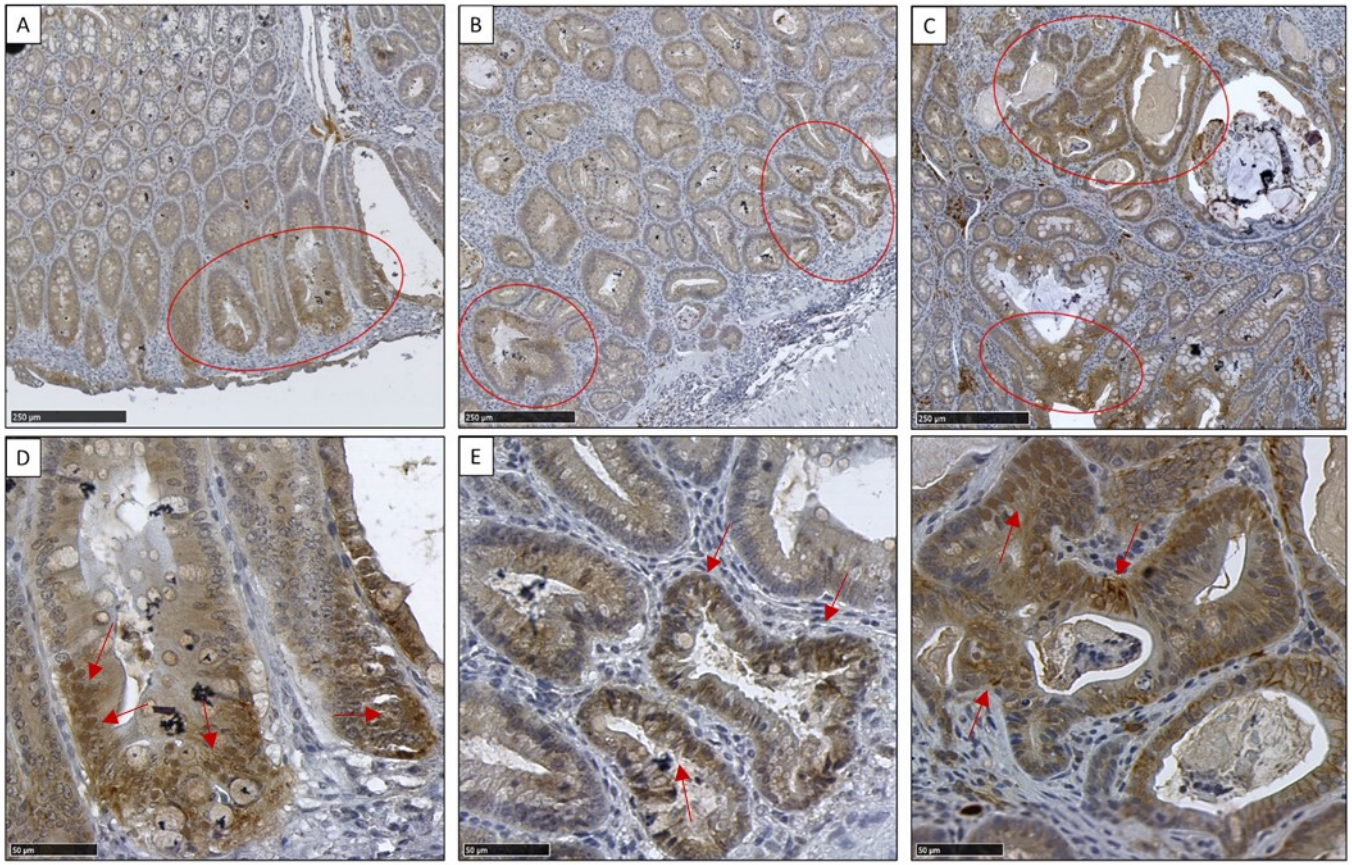

Figure 4.41: Representative images of immunohistochemical analysis of β-catenin protein expression and localisation in intestinal adenomas of *Msh2$^{flox/-}$; Lgr5CreERT2$^{+/-}$; mTmG$^{+/-}$*mice treated with 20% ethanol in drinking water. Variable areas of positive β-catenin nuclear immunostaining in adenomatous cells were observed in both caecal adenomas (A) and colonic adenomas (B and C), indicated by the red ovals. Selected areas (red ovals) within images in panels A-C are further magnified in panels D-F, and clusters of positive β-catenin nuclei are indicated by the red arrows. Images taken from sections scanned using the Hamamatsu Nanozoomer and analysed with the Hamamatsu NDP Viewer software at 10X and 40X magnification (bar at lower left indicates 250µm and 50 µm).

4.4.2.4 DNA damage response evaluation by immunohistochemistry of Msh2-LS murine small intestinal and colonic tissues

4.4.2.4.1 DNA damage response evaluation by Gamma-H2AX immunostaining of Msh2-LS murine small intestinal and colonic tissues

In order to evaluate the presence and extent of DNA damage, y-H2AX immunostaining was used. Y-H2AX is the key player in signalling and activating DNA damage repair pathways and for this it is considered a specific molecular marker for monitoring DNA damage (Mah et al., 2010).

We used colonic tissue samples from WT mice and TMZ-treated Msh2-LS mice as negative and positive y-H2AX expression controls respectively (Figure 4.42). The lack of IHC DAB-brown staining in all of the colonic crypts of the WT mice confirmed the lack of y-H2AX expression. In contrast, the widespread presence of IHC DAB-brown staining in colonic crypts of the TMZ-treated Msh2-LS murine colon confirmed positive y-H2AX immunostaining technique.

IHC analysis of y-H2AX showed large and significant differences in the number of intestinal y-H2AX-positive cells between the EtOH_*Msh2*$^{fl\ KO}$ murine colon and the H_2O_*Msh2*$^{fl\ KO}$ murine colon (Figure 4.43). The percentage of y-H2AX-positive cells per crypt was significantly higher in EtOH_*Msh2*$^{fl\ KO}$ mice (35%) compared with H_2O_*Msh2*$^{fl\ KO}$ mice (0.4%) (Figure 4.43C), consistent with ethanol/acetaldehyde induced DNA damage. The comparative analysis of SI y-H2AX expression between EtOH_*Msh2*$^{fl\ KO}$ and H_2O_*Msh2*$^{fl\ KO}$ mice didn't show any differences, as EtOH_*Msh2*$^{fl\ KO}$ and H_2O_*Msh2*$^{fl\ KO}$ murine SI showed no y-H2AX-positive cells (Figure 4.44). EtOH_*Msh2*$^{fl\ KO}$ murine large intestinal adenomas showed high y-H2AX expression (Figure 4.45).

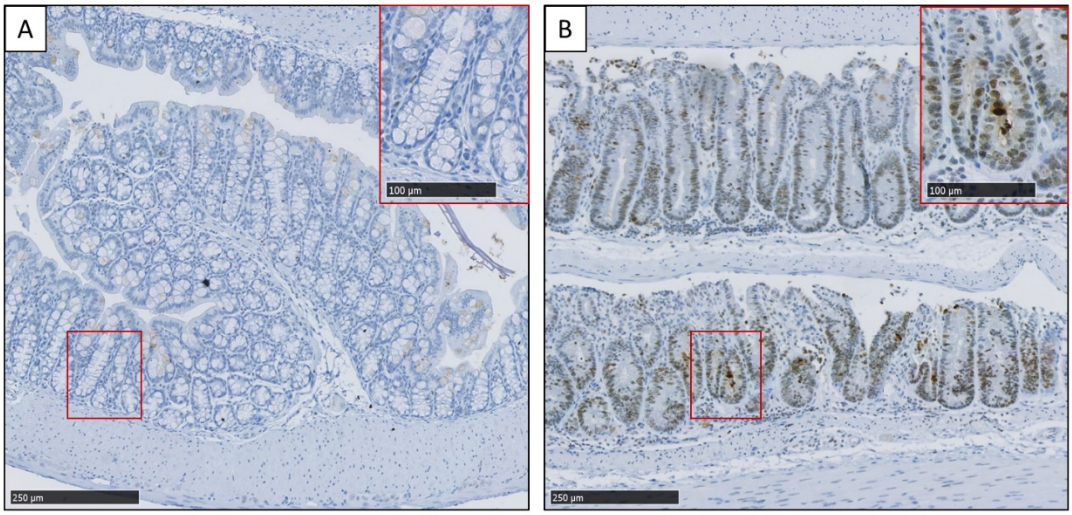

Figure 4.42: Immunohistochemical analysis of y-H2AX protein expression in large intestinal mucosal epithelium from a negative-control WT mouse (A), in which the lack of DAB brown staining indicates negative y-H2AX expression in all crypts (further magnified in the upper right inset red rectangle); and from a positive-control TMZ-treated Msh2-LS mouse (B), in which the brown staining confirms the presence of y-H2AX expression in large intestinal mucosal epithelium consistent with TMZ-induced widespread DNA damage (further magnified in the upper right inset red rectangle). Images taken from sections scanned using the Hamamatsu Nanozoomer and analysed with the Hamamatsu NDP Viewer software at 10X and 20X magnification (bar at lower left indicates 250µm, bar in red rectangle indicates 100µm).

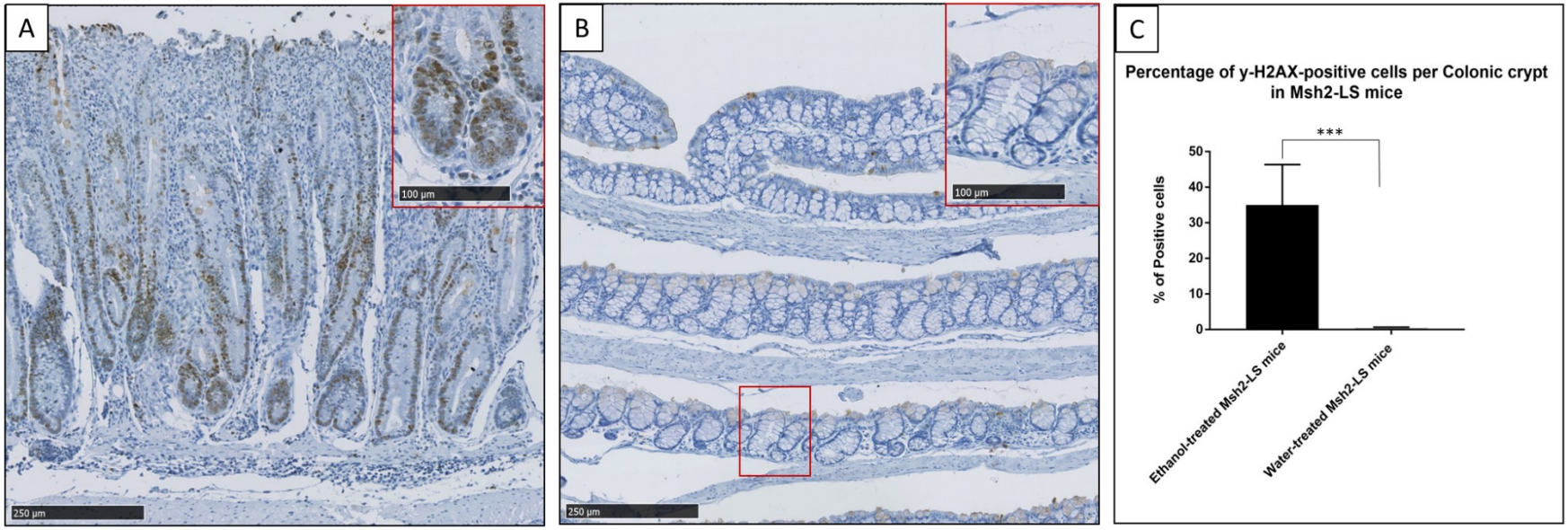

Figure 4.43: Immunohistochemical analysis of y-H2AX protein expression in large intestinal mucosal epithelium of *Msh2$^{flox/-}$; Lgr5CreERT2$^{+/-}$; mTmG$^{+/-}$* mice treated with either 20% ethanol in drinking water (A) or normal/standard water (B). Gamma-H2AX-positive cells in colonic crypts (further magnified in the upper right inset red rectangle in figure panel A) were observed in ethanol-treated Msh2-LS (EtOH_*Msh2$^{fl\,KO}$*) mice but not in water-treated Msh2-LS (H_2O_*Msh2$^{fl\,KO}$*) mice (further magnified in the upper right inset red rectangle in figure panel B). Numbers of y-H2AX-positive cells per colonic crypt were counted using QuPath (C) showing a large and statistically significant difference. Paired Students t-Test, ***p<0.0009 vs. water (data shown as mean±SD, 40 crypts per mouse were analysed, n=4 mice in each group). Images taken from sections scanned using the Hamamatsu Nanozoomer and analysed with the Hamamatsu NDP Viewer software at 10X and 20X magnification (bar at lower left indicates 250µm, bar in red rectangle indicates 100µm).

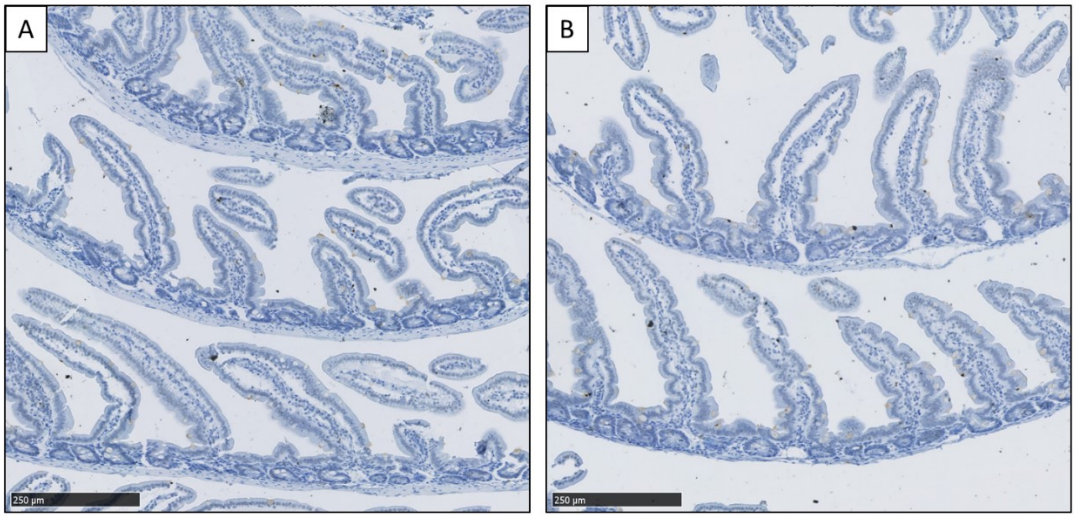

Figure 4.44: Immunohistochemical analysis of y-H2AX protein expression in small intestinal mucosa of *Msh2$^{flox/-}$; Lgr5CreERT2$^{+/-}$; mTmG$^{+/-}$*mice treated with either 20% ethanol in drinking water (A) or normal / standard drinking water (B). No y-H2AX-positive cells were observed in either sample. Images taken from sections scanned using the Hamamatsu Nanozoomer and analysed with the Hamamatsu NDP Viewer software at 10X magnification (bar at lower left indicates 250µm).

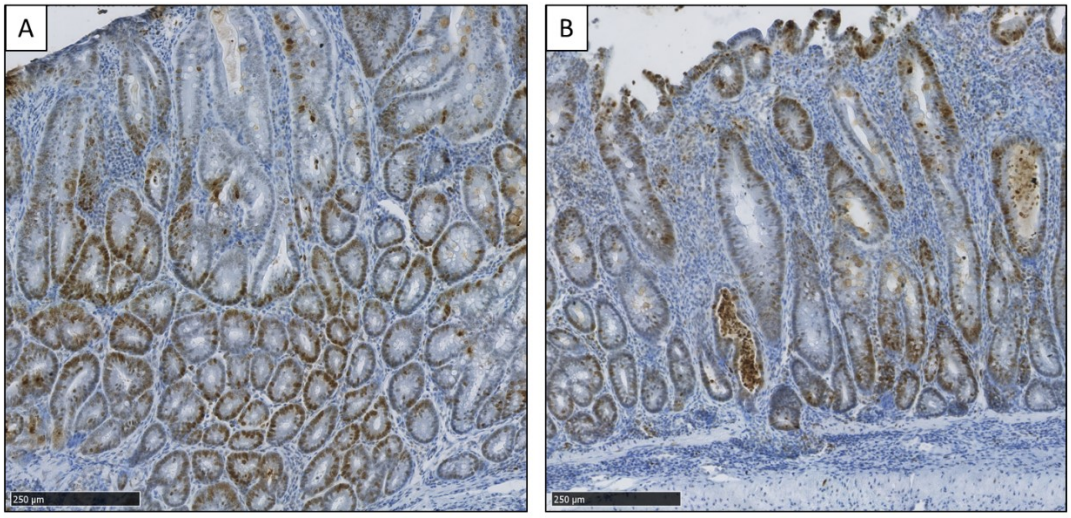

Figure 4.45: Representative images of y-H2AX immunohistochemical staining in a caecal adenoma (A) and a large intestinal adenoma (B) from 2 ethanol-treated *Msh2$^{flox/-}$; Lgr5CreERT2$^{+/-}$; mTmG$^{+/-}$* mice. In both examples, there are numerous y-H2AX-positive cells within the regions of dysplastic cells in the adenomas. Images taken from sections scanned using the Hamamatsu Nanozoomer and analysed with the Hamamatsu NDP Viewer software at 10X magnification (bar at lower left indicates 250µm).

4.4.2.4.2 DNA damage response evaluation by p53 immunostaining of Msh2-LS murine small intestinal and colonic tissues

The presence of DNA damage induces p53 pathway activation, and this is involved in maintaining genomic stability following DNA damage (and other stimuli) via transcriptional activation of a variety of response pathways, such as apoptosis, cell cycle arrest and DNA repair (Levine, 1997; Williams & Schumacher, 2016). Upon DNA damage, increased p53 levels are detected in the cell which can be demonstrated immunohistochemically as a greater proportion of cells containing moderate to high (but variable) nuclear staining of p53 in individual cells (referred as p53 "wildtype pattern") (Köbel et al., 2016; Lakin & Jackson, 1999).

We used colonic tissue samples from WT mice and TMZ-treated Msh2-LS mice as p53-normal and p53-positive expression (resulting from TMZ-induced DNA damage) controls respectively (Figure 4.46). Whereas wildtype murine colonic epithelium showed membranous and cytoplasmic p53 light immunostaining, indicating low-level non-induced expression of p53, the TMZ-treated Msh2-LS murine colonic epithelium showed moderately to highly increase brown nuclear p53 immunostaining in variable numbers of cells, confirming p53-DNA damage response activation.

IHC analysis of p53 showed large and significant differences in the number of intestinal p53-positive cells between the EtOH_*Msh2*$^{fl\ KO}$ murine colon and the H_2O_*Msh2*$^{fl\ KO}$ murine colon (Figure 4.7). The percentage of cells with either moderate or high levels of p53-positive nuclear staining per crypt was significantly higher in EtOH_*Msh2*$^{fl\ KO}$ mice (41.3%) compared with H_2O_*Msh2*$^{fl\ KO}$ mice (10.8%) (Figure 4.47C), consistent with ethanol/acetaldehyde induced DNA damage.

The percentage of small intestinal p53-positive cells per crypt was higher in EtOH_*Msh2*$^{fl\ KO}$ mice (15%) compared with H_2O_*Msh2*$^{fl\ KO}$ mice (5.2%) (Figure 4.48). EtOH_*Msh2*$^{fl\ KO}$ murine large intestinal adenomas, both colonic and caecal, showed high percentages of p53-positive cells, with variably moderate to high nuclear p53 positivity and some negative nuclei in a "p53 wildtype" pattern indicative of widespread response to DNA damage, rather than a "p53 overexpression" or "p53 null" pattern associated with p53 mutation (Figure 4.49).

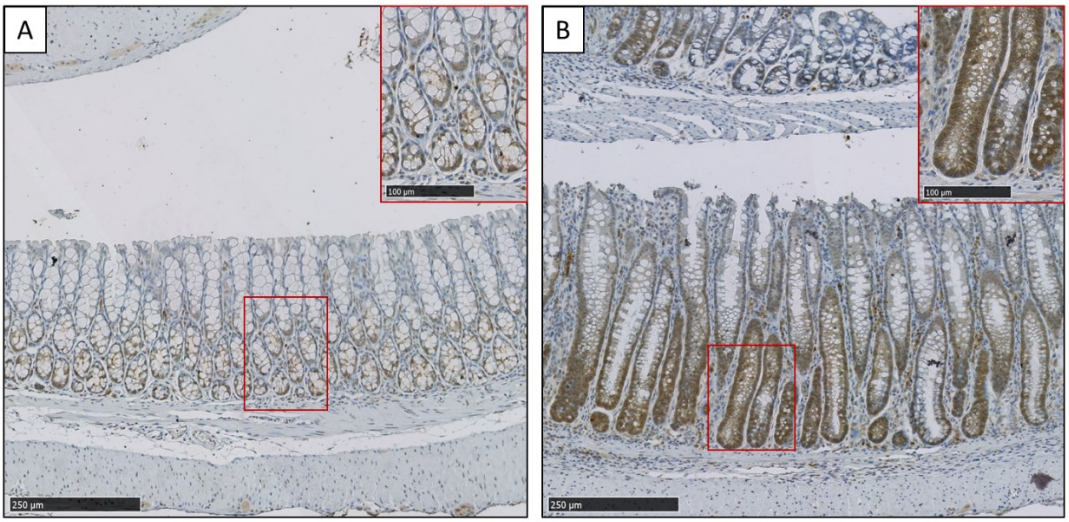

Figure 4.46: Immunohistochemical analysis of p53 protein expression and localisation in large intestinal mucosal normal epithelium from a normal control *WT* mouse (A), in which the membranous and cytoplasmic p53 light staining indicates normal low-level non-induced p53 expression (further magnified in the red rectangle); and from a positive-control TMZ-treated Msh2-LS mouse (B), in which the increased brown nuclear p53 staining in variable numbers of colonic epithelial cells confirms the presence of DNA damage (further magnified in the red rectangle). Images taken from sections scanned using the Hamamatsu Nanozoomer and analysed with the Hamamatsu NDP Viewer software at 10X and 20X magnification (bar at lower left indicates 250µm, bar in red rectangle indicates 100µm).

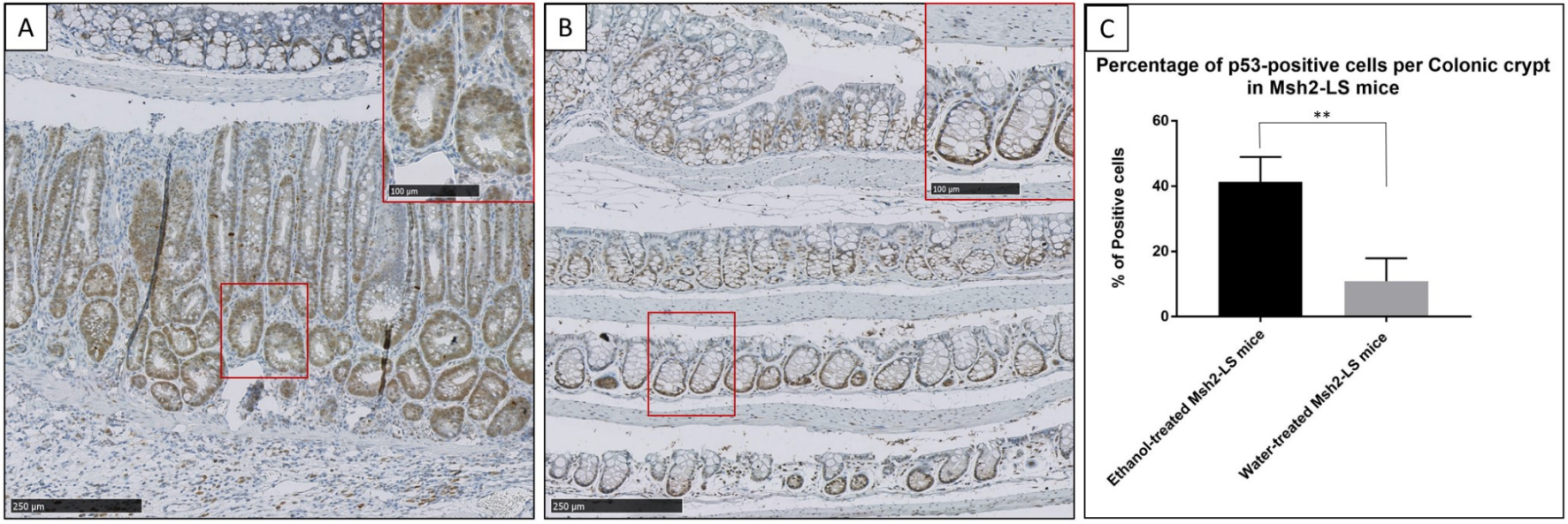

Figure 4.47: Representative images of immunohistochemical analysis of p53 protein expression in large intestinal mucosal epithelium of *Msh2$^{flox/-}$; Lgr5CreERT2$^{+/-}$; mTmG$^{+/-}$* mice treated with either 20% ethanol in drinking water (A) or normal/standard water (B). The percentage of positive p53-positive nuclei in colonic crypts in ethanol-treated Msh2-LS (EtOH_*Msh2$^{fl\ KO}$*) mice (further magnified in the upper right inset red rectangle in figure panel A) was higher compared with water-treated Msh2-LS (H_2O_*Msh2$^{fl\ KO}$*) mice (further magnified in the upper right inset red rectangle in figure panel B). Numbers of cells with positive p53 nuclear staining per colonic crypt were counted using QuPath (C), showing a statistically significant difference. Paired Students t-Test, **p<0.0011 vs. water (data shown as mean±SD, 40 crypts per mouse were analysed, n=4 mice in each group). Images taken from sections scanned using the Hamamatsu Nanozoomer and analysed with the Hamamatsu NDP Viewer software at 10X and 20X magnification (bar at lower left indicates 250µm, bar in red rectangle indicates 100µm).

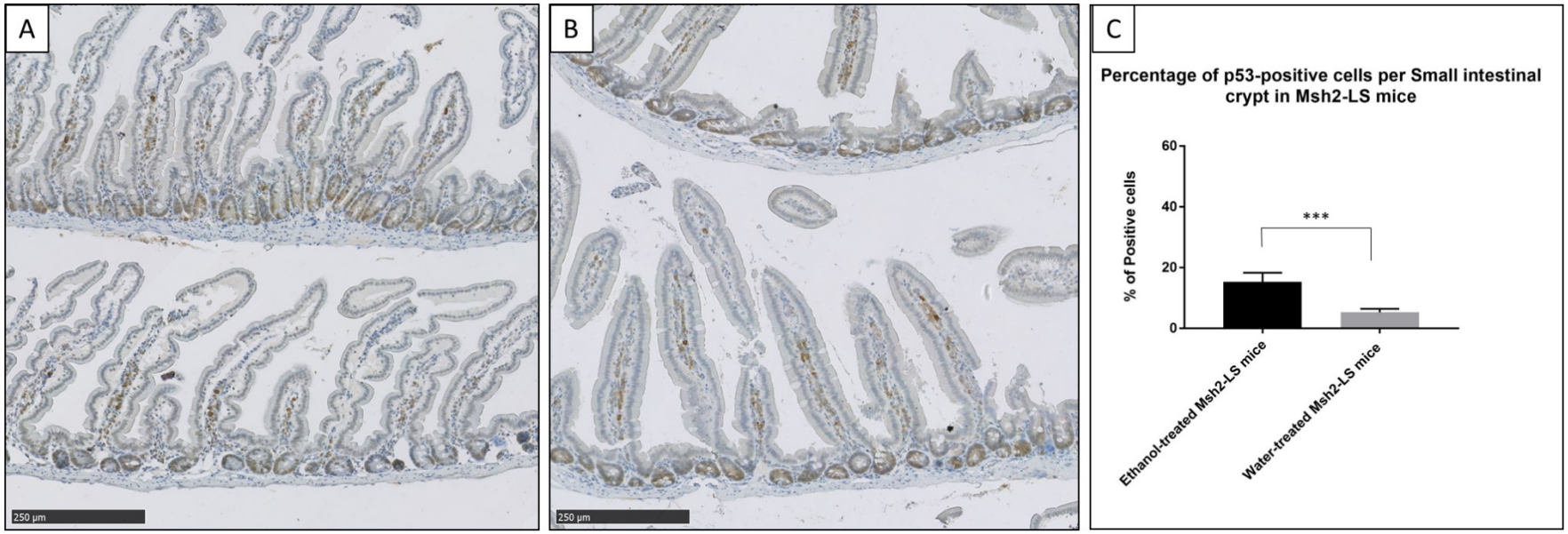

Figure 4.48: Representative images of immunohistochemical analysis of p53 protein expression in small intestinal mucosal epithelium of *Msh2$^{flox/-}$; Lgr5CreERT2$^{+/-}$; mTmG$^{+/-}$* mice treated with either 20% ethanol in drinking water (A) or normal/standard water (B). The percentage of positive p53-nuclear stained cells in small intestinal crypts was higher in ethanol-treated Msh2-LS (EtOH_*Msh2$^{fl\ KO}$*) mice compared with water-treated Msh2-LS (H_2O_*Msh2$^{fl\ KO}$*) mice. Numbers of cells with positive p53 nuclear staining per small intestinal crypt were counted using QuPath (C), showing a statistically significant difference. Paired Students t-Test, ***p<0.0008 vs. water (data shown as mean±SD, 40 crypts per mouse were analysed, n=4 mice in each group). Images taken from sections scanned using the Hamamatsu Nanozoomer and analysed with the Hamamatsu NDP Viewer software at 10X magnification (bar at lower left indicates 250µm).

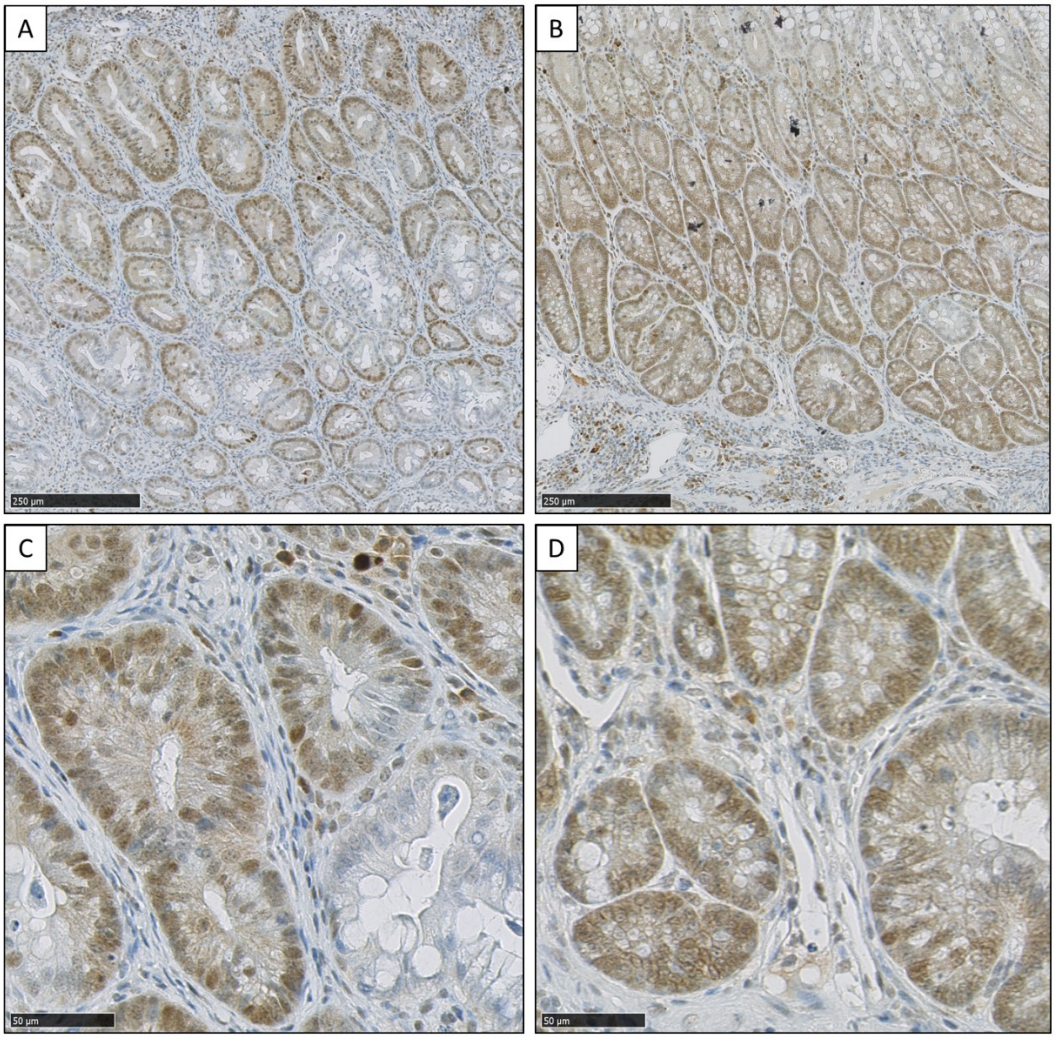

Figure 4.49: Representative images of p53 immunohistochemical staining in a colonic adenoma (A) and a caecal adenoma (B), from ethanol-treated 2 *Msh2*$^{flox/-}$*; Lgr5CreERT2*$^{+/-}$*; mTmG*$^{+/-}$ mice. In both examples, there are numerous p53-positive nuclei (variably moderate to high p53 nuclear staining with some p53-negative nuclei) within the regions of dysplastic cells in the adenomas. Images are further magnified in panels C and D. Images taken from sections scanned using the Hamamatsu Nanozoomer and analysed with the Hamamatsu NDP Viewer software at 10X and 40X magnification (bar at lower left indicates 250µm and 50 µm).

4.4.2.5 Cleaved Caspase-3 immunostaining of Msh2-LS murine small intestinal and colonic tissues

Caspase-3 (Cas3) is a key executive member of the caspase cascade, with cysteine-aspartic acid protease activity, that acts as one of the key effectors of cell death by apoptosis. IHC for cCas3 was performed to detect the incidence of apoptotic events in tumour and normal tissue samples from EtOH_*Msh2*$^{fl\ KO}$ mice and H_2O_*Msh2*$^{fl\ KO}$ mice. Colonic mucosal tissue samples from WT mice and TMZ-treated Msh2-LS mice were used as negative and positive controls respectively (Figure 4.50). In WT murine colonic mucosal epithelium, almost no apoptotic bodies were detected, apart from rare occurrences, indicating rare apoptotic events detectable in normal colonic mucosal epithelium. In contrast, the TMZ-treated Msh2-LS murine colonic mucosal epithelium showed increased easily detectable apoptotic bodies, mostly at or around the bases of colonic crypts, confirming that apoptotic events occurred in association with TMZ-exposure of the colonic mucosal epithelium.

IHC analysis of cCas3 with quantification of cCas3-positive apoptotic bodies, showed significant differences in the numbers of cCas3-positive apoptotic bodies per 30 colonic crypts per mouse between the EtOH_*Msh2*$^{fl\ KO}$ murine colonic epithelium and the H_2O_*Msh2*$^{fl\ KO}$ murine colonic epithelium, with significantly higher number of cCas3+ apoptotic bodies in EtOH_*Msh2*$^{fl\ KO}$ mice compared with no detectable cCas3+ apoptotic bodies in H_2O_*Msh2*$^{fl\ KO}$ mice (Figure 4.51), consistent with increased apoptosis associated with colonic epithelial exposure to ethanol/acetaldehyde. EtOH_*Msh2*$^{fl\ KO}$ murine large intestinal adenomas showed no detectable cCas3+ apoptotic bodies, indicating rare to no apoptotic events in dMMR colonic tumours (Figure 4.52).

IHC analysis of cCas3 of EtOH_*Msh2*$^{fl\ KO}$ murine small intestinal epithelium and the H_2O_*Msh2*$^{fl\ KO}$ murine small intestinal epithelium failed on technical grounds.

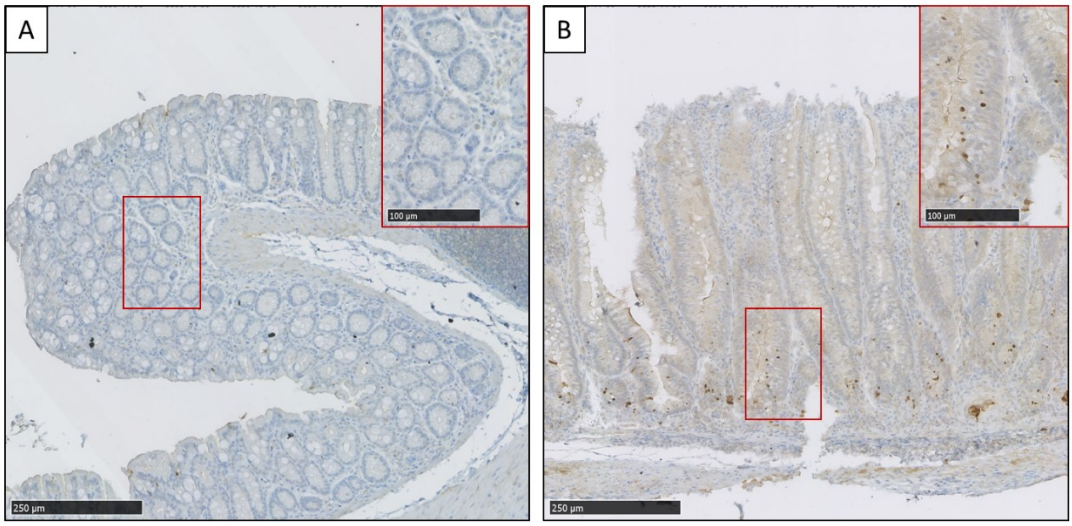

Figure 4.50: Immunohistochemical analysis of cCas3. In a representative WT negative control mouse (A), the lack of brown staining indicates absence of cCas3 positivity, reflecting the absence of apoptotic bodies in the colonic crypt epithelium analysed here (further magnified in the upper right inset red rectangle). In a representative TMZ-treated Msh2-LS positive control mouse (B), in the large intestinal mucosal crypt epithelium (mostly in the lower third of the crypt), there are scattered strongly brown staining apoptotic bodies with small round condensed chromatin nuclear particles typical of apoptosis, that are strongly positive for cCas3, on a background of pale brown non-specific staining of cellular cytoplasm (further magnified in the upper right inset red rectangle). Images taken from sections scanned using the Hamamatsu Nanozoomer and analysed with the Hamamatsu NDP Viewer software at 10X and 20X magnification (bar at lower left indicates 250µm, bar in red rectangle indicates 100µm).

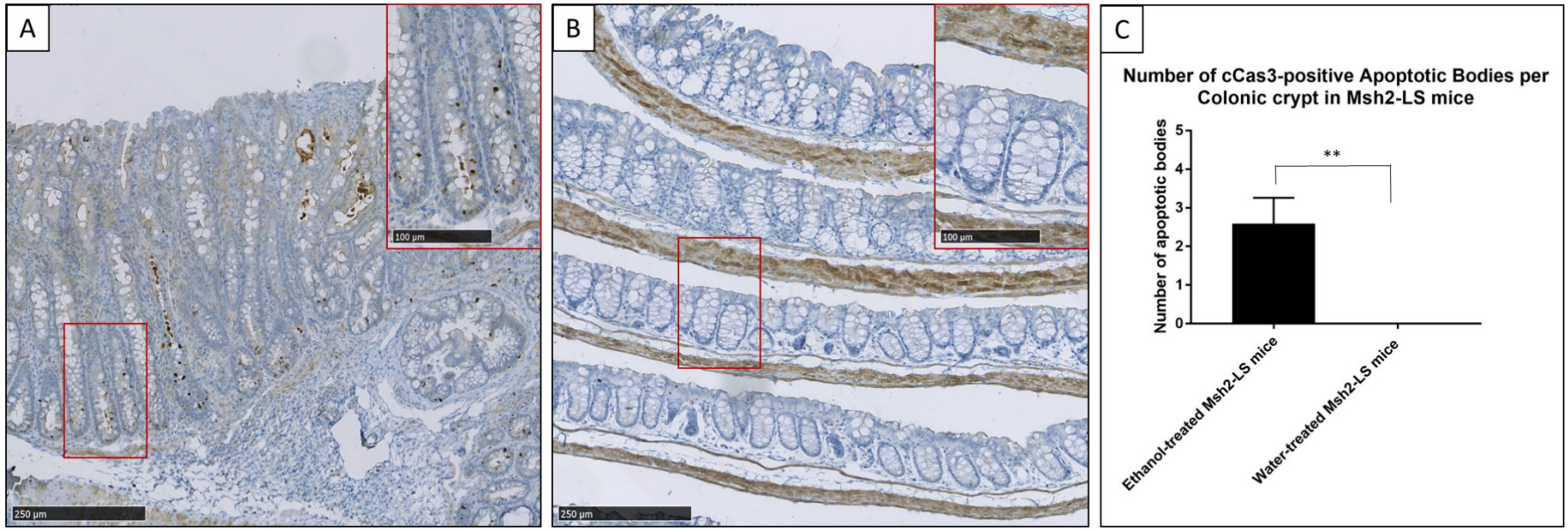

Figure 4.51: Representative images of immunohistochemical analysis of cCas3 in large intestinal mucosal epithelium of induced *Msh2$^{flox/-}$; Lgr5CreERT2$^{+/-}$; mTmG$^{+/-}$* mice treated with either 20% ethanol in drinking water (A), or normal/standard water (B). The number of apoptotic bodies positive for cCas3 in the colonic crypts of ethanol-treated Msh2-LS (EtOH_*Msh2$^{fl\ KO}$*) mice (further magnified in the upper right inset red rectangle in figure panel A) was significantly higher compared with that for water-treated Msh2-LS (H_2O_*Msh2$^{fl\ KO}$*) mice, in which no apoptotic bodies were detected (further magnified in the upper right inset red rectangle in figure panel B). Numbers of cCas3-positive apoptotic bodies per colonic crypt were counted manually (C), showing a statistically significant difference. Paired Students t-Test, **p=0.0026 vs. water (data shown as mean±SD, 30 crypts per mouse were analysed, n=3 mice in each group). Images taken from sections scanned using the Hamamatsu Nanozoomer and analysed with the Hamamatsu NDP Viewer software at 10X and 20X magnification (bar at lower left indicates 250µm, bar in red rectangle indicates 100µm).

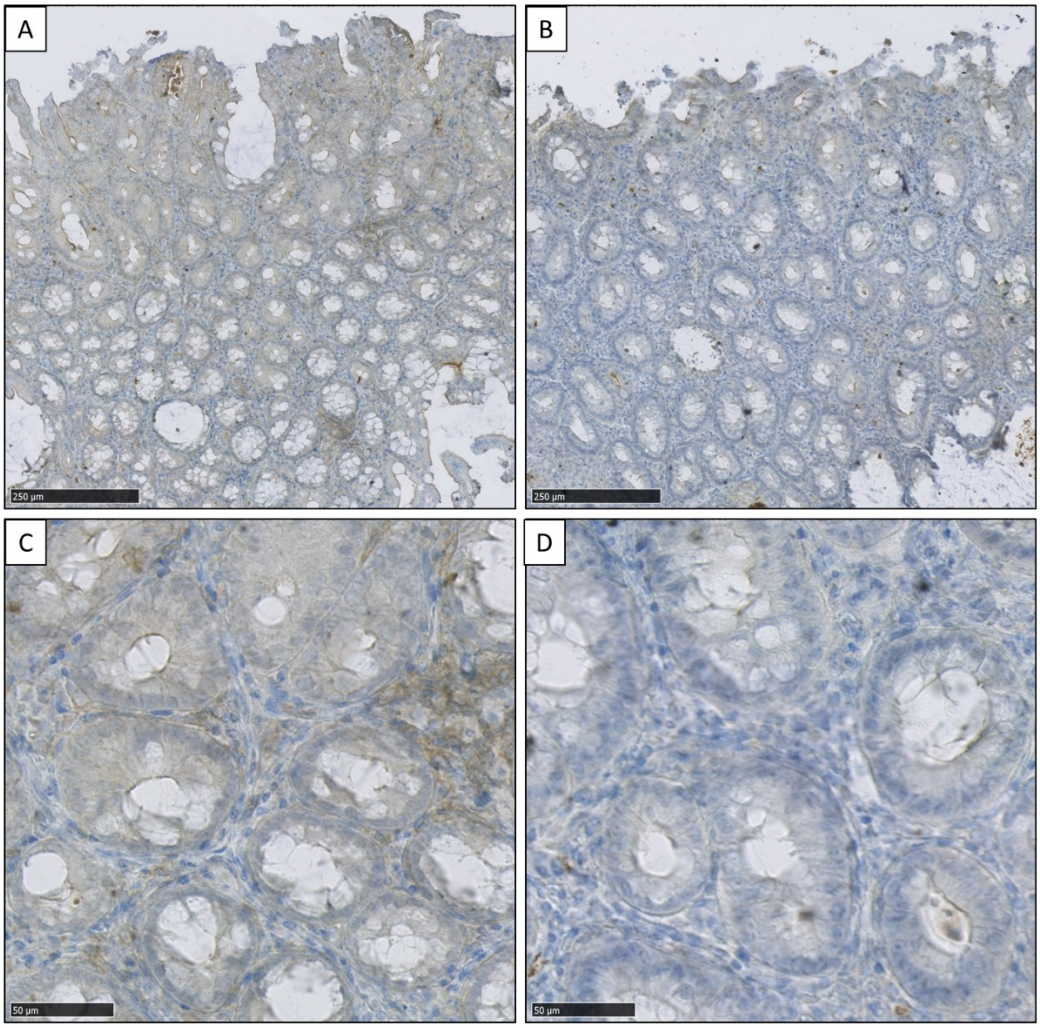

Figure 4.52: Representative images of immunohistochemical analysis of cCas3 in 2 large intestinal adenomas (A and B), from 2 ethanol-treated *Msh2$^{flox/-}$; Lgr5CreERT2$^{+/-}$; mTmG$^{+/-}$* mice. In both examples, there are almost no apoptotic bodies within the regions of dysplastic cells in the adenomas, indicating rare apoptotic events detectable in dMMR colonic adenoma. Images are further magnified in panels C and D. Images taken from sections scanned using the Hamamatsu Nanozoomer and analysed with the Hamamatsu NDP Viewer software at 10X and 40X magnification (bar at lower left indicates 250µm and 50 µm).

4.4.2.6 Immune cells infiltrating caecal adenomas from the Msh2-LS murine model

The immune system has an important role in tumour incidence, prognosis and response to immunotherapy (Gonzalez et al., 2018). In dMMR cells, predictable mutations can and do occur in repetitive protein coding sequences and result in frameshift peptides (FSPs) (Sæterdal et al., 2001). Such FSPs are novel antigens and elicit both humoral and cellular immune responses, which are seen as tumour-infiltrating lymphocytes (TILs) around the dMMR crypts in LS patients as well as in dMMR cancers, both sporadic and due to LS (Linnebacher et al., 2001; Reuschenbach et al., 2010; Seth et al., 2018).

To characterize the immune system response to Msh2-LS murine intestinal dMMR tumours, these were studied immunohistochemistry for a range of infiltrating immune cells, in collaboration with Dr. Seth Coffelt from the Beatson Cancer Institute, Glasgow. A panel of antibodies to B-cell markers, T-cell markers and macrophage markers (listed in Materials and Methods, Table 2.12) was selected and used to immunohistochemically investigate well-fixed caecal adenomas from the Msh2-LS model.

Pilot immunohistochemistry experiments were performed on EtOH_Msh2$^{fl\ KO}$ caecal adenomas. Positive immunostaining was observed for CD4 (murine T-helper cells), B220 (murine-specific B cells), CD8 (T-cytotoxic cells), F480 (murine macrophages) and Ly6G (murine myeloid cells including monocytes, macrophages, granulocytes, neutrophils) in the stroma surrounding the dysplastic crypts in EtOH_*Msh2*$^{fl\ KO}$ caecal adenomas. By contrast, we detected very few cells or no positive cells by immunostaining for any of the above immune cell markers in Msh2-LS murine morphologically normal caecal mucosa or surrounding stroma (Figure 4.53). These observations are consistent with an active immune response to dMMR adenomatous epithelial glands in this model. These pilot experiments were discontinued as a result of the COVID-19 restrictions on wet bench lab work.

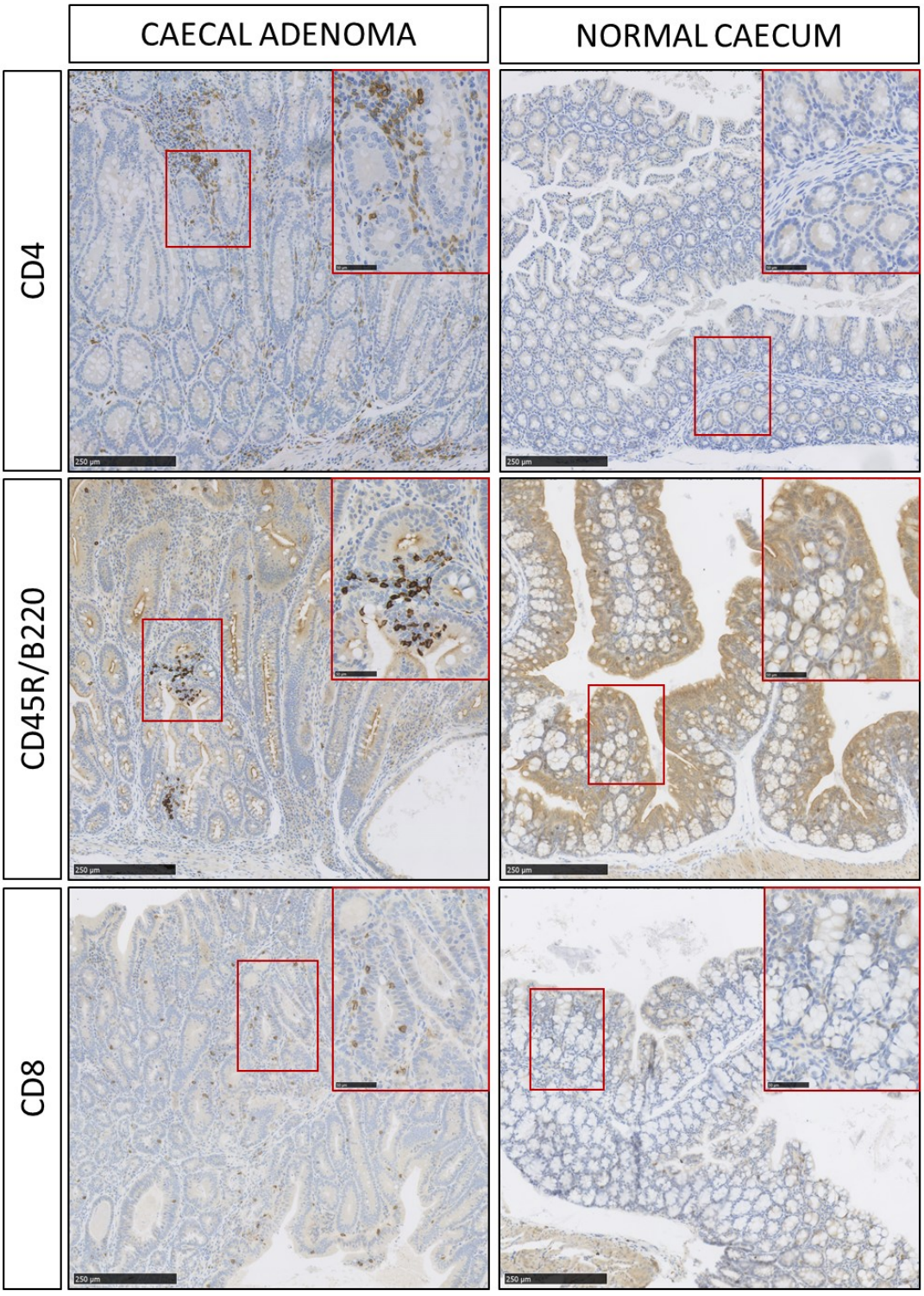
CAECAL ADENOMA
NORMAL CAECUM
CD4
CD45R/B220
CD8
250 µm

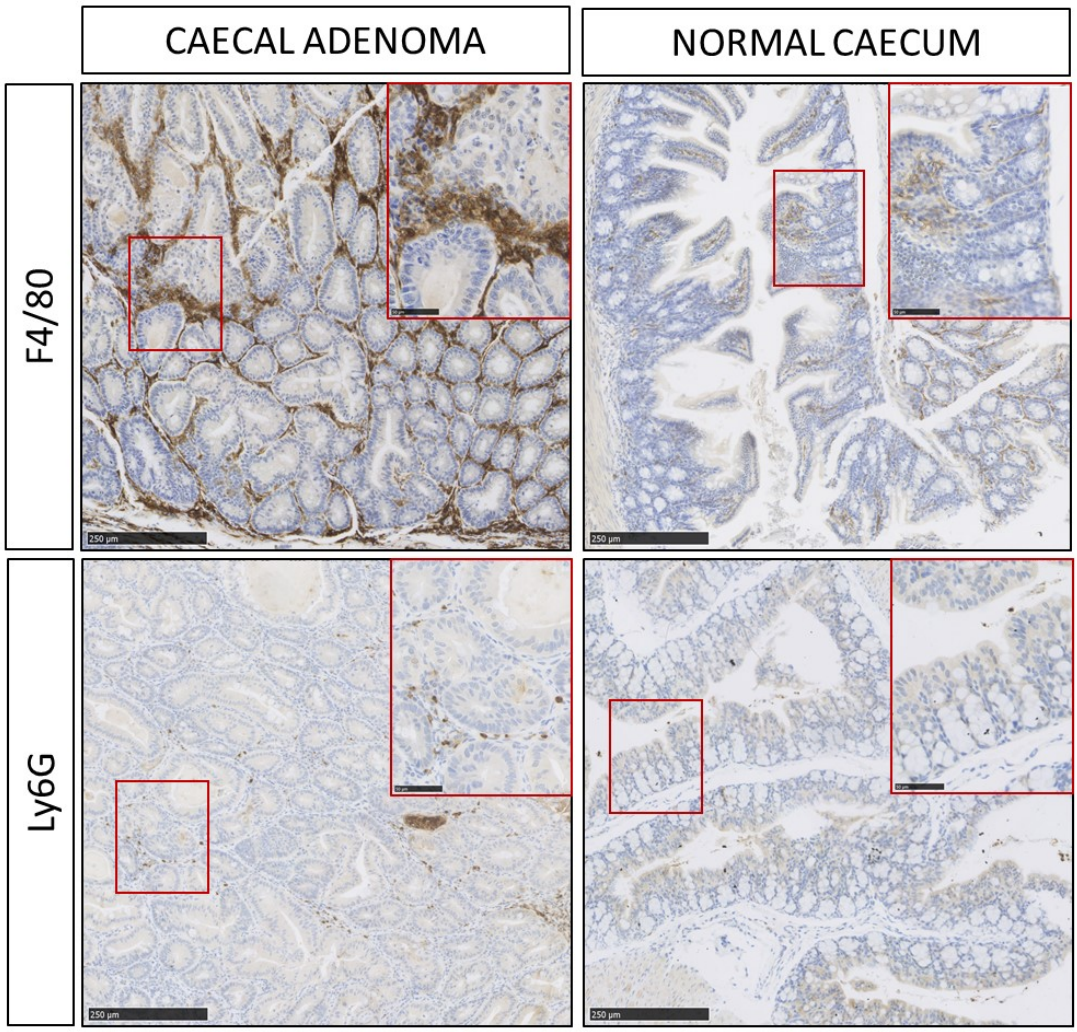

Figure 4.53: Representative images of immunohistochemical analysis of infiltrating immune cells in caecal adenomas and normal caecal mucosa, from ethanol-treated *Msh2$^{flox/-}$; Lgr5CreERT2$^{+/-}$; mTmG$^{+/-}$* mice. The images show DAB-brown staining for CD4, B220, CD8, F4/80 and Ly6G in Msh2-LS caecal neoplastic tissue (left column) compared with very few or no positive cells in Msh2-LS caecal normal tissue (right column). Images taken from sections scanned using the Hamamatsu Nanozoomer and analysed with the Hamamatsu NDP Viewer software at 10X and 40X magnification (bar at lower left indicates 250µm and 50 µm).

4.5 Plasma acetaldehyde concentrations from the Msh2-LS mouse model with and without ethanol treatment.

4.5.1 Methods

During the dissection procedure, blood was harvested from the Msh2-LS mice by post-mortem cardiac puncture. Blood was collected in a heparinized tube and centrifuged at 3000 X g for 15 min at 4℃ to allow blood fractionation. Acetaldehyde is a highly volatile compound, classified as a volatile organic compound (VOC) (Missia et al., 2010; Sarigiannis et al., 2011). To preserve the acetaldehyde concentration, plasma was collected in cryo-tubes and immediately snap-frozen in liquid nitrogen and stored at −80℃ until analysis. Plasma samples were analysed in a single batch and plasma acetaldehyde concentrations were determined using an enzymatic acetaldehyde assay kit (K-ACHYD; Megazyme), as described in Materials and Methods.

4.5.2 Results

Plasma acetaldehyde levels were analysed comparing samples from EtOH_*Msh2*$^{fl\,KO}$ mice and H_2O_*Msh2*$^{fl\,KO}$ mice as well as comparing these with EtOH_*Msh2*^{fl} mice and H_2O_*Msh2*^{fl} mice after long term ethanol treatment (experimental mice were treated with ethanol for between 8 and 48 weeks prior to sacrifice).

Plasma acetaldehyde levels were significantly higher in EtOH_*Msh2*$^{fl\,KO}$ mice compared with H_2O_*Msh2*$^{fl\,KO}$ mice (p=0.0019) (Figure 4.54). The difference in plasma acetaldehyde levels between EtOH_*Msh2*^{fl} mice and H_2O_*Msh2*^{fl} mice did not show any statistically significant difference. This is probably due to the small number of samples (n=4) used in the plasma acetaldehyde assay of non-induced Msh2-LS mice. Plasma acetaldehyde levels in EtOH_*Msh2*$^{fl\ KO}$ mice were slightly higher compared with EtOH_*Msh2*^{fl} mice, but this difference was not statistically significant.

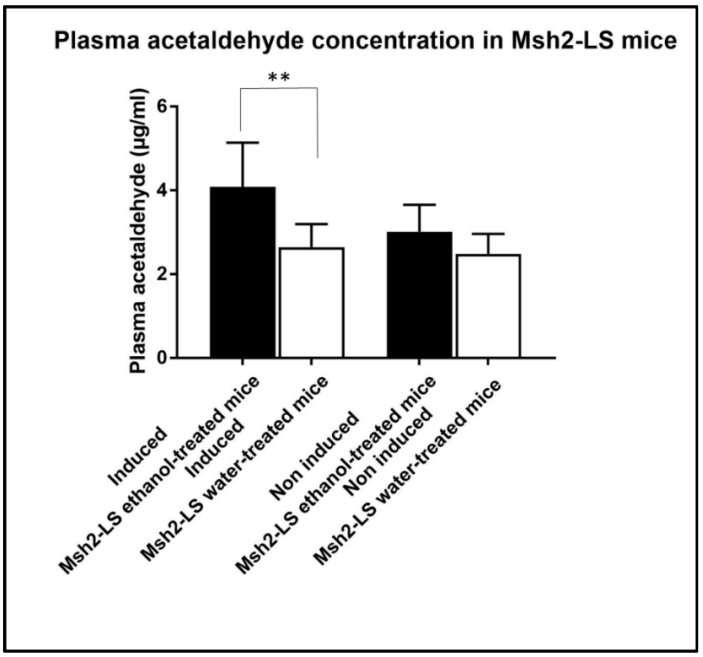

Figure 4.54: Plasma acetaldehyde concentrations in ethanol-treated Tamoxifen-induced Msh2-LS (EtOH_*Msh2*$^{fl\ KO}$) and water-treated Tamoxifen-induced Msh2-LS (H_2O_*Msh2*$^{fl\ KO}$) mice and ethanol-treated non-induced Msh2-LS (EtOH_*Msh2*^{fl}) and water-treated non-induced Msh2-LS (H_2O_*Msh2*^{fl}) mice, after long-term ethanol or water treatment. Mann-Whitney U-test was carried out to compare EtOH_*Msh2*$^{fl\ KO}$ and H_2O_*Msh2*$^{fl\ KO}$ mice (**p=0.0019) (data shown as mean±SD, n=4-6 plasma samples per group).

4.6 Detection of Microsatellite instability in Msh2-LS mouse model

4.6.1 Methods

Deficiency of MMR leads to hypermutability, resulting in an increase in the mutation rate by 100- to 1000-fold due to uncorrected base mismatches and to MSI detected as variation in the lengths of repetitive sequences (e.g. AAAAAAA… or CACACACA…. or similar, known as microsatellites) due to uncorrected insertion/deletion loops that are prone to occur as DNA replication errors in repetitive sequences (Poulogiannis et al., 2010). Detection of MSI in tumours from the Msh2-LS mouse model was performed.

We selected from the literature a panel of mononucleotide repeat murine microsatellite markers (A27, A33, mBat26, mBat37 and mBat59, primers sequences in Materials and Methods, Table 2.6) (Bacher et al., 2005; Kabbarah et al., 2003; Zou et al., 2012). In MMR-deficient mice, mononucleotide repeats showed high sensitivity for detection of MSI and MMR-deficient neoplasms exhibit more frequent instability in mononucleotide repeats than dinucleotide repeats (Kabbarah et al., 2003).

Large intestinal adenomas from *Msh2$^{flox/-}$; Lgr5CreERT2$^{+/-}$; mTmG$^{+/-}$* mice and *Msh2$^{-/-}$* mice were selected along with normal control tissue from wild-type mice. DNA was extracted from FFPE samples. PCR-based amplification of the 5 mononucleotide repeat markers was performed and PCR products were separated on 15% polyacrylamide native gels by electrophoresis and stained with GelRed (as described in Materials and Methods).

4.6.2 Results

A large intestinal adenoma from a constitutive *Msh2$^{-/-}$* mouse (Msh2 constitutive-knockout, Msh2 KO) and normal colonic tissue from a WT mouse were used as MSI-positive and MSI-negative controls respectively, for testing the 5 mononucleotide repeats markers for MSI detection (Figure 4.55). The PCR products analysed by gel electrophoresis showed no difference in banding patterns for A_{27} and mBat37 microsatellite markers between the *Msh2$^{-/-}$* adenoma and WT colonic tissue, indicating that MSI was not detectable at all microsatellite markers. However, the PCR products analysed showed differences in banding patterns with some extra bands or differences in sizes of bands, indicating the presence of microsatellite instability, detected for A_{33}, mBat26 and mBat59 microsatellite markers, between the *Msh2$^{-/-}$* adenoma and WT colonic tissue. Subsequently, in order to detect MSI in adenomas from the MSh2-LS mouse model, tumour DNA was extracted from FFPE samples of 4 large

intestinal adenomas / adenocarcinomas from EtOH_*Msh2*$^{fl\ KO}$ mice tested for MSI using the same panel of microsatellite markers (Figure 4.56). No MSI was detected at A_{27} and mBat37 in any of the large intestinal adenomas from EtOH_*Msh2*$^{fl\ KO}$ mice, and only one tumour sample showed MSI at mBat59. MSI was detected at A_{33} and mBat26 in all tumour samples from Msh2-LS mice. However, the quality of the DNA extracted from FFPE samples was not high enough to guarantee accurate results. Furthermore, Msh2-LS large intestinal tumours included a mixed cell population of MMR-proficient surrounding and intermingling reactive epithelial cells and stromal cells as well as MMR-deficient adenoma cells, complicating the interpretation of the results and thus this experimental approach was discontinued.

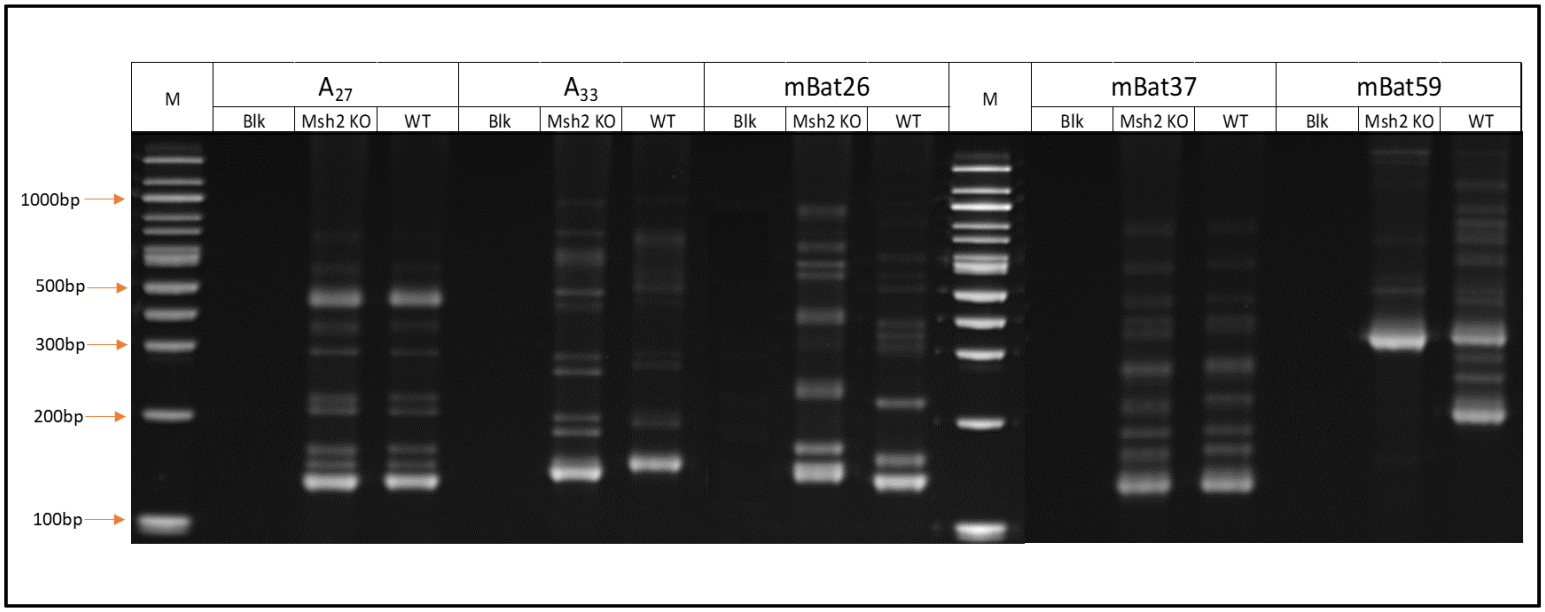

Figure 4.55: Detection of MSI using mononucleotide repeat murine microsatellite markers. A large intestinal adenoma from a constitutive *Msh2*$^{-/-}$ mouse (Msh2 KO) and compared this with normal colonic tissue from a WT mouse. The *Msh2* KO adenoma showed MSI at A_{33}, mBat26 and mBat59 confirmed by the differences in banding patterns with extra bands, between the *Msh2* KO adenoma and the WT colonic tissue. The lack of differences in banding pattern at A_{27} and mBat37 between the Msh2 KO adenoma and WT colonic tissue showed that MSI was not detectable at all markers. (M= marker; Blk=blank).

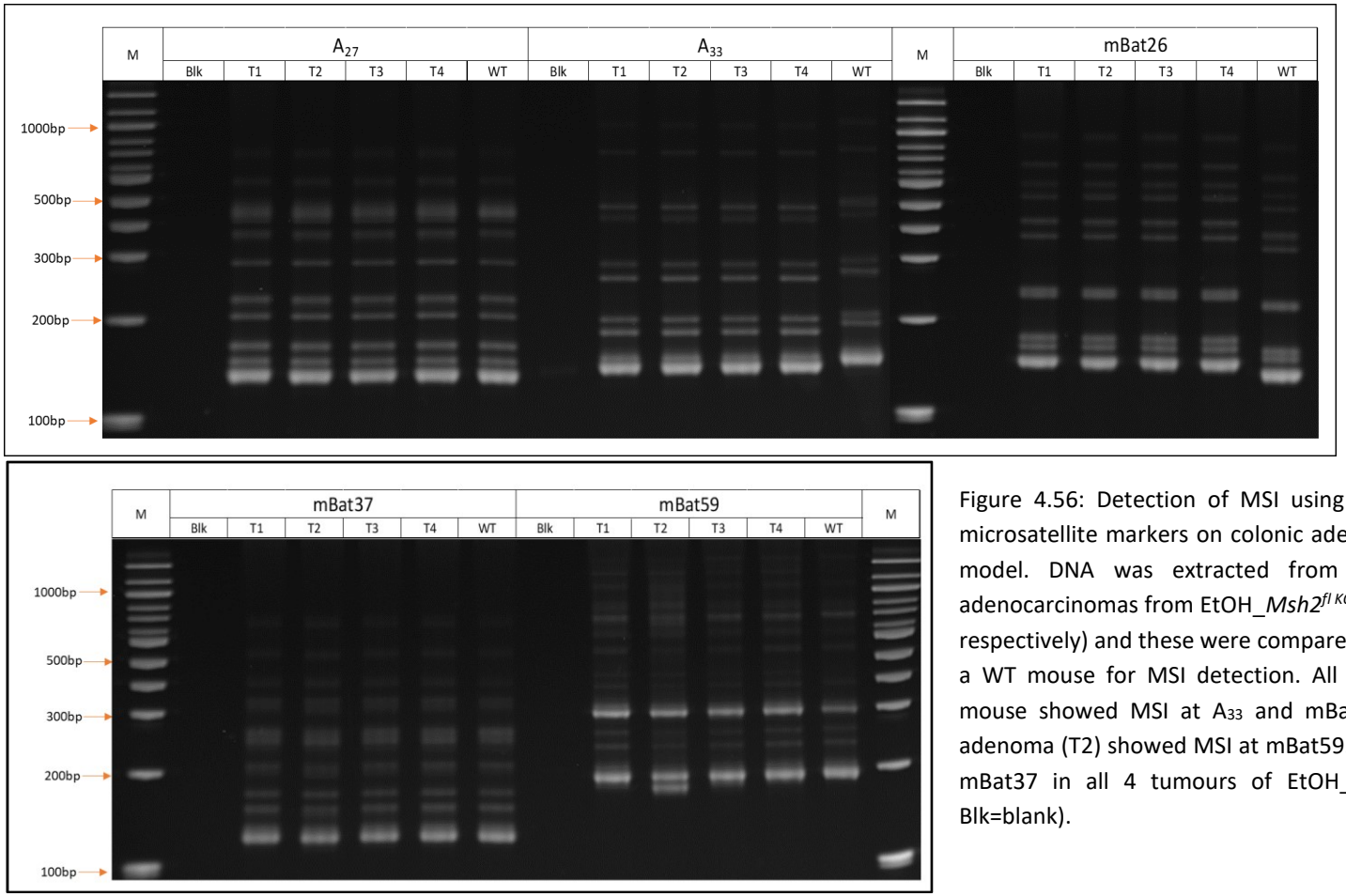

Figure 4.56: Detection of MSI using mononucleotide repeat murine microsatellite markers on colonic adenomas from the Msh2-LS mouse model. DNA was extracted from 4 large intestinal adenomas/ adenocarcinomas from EtOH_*Msh2*$^{fl\ KO}$ mice (labelled T1, T2, T3 and T4, respectively) and these were compared with normal colonic tissue from a WT mouse for MSI detection. All 4 tumours from EtOH_*Msh2*$^{fl\ KO}$ mouse showed MSI at A_{33} and mBat26 markers, whereas only one adenoma (T2) showed MSI at mBat59. No MSI was observed at A_{27} and mBat37 in all 4 tumours of EtOH_*Msh2*$^{fl\ KO}$ mouse. (M= marker; Blk=blank).

4.7 Discussion

In this chapter, the aim was to test the hypothesis that the DNA MMR system plays a role in protecting cells from some types of ethanol/acetaldehyde-induced DNA damage and that there is a gene-environment interaction between dMMR pathway and ethanol/acetaldehyde exposure that accelerates colorectal tumour development and progression.

In Müller at al., (2016), we examined intestinal tumorigenesis in WT and Aldh1b1 depleted mice after long-term ethanol treatment for one year. Ethanol was shown to initiate intestinal tumourigenesis without any additional carcinogen treatment or prior tumour suppressor gene inactivation and there was evidence for ethanol/acetaldehyde showing both carcinogenic and tumour promoting functions, in the form of increased proliferative activity of colonic mucosal epithelium. This was consistent with increased progression of ethanol-induced adenomas and adenocarcinomas. Moreover, a significant increase in DNA damage in the small and large intestinal epithelium of ethanol-treated mice was observed (Müller et al., 2016).

Wojciechowicz et al., (2014), successfully created the Msh2-LS mouse model (without the *mTmG* transgene) and characterized it for the first time. After Tamoxifen injections, *Msh2$^{flox/-}$; Lgr5CreERT2$^{+/-}$* developed more adenomas and adenocarcinomas than control mice (non-induced *Msh2$^{flox/-}$; Lgr5CreERT2$^{+/-}$*). Eight out of 20 (40%) *Msh2$^{flox/-}$; Lgr5CreERT2$^{+/-}$* mice showed intestinal tumour formation within an average of 19 months. All the tumours were located in the small intestine, no tumours were observed in the colon.

In the current investigation, long-term ethanol in drinking water treatment (compared with control water-treatment) was used to study whether ethanol causes acceleration of dMMR driven intestinal tumour formation with increased numbers of adenomas and/or adenocarcinomas.

Mice received Tamoxifen treatment by daily i.p. injection for 4 consecutive days, to activate Cre-recombinase in a low proportion of Lgr5-expressing intestinal stem cells, as described in Chapter 3. Both male and female Msh2-LS mice showed good acceptance of Tamoxifen treatment, showing no major alterations in body weights during the treatment duration.

Msh2-LS male mice showed statistically higher mean body weight compared with Msh2-LS female murine mean body weight at the same age ($p<0.0001$) (as expected due to normal sexual dimorphism for body weight observed in rodents). On the fifth day after the last Tamoxifen i.p. injection, Msh2-LS mice received 20% ethanol in drinking water or normal drinking water. We administrated ethanol in drinking water to mimic human consumption

of ethanol intake. In addition, in order to simulate the levels of toxicity and pathological effects of high ethanol consumption in humans we used a concentration of 20% ethanol in drinking water in mice, previously tested and validated by Müller et al., (2016), because it has been shown that ethanol clearance in mice is five times faster than in humans (Dole & Gentry, 1984; Holmes et al., 1986). EtOH_*Msh2*$^{fl\ KO}$ female and male mice did not show any abnormal behaviour or reduction in body weight demonstrating good acceptance of the ethanol regime.

Most of the EtOH_*Msh2*$^{fl\ KO}$ mice displayed either anal prolapse or >20% reduction in body weight as common clinical sign of distress and were culled for necropsy dissection. Long-term ethanol treatment of the Msh2-LS mice showed evidence of large intestinal hyperproliferation and adenoma formation (with 5 adenocarcinomas) in 65% (15/23 mice) of the EtOH_*Msh2*$^{fl\ KO}$ mice, for an average of 6 months of ethanol treatment. This is in stark contrast to the H_2O_*Msh2*$^{fl\ KO}$ control mice, none of which developed intestinal tumours over the same time period, with only 1 colonic adenoma observed at 15 months (4%, 1/23).

The EtOH_*Msh2*$^{fl\ KO}$ mice showed a pattern of tumour distribution of one or more large intestinal tumours mainly in the proximal colon and mid colon. A similar pattern is observed in human LS patients, in which colonic tumour formation occurs more in the caecum, ascending colon and transverse colon regions (proximal colon), than in the descending colon, sigmoid colon and rectum (distal colon), compared with sporadic colorectal tumours that are predominantly distal in location. No small intestinal adenomas were seen in the H_2O_*Msh2*$^{fl\ KO}$ or EtOH_*Msh2*$^{fl\ KO}$ mice.

Rijcken et al. (2008), described 50% of colonic adenomas in human LS cases were found in the proximal colon, compared with 26% of sporadic adenomas. In addition, proximal LS adenomas progressed to high-grade dysplasia more frequently than distal LS adenomas, and were also more often highly dysplastic than larger distal adenomas (Rijcken et al., 2008).

Hence, the Msh2-LS mouse model may be viewed as a good model of human LS in terms of the location of both the scattered dMMR crypt foci precursor lesions in the whole of the large (and small) intestines, but with colonic only tumour formation (adenomas and adenocarcinomas).

Long-term ethanol-treatment (compared with water-treatment) of the Tamoxifen-induced Msh2-LS mice provided evidence of ethanol-induced colonic adenomas that occurred at much higher numbers and at an earlier time, consistent with acceleration of dMMR-driven large intestinal tumour formation. A range of relevant control animal cohorts were also

tested for comparison with tumour formation in this test cohort. Some control animal cohorts were subjected to long-term ethanol treatment and some to water-treatment. The data on the effects of ethanol on intestinal tumourigenesis were compared for Tamoxifen-induced Msh2-LS mice, non-induced Msh2-LS mice (no Tamoxifen-treatment, hence no Cre activation and no loss of Msh2 protein expression), and WT mice (using data collected during previous work by Mike Müller and not repeated here in order to reduce animal numbers used for experiments, in line with the 3Rs principle in animal experimentation).

Non-induced Msh2-LS mice were treated with ethanol as a control group to test whether any unknown variables might affect tumour formation in the absence of induction of loss of *Msh2*. Furthermore, this control non-induced cohort would also test whether sporadic recombination (in the absence of Tamoxifen) of the $Msh2^{flox/OFF}$ allele occurred to any significant extent.

The EtOH_$Msh2^{fl}$ mice and the ethanol-treated WT mice (Müller et al., 2016) responded well to the 20% ethanol in drinking water regime with no abnormal behaviour and no significant reduction in body weight. Large intestinal tumour formation was observed in 8.4% (1/12) of the EtOH_$Msh2^{fl}$ mice after 28 weeks. In 25% (3/12) EtOH_$Msh2^{fl}$ mice hyperproliferation of the colonic crypt epithelium was observed in the mid colon. Large intestinal crypt epithelial hyperproliferation had previously been seen and described by our research group after long-term ethanol-treatment of wild-type mice and Aldh1b1-depleted mice (Müller et al., 2016). 66.6% (9/12) of the EtOH_$Msh2^{fl}$ control mice did not show any intestinal or other abnormality, or formation of intestinal adenomas or adenocarcinomas. In Group-A, 91.6% of H_2O_$Msh2^{fl}$ control mice showed no intestinal abnormality.

Long-term ethanol treatment of the cohort of WT mice (Müller et al., 2016) showed large intestinal tumour formation (and in one case a small intestinal adenoma formation) in 28.6% (4/14 mice) of after 1 year of ethanol-treatment, and 71.4% of the ethanol-treated control mice did not show any intestinal abnormality over the same time period. No intestinal abnormality was observed in the water-treated WT control mice. Hence, the non-induced Msh2-LS mice showed similar levels of colonic tumour formation to the wild-type controls with ethanol treatment and this was significantly lower than in the EtOH_$Msh2^{fl}$ mice.

The tumours and normal tissue samples from Msh2-LS model mice were characterised by IHC comparing ethanol-treated and water-treated mice. IHC was used to investigate the expression of Msh2 and other MMR proteins in tumours and tissue samples from Tamoxifen-induced Msh2-LS mice and non-induced Msh2-LS control mice. Tamoxifen treatment

induced the loss of Msh2 expression in Lgr5+ expressing crypt epithelial stem cells scattered along the entire SI and LI. The Lgr5+ expressing stem cells, located at the bottom of the crypts, generate daughter cells that can expand to fill the entire crypt-villus epithelium in SI or entire crypt in the colon (Barker et al., 2007; Wojciechowicz et al., 2014).

EtOH_*Msh2*$^{fl\ KO}$ mice showed 43% Msh2-negative small intestinal crypts and 11.2% Msh2-negative colonic crypts compared with H_2O_*Msh2*$^{fl\ KO}$ mice that showed 25.8% Msh2-negative small intestinal crypts and 5% Msh2-negative colonic crypts. The number of Msh2-negative or dMMR crypts was statistically significantly higher in both SI and colon of EtOH_*Msh2*$^{fl\ KO}$ mice compared with H_2O_*Msh2*$^{fl\ KO}$ mice, consistent with ethanol-mediated selection for survival of dMMR cells. The number of Msh2-negative crypts was higher in SI than in the colon in Msh2-LS mice, however although tumours were observed in the colon, no tumours formed in the small intestine. All large intestinal adenomas tested from EtOH_*Msh2*$^{fl\ KO}$ mice showed Msh2-negative dysplastic glands, often surrounded by or admixed with Msh2-positive crypts showing reactive or hyperproliferative changes. This confirmed colonic adenomas arose from dMMR (Msh2-negative) crypts. This is consistent with observations from human LS patients that the risk of colonic tumour formation correlates with the size of the MMR-deficient crypt clusters that grow over time in affected patients, in line with what was observed by Wojciechowicz et al, (2014) (Kloor et al., 2012; Shia et al., 2015).

No Msh2-negative crypts were observed in either small or large intestinal mucosal epithelium of non-induced Msh2-LS mice, consistent with lack of induction of Cre activity resulting in continued expression of protein from the floxed *Msh2* allele. In the MMR repair pathway, a base mismatch or single nucleotide InDel error is recognised by the MutSα complex, which is composed of Msh2 and Msh6 heterodimeric proteins. The MutLα complex, composed of Mlh1 and Pms2, is recruited by the binding of MutSα to the mismatched or InDel DNA lesion. The loss of either Msh2 or Mlh1 lead to the abrogation of all MMR activity (Poulogiannis et al., 2010). In the absence of Msh2, the heterodimeric MutSα complex cannot be formed and Msh6 is rapidly degraded. This was confirmed by the presence of Msh6-negative crypts (by IHC) scattered along both SI and colon of Tamoxifen-induced Msh2-LS mice in a very similar frequency and pattern as Msh2-negative crypts. IHC was used to explore whether the absence of Msh2 protein inhibits or modifies the expression of Mlh1 or Pms2. The IHC analysis of Mlh1 showed normal/positive expression of Mlh1 at the base of both colonic and small intestinal crypts of induced Msh2-LS mice, confirming the Msh2

absence does not inhibit Mlh1. However, the immunostaining for Pms2 proved to be technically problematic due to antibody failure and it was not possible to determine the staining pattern for Pms2.

IHC was performed to investigate Ki-67 expression in intestinal tissue samples from Tamoxifen-induced Msh2-LS mice to determine proliferative activity. The percentage of Ki-67-positive cells per crypt was significantly higher in colon in EtOH_*Msh2*$^{fl\ KO}$ mice compared with H_2O_*Msh2*$^{fl\ KO}$ mice, confirming the presence of large regions of mucosal crypt epithelial hyperproliferation observed in histological sections EtOH_*Msh2*$^{fl\ KO}$ murine colons. The percentage of Ki-67-positive cells per crypt in SI of EtOH_*Msh2*$^{fl\ KO}$ mice was slightly higher than in the SI of H_2O_*Msh2*$^{fl\ KO}$ mice. These observations confirm the previously reported association of long-term ethanol treatment of mice and colonic mucosal epithelial hyperproliferation (Müller et al., 2016).

We investigated the expression of β-catenin protein, an intracellular signal transducer in the Wnt signalling pathway (Cong et al., 2003a), on tumours and tissue samples from Tamoxifen-induced Msh2-LS mice. In the absence of the Wnt signalling, β-catenin is located mostly at the inner cell membrane bound to E-Cadherin at adherens junctions, or at very low levels in the cytoplasm, where its level is kept low through constant degradation by the β-catenin-degradation complex that includes Apc and Axin2 proteins. In the presence of Wnt signalling, the β-catenin-degradation complex is disrupted and β-catenin accumulates in the cytoplasm and translocates into the nucleus, where it binds with transcriptional co-factors and induces transcription of Wnt-responsive genes (Chen et al., 2013). Normal colorectal mucosal crypt epithelium exhibited moderate membranous and weak cytoplasmic staining for β-catenin, but absent nuclear localisation. In contrast, both colorectal adenomas and adenocarcinomas from induced Msh2-LS mice showed variably moderately to strongly positive nuclear β-catenin localisation and thus the immunostaining pattern of β-catenin is consistent with Wnt pathway activation, which is why nuclear β-catenin is regarded as a useful CRC biomarker (Lugli et al., 2007). In colonic tumours in the EtOH_*Msh2*$^{fl\ KO}$ mice, the IHC analysis of β-catenin showed a heterogeneous pattern with variable numbers of adenoma cells showing moderately to strongly positive β-catenin nuclear immunostaining due to accumulation and translocation of β-catenin in to the nuclei. This pattern has been observed in human MMR-deficient CRC (Lugli et al., 2007).

Ethanol is rapidly absorbed from the gastrointestinal tract (Brooks & Zakhari, 2014). Ethanol is metabolized to highly reactive acetaldehyde by ADHs and this is further oxidized to acetate

by ALDHs. Aldehydes are very reactive molecules and they can cause a range of DNA modifications: DNA adducts, single and double strand breaks, point mutations, increased sister chromatid exchanges, DNA-protein crosslinks or DNA ICLs (Seitz & Stickel, 2007). Langevin et al (2011) demonstrated that the Fanconi Anaemia (FA) DNA repair pathway has a crucial role in counteracting acetaldehyde-induced genotoxicity in mice, as the FA DNA repair pathway is essential for the repair of DNA ICLs (Kim & D'Andrea, 2012; Langevin et al., 2011). Recently, our research group has proposed the hypothesis that the DNA MMR repair system plays a role in protecting the cell from some types of ethanol/acetaldehyde induced DNA damage. The MMR pathway is involved in the removal of base mismatches and insertion/deletion loops caused by oxidative stress, lipid peroxidation, base deamination, methylation, certain alkylation changes and replication associated errors. Loss of MMR pathway function results in dMMR with hypermutability (increased mutation rate by 100x – 1000x due to uncorrected mismatches) and MSI (the variation in length of repetitive microsatellite sequences due to uncorrected insertion/deletion loops), but more importantly dMMR results in reduced susceptibility to either cell cycle arrest or apoptosis induced by those types of DNA damage recognised by the MMR pathway (Poulogiannis et al., 2010; Seth et al., 2018; Toft et al., 1999).

MMR is involved in a signalling cascade that leads to cell cycle arrest and/or apoptosis, if severe DNA damage has previously occurred. It has been observed that MMR-deficient cells fail to recruit ATM and ATR proteins, preventing p53 phosphorylation in response to DNA damage. MMR-deficient cells show predisposition to malignancy by failing to repair DNA damage (of MMR-recognised type) and failing to engage apoptosis to remove DNA-damaged cells (Cerretelli et al., 2020; Toft et al., 1999).

IHC analysis of y-H2AX and p53 was performed to investigate the DNA damage response in tumour and normal tissue samples from EtOH_*Msh2*$^{fl\ KO}$ and H_2O_*Msh2*$^{fl\ KO}$ mice. Upon DNA damage, an early response is the phosphorylation of the C-terminal part of the core histone protein H2AX (termed gamma-H2AX when phosphorylated) by a complex including ATM, ATR and DNA protein kinase catalytic subunit (DNA-PKcs) (Siddiqui, 2015). Y-H2AX is a key co-ordinator of signalling and activating DNA damage repair pathways and for this it is considered a specific molecular marker for monitoring DNA damage (Mah et al., 2010). At the completion of DNA repair, y-H2AX is typically de-activated (Cook et al., 2009). The immunohistochemical analysis of y-H2AX showed a higher percentage of y-H2AX positive cells in EtOH_*Msh2*$^{fl\ KO}$ murine colonic mucosal epithelium (35%) compared with H_2O_*Msh2*^{fl}

^{KO} murine colonic epithelium (0.4%). EtOH_*Msh2*$^{fl\ KO}$ murine large intestinal adenomas (both colonic and caecal) showed high y-H2AX expression. By contrast, very few or no y-H2AX positive cells were observed in H_2O_*Msh2*$^{fl\ KO}$ murine small intestinal mucosa. The high expression of y-H2AX in EtOH_*Msh2*$^{fl\ KO}$ murine colonic mucosal epithelium is consistent with DNA damage induced by ethanol/acetaldehyde suggesting that ethanol exposure has a significant mutagenic effect mainly on dMMR colonic mucosal epithelium rather than on dMMR small intestinal mucosa. This suggests that Msh2 has a key role in protecting the MMR-proficient colonic epithelial cells against this type of DNA damage, but Msh2 may not be the sole protective mechanism for small intestinal epithelium cells from ethanol/acetaldehyde-induced DNA damage.

The presence of DNA damage induces p53 pathway activation, and this is involved in maintaining genomic stability following DNA damage (and other stimuli) via transcriptional activation of a variety of response pathways, such as apoptosis, cell cycle arrest and DNA repair (Levine, 1997; Williams & Schumacher, 2016). Under normal conditions, p53 protein levels are kept low by its rapid degradation (maintaining a 20-30 minute short half-life for p53 polypeptide) and p53 is in a largely inactive state. DNA damage-mediated activation of the p53 pathway involves decreased Mdm2-mediated degradation of the p53 protein and thus stabilisation of p53 with increased p53 levels in the cell, which can be demonstrated immunohistochemically as a greater proportion of cells containing moderate to high (but variable) nuclear staining of p53 in individual cells ("wildtype pattern", distinguishable from mutated p53-associated "overexpression" or "complete absence" patterns seen in some neoplasms) (Köbel et al., 2016; Lakin & Jackson, 1999).

In the IHC analysis of p53, a higher percentage of p53 positive cells with high to moderate nuclear staining were observed in EtOH_*Msh2*$^{fl\ KO}$ murine colon (41.3%) compared with H_2O_*Msh2*$^{fl\ KO}$ murine colon (10.8%). The percentage of p53-positive cells in small intestinal mucosal epithelium was higher in EtOH_*Msh2*$^{fl\ KO}$ mice (15%) compared with H_2O_*Msh2*$^{fl\ KO}$ mice (5.2%). In EtOH_*Msh2*$^{fl\ KO}$ murine large intestinal adenomas (colonic and caecal) showed widespread variably high p53 expression. The variable pattern of p53 nuclear staining reflected the "wild-type pattern" in response to ethanol/acetaldehyde-induced genotoxic damage and there were no tumours showing either the "overexpression" or "null" patterns associated with *Tp53* mutation.

IHC analysis of cCas3 was performed to detect the incidence of apoptotic events in tumour and normal tissue samples from in EtOH_*Msh2*$^{fl\ KO}$ and H_2O_*Msh2*$^{fl\ KO}$ mice. Caspase-3 (Cas3)

is a key executive member of the caspase cascade, with cysteine-aspartic acid protease activity, that acts as one of the key effectors of cell death by apoptosis. It requires proteolytic cleavage into 2 subunits that dimerize to create the active form, cCas3 (Talmon et al., 2010, Holubec et al., 2005). Once activated, cCas3 is responsible for the cleavage of key target proteins essential in cell proliferation and survival, inducing DNA fragmentation, cell shrinkage, chromatin and cytoplasmic condensation and formation of apoptotic cells and bodies. Apoptotic bodies express ligands for phagocytic cell receptors for recognition by phagocytic cells or neighbouring cells (Elmore, 2007).

Immunohistochemical analysis of cCas3 showed significantly higher number of cCas3+ apoptotic bodies in in EtOH_*Msh2*$^{fl\ KO}$ mice compared with no detectable cCas3+ apoptotic bodies in H_2O_*Msh2*$^{fl\ KO}$ mice, consistent with increased apoptosis associated with colonic epithelial exposure to ethanol/acetaldehyde. EtOH_*Msh2*$^{fl\ KO}$ murine large intestinal adenomas showed no detectable cCas3+ apoptotic bodies, indicating rare to no apoptotic events in dMMR colonic tumours. IHC analysis of cCas3 of EtOH_*Msh2*$^{fl\ KO}$ murine small intestinal epithelium and the H_2O_*Msh2*$^{fl\ KO}$ murine small intestinal epithelium failed on technical grounds.

The increased DNA damage observed in EtOH_*Msh2*$^{fl\ KO}$ murine large intestinal mucosal epithelium is consistent with the high levels of circulating acetaldehyde detected by plasma acetaldehyde assay. We found statistically higher plasma acetaldehyde levels in EtOH_*Msh2*$^{fl\ KO}$ mice compared with H_2O_*Msh2*$^{fl\ KO}$ mice ($p=0.0019$).

Finally, we performed MSI detection using a panel of 5 mononucleotide murine microsatellite markers, validated by other studies (Bacher et al., 2005; Kabbarah et al., 2003; Zuo et al., 2012). We detected some variations in the banding patterns for three of the markers, indicating the presence of MSI in 4 colonic adenomas from EtOH_*Msh2*$^{fl\ KO}$ mice, although the MSI assay was suboptimal. However, the quality of the DNA extracted from FFPE samples was variable and often insufficiently high enough to guarantee reproducible results. Furthermore, Msh2-LS large intestinal tumours include a mixed cell population of variable ratios of surrounding and intermingling MMR-proficient reactive epithelial cells and stromal cells as well as MMR-deficient adenoma cells, complicating the interpretation of the MSI detection results and thus this experimental approach was discontinued.

In conclusion, we further characterised the Msh2-LS mouse model, demonstrating that it closely mimics the situation in human LS patients for both precursor dMMR crypt foci and tumour development in terms of colonic adenoma and (in a few cases) progression to

adenocarcinoma formation. Ethanol-treatment was shown to cause DNA damage and induce colonic crypt epithelial hyperproliferation in this Msh2-LS model, confirming similar observations made by others and our own research group (Brooks & Zakhari, 2014; Müller et al., 2016). We provided evidence that ethanol-treatment can induce regions of hyperproliferation of the large intestinal mucosal epithelium (but not the small intestinal mucosal epithelium) and this appears to contribute to intestinal adenoma formation by acting as a tumour promoter, which occurs mostly in the parts of the colon (proximal and mid colon) affected by hyperproliferation in this Msh2-LS mouse model (*Msh2*$^{flox/-}$; *Lgr5CreERT2*$^{+/-}$) following ethanol-treatment, but not water-treatment. EtOH_Msh2$^{fl\ KO}$ mice showed accelerated formation of large intestinal tumours within ~6 months of starting ethanol exposure, compared with the control cohorts of H_2O_*Msh2*$^{fl\ KO}$ mice, EtOH_*Msh2*^{fl} mice and ethanol-treated WT mice, with these control cohorts developing significantly fewer large intestinal tumours after 12 months of the ethanol-treatment or water-treatment regimes.

The data shown here are consistent with the hypothesis that in normal pMMR intestinal epithelial stem cells, ethanol/acetaldehyde-induced DNA damage results in activation of the DNA mismatch repair pathway, inducing either cell cycle arrest in the case of mild DNA damage to allow DNA repair, or cell death by apoptosis in the case of more severe DNA damage. In this way, tissue homeostasis is maintained. We propose that in dMMR cells, modelled in this Msh2-LS mouse model, ethanol/acetaldehyde caused DNA damage that was not recognised or repaired by the dMMR intestinal epithelial stem cells (and their daughter cells) as they are unable to activate the MMR signalling pathway. Hence, dMMR cells showed inappropriate survival of these ethanol-damaged cells, compared with proficient MMR cells. These aberrantly surviving DNA-damaged dMMR colonic epithelial cells were stimulated to hyperproliferate by ethanol, leading to an increased probability of acquisition and fixation of DNA mutations explaining the accelerated colonic adenoma formation. Hence, there is evidence for a selective advantage of the dMMR/ethanol/acetaldehyde interaction, as a gene/environment interaction, that explains the acceleration of colonic adenoma development and further progression to adenocarcinoma (in some cases) in ethanol-treated Msh2-LS (EtOH_*Msh2*$^{fl\ OK}$) mice (Figure 4.57). This process is observed mostly in the proximal colon and mid colon, but not in the small intestine, very similar to the anatomical tumour distribution seen in human LS patients.

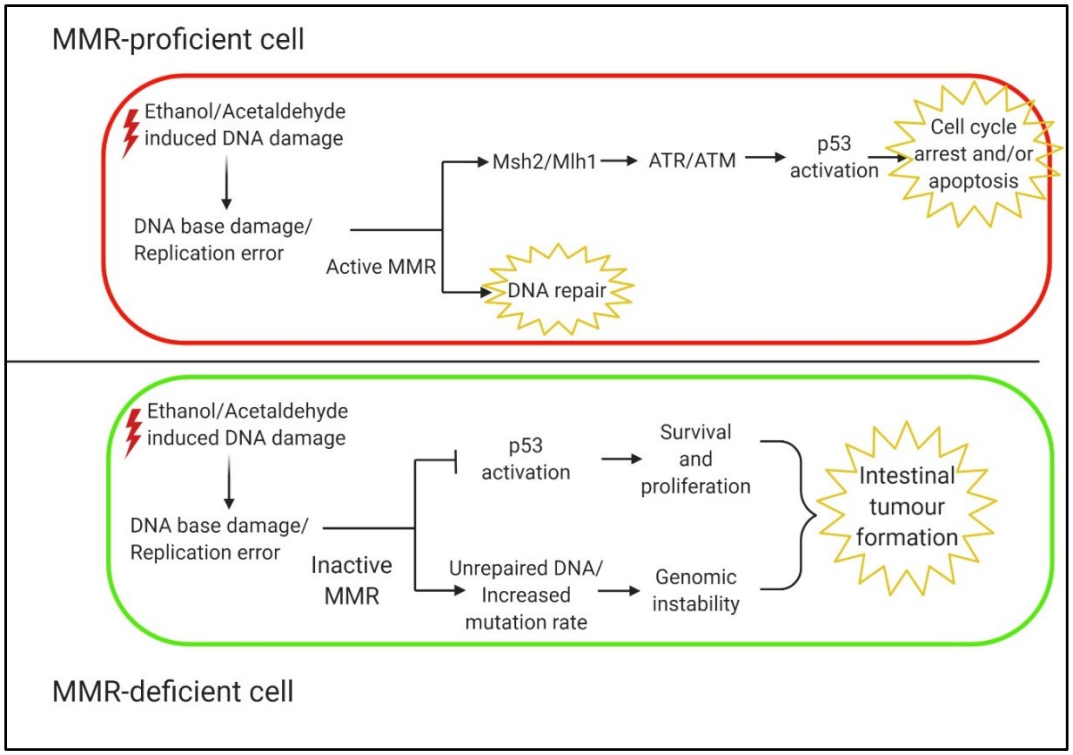

Figure 4.57: Schematic diagram of the proposed model of the MMR/ethanol/acetaldehyde gene/environment interactions in both MMR-proficient (pMMR) and MMR-deficient (dMMR) intestinal epithelial cells. Upon ethanol/acetaldehyde exposure, in some intestinal epithelial stem cells there is some DNA base damage that normally would be recognised and repaired by the MMR system, or if unrepaired this base damage may induce replication errors, such as base mismatches or InDels, during S-phase of the cell cycle. Here, the pMMR cell (red cell membrane) is able to activate DNA mismatch repair of the (MMR-recognised) base damage bringing about either cell cycle arrest in the case of mild DNA damage to allow DNA repair, or cell death by apoptosis in the case of more severe DNA damage. By contrast, the dMMR cell (green cell membrane) is unable to activate the MMR signalling pathway and so there is neither cell cycle arrest nor apoptosis, resulting in aberrant survival of DNA-damaged cells and their subsequent proliferation. These proliferating dMMR stem cells populate the crypt and expand further (by crypt fission) to form dMMR crypt foci. Stimulated by ethanol to undergo increased proliferation, these cells form hyperproliferative crypts whilst remaining subject to ongoing DNA damage from continued exposure to ethanol/acetaldehyde. Thus, these dMMR cells can accumulate mutations reflecting a form of dMMR genomic instability, and are consequently at increased risk of tumour formation, thus explaining the acceleration of colonic adenoma formation and increased probability of evolution to adenocarcinoma.

Chapter 5: Effects of Temozolomide Treatment on the Msh2-LS Mouse Model

5.1 Introduction

The carcinogenic and tumour promoting/hyperproliferative effects of ethanol on the murine colon were previously studied by comparing Aldh1b1-depleted mice and WT mice treated with 20% ethanol in drinking water (Müller et al., 2016). 27% of ethanol-treated Aldh1b1-depleted mice showed large intestinal adenomas (with a few adenocarcinomas) after 1 year of treatment, compared with 29% of ethanol-treated WT mice that showed large intestinal adenomas after 1 year. Ethanol was shown to initiate intestinal tumorigenesis without any additional chemical carcinogen treatment or prior tumour suppressor gene inactivation or oncogene activation, and there was evidence for both carcinogenic and tumour promoting functions of ethanol and its main metabolite acetaldehyde, including increased progression of ethanol-induced adenomas to early adenocarcinomas in some cases (Müller et al., 2016).

In LS patients, dMMR tumours arise from somatic cells that acquire inactivation of the MMR gene's wild-type allele (on the background of inheritance of a mutation in that MMR gene's other allele). It has been observed that the number and size of dMMR crypt foci that accumulate in LS patients' colons over time influences their risk of tumour development (Kloor et al., 2012).

A Msh2-LS mouse model (*Msh2*$^{flox/-}$*; Lgr5CreERT2*$^{+/-}$*)* was generated, in which it was observed that loss of Msh2 expression occurs in approximately 10% of intestinal crypts after Tamoxifen treatment to induce inactivation of the second conditional knockout *Msh2* allele in scattered intestinal stem cells, leading to intestinal tumour formation in 40% of the mice after 1.5 years (Wojciechowicz et al., 2014). To increase the number of dMMR crypts and accelerate the tumourigenesis process, a methylating chemotherapy agent, Temozolomide, was used because MMR-deficient cells are known to be resistant to killing by methylating agents (Karran, 2001). Temozolomide (TMZ) treatments were applied to Msh2-LS mice after Tamoxifen treatment, resulting in gastrointestinal intraepithelial neoplasms developing 3 weeks or more after the last TMZ administration. Intestinal adenomas and/or adenocarcinomas were observed between 13 and 19 weeks after TMZ administration. In the TMZ-treated tumour-bearing mice, loss of Msh2 expression was observed in approximately

32% of intestinal crypts compared with 10% in non-TMZ-treated control mice (Wojciechowicz et al., 2014). Data provided were interpreted as showing evidence that TMZ confers upon dMMR cells a proliferative advantage over WT cells, resulting in an expansion of the pool of dMMR cells, with TMZ inducing increases in both dMMR crypt foci and DNA mutation load causing the acceleration of tumourigenesis.

TMZ is converted (by non-enzymatic chemical conversion) to the active metabolite 5-(3-methyltriazen-1-yl) imidazole-4-carboxamide (MTIC) which can cause several base methylation events, such as at the *O*6 position of guanine (O^6-MeG) (Zhang et al., 2012). In normal cells, O^6-MeG is directly repaired by the enzyme MGMT that removes the methyl adduct. When MGMT fails, the O^6-MeG lesions are replicated during DNA synthesis generating an aberrant base pair. This stimulates activation of the DNA MMR pathway and is processed into a double-stranded DNA break, eventually resulting in apoptosis. MMR-deficient cells do not detect such alkylation adducts and hence are resistant to TMZ (Thomas et al., 2017).

In this chapter, the aim was to accelerate the process of intestinal tumourigenesis in the Msh2-LS mice used in this research work, by combining the effects of TMZ, as described by Wojciechowicz et al. (2014), with the effects of long-term 20% ethanol in drinking water, as described by Mueller et al., (2016). A new protocol was designed to apply to the Msh2-LS mouse model in order to try to accelerate intestinal tumour formation to around 2-4 months, in contrast to the 1 year of ethanol treatment required for intestinal adenoma formation in WT and Aldh1b1-depeleted mice (Müller et al., 2016) and the 1.5 years for intestinal adenoma development in induced conditional *Msh2* knockout Msh2-LS model mice without any treatments (Wojciechowicz et al., 2014).

5.2 Potential Acceleration of the Msh2-LS Mouse Model Using Temozolomide treatment

5.2.1 Methods

Experiments were designed firstly to establish the most appropriate TMZ dose and treatment regime, and secondly, to observe the effects of TMZ on tumour development in the Msh2-LS mice.

Msh2$^{flox/-}$; Lgr5CreERT2$^{+/-}$; mTmG$^{+/-}$ 7-9 weeks old mice were divided into 6 Groups A-F (Figure 5.1). During the first week of treatment, Group-A mice received an i.p injection of 0.15mg Tamoxifen/g bw on day 1 and 0.1mg Tamoxifen/g bw on day 2, from the second week to the fourth week these mice were treated with 10 daily doses of 0.1mg TMZ/g bw by oral gavage (o.g.), followed by the 20% ethanol in drinking water regime from the 5th week onwards. Group-B mice received 2 i.p injections of tamoxifen in the first week (the same as for Group-A mice), from the second week to the third week these mice were given 5 daily doses of 0.1mg TMZ/g bw by o.g., followed by the 20% ethanol in drinking water regime from the 3rd week onwards (Figure 5.1). The Group-A and -B mice were sacrificed after 4 weeks of the ethanol regime to investigate the presence of any intestinal abnormalities or early signs of intestinal tumour formation.

To observe the combined effects of TMZ and long-term ethanol treatment (compared with water-treated controls) on the Msh2-LS mice, a further 4 groups were included in the study. Group-C to Group-F mice followed the same Tamoxifen treatment protocol as Group-A and -B, receiving an i.p injection of 0.15mg Tamoxifen/g bw on day 1 and 0.1mg Tamoxifen/g bw on day 2. Group-C and -E mice were treated with 10 daily doses of 0.1mg TMZ/g bw by o.g. over 3 weeks (from the second week to the fourth week), followed by either 20% ethanol in drinking water regime for Group-C mice or normal / standard drinking water for Group-E mice until signs of tumour formation were observed. Group-D and -F mice were given 5 daily doses of TMZ by o.g. over 2 weeks from the second week to the third week, followed by either 20% ethanol in drinking water regime for Group-D mice or normal / standard drinking water for Group-F mice, until signs of tumour formation were observed (Figure 5.1).

Animals in Group-C to -F were culled and tissues collected when either clinical signs of distress were visible or they displayed >20% body weight loss compared with the initial body weight. The small and large intestines, caecum, stomach, liver, spleen, thymus, lymph nodes (if visible) and any other organ or tissue showing abnormalities, were collected following

schedule 1 culling and necropsy dissection (as described in Materials and Methods). Tissues were fixed in 10% NBF, processed using standard tissue processing protocols and paraffin embedded in preparation for section cutting and staining. The acronyms used for Msh2-LS model mice and their relevant treatments are shown in Table 2.2.

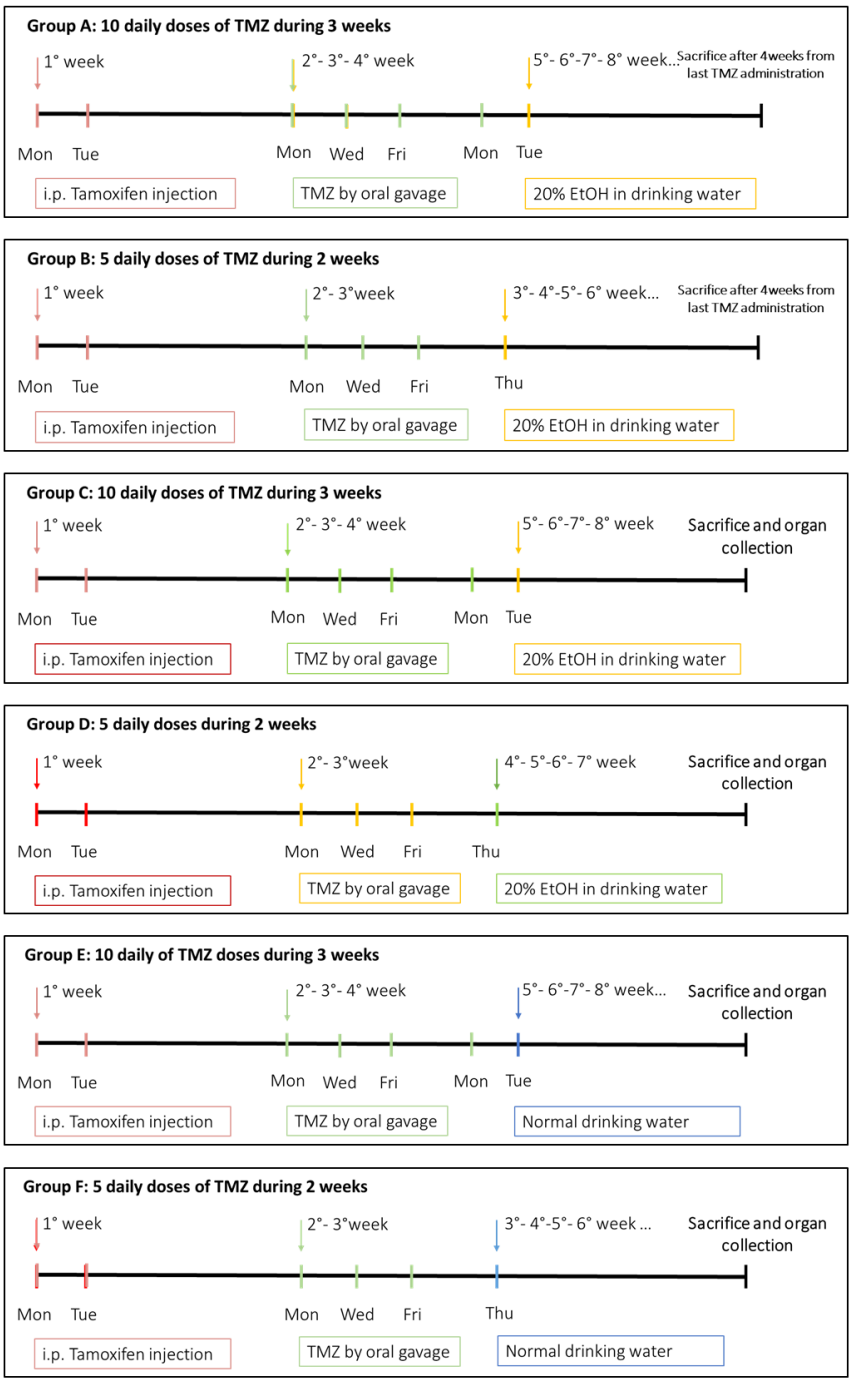

Figure 5.1: Experimental treatment protocols and timelines for Group-A to -F using Msh2-LS mice. Animals in all groups received i.p Tamoxifen injections over two days (0.15mg Tamoxifen/g bw on day 1 and 0.1mg Tamoxifen/g bw on day 2). Animals in Group-A (10 TMZ doses over 3 weeks, 0.1mg TMZ/g bw by o.g) and Group-B (5 TMZ doses over 2 weeks, 0.1mg TMZ/g bw by o.g) were culled after 4 weeks of 20% ethanol in drinking water regime. Animals in Group-C and -D followed the same Tamoxifen and TMZ treatment protocol as Group-A and -B respectively, but they were kept alive until sign until signs of tumour formation were observed. Group-E and -F mice received the same Tamoxifen and TMZ treatment protocol as Group-C and -D respectively, but were water-treated controls for Group-C and -D respectively. (TMZ = Temozolomide; i.p. = intraperitoneal; EtOH= Ethanol; o.g. = oral gavage).

5.2.2 Results

5.2.2.1 Experimental Group Organization and Comparisons of Body Weight Changes.

The first experiment was designed to determine the most appropriate TMZ dose and treatment regime, starting with the protocols set out by Wojciechowicz et al (2014). Six experimental subjects (3 females and 3 males) were divided into two groups: Group-A (3 mice: 2 females and 1 male, receiving 10 TMZ doses over 3 weeks) and Group-B (3 mice: 1 female and 2 males, receiving 5 TMZ doses over 2 weeks). Animals from Group-A and -B were culled 4 weeks after the last TMZ administration. The second experiment was designed to include 4 groups to study the combined effects of TMZ and ethanol treatment on the Msh2-LS mice. Animals were divided into ethanol-treated groups, Group-C (7 mice: 3 females and 4 males, receiving 10 TMZ doses over 3 weeks), and Group-D (7 mice: 2 females and 5 males, receiving 5 TMZ doses over 2 weeks); and water-treated groups, Group-E (4 mice: 3 females and 1 male, receiving 10 TMZ doses over 3 weeks) and Group-F (7 mice: 3 females and 4 males, receiving 5 TMZ doses over 2 weeks).

During the first week, Msh2-LS mice (Group-A to -F) started the Tamoxifen treatment (daily Tamoxifen i.p injections for 2 consecutive days), and body weight and health status were recorded. Body weights of the female and male mice didn't significantly differ during the Tamoxifen treatment (Figure 5.2), showing successful drug administration and acceptance of the experimental procedures by the mice. Body weights of Msh2-LS males (~28g) were significantly higher than body weights of Msh2-LS females (~21g) both before and during the Tamoxifen treatments (Figure 5.2), in line with data shown in Chapter 4 (4.2.2.1).

In the second week, mice started the TMZ treatment with either 5 daily doses of 0.1mg TMZ/g bw by o.g. over 2 weeks or 10 daily doses of 0.1mg TMZ/g bw by o.g. over 3 weeks. Body weights and health status of the mice were recorded (Figure 5.3). Body weights of the female and male mice receiving both treatments (5 or 10 TMZ doses) didn't significantly differ during the TMZ treatment (Figure 5.3). However, 4 mice died (1 female from Group-C, one male from Group-D, 1 female from Group-E and 1 female from Group-F) due to gastrointestinal paralysis after the administration of TMZ via oral gavage and these mice were excluded from the study. Body weights of Msh2-LS males were significantly higher than body weights of Msh2-LS females during both the Tamoxifen and the TMZ treatment as expected.

After TMZ treatment, animals received either 20% ethanol in drinking water or normal / standard drinking water regimes, with continued monitoring of body weights and health status twice a week (Figure 5.4). Ethanol-treated Msh2-LS female mice did not show abnormal behaviour or reduced body weight compared with the water-treated female mice, indicating good acceptance of the ethanol regime. Ethanol-treated Msh2-LS female mice weighed on average 23.14g compared with 23.28g of the water-treated Msh2-LS female mice (Figure 5.4B).

By contrast, ethanol-treated and water-treated Msh2-LS male mice, showed statistically significant differences between the two groups. Ethanol-treated Msh2-LS male murine body weights changed from ~30g to ~25g over 13 weeks of the ethanol treatment regime, whereas water-treated Msh2-LS male mice showed a general increase in body weight (to ~34g) over the same time with some fluctuation between weeks 15 and 21 of the water treatment regime (Figure 5.4A).

Drinking bottles were changed and bottle weights were recorded once a week to allow measurement of liquid consumption. Liquid consumption per mouse was estimated by analysing the weights of the drinking bottles (per cage) and calculating the average weight of consumed liquid per mouse per day (Figure 5.5). Water-treated and ethanol-treated Msh2-LS male mice consumed around the same amount of liquid per day, 13.5 and 13.8 ml respectively. On average water-treated Msh2-LS female mice consumed around 8.9ml of water per day, whereas on average ethanol-treated Msh2-LS female mice consumed around 11.2ml of 20% ethanol in drinking water per day. No significant differences were observed between ethanol- and water-treated males or females.

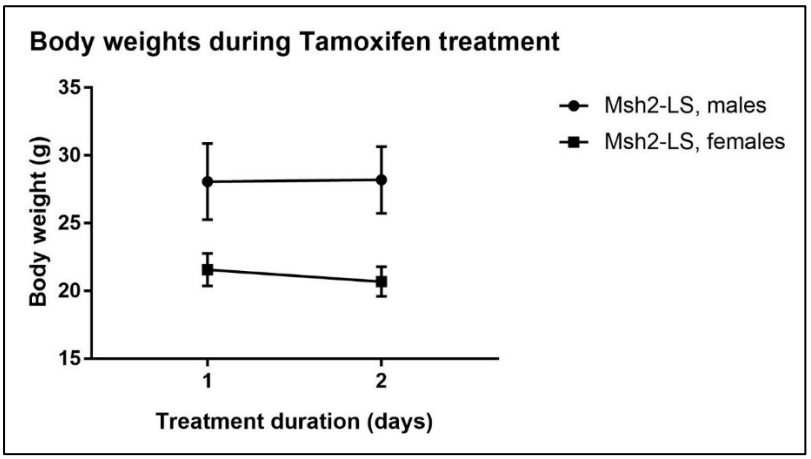

Figure5.2: Murine body weights during Tamoxifen treatment. Body weights of Msh2-LS males (circles) were significantly higher than body weights of Msh2-LS females (squares), before and during Tamoxifen treatments, although both showed no significant change over the two days of Tamoxifen treatment. 2-way-ANOVA test with Bonferroni post-test correction showed statistically significant differences between the two sex cohorts, $p<0.0001$ on day 1 and day 2 (data shown as mean ± SD, n=10 mice in each group).

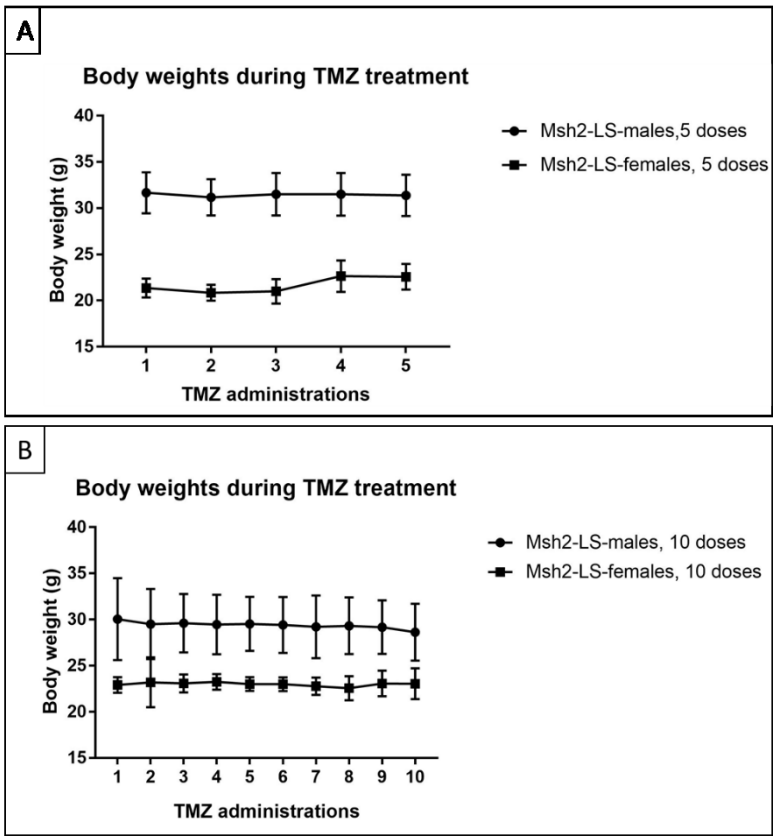

Figure 5.3: Murine body weights during Temozolomide (TMZ) treatment. Body weights of Msh2-LS males (circles) and females (squares) that received either 5 TMZ doses (A) or 10 TMZ doses (B). Body weights of Msh2-LS males were significantly higher than body weights of Msh2-LS females, although all 4 groups of mice showed no significant change over the period of TMZ treatment. 2-way-ANOVA test with Bonferroni post-test correction showed statistically significant differences between these two sex cohorts, $p<0.0001$ on days 1 -5 in graph A and on day 1 in graph B, $p=0.0004$ on days 2-9 in graph B and $p=0.0025$ on day 10 in graph B (data shown as mean ± SD, n=10 mice in each group).

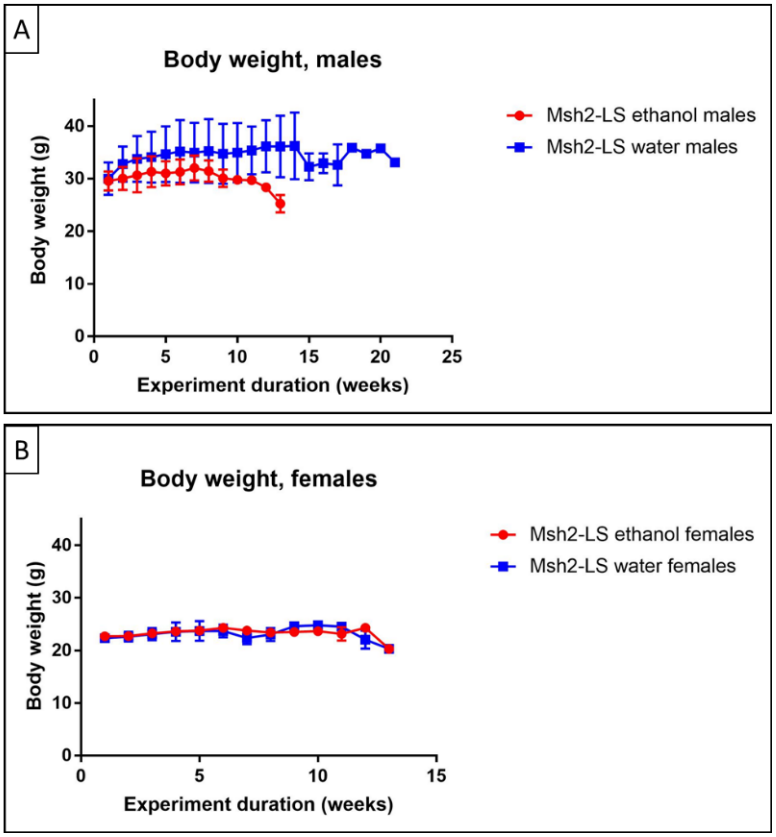

Figure 5.4: Murine body weights for males and females during 20% ethanol or standard/normal drinking water regimes. A statistically significant difference was observed between the ethanol-treated Msh2-LS males (red circles) body weights curve and the water-treated Msh2-LS males (blue squares) body weights curve, $p<0.0001$. There were no significant differences between the body weights curves of ethanol-treated Msh2-LS females versus water-treated Msh2-LS females. 2-way-ANOVA with Bonferroni post-test correction analysis (data shown as mean±SD).

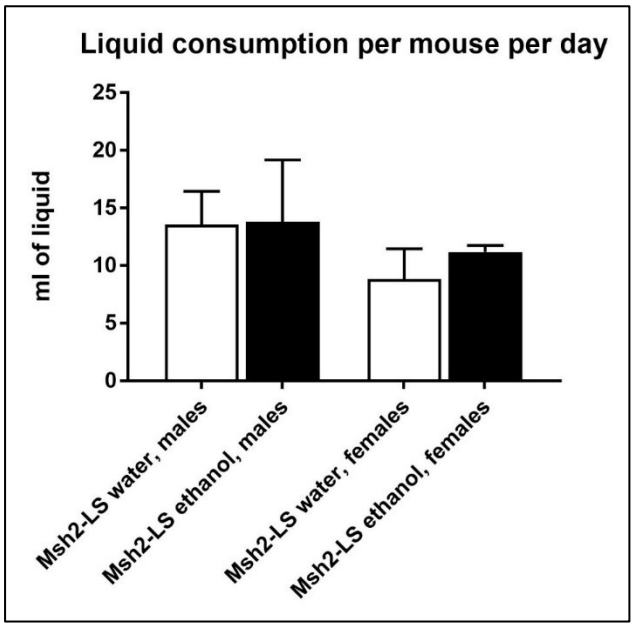

Figure 5.5: Liquid consumption of either 20% ethanol containing drinking water (black bars) or standard/normal water (white bars) per mouse per day for Msh2-LS males and females. No significant differences were observed for any of the comparisons of ethanol versus water treatment or males versus females. 2-way-ANOVA with Bonferroni post-test correction analysis (data shown as mean±SD).

5.2.2.2 Tumour Development in the Msh2-LS Mouse Model after Temozolomide and Ethanol Treatment

The ethanol-treated Msh2-LS mice in Group-A (10 TMZ doses over 3 weeks) and in Group-B (5 TMZ doses over 2 weeks), were culled after 4-5 weeks of 20% ethanol in drinking water regime to investigate the presence of any intestinal abnormalities or early signs of intestinal tumour formation. In both Group-A and Group-B mice, no gastrointestinal abnormalities or tumours were observed after 4 weeks from the last TMZ administration.

The other 4 cohorts (C-F) of Msh2-LS mice were monitored every day for signs of intestinal tumour development or other pathological abnormalities, using the clinical scoring system described in Chapter 4 (Table 4.1). Most of the mice in Group-C to -F displayed irregular breathing or >20% reduction in body weight as common clinical signs of distress, at varying lengths of time from the start of the experimental protocol and these mice were then culled for necropsy dissection.

During necropsy dissection, the majority of the Msh2-LS mice treated with either 5 TMZ doses or 10 TMZ doses, and either water or ethanol, showed an expansion of the thymus covering the heart and lungs in the thorax (Figure 5.6). Histopathological analyses revealed the presence of thymic lymphomas in these cases, with many showing evidence of lymphoma infiltrating into other tissues (mostly liver, spleen and in few cases into the small intestinal mucosa and submucosa). The H&E analyses revealed some cases of small and large intestinal adenoma formation (Figure 5.7).

Group-C (10 TMZ doses, ethanol-treated cohort; 10TMZ_EtOH_*Msh2*$^{fl\ KO}$) mice were sacrificed after 8-10 weeks of starting the 20% ethanol regime. Four out of 6 10TMZ_EtOH_*Msh2*$^{fl\ KO}$ mice showed primary thymic lymphoma, with lymphoma infiltration in liver and spleen, 2 out of 6 showed monocryptal adenomas in the small intestine and in one case a caecal adenoma (Figure 5.7). In the corresponding water-treated control group (Group-E: 10 TMZ doses, water-treated cohort; 10TMZ_H_2O_*Msh2*$^{fl\ KO}$), 2 mice were culled 8 weeks after the last TMZ dose, in one of which a thymic lymphoma was observed together with a few small adenomas in the small intestine, and the other case showed lymphoma formation with infiltration into the lamina propria of the mucosa and into the submucosa of the small intestine. The remaining mice were sacrificed after 17 weeks from the last TMZ dose because of discomfort due to axillary squamous carcinoma. In both 10TMZ_EtOH_*Msh2*$^{fl\ KO}$ mice and 10TMZ_H_2O_*Msh2*$^{fl\ KO}$ mice, the incidence of lymphomas (in the thymus with some showing infiltration into the small intestine) was 66% and the

incidence of intestinal tumour formation was 30% (Figure 5.8). In total, there were 3 intestinal neoplasms and 4 thymic lymphomas in 10TMZ_EtOH_*Msh2*$^{fl\ KO}$ mice compared with 4 intestinal neoplasms and 1 thymic lymphoma in 10TMZ_H_2O_*Msh2*$^{fl\ KO}$ mice (Figure 5.9).

In Group-D (5 TMZ doses, ethanol-treated cohort; 5TMZ_EtOH_*Msh2*$^{fl\ KO}$), Msh2-LS mice were culled between 8 and 12 weeks of the start of the 20% ethanol in drinking water regime. Four out of 6 5TMZ_EtOH_*Msh2*$^{fl\ KO}$ mice showed primary thymic lymphoma with infiltration of lymphoma into liver and spleen, one showed a colonic adenoma, and one showed an adenoma in the duodenum and an adenoma in the caecum. In the remaining 2 animals, extended colonic mucosal hyperproliferative areas and small adenomas were observed in the proximal colon and mid colon. In the corresponding water-treated control group (Group-F, 5 TMZ doses, water-treated cohort; 5TMZ_H_2O_*Msh2*$^{fl\ KO}$), 4 out of 6 mice were culled between 10 and 14 weeks after the last TMZ administration because of discomfort or distress due to thymic lymphoma with lymphoma infiltration into liver and spleen. In addition, 1 of the mice showed a small intestinal adenoma and another one of the mice developed small adenomas in the proximal colon and mid colon (with no evidence of colonic mucosal hyperproliferation). The remaining 2 5TMZ_H_2O_*Msh2*$^{fl\ KO}$ mice showed small adenomas in the small intestine, colon and caecum after 18 and 15 weeks following the last TMZ dose, respectively. In both 5TMZ_EtOH_*Msh2*$^{fl\ KO}$ and 5TMZ_H_2O_*Msh2*$^{fl\ KO}$ mice, the incidence of thymic lymphomas was 66%, and the incidence of intestinal tumour formation was 66% (Figure 5.10). In total, 4 thymic lymphomas and 10 intestinal neoplasms were observed in both 5TMZ_EtOH_*Msh2*$^{fl\ KO}$ and 5TMZ_H_2O_*Msh2*$^{fl\ KO}$ mice (Figure 5.11).

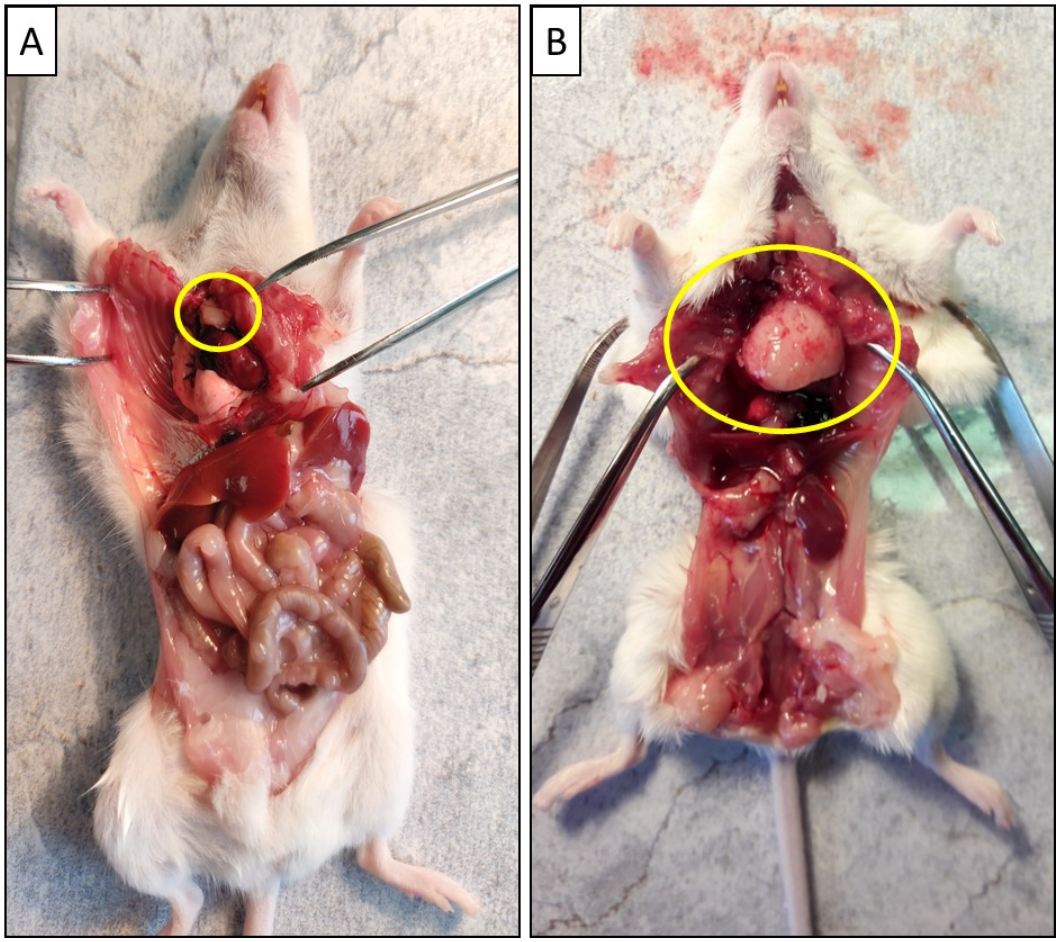

Figure 5.6: Representative necropsy images of normal thymus (A, highlighted in the yellow circle) from a wildtype mouse and thymus expanded by lymphoma (B, highlighted in the yellow circle) from a TMZ- and ethanol-treated Msh2-LS mouse.

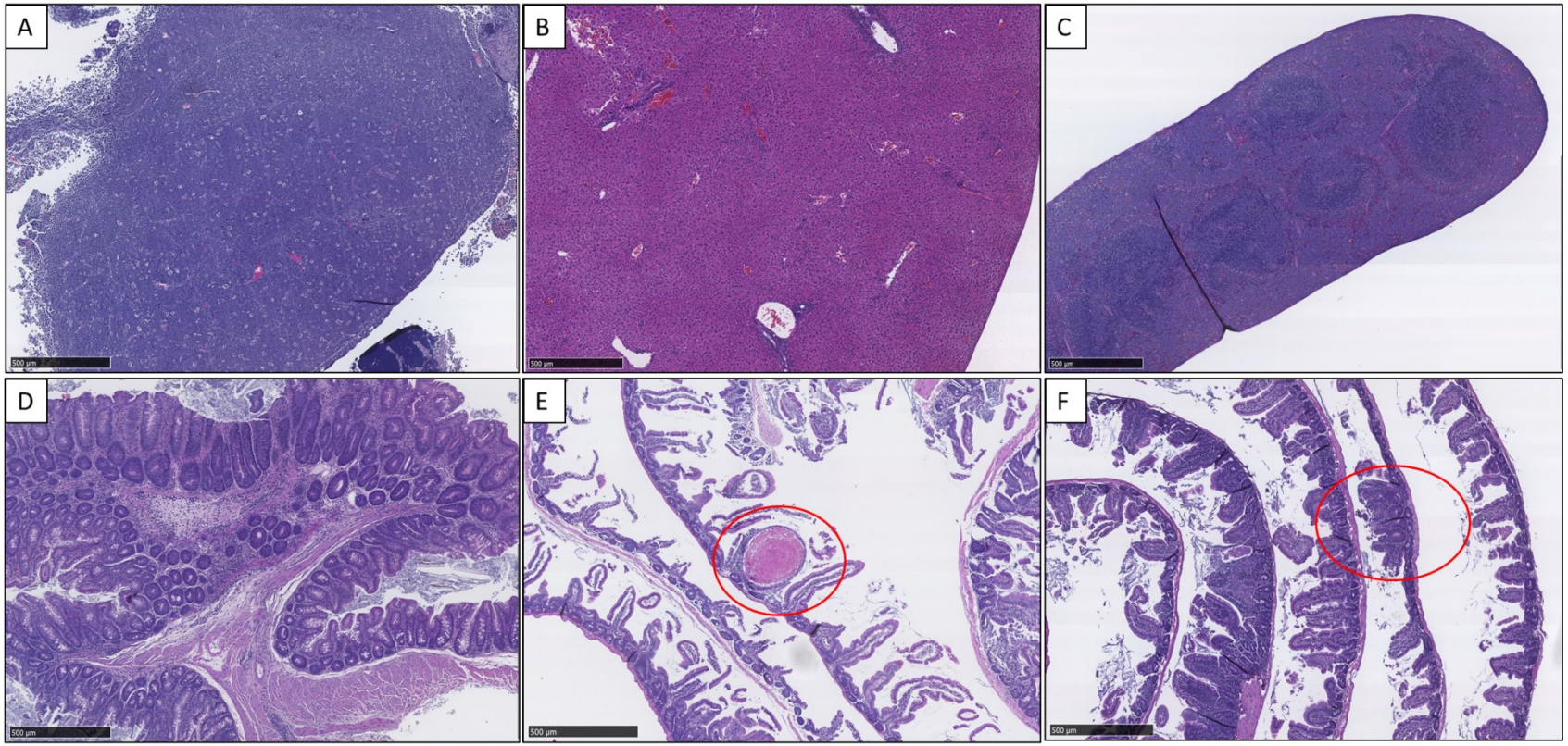

Figure 5.7: Representative images of histopathological sections of tumours observed in TMZ- and ethanol-treated Msh2-LS mice. In the first row, images are shown of H&E stained sections of thymic lymphoma (A), lymphoma infiltrating liver (B), and lymphoma infiltrating spleen (C). In the second row, images are shown of H&E stained sections of caecal adenoma (D), small intestinal monocryptal adenoma (red oval) (E), and colonic adenoma (red oval) with surrounding infiltration by lymphoma in mucosal and submucosal regions (F). Images taken from stained sections that were subsequently scanned using the Hamamatsu Nanozoomer and analysed with photographic image export using the Hamamatsu NDP Viewer software at 5X magnification (bar at lower left indicates 500µm).

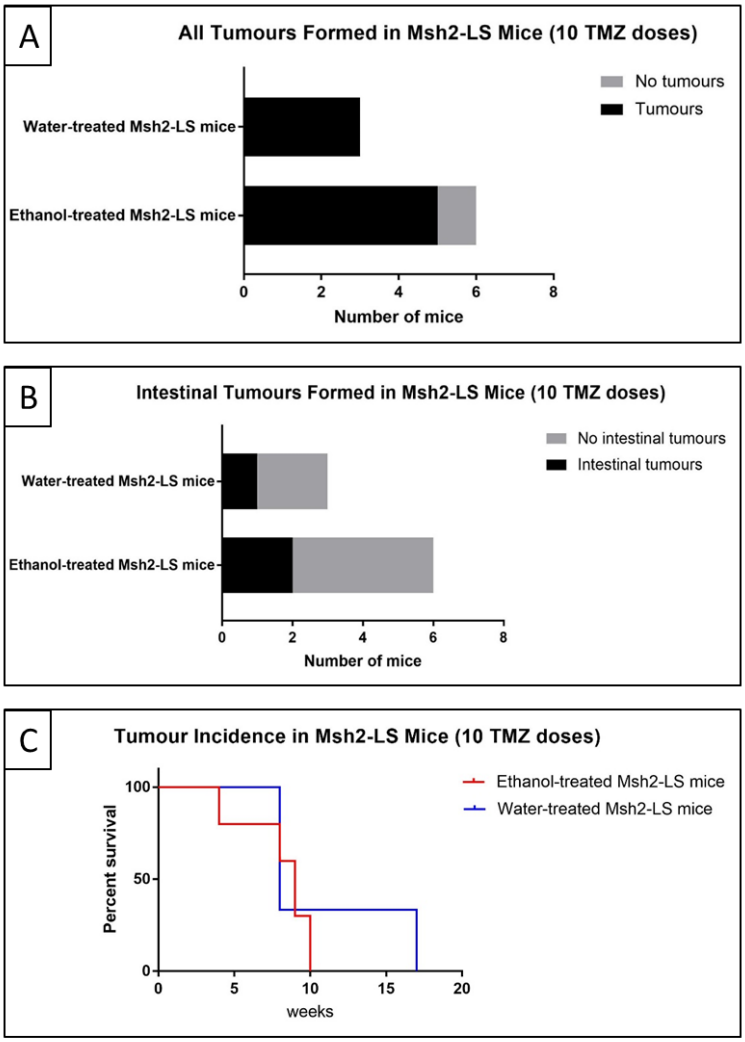

Figure 5.8: A) Bar chart of the number of Msh2-LS mice in Group-C (ethanol-treated, 10TMZ_EtOH_*Msh2*$^{fl\ KO}$) and Group-E (water-treated, 10TMZ_H_2O_*Msh2*$^{fl\ KO}$) that developed any tumours (lymphomas and intestinal adenomas) after receiving 10 TMZ doses and either 20% ethanol in drinking water or regular drinking water: 5/6 (83%) 10TMZ_EtOH_*Msh2*$^{fl\ KO}$ mice developed tumours compared with 3/3 (100%) 10TMZ_H_2O_*Msh2*$^{fl\ KO}$ mice that developed tumours. Fisher's exact test, no significant differences observed. B) Bar chart of the number of Msh2-LS mice in Group-C (10TMZ_EtOH_*Msh2*$^{fl\ KO}$) and Group-E (10TMZ_H_2O_*Msh2*$^{fl\ KO}$) that developed intestinal tumours after receiving 10 TMZ doses and either 20% ethanol in drinking water or regular drinking water: 2/6 (33%) 10TMZ_EtOH_*Msh2*$^{fl\ KO}$ mice developed intestinal tumours compared with 1/3 (33%) 10TMZ_H_2O_*Msh2*$^{fl\ KO}$ mice that developed intestinal tumours. Fisher's exact test, no significant differences observed. C) Tumour incidence in Msh2-LS mice in Group-C (10TMZ_EtOH_*Msh2*$^{fl\ KO}$) and Group-E (10TMZ_H_2O_*Msh2*$^{fl\ KO}$) following 10 TMZ doses and either 20% ethanol or normal drinking water. The survival plot shows development of tumours (both lymphomas and intestinal adenomas) in the ethanol-treated group (red) compared with the water-treated group (blue), Log-rank (Mantel-Cox) test showed no significant differences.

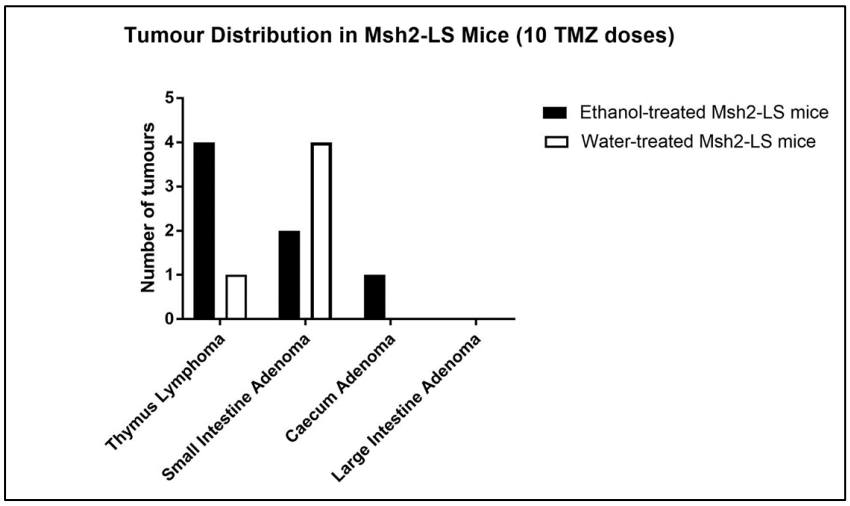

Figure 5.9: Tumour distribution in Msh2-LS mice in Group-C (ethanol-treated, 10TMZ_EtOH_ *Msh2*$^{fl\,KO}$ mice, black bars) and Group-E (water-treated, 10TMZ_H_2O_ *Msh2*$^{fl\,KO}$ mice, white bars) after 10 doses of TMZ treatment. In 10TMZ_EtOH_ *Msh2*$^{fl\,KO}$ mice (Group-C), 4 thymus lymphomas, 2 small intestinal adenomas and 1 caecal adenoma were observed. In 10TMZ_H_2O_ *Msh2*$^{fl\,KO}$ mice (Group-E), 1 thymus lymphoma and 4 small intestinal adenomas were seen.

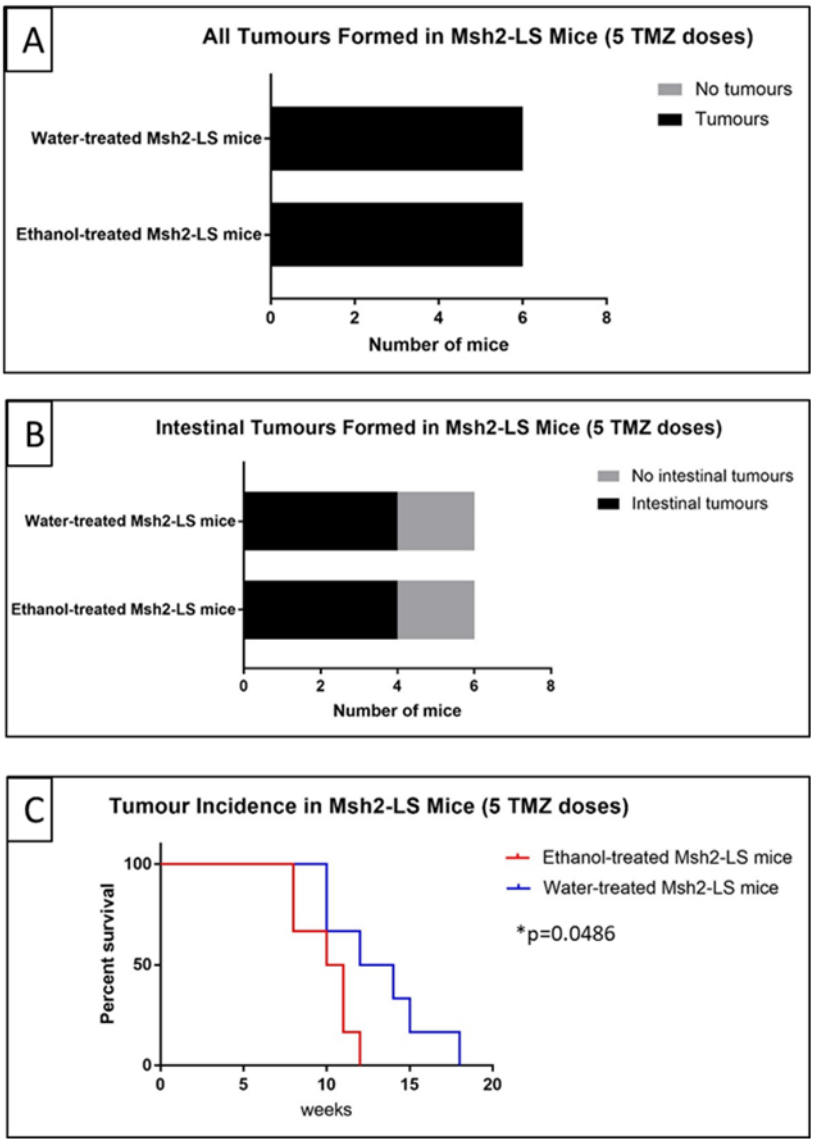

Figure 5.10: A) Bar chart of the number of Msh2-LS mice in Group-D (ethanol-treated, 5TMZ_EtOH_ *Msh2*$^{fl\ KO}$) and Group-F (water-treated, 5TMZ_H_2O_ *Msh2*$^{fl\ KO}$) that developed tumours (lymphomas and intestinal adenomas) after receiving 5 TMZ doses and either 20% ethanol in drinking water or regular drinking water: 6/6 (100%) 5TMZ_EtOH_ *Msh2*$^{fl\ KO}$ mice and 6/6 (100%) 5TMZ_H_2O_ *Msh2*$^{fl\ KO}$ mice developed tumours. Fisher's exact test, no significant differences observed. B) Bar chart of the number of Msh2-LS mice in Group-D (5TMZ_EtOH_ *Msh2*$^{fl\ KO}$) and Group-F (5TMZ_H_2O_ *Msh2*$^{fl\ KO}$) that developed intestinal tumours after receiving 5 TMZ doses and either 20% ethanol in drinking water or regular drinking water: 4/6 (66%) 5TMZ_EtOH_ *Msh2*$^{fl\ KO}$ and 4/6 (66%) 5TMZ_H_2O_ *Msh2*$^{fl\ KO}$ mice developed intestinal tumours. Fisher's exact test, no significant differences observed. C) Tumour incidence in Msh2-LS mice in Group-D (5TMZ_EtOH_ *Msh2*$^{fl\ KO}$) and Group-F (5TMZ_H_2O_ *Msh2*$^{fl\ KO}$) following 5 TMZ doses and either 20% ethanol or normal drinking water. The survival plot shows development of tumours (both lymphomas and intestinal adenomas) in the ethanol-treated group (red) compared with the water-treated group (blue). Log-rank (Mantel-Cox) test showed a statistically significant difference between the two curves, *p=0.0486.

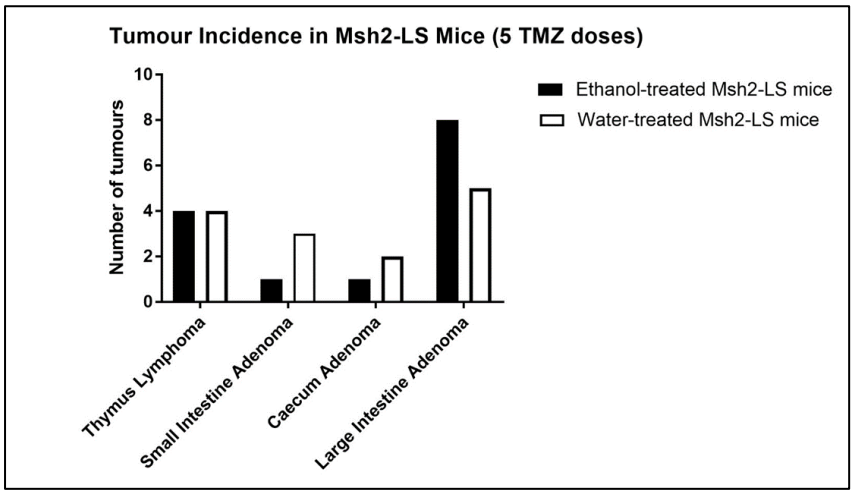

Figure 5.11: Tumour distribution in Msh2-LS mice in Group-D (ethanol-treated, 5TMZ_EtOH_ *Msh2*$^{fl\ KO}$ mice, black bars) and Group-F (water-treated, 5TMZ_H_2O_ *Msh2*$^{fl\ KO}$ mice, white bars) after 5 doses of TMZ treatment. In 5TMZ_EtOH_ *Msh2*$^{fl\ KO}$ mice (Group-D), 4 thymic lymphomas, 1 small intestinal adenoma, 8 colonic adenomas and 1 caecal adenoma were observed. In 5TMZ_H_2O_ *Msh2*$^{fl\ KO}$ mice (Group-F), 4 thymic lymphomas, 3 small intestinal adenomas, 5 colonic adenomas and 2 caecal adenomas were seen.

5.2.2.3 Immunohistochemical characterization of tumours and tissues from the Msh2-LS mouse model after Temozolomide and ethanol treatment

5.2.2.3.1 Msh2 immunostaining of Msh2-LS murine small intestinal and colonic tissues

Msh2 expression was analysed in murine tumour and normal intestinal tissues and other tissues in *Msh2$^{flox/+}$; Lgr5CreERT2$^{+/-}$; mTmG$^{+/-}$*mice following Cre activation by Tamoxifen treatment, either 5 or 10 daily TMZ doses, and either ethanol or water treatments. Small and large intestinal tissues were harvested, prepared as Swiss-rolls and fixed in 10% NBF (as described in Materials and Methods). They were processed using standard tissue processing protocols for paraffin wax embedding and microtome sectioning. Immunohistochemical staining for Msh2 was performed using protocols described in Materials and Methods (2.2.3) followed by manual counting of Msh2-positive and negative crypts. Tamoxifen treatment induced the loss of Msh2 expression in Lgr5+ expressing crypt epithelial stem cells scattered along the entire intestines, as previously shown in Chapter 4 (4.4.2.1). We used small intestinal tissue samples of *Msh2$^{-/-}$* and WT mice as Msh2-negative and -positive expression controls respectively (Figure 5.12). The lack of IHC DAB-brown staining in the *Msh2$^{-/-}$* tissues confirmed complete loss of Msh2 expression in the Msh2-null control tissues and similar patterns of Msh2 expression loss were observed in the intestinal epithelium in scattered crypts of the Msh2-LS mice.

In the colon, the number of Msh2-negative crypts was slightly higher (but not significantly so) in the ethanol-treated mice compared with the water-treated mice in both Msh2-LS mice treated with 5 and 10 TMZ doses (Figure 5.13). In 5TMZ_EtOH_*Msh2$^{fl\ KO}$* mice, 23% Msh2-negative colonic crypts were observed compared with 20% Msh2-negative colonic crypts found in 5TMZ_H_2O_*Msh2$^{fl\ KO}$* controls. In 10TMZ_EtOH_*Msh2$^{fl\ KO}$* mice, 32% Msh2-negative colonic crypts were observed compared with 27% Msh2-negative colonic crypts found in 10TMZ_H_2O_*Msh2$^{fl\ KO}$* controls (Figure 5.14). The number of Msh2-negative crypts was higher in the SI than in the colon; the number of Msh2-negative crypts in the SI was slightly higher (but not significantly so) in the ethanol-treated mice compared with the water-treated mice, in both Msh2-LS mice treated with 5 and 10 TMZ doses (Figure 5.15). In 5TMZ_EtOH_*Msh2$^{fl\ KO}$* mice, 48% Msh2-negative colonic crypts were observed compared with 40% Msh2-negative colonic crypts found in 5TMZ_H_2O_*Msh2$^{fl\ KO}$* mice. In 10TMZ_EtOH_*Msh2$^{fl\ KO}$*, 48% Msh2-negative colonic crypts were observed compared with

41% Msh2-negative colonic crypts found in 10TMZ_H_2O_*Msh2*$^{fl\ KO}$ mice (Figure 5.16). No significant differences were observed in any of these comparisons.

Due to the small size of large intestinal adenomas that were found in these Msh2-LS mice, there was insufficient adenoma tissue remaining in the tissue blocks for anti-Msh2 IHC analysis. However, some small intestinal adenomas showed Msh2-negative dysplastic glands often surrounded by or admixed with Msh2-positive crypts showing reactive or hyperproliferative changes (Figure 5.17).

Msh2 protein expression was examined by IHC in both normal thymus tissue and thymic lymphomas in order to investigate whether TMZ treatment can induce loss of the second *Msh2* allele (*Msh2*$^{flox/OFF}$) leading to MMR abrogation in Lgr5- thymus cells in the Msh2-LS mouse model, contributing to tumour formation outside of the intestinal Lgr5+ stem cells. Thymic lymphoma and normal thymus tissue samples from Msh2-LS model mice were investigated and no evidence of loss of Msh2 expression (no lack of brown IHC DAB staining) was found in either thymic lymphomas or normal thymus samples from *Msh2*$^{flox/-}$; *Lgr5CreERT2*$^{+/-}$; *mTmG*$^{+/-}$ mice treated with Tamoxifen and either 5 or 10 TMZ doses, including both ethanol-treated and water-treated mice (Figure 5.18).

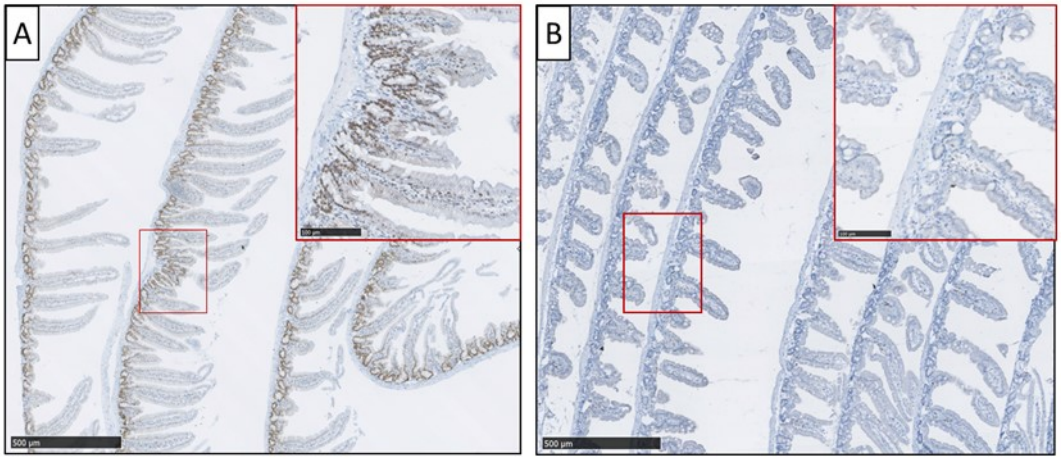

Figure 5.12: Immunohistochemical analysis of Msh2 protein expression in small intestinal mucosal epithelium from a positive-control WT mouse (A), in which the brown staining indicates positive Msh2 expression in all crypts (further magnified in the red rectangle); and from a negative-control *Msh2*$^{-/-}$ mouse (B), in which the lack of brown staining confirms the absence of Msh2 expression in intestinal mucosal epithelium (further magnified in the red rectangle). Images taken from anti-Msh2 IHC stained sections scanned using the Hamamatsu Nanozoomer and analysed with the Hamamatsu NDP Viewer software at 5X and 20X magnification (bar at lower left indicates 500µm, bar in red rectangle indicates 100µm).

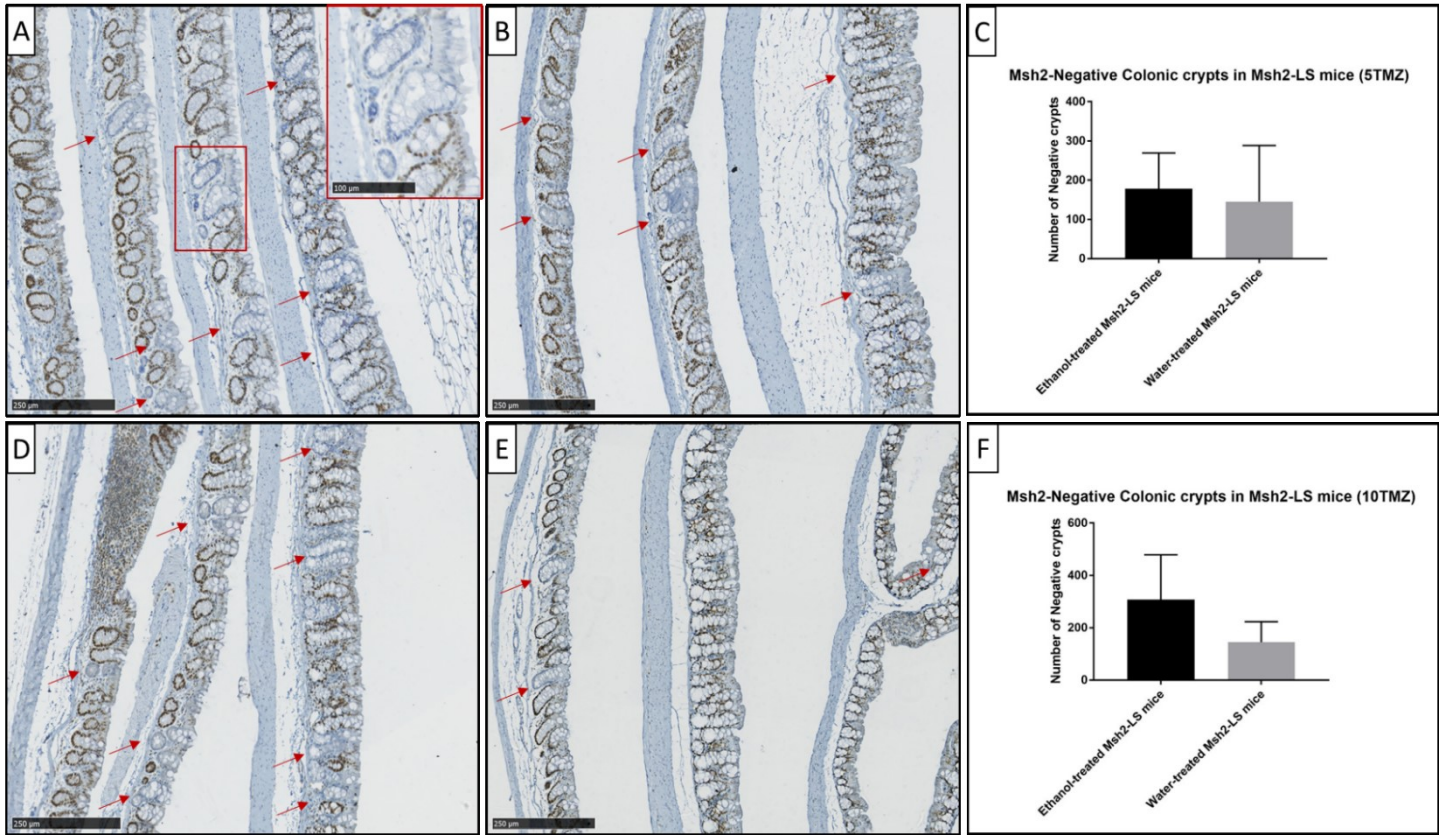

Figure 5.13: Immunohistochemical analysis of Msh2 protein expression in large intestinal mucosal epithelium of 5TMZ_EtOH_*Msh2*$^{fl\ KO}$ mice (A), compared with 5TMZ_H_2O_*Msh2*$^{fl\ KO}$ mice (B) and 10TMZ_EtOH_*Msh2*$^{fl\ KO}$ mice (D), compared with 10TMZ_H_2O_*Msh2*$^{fl\ KO}$ mice (E). Msh2-negative crypts (indicated by the red arrows and further magnified in the red rectangle in figure A) were manually counted along the entire colon for all four of these groups of treated Msh2-LS mice (shown in C and F, respectively). No significant differences were observed between ethanol-treated versus water-treated mice following either 5 or 10 doses of TMZ. Mann-Whitney U Test (data shown as mean±SD, n=3 mice each group). Images taken from sections scanned using the Hamamatsu Nanozoomer and analysed with the Hamamatsu NDP Viewer software at 10X and 20X magnification (bar at lower left indicates 250µm, bar in red rectangle indicates 100µm).

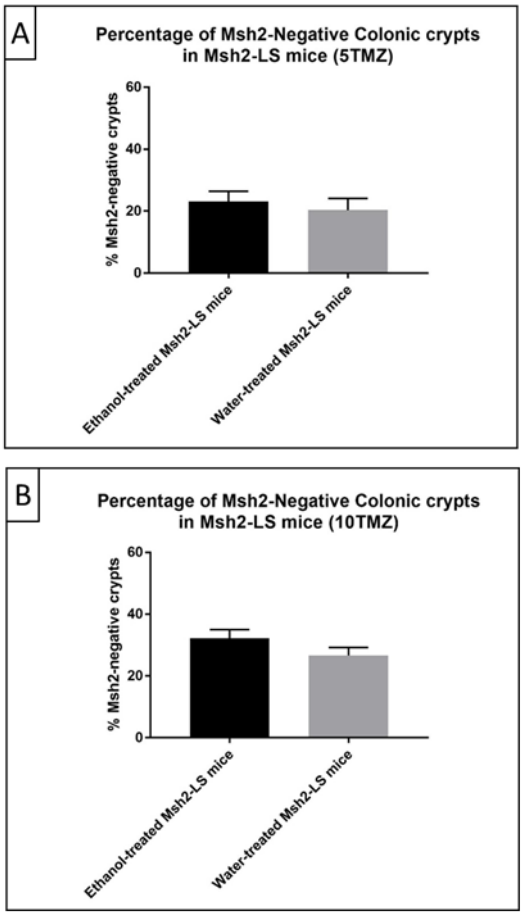

Figure 5.14: Percentage of Msh2 protein-non-expressing crypts in large intestinal mucosal epithelium of 5TMZ_EtOH_*Msh2*$^{fl\ KO}$ mice compared with 5TMZ_H_2O_*Msh2*$^{fl\ KO}$ mice (A), and 10TMZ_EtOH_*Msh2*$^{fl\ KO}$ compared with 10TMZ_H_2O_*Msh2*$^{fl\ KO}$ mice (B). No significant differences were observed between ethanol-treated versus water-treated mice following either 5 or 10 doses of TMZ. Mann-Whitney U Test (data shown as mean±SD, 300 crypts counted in 3 mice from each group).

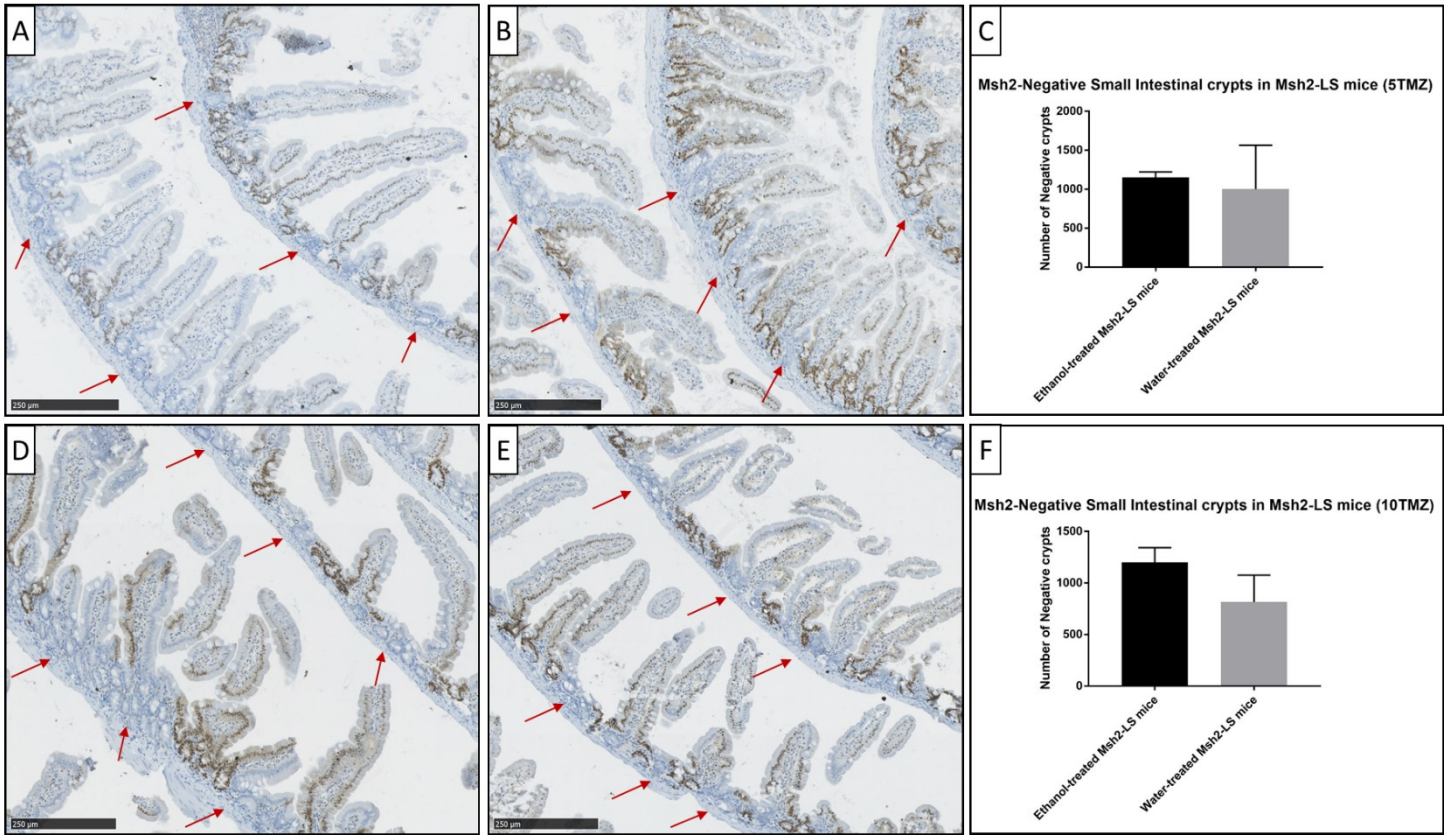

Figure 5.15: Immunohistochemical analysis of Msh2 protein expression in small intestinal mucosal epithelium of 5TMZ_EtOH_*Msh2*$^{fl\ KO}$ mice (A), compared with 5TMZ_H_2O_*Msh2*$^{fl\ KO}$ mice (B), and 10TMZ_EtOH_*Msh2*$^{fl\ KO}$ mice (D), compared with 10TMZ_EtOH_*Msh2*$^{fl\ KO}$ mice (E). Msh2-negative crypts were manually counted along the entire small intestine for both of these groups of treated Msh2-LS mice (C and F, respectively). No significant differences were observed between ethanol-treated versus water-treated mice following either 5 or 10 doses of TMZ. Mann-Whitney U Test (data shown as mean±SD, n=3 mice each group). Images taken from sections scanned using the Hamamatsu Nanozoomer and analysed with the Hamamatsu NDP Viewer software at 10X magnification (bar at lower left indicates 250µm).

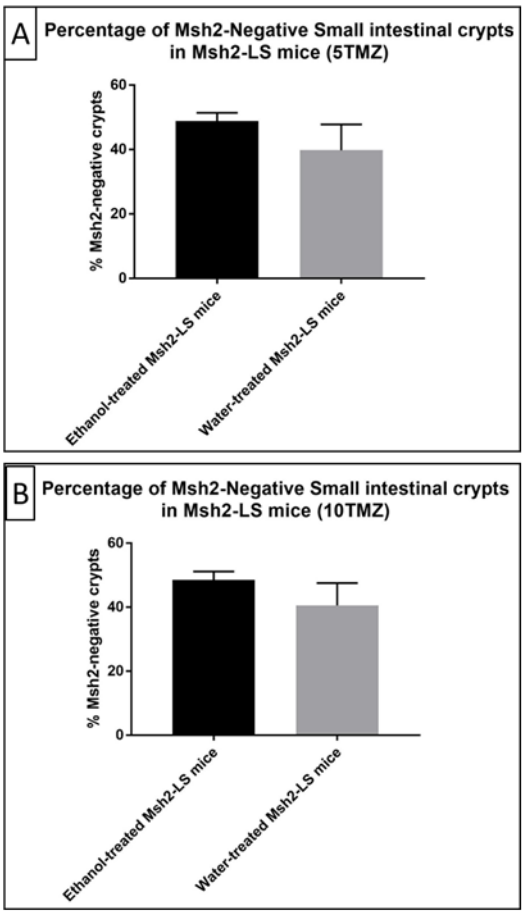

Figure 5.16: Percentage of Msh2 protein-non-expressing crypts in small intestinal mucosal epithelium of 5TMZ_EtOH_*Msh2*$^{fl\ KO}$ mice compared with 5TMZ_H_2O_*Msh2*$^{fl\ KO}$ mice (A), and 10TMZ_EtOH_*Msh2*$^{fl\ KO}$ mice compared with 10TMZ_H_2O_*Msh2*$^{fl\ KO}$ mice (B). No significant differences were observed between ethanol-treated versus water-treated mice following either 5 or 10 doses of TMZ. Mann-Whitney U Test (data shown as mean±SD, 300 crypts counted in 3 mice from each group).

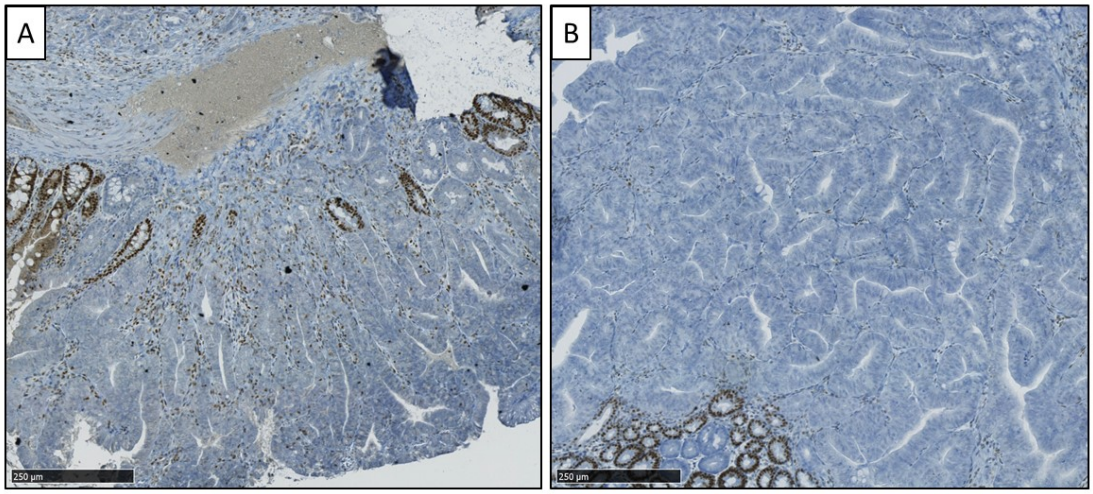

Figure 5.17: Representative images of Msh2 immunohistochemical staining for Msh2 in small intestinal adenomas from 5TMZ_EtOH_*Msh2*$^{fl\,KO}$ mice (A) and from 5TMZ_H_2O_*Msh2*$^{fl\,KO}$ mice (B). In both examples, there are Msh2-negative dysplastic or adenomatous glands, either surrounded by or admixed with reactive crypts or hyperproliferative crypts that are staining positively for Msh2. Images taken from sections scanned using the Hamamatsu Nanozoomer and analysed with the Hamamatsu NDP Viewer software at 10X magnification (bar at lower left indicates 250µm).

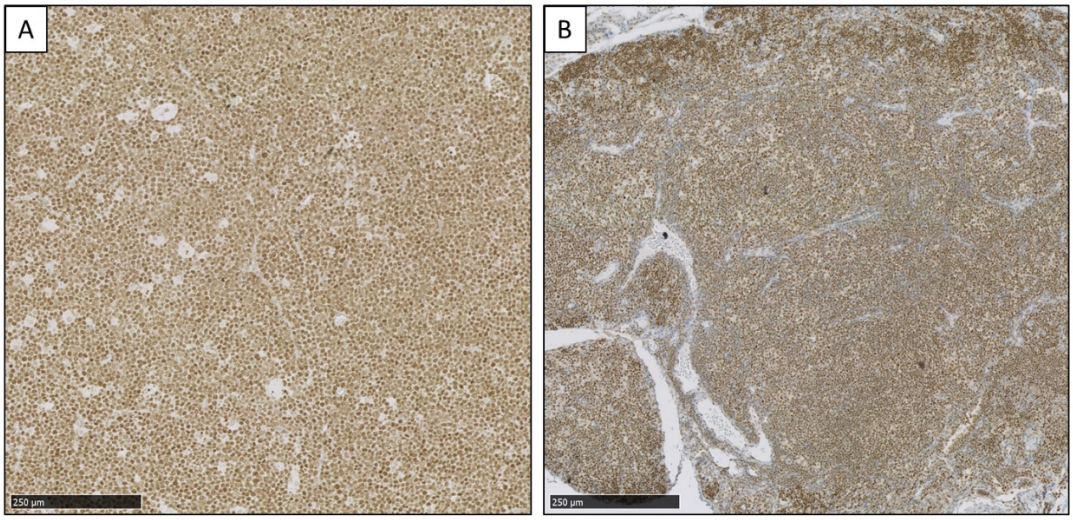

Figure 5.18: Immunohistochemical analysis of Msh2 protein expression in thymic lymphoma (A), and in normal thymus tissue (B), from *Msh2$^{flox/-}$; Lgr5CreERT2$^{+/-}$; mTmG$^{+/-}$*mice, showing no evidence of loss of Msh2 expression in thymic lymphoma or normal thymus.

5.2.2.3.2 Ki-67 and Beta-Catenin immunostaining of Msh2-LS murine small intestinal and colonic tissues

Immunohistochemical staining for Ki-67 was performed using protocols described in Materials and Methods (2.2.3). This was used to investigate Ki-67 expression in *Msh2$^{flox/-}$; Lgr5CreERT2$^{+/-}$; mTmG$^{+/-}$* mice treated with TMZ and either 20% ethanol in drinking water or normal water. This was observed in normal large and small intestinal tissues of Msh2-LS mice, indicating absence of aberrant cell proliferation taking place outside the stem cell at the base of crypts (Figure 5.19B and C). By contrast, large regions of colonic mucosal crypt hyperproliferation and small intestinal adenomas of Msh2-LS mice showed Ki-67-positive crypts all along the extended crypts, confirming the presence of neoplastic tissue (Figure 5.19A and B).

Immunohistochemical staining for β-catenin was performed using protocols described in Materials and Methods (2.2.3). β-catenin is the key signalling intermediate of the Wnt pathway and is sometimes used as a CRC biomarker (Lugli et al., 2007), as described in Chapter 4 (4.4.2.3). This was used to investigate β-catenin and expression in tumour tissue of *Msh2$^{flox/-}$; Lgr5CreERT2$^{+/-}$; mTmG$^{+/-}$* mice treated with TMZ and either 20% ethanol in drinking water or normal water. β-catenin IHC was performed with assistance from Marion Bacou using large intestinal samples from *Apc Min* mice that contained large intestinal adenomas (provided by Vidya Rajasekaran), and WT mice as β-catenin-positive and β-catenin-normal expression controls respectively (Figure 4.41). The immunohistochemical analysis of β-catenin was performed on small and large intestinal adenomas from Msh2-LS mice. Analysed samples showed a heterogeneous pattern with variable numbers of adenoma cells showing positive β-catenin nuclear immunostaining due to accumulation and translocation of β-catenin in the nuclei (Figure 5.20).

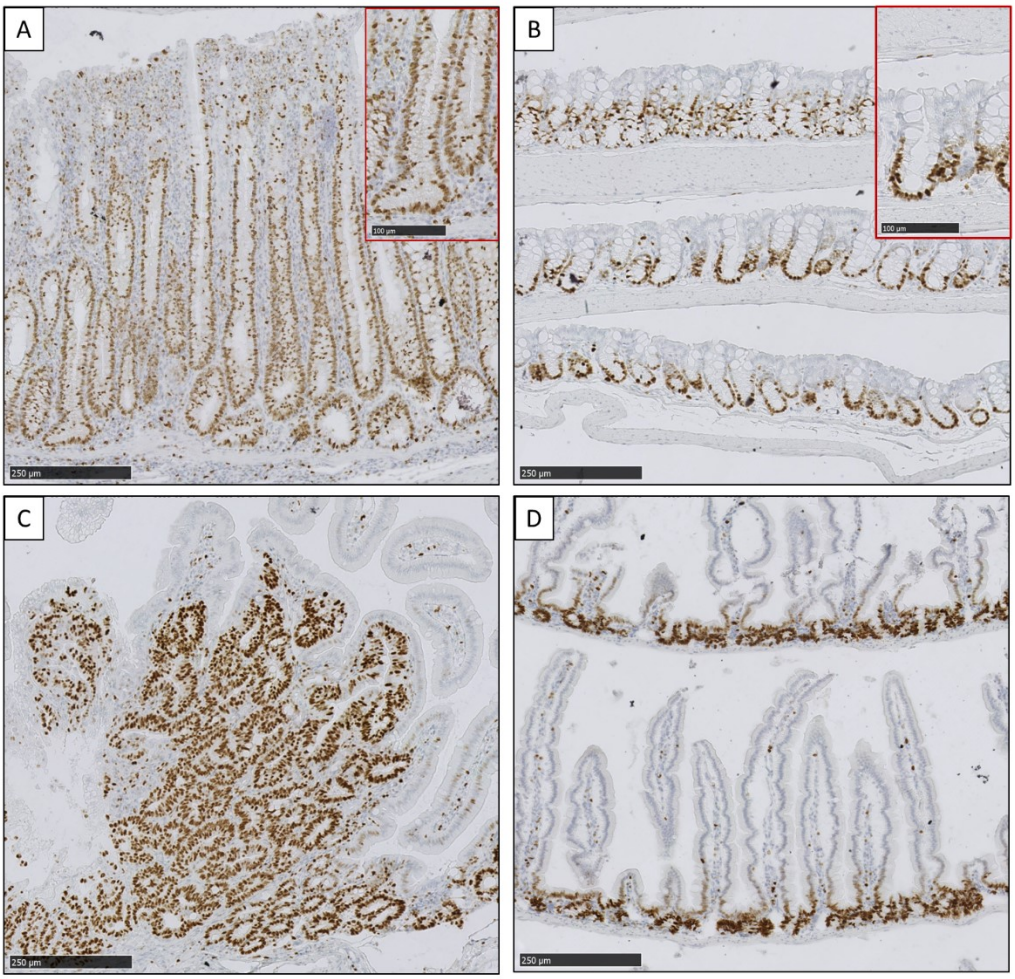

Figure 5.19: Immunohistochemical analysis of Ki-67 protein expression in normal large and small intestinal mucosal epithelium of *Msh2$^{flox/-}$; Lgr5CreERT2$^{+/-}$; mTmG$^{+/-}$*mice treated with TMZ (B and D) and neoplastic large and small intestinal mucosal epithelium of *Msh2$^{flox/-}$; Lgr5CreERT2$^{+/-}$; mTmG$^{+/-}$* mice treated with TMZ (A and C). Images taken from sections scanned using the Hamamatsu Nanozoomer and analysed with the Hamamatsu NDP Viewer software at 10X and 20X magnification (bar at lower left indicates 250µm, bar in red rectangle indicates 100µm).

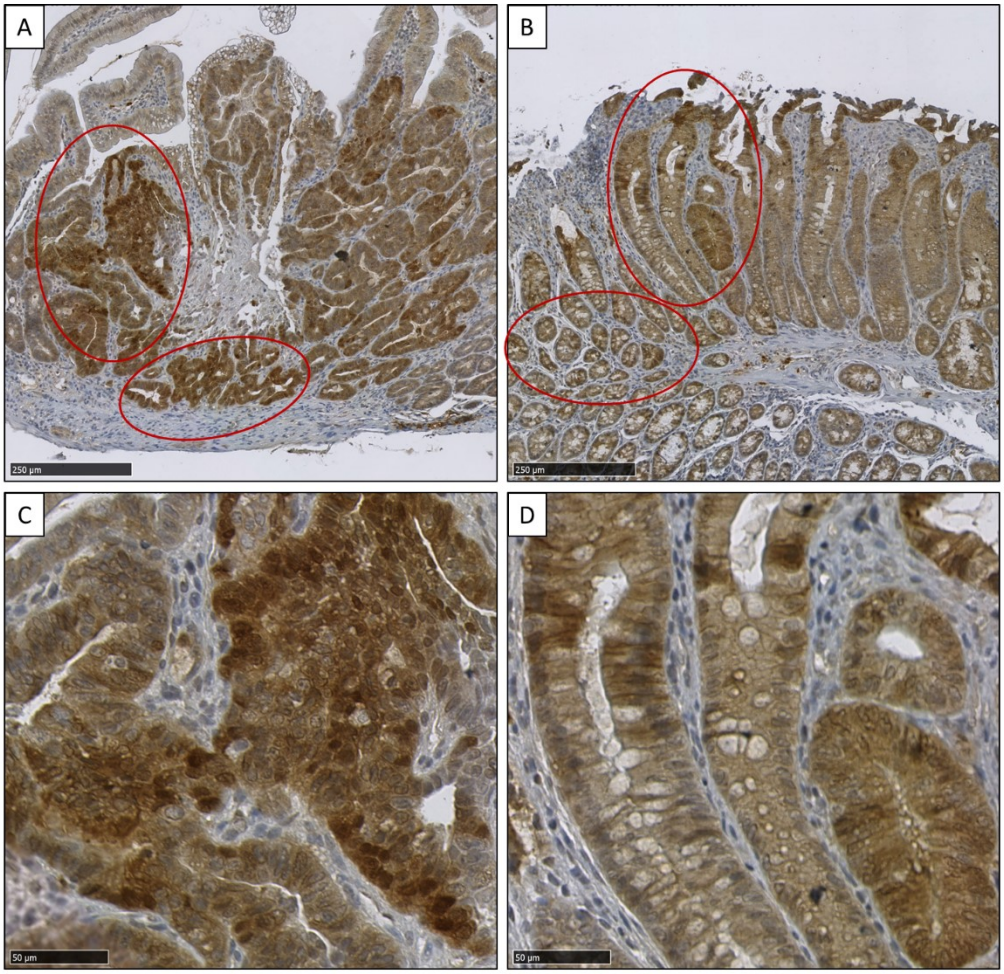

Figure 5.20: Representative images of immunohistochemical analysis of β-catenin protein expression and localisation in intestinal adenomas of *Msh2$^{flox/-}$; Lgr5CreERT2$^{+/-}$; mTmG$^{+/-}$* mice treated with TMZ. Variable areas of positive β-catenin nuclear immunostaining in adenomatous cells were observed in both small intestinal adenomas (A) and colonic adenomas (B), indicated by the red ovals. Images are further magnified in panel figures C and D. Images taken from sections scanned using the Hamamatsu Nanozoomer and analysed with the Hamamatsu NDP Viewer software at 10X and 40X magnification (bar at lower left indicates 250µm and 50 µm).

5.3 Discussion

In this work, the aim was to potentially accelerate dMMR-driven intestinal tumour formation in the Msh2-LS mouse model by applying TMZ treatment, as used by Wojciechowicz et al. (2014).

Wojciechowicz et al. (2014) generated the Msh2-LS mouse model in which Tamoxifen-induced loss of Msh2 expression in approximately 10% of intestinal crypts, without any additional carcinogen treatment, and this led to intestinal tumours in 40% of the mice after 1.5 years. Wojciechowicz et al. (2014) showed that Msh2-LS (*Msh2$^{flox/-}$; Lgr5CreERT2$^{+/-}$*) mice of 6–7 weeks age received either 5 or 10 daily doses of TMZ over three weeks (100mg/kg of TMZ) after Tamoxifen treatment, resulting in early gastrointestinal intra-epithelial neoplasms and later intestinal adenomas and/or adenocarcinomas, with some thymic lymphomas (no quantitative data on lymphomas were provided). It is known that the number of dMMR crypt foci influences the risk of tumour development in LS patients. The size and growth rate of the dMMR cell pool appears to vary with time (as consequence of an increased mutation rate) and with exposure to some environmental factors (Kloor et al., 2012). TMZ is a methylating agent and MMR-deficient cells are known to be resistant to killing by methylating agents. TMZ exposure caused an expansion of pre-existing Msh2-deficient colonic crypt foci increasing the number of fully Msh2-deficient crypts in a statistically significant way (Wojciechowicz et al., 2014).
In this chapter, a modification of the standard protocol was designed by introducing an additional treatment with TMZ with the aim of potentially accelerating intestinal tumour formation to around 2-4 months, when combined with ethanol.

In these preliminary experiments, Tamoxifen treatment was halved from that used in the Chapter 4 procedure, to a daily i.p injection for 2 consecutive days, in line with Wojciechowicz et al (2014). This change in Tamoxifen treatment was made to reduce the probability of very large numbers of tumours arising from widespread dMMR foci induced by Tamoxifen-mediated Cre activation followed by TMZ treatment. This change also reduced the number of procedures applied to the experimental subjects in line with 3Rs. However, it had already been demonstrated in Chapter 3 that 2 i.p. Tamoxifen injections were sufficient to activate Cre-recombinase in an acceptable number of Lgr5-expressing intestinal stem cells. Both male and female Msh2-LS mice showed good acceptance of Tamoxifen treatment, showing stable body weights during the treatment duration. Msh2-LS male mice showed statistically higher

mean body weight compared with Msh2-LS female mice mean body weight at the same age ($p<0.0001$). Subsequently, in order to identify the most appropriate TMZ dose and treatment regime to induce tumorigenesis in around 2-4 months, animals were divided into groups that received either 5 or 10 daily doses of TMZ (100mg/kg) by o.g. over 2 or 3 weeks respectively, as described by Wojciechowicz et al. (2014).

TMZ treatment was commenced the following week to allow time for the activated Cre to inactivate the second conditional knockout Msh2 allele. In this way, the dMMR stem cells at the crypt bases had time to expand into many dMMR daughter cells passing through the transit-amplifying compartment into the differentiation compartment, moving up the crypts and on to the table surface of the colonic mucosa or onto the small intestinal villi. Most of the mice accepted the TMZ administrations well. During TMZ treatment with either 5 or 10 TMZ doses treatment, body-weights of Msh2-LS female and male mice did not significantly change. Body weights of Msh2-LS males were significantly higher than body weights of Msh2-LS females (as expected due to normal sexual dimorphism observed in rodents), but no major fluctuations in body weights were observed during the treatments. However, a few mice died during the treatments likely due to presumed hypersensitivity to the methylating agent, which has been reported by others.

After TMZ, Msh2-LS mice received either 20% ethanol in drinking water or normal drinking water. Msh2-LS female and male mice did not show any reduction in body weight during the first weeks showing good acceptance of the ethanol regime. Ethanol-treated and water-treated Msh2-LS female mice showed similar mean body weights (23.14g and 23.28g respectively) and no significant differences were observed between these two cohorts. By contrast, Msh2-LS ethanol-treated mice showed a decrease of an average of 5g over 13 weeks (from ~30g to ~25g), whereas the water-treated mice showed a general increase in body weight over the same time period. The trend over time of the body weights curves between these two cohorts showed a statistically significant difference of $p<0.0001$. The female Msh2-LS mice survived only 13-14 weeks under either liquid regime. Similarly, the ethanol-treated male Msh2-LS mice survived 13-14 weeks, whereas water-treated male Msh2-LS mice survived until 21-22 weeks. However, the average ml of liquid consumption per mouse (13.5ml for water-treated Msh2-LS males, 13.8ml for ethanol-treated Msh2-LS males, 8.9ml for water-treated Msh2-LS females, and 11.2ml for ethanol-treated Msh2-LS females) did not significantly differ from the data obtained in the previous experiments (13.85ml for water-treated Msh2-LS males, 11.65ml for ethanol-treated Msh2-LS males,

10.33ml for water-treated Msh2-LS females, and 9.65ml for ethanol-treated Msh2-LS females; see Chapter 4; Figure 4.4).

Msh2-LS mice in this experiment did not survive as long as the mice in the previous experiment due to the carcinogenic effects of TMZ treatment. The main reason for early death of the mice was that in most cases Msh2-LS mice receiving either 5 or 10 daily TMZ doses, and either ethanol or water treatments, needed to be culled because of clinical signs relating to thymic lymphoma. Wojciechowicz et al. (2014) treated Msh2-LS mice with TMZ and they survived only 19 weeks from the last TMZ administration: 11 out of 13 Msh2-LS TMZ-treated mice displayed extended extra-intestinal lymphoid formations or lymphomas that were the main cause of death. Only two mice were culled for clinical signs of large intestinal neoplasms. In most cases, gastrointestinal abnormalities and neoplasms were only discovered during histopathological analysis suggesting secondary relevance.

In all cohorts, we observed thymic lymphomas in 66% of the cases in each group. By contrast, 10TMZ_EtOH_*Msh2*$^{fl\ KO}$ and 10TMZ_H_2O_*Msh2*$^{fl\ KO}$ mice showed only 33% intestinal tumour incidence, while in 5TMZ_EtOH_*Msh2*$^{fl\ KO}$ and 5TMZ_H_2O_*Msh2*$^{fl\ KO}$ mice showed 66% intestinal tumour incidence. When tested for presence or absence of Msh2 protein expression by IHC, the thymic lymphomas showed positive expression of Msh2, indicating that these tumours had arisen from MMR-proficient cells, most likely as a result of the carcinogenic effects of TMZ rather than by selection of dMMR cells for neoplastic growth. The results obtained from these experiments were similar to those described by Wojciechowicz et al. (2014), suggesting that both the lymphomas and the intestinal tumours observed were most likely a consequence of TMZ carcinogenic effects and not related to any ethanol effects. The TMZ carcinogenic properties appear to be too potent and mask any ethanol tumour-inducing effects. In 5TMZ_EtOH_*Msh2*$^{fl\ KO}$ and 5TMZ_H_2O_*Msh2*$^{fl\ KO}$ mice, the intestinal tumour incidence was higher than that in 10TMZ_EtOH_*Msh2*$^{fl\ KO}$ and 10TMZ_H_2O_*Msh2*$^{fl\ KO}$ mice, demonstrating that the TMZ carcinogenic and toxic properties appeared to vary amongst these four groups to an extent that this prevented experimental revelation of any tumour-initiating or tumour-promoting ethanol effects on the Msh2-LS mice. In 5TMZ_EtOH_*Msh2*$^{fl\ KO}$ mice and 5TMZ_H_2O_*Msh2*$^{fl\ KO}$ mice, the lower dose TMZ treatment slightly extended the survival allowing time for the Tamoxifen-induced Msh2-LS mice to express in part their intestinal tumour prone phenotype. By contrast, in 10TMZ_EtOH_*Msh2*$^{fl\ KO}$ mice and 10TMZ_H_2O_*Msh2*$^{fl\ KO}$ mice, we observed a lower number

of intestinal tumours largely because these mice died earlier from extra-intestinal tumours (thymic lymphomas) induced by the higher dose of carcinogenic TMZ.

Some environmental factors (such as methylating compounds either naturally produced by the intestinal flora or absorbed with food) can promote survival of dMMR intestinal cells and their expansion (Stojic et al., 2004). Wojciechowicz et al. (2014) performed anti-Msh2 IHC on tumour and normal tissue samples comparing Msh2-LS mice treated with Tamoxifen followed by TMZ treatment with Msh2-LS mice treated only with Tamoxifen. They observed a higher number of crypts lacking Msh2 staining in the TMZ-treated Msh2-LS mice than in the non-TMZ treated Msh2-LS mice. Furthermore, the gastrointestinal intra-epithelial neoplasms showed lack of Msh2 expression IHC staining in crypts, thus forming dMMR crypts in around 68% around the tumour area. They demonstrated that TMZ treatment conferred a proliferative advantage upon dMMR cells over wild-type intestinal epithelial cells, leading to expansion of the dMMR crypt compartment.

We performed anti-Msh2-LS IHC on tumour and tissue samples from the Msh2-LS mice treated with TMZ and ethanol. We analysed Msh2 expression in murine small and large intestinal samples in *Msh2$^{flox/-}$; Lgr5CreERT2$^{+/-}$; mTmG$^{+/-}$* mice after either 5 or 10 daily TMZ doses, and either ethanol or water treatments. In both colon and SI, we did not observe any statistically significant differences in the numbers of Msh2-negative crypts between ethanol-treated and water-treated mice in Msh2-LS mice treated with either 5 or 10 daily TMZ doses. The number of dMMR crypts was higher in the SI than in the colon, as expected from previous experiments (see Chapter 4; 4.4.2.1). However, Msh2-LS mice treated with TMZ showed higher numbers of Msh2-negative crypt foci compared with those observed in the absence of TMZ-treatment in the Msh2-LS mice in the previous experiments (see Chapter 4; Figure 4.26 and Figure 4.30), suggesting a dominant effect due to selection for survival and expansion of dMMR crypt foci by the methylating agent TMZ.

TMZ is a strongly carcinogenic tumour-inducer and for this reason, the mice died prematurely from extra-intestinal tumours, predominantly thymic lymphomas, before intestinal tumours had time to develop. Due to the small size of large intestinal adenomas that were found in these Msh2-LS mice, there was insufficient adenoma tissue remaining in the tissue blocks for anti-Msh2 IHC analysis. However, some small intestinal adenomas showed Msh2-negative dysplastic glands often surrounded by or admixed with Msh2-positive crypts showing reactive or hyperproliferative changes.

Msh2 protein expression was examined by IHC in both normal thymus tissue and thymic lymphomas in order to investigate whether TMZ treatment can induce loss of the second *Msh2* allele (*Msh2*$^{flox/OFF}$) leading to MMR abrogation in Lgr5- thymus cells in the Msh2-LS mouse model, potentially contributing to tumour formation from other sources outside of the intestinal Lgr5+ stem cells. The immunostaining for Msh2 proved to be technically difficult on thymus tissue, therefore we relied on the samples that showed a reliable result. No evidence of loss of Msh2 expression (no lack of brown IHC DAB staining) was found in either thymic lymphomas or normal thymus control samples from *Msh2*$^{flox/-}$*; Lgr5CreERT2*$^{+/-}$*; mTmG*$^{+/-}$mice treated with either 5 or 10 TMZ doses, including both ethanol-treated and water-treated mice, indicating that inactivation of mismatch repair was not involved in this pathway of thymic lymphoma formation.

Immunohistochemistry was performed to investigate Ki-67 expression in intestinal tissue samples from *Msh2*$^{flox/-}$*; Lgr5CreERT2*$^{+/-}$*; mTmG*$^{+/-}$mice treated with TMZ and either 20% ethanol in drinking water or normal water to determine proliferative activity. In normal large and small intestinal tissue, Ki-67 is expressed only in the proliferating cells at the base of crypts as previously reported (Johnston et al., 1989). Large regions of colonic mucosal crypt hyperproliferation and small intestinal adenomas of Msh2-LS mice showed Ki-67-positive crypts all along the extended crypts, confirming the presence of neoplastic tissue.

We investigated the expression of β-catenin protein, an intracellular signal transducer in the Wnt signalling pathway (Cong et al., 2003a), on tumours and tissue samples from *Msh2*$^{flox/-}$*; Lgr5CreERT2*$^{+/-}$*; mTmG*$^{+/-}$mice treated with TMZ and either 20% ethanol in drinking water or normal water. Normal colorectal tissue exhibits membranous localisation of β catenin whereas colorectal adenoma/adenocarcinoma shows nuclear β catenin localization, nuclear β-catenin is regarded as a useful CRC biomarker (Lugli et al., 2007). Small intestinal and colon adenomas showed a heterogeneous pattern with variable numbers of adenoma cells showing positive β-catenin nuclear immunostaining due to accumulation and translocation of β-catenin in the nuclei.

In conclusion, TMZ is a powerful methylating agent and carcinogen that can confer a proliferative advantage upon established dMMR crypt foci leading to selection for survival and expansion in the Msh2-LS murine intestines that could, potentially, lead to an acceleration of intestinal tumorigenesis. However, the carcinogenic properties of TMZ appear to be too potent in these experiments, inducing a variety of extra-intestinal tumours (independent from dMMR), predominantly thymic lymphomas, that mask any carcinogenic

ethanol effects. The data obtained were inconclusive and the use of TMZ was misleading for the purpose of exploring the carcinogenic and tumour-promoting effects of ethanol and its major metabolite acetaldehyde, particularly in combination with deficient MMR. For this reason, it was decided to discontinue the experimental investigation of TMZ in combination with ethanol in the Msh2-LS mouse model.

Chapter 6: Investigation of long-term ethanol consumption effects on Aldh1b1 conditional-knockout Msh2-LS mice and Aldh1b1 constitutive-knockout Msh2-LS mice

6.1 Introduction

The mechanisms of how ethanol induces intestinal carcinogenesis include involvement of its metabolite acetaldehyde. Acetaldehyde is a highly reactive molecule able to induce a wide range of DNA damage, as described in Chapter 1, 1.3.3. Evidence of acetaldehyde involvement in ethanol-related cancers emerged from the study of human polymorphisms in ADH and ALDH enzymes. A polymorphism of ALDH1B1 causes reduced enzyme activity and has been associated with altered drinking habits and alcohol sensitivity in Caucasians. ALDH1B1 plays a key role in acetaldehyde detoxification in the gastrointestinal epithelium (Stagos et al., 2010), as we previously explained in Chapter 1, 1.3.2.

As already mentioned in Chapter 4, our group demonstrated an important role of murine Aldh1b1 in acetaldehyde detoxification in vivo during intestinal tumorigenesis in wildtype and *Aldh1b1*-depleted mice after long-term ethanol treatment for one year (Müller et al., 2016).

Aldh1b1-depleted mice were generated using the 'knockout-first' *Aldh1b1* allele (tm1a) (Figure 6.1) (Skarnes et al., 2011). This contains an IRES:lacZ trapping cassette and a floxed promoter-driven neo cassette inserted into the intron of *Aldh1b1*, disrupting gene function. *Aldh1b1* tm1a was shown previously to be a hypomorph (Müller et al., 2016). The knockout-first allele can be easily modified in ES cells or in adult murine crosses with transgenic Flp and/or Cre transgenic mice. Conditional alleles (*Aldh1b1*$^{flox/flox}$) are generated by removal of the gene-trap cassette by Flp recombinase, which reverts the mutation to wild type, leaving loxP sites on either side of a critical exon creating a conditional allele (tm1c). Subsequent exposure to Cre deletes the critical exon to induce an exon deletion knockout mutation (tm1d) and this triggers nonsense-mediated decay of the mutant transcript, with production of no functional Aldh1b1 protein (Figure 6.1). If whole mouse Cre activation is used, this generates a complete knockout in every cell of the mouse (*Aldh1b1*$^{-/-}$ or constitutive knockout).

In this chapter, the first aim is to introduce the conditional *Aldh1b1* allele (*Aldh1b1*$^{flox/flox}$) and the constitutive *Aldh1b1* knockout allele (*Aldh1b1*$^{-/-}$), by cross-breeding of the Msh2-LS mouse model in order to establish an *Msh2*$^{flox/-}$*; Lgr5CreERT2*$^{+/-}$*; mTmG*$^{+/-}$*; Aldh1b1*$^{flox/flox}$ colony and an *Msh2*$^{flox/-}$*; Lgr5CreERT2*$^{+/-}$*; mTmG*$^{+/-}$*; Aldh1b1*$^{-/-}$ colony. In this chapter, the generation and characterization of these mouse models are described.

The second aim is to study the combined effects of inactivation of *Msh2* and *Aldh1b1* in mice with long-term ethanol treatment. We hypothesised that loss of Aldh1b1 function increases the levels of acetaldehyde in the intestinal epithelial cells, causing more acetaldehyde-mediated DNA damage that may interact with defective mismatch repair to influence intestinal tumour formation in these Msh2-LS mouse models.

In *Msh2*$^{flox/-}$*; Lgr5CreERT2*$^{+/-}$*; mTmG*$^{+/-}$*; Aldh1b1*$^{flox/flox}$ mice, the conditional loss of Aldh1b1 expression is dependent on Tamoxifen-induced Cre recombinase activation and this only occurs in Lgr5-expressing small intestinal and large intestinal stem cells along with loss of Msh2 expression. We predicted that Lgr5-expressing intestinal cells and their daughter cells would acquire a high number of DNA mutations due to the combined lack of MMR pathway activity and increased levels of acetaldehyde.

In contrast, *Msh2*$^{flox/-}$*; Lgr5CreERT2*$^{+/-}$*; mTmG*$^{+/-}$*; Aldh1b1*$^{-/-}$ constitutive knockout mice are characterized by complete loss of Aldh1b1 expression in all cells of the organism (Tamoxifen independent). We hypothesised that this would cause a further increase in acetaldehyde levels (above that in the conditional model), resulting in more acetaldehyde-mediated DNA damage in all cells of the organism, including a higher level of acetaldehyde-induced DNA mutations in the MMR-deficient intestinal cells, (loss of Msh2 expression in scattered induced-Lgr5-expressing intestinal stem cells) manifested by accelerated or increased tumour formation in these cells.

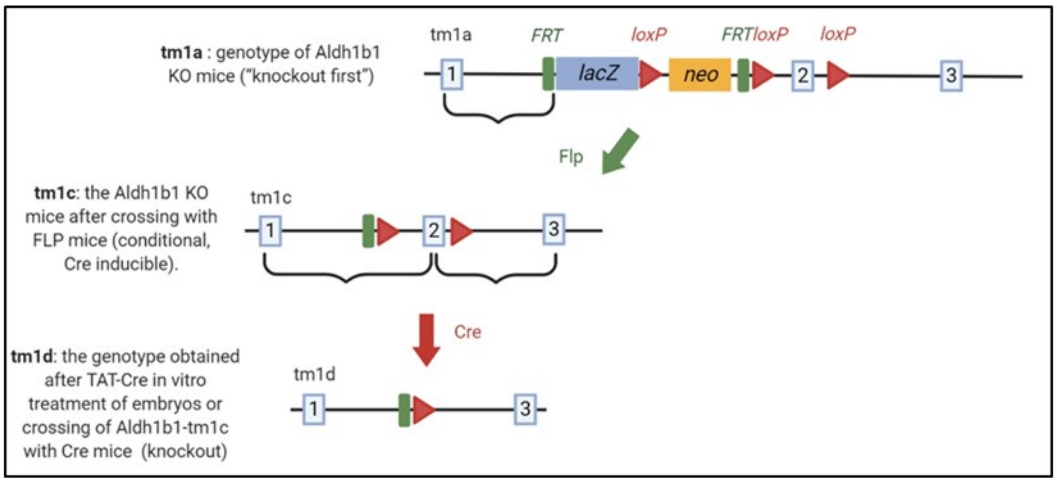

Figure 6.1: Schematic representation of the 'knockout-first' allele (tm1a) and its modifications. The tm1a allele contains an IRES:*lacZ* trapping cassette and a floxed promoter-driven *neo* cassette inserted into the intron of the target gene, disrupting gene function (in this case, the gene is *Aldh1b1*). Following breeding with an Flp expressing mouse, Flp recombines the two FRT sites and converts the 'knockout-first' allele to a conditional allele (tm1c, $Aldh1b1^{flox/flox}$), restoring normal gene activity. After subsequently breeding with a Cre expressing mouse, Cre recombines the two loxP sites and deletes the floxed exon of the tm1c allele to inactivate the gene (tm1d, $Aldh1b1^{-/-}$), triggering nonsense mediated decay of the exon-deleted transcript with complete loss of gene function (adapted and modified from Skarnes et al., 2011).

6.2 Establishment of the colony of combined Aldh1b1-knockout and Msh2-LS model mice

6.2.1 Methods

Mice were housed in IVCs with group sizes and enrichment according to Home Office regulations. Further details on the mice housing conditions and maintenance can be found in Chapter 2, 2.1.1.

6.2.2 Results

To generate the *Aldh1b1* conditional-knockout (*Aldh1b1*$^{flox/flox}$) mice, (Zhu & Sadowski, 1995) the *Aldh1b1* tm1a mice were cross-bred with Flpe mice obtained from Professor Ian Jackson (University of Edinburgh, Institute of Genetics & Molecular Medicine) (Zhu & Sadowski, 1995). Subsequently, the *Msh2*$^{+/+}$*; Lgr5CreERT2*$^{-/-}$*; mTmG*$^{-/-}$*; Aldh1b1*$^{flox/flox}$ mice were cross-bred with *Msh2*$^{flox/-}$*; Lgr5CreERT2*$^{+/-}$*; mTmG*$^{+/+}$*; Aldh1b1*$^{+/+}$ mice (Figure 6.2). The genotype frequencies that resulted from this breeding almost perfectly reflected the expected Mendelian ratios (Figure 6.2). Subsequently, the resulting progeny were used as breeders for the creation of the correct genotype for Aldh1b1 conditional-knockout Msh2-LS experimental subject mice: *Msh2*$^{flox/-}$*; Lgr5CreERT2*$^{+/-}$*; mTmG*$^{+/-}$*; Aldh1b1*$^{flox/flox}$. The mice resulting from these matings showed 1.5% progeny with *Msh2*$^{flox/-}$*; Lgr5CreERT2*$^{+/-}$; *mTmG*$^{+/-}$*; Aldh1b1*$^{flox/flox}$ genotypes and 0.8% progeny with *Msh2*$^{flox/flox}$*; Lgr5CreERT2*$^{+/-}$*; mTmG*$^{-/-}$*; Aldh1b1*$^{flox/flox}$ genotypes (Figure 6.3). Tabular representation of the inter-cross to generate the *Aldh1b1* conditional-knockout Msh2-LS mouse model experimental subjects is shown in the Appendix (Supplementary Table 6.1-6.2). Mice with these genotypes were used as experimental subject mice or breeders. *Msh2*$^{flox/-}$*; Lgr5CreERT2*$^{+/-}$*; mTmG*$^{+/-}$*; Aldh1b1*$^{flox/flox}$ mice only show loss of Aldh1b1 activity following Cre recombinase activation and this only occurs in the scattered Lgr5-expressing intestinal epithelial stem cells (that go on to form crypt foci) along with inactivation of the second allele of Msh2 and conversion to mG expression by Cre following Tamoxifen treatment (Figure 6.4).

To generate the *Aldh1b1* constitutive-knockout (*Aldh1b1*$^{-/-}$) mice, embryos from the *Aldh1b1* conditional-knockout (*Aldh1b1*$^{flox/flox}$) mice were treated with TAT-Cre *in vitro* and implanted into surrogate mothers using standard techniques (performed by Matt Sharp, Ailsa Travers and Julie Thomson, Bioresearch & Veterinary Services, Central Transgenic Core, University of

Edinburgh) (Ryder et al., 2014). The resulting *Aldh1b1*$^{-/-}$ mice (with genotype *Msh2*$^{+/+}$*; Lgr5CreERT2*$^{-/-}$*; mTmG*$^{-/-}$*; Aldh1b1*$^{-/-}$*)* obtained from the surrogate mothers were cross-bred with *Msh2*$^{flox/-}$*; Lgr5CreERT2*$^{+/-}$*; mTmG*$^{+/+}$*; Aldh1b1*$^{+/+}$ mice. The genotype frequencies that resulted from this breeding almost perfectly reflected the expected Mendelian ratios (Figure 6.5). Subsequently, the resulting progeny were used as breeders for the generation of the correct genotype for *Aldh1b1* constitutive-knockout Msh2-LS experimental subject mice with the genotype *Msh2*$^{flox/-}$*; Lgr5CreERT2*$^{+/-}$*; mTmG*$^{+/-}$*; Aldh1b1*$^{-/-}$. The mice resulting from these matings showed 1.5% progeny with *Msh2*$^{flox/-}$*; Lgr5CreERT2*$^{+/-}$; *mTmG*$^{+/-}$*; Aldh1b1*$^{-/-}$ genotypes and 0.8% progeny with *Msh2*$^{flox/flox}$*; Lgr5CreERT2*$^{+/-}$*; mTmG*$^{-/-}$*; Aldh1b1*$^{-/-}$ genotypes (Figure 6.6). Tabular representation of the inter-cross to generate the *Aldh1b1* constitutive-knockout Msh2-LS mouse model experimental subjects is shown in the Appendix (Supplementary Table 6.3-6.4). Mice with these genotypes were used as experimental subject mice or breeders. *Msh2*$^{flox/-}$*; Lgr5CreERT2*$^{+/-}$*; mTmG*$^{+/-}$*; Aldh1b1*$^{-/-}$ mice have complete loss of Aldh1b1 in all cells (Figure 6.7).

Genotype	Probability
Msh2 fl/+, Lgr5Cre+/-, mTmG +/-, Aldh1b1fl/+	25%
Msh2 fl/+, Lgr5Cre-/-, mTmG +/-, Aldh1b1fl/+	25%
Msh2 -/+ Lgr5Cre+/- mTmG +/- Aldh1b1fl/+	25%
Msh2 -/+ Lgr5Cre-/- mTmG +/- Aldh1b1fl/+	25%

Figure 6.2: Percentage of resulting genotypes from the breeding between the *Msh2$^{+/+}$; Lgr5CreERT2$^{-/-}$; mTmG$^{-/-}$; Aldh1b1$^{flox/flox}$ with Msh2$^{flox/-}$; Lgr5CreERT2$^{+/-}$; mTmG$^{+/+}$; Aldh1b1$^{+/+}$* mice

Genotype	Probability	Msh2+/+ Lgr5Cre+/- mTmG+/+ Aldh1b1fl/+	1.5
Msh2+/- Lgr5Cre+/- mTmG+/+ Aldh1b1fl/fl	0.8	Msh2+/+ Lgr5Cre-/- mTmG+/+ Aldh1b1fl/fl	0.8
Msh2+/- Lgr5Cre+/- mTmG+/+ Aldh1b1fl/+	1.5	Msh2+/+ Lgr5Cre-/- mTmG+/+ Aldh1b1fl/+	1.5
Msh2+/- Lgr5Cre-/- mTmG+/+ Aldh1b1fl/fl	0.8	Msh2+/+ Lgr5Cre+/- mTmG+/- Aldh1b1fl/fl	0.8
Msh2+/- Lgr5Cre-/- mTmG+/+ Aldh1b1fl/+	1.5	Msh2+/+ Lgr5Cre+/- mTmG+/-Aldh1b1fl/+	0.8
Msh2+/- Lgr5Cre+/- mTmG+/- Aldh1b1fl/fl	1.5	Msh2+/+ Lgr5Cre-/- mTmG+/- Aldh1b1fl/fl	1.5
Msh2+/- Lgr5Cre+/- mTmG+/- Aldh1b1fl/+	3.9	Msh2+/+ Lgr5Cre-/- mTmG+/- Aldh1b1fl/+	3.1
Msh2+/- Lgr5Cre-/- mTmG+/- Aldh1b1fl/fl	1.5	Msh2+/+ Lgr5Cre+/- mTmG+/+ Aldh1b1+/+	0.8
Msh2+/- Lgr5Cre-/- mTmG+/- Aldh1b1fl/+	3.1	Msh2+/+ Lgr5Cre-/- mTmG+/+ Aldh1b1+/+	0.8
Msh2+/- Lgr5Cre+/- mTmG+/+ Aldh1b1+/+	0.8	Msh2+/+ Lgr5Cre+/- mTmG+/- Aldh1b1fl/+	2.3
Msh2+/- Lgr5Cre-/- mTmG+/+ Aldh1b1+/+	0.8	Msh2+/+ Lgr5Cre+/- mTmG+/-Aldh1b1+/+	0.8
Msh2+/- Lgr5Cre+/- mTmG+/- Aldh1b1+/+	2.3	Msh2+/+ Lgr5Cre-/- mTmG+/- Aldh1b1+/+	1.5
Msh2+/- Lgr5Cre-/- mTmG+/- Aldh1b1+/+	1.5	Msh2+/+ Lgr5Cre+/- mTmG+/-Aldh1b1fl/fl	0.8
Msh2+/- Lgr5Cre+/- mTmG-/- Aldh1b1fl/fl	0.8	Msh2+/+ Lgr5Cre+/- mTmG-/- Aldh1b1fl/fl	0.8
Msh2+/- Lgr5Cre+/- mTmG-/- Aldh1b1fl/+	0.8	Msh2+/+ Lgr5Cre+/- mTmG-/-Aldh1b1fl/+	0.8
Msh2+/- Lgr5Cre-/- mTmG-/- Aldh1b1fl/fl	0.8	Msh2+/+ Lgr5Cre-/- mTmG-/- Aldh1b1fl/fl	0.8
Msh2+/- Lgr5Cre-/- mTmG-/- Aldh1b1fl/+	1.5	Msh2+/+ Lgr5Cre-/- mTmG-/- Aldh1b1fl/+	1.5
Msh2+/- Lgr5Cre-/- mTmG-/- Aldh1b1+/+	0.8	Msh2+/+ Lgr5Cre+/- mTmG+/- Aldh1b1+/+	0.8
Msh2fl/- Lgr5Cre+/- mTmG+/+ Aldh1b1fl/fl	0.8	Msh2+/+ Lgr5Cre+/- mTmG-/- Aldh1b1fl/+	0.8
Msh2fl/- Lgr5Cre+/- mTmG+/+ Aldh1b1fl/+	1.5	Msh2+/+ Lgr5Cre+/- mTmG-/-Aldh1b1+/+	0.8
Msh2fl/- Lgr5Cre-/- mTmG+/+ Aldh1b1fl/fl	0.8	Msh2+/+ Lgr5Cre-/- mTmG-/- Aldh1b1+/+	0.8
Msh2fl/- Lgr5Cre-/- mTmG+/+ Aldh1b1fl/+	1.5	Msh2fl/+ Lgr5Cre+/- mTmG+/+ Aldh1b1fl/fl	0.8
Msh2fl/- Lgr5Cre+/- mTmG+/- Aldh1b1fl/fl	1.5	Msh2fl/+ Lgr5Cre+/- mTmG+/+ Aldh1b1fl/+	1.5
Msh2fl/- Lgr5Cre+/- mTmG+/-Aldh1b1fl/+	0.8	Msh2fl/+ Lgr5Cre-/- mTmG+/+ Aldh1b1fl/fl	0.8
Msh2fl/- Lgr5Cre-/- mTmG+/- Aldh1b1fl/fl	1.5	Msh2fl/+ Lgr5Cre-/- mTmG+/+ Aldh1b1fl/+	1.5
Msh2fl/- Lgr5Cre-/- mTmG+/- Aldh1b1fl/+	2.3	Msh2fl/+ Lgr5Cre+/- mTmG+/- Aldh1b1fl/fl	1.5
Msh2fl/- Lgr5Cre+/- mTmG+/+ Aldh1b1+/+	0.8	Msh2fl/+ Lgr5Cre+/- mTmG+/- Aldh1b1fl/+	3.1
Msh2fl/- Lgr5Cre-/- mTmG+/+ Aldh1b1+/+	0.8	Msh2fl/+ Lgr5Cre-/- mTmG+/- Aldh1b1fl/fl	1.5
Msh2fl/- Lgr5Cre+/- mTmG+/- Aldh1b1fl/+	1.5	Msh2fl/+ Lgr5Cre-/- mTmG+/- Aldh1b1fl/+	3.1
Msh2fl/- Lgr5Cre+/- mTmG+/-Aldh1b1+/+	0.8	Msh2fl/+ Lgr5Cre+/- mTmG+/+ Aldh1b1+/+	0.8
Msh2fl/- Lgr5Cre-/- mTmG+/- Aldh1b1+/+	0.8	Msh2fl/+ Lgr5Cre-/- mTmG+/+ Aldh1b1+/+	0.8
Msh2fl/- Lgr5Cre+/- mTmG-/- Aldh1b1fl/fl	0.8	Msh2fl/+ Lgr5Cre+/- mTmG+/- Aldh1b1+/+	0.8
Msh2fl/- Lgr5Cre+/- mTmG-/- Aldh1b1fl/+	0.8	Msh2fl/+ Lgr5Cre-/- mTmG+/- Aldh1b1+/+	0.8
Msh2fl/- Lgr5Cre-/- mTmG-/- Aldh1b1fl/fl	0.8	Msh2fl/+ Lgr5Cre+/- mTmG-/- Aldh1b1fl/fl	0.8
Msh2fl/- Lgr5Cre-/- mTmG-/- Aldh1b1fl/+	0.8	Msh2fl/+ Lgr5Cre+/- mTmG-/- Aldh1b1fl/+	1.5
Msh2fl/-Lgr5Cre+/- mTmG+/- Aldh1b1fl/+	0.8	Msh2fl/+ Lgr5Cre-/- mTmG-/- Aldh1b1fl/fl	0.8
Msh2fl/- Lgr5Cre+/- mTmG+/- Aldh1b1+/+	0.8	Msh2fl/+ Lgr5Cre-/- mTmG-/- Aldh1b1fl/+	1.5
Msh2fl/-Lgr5Cre-/- mTmG+/- Aldh1b1fl/+	0.8	Msh2fl/+ Lgr5Cre+/- mTmG+/-Aldh1b1+/+	0.8
Msh2fl/-Lgr5Cre+/- mTmG-/- Aldh1b1fl/+	1.5	Msh2fl/+ Lgr5Cre-/- mTmG+/-Aldh1b1+/+	0.8
Msh2fl/- Lgr5Cre+/- mTmG-/- Aldh1b1+/+	1.5	Msh2fl/+ Lgr5Cre+/- mTmG-/- Aldh1b1+/+	0.8
Msh2+/+ Lgr5Cre+/- mTmG+/+ Aldh1b1fl/fl	0.8	Msh2fl/+ Lgr5Cre-/- mTmG-/- Aldh1b1+/+	0.8

Figure 6.3: Percentage of resulting genotypes from the breeding between the *Msh2$^{+/-}$; Lgr5CreERT2$^{-/-}$; mTmG$^{+/-}$; Aldh1b1$^{flox/+}$ with Msh2$^{flox/+}$; Lgr5CreERT2$^{+/-}$; mTmG$^{+/-}$; Aldh1b1$^{flox/+}$* mice.

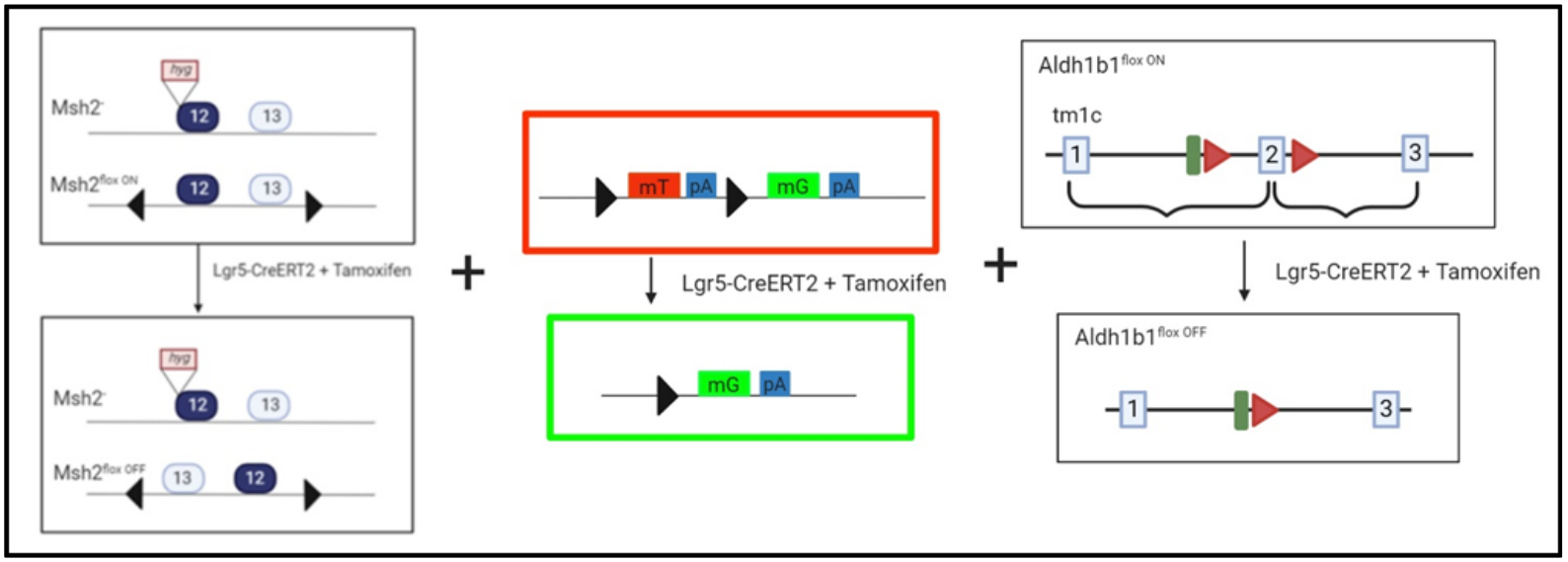

Figure 6.4: Schematic diagram of the *Msh2$^{flox/-}$; Lgr5CreERT2$^{+/-}$; mTmG$^{+/-}$; Aldh1b1$^{flox/flox}$* genotype before and after Cre activation. On the left, the schematic diagram of the *Msh2$^{fl/-}$* alleles before and after Cre activation, showing constitutive inactivation (*Msh2^{-}*) and conditional knockout (before: *Msh2 $^{flox\ ON}$* and after: *Msh2 $^{flox\ OFF}$*) alleles of Msh2 (adapted and modified from Wojciechowicz et al., 2014). In the middle, the schematic diagram of the mTmG coloured fluorescent protein reporter construct shows the status before (cell expresses mT and appears red) and after (cell expresses mG and appears green) Cre-mediated recombination (adapted and modified from Muzumdar et al., 2007). On the right, the schematic diagram of the *Aldh1b1$^{flox/flox}$* alleles before and after Cre activation: Cre-mediated recombination of the loxP sites flanking the critical exon induces loss of Aldh1b1 expression only in Lgr5-driven Cre-expressing intestinal epithelial stem cells (adapted and modified from Skarnes et al., 2011).

Genotype	Probability
Msh2 fl/+, Lgr5Cre+/-, mTmG +/-, Aldh1b1+/-	25%
Msh2 fl/+, Lgr5Cre-/-, mTmG +/-, Aldh1b1+/-	25%
Msh2 -/+ Lgr5Cre+/- mTmG +/- Aldh1b1+/-	25%
Msh2 -/+ Lgr5Cre-/- mTmG +/- Aldh1b1+/-	25%

Figure 6.5: Percentage of resulting genotypes from the breeding between the *Msh2$^{+/+}$; Lgr5CreERT2$^{-/-}$; mTmG$^{-/-}$; Aldh1b1$^{-/-}$* with *Msh2$^{flox/-}$; Lgr5CreERT2$^{+/-}$; mTmG$^{+/+}$; Aldh1b1$^{+/+}$* mice.

Genotype	Probability	Msh2+/+ Lgr5Cre+/- mTmG+/+ Aldh1b1-/+	1.5
Msh2+/- Lgr5Cre+/- mTmG+/+ Aldh1b1-/-	0.8	Msh2+/+ Lgr5Cre-/- mTmG+/+ Aldh1b1-/-	0.8
Msh2+/- Lgr5Cre+/- mTmG+/+ Aldh1b1-/+	1.5	Msh2+/+ Lgr5Cre-/- mTmG+/+ Aldh1b1-/+	1.5
Msh2+/- Lgr5Cre-/- mTmG+/+ Aldh1b1-/-	0.8	Msh2+/+ Lgr5Cre+/- mTmG+/- Aldh1b1-/-	0.8
Msh2+/- Lgr5Cre-/- mTmG+/+ Aldh1b1-/+	1.5	Msh2+/+ Lgr5Cre+/- mTmG+/-Aldh1b1-/+	0.8
Msh2+/- Lgr5Cre+/- mTmG+/- Aldh1b1-/-	1.5	Msh2+/+ Lgr5Cre-/- mTmG+/- Aldh1b1-/-	1.5
Msh2+/- Lgr5Cre+/- mTmG+/- Aldh1b1-/+	3.9	Msh2+/+ Lgr5Cre-/- mTmG+/- Aldh1b1-/+	3.1
Msh2+/- Lgr5Cre-/- mTmG+/- Aldh1b1-/-	1.5	Msh2+/+ Lgr5Cre+/- mTmG+/+ Aldh1b1+/+	0.8
Msh2+/- Lgr5Cre-/- mTmG+/- Aldh1b1-/+	3.1	Msh2+/+ Lgr5Cre-/- mTmG+/+ Aldh1b1+/+	0.8
Msh2+/- Lgr5Cre+/- mTmG+/+ Aldh1b1+/+	0.8	Msh2+/+ Lgr5Cre+/- mTmG+/- Aldh1b1-/+	2.3
Msh2+/- Lgr5Cre-/- mTmG+/+ Aldh1b1+/+	0.8	Msh2+/+ Lgr5Cre+/- mTmG+/-Aldh1b1+/+	0.8
Msh2+/- Lgr5Cre+/- mTmG+/- Aldh1b1+/+	2.3	Msh2+/+ Lgr5Cre-/- mTmG+/- Aldh1b1+/+	1.5
Msh2+/- Lgr5Cre-/- mTmG+/- Aldh1b1+/+	1.5	Msh2+/+ Lgr5Cre+/- mTmG+/-Aldh1b1-/-	0.8
Msh2+/- Lgr5Cre+/- mTmG-/- Aldh1b1-/-	0.8	Msh2+/+ Lgr5Cre+/- mTmG-/- Aldh1b1-/-	0.8
Msh2+/- Lgr5Cre+/- mTmG-/- Aldh1b1-/+	0.8	Msh2+/+ Lgr5Cre+/- mTmG-/-Aldh1b1-/+	0.8
Msh2+/- Lgr5Cre-/- mTmG-/- Aldh1b1-/-	0.8	Msh2+/+ Lgr5Cre-/- mTmG-/- Aldh1b1-/-	0.8
Msh2+/- Lgr5Cre-/- mTmG-/- Aldh1b1-/+	1.5	Msh2+/+ Lgr5Cre-/- mTmG-/- Aldh1b1-/+	1.5
Msh2+/- Lgr5Cre-/- mTmG-/- Aldh1b1+/+	0.8	Msh2+/+ Lgr5Cre+/- mTmG+/- Aldh1b1+/+	0.8
Msh2fl/- Lgr5Cre+/- mTmG+/+ Aldh1b1-/-	0.8	Msh2+/+ Lgr5Cre+/- mTmG-/- Aldh1b1-/+	0.8
Msh2fl/- Lgr5Cre+/- mTmG+/+ Aldh1b1-/+	1.5	Msh2+/+ Lgr5Cre+/- mTmG-/-Aldh1b1+/+	0.8
Msh2fl/- Lgr5Cre-/- mTmG+/+ Aldh1b1-/-	0.8	Msh2+/+ Lgr5Cre-/- mTmG-/- Aldh1b1+/+	0.8
Msh2fl/- Lgr5Cre-/- mTmG+/+ Aldh1b1-/+	1.5	Msh2fl/+ Lgr5Cre+/- mTmG+/+ Aldh1b1-/-	0.8
Msh2fl/- Lgr5Cre+/- mTmG+/- Aldh1b1-/-	1.5	Msh2fl/+ Lgr5Cre+/- mTmG+/+ Aldh1b1-/+	1.5
Msh2fl/- Lgr5Cre+/- mTmG+/-Aldh1b1-/+	0.8	Msh2fl/+ Lgr5Cre-/- mTmG+/+ Aldh1b1-/-	0.8
Msh2fl/- Lgr5Cre-/- mTmG+/- Aldh1b1-/-	1.5	Msh2fl/+ Lgr5Cre-/- mTmG+/+ Aldh1b1-/+	1.5
Msh2fl/- Lgr5Cre-/- mTmG+/- Aldh1b1-/+	2.3	Msh2fl/+ Lgr5Cre+/- mTmG+/- Aldh1b1-/-	1.5
Msh2fl/- Lgr5Cre+/- mTmG+/+ Aldh1b1+/+	0.8	Msh2fl/+ Lgr5Cre+/- mTmG+/- Aldh1b1-/+	3.1
Msh2fl/- Lgr5Cre-/- mTmG+/+ Aldh1b1+/+	0.8	Msh2fl/+ Lgr5Cre-/- mTmG+/- Aldh1b1-/-	1.5
Msh2fl/- Lgr5Cre+/- mTmG+/- Aldh1b1-/+	1.5	Msh2fl/+ Lgr5Cre-/- mTmG+/- Aldh1b1-/+	3.1
Msh2fl/- Lgr5Cre+/- mTmG+/-Aldh1b1+/+	0.8	Msh2fl/+ Lgr5Cre+/- mTmG+/+ Aldh1b1+/+	0.8
Msh2fl/- Lgr5Cre-/- mTmG+/- Aldh1b1+/+	0.8	Msh2fl/+ Lgr5Cre-/- mTmG+/+ Aldh1b1+/+	0.8
Msh2fl/- Lgr5Cre+/- mTmG-/- Aldh1b1-/-	0.8	Msh2fl/+ Lgr5Cre+/- mTmG+/- Aldh1b1+/+	0.8
Msh2fl/- Lgr5Cre+/- mTmG-/- Aldh1b1-/+	0.8	Msh2fl/+ Lgr5Cre-/- mTmG+/- Aldh1b1+/+	0.8
Msh2fl/- Lgr5Cre-/- mTmG-/- Aldh1b1-/-	0.8	Msh2fl/+ Lgr5Cre+/- mTmG-/- Aldh1b1-/-	0.8
Msh2fl/- Lgr5Cre-/- mTmG-/- Aldh1b1-/+	0.8	Msh2fl/+ Lgr5Cre+/- mTmG-/- Aldh1b1-/+	1.5
Msh2fl/-Lgr5Cre+/- mTmG+/- Aldh1b1-/+	0.8	Msh2fl/+ Lgr5Cre-/- mTmG-/- Aldh1b1-/-	0.8
Msh2fl/- Lgr5Cre+/- mTmG+/- Aldh1b1+/+	0.8	Msh2fl/+ Lgr5Cre-/- mTmG-/- Aldh1b1-/+	1.5
Msh2fl/-Lgr5Cre-/- mTmG+/- Aldh1b1-/+	0.8	Msh2fl/+ Lgr5Cre+/- mTmG+/-Aldh1b1+/+	0.8
Msh2fl/-Lgr5Cre+/- mTmG-/- Aldh1b1-/+	1.5	Msh2fl/+ Lgr5Cre-/- mTmG+/-Aldh1b1+/+	0.8
Msh2fl/- Lgr5Cre+/- mTmG-/- Aldh1b1+/+	1.5	Msh2fl/+ Lgr5Cre+/- mTmG-/- Aldh1b1+/+	0.8
Msh2+/+ Lgr5Cre+/- mTmG+/+ Aldh1b1-/-	0.8	Msh2fl/+ Lgr5Cre-/- mTmG-/- Aldh1b1+/+	0.8

Figure 6.6: Percentage of resulting genotypes from the breeding between the *Msh2$^{+/-}$; Lgr5CreERT2$^{-/-}$; mTmG$^{+/-}$; Aldh1b1$^{+/-}$* with *Msh2$^{flox/+}$; Lgr5CreERT2$^{+/-}$; mTmG$^{+/-}$; Aldh1b1$^{+/-}$* mice.

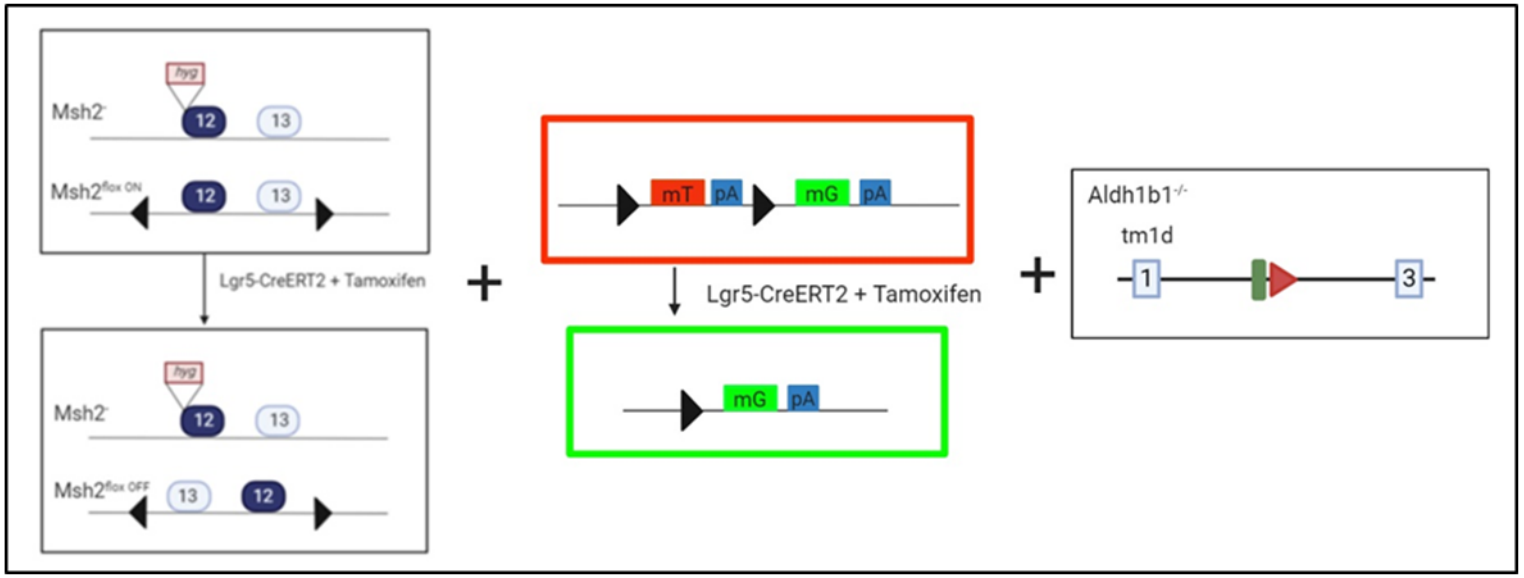

Figure 6.7: Schematic diagram of the *Msh2$^{flox/-}$; Lgr5CreERT2$^{+/-}$; mTmG$^{+/-}$; Aldh1b1$^{-/-}$* genotype before and after Cre activation. On the left, the schematic diagram of the *Msh2$^{fl/-}$* alleles before and after Cre activation: constitutive-knockout (*Msh2^{-}*) and conditional-knockout (before: *Msh2 $^{flox\ ON}$*; and after: *Msh2 $^{flox\ OFF}$*) alleles of Msh2 (adapted and modified from Wojciechowicz et al., 2014). In the middle, the schematic diagram of the mTmG coloured fluorescent protein reporter construct before (cell expresses mT and appears red) and after (cell expresses mG and appears green) Cre-mediated recombination (adapted and modified from Muzumdar et al., 2007). On the right, the schematic diagram of the *Aldh1b1$^{-/-}$* alleles. In *Aldh1b1* constitutive-knockout mice, all cells have complete loss of Aldh1b1.

6.3 Long-term ethanol effects on intestinal tumourigenesis in the combined *Aldh1b1*-knockout and Msh2-LS mouse model

6.3.1 Methods

Groups of 7-9 weeks old mice with either *Aldh1b1* conditional-knockout or *Aldh1b1* constitutive-knockout alleles were used in combination with the Msh2-LS mice. The combined *Aldh1b1* conditional-knockout and Msh2-LS experimental mice had the genotypes *Msh2$^{flox/-}$; Lgr5CreERT2$^{+/-}$; Aldh1b1$^{flox/flox}$* or *Msh2$^{flox/-}$; Lgr5CreERT2$^{+/-}$; mTmG$^{+/-}$; Aldh1b1$^{flox/flox}$*. Whereas, the combined *Aldh1b1* constitutive-knockout and Msh2-LS experimental mice had the genotypes *Msh2$^{flox/-}$; Lgr5CreERT2$^{+/-}$; Aldh1b1$^{-/-}$* or *Msh2$^{flox/-}$; Lgr5CreERT2$^{+/-}$; mTmG$^{+/-}$; Aldh1b1$^{-/-}$*. All experiments involved these mice being divided into two groups for treatment with either standard / conventional drinking water (Group-A) or 20% ethanol in drinking water (Group-B). Group-A mice received i.p. injections of 0.15mg Tamoxifen/g bw on day 1 and 0.1mg Tamoxifen/g bw on days 2, 3 and 4; on day 5 mice were provided with standard/normal drinking water. By contrast, Group-B received i.p. injections of 0.15mg Tamoxifen/g bw on day 1 and 0.1mg Tamoxifen/g bw on days 2, 3 and 4; but on day 5 the Group-B mice were provided with 20% ethanol in drinking water (as previously validated by our group; (Müller et al., 2016)) (Figure 6.8). Animals were culled and tissues collected when either clinical signs of distress were visible or they displayed >20% body weight loss compared with the initial weight. The small and large intestines, caecum, stomach, liver, spleen, thymus, lymph nodes (if visible) and any other organ or tissue showing abnormalities, were collected following schedule 1 culling and necropsy dissection. Tissues were fixed in 10% NBF, processed using standard tissue processing protocols and paraffin embedded in preparation for section cutting and staining. The acronyms used for the Msh2-LS model mice and their relevant treatments are shown in Table 2.2.

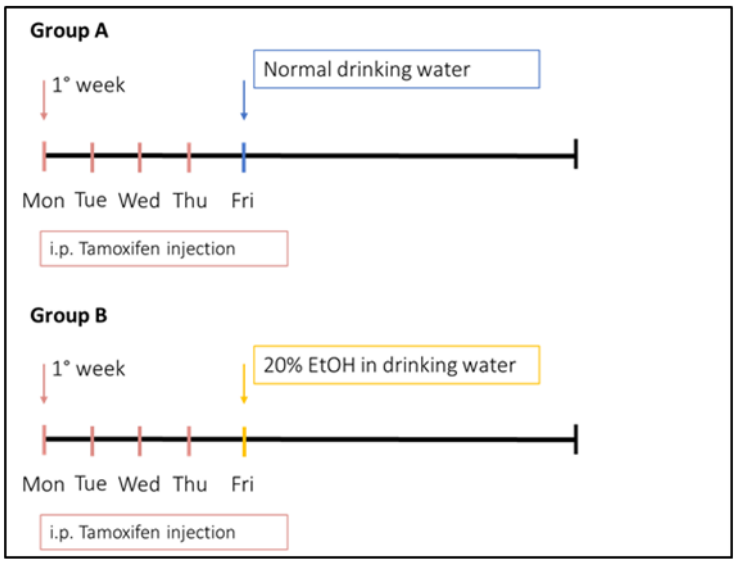

Figure 6.8: Experimental treatment protocols and timelines for Group-A (water-treated) and -B (ethanol-treated) mice, showing 4 days of i.p. injections of Tamoxifen, followed by either standard / normal drinking water (Group-A) or drinking water containing 20% ethanol (Group-B). (EtOH = Ethanol).

6.3.2 Results

6.3.2.1 Experimental group organization and observations

Msh2$^{flox/-}$; Lgr5CreERT2$^{+/-}$; mTmG$^{+/-}$; Aldh1b1$^{flox/flox}$ experimental subjects (18 females and 6 males) were divided into two groups: Group-A (12 mice: 9 females and 3 males; water-treated control group) and Group-B (12 mice: 9 females and 3 males; ethanol-treated test group).

Msh2$^{flox/-}$; Lgr5CreERT2$^{+/-}$; mTmG$^{+/-}$; Aldh1b1$^{-/-}$ experimental subjects (8 females and 16 males) were divided into in two groups: Group-A (12 mice: 4 females and 8 males; water-treated control group) and Group-B (12 mice: 4 females and 8 males; ethanol-treated test group).

Ethanol-treated animals from both groups were culled when either clinical signs of distress were visible or they displayed >20% body weight loss compared with the initial weight, whereas water-treated mice (pair matched for age and sex) were culled at the same timepoints as ethanol-treated mice. During Tamoxifen treatment (daily Tamoxifen i.p injections for 4 consecutive days), body weights and health status were recorded. In both *Aldh1b1* conditional-knockout Msh2-LS mice and *Aldh1b1* constitutive-knockout Msh2-LS mice, body weights of the female and male mice didn't significantly differ during the Tamoxifen treatment (Figure 6.9), showing successful drug administration and acceptance of the experimental procedures by the mice.

In *Aldh1b1$^{flox/flox}$* Msh2-LS mice, body weights of males (~25g) were significantly higher than body weights of females (~21g) both before and during the Tamoxifen treatments (Figure 6.9A). In *Aldh1b1$^{-/-}$* Msh2-LS mice, body weights of males (~26.4g) were significantly higher than body weights of females (~22g), both before and during the Tamoxifen treatments (Figure 6.9B).

After Tamoxifen treatment mice received either 20% ethanol in drinking water or normal drinking water regimes and the body weights and health status of the mice were recorded twice a week (Figure 6.10-6.11).

EtOH_*Aldh1b1$^{fl/fl}$*_*Msh2$^{fl\ KO}$* female mice did not show abnormal behaviour or reduced weight compared with H_2O_*Aldh1b1$^{fl/fl}$*_*Msh2$^{fl\ KO}$* female mice, indicating good acceptance of the ethanol regime (Figure 6.10A). In EtOH_*Aldh1b1$^{fl/fl}$*_*Msh2$^{fl\ KO}$* and H_2O_*Aldh1b1$^{fl/fl}$*_*Msh2$^{fl\ KO}$* male mice showed some variation in body weight most likely reflecting the low number of male experimental mice in this experiment (Figure 6.10B). EtOH_*Aldh1b1$^{fl/fl}$*_*Msh2$^{fl\ KO}$* mice weighed on average 31g for the males and 31g for the females, whereas

H_2O_*Aldh1b1*$^{fl/fl}$_*Msh2*$^{fl\ KO}$ mice weighed on average 34g for the males and 33g for the females (Figure 6.10).

EtOH_*Aldh1b1*$^{-/-}$_*Msh2*$^{fl\ KO}$ female and male mice did not show abnormal behaviour or reduced body weight compared with H_2O_*Aldh1b1*$^{-/-}$_*Msh2*$^{fl\ KO}$ female and male mice, indicating good acceptance of the ethanol regime (Figure 6.11). EtOH_*Aldh1b1*$^{-/-}$_ *Msh2*$^{fl\ KO}$ mice weighed on average 36g for the males and 27g for the females, whereas H_2O_*Aldh1b1*$^{-/-}$_*Msh2*$^{fl\ KO}$ mice weighed on average 39g for the males and 30g for the females (Figure 6.11).

Drinking bottles were changed and bottle weights were recorded once a week. Liquid consumption per mouse was estimated by analysing the weights of the drinking bottles (per cage) and calculating the average weight of consumed liquid per mouse per day (Figure 6.12-6.13). In *Aldh1b1*$^{flox/flox}$ Msh2-LS mice, an average H_2O_*Aldh1b1*$^{fl/fl}$_*Msh2*$^{fl\ KO}$ male mouse consumed around 12.83ml of drinking water per day, whereas an average EtOH_*Aldh1b1*$^{fl/fl}$_*Msh2*$^{fl\ KO}$ male mouse consumed around 13.4ml of 20% ethanol in drinking water. In *Aldh1b1*$^{flox/flox}$ Msh2-LS mice, an average H_2O_*Aldh1b1*$^{fl/fl}$_*Msh2*$^{fl\ KO}$ female mouse consumed around 12.87ml of water per day, whereas an average EtOH_*Aldh1b1*$^{fl/fl}$_*Msh2*$^{fl\ KO}$ female mouse consumed around 9ml of 20% ethanol in drinking water per day (Figure 6.12). In *Aldh1b1*$^{-/-}$ Msh2-LS mice, an average H_2O_*Aldh1b1*$^{-/-}$_*Msh2*$^{fl\ KO}$ male mouse consumed around 10.4ml of drinking water per day, whereas an average EtOH_*Aldh1b1*$^{-/-}$_*Msh2*$^{fl\ KO}$ male mouse consumed around 10.5ml of 20% ethanol in drinking water. In *Aldh1b1*$^{-/-}$ Msh2-LS mice, an average H_2O_*Aldh1b1*$^{-/-}$_*Msh2*$^{fl\ KO}$ female mouse consumed around 10.2ml of water per day, whereas an average EtOH_*Aldh1b1*$^{-/-}$_*Msh2*$^{fl\ KO}$ female mouse consumed around 11.5ml of 20% ethanol in drinking water per day (Figure 6.13). In both experiments, no significant differences were observed between any of the comparisons of ethanol-treated versus water-treated males or females.

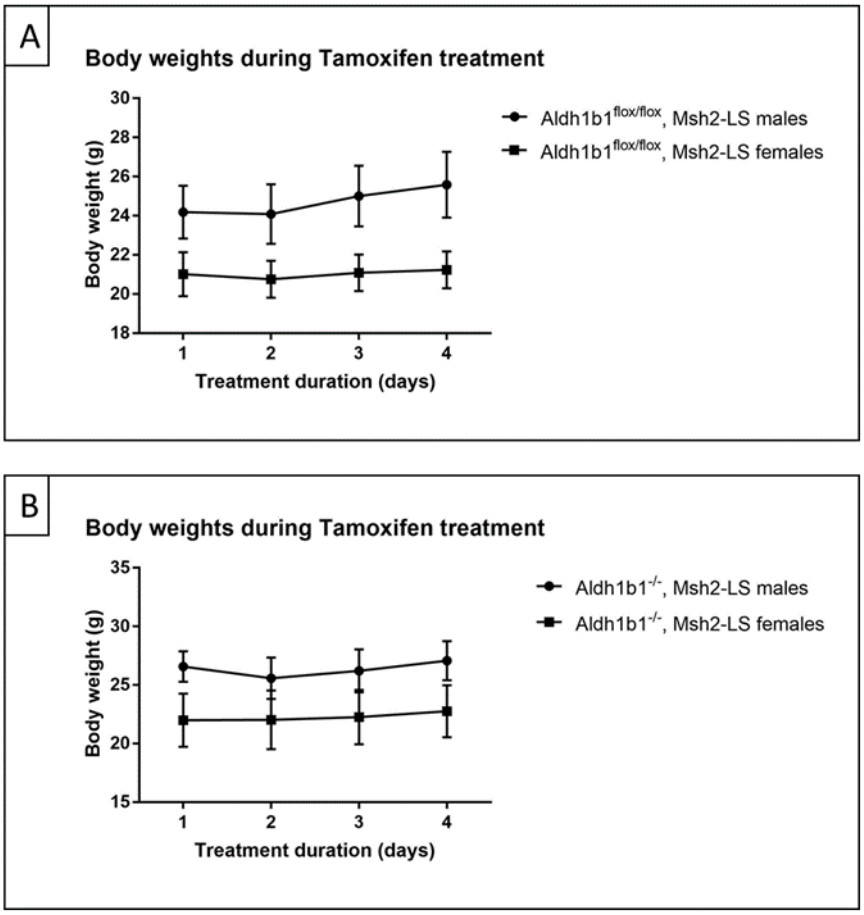

Figure 6.9: Body weights during Tamoxifen treatment. A) Body weights of *Aldh1b1*$^{flox/flox}$ Msh2-LS males were significantly higher than body weights of females, before and during Tamoxifen treatments. 2-way-ANOVA test with Bonferroni post-test correction, p=0.0005 on days 1 and 2, p<0.0001 on days 3 and 4 (data shown as mean ± SD, n=6 mice in each group). B) Body weights of *Aldh1b1*$^{-/-}$ Msh2-LS males were significantly higher than body weights of females, before and during Tamoxifen treatments. 2-way-ANOVA test with Bonferroni post-test correction, p=0.0014 on day 1, p=0.0169 on day 2, p=0.0066 on day 3, and p=0.0027 on day 4 (data shown as mean ± SD, n=6 mice in each group).

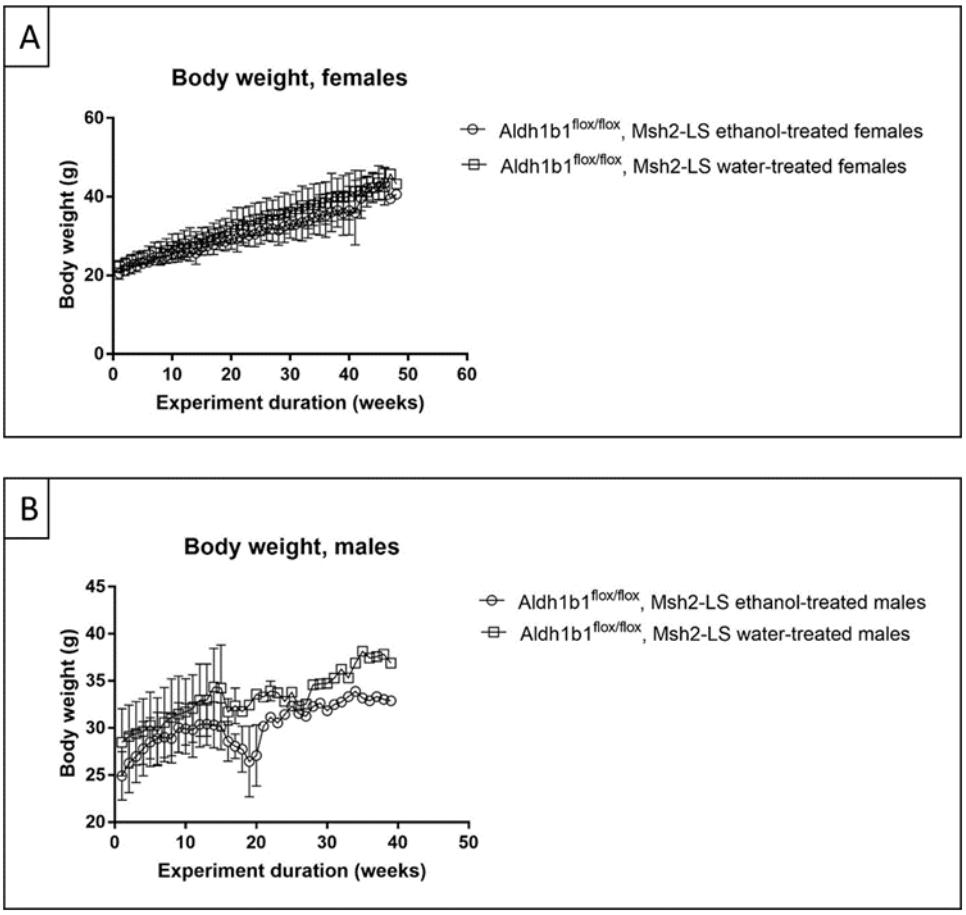

Figure 6.10: Body weights for *Aldh1b1*$^{flox/flox}$ Msh2-LS males and females during 20% ethanol or standard/normal drinking water regimes. The data distribution for the body weight curves for the *Aldh1b1*$^{flox/flox}$ Msh2-LS male mice were influenced by the low number of male animals used in the experiment. There were no significant differences between the body weights of *Aldh1b1*$^{flox/flox}$ Msh2-LS ethanol-treated (EtOH_*Aldh1b1*$^{fl/fl}$_Msh2$^{fl\ KO}$) males (or females) versus *Aldh1b1*$^{flox/flox}$ Msh2-LS water-treated (H_2O_*Aldh1b1*$^{fl/fl}$_*Msh2*$^{fl\ KO}$) males (or females). 2-way-ANOVA with Bonferroni post-test correction analysis (data shown as mean±SD, n=6 mice each group).

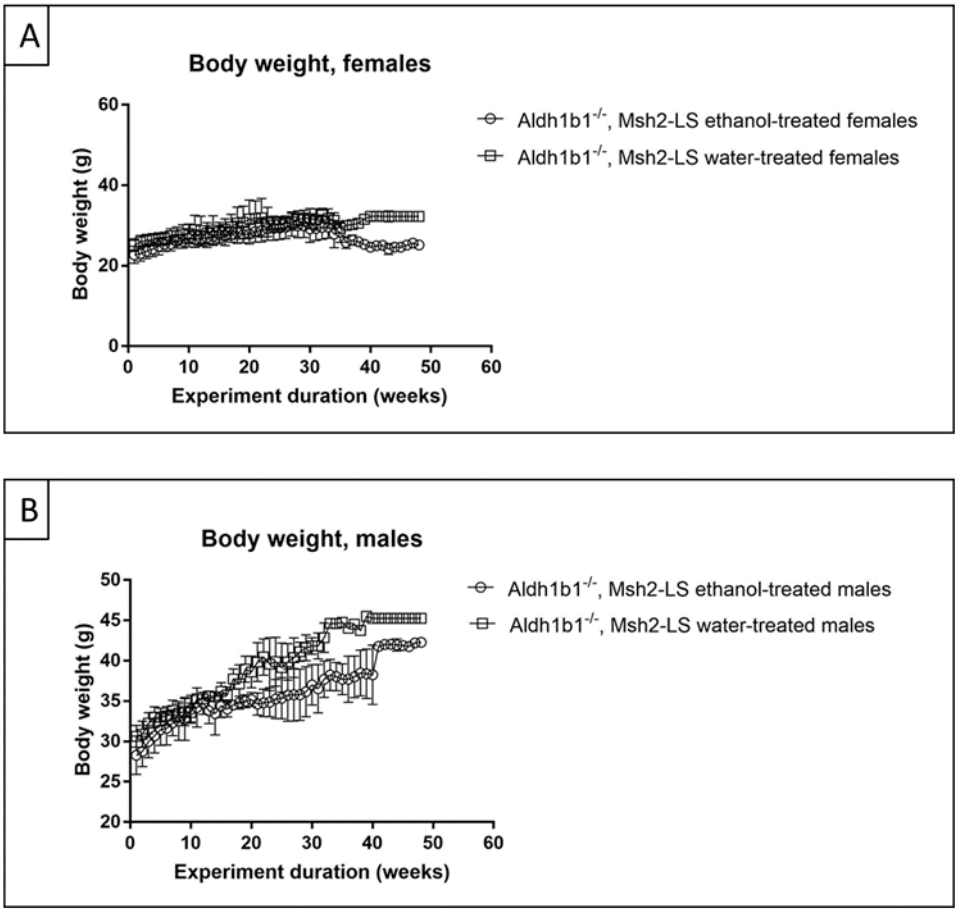

Figure 6.11: Body weights for *Aldh1b1*$^{-/-}$ Msh2-LS males and females during 20% ethanol or standard / normal drinking water regimes. There were no significant differences between the body weights of *Aldh1b1*$^{-/-}$ Msh2-LS ethanol-treated (EtOH_*Aldh1b1*$^{-/-}$_*Msh2*$^{fl\ KO}$) males (or females) versus *Aldh1b1*$^{-/-}$ Msh2-LS water-treated (H_2O_*Aldh1b1*$^{-/-}$_*Msh2*$^{fl\ KO}$) males (or females). 2-way-ANOVA with Bonferroni post-test correction analysis (data shown as mean±SD, n=6 mice each group).

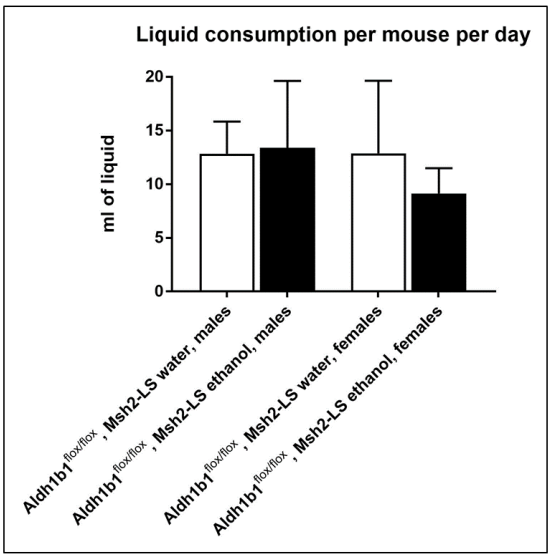

Figure 6.12: Liquid consumption of *Aldh1b1*$^{flox/flox}$ Msh2-LS males and females treated with either 20% ethanol in drinking water or standard / normal water per mouse per day. 2-way-ANOVA with Bonferroni post-test correction analysis (data shown as mean±SD, n=6 mice in each group). No significant differences were observed for any of the comparisons of ethanol versus water treatment, or males versus females.

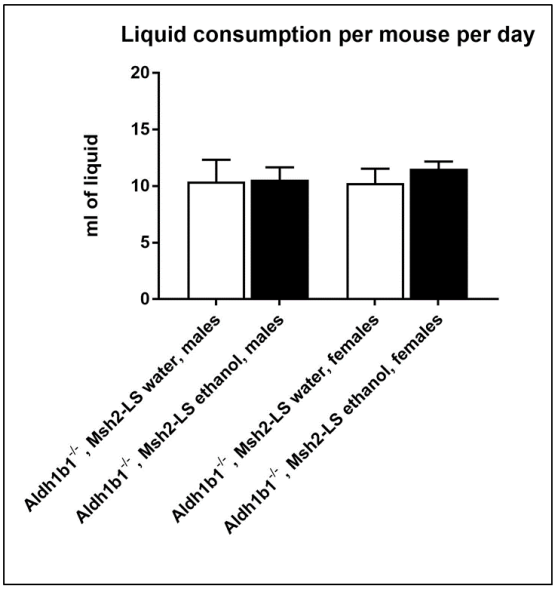

Figure 6.13: Liquid consumption of *Aldh1b1*$^{-/-}$ Msh2-LS males and females treated with either 20% ethanol in drinking water or standard / normal water per mouse per day. 2-way-ANOVA with Bonferroni post-test correction analysis (data shown as mean±SD, n=6 mice in each group). No significant differences were observed for any of the comparisons of ethanol versus water treatment, or males versus females.

6.3.2.2 Tumour development in *Aldh1b1* conditional-knockout Msh2-LS mice under long-term ethanol treatment

The two cohorts of *Aldh1b1*$^{flox/flox}$ Msh2-LS model mice, Group-A (water-treated, H_2O_*Aldh1b1*$^{fl.fl}$_*Msh2*$^{fl\ KO}$) and Group-B (ethanol-treated, EtOH_*Aldh1b1*$^{fl.fl}$_*Msh2*$^{fl\ KO}$), were monitored for up to 12 months for signs of intestinal tumour development or other pathological abnormalities, using a clinical scoring system that included known clinical signs of distress seen in mice that develop intestinal neoplasms, to determine when the mice should be culled for necropsy dissection and tumour analysis (Table 4.1). Most of the mice in Group-B (ethanol experimental group) displayed either anal prolapse or >20% reduction in body weight as common clinical signs of distress, at varying lengths of time from the start of the experimental protocol and were then culled for necropsy dissection. During necropsy dissection, naked eye inspection revealed that the majority of the EtOH_*Aldh1b1*$^{fl.fl}$_*Msh2*$^{fl\ KO}$ mice showed a thicker colonic wall compared with the colonic walls of the H_2O_*Aldh1b1*$^{fl.fl}$_*Msh2*$^{fl\ KO}$ mice, but no gross morphological differences were observed in the small intestines. The lengths of the small intestines and colons were measured and recorded, but no significant differences in length were observed between the ethanol-treated and the water-treated groups.

The histopathological analyses of *Aldh1b1*$^{flox/flox}$ Msh2-LS large intestines and small intestines confirmed the macroscopic observations of no significant morphological differences between the two groups in the small intestines, but increased colonic wall thickness in EtOH_*Aldh1b1*$^{fl.fl}$_*Msh2*$^{fl\ KO}$ mice, due to a widespread increase in the colon crypt length as a result of extended zones of crypt epithelial hyperproliferation that were not observed in H_2O_*Aldh1b1*$^{fl.fl}$_*Msh2*$^{fl\ KO}$ murine colons (Figure 6.14). These extended zones of colonic crypt hyperproliferation were seen to affect 50% – 90% of the whole colonic length, usually involving proximal colon and mid colon more than distal colon and rectum, in most of the EtOH_*Aldh1b1*$^{fl.fl}$_*Msh2*$^{fl\ KO}$ mice who survived more than 3 months of the ethanol treatment protocol. By contrast, histopathological analyses of the small intestines did not show any significant morphological differences between the two groups of animals using H&E-stained Swiss rolls of the intestines (Figure 6.15).

In total, 5 out of 12 EtOH_*Aldh1b1*$^{fl.fl}$_*Msh2*$^{fl\ KO}$ mice demonstrated zones of large intestinal crypt epithelial hyperproliferation, with adenoma formation and, in 1 case, invasive

adenocarcinoma was present, forming within an average of 4.5 months (minimum 13 weeks and maximum 39 weeks) of the start of the experimental protocol, compared with no cases of large intestinal adenoma formation in the 12 H_2O_*Aldh1b1*$^{fl.fl}$_*Msh2*$^{fl\ KO}$ control mice, in the same time-period (Figure 6.16).

Almost all 5 EtOH_*Aldh1b1*$^{fl.fl}$_*Msh2*$^{fl\ KO}$ adenoma-bearing mice showed colonic crypt hyperproliferative changes along the whole colon. Only one *Aldh1b1*$^{flox/flox}$ Msh2-LS mouse showed only colonic hyperproliferation without tumour formation (after 35 weeks of ethanol treatment). One out of these 5 EtOH_*Aldh1b1*$^{fl.fl}$_*Msh2*$^{fl\ KO}$ adenoma-bearing mice was diagnosed with invasive adenocarcinoma in the proximal colon. In addition, in 2 out of these 5 mice, caecal adenomas were found. Among these 5 EtOH_*Aldh1b1*$^{fl.fl}$_*Msh2*$^{fl\ KO}$ mice, 2 were diagnosed with rectal adenoma. In total, we observed 21 neoplasms distributed across the caecum, colon and rectum (Figure 6.17). Additionally, 1 out of these 5 mice developed a cutaneous sebaceous adenoma (a type of skin tumour that occurs in LS patients).

Seven out of 12 EtOH_*Aldh1b1*$^{fl.fl}$_*Msh2*$^{fl\ KO}$ mice did not show any intestinal adenoma formation, but in one of these cases there was a uterine endometrial adenocarcinoma (after 13 weeks of ethanol treatment). Endometrial adenocarcinoma was also observed in EtOH_*Msh2*^{fl} and H_2O_*Msh2*^{fl} mice, after 12 and 15 months, under 20% ethanol in drinking water and normal water treatment respectively (Chapter 4, 4.2.2.2).

In Group-A (water-treated control cohort, H_2O_*Aldh1b1*$^{fl.fl}$_*Msh2*$^{fl\ KO}$), no abnormalities or tumours were found in the large intestines in any of the 12 H_2O_*Aldh1b1*$^{fl.fl}$_*Msh2*$^{fl\ KO}$ mice. No morphological abnormalities or tumours were observed following necropsy and histopathological analysis of the H&E-stained sections of the small intestines, stomach, liver, spleen, lymph nodes and thymus, of any of the 12 EtOH_*Aldh1b1*$^{fl.fl}$_*Msh2*$^{fl\ KO}$ mice or 12 H_2O_*Aldh1b1*$^{fl.fl}$_*Msh2*$^{fl\ KO}$ mice.

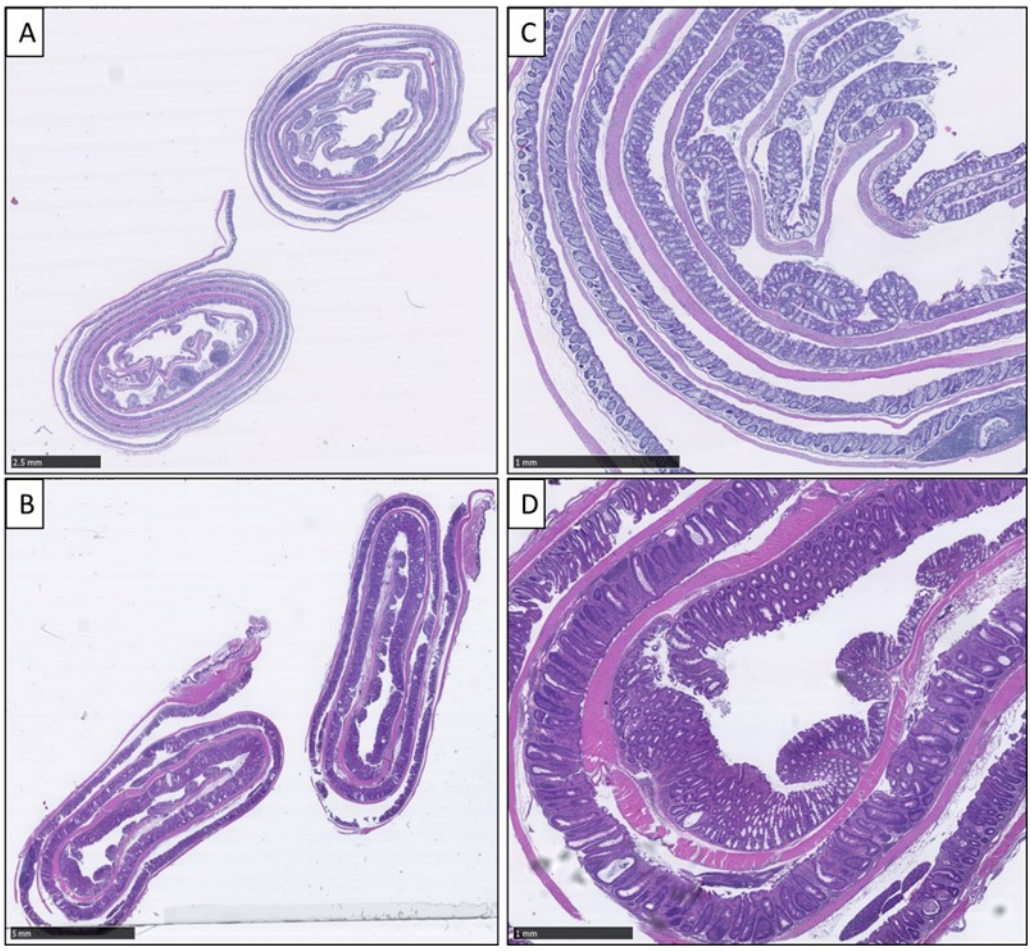

Figure 6.14: Representative images of H&E stained colon Swiss rolls. A) Images of H&E stained LI Swiss rolls from water-treated *Aldh1b1*$^{flox/flox}$ Msh2-LS (H_2O_*Aldh1b1*$^{fl.fl}$_*Msh2*$^{fl\ KO}$) mice, further magnified in image (C) showing normal large intestinal mucosal appearances. Images taken from scanned slide files with the Hamamatsu Nanozoomer NDP Viewer software at 0.7X and 2.5X magnification respectively (bar at lower left indicates 2.5mm and 1mm). B) Images of H&E stained LI Swiss rolls from ethanol-treated *Aldh1b1*$^{flox/flox}$ Msh2-LS (EtOH_*Aldh1b1*$^{fl.fl}$_*Msh2*$^{fl\ KO}$) mice, further magnified in image (D) showing widespread hyperproliferation of the elongated colonic crypts. Images taken from scanned slide files with the Hamamatsu Nanozoomer NDP Viewer software at 0.6X and 2.5X magnification respectively (bar at lower left indicates 2.5mm and 1mm).

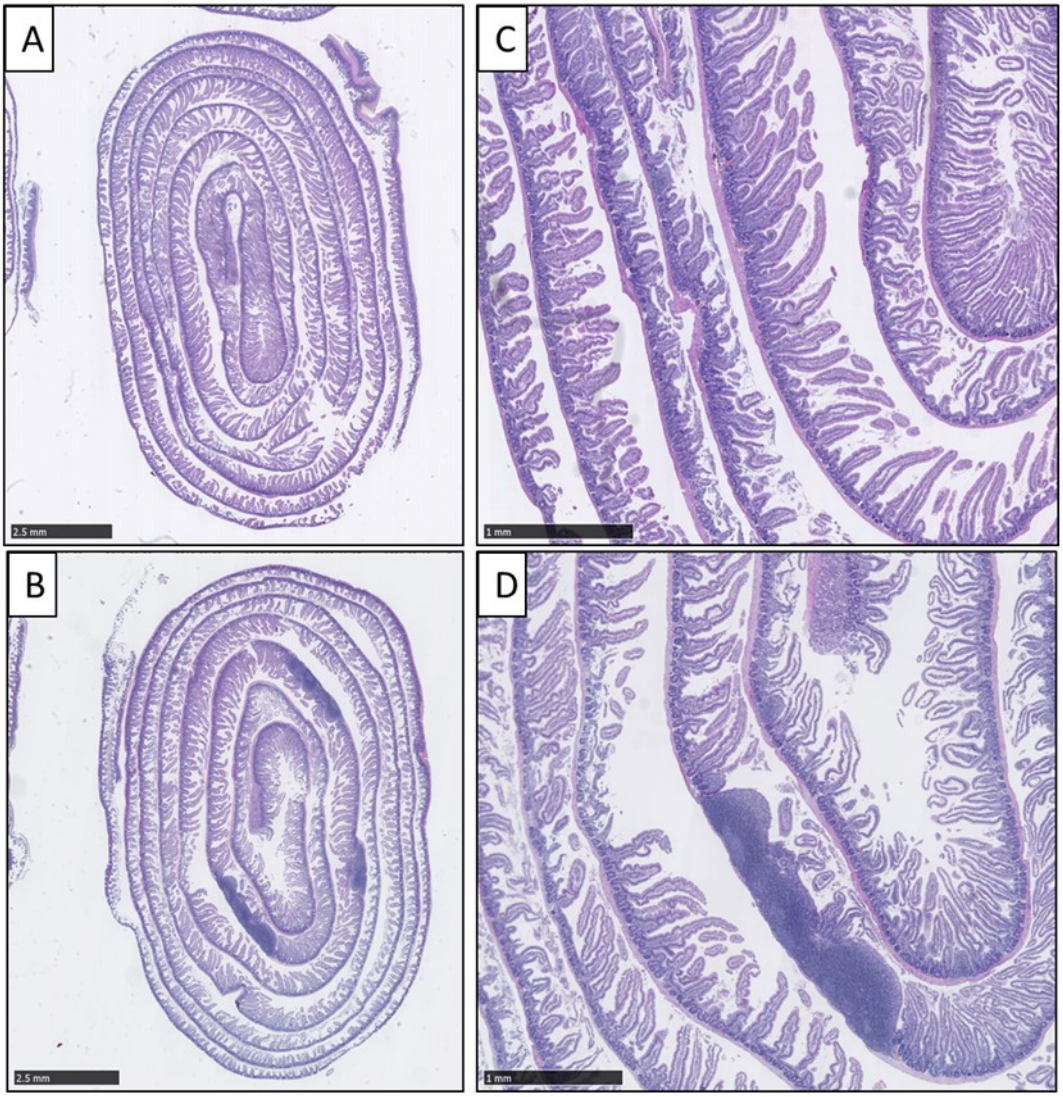

Figure 6.15: Representative images of H&E stained SI Swiss rolls. A) Image of H&E stained SI Swiss roll from a water-treated *Aldh1b1*$^{flox/flox}$ Msh2-LS (H_2O_*Aldh1b1*$^{fl.fl}$_*Msh2*$^{fl\ KO}$) mouse, further magnified in image (C). Images taken from scanned slide files with the Hamamatsu Nanozoomer NDP Viewer software at 0.7X and 2.5X magnification respectively. B) Image of H&E stained small intestine Swiss roll from an ethanol-treated *Aldh1b1*$^{flox/flox}$ Msh2-LS (EtOH_*Aldh1b1*$^{fl.fl}$_*Msh2*$^{fl\ KO}$) mouse, further magnified in image (D). Images taken from scanned slide files with the Hamamatsu Nanozoomer NDP Viewer software at 0.7X and 2.5X magnification respectively (bar at lower left indicates 2.5mm and 1mm). All images show normal small intestinal mucosal appearances. SI: Small Intestine.

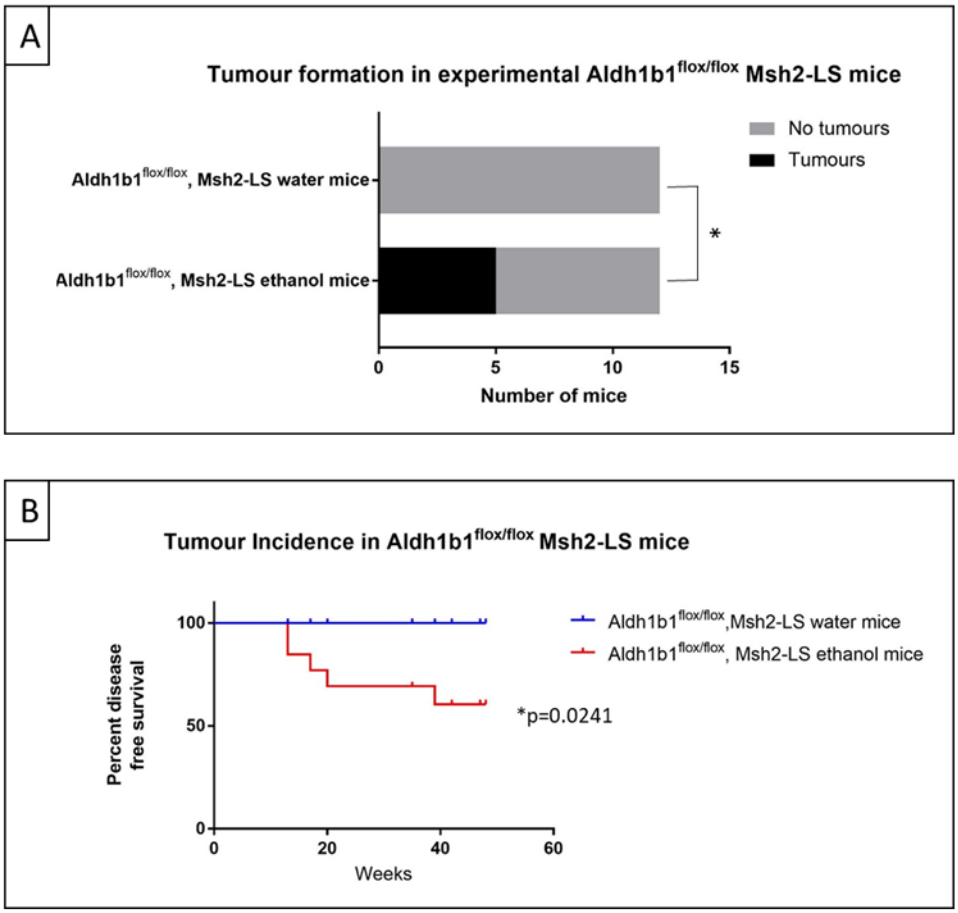

Figure 6.16: A) Bar chart of the number of *Aldh1b1*$^{flox/flox}$ Msh2-LS mice that developed intestinal tumours (both adenomas and adenocarcinomas) after receiving either 20% ethanol in drinking water or normal/regular drinking water. 5/12 (41.7%) *Aldh1b1*$^{flox/flox}$ Msh2-LS ethanol-treated (EtOH_*Aldh1b1*$^{fl.fl}$_*Msh2*$^{fl\ KO}$) mice developed large intestinal tumours compared with 0/12 (0%) *Aldh1b1*$^{flox/flox}$ Msh2-LS water-treated (H_2O_*Aldh1b1*$^{fl.fl}$_*Msh2*$^{fl\ KO}$) mice that developed large intestinal tumours. Fisher's exact test, *p=0.0373. B) Survival chart showing tumour incidence in *Aldh1b1*$^{flox/flox}$ Msh2-LS mice treated with either 20% ethanol or water. The survival plot shows the development of tumours (both adenomas and adenocarcinomas) in the *Aldh1b1*$^{flox/flox}$ Msh2-LS ethanol-treated (EtOH_*Aldh1b1*$^{fl.fl}$_*Msh2*$^{fl\ KO}$) group (red) compared with the lack of intestinal tumours over the same time period in the *Aldh1b1*$^{flox/flox}$ Msh2-LS water-treated (H_2O_*Aldh1b1*$^{fl.fl}$_*Msh2*$^{fl\ KO}$) group (blue). Log-rank (Mantel-Cox) test, *p=0.0241.

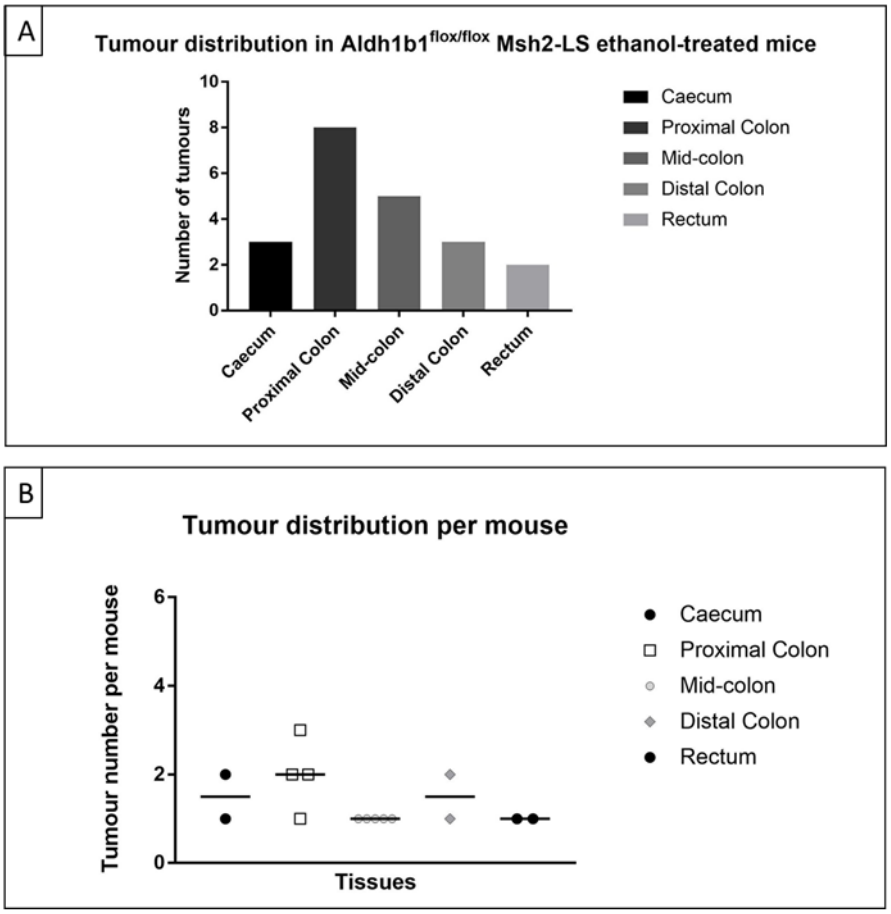

Figure 6.17: Tumour distribution in ethanol-treated *Aldh1b1*$^{flox/flox}$ Msh2-LS (EtOH_*Aldh1b1*$^{fl.fl}$_*Msh2*$^{fl\ KO}$) tumour-bearing mice. A) Numbers of adenomas and adenocarcinomas found and their locations. In total, 21 neoplasms were observed: 3 adenomas in the caecum; 8 adenomas in the proximal colon (1/8 was an invasive adenocarcinomas); 5 adenomas in the mid-colon; 3 adenomas in the distal colon; and 2 adenomas in the rectum. B) Tumour distribution and number per EtOH_*Aldh1b1*$^{fl.fl}$_*Msh2*$^{fl\ KO}$ tumour-bearing mouse: 1/5 tumour-bearing mice showed one caecal adenoma and 1/5 mice showed two adenomas in the caecum; 1/5 tumour-bearing mice showed one proximal colonic adenoma; 2/5 showed two adenomas and 1/5 showed three adenomas in the proximal colon; 5/5 tumour-bearing mice showed one mid-colonic adenoma; 1/5 tumour-bearing mice showed 2 distal colonic adenomas and 1/5 showed one adenoma in the distal colon; 2/5 tumour-bearing mice showed one rectal adenoma.

6.3.2.3 Tumour development in *Aldh1b1* constitutive-knockout Msh2-LS mice under long-term ethanol treatment

The two cohorts of *Aldh1b1*$^{-/-}$ Msh2-LS model mice, Group-A (water-treated, H_2O_*Aldh1b1*$^{-/-}$_*Msh2*$^{fl\ KO}$) and Group-B (ethanol-treated, EtOH_*Aldh1b1*$^{-/-}$_*Msh2*$^{fl\ KO}$), were monitored for up to 12 months for signs of intestinal tumour development or other pathological abnormalities, using a clinical scoring system that included known clinical signs of distress seen in mice that develop intestinal neoplasms, to determine when the mice should be culled for necropsy dissection and tumour analysis (Table 4.1). Most of the mice in Group-B (ethanol-treated experimental group) displayed either anal prolapse or >20% reduction in body weight as common clinical signs of distress, at varying lengths of time from the start of the experimental protocol and were then culled for necropsy dissection. During necropsy dissection, naked eye inspection revealed that the majority of the EtOH_*Aldh1b1*$^{-/-}$_*Msh2*$^{fl\ KO}$ mice showed a thicker colonic wall compared with the normal colonic walls of the H_2O_*Aldh1b1*$^{-/-}$_*Msh2*$^{fl\ KO}$ mice, but no gross morphological differences were observed in the small intestines. The lengths of the small intestines and colons were measured and recorded, but no significant differences in length were observed between the ethanol-treated mice and the water-treated mice.

The histopathological analyses of *Aldh1b1*$^{-/-}$ Msh2-LS large intestines and small intestines confirmed the macroscopic observations of no significant morphological differences between the two groups in the small intestines, but increased colonic wall thickness in EtOH_*Aldh1b1*$^{-/-}$_*Msh2*$^{fl\ KO}$ mice, due to a widespread increase in the colonic crypt length as a result of extended zones of crypt epithelial hyperproliferation that were not observed in H_2O_*Aldh1b1*$^{-/-}$_*Msh2*$^{fl\ KO}$ murine colons (Figure 6.18). These extended zones of colonic crypt hyperproliferation were seen to affect 50% – 90% of the whole colonic length, usually involving proximal colon and mid colon, more than distal colon and rectum, in most of the EtOH_*Aldh1b1*$^{-/-}$_*Msh2*$^{fl\ KO}$ mice who survived more than 2 months of the ethanol treatment protocol. By contrast, histopathological analyses of the small intestines showed normal mucosal appearances with no significant morphological differences between the two groups of animals using H&E-stained Swiss rolls of the small intestines (Figure 6.19).

In total, 8 out of 12 EtOH_*Aldh1b1*$^{-/-}$_*Msh2*$^{fl\ KO}$ mice demonstrated zones of large intestinal crypt elongation with epithelial hyperproliferation, and with adenoma formation, all within

an average of 6 months (minimum 9 weeks and maximum 42 weeks) of the start of the experimental protocol, compared with no cases of either colonic crypt hyperproliferation or large intestinal adenoma formation in the 12 H_2O_*Aldh1b1*$^{-/-}$_*Msh2*$^{fl\ KO}$ control mice, over the same time-period (Figure 6.20).

Almost all of the 8 EtOH_*Aldh1b1*$^{-/-}$_*Msh2*$^{fl\ KO}$ tumour-bearing mice showed colonic crypt hyperproliferative changes along the whole colon. No *Aldh1b1*$^{-/-}$ Msh2-LS mice showed only colonic hyperproliferation without tumour formation. In addition, in 4 out of 8 EtOH_*Aldh1b1*$^{-/-}$_*Msh2*$^{fl\ KO}$ mice, caecal adenomas were found. Among these 8 EtOH_*Aldh1b1*$^{-/-}$_*Msh2*$^{fl\ KO}$ mice, 5 were diagnosed with rectal adenoma. In total, 35 neoplasms were observed, distributed between both the caecum and the colon (Figure 6.21). Four out of 12 EtOH_*Aldh1b1*$^{-/-}$_*Msh2*$^{fl\ KO}$ mice did not show any intestinal adenoma formation or extra-intestinal abnormality or tumour.

In Group-A (water-treated control cohort), no abnormalities or tumours in the large intestines were found in any of the 12 H_2O_*Aldh1b1*$^{-/-}$_*Msh2*$^{fl\ KO}$ mice.

No morphological abnormalities or tumours were observed following necropsy and histopathological analysis of the H&E-stained sections of the small intestines, stomach, liver, spleen, lymph nodes and thymus, in any of the 12 EtOH_*Aldh1b1*$^{-/-}$_*Msh2*$^{fl\ KO}$ mice or in any of the 12 H_2O_*Aldh1b1*$^{-/-}$_*Msh2*$^{fl\ KO}$ mice.

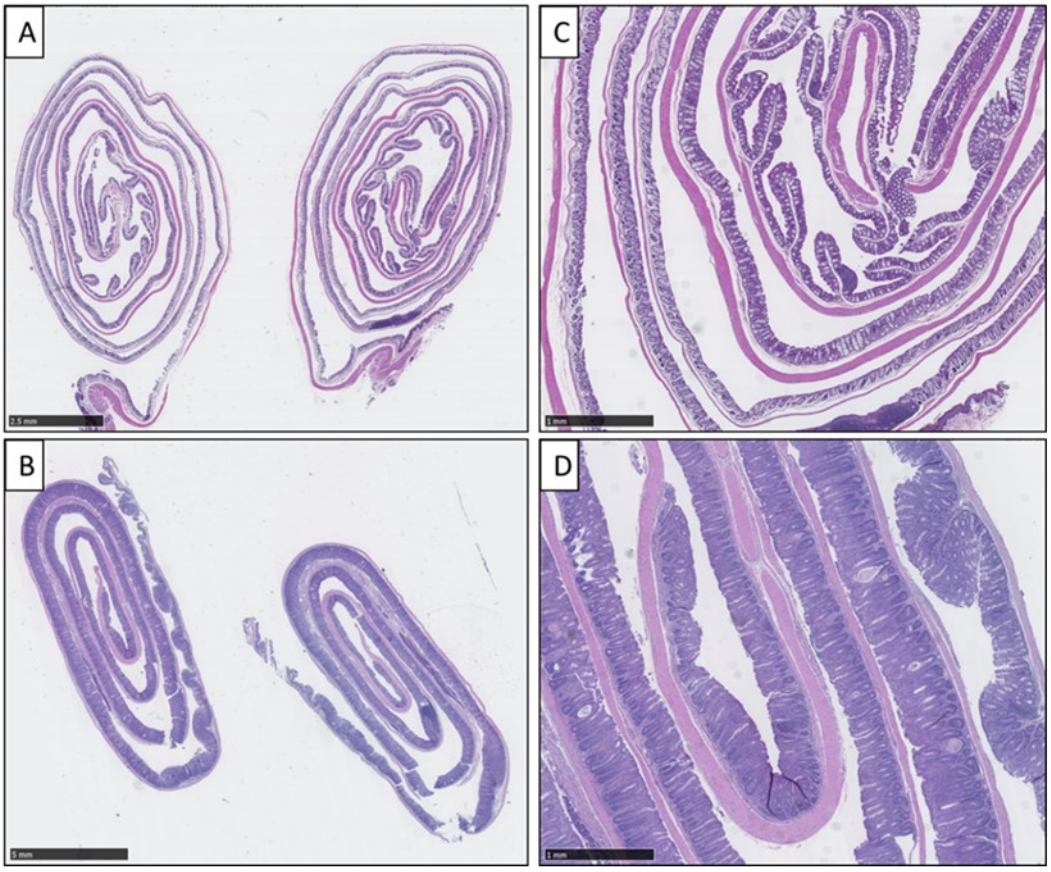

Figure 6.18: Representative images of H&E stained colon Swiss rolls. A) Images of H&E stained LI Swiss rolls from water-treated *Aldh1b1*$^{-/-}$ Msh2-LS (H_2O_*Aldh1b1*$^{-/-}$_*Msh2*$^{fl\ KO}$) mice, further magnified in image (C) showing normal large intestinal mucosal appearances. Images taken from scanned slide files with the Hamamatsu Nanozoomer NDP Viewer software at 0.7X and 2.5X magnification respectively. B) Images of H&E stained LI Swiss rolls from ethanol-treated *Aldh1b1*$^{-/-}$ Msh2-LS (EtOH_*Aldh1b1*$^{-/-}$_*Msh2*$^{fl\ KO}$) mice, further magnified in image (D) showing widespread hyperproliferative changes with colonic crypt elongation. Images taken from scanned slide files with the Hamamatsu Nanozoomer NDP Viewer software at 0.5X and 2.5X magnification respectively (bar at lower left indicates 5mm and 1mm).

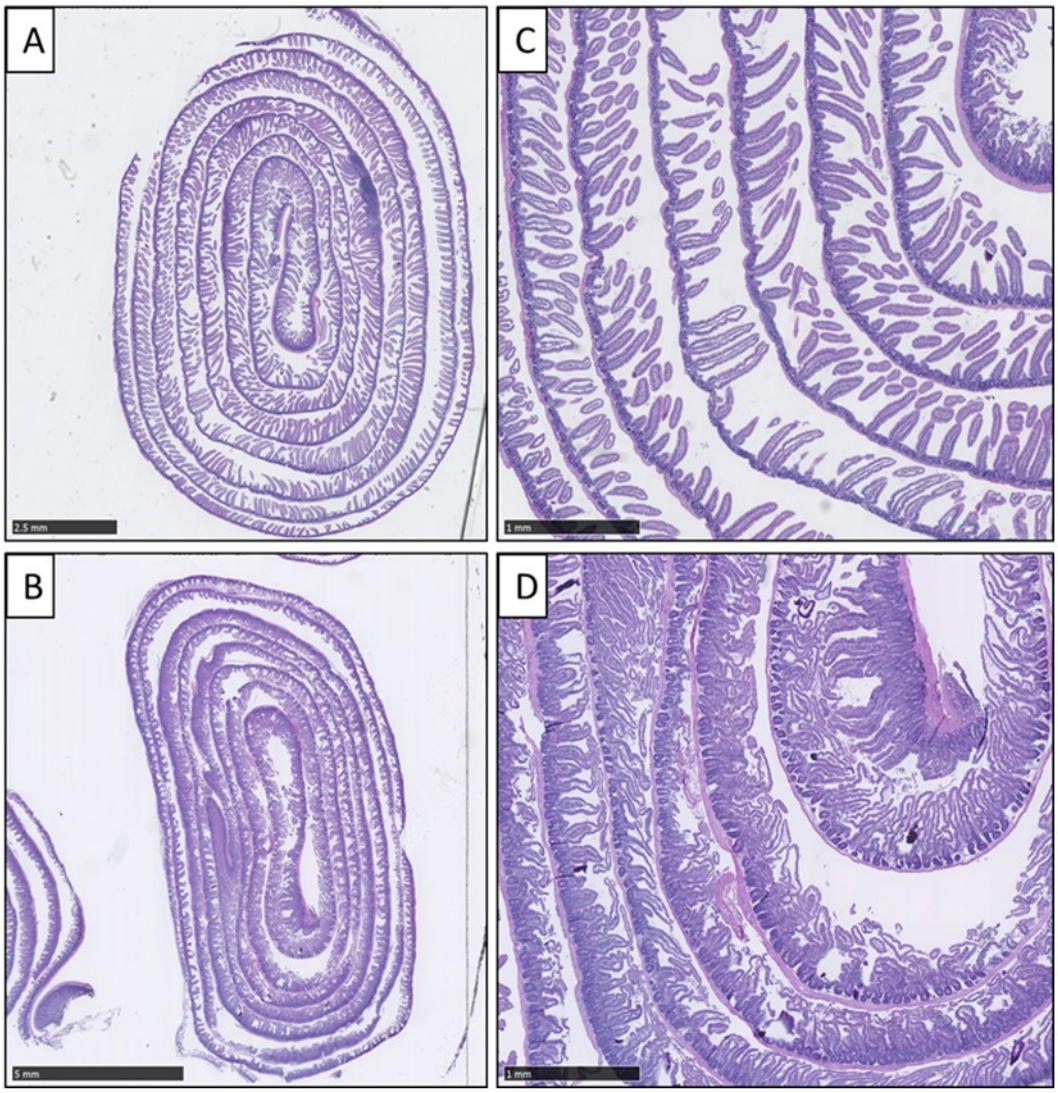

Figure 6.19: Representative images of H&E stained SI Swiss rolls. A) Image of H&E stained SI Swiss roll from a water-treated *Aldh1b1*$^{-/-}$ Msh2-LS (H_2O_*Aldh1b1*$^{-/-}$_*Msh2*$^{fl\ KO}$) mouse, further magnified in image (C). Images taken from scanned slide files with the Hamamatsu Nanozoomer NDP Viewer software at 0.7X and 2.5X magnification respectively. B) Image of H&E stained small intestine Swiss roll from an ethanol-treated *Aldh1b1*$^{-/-}$ Msh2-LS (EtOH_*Aldh1b1*$^{-/-}$_*Msh2*$^{fl\ KO}$) mouse, further magnified in image (D). Images taken from scanned slide files with the Hamamatsu Nanozoomer NDP Viewer software at 0.5X and 2.5X magnification respectively magnification (bar at lower left indicates 5mm and 1mm). All images show normal small intestinal mucosal appearances.SI: Small Intestine.

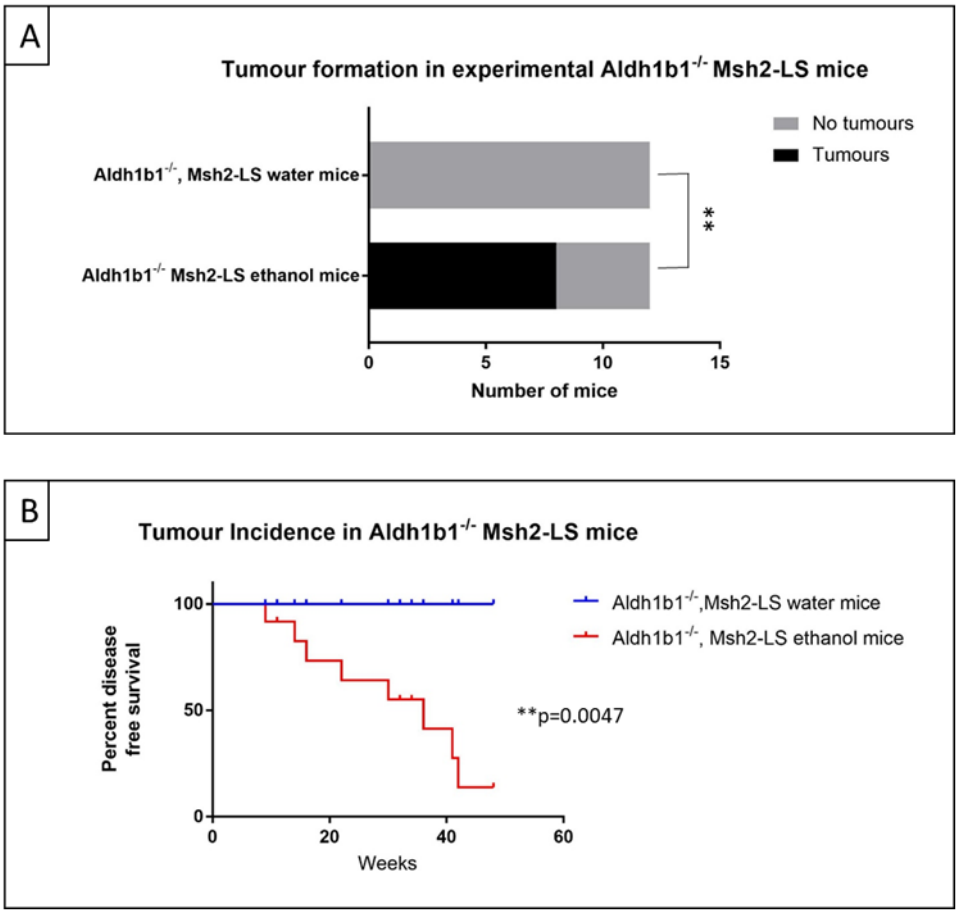

Figure 6.20: A) Bar chart of the number of *Aldh1b1*$^{-/-}$ Msh2-LS mice that developed intestinal tumours after receiving either 20% ethanol in drinking water or normal/regular drinking water. 8/12 (66.7%) ethanol-treated *Aldh1b1*$^{-/-}$ Msh2-LS (EtOH_*Aldh1b1*$^{-/-}$_*Msh2*$^{fl\ KO}$) mice developed large intestinal tumours compared with 0/12 (0%) water-treated *Aldh1b1*$^{-/-}$ Msh2-LS (H_2O_*Aldh1b1*$^{-/-}$_*Msh2*$^{fl\ KO}$) mice. Fisher's exact test, **p=0.0013.

B) Survival chart showing tumour incidence in *Aldh1b1*$^{-/-}$ Msh2-LS mice treated with either 20% ethanol or water. The survival plot shows the development of tumours (both adenomas and adenocarcinomas) in the ethanol-treated *Aldh1b1*$^{-/-}$ Msh2-LS (EtOH_*Aldh1b1*$^{-/-}$_*Msh2*$^{fl\ KO}$) group (red) compared with the lack of intestinal tumours over the same time period in the water-treated *Aldh1b1*$^{-/-}$ Msh2-LS (H_2O_*Aldh1b1*$^{-/-}$_*Msh2*$^{fl\ KO}$) group (blue). Log-rank (Mantel-Cox) test, **p=0.0047.

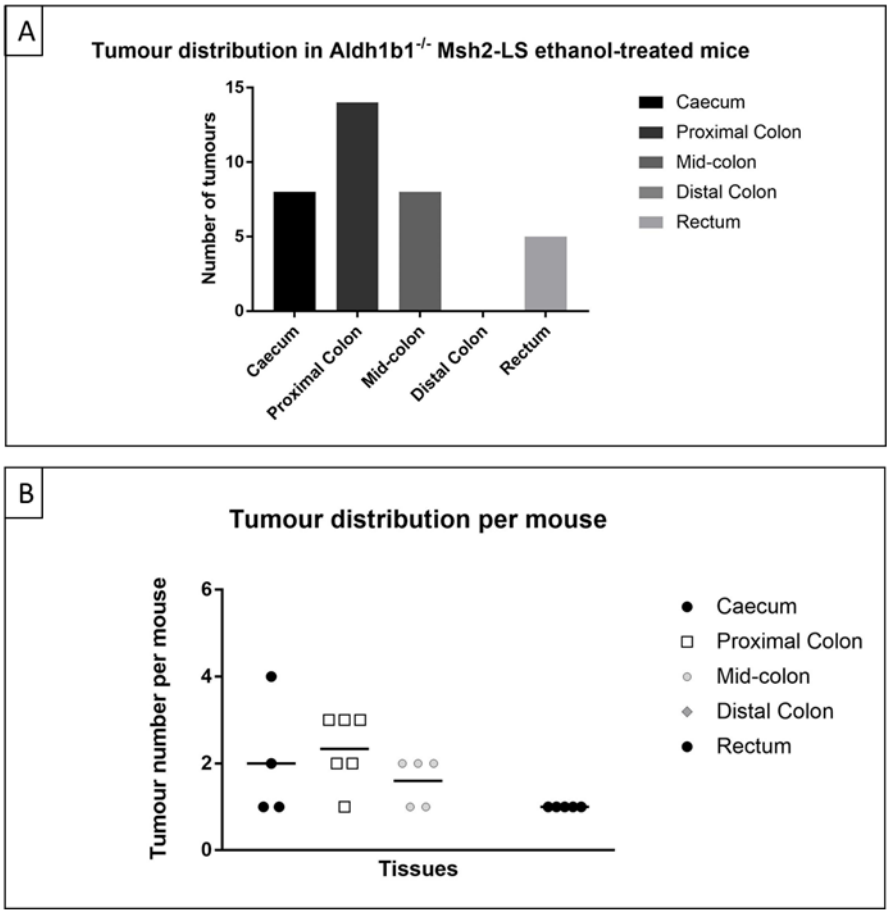

Figure 6.21: Tumour distribution in ethanol-treated *Aldh1b1*$^{-/-}$ Msh2-LS (EtOH_*Aldh1b1*$^{-/-}$_*Msh2*$^{fl\ KO}$) tumour-bearing mice. A) Numbers of adenomas (no adenocarcinomas observed in this group) found and their locations. In total, 35 neoplasms were observed: 8 adenomas in the caecum; 14 adenomas in the proximal colon; 8 adenomas in the mid-colon; 0 adenomas in the distal colon; and 5 adenomas in the rectum. B) Tumour distribution and number per EtOH_*Aldh1b1*$^{-/-}$_*Msh2*$^{fl\ KO}$ tumour-bearing mouse: 2/8 tumour-bearing mice showed one caecal adenoma, 1/8 mice showed two caecal adenomas and 1/8 showed 4 adenomas in the caecum; 1/8 tumour-bearing mice showed one proximal colonic adenoma, 2/8 showed two adenomas and 3/8 showed three adenomas in the proximal colon; 2/8 tumour-bearing mice showed one mid-colonic adenoma and 3/8 showed 2 adenomas in the mid-colon. No EtOH_*Aldh1b1*$^{-/-}$_Msh2$^{fl\ KO}$ mice showed adenoma formation in the distal colon. However, 5/8 tumour-bearing mice showed one rectal adenoma.

6.3.2.4 Comparative analysis of tumour development between in *Aldh1b1* conditional-knockout Msh2-LS mice, *Aldh1b1* constitutive-knockout Msh2-LS mice and *Aldh1b1* wild-type Msh2-LS mice under long-term ethanol treatment

In *Aldh1b1*$^{flox/flox}$ Msh2-LS subjects, 41.7% (5/12 mice) of EtOH_*Aldh1b1*$^{fl/fl}$_*Msh2*$^{fl\ KO}$ mice demonstrated adenoma formation (with 1 case of invasive adenocarcinoma), forming within an average of 4.5 months (minimum 13 weeks and maximum 39 weeks), compared with *Aldh1b1* wild-type (*Aldh1b1*^{wt}) Msh2-LS in which 65% (15/23) of EtOH_*Msh2*$^{fl\ KO}$ mice showed adenoma formation (5 cases of invasive adenocarcinoma), all within an average of 6 months (minimum 4 weeks and maximum 48 weeks) (Figure 6.22). EtOH_*Aldh1b1*$^{fl/fl}$_*Msh2*$^{fl\ KO}$mice showed tumour formation slightly earlier than EtOH_*Msh2*$^{fl\ KO}$ mice, but no statistically significant difference was observed. However, tumour-bearing EtOH_*Aldh1b1*$^{fl/fl}$_*Msh2*$^{fl\ KO}$ mice showed statistically significantly higher numbers of tumour per mouse (21 neoplasms were observed in 5 tumour-bearing mice) compared with tumour-bearing e EtOH_*Msh2*$^{fl\ KO}$ mice (36 neoplasms were observed in 15 tumour-bearing mice) (Figure 6.23).

In *Aldh1b1*$^{-/-}$ Msh2-LS subjects, 66.7% (8/12 mice) of EtOH_*Aldh1b1*$^{-/-}$_*Msh2*$^{fl\ KO}$ mice demonstrated adenoma formation (no adenocarcinomas observed in this group), forming within an average of 6 months (minimum 9 weeks and maximum 42 weeks), compared with *Aldh1b1*^{wt} Msh2-LS in which 65% (15/23) of EtOH_*Msh2*$^{fl\ KO}$ mice showed adenoma formation (5 cases of invasive adenocarcinoma), all within an average of 6 months (minimum 4 weeks and maximum 48 weeks) (Figure 6.24). Tumour-bearing EtOH_*Aldh1b1*$^{-/-}$_*Msh2*$^{fl\ KO}$ mice showed statistically higher numbers of tumours per mouse (35 neoplasms were observed in 8 tumour-bearing mice) compared with tumour-bearing EtOH_*Msh2*$^{fl\ KO}$ mice (36 neoplasms were observed in 15 tumour-bearing mice) (Figure 6.25).

We performed the same comparative analyses of tumour development between EtOH_*Aldh1b1*$^{fl/fl}$_*Msh2*$^{fl\ KO}$ and EtOH_*Aldh1b1*$^{-/-}$_*Msh2*$^{fl\ KO}$ mice, but no statistically significant differences were found between these two cohorts (Figure 6.27-6.28).

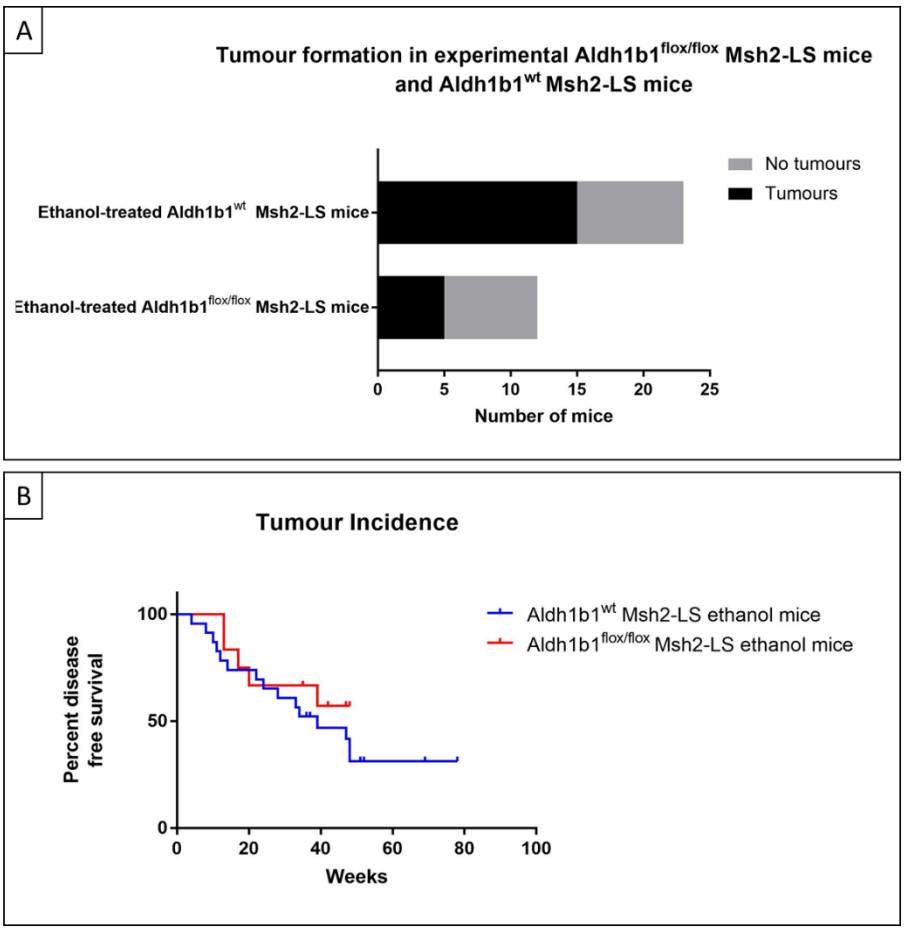

Figure 6.22: A) Bar chart of the number of ethanol-treated *Aldh1b1*^{wt} Msh2-LS (EtOH_*Msh2*$^{fl\ KO}$) tumour-bearing mice (15/23, 65%) compared with ethanol-treated *Aldh1b1*$^{flox/flox}$ Msh2-LS (EtOH_*Aldh1b1*$^{fl/fl}$_*Msh2*$^{fl\ KO}$) tumour-bearing mice (5/12, 41.7%). No significant differences were observed between these groups. B) Survival chart showing tumour incidence in ethanol-treated *Aldh1b1*^{wt} Msh2-LS (EtOH_*Msh2*$^{fl\ KO}$) mice compared with ethanol-treated *Aldh1b1*$^{flox/flox}$ Msh2-LS (EtOH_*Aldh1b1*$^{fl/fl}$_*Msh2*$^{fl\ KO}$) mice. The survival plot shows the development of tumours (both adenomas and adenocarcinomas) in both EtOH_*Msh2*$^{fl\ KO}$ mice (blue) and EtOH_*Aldh1b1*$^{fl/fl}$_*Msh2*$^{fl\ KO}$ mice (red). No statistically significant differences were observed between these groups.

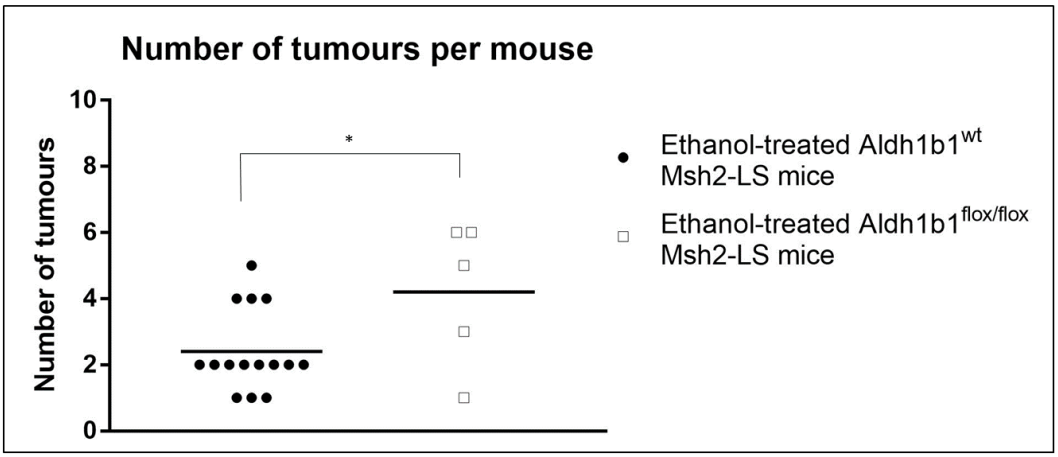

Figure 6.23: Number of tumours per mouse in ethanol-treated *Aldh1b1*^{wt} Msh2-LS (EtOH_*Msh2*$^{fl\ KO}$) tumour-bearing mice compared with ethanol-treated *Aldh1b1*$^{flox/flox}$ Msh2-LS (EtOH_*Aldh1b1*$^{fl/fl}$_*Msh2*$^{fl\ KO}$) tumour-bearing mice. EtOH_*Msh2*$^{fl\ KO}$ tumour-bearing mice showed an average of 2.4 tumours per mouse compared with EtOH_*Aldh1b1*$^{fl/fl}$_*Msh2*$^{fl\ KO}$ tumour-bearing mice with an average 4.2 tumours per mouse. Student t test, *p=0.0319.

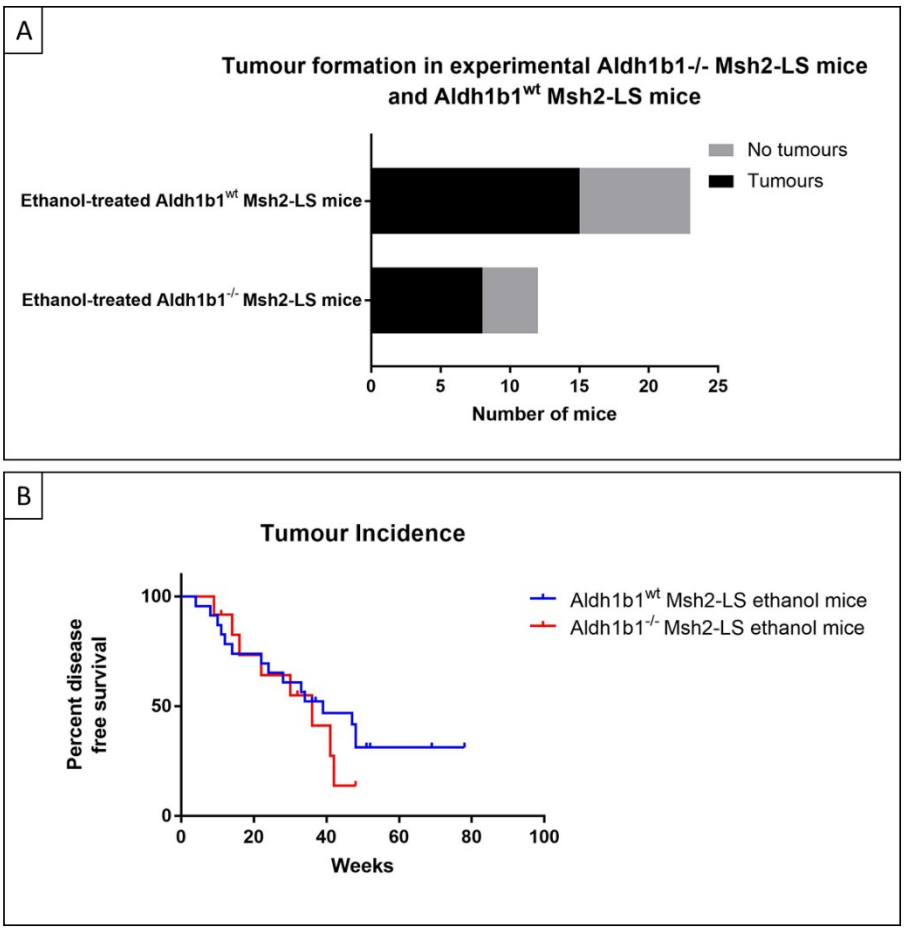

Figure 6.24: A) Bar chart of the number of ethanol-treated *Aldh1b1*^{wt} Msh2-LS (EtOH_*Msh2*$^{fl\ KO}$) tumour-bearing mice (15/23, 65%) compared with ethanol-treated *Aldh1b1*$^{-/-}$ Msh2-LS (EtOH_*Aldh1b1*$^{-/-}$_*Msh2*$^{fl\ KO}$) tumour-bearing mice (8/12, 66.7%). No statistically significant differences were observed between these groups. B) Survival chart showing tumour incidence in ethanol-treated *Aldh1b1*^{wt} Msh2-LS (EtOH_*Msh2*$^{fl\ KO}$) mice compared with ethanol-treated *Aldh1b1*$^{-/-}$ Msh2-LS (EtOH_*Aldh1b1*$^{-/-}$_*Msh2*$^{fl\ KO}$) mice. The survival plot shows the development of tumours (both adenomas and adenocarcinomas) in both EtOH_*Msh2*$^{fl\ KO}$ mice (blue) and EtOH_*Aldh1b1*$^{-/-}$_*Msh2*$^{fl\ KO}$ (red). No statistically significant differences were observed between these groups.

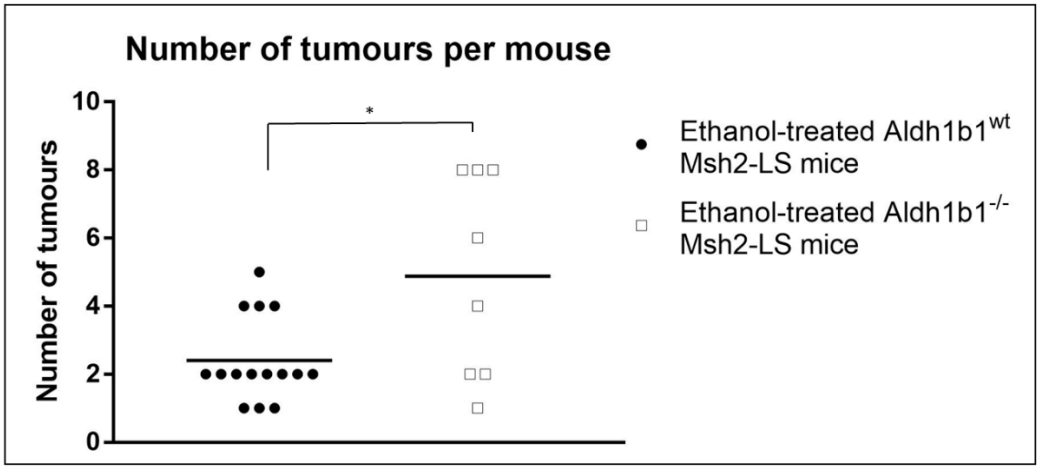

Figure 6.25: Number of tumours per mouse in ethanol-treated *Aldh1b1*^{wt} Msh2-LS (EtOH_*Msh2*$^{fl\ KO}$) tumour-bearing mice compared with ethanol-treated *Aldh1b1*$^{-/-}$ Msh2-LS (EtOH_*Aldh1b1*$^{-/-}$_*Msh2*$^{fl\ KO}$) tumour-bearing mice. EtOH_*Msh2*$^{fl\ KO}$ tumour-bearing mice showed on average 2.4 tumours per mouse compared with EtOH_*Aldh1b1*$^{-/-}$_*Msh2*$^{fl\ KO}$ tumour-bearing mice with an average of 4.8 tumours per mouse. Student t test, *p=0.0103.

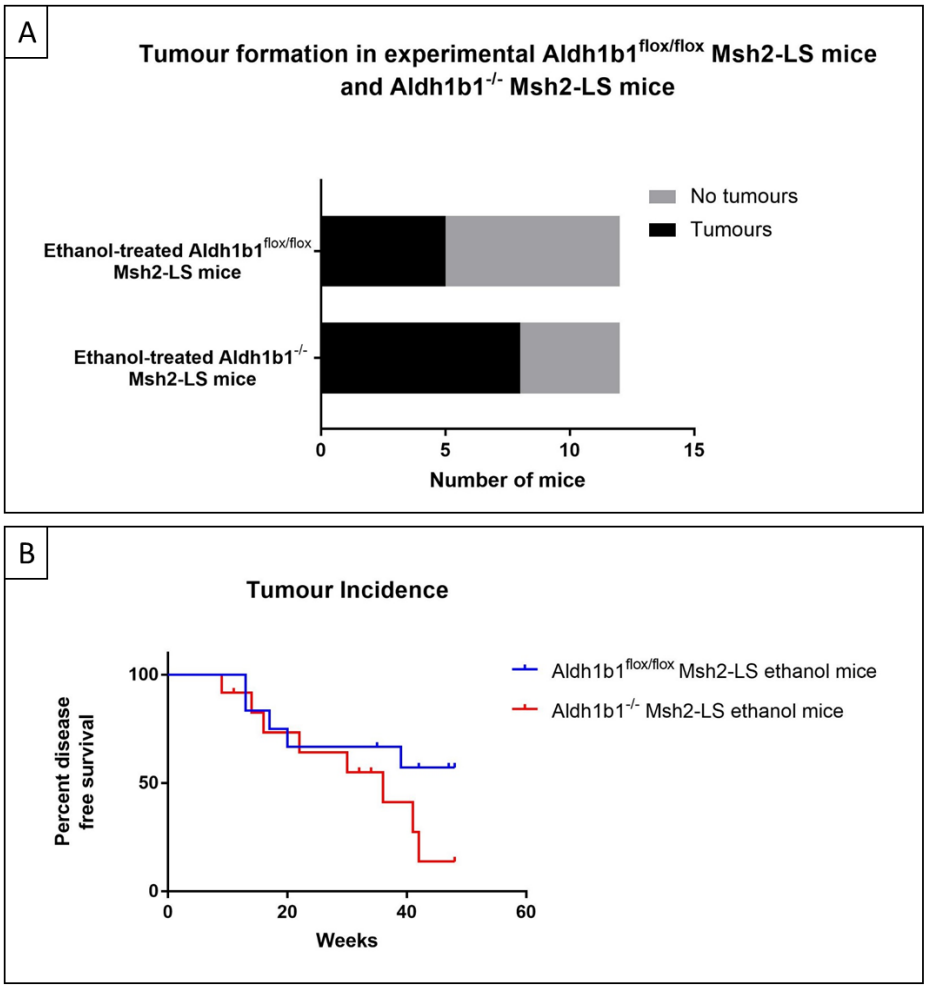

Figure 6.26: A) Bar chart of the number of ethanol-treated *Aldh1b1*$^{flo/flox}$ Msh2-LS (EtOH_*Aldh1b1*$^{fl/fl}$_*Msh2*$^{fl\ KO}$) tumour-bearing mice (5/12, 41.7%) compared with ethanol-treated *Aldh1b1*$^{-/-}$ Msh2-LS (EtOH_*Aldh1b1*$^{-/-}$_*Msh2*$^{fl\ KO}$) tumour-bearing mice (8/12, 66.7%). No statistically significant differences were observed between these groups. B) Survival chart showing tumour incidence in ethanol-treated *Aldh1b1*$^{flox/flox}$ Msh2-LS (EtOH_*Aldh1b1*$^{fl/fl}$_*Msh2*$^{fl\ KO}$) mice compared with ethanol-treated *Aldh1b1*$^{-/-}$ Msh2-LS (EtOH_*Aldh1b1*$^{-/-}$_*Msh2*$^{fl\ KO}$) mice. The survival plot shows the development of tumours (both adenomas and adenocarcinomas) in both EtOH_*Aldh1b1*$^{fl/fl}$_*Msh2*$^{fl\ KO}$ mice (blue) and EtOH_*Aldh1b1*$^{-/-}$_*Msh2*$^{fl\ KO}$ (red). No statistically significant differences were observed between these groups.

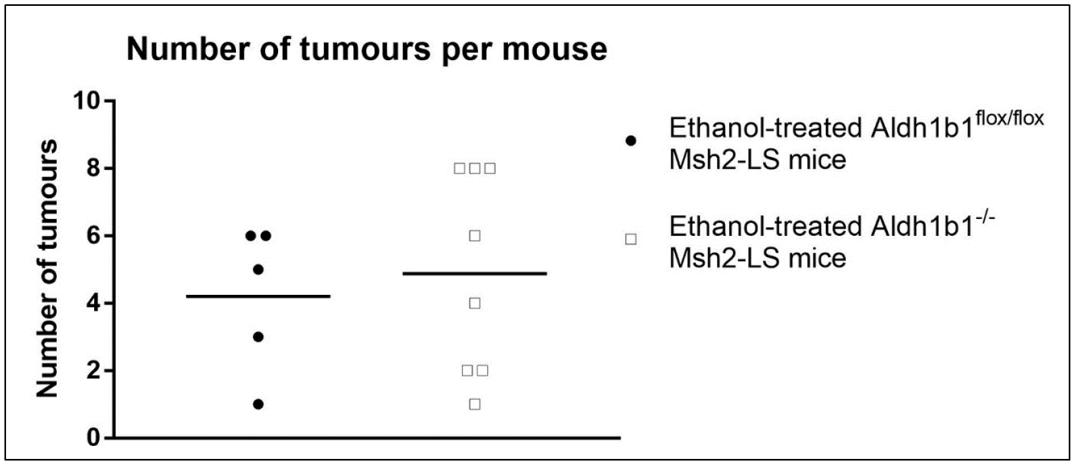

Figure 6.27: Number of tumours per mouse in ethanol-treated *Aldh1b1*$^{flox/flox}$ Msh2-LS (EtOH_*Aldh1b1*$^{fl/fl}$_*Msh2*$^{fl\ KO}$) tumour-bearing mice compared with ethanol-treated *Aldh1b1*$^{-/-}$ Msh2-LS (EtOH_*Aldh1b1*$^{-/-}$_*Msh2*$^{fl\ KO}$) tumour-bearing mice. EtOH_*Aldh1b1*$^{fl/fl}$_*Msh2*$^{fl\ KO}$ tumour-bearing mice showed an average of 4.2 tumours per mouse compared with EtOH_*Aldh1b1*$^{-/-}$_*Msh2*$^{fl\ KO}$ tumour-bearing mice with an average of 4.8 tumours. No statistically significant difference was observed between these groups.

6.4 Long-term ethanol effects in *Aldh1b1*-knockout Msh2-LS mouse model control mice.

6.4.1 Methods

We introduced negative control experimental groups to study the ethanol effect in Msh2-LS mice without treating them with Tamoxifen.

Groups of 7-9 weeks old *Aldh1b1*$^{flox/flox}$ Msh2-LS control mice (*Msh2*$^{flox/-}$*; Lgr5CreERT2*$^{+/-}$*; Aldh1b1*$^{flox/flox}$ or *Msh2*$^{flox/-}$*; Lgr5CreERT2*$^{+/-}$*; mTmG*$^{+/-}$*; Aldh1b1*$^{flox/flox}$) and *Aldh1b1*$^{-/-}$ Msh2-LS control mice (*Msh2*$^{flox/-}$*; Lgr5CreERT2*$^{+/-}$*; Aldh1b1*$^{-/-}$ or *Msh2*$^{flox/-}$*; Lgr5CreERT2*$^{+/-}$*; mTmG*$^{+/-}$*; Aldh1b1*$^{-/}$*)* were divided into two groups (A and B) prior to treatment with corn oil (without Tamoxifen).

Both Group-A and Group-B mice received i.p. injections of corn oil on days 1, 2, 3, and 4 (using the same volume of corn oil as used in treatments of the experimental subjects). On day 5 Group-A mice were provided with normal drinking water and Group-B mice with 20% ethanol in drinking water (Figure 6.28).

These control animals were culled when they reached the same end-timepoint as the age- and sex-matched experimental Tamoxifen-induced mice (following tumour development or clinical distress in these experimental subjects), or when the control mice showed either clinical signs of distress or they displayed >20% body weight loss compared with the initial weight. Following schedule 1 culling and necropsy dissection of the control mice, tissues were collected and fixed in 10% NBF (as described in Materials and Methods). Following standard tissue processing protocols, the tissue blocks were paraffin-embedded in preparation for section cutting and staining.

In previous work, *Aldh1b1*-depleted mice were used as experimental subjects, along with wild-type control mice, under long-term (>1 year) treatment with 20% ethanol in drinking water or normal/standard drinking water (Müller et al., 2016). The data related to wild-type control mice have already been discussed in Chapter 4 (4.3.2.1). Here, the data are shown for the ethanol/acetaldehyde effects on intestinal tumourigenesis, comparing both *Aldh1b1* conditional-knockout Tamoxifen-induced Msh2-LS mice and *Aldh1b1* constitutive-knockout Tamoxifen-induced Msh2-LS mice with *Aldh1b1* conditional-knockout non-induced Msh2-LS mice and *Aldh1b1* constitutive-knockout non-induced Msh2-LS mice. The acronyms used for the Msh2-LS model mice and their relevant treatments are shown in Table 2.2.

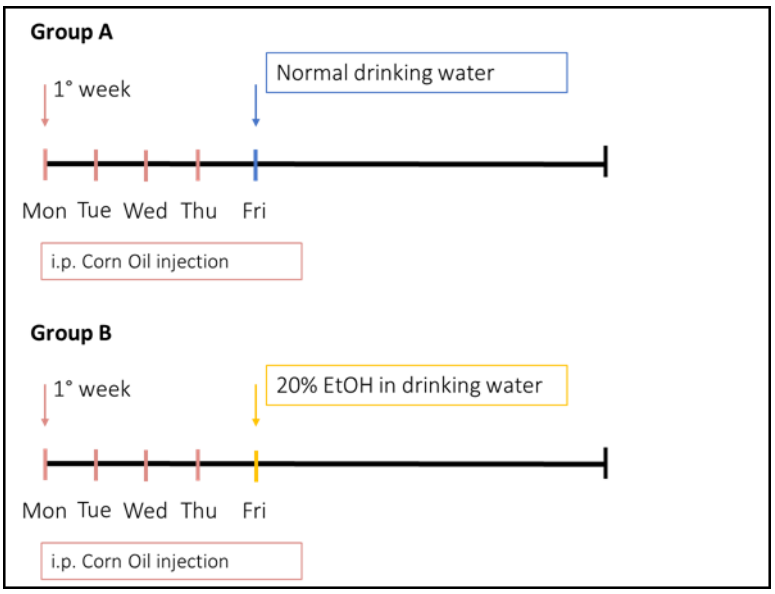

Figure 6.28: Experimental treatment protocols and timelines for Group-A (water-treated) and -B ethanol-treated) mice, showing 4 days of i.p. injections of corn oil (without Tamoxifen), followed by either standard/normal drinking water (Group-A) or drinking water containing 20% ethanol (Group-B). (EtOH = Ethanol).

6.4.2 Results

6.4.2.1 Control group organization and observations.

We studied the effects of ethanol/acetaldehyde (compared with water-treatment) on intestinal tumour formation in *Aldh1b1* conditional-knockout non-induced Msh2-LS mice and *Aldh1b1* constitutive-knockout non-induced Msh2-LS mice.

Fourteen non-induced *Aldh1b1*$^{flox/flox}$ Msh2-LS control mice were divided into two groups: 7 mice in Group-A (4 females and 3 males, water-treated control group) and 7 mice in Group-B (4 females and 3 males, ethanol-treated group).

Twelve non-induced *Aldh1b1*$^{-/-}$ Msh2-LS control mice were divided into two groups: 6 mice in Group-A (2 females and 4 males, water-treated control group) and 6 mice in Group-B (2 females and 4 males, ethanol-treated group).

Animals were culled, necropsy dissected and tissues were collected when they reached the same end-timepoint as the age- and sex-matched experimental Tamoxifen-induced ethanol-treated *Aldh1b1* conditional- or constitutive-knockout Msh2-LS mice.

During corn oil administration (daily corn oil i.p injections for 4 consecutive days), body weights and health status were recorded. In both *Aldh1b1* conditional-knockout Msh2-LS mice and *Aldh1b1* constitutive-knockout Msh2-LS mice, body weights of the female and male mice didn't significantly differ during the corn oil treatment (Figure 6.29), showing successful drug administration and acceptance of the experimental procedures by the mice. In non-induced *Aldh1b1*$^{flox/flox}$ Msh2-LS mice, body weights of males (~22.5g) were significantly higher than body weights of females (~18.9g) both before and during the corn oil treatments (Figure 6.29A). In non-induced *Aldh1b1*$^{-/-}$ Msh2-LS mice, body weights of males (~22.2g) were slightly lower than body weights of females (~22.8g), both before and during the corn oil treatments (Figure 6.29B).

After corn oil treatment, mice received either 20% ethanol in drinking water regime or standard/normal drinking water regime and the body weights and health status of the mice were monitored and recorded twice per week.

EtOH_*Aldh1b1*$^{fl/fl}$_*Msh2*^{fl} female and male mice did not show abnormal behaviour or reduced weight compared with H_2O_*Aldh1b1*$^{fl/fl}$_*Msh2*^{fl} female and male mice, indicating good acceptance of the ethanol regime (Figure 6.30A). The EtOH_*Aldh1b1*$^{fl/fl}$_*Msh2*^{fl} and H_2O_*Aldh1b1*$^{fl/fl}$_*Msh2*^{fl} male mice showed some variation in body weight within the groups, most likely reflecting the use of small numbers of mice from different litters starting at

different times (Figure 6.31B). EtOH_*Aldh1b1*$^{fl/fl}$_*Msh2*^{fl} mice weighed on average 32.4g for the males and 27g for the females, whereas H_2O_*Aldh1b1*$^{fl/fl}$_*Msh2*^{fl} mice weighed on average 29.5g for the males and 23g for the females (Figure 6.30).

EtOH_*Aldh1b1*$^{-/-}$_*Msh2*^{fl} female and male mice did not show abnormal behaviour or reduced body weight compared with H_2O_*Aldh1b1*$^{-/-}$_*Msh2*^{fl} female and male mice, indicating good acceptance of the ethanol regime (Figure 6.31). The EtOH_*Aldh1b1*$^{-/-}$_*Msh2*^{fl} and H_2O_*Aldh1b1*$^{-/-}$_*Msh2*^{fl} female and male mice showed some variation in body weight within the groups, most likely reflecting the use of small numbers of mice from different litters starting at different times. EtOH_*Aldh1b1*$^{-/-}$_*Msh2*^{fl} mice weighed on average 30g for the males and 31g for the females, whereas H_2O_*Aldh1b1*$^{-/-}$_*Msh2*^{fl} mice weighed on average 30.3g for the males and 26.3g for the females (Figure 6.31).

The body weights of both Tamoxifen-induced *Aldh1b1* conditional-knockout and *Aldh1b1* constitutive-knockout Msh2-LS mice, were compared with both non-induced *Aldh1b1* conditional-knockout and *Aldh1b1* constitutive-knockout Msh2-LS mice, during either 20% ethanol treatment or normal drinking water treatment (Figure 6.32-6.33). In every study group, ethanol-treated Msh2-LS female and male mice did not show significant differences in body weight, or abnormal behaviour, indicating good acceptance of the 20% ethanol treatment regime.

Drinking bottles were changed and bottle weights were recorded once a week. Liquid consumption per mouse was estimated by analysing the weights of the drinking bottles (per cage) and calculating the average weight of consumed liquid per mouse per day (Figure 6.34). H_2O_*Aldh1b1*$^{fl/fl}$_*Msh2*^{fl} female mice consumed on average 12ml of drinking water per day, compared with 7.7ml of 20% ethanol in drinking water consumed by EtOH_*Aldh1b1*$^{fl/fl}$_*Msh2*^{fl} female mice. The difference in liquid consumption between EtOH_*Aldh1b1*$^{fl/fl}$_*Msh2*^{fl} and H_2O_*Aldh1b1*$^{fl/fl}$_*Msh2*^{fl} females is statistically significant ($p = 0.0018$). H_2O_*Aldh1b1*$^{fl/fl}$_*Msh2*^{fl} male mice consumed on average 12.7ml of drinking water per day, compared with 11.2ml of 20% ethanol in drinking water consumed by EtOH_*Aldh1b1*$^{fl/fl}$_*Msh2*^{fl} male mice, with no significant differences observed (Figure 6.34A). In non-induced *Aldh1b1*$^{-/-}$ Msh2-LS mice, an average H_2O_*Aldh1b1*$^{-/-}$_*Msh2*^{fl} male mouse consumed around 11.3ml of drinking water per day, whereas an average EtOH_*Aldh1b1*$^{-/-}$_*Msh2*^{fl} male mouse consumed around 13ml of 20% ethanol in drinking water. In *Aldh1b1*$^{-/-}$ Msh2-LS mice, an average H_2O_*Aldh1b1*$^{-/-}$_*Msh2*^{fl} female mouse consumed around 11.5ml of

water per day, whereas an average EtOH_*Aldh1b1*$^{-/-}$_*Msh2*^{fl} female mouse consumed around 7ml of 20% ethanol in drinking water per day (Figure 6.34B). No significant differences were observed between any of the comparisons of EtOH_*Aldh1b1*$^{-/-}$_*Msh2*^{fl} versus H_2O_*Aldh1b1*$^{-/-}$_*Msh2*^{fl} males or females.

.

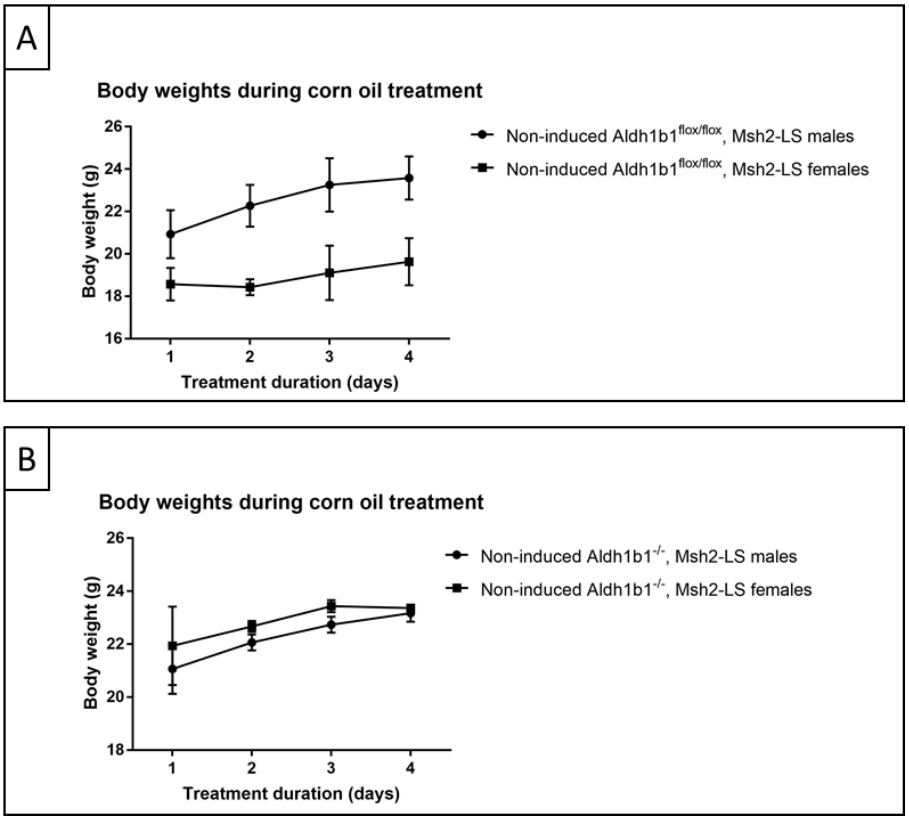

Figure 6.29: Body weights during corn oil treatment. A) Body weights of non-induced (no Tamoxifen) *Aldh1b1*$^{flox/flox}$ Msh2-LS males were significantly higher than body weights of non-induced *Aldh1b1*$^{flox/flox}$ Msh2-LS females, before and during corn oil treatments. 2-way-ANOVA test with Bonferroni post-test correction, p=0.0145 on day 1 and p<0.0001 on days 2-4 (data shown as mean ± SD, n=6 mice in each group). B) Body weights of non-induced *Aldh1b1*$^{-/-}$ Msh2-LS males were similar to body weights of females, before and during corn oil treatments. 2-way-ANOVA test with Bonferroni post-test correction, no significant differences observed (data shown as mean ± SD, n=6 mice in each group).

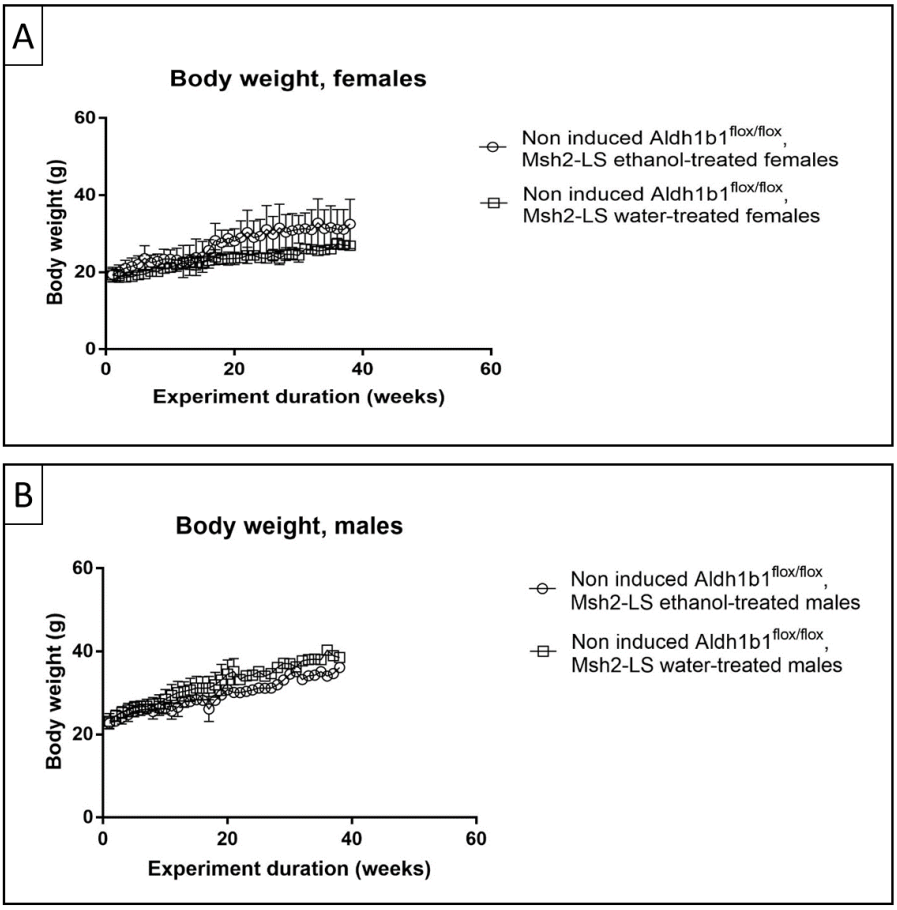

Figure 6.30: Body weights for non-induced *Aldh1b1*$^{flox/flox}$ Msh2-LS males and females during 20% ethanol or standard/normal drinking water regimes. The data distribution for the body weight curves of the *Aldh1b1*$^{flox/flox}$ Msh2-LS mice were influenced by the small numbers of mice coming from different litters and starting at different time points. There were no significant differences between the body weights of non-induced ethanol-treated *Aldh1b1*$^{flox/flox}$ Msh2-LS (EtOH_*Aldh1b1*$^{fl/fl}$_*Msh2*^{fl}) males (or females) versus non-induced water-treated *Aldh1b1*$^{flox/flox}$ Msh2-LS (H_2O_*Aldh1b1*$^{fl/fl}$_*Msh2*^{fl}) males (or females). 2-way-ANOVA with Bonferroni post-test correction analysis (data shown as mean±SD, n=4 mice each group for the females and n=3 each group for the males).

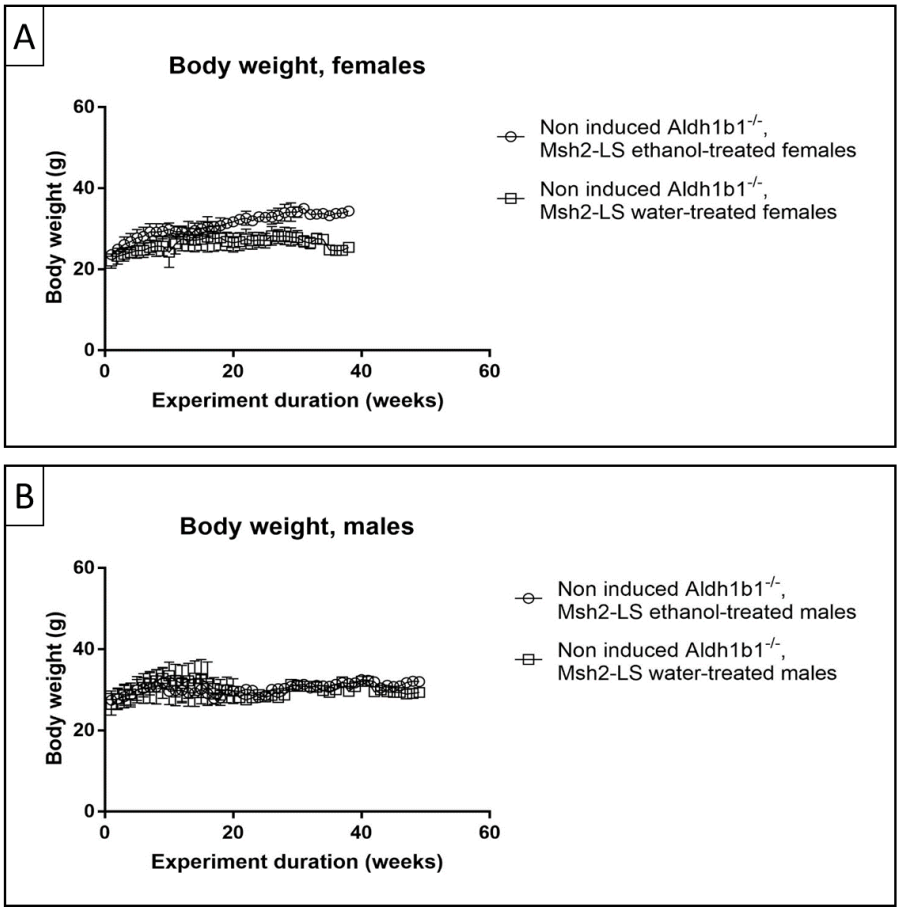

Figure 6.31: Body weights for non-induced *Aldh1b1*$^{-/-}$ Msh2-LS males and females during 20% ethanol or standard/normal drinking water regimes. The data distribution for the body weight curves for the *Aldh1b1*$^{-/-}$ Msh2-LS mice were influenced by the small numbers of mice coming from different litters and starting at different time points. There were no significant differences between the body weights of non-induced ethanol-treated *Aldh1b1*$^{-/-}$ Msh2-LS (EtOH_*Aldh1b1*$^{-/-}$_*Msh2*^{fl}) males (or females) versus non-induced water-treated *Aldh1b1*$^{-/-}$ Msh2-LS (H_2O_*Aldh1b1*$^{-/-}$_*Msh2*^{fl}) males (or females). 2-way-ANOVA with Bonferroni post-test correction analysis (data shown as mean±SD, n=2 mice each group for the females and n=4 each group for the males).

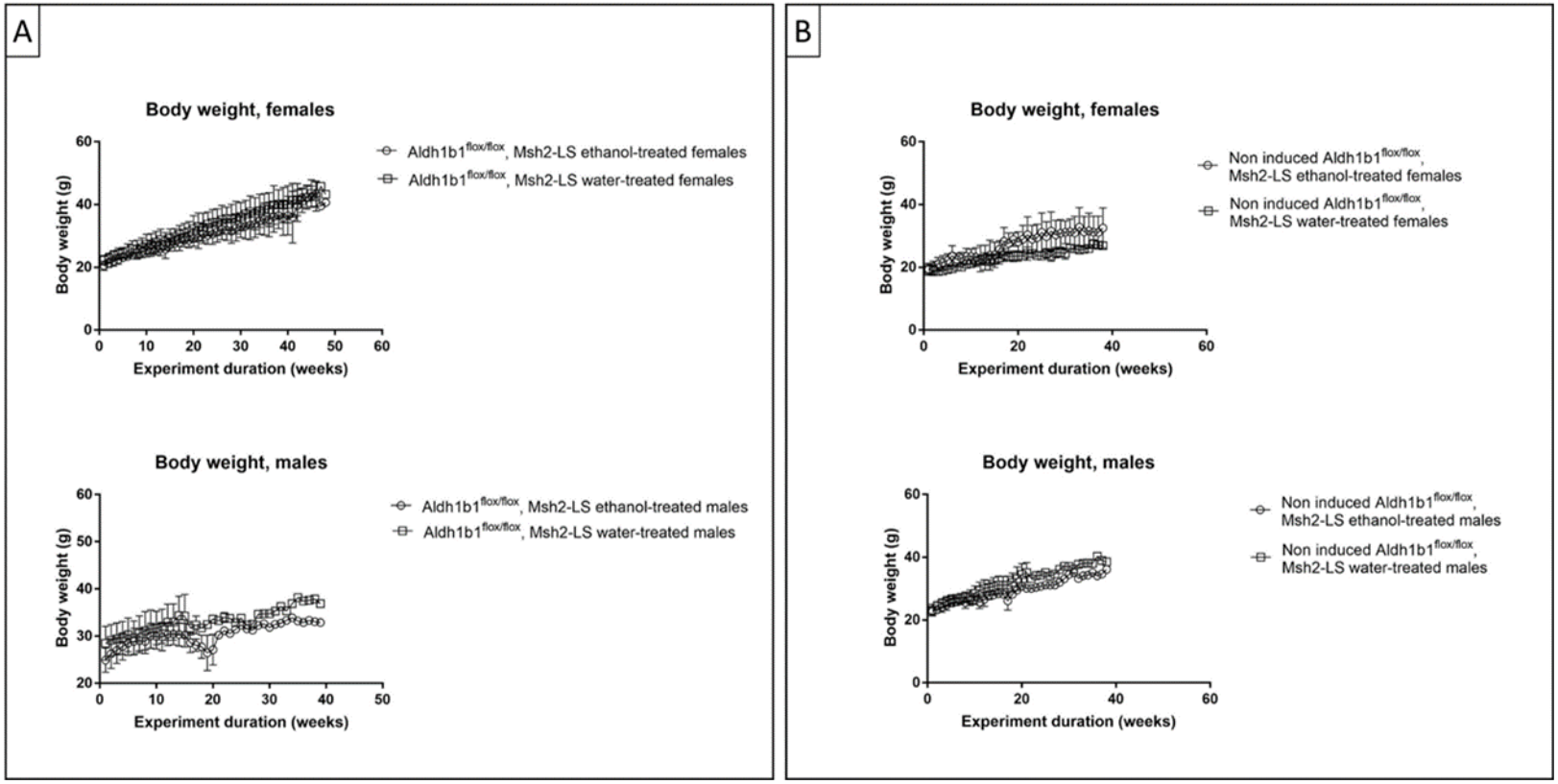

Figure 6.32: Body weights for males and females during 20% ethanol or standard/normal drinking water regimes. Body weight graphs of Tamoxifen-induced *Aldh1b1*$^{flox/flox}$ Msh2-LS experimental subject mice (A), non-induced *Aldh1b1*$^{flox/flox}$ Msh2-LS control mice (B), during 20% ethanol or standard/normal drinking water regimes. In each group, there were no significant differences between the body weights of ethanol-treated versus water-treated groups of mice for either males or females. 2-way-ANOVA test with Bonferroni post-test correction analysis (data shown as mean±SD, n=6, n=3-4; SD too small to show as bars in some experiments).

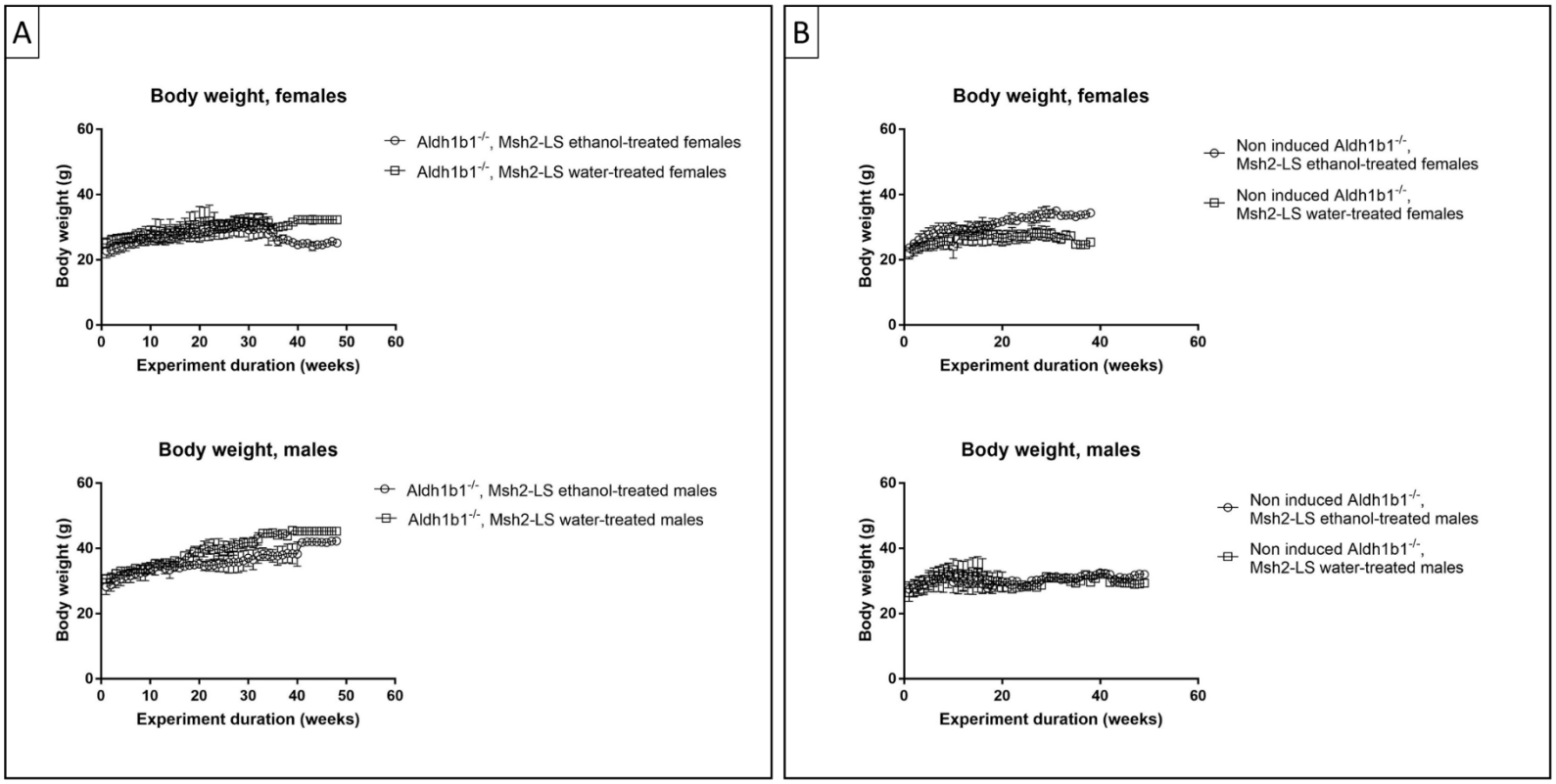

Figure 6.33: Body weights for males and females during 20% ethanol or standard/normal drinking water regimes. Body weight graphs of Tamoxifen-induced *Aldh1b1*$^{-/-}$ Msh2-LS experimental subject mice (A), non-induced *Aldh1b1*$^{-/-}$ Msh2-LS control mice (B), during 20% ethanol or standard/normal drinking water regimes. In each group, there were no significant differences between the body weights of ethanol-treated versus water-treated groups of mice for either males or females. 2-way-ANOVA test with Bonferroni post-test correction analysis (data shown as mean±SD, n=6, n=2-4; SD too small to show as bars in some experiments).

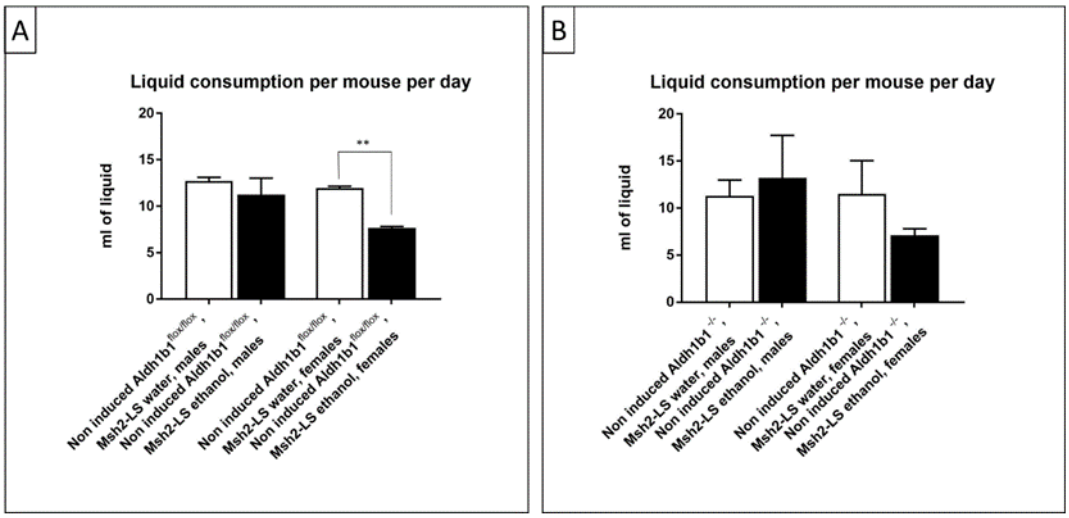

Figure 6.34: Liquid consumption of either 20% ethanol containing drinking water or standard/normal water per mouse per day of non-induced *Aldh1b1*$^{flox/flox}$ Msh2-LS control mice (A), and non-induced *Aldh1b1*$^{-/-}$ Msh2-LS control mice (B). 2-way-ANOVA with Bonferroni post-test correction analysis, **p=0.0018 (data shown as mean±SD).

6.4.2.2 Tumour development in control mice exposed to long-term ethanol treatment

Both non-induced *Aldh1b1* conditional-knockout and *Aldh1b1* constitutive-knockout Msh2-LS control mice treated with either ethanol or water, were culled when they reached the same end-timepoint as age- and sex-matched Tamoxifen-induced ethanol-treated *Aldh1b1* conditional-knockout and *Aldh1b1* constitutive-knockout Msh2-LS experimental mice.

These control mice underwent necropsy dissection and organ/tissue collection in the same way as the experimental mice.

In non-induced *Aldh1b1*$^{flox/flox}$ Msh2-LS control mice, Group-B (ethanol-treated cohort, EtOH_*Aldh1b1*$^{fl/fl}$_*Msh2*^{fl}), 3 out of 7 (43%) mice showed zones of colonic crypt epithelial hyperproliferation involving mainly the proximal and mid colon (after 13, 15 and 39 weeks of 20% ethanol in drinking water regime, respectively). None of the EtOH_*Aldh1b1*$^{fl/fl}$_*Msh2*^{fl} control mice showed intestinal adenoma formation. In Group-A (water-treated control cohort, H_2O_*Aldh1b1*$^{fl/fl}$_*Msh2*^{fl}), no intestinal hyperproliferation, adenoma or other abnormality was observed in any of the 7 H_2O_*Aldh1b1*$^{fl/fl}$_*Msh2*^{fl} control mice (Figure 6.35). The tumour incidence was compared between Tamoxifen-induced *Aldh1b1*$^{flox/flox}$ Msh2-LS experimental cohort mice and non-induced *Aldh1b1*$^{flox/flox}$ Msh2-LS control mice (Figure 6.36).

In non-induced *Aldh1b1*$^{-/-}$ Msh2-LS control mice, Group-B (ethanol-treated cohort, EtOH_*Aldh1b1*$^{-/-}$_*Msh2*^{fl}), 2 out of 6 (33.4%) mice showed zones of colonic crypt epithelial hyperproliferation involving mainly the mid colon (after 14 and 22 weeks of 20% ethanol in drinking water regime, respectively). None of the EtOH_*Aldh1b1*$^{-/-}$_*Msh2*^{fl} control mice showed intestinal adenoma formation. In Group-A (water-treated control cohort, H_2O_*Aldh1b1*$^{-/-}$_*Msh2*^{fl}), no intestinal hyperproliferation, adenoma or other abnormality was observed in any of the 6 H_2O_*Aldh1b1*$^{-/-}$_*Msh2*^{fl} control mice (Figure 6.36). The tumour incidence was compared between Tamoxifen-induced *Aldh1b1*$^{-/-}$ Msh2-LS experimental cohort mice and non-induced *Aldh1b1*$^{-/-}$ Msh2-LS control mice (Figure 6.37).

No morphological abnormalities or tumours were observed following necropsy dissection and histopathological analysis of the H&E-stained sections of the caecum, small intestines, stomach, anal canal, liver, spleen, lymph nodes and thymus, of any of the 14 EtOH_*Aldh1b1*$^{fl/fl}$_*Msh2*^{fl} or H_2O_*Aldh1b1*$^{fl/fl}$_*Msh2*^{fl} mice, and of any of the 12 EtOH_*Aldh1b1*$^{-/-}$_*Msh2*^{fl} or H_2O_*Aldh1b1*$^{fl/fl}$_*Msh2*^{fl} mice. The intestinal tumour formation in the Tamoxifen-induced Aldh1b1$^{flox/flox}$ MSh2-LS experimental mice was compared with that

for non-induced *Aldh1b1*$^{flox/flox}$ Msh2-LS control mice, treated with either 20% ethanol in drinking water or normal/standard drinking water (Figure 6.38). The intestinal tumour formation in the Tamoxifen-induced *Aldh1b1*$^{-/-}$ MSh2-LS experimental mice was compared with that for the non-induced *Aldh1b1*$^{-/-}$ Msh2-LS control mice (Figure 6.39).

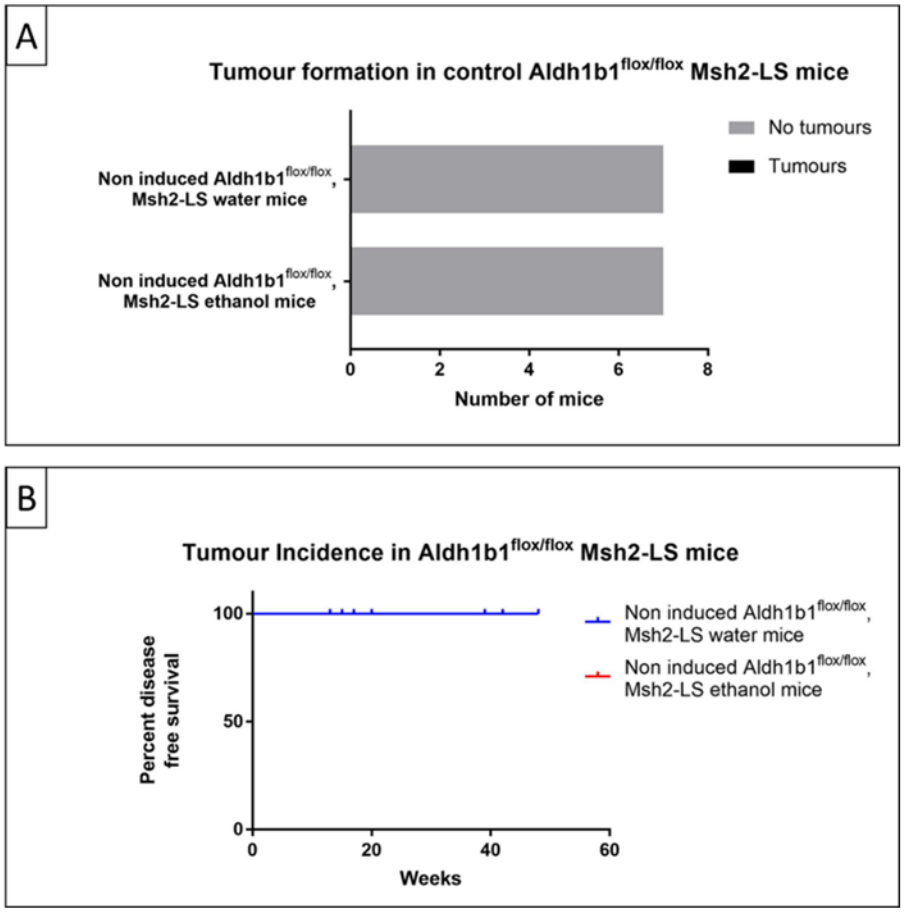

Figure 6.35: A) Bar chart of the number of non-induced *Aldh1b1*$^{flox/flox}$ Msh2-LS control mice that developed intestinal tumours (adenomas or adenocarcinomas) after receiving either 20% ethanol in drinking water or normal/standard drinking water. In both groups (water-treated cohort and ethanol-treated cohort) 0/7 non-induced *Aldh1b1*$^{flox/flox}$ Msh2-LS control mice developed large intestinal adenomas. Fisher's exact test showed no significant differences were observed. B) Tumour incidence shown as a survival plot in non-induced *Aldh1b1*$^{flox/flox}$ Msh2-LS control mice treated with either 20% ethanol (red) or water (blue). The blue curve (water-treated control mice) completely overlaps the red curve (ethanol-treated control mice) such that it can't be seen in the graph. Log-rank (Mantel-Cox) test, no significant differences observed.

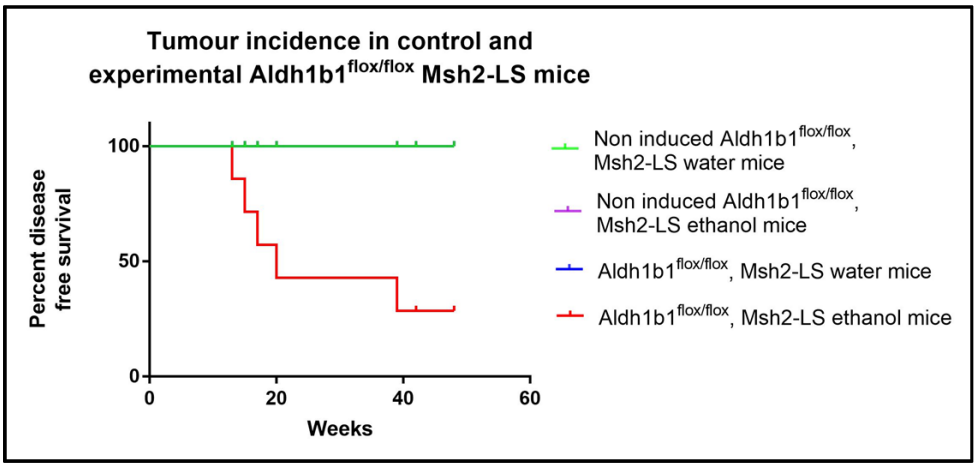

Figure 6.36: Tumour incidence, shown as survival plots, in non-induced *Aldh1b1*$^{flox/flox}$ Msh2-LS control mice both water-treated (H2O_*Aldh1b1*$^{fl/fl}$_*Msh2*^{fl}) (green) and ethanol-treated (EtOH_*Aldh1b1*$^{fl/fl}$_*Msh2*^{fl}) (violet), compared with Tamoxifen-induced *Aldh1b1*$^{flox/flox}$ Msh2-LS experimental mice, both water-treated (H2O_*Aldh1b1*$^{fl/fl}$_*Msh2*$^{fl\ KO}$) (blue) and 20% ethanol-treated (EtOH_*Aldh1b1*$^{fl/fl}$_*Msh2*$^{fl\ KO}$) (red). The green curve completely overlaps both violet and blue curves, such that these curves can't be seen in the graph. Log-rank (Mantel-Cox) test, p = 0.0018 indicating significant differences observed between the ethanol-treated Tamoxifen-induced *Aldh1b1*$^{flox/flox}$ Msh2-LS (EtOH_*Aldh1b1*$^{fl/fl}$_*Msh2*$^{fl\ KO}$) experimental mice and each of the three control cohorts.

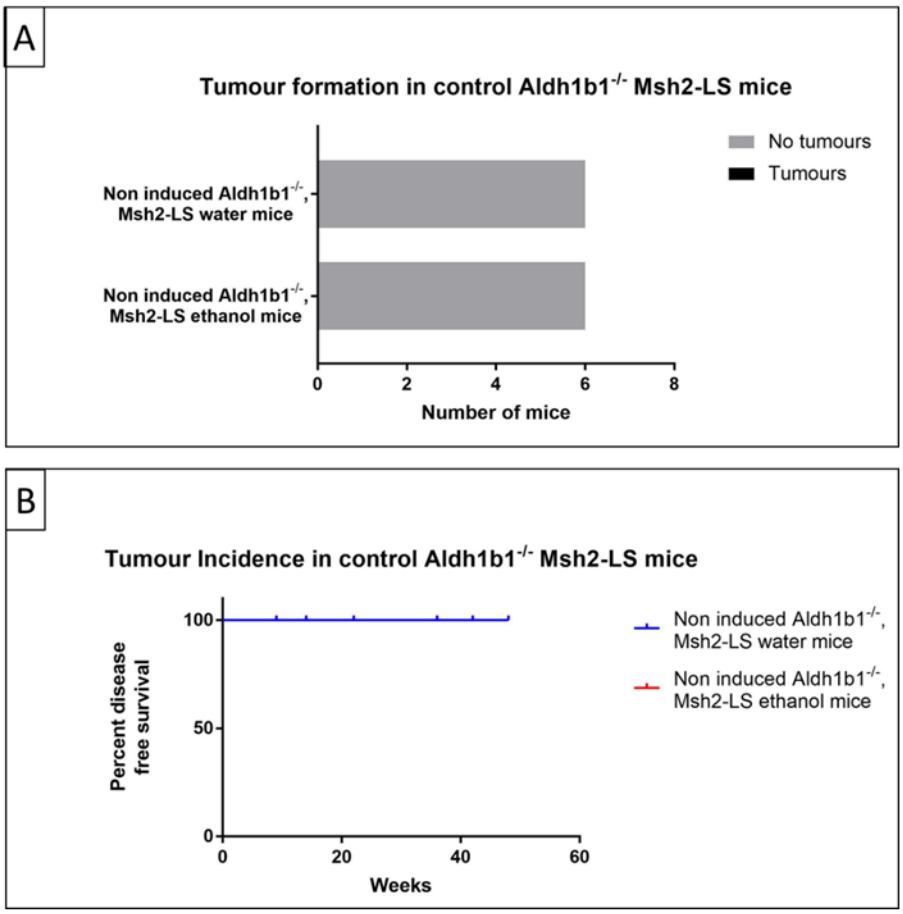

Figure 6.37: A) Bar chart of the number of non-induced *Aldh1b1*$^{-/-}$ Msh2-LS control mice that developed intestinal tumours (adenomas or adenocarcinomas) after receiving either 20% ethanol in drinking water or normal/standard drinking water. In both groups (water-treated cohort and ethanol-treated cohort) 0/6 non-induced *Aldh1b1*$^{-/-}$ Msh2-LS control mice developed large intestinal adenomas. Fisher's exact test, no significant differences observed. B) Tumour incidence shown as a survival plot in non-induced *Aldh1b1*$^{-/-}$ Msh2-LS control mice treated with either 20% ethanol (red) or water (blue). The blue curve (water-treated control mice) completely overlaps the red curve (ethanol-treated control mice) such that it can't be seen in the graph. Log-rank (Mantel-Cox) test, no significant differences observed.

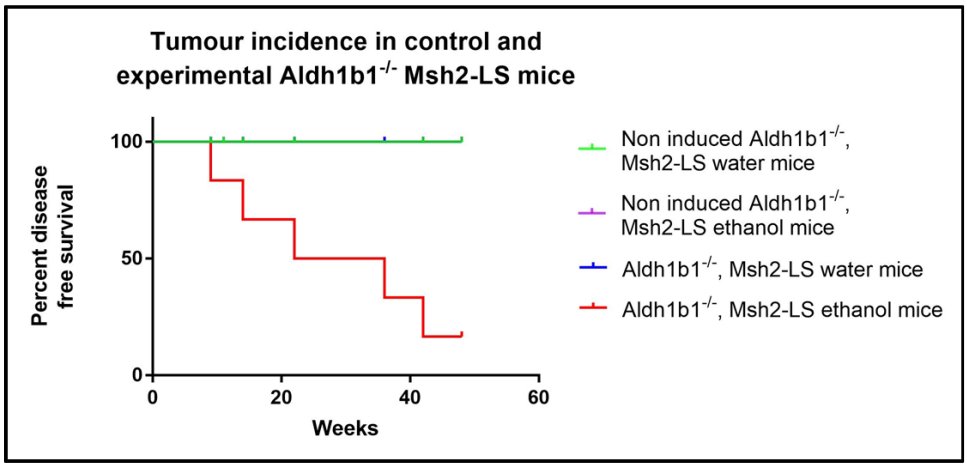

Figure 6.38: Tumour incidence, shown as survival plots, in non-induced *Aldh1b1*$^{-/-}$ Msh2-LS control mice both water-treated (H2O_*Aldh1b1*$^{-/-}$_*Msh2*^{fl}) (green) and ethanol-treated (EtOH_*Aldh1b1*$^{-/-}$_*Msh2*^{fl}) (violet), compared with Tamoxifen-induced *Aldh1b1*$^{-/-}$ Msh2-LS experimental mice, both water-treated (H2O_*Aldh1b1*$^{-/-}$_*Msh2*$^{fl\,KO}$) (blue) and 20% ethanol-treated (EtOH_*Aldh1b1*$^{-/-}$_*Msh2*$^{fl\,KO}$) (red). The green curve completely overlaps both violet and blue curves, such that these curves can't be seen in the graph. Log-rank (Mantel-Cox) test, p = 0.0039 indicating significant differences observed between the ethanol-treated Tamoxifen-induced *Aldh1b1*$^{-/-}$ Msh2-LS (EtOH_*Aldh1b1*$^{-/-}$_*Msh2*$^{fl\ KO}$) experimental mice and each of the three control cohorts.

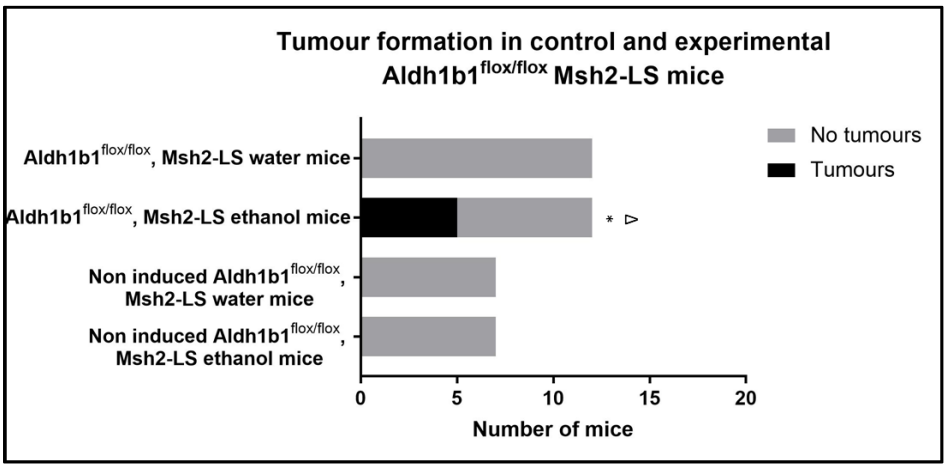

Figure 6.39: Bar chart of the numbers of non-induced *Aldh1b1*$^{flox/flox}$ Msh2-LS control mice, and Tamoxifen-induced *Aldh1b1*$^{flox/flox}$ Msh2-LS experimental mice that developed intestinal tumours after receiving either 20% ethanol in drinking water or normal/standard drinking water. Fisher's exact test was carried out to compare the effects of ethanol in the three different pairs of cohorts: 5/12 (41.7%) ethanol-treated Tamoxifen-induced *Aldh1b1*$^{flox/flox}$ Msh2-LS (EtOH_*Aldh1b1*$^{fl/fl}$_*Msh2*$^{fl\ KO}$) mice developed large intestinal tumours compared with 0/12 (0%) water-treated *Aldh1b1*$^{flox/flox}$ Msh2-LS (H_2O_*Aldh1b1*$^{fl/fl}$_*Msh2*$^{fl\ KO}$) mice (Fisher's exact test, *p=0.0373), 0/7 (0%) ethanol-treated non-induced *Aldh1b1*$^{flox/flox}$ Msh2-LS (EtOH_*Aldh1b1*$^{fl/fl}$_*Msh2*^{fl}) mice, and 0/7 (0%) water-treated non-induced *Aldh1b1*$^{flox/flox}$ Msh2-LS (H_2O_*Aldh1b1*$^{fl/fl}$_*Msh2*^{fl}) mice. Fisher's exact test was carried out to

compare the tumour incidence between EtOH_*Aldh1b1*$^{fl/fl}$_*Msh2*$^{fl\ KO}$ and EtOH_*Aldh1b1*$^{fl/fl}$_*Msh2*^{fl} mice ($^{\Delta}$p=0.0466).

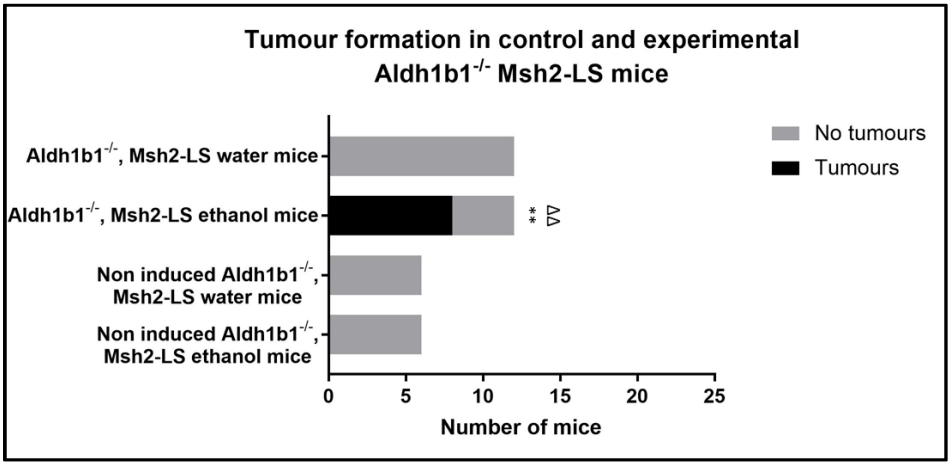

Figure 3.40: Bar chart of the numbers of non-induced *Aldh1b1*$^{-/-}$ Msh2-LS control mice, and Tamoxifen-induced *Aldh1b1*$^{-/-}$ Msh2-LS experimental mice that developed intestinal tumours after receiving either 20% ethanol in drinking water or normal/standard drinking water. Fisher's exact test was carried out to compare the effects of ethanol in the three different pairs of cohorts: 8/12 (66.7%) ethanol-treated Tamoxifen-induced *Aldh1b1*$^{-/-}$ Msh2-LS (EtOH_*Aldh1b1*$^{-/-}$_*Msh2*$^{fl\ KO}$) mice developed large intestinal tumours compared with 0/12 (0%) water-treated induced *Aldh1b1*$^{-/-}$ Msh2-LS (H_2O_*Aldh1b1*$^{-/-}$_*Msh2*$^{fl\ KO}$) mice (Fisher's exact test,**p=0.0013), 0/6 (0%) ethanol-treated non-induced *Aldh1b1*$^{-/-}$ Msh2-LS (EtOH_*Aldh1b1*$^{-/-}$_*Msh2*^{fl}) mice, and 0/6 (0%) water-treated non-induced *Aldh1b1*$^{-/-}$ Msh2-LS (H_2O_*Aldh1b1*$^{-/-}$_*Msh2*^{fl}) mice. Fisher's exact test was carried out to compare the tumour incidence between EtOH_*Aldh1b1*$^{-/-}$_*Msh2*$^{fl\ KO}$ and EtOH_*Aldh1b1*$^{-/-}$_*Msh2*^{fl} mice ($^{\Delta\Delta}$p=0.0073).

6.5 Immunohistochemical characterization of tumours and tissues from the *Aldh1b1* conditional-knockout Msh2-LS and *Aldh1b1* constitutive-knockout Msh2-LS model mice with and without ethanol treatment

6.5.1 Methods

We performed IHC analyses in FFPE colonic and small intestinal tissues from induced *Aldh1b1* conditional-knockout Msh2-LS mice, *Aldh1b1* constitutive-knockout Msh2-LS mice, non-induced *Aldh1b1* conditional-knockout Msh2-LS control mice and non-induced *Aldh1b1* constitutive-knockout Msh2-LS control mice to verify or investigate the expression of various proteins of interest. We performed the same analysis on the colonic and SI tissues comparing ethanol-treated mice with water-treated mice. Small and large intestinal tissues were harvested, prepared as Swiss-rolls and fixed in 10% NBF (as described in Materials and Methods). They were processed using standard tissue processing protocols for paraffin wax embedding and microtome sectioning.

IHC was performed to confirm changes to the expression of Msh2 and Aldh1b1 (target proteins), the proliferation marker Ki-67, the Wnt pathway marker β-Catenin, the DNA damage marker γ-H2AX, the DNA damage / tumour suppressor marker p53, and cCas-3 a critical executioner of apoptosis. DAB was used to visualise positive staining by these antibodies. IHC staining for these antibodies was performed using protocols described in Materials and Methods (Chapter 2, 2.2.3). Staining and quantification was performed either by manual scoring or using the bioimage analysis software for digital pathology images, QuPath.

6.5.2 Results

6.5.2.1 Msh2 immunohistochemical analyses of intestinal samples from *Aldh1b1* conditional-knockout Msh2-LS and *Aldh1b1* constitutive-knockout Msh2-LS mouse models

6.5.2.1.1 Msh2 immunostaining of *Aldh1b1* conditional-knockout Msh2-LS murine small intestinal and colonic tissues

We investigated Msh2 expression in *Aldh1b1*$^{flox/flox}$; Msh2$^{flox/-}$; Lgr5CreERT2$^{+/-}$; mTmG$^{+/-}$mice. We used small intestinal samples of *Msh2*$^{-/-}$ and WT mice as Msh2-negative and -positive expression controls respectively (Figure 6.41). The lack of IHC DAB-brown staining in all of the SI crypts and villi and in all of the colonic crypts of the *Msh2*$^{-/-}$ mice confirmed complete loss of Msh2 expression in the Msh2-null control tissues. In contrast, scattered crypts, in both SI and colon, showed Msh2 expression loss in the Msh2-LS model mice.

The number of Msh2-negative crypts was higher in the SI than in the colon in EtOH_*Aldh1b1*$^{fl/fl}$_*Msh2*$^{fl\ KO}$ mice, however no tumours were observed in the small intestine. The number of Msh2-negative crypts in the SI was statistically significantly higher in the EtOH_*Aldh1b1*$^{fl/fl}$_*Msh2*$^{fl\ KO}$ mice compared with the H_2O_*Aldh1b1*$^{fl/fl}$_*Msh2*$^{fl\ KO}$ mice (Figure 6.42). In EtOH_*Aldh1b1*$^{fl/fl}$_*Msh2*$^{fl\ KO}$ mice, 43% Msh2-negative small intestinal crypts were observed compared with 24% Msh2-negative small intestinal crypts found in H_2O_*Aldh1b1*$^{fl/fl}$_*Msh2*$^{fl\ KO}$ mice (Figure 6.43).

IHC analysis of Msh2 expression in the intestinal tissue samples from EtOH_*Aldh1b1*$^{fl/fl}$_*Msh2*^{fl} mice and H_2O_*Aldh1b1*$^{fl/fl}$_*Msh2*^{fl} mice showed no Msh2-negative crypts in either small or large intestinal mucosal epithelium (Figures 6.44-6.45), consistent with lack of induction of Cre activity with continued expression of protein from the floxed Msh2 allele.

In the colon, the number of Msh2-negative crypts was statistically significantly higher in the EtOH_*Aldh1b1*$^{fl/fl}$_*Msh2*$^{fl\ KO}$ mice compared with the H_2O_*Aldh1b1*$^{fl/fl}$_*Msh2*$^{fl\ KO}$ control mice (Figure 6.46). In EtOH_*Aldh1b1*$^{fl/fl}$_*Msh2*$^{fl\ KO}$ mice 17% Msh2-negative colonic crypts were observed compared with 7% Msh2-negative colonic crypts found in H_2O_*Aldh1b1*$^{fl/fl}$_*Msh2*$^{fl\ KO}$ control mice (Figure 6.47). EtOH_*Aldh1b1*$^{fl/fl}$_*Msh2*$^{fl\ KO}$ mice formed some caecal and some colonic adenomas that were characterized by Msh2-negative dysplastic glands often surrounded by or admixed with Msh2-positive crypts showing reactive or hyperproliferative changes (Figure 6.48).

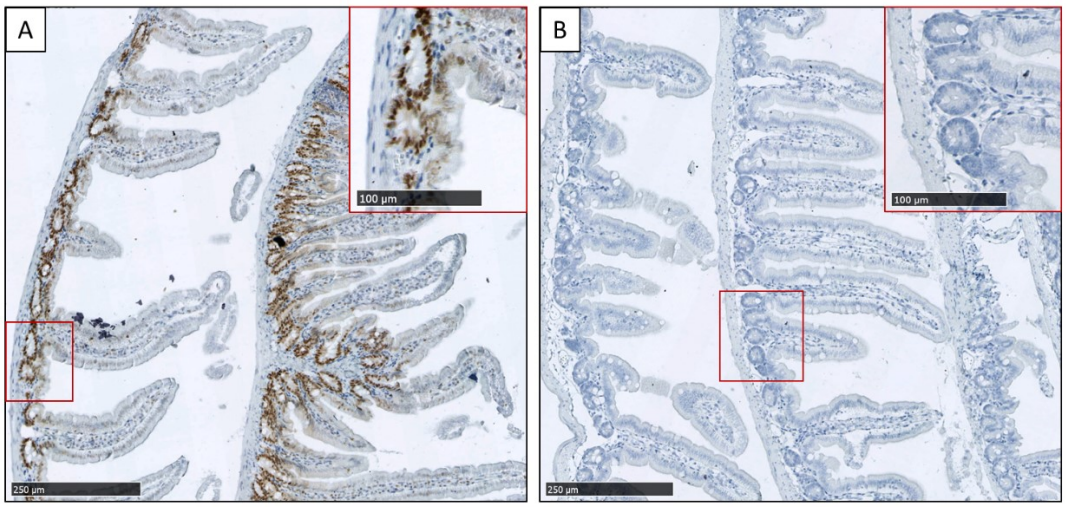

Figure 6.41: Immunohistochemical analysis of Msh2 protein expression in small intestinal mucosal epithelium from a positive-control WT mouse (A), in which the brown staining indicates positive Msh2 expression in all crypts (further magnified in the red rectangle); and from a negative-control *Msh2*$^{-/-}$ mouse (B), in which the lack of brown staining confirms the absence of Msh2 expression in small intestinal mucosal epithelium (further magnified in the red rectangle). Images taken from anti-Msh2 IHC stained sections scanned using the Hamamatsu Nanozoomer and analysed with the Hamamatsu NDP Viewer software at 10X and 20X magnification (bar at lower left indicates 250µm, bar in red rectangle indicates 100µm).

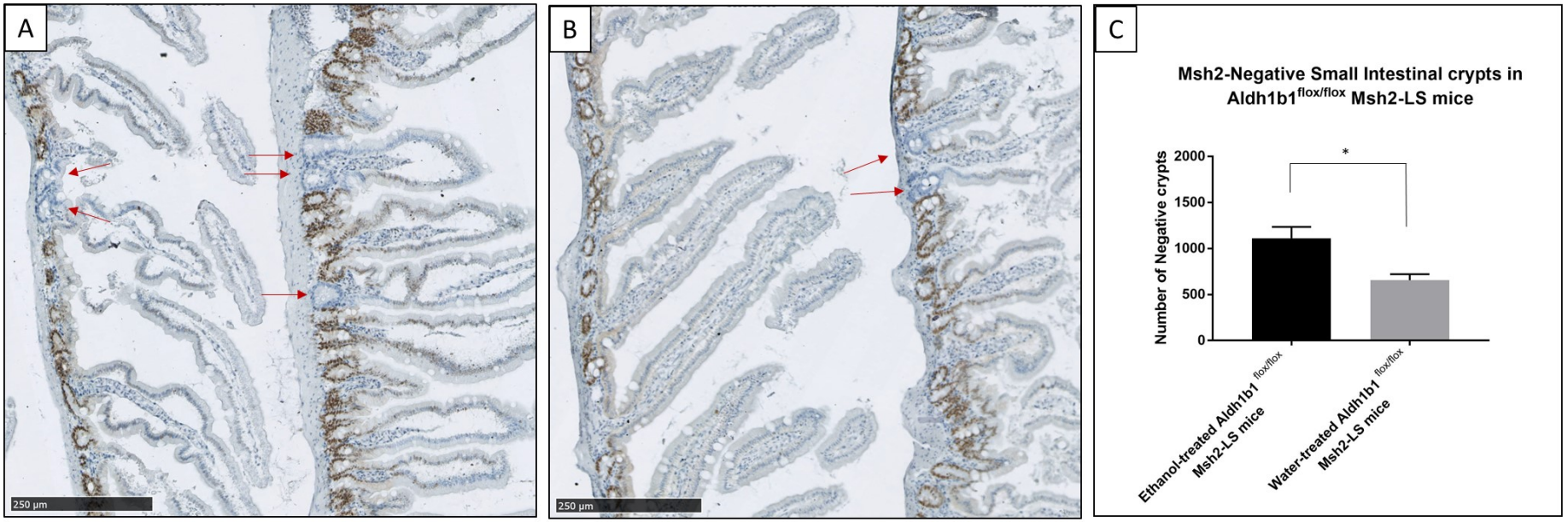

Figure 6.42: Immunohistochemical analysis of Msh2 protein expression in small intestinal mucosal epithelium of *Aldh1b1*$^{flox/flox}$; Msh2$^{flox/-}$; Lgr5CreERT2$^{+/-}$; mTmG$^{+/-}$mice treated with either 20% ethanol in drinking water (A) or normal / standard drinking water (B). Msh2-negative crypts (indicated by the red arrows) were manually counted along the entire small intestine of treated *Aldh1b1*$^{flox/flox}$; Msh2-LS mice (C). Paired Students t Test, *p= 0.0169 vs. water (data shown as mean±SD, n=3 mice in each group). Images taken from sections scanned using the Hamamatsu Nanozoomer and analysed with the Hamamatsu NDP Viewer software at 10X magnification (bar at lower left indicates 250µm).

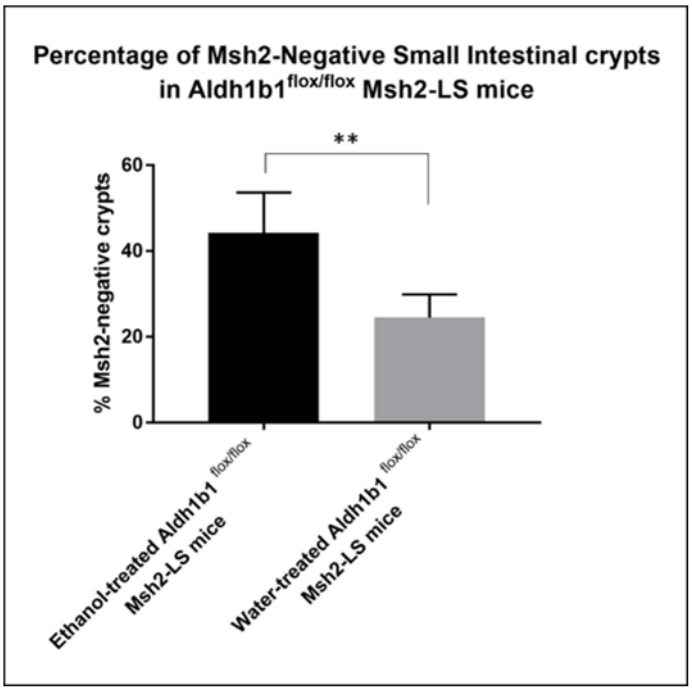

Figure 6.43: Percentage of Msh2 protein-non-expressing crypts in small intestinal mucosa of *Aldh1b1*$^{flox/flox}$*; Msh2*$^{flox/-}$*; Lgr5CreERT2*$^{+/-}$*; mTmG*$^{+/-}$ mice treated with either 20% ethanol in drinking water or normal / standard water. Paired Students t Test, **p=0.0056 vs. water (data shown as mean±SD, 200 crypts counted in 3 mice from each group).

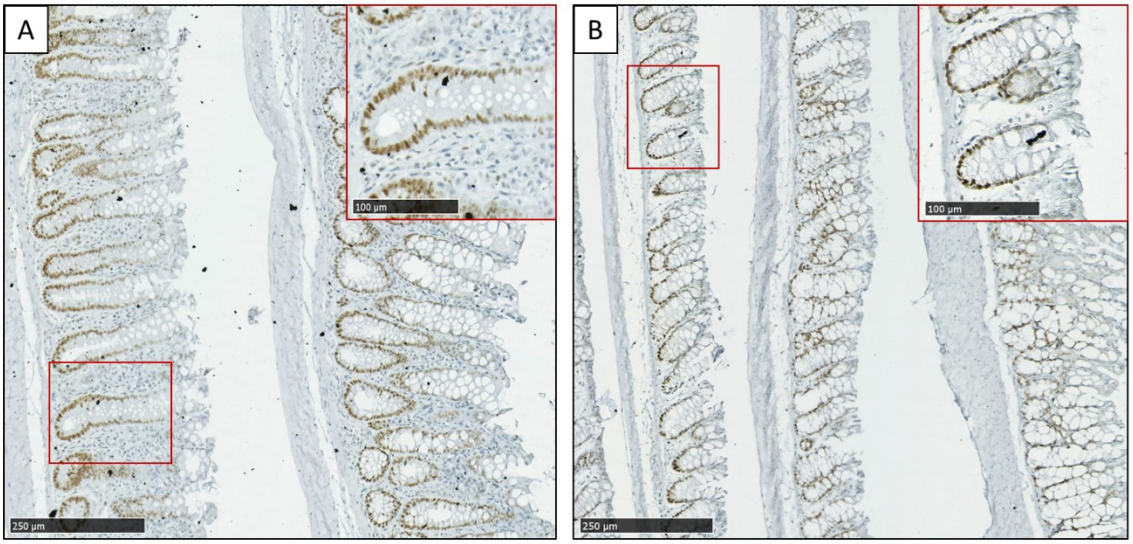

Figure 6.44: Immunohistochemical analysis of Msh2 protein expression in large intestinal mucosal epithelium of non-induced *Aldh1b1* conditional-knockout Msh2-LS control mice treated with either 20% of ethanol in drinking water (A) or normal / standard water (B). No Msh2-negative crypts were observed along the entire colon of non-induced *Aldh1b1* conditional-knockout Msh2-LS mice in either the ethanol- or water-treated groups (n=3 mice in each group). Images taken from sections scanned using the Hamamatsu Nanozoomer and analysed with the Hamamatsu NDP Viewer software at 10X and 20X magnification (bar at lower left indicates 250µm, bar in red rectangle indicates 100µm).

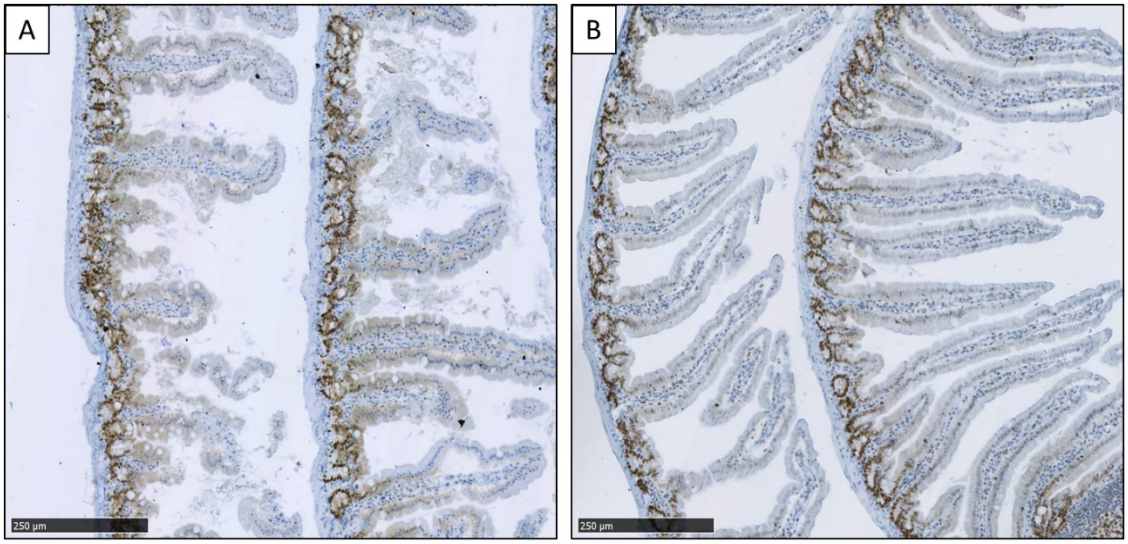

Figure 6.45: Immunohistochemical analysis of Msh2 protein expression in small intestinal mucosal epithelium of non-induced *Aldh1b1* conditional-knockout Msh2-LS control mice treated with either 20% ethanol in drinking water (A) or normal / standard drinking water (B). No Msh2-negative crypts were observed along the entire small intestine of non-induced *Aldh1b1* conditional-knockout Msh2-LS mice in either the ethanol- or water-treated groups (n=3 mice in each group). Images taken from sections scanned using the Hamamatsu Nanozoomer and analysed with the Hamamatsu NDP Viewer software at 10X magnification (bar at lower left indicates 250µm).

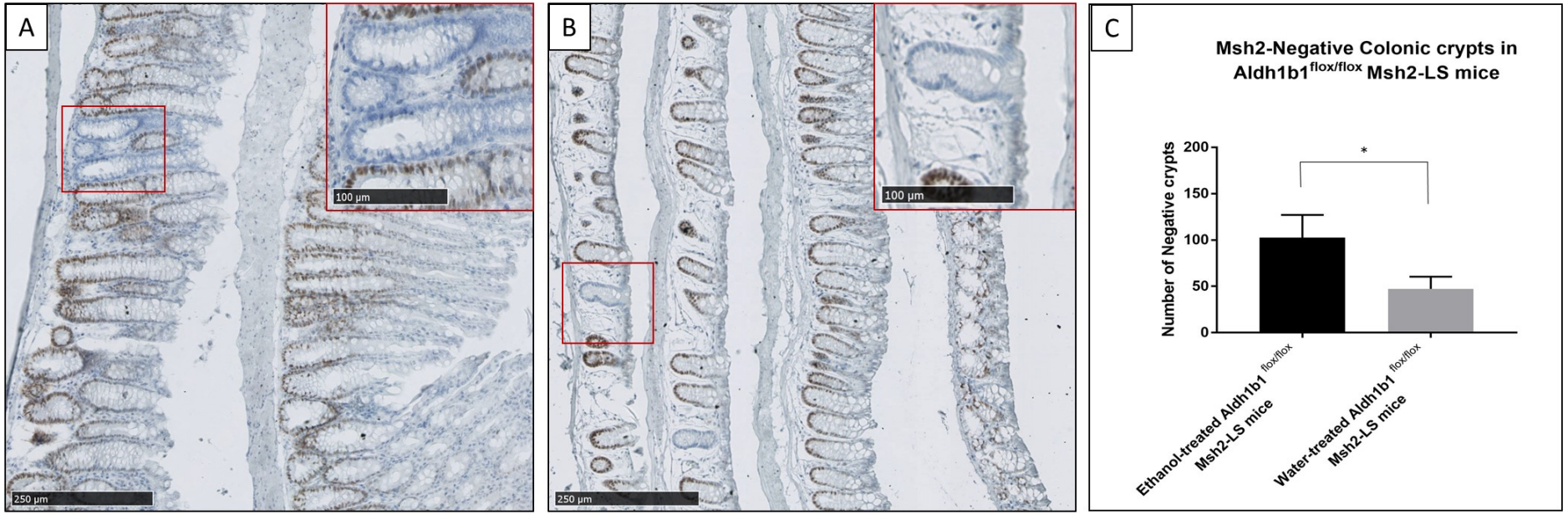

Figure 6.46: Immunohistochemical analysis of Msh2 protein expression in large intestinal mucosal epithelium of of *Aldh1b1*$^{flox/flox}$*; Msh2*$^{flox/-}$*; Lgr5CreERT2*$^{+/-}$*; mTmG*$^{+/-}$ mice treated with either 20% ethanol in drinking water (A) or normal/standard water (B). Msh2-negative crypts (indicated by the red rectangle and further magnified in the upper right inset red rectangle in Figures A and B) were manually counted along the entire colon of treated *Aldh1b1*$^{flox/flox}$ Msh2-LS mice (C). Mann-Whitney U Test, *p=0.0210 vs. water (data shown as mean±SD, n=5 mice each group). Images taken from sections scanned using the Hamamatsu Nanozoomer and analysed with the Hamamatsu NDP Viewer software at 10X and 20X magnification (bar at lower left indicates 250µm, bar in red rectangle indicates 100µm).

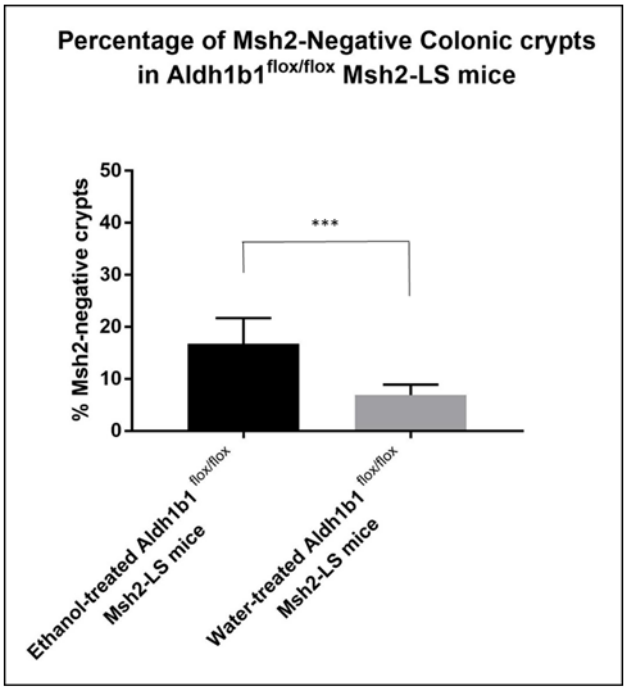

Figure 6.47: Percentage of Msh2 protein-non-expressing crypts in large intestinal mucosa of *Aldh1b1$^{flox/flox}$; Msh2$^{flox/-}$; Lgr5CreERT2$^{+/-}$; mTmG$^{+/-}$* mice treated with either 20% ethanol in drinking water or normal/standard water. Paired Students t Test, ***p=0.0006 vs. water (data shown as mean±SD, 200 crypts counted in 5 mice from each group).

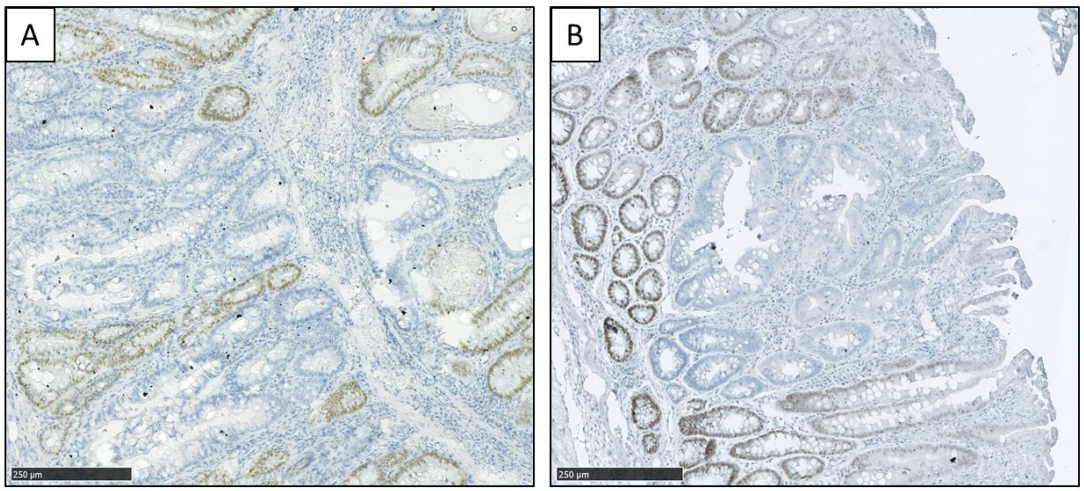

Figure 6.48: Representative images of immunohistochemical staining for Msh2 in adenomas from 2 ethanol-treated *Aldh1b1$^{flox/flox}$; Msh2$^{flox/-}$; Lgr5CreERT2$^{+/-}$; mTmG$^{+/-}$* mice. In both examples, a caecal adenoma (A) and a colonic adenoma (B), there are Msh2-negative dysplastic or adenomatous glands, either surrounded by or admixed with reactive crypts or hyperproliferative crypts that are staining positively for Msh2. Images taken from sections scanned using the Hamamatsu Nanozoomer and analysed with the Hamamatsu NDP Viewer software at 10X magnification (bar at lower left indicates 250µm).

6.5.2.1.2 Msh2 immunostaining of *Aldh1b1* constitutive-knockout Msh2-LS murine small intestinal and colonic tissues

Msh2 IHC analyses were performed to verify or investigate Msh2 expression in *Aldh1b1*$^{-/-}$; Msh2$^{flox/-}$; Lgr5CreERT2$^{+/-}$; mTmG$^{+/-}$mice. Details of the positive and negative controls are reported in the previous section (6.5.2.1.1, Figure 6.41). The number of Msh2-negative crypts was higher in the SI than in the colon in EtOH_*Aldh1b1*$^{-/-}$_*Msh2*$^{fl\ KO}$ mice, however no tumours were observed in the small intestine. The number of Msh2-negative crypts in the SI was statistically significantly higher in the EtOH_*Aldh1b1*$^{-/-}$_*Msh2*$^{fl\ KO}$ mice compared with the H_2O_*Aldh1b1*$^{-/-}$_*Msh2*$^{fl\ KO}$ mice (Figure 6.49). In EtOH_*Aldh1b1*$^{-/-}$_*Msh2*$^{fl\ KO}$ mice, 55.7% Msh2-negative small intestinal crypts were observed compared with 28% Msh2-negative small intestinal crypts found in H_2O_*Aldh1b1*$^{-/-}$_*Msh2*$^{fl\ KO}$ mice (Figure 4.50).

IHC analysis of Msh2 expression in the intestinal tissue samples from EtOH_*Aldh1b1*$^{-/-}$_*Msh2*^{fl} mice and H_2O_*Aldh1b1*$^{-/-}$_*Msh2*^{fl} mice showed no Msh2-negative crypts in either small or large intestinal mucosal epithelium (Figure 6.51-6.52), consistent with lack of induction of Cre activity with continued expression of protein from the floxed Msh2 allele.

In the colon, the number of Msh2-negative crypts was statistically significantly higher in the EtOH_*Aldh1b1*$^{-/-}$_*Msh2*$^{fl\ KO}$ mice compared with the H_2O_*Aldh1b1*$^{-/-}$_*Msh2*$^{fl\ KO}$ (Figure 6.53). In EtOH_*Aldh1b1*$^{-/-}$_*Msh2*$^{fl\ KO}$ mice 29% Msh2-negative colonic crypts were observed compared with 10% Msh2-negative colonic crypts found in H_2O_*Aldh1b1*$^{-/-}$_*Msh2*$^{fl\ KO}$ control mice (Figure 6.54). EtOH_*Aldh1b1*$^{-/-}$_*Msh2*$^{fl\ KO}$ mice formed some caecal and some colonic adenomas that were characterized by Msh2-negative dysplastic glands often surrounded by or admixed with Msh2-positive crypts showing reactive or hyperproliferative changes (Figure 6.55).

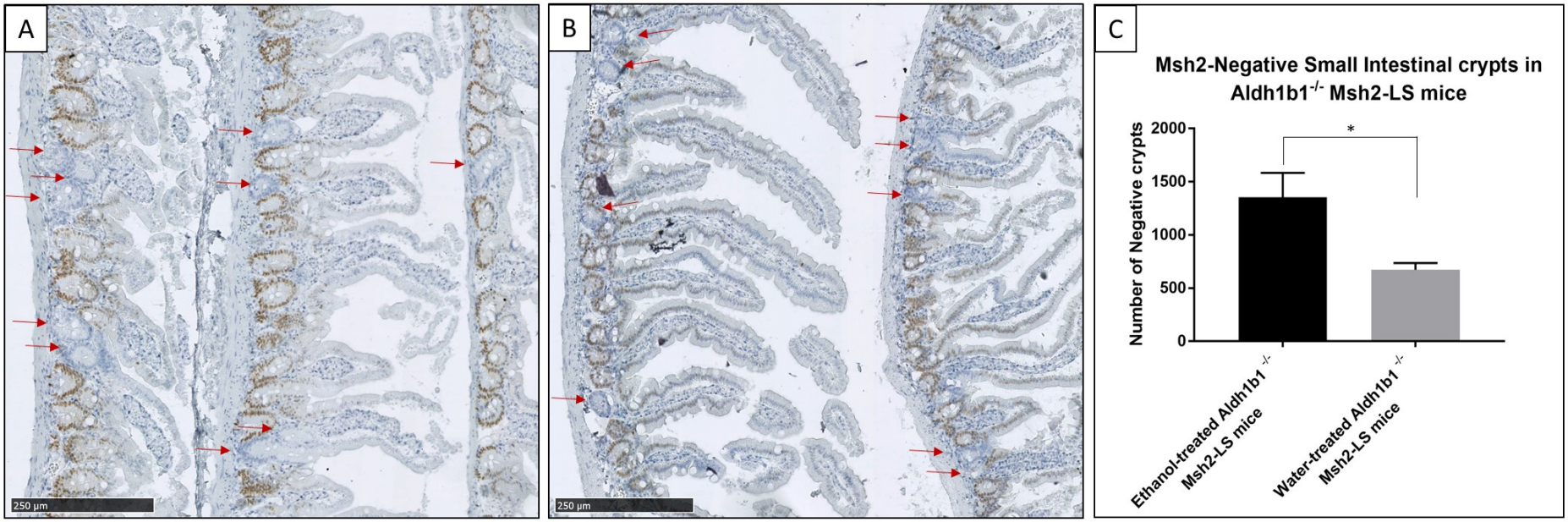

Figure 6.49 Immunohistochemical analysis of Msh2 protein expression in small intestinal mucosal epithelium of *Aldh1b1*$^{-/-}$; Msh2$^{flox/-}$; Lgr5CreERT2$^{+/-}$; mTmG$^{+/-}$mice treated with either 20% ethanol in drinking water (A) or normal / standard drinking water (B). Msh2-negative crypts (indicated by the red arrows) were manually counted along the entire small intestine of treated *Aldh1b1*$^{-/-}$ Msh2-LS mice (C). Paired Students t Test, *p= 0.0246 vs. water (data shown as mean±SD, n=3 mice in each group). Images taken from sections scanned using the Hamamatsu Nanozoomer and analysed with the Hamamatsu NDP Viewer software at 10X magnification (bar at lower left indicates 250µm).

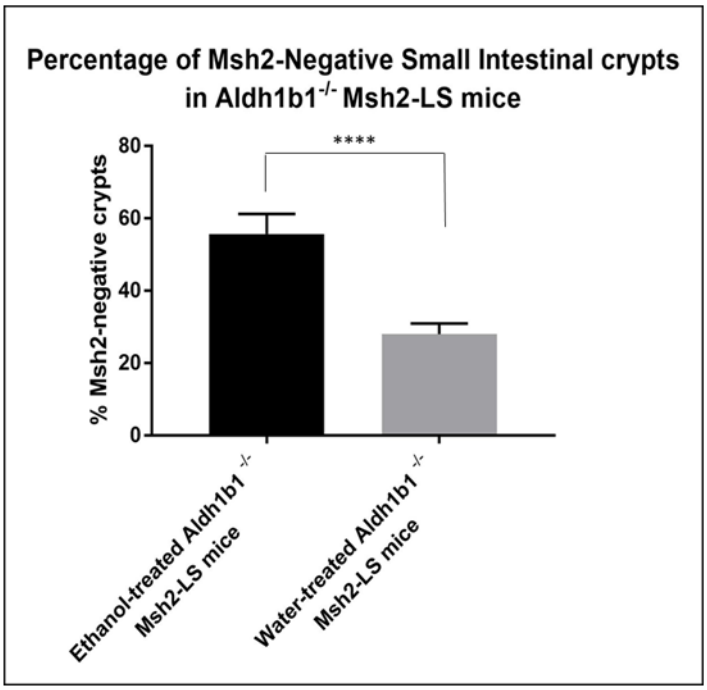

Figure 6.50: Percentage of Msh2 protein-non-expressing crypts in small intestinal mucosa of *Aldh1b1*$^{-/-}$; *Msh2*$^{flox/-}$; *Lgr5CreERT2*$^{+/-}$; *mTmG*$^{+/-}$ mice treated with either 20% ethanol in drinking water or normal / standard water. Paired Students t Test, ****p<0.0001 vs. water (data shown as mean±SD, 200 crypts counted in 3 mice from each group).

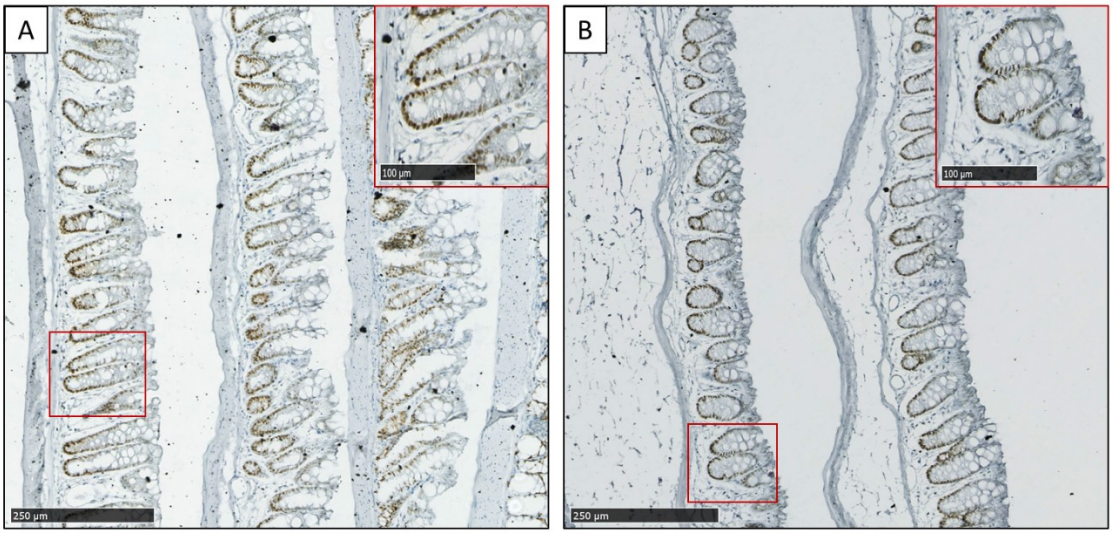

Figure 6.51: Immunohistochemical analysis of Msh2 protein expression in large intestinal mucosal epithelium of non-induced Aldh1b1 constitutive-knockout Msh2-LS control mice treated with either 20% of ethanol in drinking water (A) or normal / standard water (B). No Msh2-negative crypts were observed along the entire colon of non-induced *Aldh1b1*$^{-/-}$ Msh2-LS mice (n=3 mice in each group). Images taken from sections scanned using the Hamamatsu Nanozoomer and analysed with the Hamamatsu NDP Viewer software at 10X and 20X magnification (bar at lower left indicates 250µm, bar in red rectangle indicates 100µm).

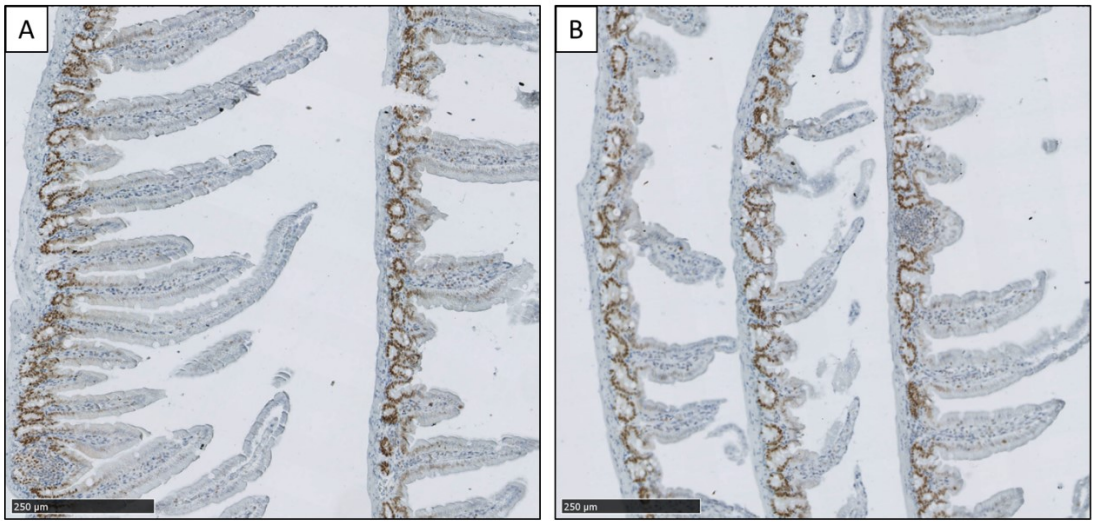

Figure 6.52: Immunohistochemical analysis of Msh2 protein expression in small intestinal mucosal epithelium of non-induced *Aldh1b1* constitutive-knockout Msh2-LS control mice treated with either 20% ethanol in drinking water (A) or normal / standard drinking water (B). No Msh2-negative crypts were observed along the entire small intestine of non-induced *Aldh1b1*$^{-/-}$ Msh2-LS mice (n=3 mice in each group). Images taken from sections scanned using the Hamamatsu Nanozoomer and analysed with the Hamamatsu NDP Viewer software at 10X magnification (bar at lower left indicates 250µm).

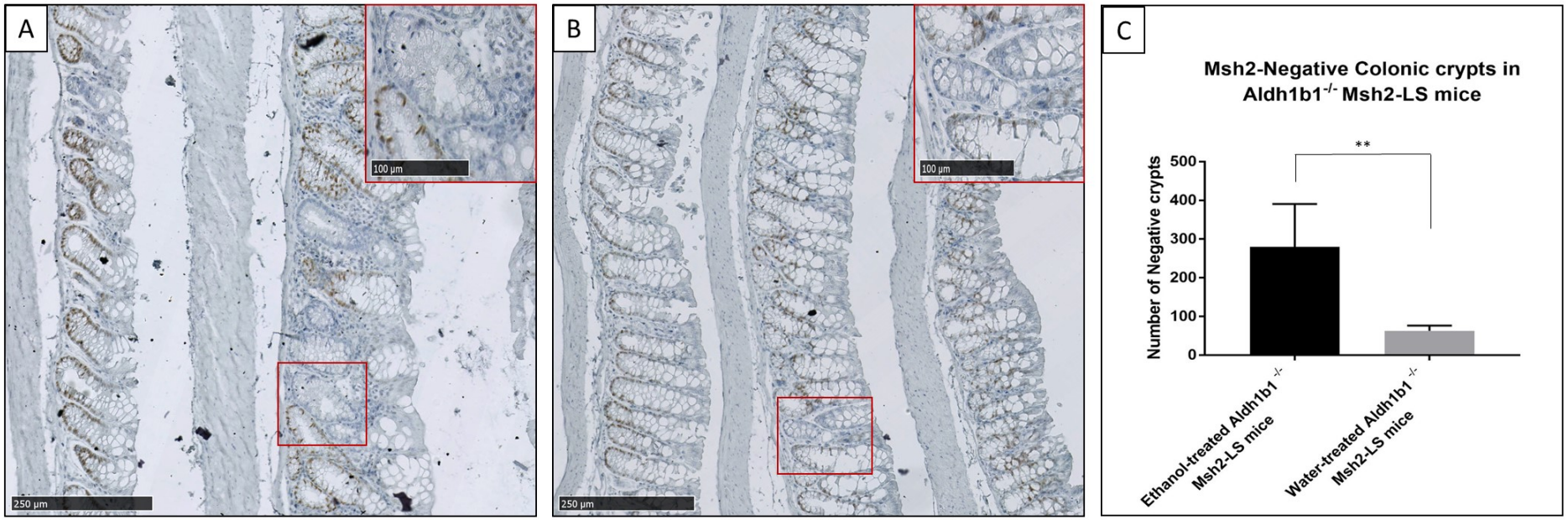

Figure 6.53: Immunohistochemical analysis of Msh2 protein expression in large intestinal mucosal epithelium of *Aldh1b1*$^{-/-}$*; Msh2*$^{flox/-}$*; Lgr5CreERT2*$^{+/-}$*; mTmG*$^{+/-}$ mice treated with either 20% ethanol in drinking water (A) or normal/standard water (B). Msh2-negative crypts (indicated by the red square/rectangle and further magnified in the upper right inset red rectangle in figures A and B) were manually counted along the entire colon of treated *Aldh1b1*$^{-/-}$ Msh2-LS mice (C). Mann-Whitney U Test, **p=0.0085 vs. water (data shown as mean±SD, n=5 mice each group). Images taken from sections scanned using the Hamamatsu Nanozoomer and analysed with the Hamamatsu NDP Viewer software at 10X and 20X magnification (bar at lower left indicates 250µm, bar in red rectangle indicates 100µm).

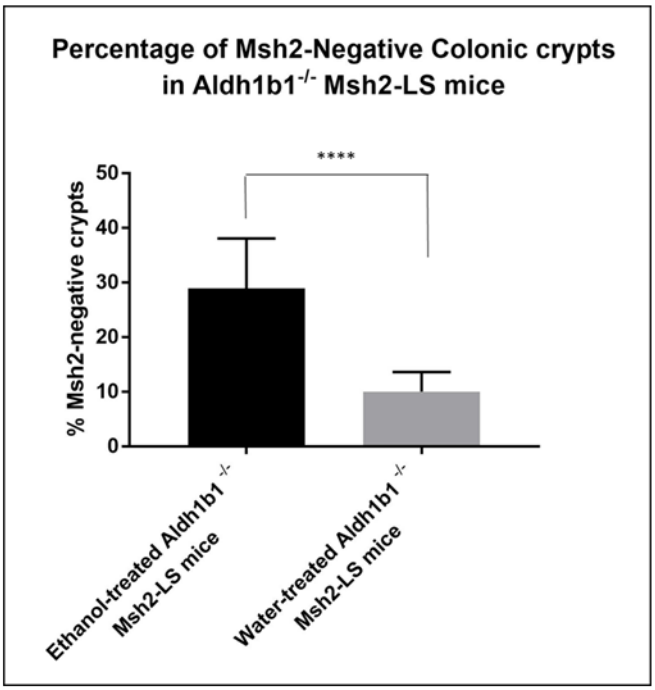

Figure 6.54: Percentage of Msh2 protein-non-expressing crypts in large intestinal mucosa of *Aldh1b1*$^{-/-}$*; Msh2*$^{flox/-}$*; Lgr5CreERT2*$^{+/-}$*; mTmG*$^{+/-}$mice treated with either 20% ethanol in drinking water or normal/standard water. Paired Students t Test, ****p<0.0001 vs. water (data shown as mean±SD, 200 crypts counted in 5 mice from each group).

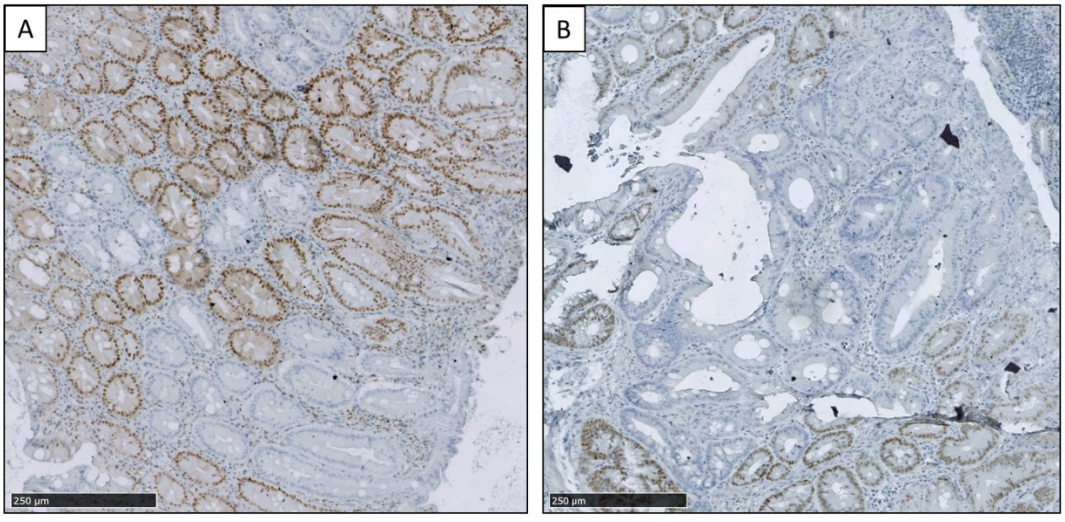

Figure 6.55: Representative images of immunohistochemical staining for Msh2 in adenomas from 2 *Aldh1b1*$^{-/-}$*; Msh2*$^{flox/-}$*; Lgr5CreERT2*$^{+/-}$*; mTmG*$^{+/-}$ ethanol-treated mice. In both examples, a caecal adenoma (A) and a colonic adenoma (B), there are Msh2-negative dysplastic or adenomatous glands, either surrounded by or admixed with reactive crypts or hyperproliferative crypts that are staining positively for Msh2. Images taken from sections scanned using the Hamamatsu Nanozoomer and analysed with the Hamamatsu NDP Viewer software at 10X magnification (bar at lower left indicates 250µm).

6.5.2.2 Aldh1b1 immunostaining of *Aldh1b1* conditional-knockout Msh2-LS and *Aldh1b1* constitutive-knockout Msh2-LS murine small intestinal and colonic tissues

Aldh1b1 protein is highly expressed in the intestinal epithelial cells. In normal small intestines, there is strong Aldh1b1 cytoplasmic immunostaining in the crypt epithelial cells, but this fades in the non-dividing differentiated SI villus cells. In contrast in normal colon, Aldh1b1 cytoplasmic immunostaining appears homogeneous along the crypt axis (Müller et al., 2016). We used colonic tissue samples of WT and *Aldh1b1*$^{tm2a(EUCOMM)Wtsi}$ mice (mice with depletion of *Aldh1b1*, used by Müller at al., 2016) as Aldh1b1-positive and Aldh1b1-negative expression controls respectively (Figure 6.56).

In *Aldh1b1*$^{flox/flox}$ conditional-knockout Msh2-LS mice, Tamoxifen treatment induced the loss of Aldh1b1 expression, together with the loss of Msh2, in Lgr5+ expressing crypt epithelial stem cells scattered along the entire small and large intestines (Figure 6.57). Aldh1b1-negative crypts were observed in the intestinal samples of EtOH_*Aldh1b1*$^{fl/fl}$_*Msh2*$^{fl\ KO}$ and H_2O_*Aldh1b1*$^{fl/fl}$_*Msh2*$^{fl\ KO}$ mice (Figure 6.58). IHC analysis of Aldh1b1 expression in the intestinal tissue samples from EtOH_*Aldh1b1*$^{fl/fl}$_*Msh2*^{fl} mice and H_2O_*Aldh1b1*$^{fl/fl}$_*Msh2*^{fl} mice showed no Aldh1b1-negative crypts in either small or large intestinal mucosal epithelium (Figure 6.59), consistent with lack of induction of Cre activity with continued expression of protein from the floxed *Aldh1b1* allele.

In *Aldh1b1*$^{-/-}$ constitutive-knockout Msh2-LS mice, Aldh1b1 is permanently inactivated in all tissues and cells (Tamoxifen treatment is not required to induce the loss of Aldh1b1 expression). Immunohistochemical analysis of Aldh1b1 expression in the intestinal tissue samples from both Tamoxifen induced and non-induced (no Tamoxifen treatment) *Aldh1b1*$^{-/-}$ Msh2-LS model mice treated with either 20% ethanol in drinking water or normal water showed only Aldh1b1-negative crypts in both small intestinal and large intestinal mucosal epithelium (Figure 6.60-6.61).

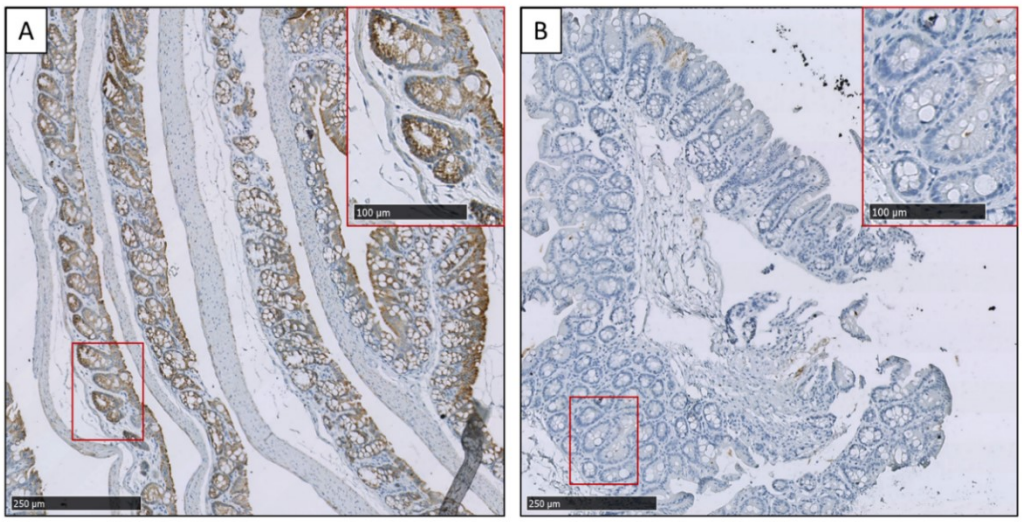

Figure 6.56: Immunohistochemical analysis of Aldh1b1 protein expression in colonic mucosal epithelium from a positive-control WT mouse (A), in which the brown staining indicates positive Aldh1b1 expression in all crypts (further magnified in the red rectangle); and from a negative-control *Aldh1b1*$^{tm2a\,(EUCOMM)Wtsi}$ mouse (B), in which the lack of brown staining confirms the absence of Aldh1b1 expression in colonic mucosal epithelium (further magnified in the red rectangle). The Aldh1b1 protein is predominantly located in the cytoplasm of epithelial cells. Images taken from anti-Aldh1b1 IHC stained sections scanned using the Hamamatsu Nanozoomer and analysed with the Hamamatsu NDP Viewer software at 10X and 20X magnification (bar at lower left indicates 250µm, bar in red rectangle indicates 100µm).

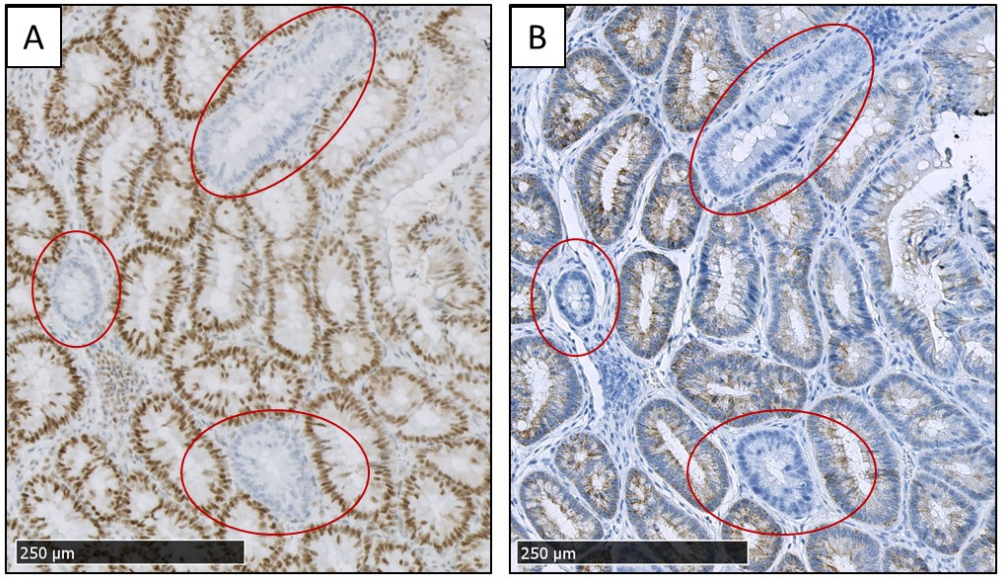

Figure 6.57: Representative comparison between Msh2 and Aldh1b1 immunostaining of adjacent serial sections of caecum of *Aldh1b1*$^{flox/flox}$*; Msh2*$^{flox/-}$*; Lgr5CreERT2*$^{+/-}$*; mTmG*$^{+/-}$ mice treated with Tamoxifen to activate Cre in scattered crypts. The same dMMR crypt foci (A) are negative for Msh2 and negative for Aldh1b1 (B) (red ovals). Images taken using the Hamamatsu Nanozoomer and

analysed with the Hamamatsu NDP Viewer software at 10X magnification (bar at lower left indicates 250µm).

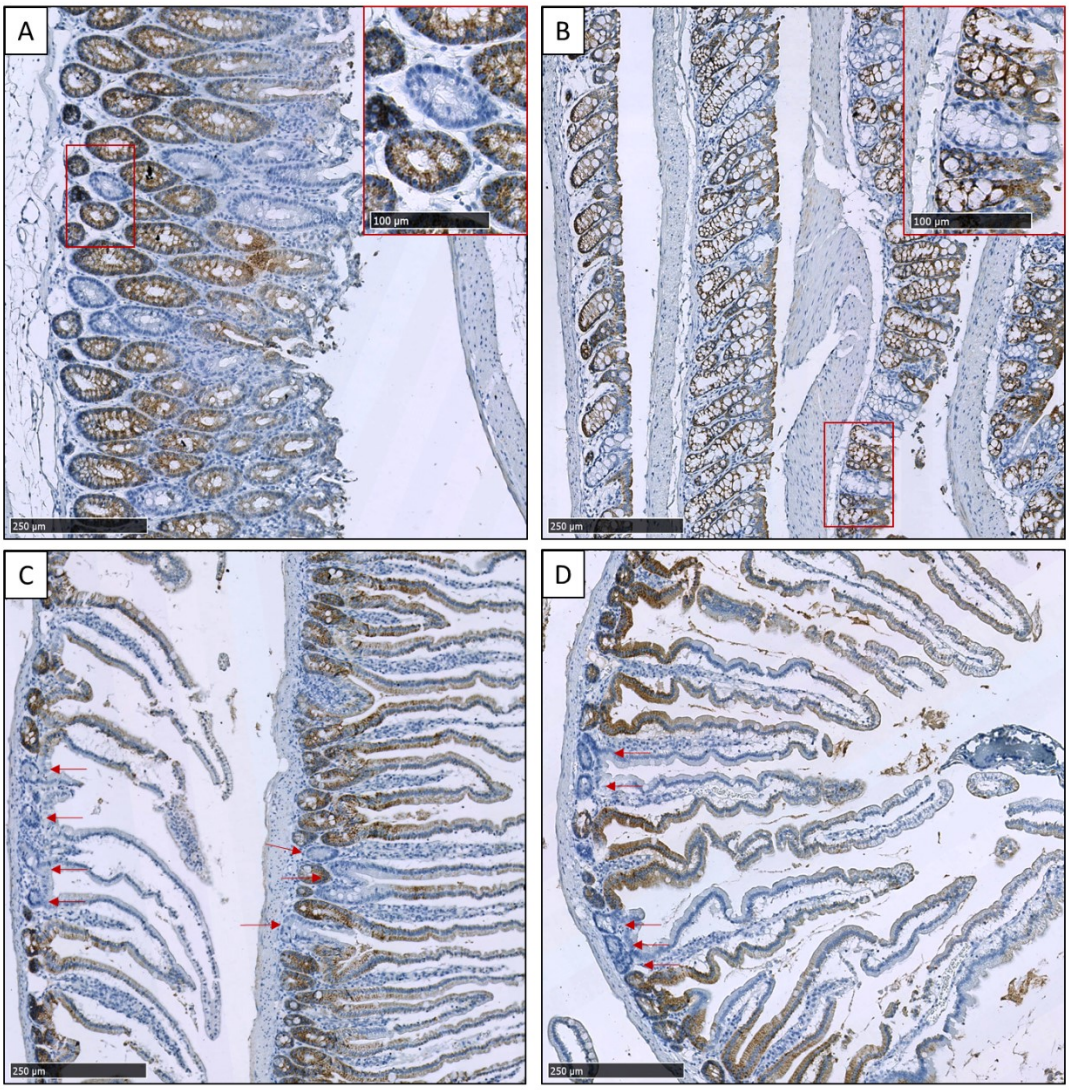

Figure 6.58: Immunohistochemical analysis of Aldh1b1 protein expression in large intestinal (A&B) and small intestinal (C and D) mucosal epithelium of *Aldh1b1*$^{flox/flox}$*; Msh2*$^{flox/-}$*; Lgr5CreERT2*$^{+/-}$*; mTmG*$^{+/-}$ mice treated with either 20% ethanol in drinking water (A and C) or normal/standard water (B and D). Colonic Aldh1b1-negative crypts are indicated by the red rectangle and further magnified in the upper right inset red rectangle in figure panels A and B and small intestinal Aldh1b1-negative crypts are indicated by the red arrows in figure panels C and D. Images taken from sections scanned using the Hamamatsu Nanozoomer and analysed with the Hamamatsu NDP Viewer software at 10X and 20X magnification (bar at lower left indicates 250µm, bar in red rectangle indicates 100µm).

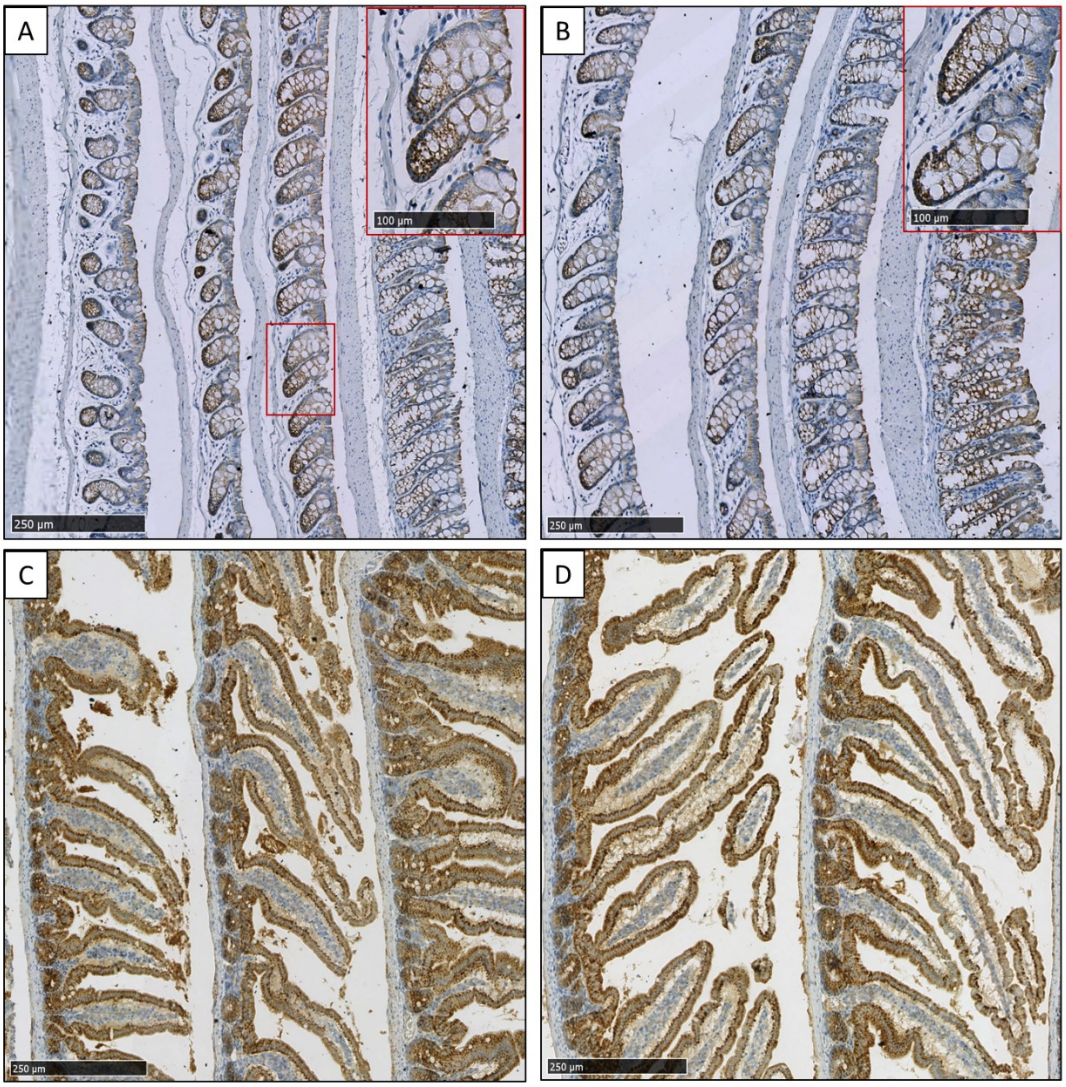

Figure 6.59: Immunohistochemical analysis of Aldh1b1 protein expression in intestinal mucosal epithelium of non-induced (no Tamoxifen treatment) *Aldh1b1$^{flox/flox}$; Msh2$^{flox/-}$; Lgr5CreERT2$^{+/-}$; mTmG$^{+/-}$* mice treated with either 20% ethanol in drinking water (A and C) or normal/standard water (B and D). Normal Aldh1b1 expression is observed in colonic mucosal epithelium (Aldh1b1-positive crypts indicated by the red rectangle and further magnified in the upper right inset red rectangle in figure panels A and B) and in small intestinal mucosal epithelium (C and D). Images taken from sections scanned using the Hamamatsu Nanozoomer and analysed with the Hamamatsu NDP Viewer software at 10X and 20X magnification (bar at lower left indicates 250µm, bar in red rectangle indicates 100µm).

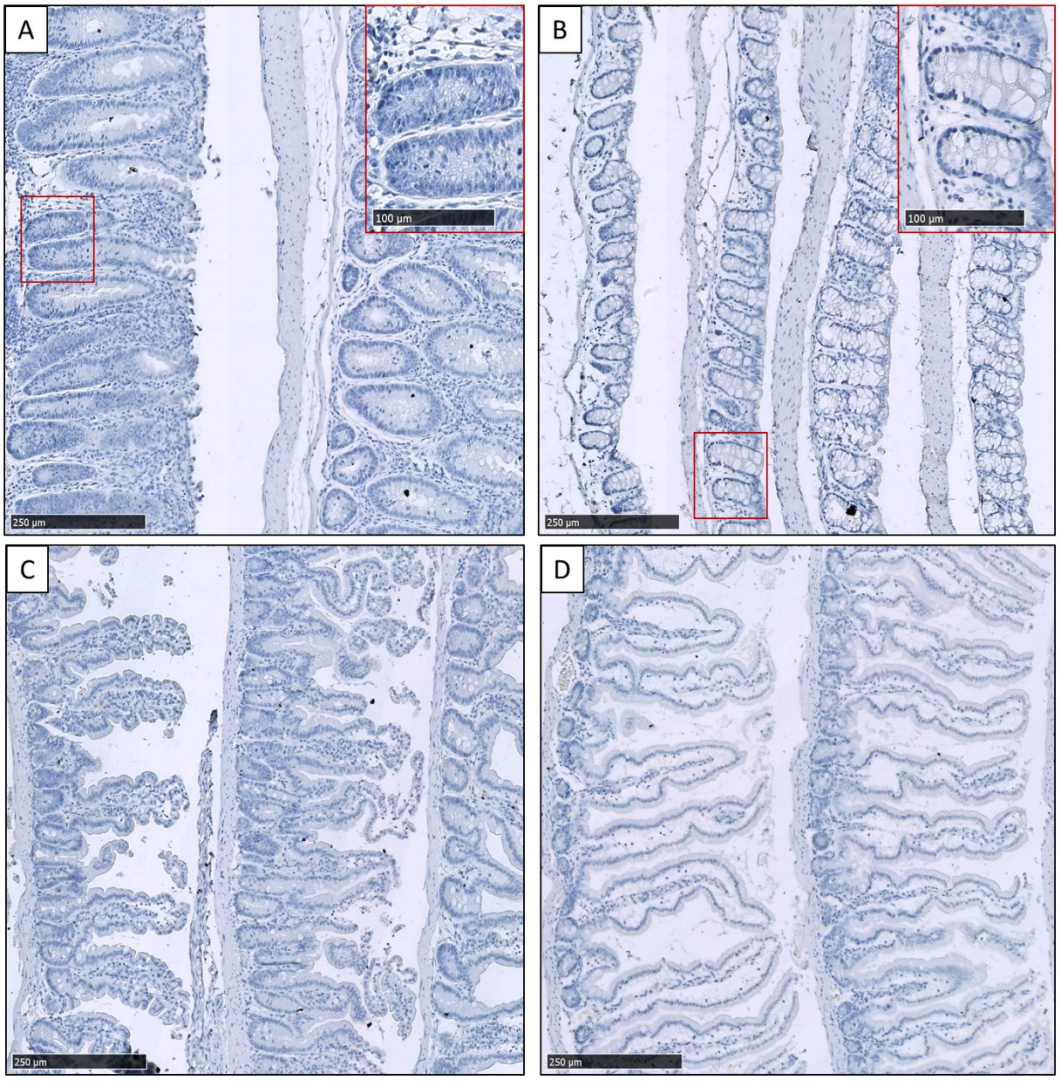

Figure 6.60: Immunohistochemical analysis of Aldh1b1 protein expression in intestinal mucosal epithelium of *Aldh1b1*$^{-/-}$; *Msh2*$^{flox/-}$; *Lgr5CreERT2*$^{+/-}$; *mTmG*$^{+/-}$ mice treated with either 20% ethanol in drinking water (A and C) or normal/standard water (B and D). Complete loss of Aldh1b1 expression is observed in colonic mucosal epithelium (Aldh1b1-negative crypts are indicated by the red rectangle and further magnified in the upper right inset red rectangle in figure panels A and B) and in small intestinal mucosal epithelium (C and D). Images taken from sections scanned using the Hamamatsu Nanozoomer and analysed with the Hamamatsu NDP Viewer software at 10X and 20X magnification (bar at lower left indicates 250µm, bar in red rectangle indicates 100µm).

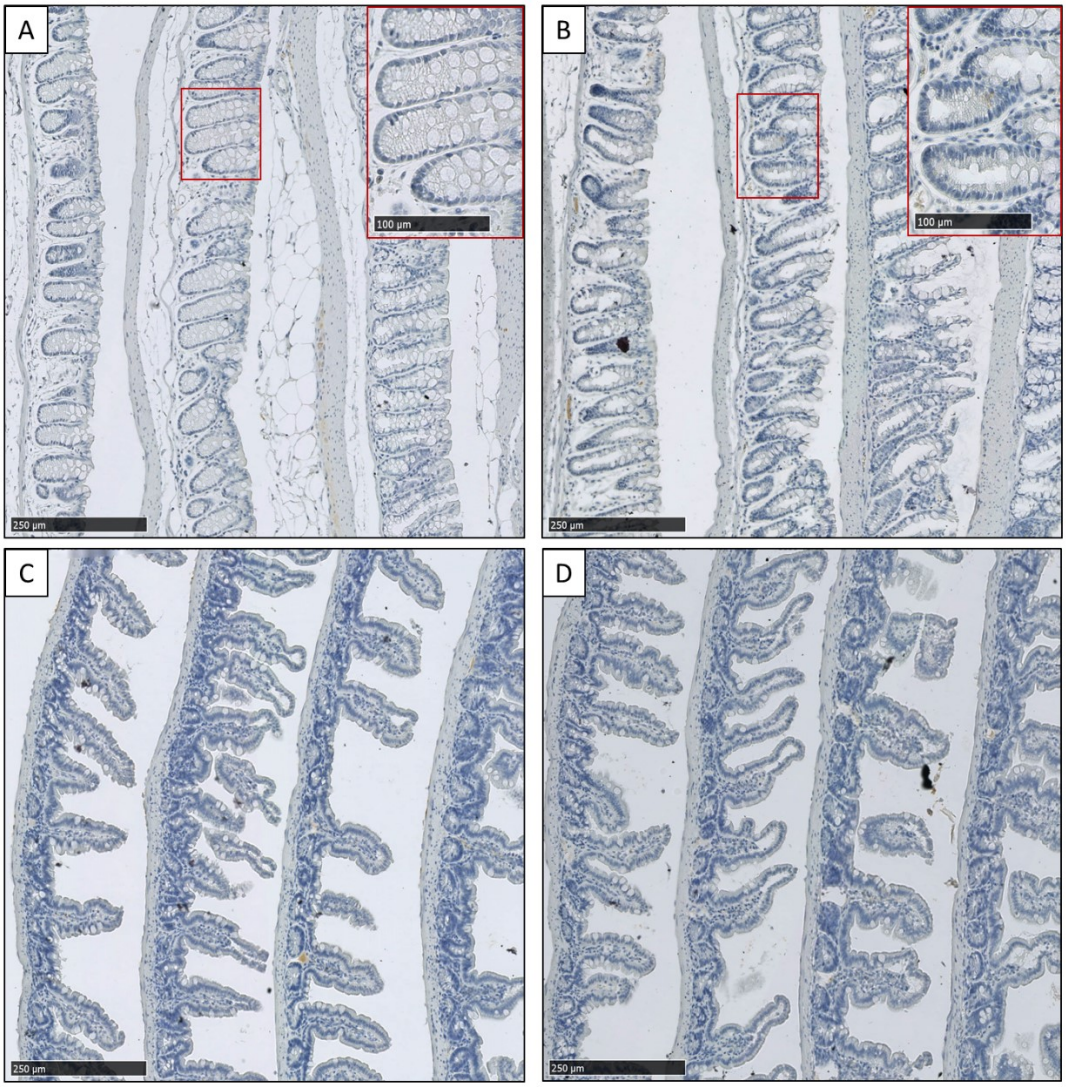

Figure 6.61: Immunohistochemical analysis of Aldh1b1 protein expression in intestinal mucosal epithelium of non-induced (no Tamoxifen treatment) *Aldh1b1*$^{-/-}$; *Msh2*$^{flox/-}$; *Lgr5CreERT2*$^{+/-}$; *mTmG*$^{+/-}$ mice treated with either 20% ethanol in drinking water (A and C) or normal/standard water (B and D). Complete loss of Aldh1b1 expression is observed in colonic mucosal epithelium (Aldh1b1-negative crypts are indicated by the red rectangle and further magnified in the upper right inset red rectangle in A and B) and in small intestinal mucosal epithelium (C and D). Images taken from sections scanned using the Hamamatsu Nanozoomer and analysed with the Hamamatsu NDP Viewer software at 10X and 20X magnification (bar at lower left indicates 250µm, bar in red rectangle indicates 100µm).

6.5.2.2 Ki-67 immunohistochemical analyses of intestinal samples from *Aldh1b1* conditional-knockout Msh2-LS and *Aldh1b1* constitutive-knockout Msh2-LS mouse models

6.5.2.2.1 Ki-67 immunostaining of *Aldh1b1* conditional-knockout Msh2-LS murine small intestinal and colonic tissues

Immunohistochemical analysis of Ki-67 showed large and significant differences in the number of intestinal Ki-67-positive cells between EtOH_*Aldh1b1*$^{fl/fl}$_*Msh2*$^{fl\ KO}$ murine colon and H_2O_*Aldh1b1*$^{fl/fl}$_*Msh2*$^{fl\ KO}$ murine colon (Figure 6.62). The percentage of Ki-67-positive cells per crypt was significantly higher in EtOH_*Aldh1b1*$^{fl/fl}$_*Msh2*$^{fl\ KO}$ mice (80.6%) compared with H_2O_*Aldh1b1*$^{fl/fl}$_*Msh2*$^{fl\ KO}$ mice (27.3%) (Figure 6.63), consistent with the large regions of mucosal crypt hyperproliferation, that show extended crypt lengths, observed in H&E stained sections of EtOH_*Aldh1b1*$^{fl/fl}$_*Msh2*$^{fl\ KO}$ murine colons (Figure 6.64).

The comparative analysis of SI Ki-67 expression between EtOH_*Aldh1b1*$^{fl/fl}$_*Msh2*$^{fl\ KO}$ and H_2O_*Aldh1b1*$^{fl/fl}$_*Msh2*$^{fl\ KO}$ mice didn't show the same large differences. EtOH_*Aldh1b1*$^{fl/fl}$_*Msh2*$^{fl\ KO}$ murine SI showed similar numbers of Ki-67-positive cells per crypt when compared with H_2O_*Aldh1b1*$^{fl/fl}$_*Msh2*$^{fl\ KO}$ mice SI, with no significant differences observed between the two groups (Figure 6.65). However, the percentage of Ki-67-positive cells per crypt was significantly higher in SI of EtOH_*Aldh1b1*$^{fl/fl}$_*Msh2*$^{fl\ KO}$ mice (13.5%) compared with H_2O_*Aldh1b1*$^{fl/fl}$_*Msh2*$^{fl\ KO}$ mice (8.3%) (Figure 6.66).

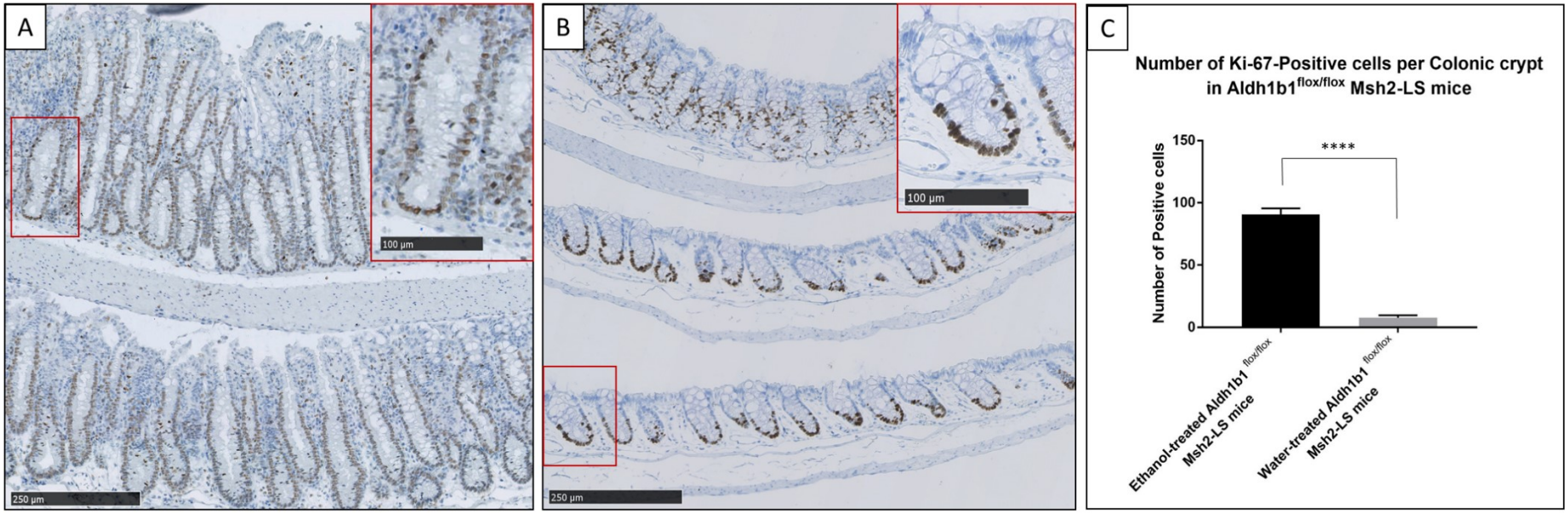

Figure 6.62: Immunohistochemical analysis of Ki-67 protein expression in large intestinal mucosal epithelium of *Aldh1b1*$^{flox/flox}$; *Msh2*$^{flox/-}$; *Lgr5CreERT2*$^{+/-}$; *mTmG*$^{+/-}$mice treated with either 20% of ethanol in drinking water (A) or normal/standard water (B) (magnified in the upper right inset red rectangles in figure panels A and B). Numbers of Ki-67-positive cells per colonic crypt were manually counted (C). Paired Students t Test, ****p<0.0001 vs. water (data shown as mean±SD, 30 crypts per mouse were analysed, n=4 mice in each group). Images taken from sections scanned using the Hamamatsu Nanozoomer and analysed with the Hamamatsu NDP Viewer software at 10X and 20X magnification (bar at lower left indicates 250µm, bar in red rectangle indicates 100µm).

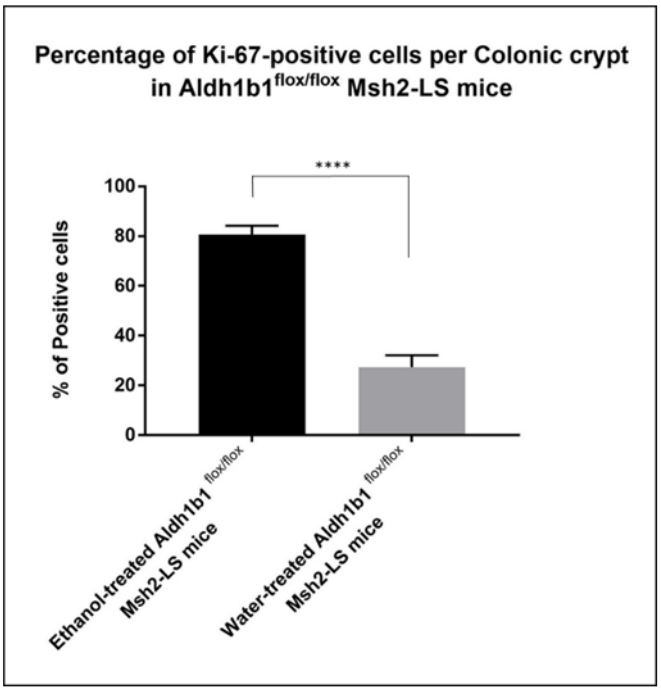

Figure 6.63: Percentage of Ki-67 protein expressing cells in large intestinal mucosal crypts of *Aldh1b1*$^{flox/flox}$; *Msh2*$^{flox/-}$; *Lgr5CreERT2*$^{+/-}$; *mTmG*$^{+/-}$mice treated with either 20% ethanol in drinking water or normal / standard water. Paired Students t Test, ****p<0.0001 vs. water (data shown as mean±SD, 30 crypts per mouse counted, n=4 mice from each group).

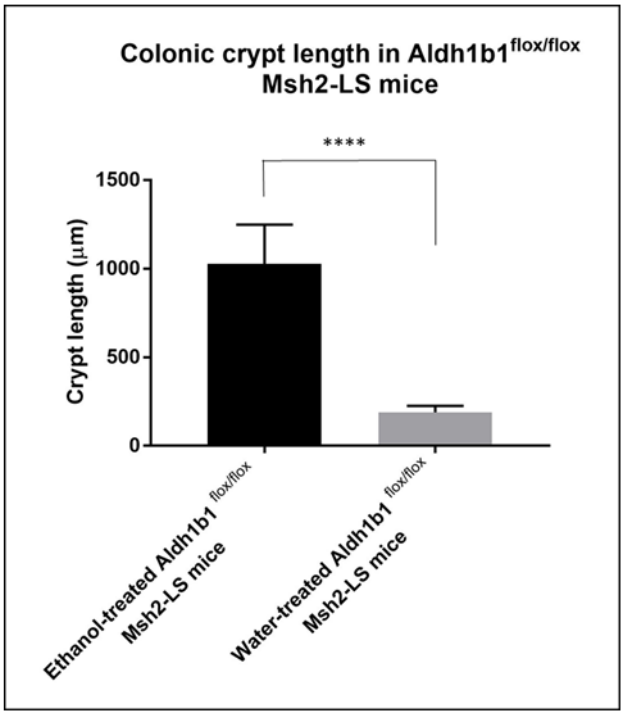

Figure 6.64: Quantification of the colonic crypt lengths (in µm) comparing colons from ethanol-treated versus water-treated *Aldh1b1*$^{flox/flox}$ Msh2-LS mice. Mann-Whitney U test analysis, ****p<0.0001 vs. water (data shown as mean ± SD).

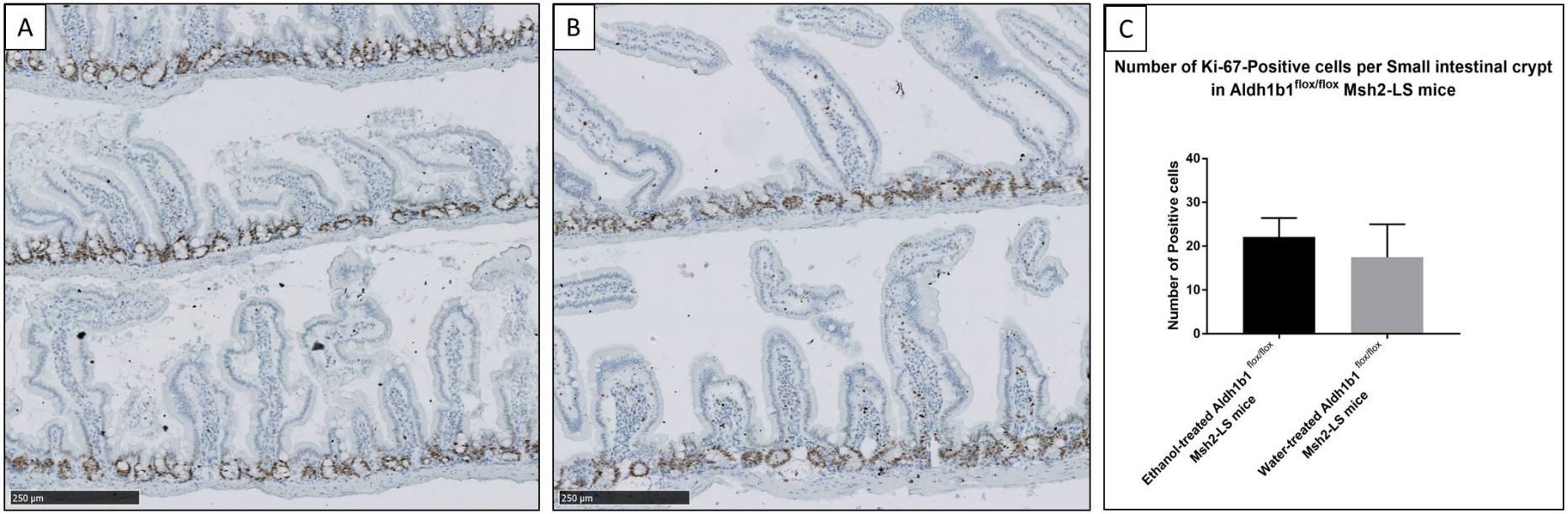

Figure 6.65: Immunohistochemical analysis of Ki-67 protein expression in small intestinal mucosa of *Aldh1b1*$^{flox/flox}$; *Msh2*$^{flox/-}$; *Lgr5CreERT2*$^{+/-}$; *mTmG*$^{+/-}$mice treated with either 20% ethanol in drinking water (A) or normal / standard drinking water (B). Ki-67-positive cells per colonic crypt/villus were counted using QuPath (C). Paired Students t Test, (data shown as mean±SD, 30 crypts/villi per mouse were analysed, n=3 mice in each group) showed no statistical differences were observed between these 2 groups. Images taken from sections scanned using the Hamamatsu Nanozoomer and analysed with the Hamamatsu NDP Viewer software at 10X magnification (bar at lower left indicates 250µm).

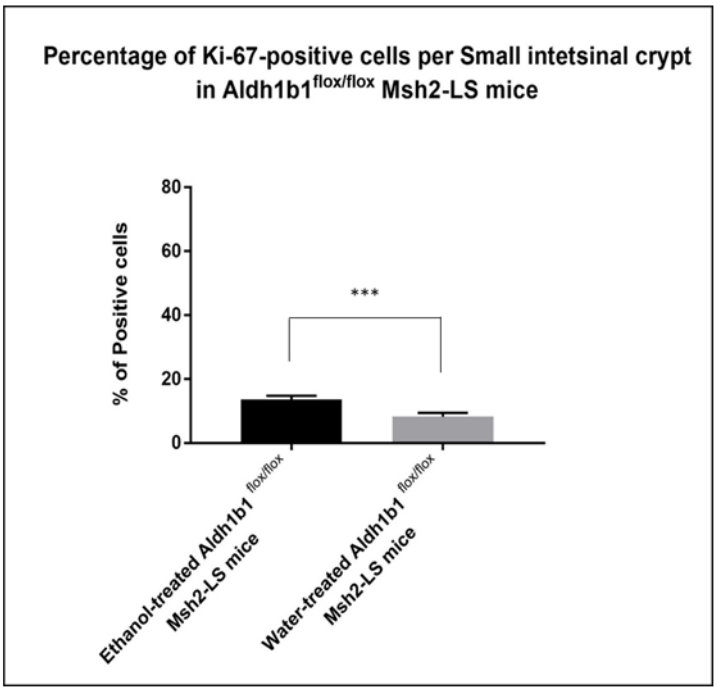

Figure 6.66: Percentage of Ki-67 protein expressing cells in small intestinal mucosa of *Aldh1b1*$^{flox/flox}$; *Msh2*$^{flox/-}$; *Lgr5CreERT2*$^{+/-}$; *mTmG*$^{+/-}$ mice treated with either 20% ethanol in drinking water or normal / standard water. Paired Students t Test, ***p=0.0005 vs. water (data shown as mean±SD, 30 crypts per mouse counted, n=3 mice from each group).

6.5.2.2.2 Ki-67 immunostaining of *Aldh1b1* constitutive-knockout Msh2-LS murine small intestinal and colonic tissues

Immunohistochemical analysis of Ki-67 showed large and significant differences in the number of intestinal Ki-67-positive cells between the EtOH_*Aldh1b1*$^{-/-}$_*Msh2*$^{fl\ KO}$ murine colon and the H_2O_*Aldh1b1*$^{-/-}$_*Msh2*$^{fl\ KO}$ murine colon (Figure 6.67). The percentage of Ki-67-positive cells per crypt was significantly higher in EtOH_*Aldh1b1*$^{-/-}$_*Msh2*$^{fl\ KO}$ mice (87%) compared with H_2O_*Aldh1b1*$^{-/-}$_*Msh2*$^{fl\ KO}$ mice (25.3%) (Figure 6.68), consistent with the large regions of crypt hyperproliferation, that show extended crypt lengths, observed in H&E stained sections of EtOH_*Aldh1b1*$^{-/-}$_*Msh2*$^{fl\ KO}$ murine colons (Figure 6.69).

The comparative analysis of SI Ki-67 expression between EtOH_*Aldh1b1*$^{-/-}$_*Msh2*$^{fl\ KO}$ and H_2O_*Aldh1b1*$^{-/-}$_*Msh2*$^{fl\ KO}$ mice didn't show the same large differences. EtOH_*Aldh1b1*$^{-/-}$_*Msh2*$^{fl\ KO}$ murine SI showed similar numbers of Ki-67-positive cells per crypt compared with H_2O_*Aldh1b1*$^{-/-}$_*Msh2*$^{fl\ KO}$ mice SI, with no significant differences observed between the two groups (Figure 6.70). The percentage of Ki-67-positive cells per crypt was significantly higher in SI of EtOH_*Aldh1b1*$^{-/-}$_*Msh2*$^{fl\ KO}$ mice (17.8%) compared with H_2O_*Aldh1b1*$^{-/-}$_*Msh2*$^{fl\ KO}$ mice (13.2%), but with only a small difference between the two groups (Figure 6.71).

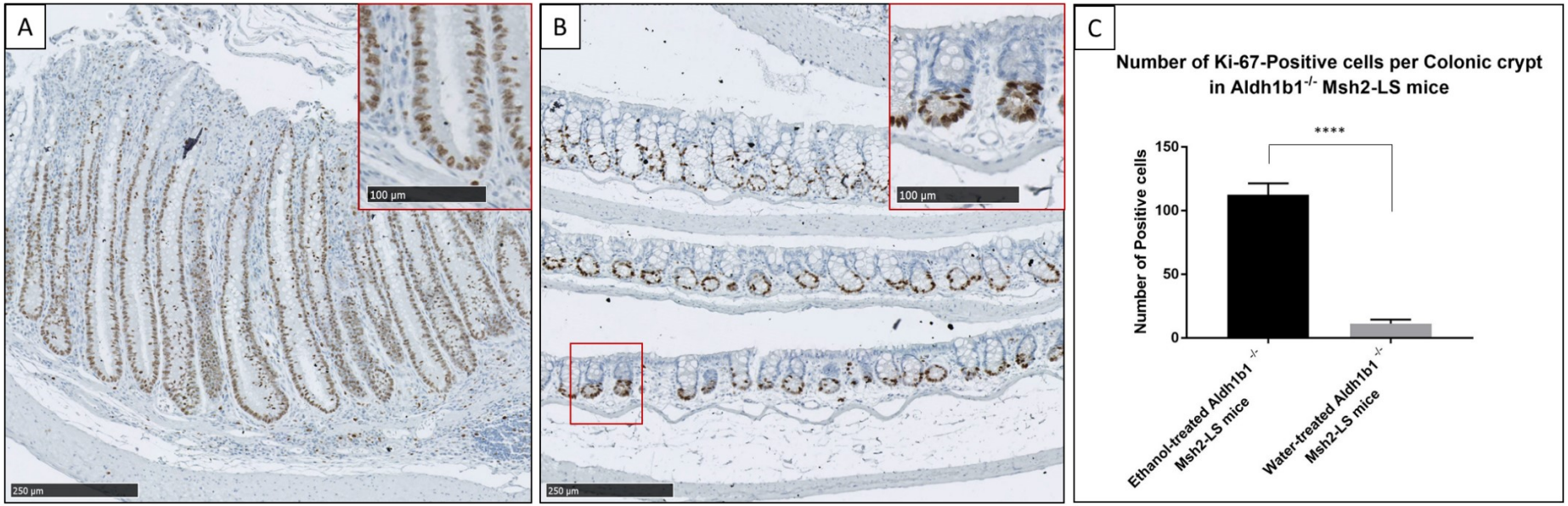

Figure 6.67: Immunohistochemical analysis of Ki-67 protein expression in large intestinal mucosal epithelium of *Aldh1b1*$^{-/-}$; *Msh2*$^{flox/-}$; *Lgr5CreERT2*$^{+/-}$; *mTmG*$^{+/-}$mice treated with either 20% of ethanol in drinking water (A) or normal/standard water (B). Numbers of Ki-67-positive cells per colonic crypt (magnified in the upper right inset red rectangles in figure panels A and B) were manually counted (C). Paired Students t Test, ****p<0.0001 vs. water (data shown as mean±SD, 30 crypts per mouse were analysed, n=4 mice in each group). Images taken from sections scanned using the Hamamatsu Nanozoomer and analysed with the Hamamatsu NDP Viewer software at 10X and 20X magnification (bar at lower left indicates 250µm, bar in red rectangle indicates 100µm).

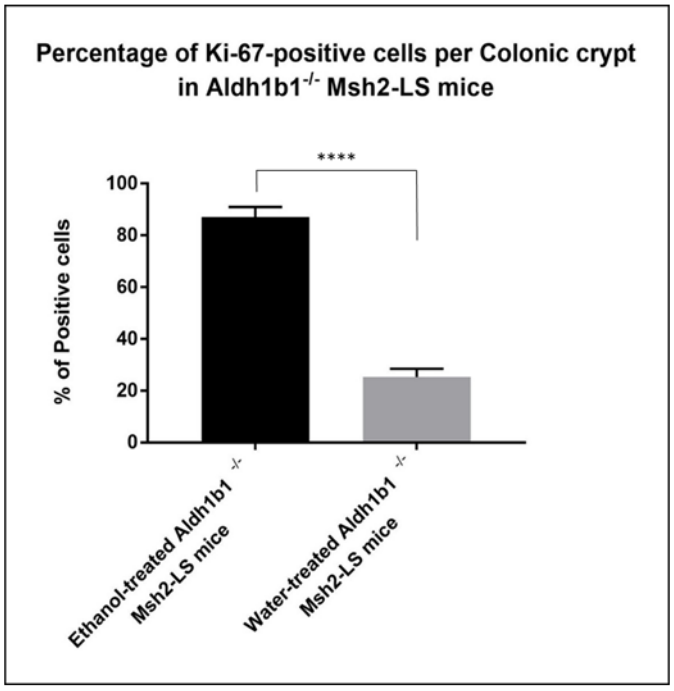

Figure 6.68: Percentage of Ki-67 protein expressing cells in large intestinal mucosal crypts of *Aldh1b1*$^{-/-}$; *Msh2*$^{flox/-}$; *Lgr5CreERT2*$^{+/-}$; *mTmG*$^{+/-}$mice treated with either 20% ethanol in drinking water or normal / standard water. Paired Students t Test, ****p<0.0001 vs. water (data shown as mean±SD, 30 crypts per mouse counted, n=4 mice from each group).

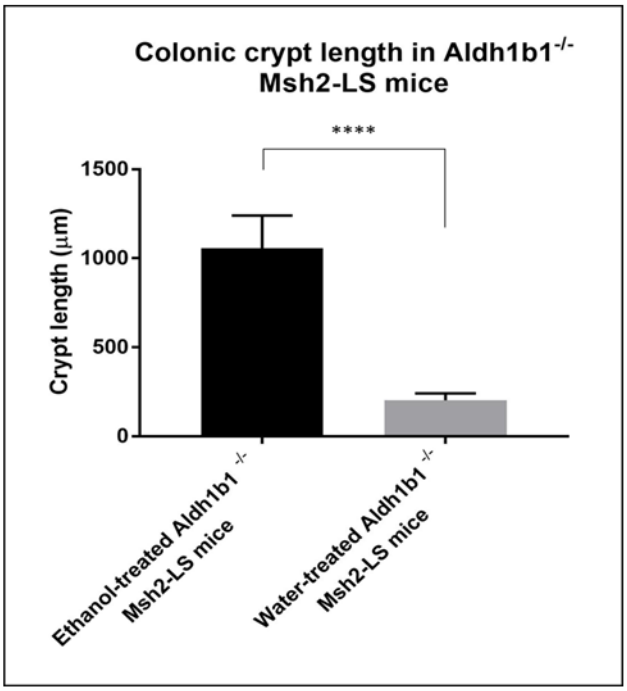

Figure 6.69: Quantification of the colonic crypt lengths (in µm) comparing colons from ethanol-treated versus water-treated *Aldh1b1*$^{-/-}$ Msh2-LS mice. Paired Students t Test, ****p<0.0001 vs. water (data shown as mean ± SD).

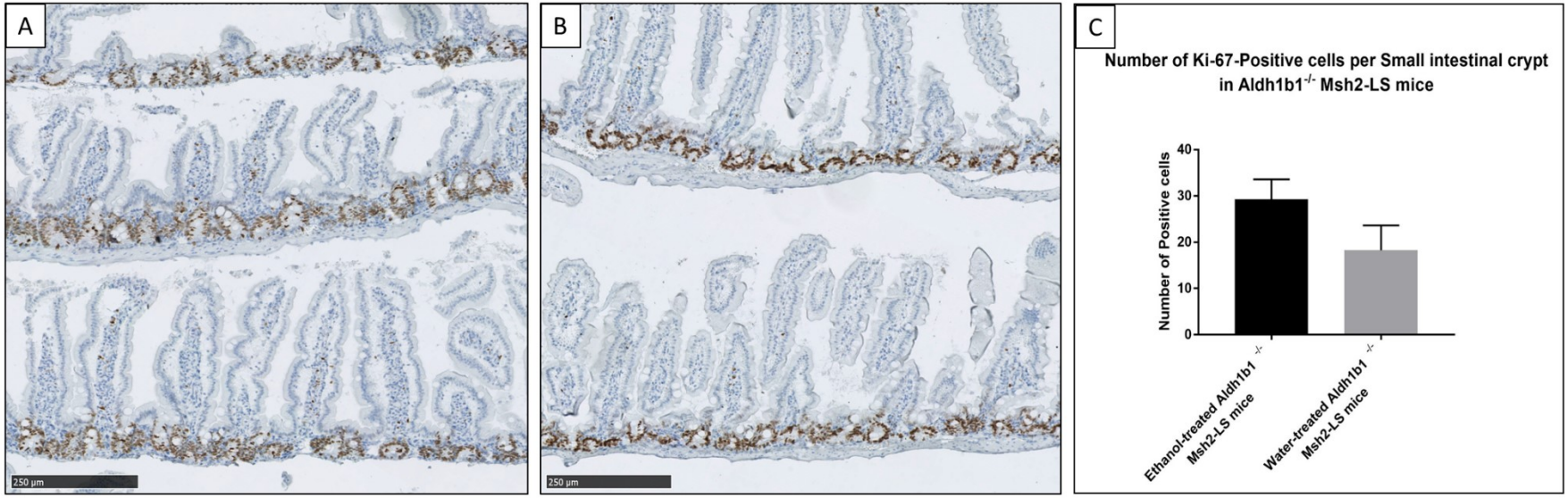

Figure 6.70: Immunohistochemical analysis of Ki-67 protein expression in small intestinal mucosa of *Aldh1b1*$^{-/-}$; *Msh2*$^{flox/-}$; *Lgr5CreERT2*$^{+/-}$; *mTmG*$^{+/-}$mice treated with either 20% ethanol in drinking water (A) or normal / standard drinking water (B). Ki-67-positive cells per colonic crypt/villus were counted using QuPath (C). Paired Students t test, (data shown as mean±SD, 30 crypts/villi per mouse were analysed, n=3 mice in each group) showed no statistical differences were observed between the 2 groups. Images taken from sections scanned using the Hamamatsu Nanozoomer and analysed with the Hamamatsu NDP Viewer software at 10X magnification (bar at lower left indicates 250µm).

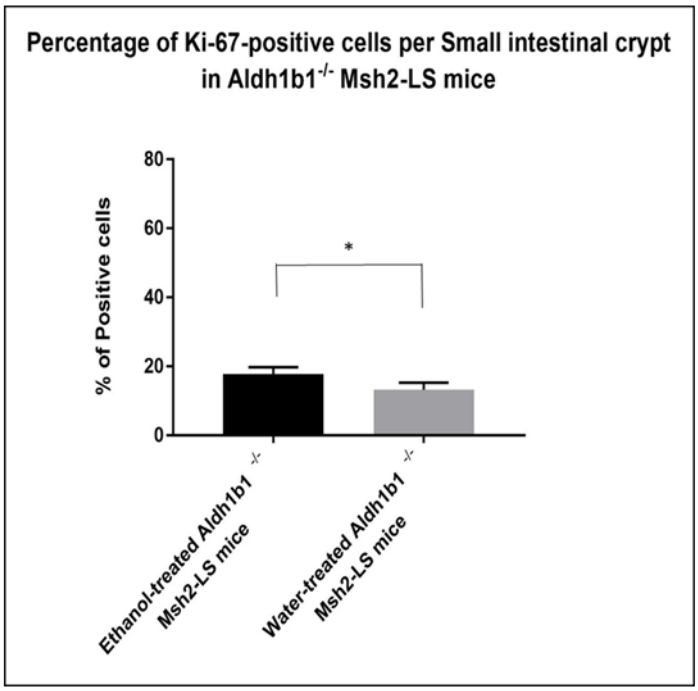

Figure 6.71: Percentage of Ki-67 protein expressing cells in small intestinal mucosa of *Aldh1b1*$^{-/-}$; *Msh2*$^{flox/-}$; *Lgr5CreERT2*$^{+/-}$; *mTmG*$^{+/-}$mice treated with either 20% ethanol in drinking water or normal / standard water. Paired Students t test, *p=0.0127 vs. water (data shown as mean±SD, 30 crypts per mouse counted, n=3 mice from each group).

6.5.2.3 Beta-Catenin immunostaining of *Aldh1b1* conditional-knockout Msh2-LS and *Aldh1b1* constitutive-knockout Msh2-LS murine small intestinal and colonic tissues

We investigated β-catenin expression in *Aldh1b1*$^{flox/flox;}$ Msh2$^{flox/-}$; Lgr5CreERT2$^{+/-}$; mTmG$^{+/-}$ mice and *Aldh1b1*$^{-/-;}$ Msh2$^{flox/-}$; Lgr5CreERT2$^{+/-}$; mTmG$^{+/-}$. β-catenin IHC was performed with assistance from Marion Bacou using large intestinal samples from *Apc Min* mice that contained large intestinal adenomas (provided by Vidya Rajasekaran), and WT mice as β-catenin-positive and β-catenin-normal expression controls respectively (Figure 4.41). Details of the IHC positive and normal β-catenin expression controls were reported in Chapter 4 (4.4.2.3). The IHC analysis of β-catenin was performed on large intestinal adenomas and caecal adenomas from *Aldh1b1*$^{flox/flox;}$ Msh2$^{flox/-}$; Lgr5CreERT2$^{+/-}$; mTmG$^{+/-}$mice (Figure 6.72) and *Aldh1b1*$^{-/-;}$ Msh2$^{flox/-}$; Lgr5CreERT2$^{+/-}$; mTmG$^{+/-}$ (Figure 6.73). Analysed samples showed a heterogeneous pattern with variable numbers of adenoma cells showing positive β-catenin nuclear immunostaining due to accumulation and translocation of β-catenin in the nuclei.

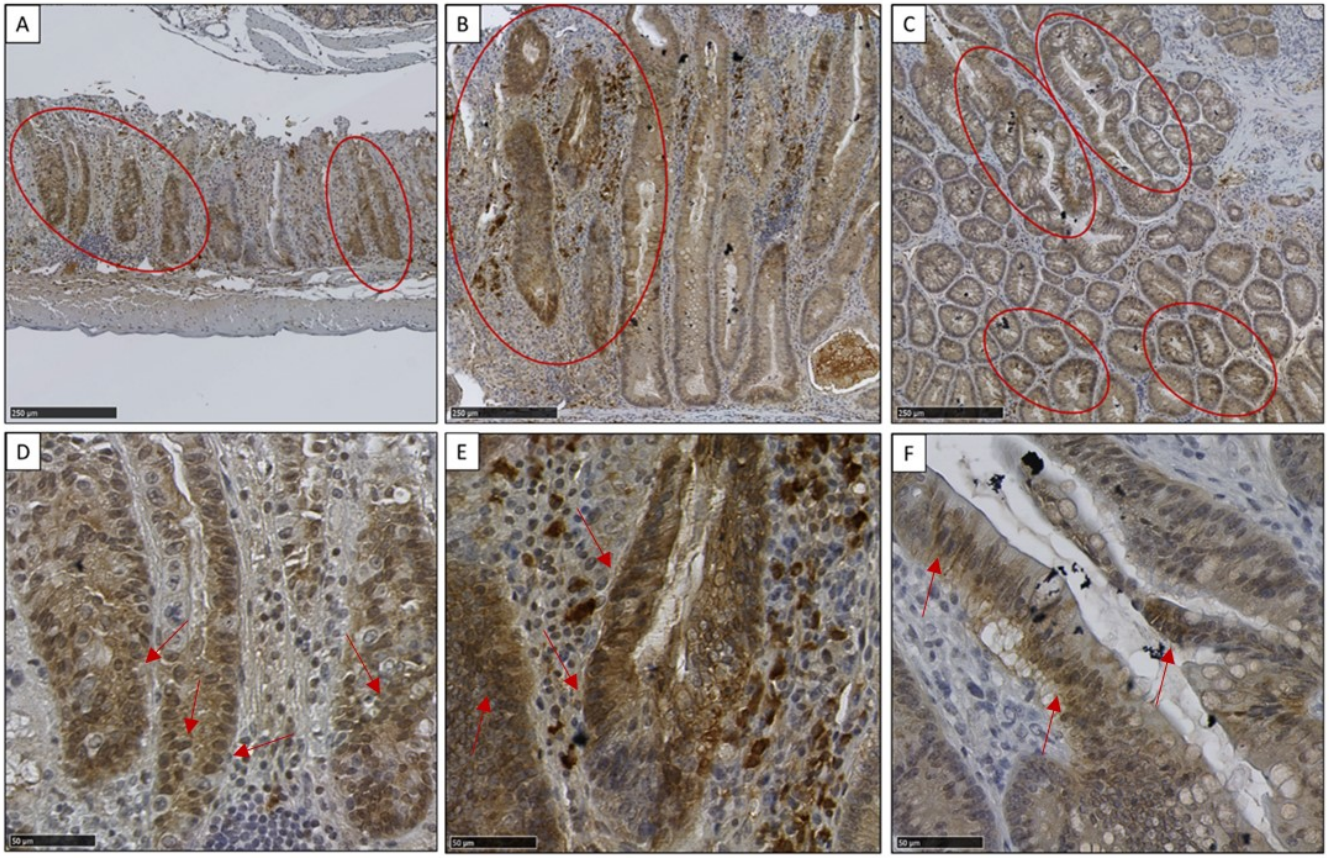

Figure 6.72: Representative images of immunohistochemical analysis of β-catenin protein expression and localisation in large intestinal adenomas of *Aldh1b1*$^{-/-}$; *Msh2*$^{flox/-}$; *Lgr5CreERT2*$^{+/-}$; *mTmG*$^{+/-}$mice treated with 20% ethanol in drinking water. Variable areas of positive β-catenin nuclear immunostaining in adenomatous cells were observed in colonic adenomas (A-C), indicated by the red ovals. Selected areas (red ovals) within images in panels A-C are further magnified in panels D-F, and clusters of cells with nuclei positive for β-catenin are indicated by the red arrows. Images taken from sections scanned using the Hamamatsu Nanozoomer and analysed with the Hamamatsu NDP Viewer software at 10X and 40X magnification (bar at lower left indicates 250µm and 50µm).

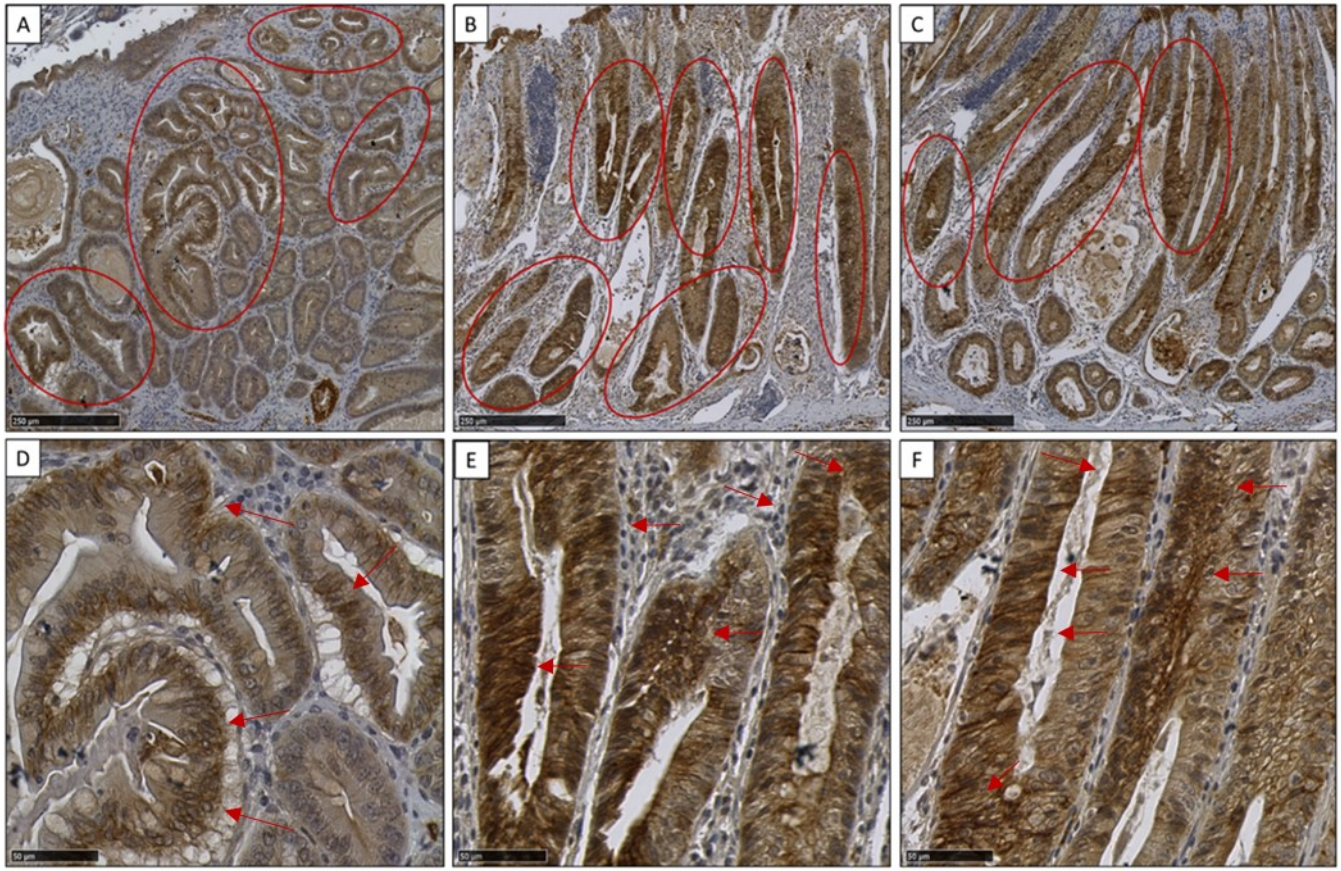

Figure 6.73: Representative images of immunohistochemical analysis of β-catenin protein expression and localisation in intestinal adenomas of *Aldh1b1*$^{-/-}$; *Msh2*$^{flox/-}$; *Lgr5CreERT2*$^{+/-}$; *mTmG*$^{+/-}$mice treated with 20% ethanol in drinking water. Variable areas of positive β-catenin nuclear immunostaining in adenomatous cells were observed in both caecal adenomas (A) and colonic adenomas (B&C), indicated by the red ovals. Selected areas (red ovals) within images in panels A-C are further magnified in panels D-F, and clusters of cells with nuclei positive for β-catenin are indicated by the red arrows. Images taken from sections scanned using the Hamamatsu Nanozoomer and analysed with the Hamamatsu NDP Viewer software at 10X and 40X magnification (bar at lower left indicates 250µm and 50µm).

6.5.2.4 DNA damage response evaluation by immunohistochemistry of *Aldh1b1* conditional-knockout Msh2-LS and *Aldh1b1* constitutive-knockout Msh2-LS murine small intestinal and colonic tissues

6.5.2.4.1 DNA damage response evaluation by Gamma-H2AX immunostaining of *Aldh1b1* conditional-knockout Msh2-LS murine small intestinal and colonic tissues

In order to evaluate the presence and extent of DNA damage, y-H2AX immunostaining was used. We used colonic tissue samples from WT mice and TMZ-treated Msh2-LS mice as negative and positive y-H2AX expression controls, respectively. Details of the negative and positive y-H2AX expression controls can be found in Chapter 4 (4.4.2.4.1; Figure 4.43). IHC analysis of y-H2AX showed large and significant differences in the number of intestinal y-H2AX-positive cells between the EtOH_*Aldh1b1*$^{fl/fl}$_*Msh2*$^{fl\ KO}$ murine colon and the H_2O_*Aldh1b1*$^{fl/fl}$_*Msh2*$^{fl\ KO}$ murine colon (Figure 6.74). The percentage of y-H2AX-positive cells per crypt was significantly higher in EtOH_*Aldh1b1*$^{fl/fl}$_*Msh2*$^{fl\ KO}$ mice (38.7%) compared with H_2O_*Aldh1b1*$^{fl/fl}$_*Msh2*$^{fl\ KO}$ mice (0.5%) (Figure 6.74), consistent with ethanol/acetaldehyde induced DNA damage. The comparative analysis of SI y-H2AX expression between EtOH_*Aldh1b1*$^{fl/fl}$_*Msh2*$^{fl\ KO}$ and H_2O_*Aldh1b1*$^{fl/fl}$_*Msh2*$^{fl\ KO}$ mice didn't show any differences, as EtOH_*Aldh1b1*$^{fl/fl}$_*Msh2*$^{fl\ KO}$ and H_2O_*Aldh1b1*$^{fl/fl}$_*Msh2*$^{fl\ KO}$ murine SI showed no y-H2AX-positive cells (Figure 6.75). EtOH_*Aldh1b1*$^{fl/fl}$_*Msh2*$^{fl\ KO}$ Msh2-LS murine large intestinal adenomas, both colonic and caecal, showed high levels of y-H2AX expression (Figure 6.76).

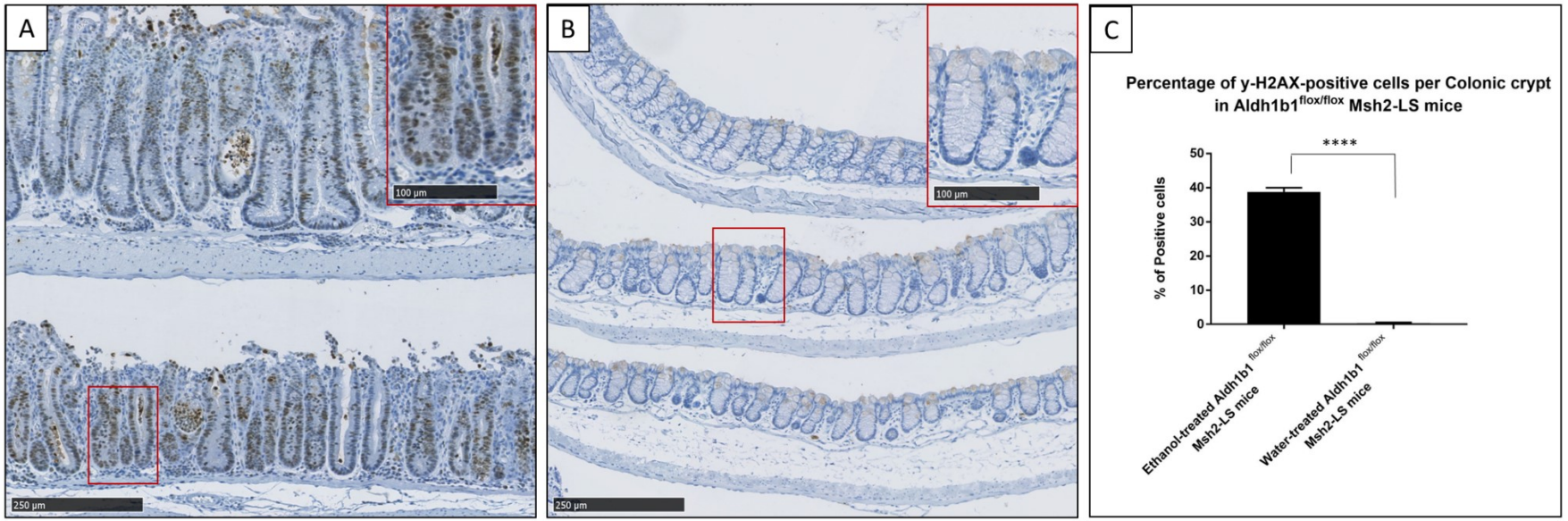

Figure 6.74: Immunohistochemical analysis of y-H2AX protein expression in large intestinal mucosal epithelium of *Aldh1b1*$^{flox/flox}$*; Msh2*$^{flox/-}$*; Lgr5CreERT2*$^{+/-}$*; mTmG*$^{+/-}$ mice treated with either 20% ethanol in drinking water (A) or normal/standard water (B). Gamma-H2AX-positive cells in colonic crypts (further magnified in the upper right inset red rectangle in figure panel A) were observed in ethanol-treated *Aldh1b1*$^{flox/flox}$ Msh2-LS (EtOH_*Aldh1b1*$^{fl/fl}$_*Msh2*$^{fl\ KO}$) mice but not in water-treated *Aldh1b1*$^{flox/flox}$ Msh2-LS (H_2O_*Aldh1b1*$^{fl/fl}$_*Msh2*$^{fl\ KO}$) mice (further magnified in the upper right inset red rectangle in figure panel B). Numbers of y-H2AX-positive cells per colonic crypt were counted using QuPath to calculate the percentage of y-H2AX-positive cells (C) and these showed a large and statistically significant difference. Paired Students t-Test, ****p<0.0001 vs. water (data shown as mean±SD, 40 crypts per mouse were analysed, n=4 mice in each group). Images taken from sections scanned using the Hamamatsu Nanozoomer and analysed with the Hamamatsu NDP Viewer software at 10X and 20X magnification (bar at lower left indicates 250µm, bar in red rectangle indicates 100µm).

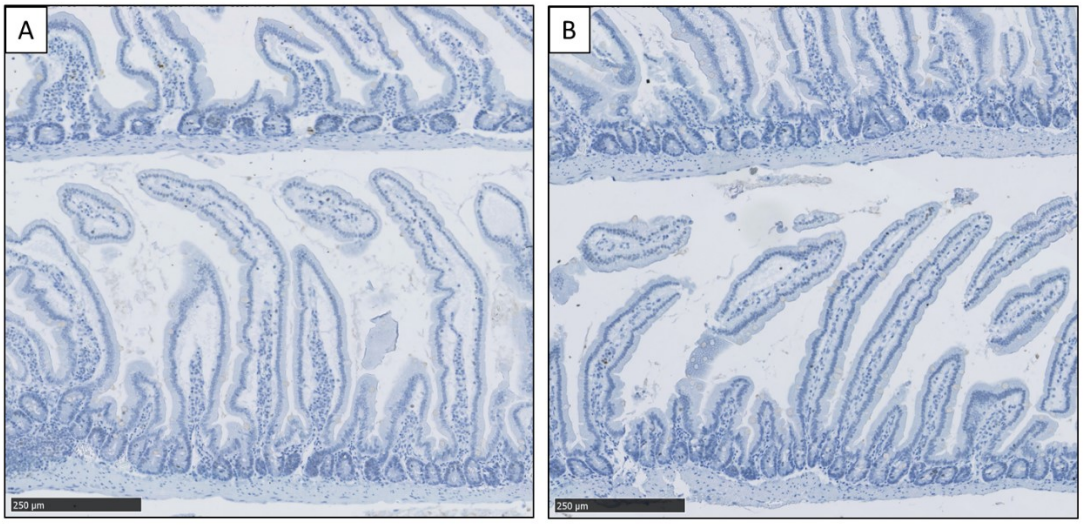

Figure 6.75: Immunohistochemical analysis of y-H2AX protein expression in small intestinal mucosa of *Aldh1b1*$^{flox/flox}$*; Msh2*$^{flox/-}$*; Lgr5CreERT2*$^{+/-}$*; mTmG*$^{+/-}$mice treated with either 20% ethanol in drinking water (A) or normal / standard drinking water (B). No y-H2AX-positive cells were observed in either sample. Images taken from sections scanned using the Hamamatsu Nanozoomer and analysed with the Hamamatsu NDP Viewer software at 10X magnification (bar at lower left indicates 250µm).

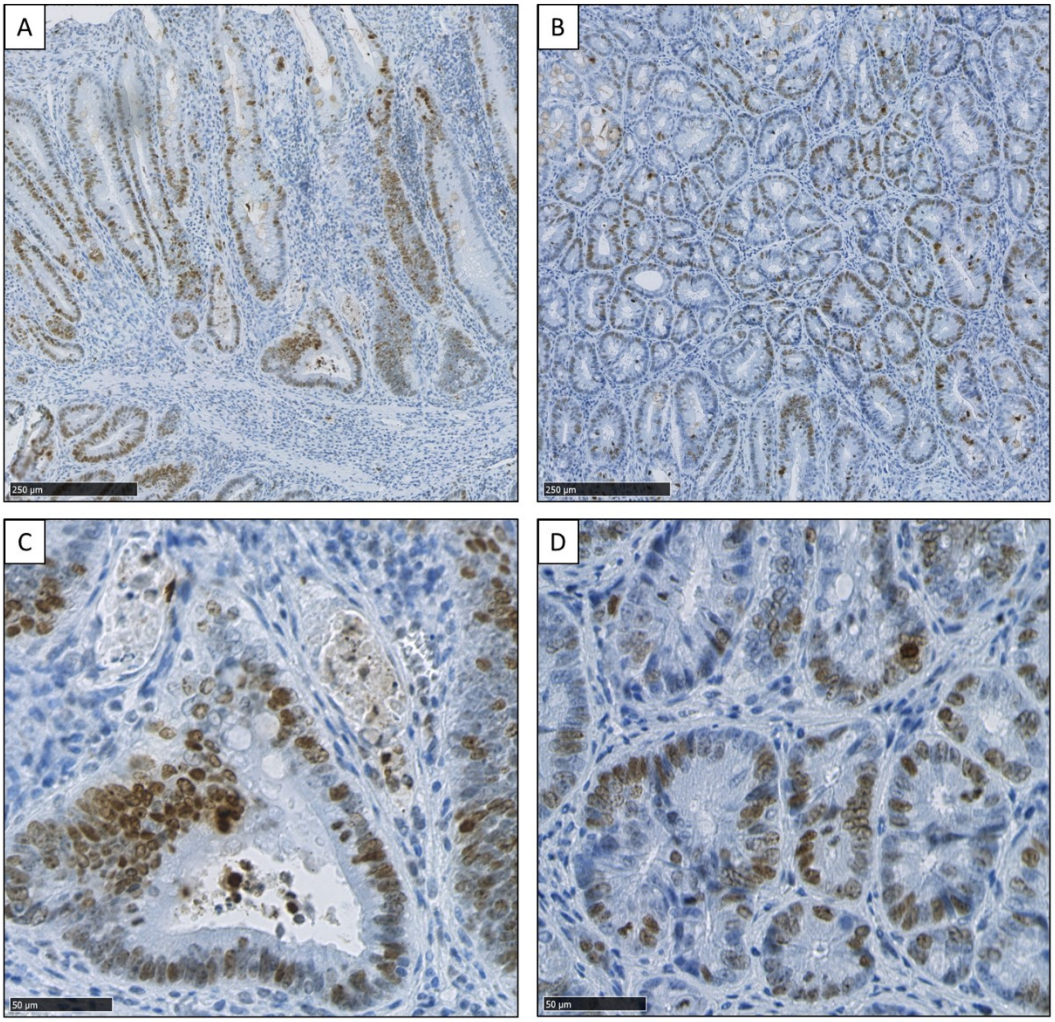

Figure 6.76: Representative images of y-H2AX immunohistochemical staining in a large intestinal adenoma (A) and a caecal adenoma (B) from 2 ethanol-treated *Aldh1b1*$^{flox/flox}$; *Msh2*$^{flox/-}$; *Lgr5CreERT2*$^{+/-}$; *mTmG*$^{+/-}$ mice. In both examples, there are numerous y-H2AX-positive cells within the regions of dysplastic cells in the adenomas. Images are further magnified in panels C and D. Images taken from sections scanned using the Hamamatsu Nanozoomer and analysed with the Hamamatsu NDP Viewer software at 10X and 40X magnification (bar at lower left indicates 250µm and 50 µm).

6.5.2.4.2 DNA damage response evaluation by Gamma-H2AX immunostaining of *Aldh1b1* constitutive-knockout Msh2-LS murine small intestinal and colonic tissues

Details of the negative and positive y-H2AX IHC expression controls can be found in Chapter 4 (4.4.2.4.1; Figure 4.43). IHC analysis of y-H2AX showed large and significant differences in the number of intestinal y-H2AX-positive cells between the EtOH_*Aldh1b1*$^{-/-}$_*Msh2*$^{fl\ KO}$ murine colon and the H_2O_*Aldh1b1*$^{-/-}$_*Msh2*$^{fl\ KO}$ murine colon (Figure 6.77). The percentage of y-H2AX-positive cells per crypt was significantly higher in EtOH_*Aldh1b1*$^{-/-}$_*Msh2*$^{fl\ KO}$ mice (46%) compared with H_2O_*Aldh1b1*$^{-/-}$_*Msh2*$^{fl\ KO}$ mice (0.5%) (Figure 6.77), consistent with ethanol/acetaldehyde induced DNA damage. The percentage of SI y-H2AX-positive cells was higher in EtOH_*Aldh1b1*$^{-/-}$_Msh2$^{fl\ KO}$ mice (3.4%) compared with H_2O_*Aldh1b1*$^{-/-}$_*Msh2*$^{fl\ KO}$ mice (0.1%) (Figure 6.78). EtOH_*Aldh1b1*$^{-/-}$_*Msh2*$^{fl\ KO}$ murine large intestinal adenomas, both colonic and caecal, showed high levels of y-H2AX expression (Figure 6.79).

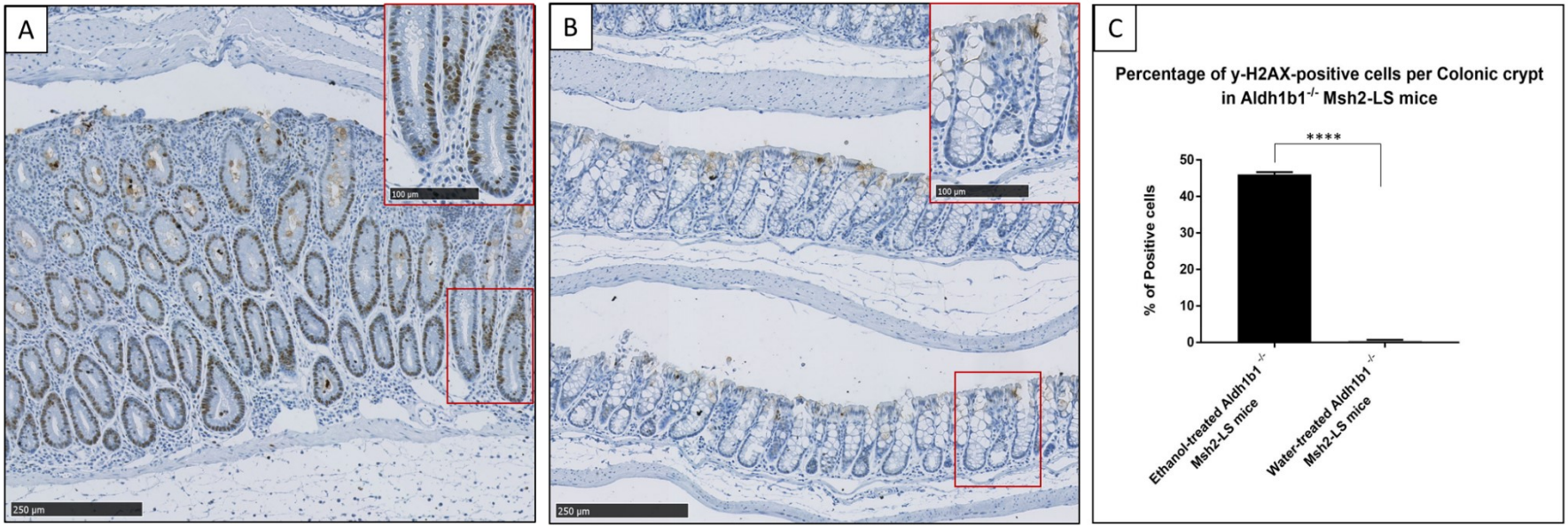

Figure 6.77: Immunohistochemical analysis of y-H2AX protein expression in large intestinal mucosal epithelium of *Aldh1b1*$^{-/-}$*; Msh2*$^{flox/-}$*; Lgr5CreERT2*$^{+/-}$*; mTmG*$^{+/-}$mice treated with either 20% ethanol in drinking water (A) or normal/standard water (B). Gamma-H2AX-positive cells in colonic crypts (further magnified in the upper right inset red rectangle in figure panel A) were observed in ethanol-treated *Aldh1b1*$^{-/-}$ Msh2-LS (EtOH_*Aldh1b1*$^{-/-}$_*Msh2*$^{fl\ KO}$) mice but not in water-treated *Aldh1b1*$^{-/-}$ Msh2-LS (H_2O_*Aldh1b1*$^{-/-}$_*Msh2*$^{fl\ KO}$) mice (further magnified in the upper right inset red rectangle in figure panel B). Numbers of y-H2AX-positive cells per colonic crypt were counted using QuPath to calculate the percentage of y-H2AX-positive cells (C) and these showed a large and statistically significant difference. Paired Students t-Test, ****p<0.0001 vs. water (data shown as mean±SD, 40 crypts per mouse were analysed, n=4 mice in each group). Images taken from sections scanned using the Hamamatsu Nanozoomer and analysed with the Hamamatsu NDP Viewer software at 10X and 20X magnification (bar at lower left indicates 250µm, bar in red rectangle indicates 100µm).

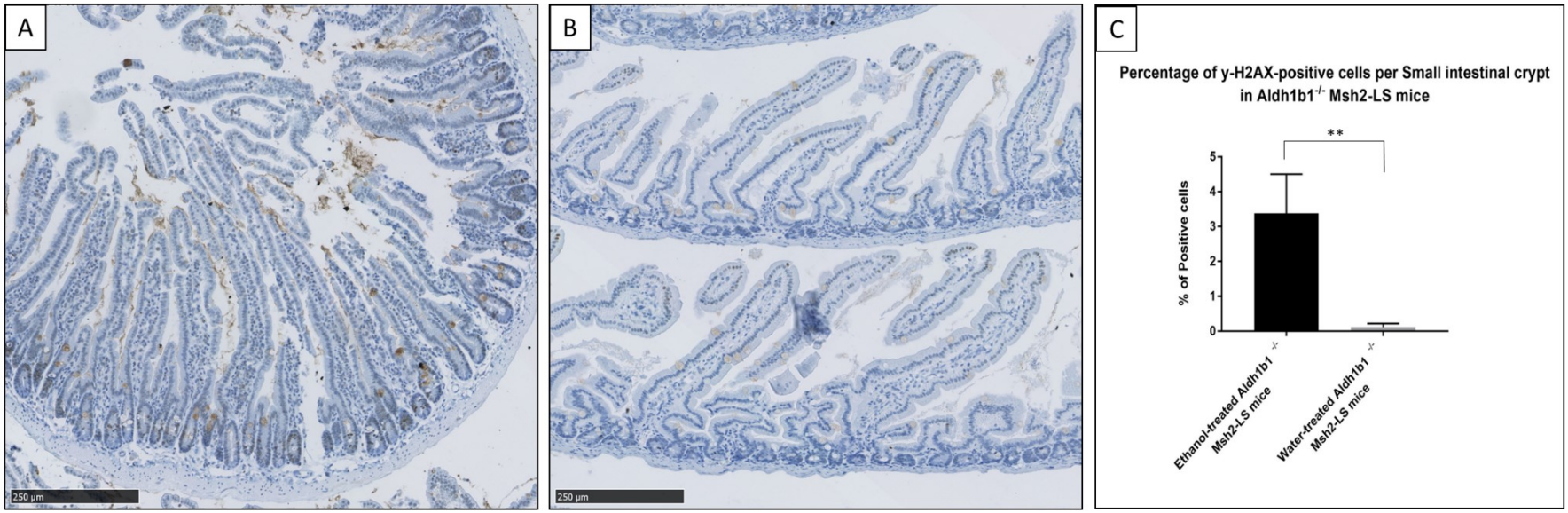

Figure 6.78: Immunohistochemical analysis of y-H2AX protein expression in small intestinal mucosal epithelium of *Aldh1b1*$^{-/-}$*; Msh2*$^{flox/-}$*; Lgr5CreERT2*$^{+/-}$*; mTmG*$^{+/-}$mice treated with either 20% ethanol in drinking water (A) or normal/standard water (B). Gamma-H2AX-positive cells in small intestinal crypts (further magnified in the upper right inset red rectangle in figure panel A) were observed in ethanol-treated *Aldh1b1*$^{-/-}$ Msh2-LS (EtOH_*Aldh1b1*$^{-/-}$_*Msh2*$^{fl\ KO}$) mice but not in water-treated *Aldh1b1*$^{-/-}$ Msh2-LS (H_2O_*Aldh1b1*$^{-/-}$_*Msh2*$^{fl\ KO}$) mice (further magnified in the upper right inset red rectangle in figure panel B). Numbers of y-H2AX-positive cells per small intetsinal crypt were counted using QuPath to calculate the percentage of y-H2AX-positive cells (C) and these showed a large and statistically significant difference. Paired Students t-Test, **p<0.0012 vs. water (data shown as mean±SD, 40 crypts per mouse were analysed, n=4 mice in each group). Images taken from sections scanned using the Hamamatsu Nanozoomer and analysed with the Hamamatsu NDP Viewer software at 10X and 20X magnification (bar at lower left indicates 250µm, bar in red rectangle indicates 100µm).

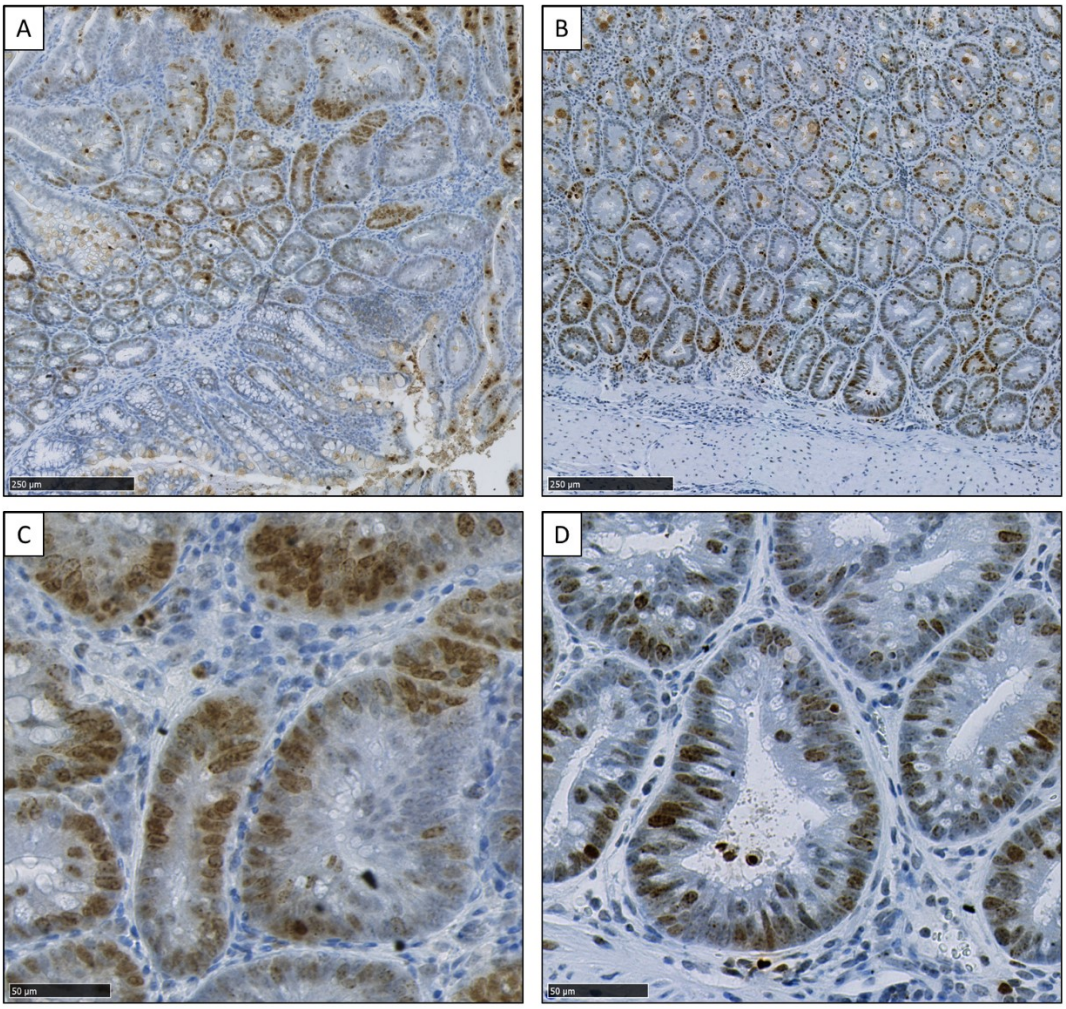

Figure 6.79: Representative images of y-H2AX immunohistochemical staining in a caecal adenoma (A) and a large intestinal adenoma (B) from 2 ethanol-treated *Aldh1b1*$^{-/-}$; *Msh2*$^{flox/-}$; *Lgr5CreERT2*$^{+/-}$; *mTmG*$^{+/-}$ mice. In both examples, there are numerous y-H2AX-positive cells within the regions of dysplastic cells in the adenomas. Images are further magnified in panels C and D. Images taken from sections scanned using the Hamamatsu Nanozoomer and analysed with the Hamamatsu NDP Viewer software at 10X and 40X magnification (bar at lower left indicates 250µm and 50 µm).

6.5.2.4.3 DNA damage response evaluation by p53 immunostaining of *Aldh1b1* conditional-knockout Msh2-LS murine small intestinal and colonic tissues

As reported in Chapter 4 (4.4.2.4.2), p53 IHC was performed to detect activation of DNA damage response mechanisms (referred as p53 "wildtype pattern") (Köbel et al., 2016; Lakin & Jackson, 1999). We used colonic tissue samples from WT mice and TMZ-treated Msh2-LS mice as p53-wildtype and p53-positive expression (resulting from TMZ-induced DNA damage) controls, respectively. Details of the wildtype and positive p53 expression controls can be found in Chapter 4 (4.4.2.4.2, Figure 4.47).

In *Aldh1b1*$^{flox/flox}$ Msh2-LS mice, IHC analysis of p53 showed large and significant differences in the number of intestinal p53-positive cells between the EtOH_*Aldh1b1*$^{fl/fl}$_*Msh2*$^{fl\ KO}$ murine colon and the H_2O_*Aldh1b1*$^{fl/fl}$_*Msh2*$^{fl\ KO}$ murine colon (Figure 6.80). The percentage of cells with either moderate or high levels of p53-positive nuclear staining per crypt was significantly higher in EtOH_*Aldh1b1*$^{fl/fl}$_*Msh2*$^{fl\ KO}$ mice (52.7%) compared with H_2O_*Aldh1b1*$^{fl/fl}$_*Msh2*$^{fl\ KO}$ mice (6.3%) (Figure 6.80), consistent with an ethanol/acetaldehyde induced DNA damage response.

The percentage of small intestinal p53-positive cells per crypt was higher in EtOH_*Aldh1b1*$^{fl/fl}$_*Msh2*$^{fl\ KO}$ mice (21.7%) compared with H_2O_*Aldh1b1*$^{fl/fl}$_*Msh2*$^{fl\ KO}$ mice (3.3%) (Figure 6.81). EtOH_*Aldh1b1*$^{fl/fl}$_*Msh2*$^{fl\ KO}$ murine large intestinal adenomas, both colonic and caecal, showed high percentages of p53-positive cells, with variably moderate to marked nuclear p53 positivity with some surrounding or mixed cells showing p53-negative nuclei in a "p53 wildtype" pattern, indicative of a widespread response to DNA damage, rather than a "p53 overexpression" or "null" pattern associated with p53 mutation (Figure 6.82).

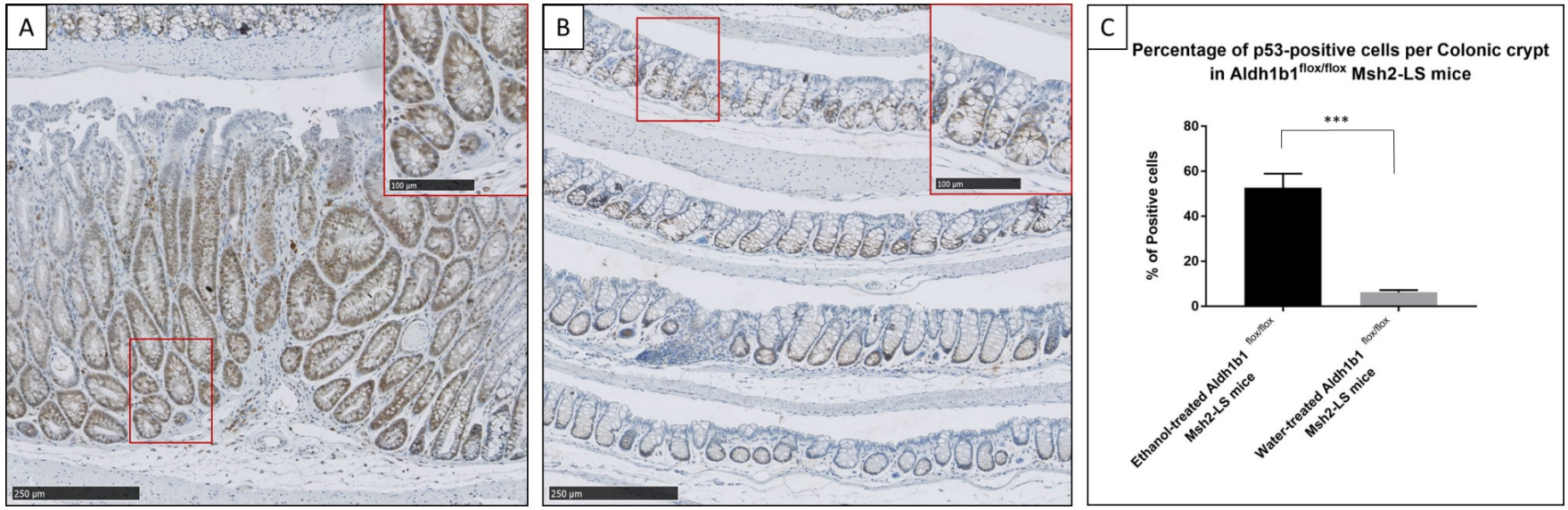

Figure 6.80: Representative images of immunohistochemical analysis of p53 protein expression in large intestinal mucosal epithelium of *Aldh1b1*$^{flox/flox}$*; Msh2*$^{flox/-}$*; Lgr5CreERT2*$^{+/-}$*; mTmG*$^{+/-}$mice treated with either 20% ethanol in drinking water (A) or normal/standard water (B). The percentage of positive p53-positive nuclei in colonic crypts in ethanol-treated *Aldh1b1*$^{flox/flox}$ Msh2-LS (EtOH_*Aldh1b1*$^{fl/fl}$_*Msh2*$^{fl\ KO}$) mice (further magnified in the upper right inset red rectangle in figure panel A) was higher compared with water-treated *Aldh1b1*$^{flox/flox}$ Msh2-LS (H_2O_*Aldh1b1*$^{fl/fl}$_*Msh2*$^{fl\ KO}$) mice (further magnified in the upper right inset red rectangle in figure panel B). Numbers of cells with positive p53 nuclear staining per colonic crypt were counted using QuPath to calculate the percentage of p53-positive cells (C) and these showed a statistically significant difference. Paired Students t-Test, ***p<0.0002 vs. water (data shown as mean±SD, 40 crypts per mouse were analysed, n=4 mice in each group). Images taken from sections scanned using the Hamamatsu Nanozoomer and analysed with the Hamamatsu NDP Viewer software at 10X and 20X magnification (bar at lower left indicates 250µm, bar in red rectangle indicates 100µm).

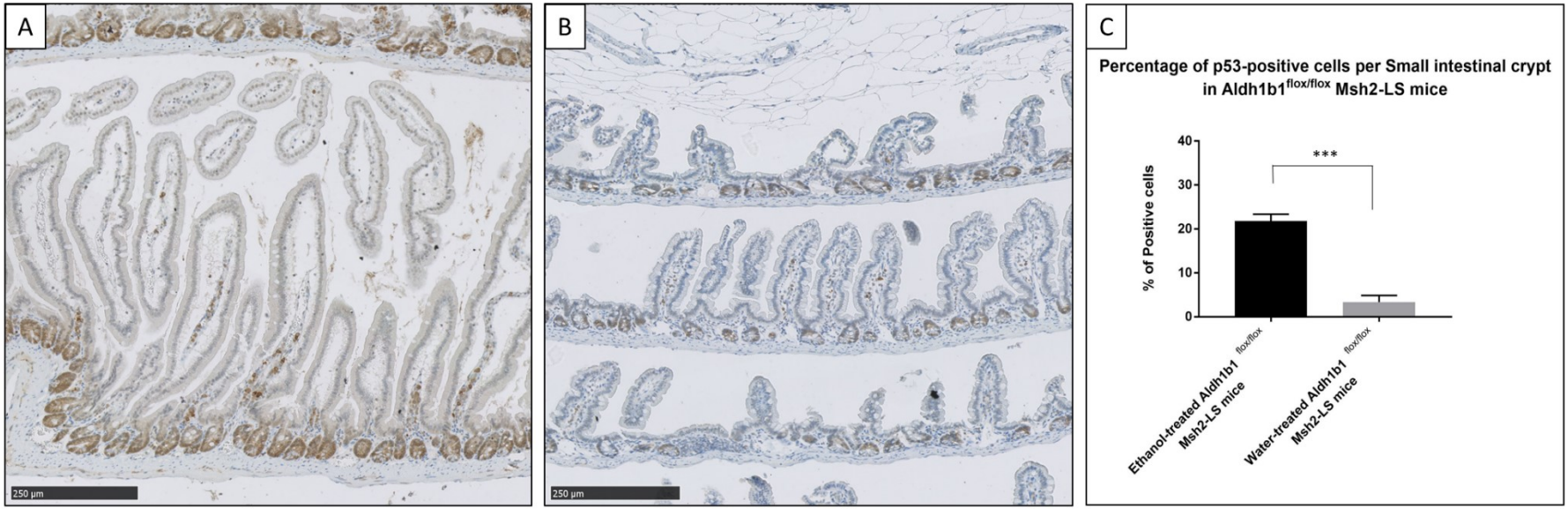

Figure 6.81: Representative images of immunohistochemical analysis of p53 protein expression in small intestinal mucosal epithelium of *Aldh1b1*$^{flox/flox}$*; Msh2*$^{flox/-}$*; Lgr5CreERT2*$^{+/-}$*; mTmG*$^{+/-}$mice treated with either 20% ethanol in drinking water (A) or normal/standard water (B). The percentage of positive p53-nuclear stained cells in small intestinal crypts was higher in ethanol-treated *Aldh1b1*$^{flox/flox}$ Msh2-LS (EtOH_*Aldh1b1*$^{fl/fl}$_*Msh2*$^{fl\ KO}$) mice compared with water-treated *Aldh1b1*$^{flox/flox}$ Msh2-LS (H_2O_*Aldh1b1*$^{fl/fl}$_*Msh2*$^{fl\ KO}$) mice. Numbers of cells with positive p53 nuclear staining per small intestinal crypt were counted using QuPath to calculate the percentage of p53-positive cells (C) and these showed a statistically significant difference. Paired Students t-Test, ***p<0.0001 vs. water (data shown as mean±SD, 40 crypts per mouse were analysed, n=4 mice in each group). Images taken from sections scanned using the Hamamatsu Nanozoomer and analysed with the Hamamatsu NDP Viewer software at 10X magnification (bar at lower left indicates 250µm).

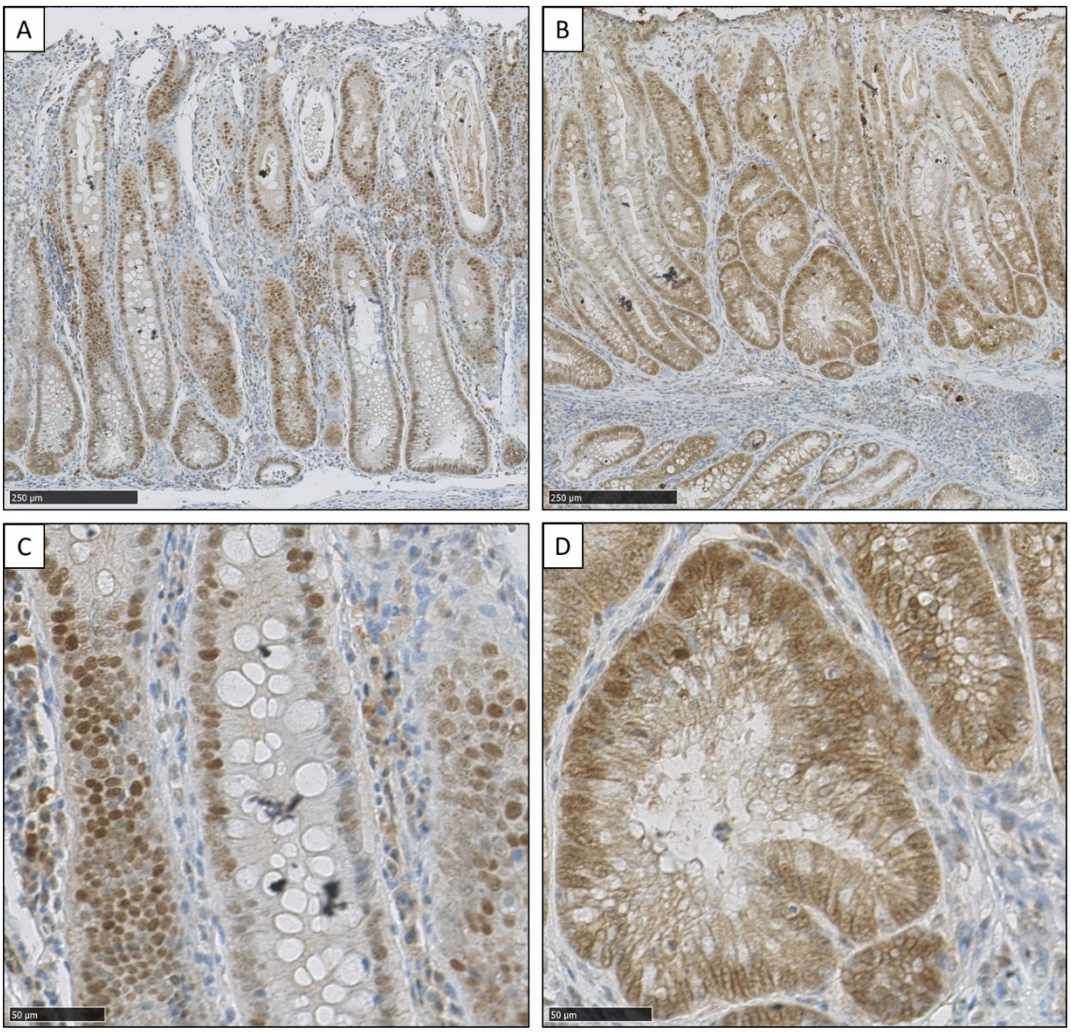

Figure 6.82: Representative images of p53 immunohistochemical staining in a colonic adenoma (A and C) and a caecal adenoma (B and D), from 2 ethanol-treated *Aldh1b1*$^{flox/flox}$*; Msh2*$^{flox/-}$*; Lgr5CreERT2*$^{+/-}$*; mTmG*$^{+/-}$ mice. In both examples, there are numerous p53-positive nuclei (variably moderate to high p53 nuclear staining with some p53-negative nuclei) within the regions of dysplastic cells in the adenomas. Images taken from sections scanned using the Hamamatsu Nanozoomer and analysed with the Hamamatsu NDP Viewer software at 10X (A and B) and 40X (C and D) magnification (bar at lower left indicates 250µm and 50 µm).

6.5.2.4.4 DNA damage response evaluation by p53 immunostaining of Aldhd1b1 constitutive-knockout Msh2-LS murine small intestinal and colonic tissues

Details of the normal and positive p53 expression controls can be found in Chapter 4 (4.4.2.4.2, Figure 4.47).

In *Aldh1b1*$^{-/-}$ Msh2-LS mice, IHC analysis of p53 showed large and significant differences in the number of intestinal p53-positive cells between the EtOH_*Aldh1b1*$^{-/-}$_*Msh2*$^{fl\ KO}$ murine colon and the H_2O_*Aldh1b1*$^{-/-}$_*Msh2*$^{fl\ KO}$ murine colon (Figure 6.83). The percentage of cells with either moderate or high levels of p53-positive nuclear staining per crypt was significantly higher in EtOH_*Aldh1b1*$^{-/-}$_*Msh2*$^{fl\ KO}$ mice (47.5%) compared with H_2O_*Aldh1b1*$^{-/-}$_*Msh2*$^{fl\ KO}$ mice (3.3%) (Figure 6.83), consistent with ethanol/acetaldehyde induced DNA damage.

The percentage of small intestinal p53-positive cells per crypt was higher in EtOH_*Aldh1b1*$^{-/-}$_*Msh2*$^{fl\ KO}$ mice (20%) compared with H_2O_*Aldh1b1*$^{-/-}$_*Msh2*$^{fl\ KO}$ mice (4%) (Figure 6.84). EtOH_*Aldh1b1*$^{-/-}$_*Msh2*$^{fl\ KO}$ murine large intestinal adenomas, both colonic and caecal, showed high percentages of p53-positive cells, with variably moderate to marked nuclear p53 positivity and some negative nuclei in a “p53 wildtype” pattern, as observed previously in the section 6.5.2.4.3 (Figure 6.85).

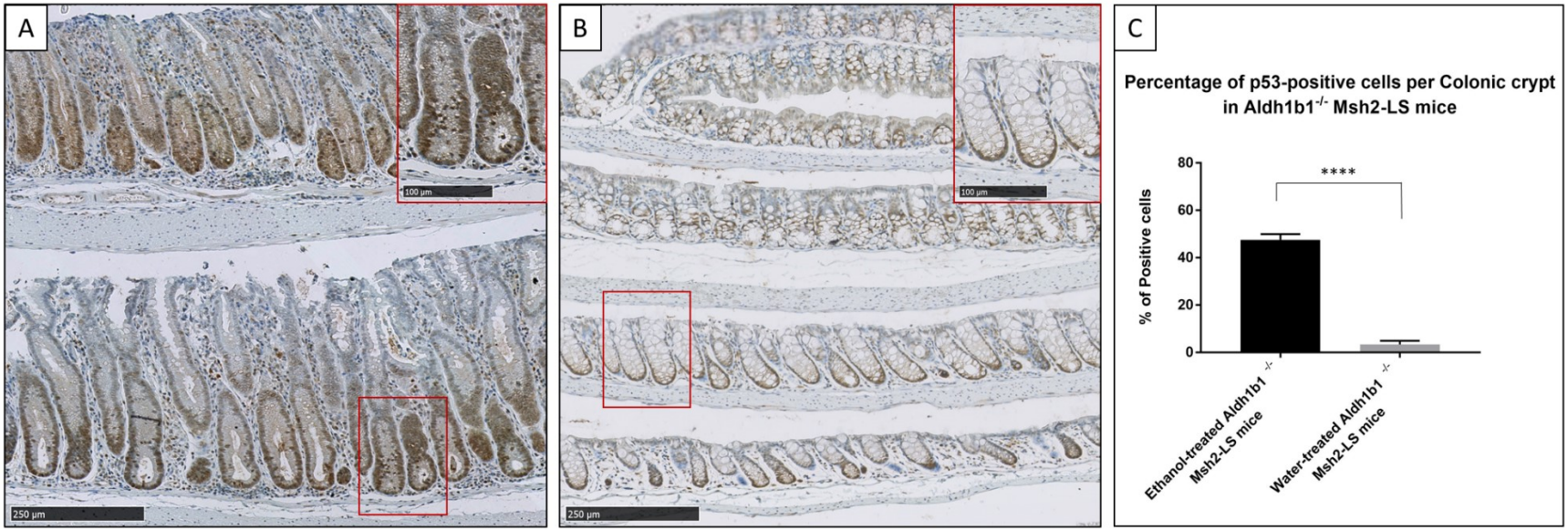

Figure 6.83: Representative images of immunohistochemical analysis of p53 protein expression in large intestinal mucosal epithelium of *Aldh1b1*$^{-/-}$*; Msh2*$^{flox/-}$*; Lgr5CreERT2*$^{+/-}$*; mTmG*$^{+/-}$ mice treated with either 20% ethanol in drinking water (A) or normal/standard water (B). The percentage of p53-positive nuclei in colonic crypts in ethanol-treated *Aldh1b1*$^{-/-}$ Msh2-LS (EtOH_*Aldh1b1*$^{-/-}$_*Msh2*$^{fl\ KO}$) mice (further magnified in the upper right inset red rectangle in figure panel A) was higher compared with water-treated *Aldh1b1*$^{-/-}$ Msh2-LS (H_2O_*Aldh1b1*$^{-/-}$_*Msh2*$^{fl\ KO}$) mice (further magnified in the upper right inset red rectangle in figure panel B). Numbers of cells with positive p53 nuclear staining per colonic crypt were counted using QuPath to calculate the percentage of p53-positive cells (C) and these showed a statistically significant difference. Paired Students t-Test, ****p<0.0001 vs. water (data shown as mean±SD, 40 crypts per mouse were analysed, n=4 mice in each group). Images taken from sections scanned using the Hamamatsu Nanozoomer and analysed with the Hamamatsu NDP Viewer software at 10X and 20X magnification (bar at lower left indicates 250µm, bar in red rectangle indicates 100µm).

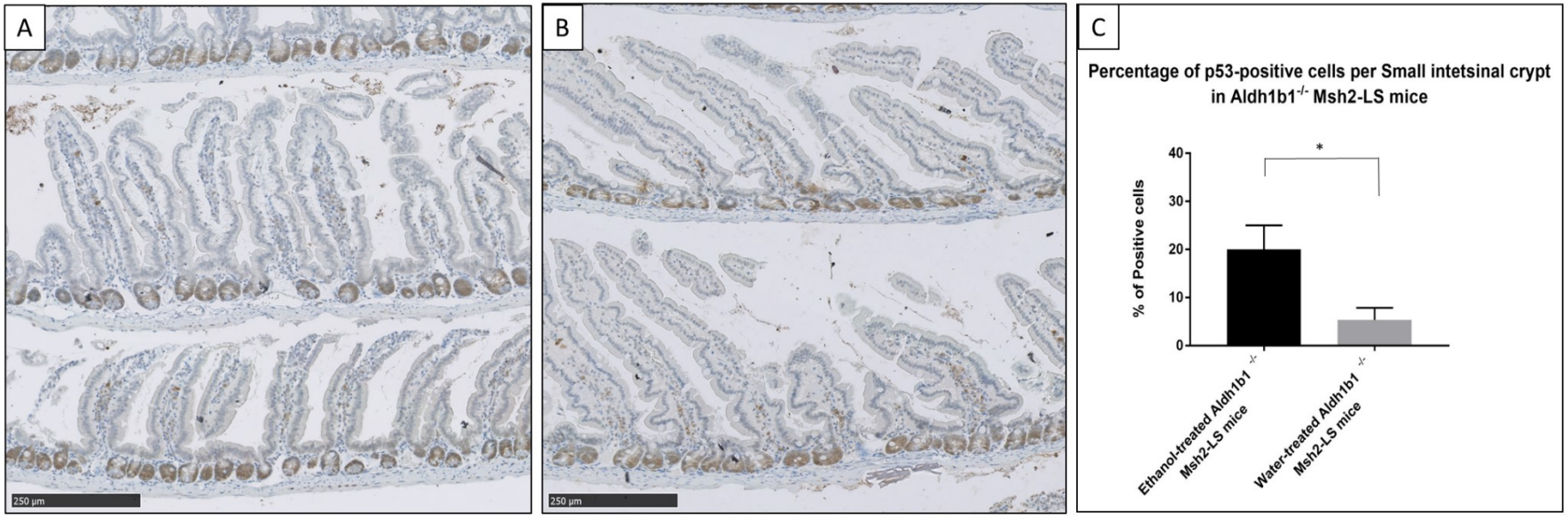

Figure 6.84: Representative images of immunohistochemical analysis of p53 protein expression in small intestinal mucosal epithelium of *Aldh1b1*$^{-/-}$; *Msh2*$^{flox/-}$; *Lgr5CreERT2*$^{+/-}$; *mTmG*$^{+/-}$ mice treated with either 20% ethanol in drinking water (A) or normal/standard water (B). The percentage of positive p53-nuclear stained cells in small intestinal crypts was higher in ethanol-treated *Aldh1b1*$^{-/-}$ Msh2-LS (EtOH_*Aldh1b1*$^{-/-}$_*Msh2*$^{fl\ KO}$) mice compared with water-treated *Aldh1b1*$^{-/-}$ Msh2-LS (H_2O_*Aldh1b1*$^{-/-}$_*Msh2*$^{fl\ KO}$) mice. Numbers of cells with positive p53 nuclear staining per small intestinal crypt were counted using QuPath to calculate the percentage of p53-positive cells (C) and these showed a statistically significant difference. Paired Students t-Test, *p<0.0105 vs. water (data shown as mean±SD, 40 crypts per mouse were analysed, n=4 mice in each group). Images taken from sections scanned using the Hamamatsu Nanozoomer and analysed with the Hamamatsu NDP Viewer software at 10X magnification (bar at lower left indicates 250µm).

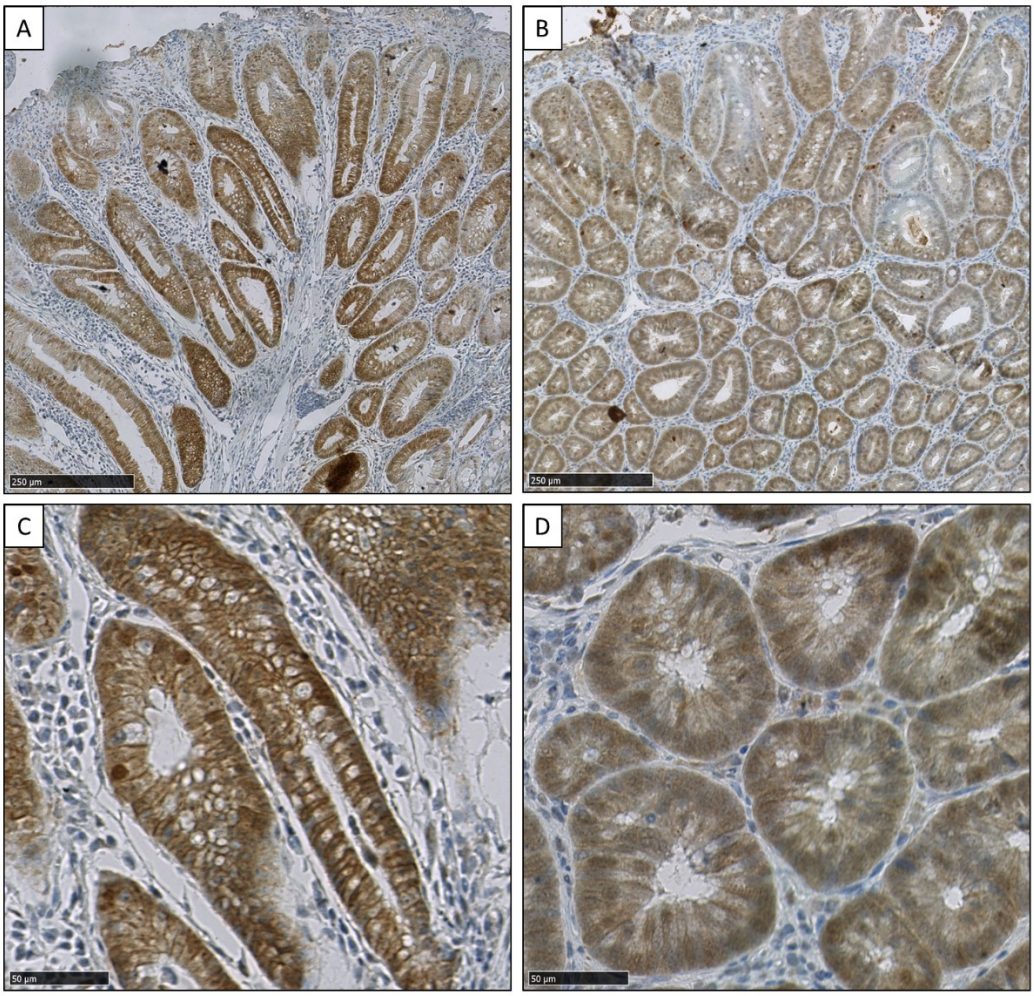

Figure 6.85: Representative images of p53 immunohistochemical staining in a colonic adenoma (A and C) and a caecal adenoma (B and D), from 2 ethanol-treated *Aldh1b1*$^{-/-}$; *Msh2*$^{flox/-}$; *Lgr5CreERT2*$^{+/-}$; *mTmG*$^{+/-}$ mice. In both examples, there are numerous p53-positive nuclei (variably moderate to high p53 nuclear staining with some p53-negative nuclei) within the regions of dysplastic cells in the adenomas. Images taken from sections scanned using the Hamamatsu Nanozoomer and analysed with the Hamamatsu NDP Viewer software at 10X (A and B) and 40X (C and D) magnification (bar at lower left indicates 250µm and 50 µm).

6.5.2.5 Cleaved Caspase-3 immunostaining of *Aldh1b1* conditional-knockout Msh2-LS and *Aldh1b1* constitutive-knockout Msh2-LS murine small intestinal and colonic tissues

Caspase-3 (Cas3) IHC was performed to identify cCas3-positive apoptotic bodies, as explained in Chapter 4 (4.4.2.5). Colonic mucosal tissue samples from WT mice and TMZ-treated Msh2-LS mice were used as negative and positive controls, respectively. Details of the positive and negative controls can be found in Chapter 4 (4.4.2.5; Figure 4.51).

In *Aldh1b1*$^{flox/flox}$ Msh2-LS mice, IHC analysis of cCas3 with quantification of cCas3-positive apoptotic bodies, showed significant differences in the numbers of cCas3-positive apoptotic bodies per 30 colonic crypts per mouse between the EtOH_*Aldh1b1*$^{fl/fl}$_*Msh2*$^{fl\ KO}$ murine colonic epithelium and the H_2O_*Aldh1b1*$^{fl/fl}$_*Msh2*$^{fl\ KO}$ murine colonic epithelium. There were significantly higher numbers of cCas3+ apoptotic bodies in EtOH_*Aldh1b1*$^{fl/fl}$_*Msh2*$^{fl\ KO}$ mice compared with no detectable cCas3+ apoptotic bodies in H_2O_*Aldh1b1*$^{fl/fl}$_*Msh2*$^{fl\ KO}$ mice (Figure 6.86), consistent with increased apoptosis associated with colonic epithelial exposure to ethanol/acetaldehyde. EtOH_*Aldh1b1*$^{fl/fl}$_*Msh2*$^{fl\ KO}$ murine large intestinal adenomas showed no detectable cCas3+ apoptotic bodies, indicating rare to no apoptotic events in dMMR colonic tumours (Figure 6.87).

In *Aldh1b1*$^{-/-}$ Msh2-LS mice, IHC analysis of cCas3 with quantification of cCas3-positive apoptotic bodies, showed significantly higher number of cCas3+ apoptotic bodies in EtOH_*Aldh1b1*$^{-/-}$_*Msh2*$^{fl\ KO}$ mice compared with no detectable cCas3+ apoptotic bodies in H_2O_*Aldh1b1*$^{-/-}$_*Msh2*$^{fl\ KO}$ mice (Figure 6.89), consistent with increased apoptosis associated with colonic epithelial exposure to ethanol/acetaldehyde. EtOH_*Aldh1b1*$^{-/-}$_*Msh2*$^{fl\ KO}$ murine large intestinal adenomas showed no detectable cCas3+ apoptotic bodies, indicating rare to no apoptotic events in dMMR colonic tumours (Figure 6.90). In both *Aldh1b1*$^{flox/flox}$ Msh2-LS mice and *Aldh1b1*$^{-/-}$ Msh2-LS mice, IHC analysis of cCas3 of small intestinal epithelium failed on technical grounds.

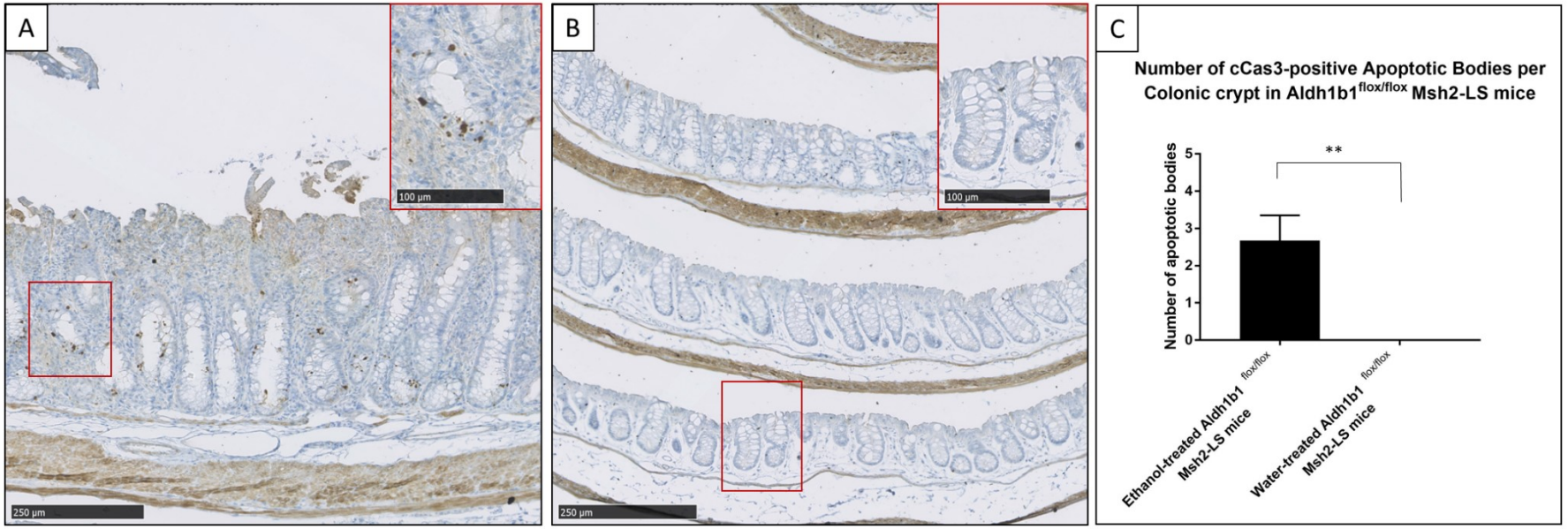

Figure 6.86: Representative images of immunohistochemical analysis of cCas3 in large intestinal mucosal epithelium of induced *Aldh1b1*$^{flox/flox}$*; Msh2*$^{flox/-}$*; Lgr5CreERT2*$^{+/-}$*; mTmG*$^{+/-}$ mice treated with either 20% ethanol in drinking water (A), or normal/standard water (B). The number of apoptotic bodies positive for cCas3 in the colonic crypts of ethanol-treated *Aldh1b1*$^{flox/flox}$ Msh2-LS (EtOH_*Aldh1b1*$^{fl/fl}$_*Msh2*$^{fl\ KO}$) mice (further magnified in the upper right inset red rectangle in figure panel A) was significantly higher compared with that for water-treated *Aldh1b1*$^{flox/flox}$ Msh2-LS (H_2O_*Aldh1b1*$^{fl/fl}$_*Msh2*$^{fl\ KO}$) mice, in which no apoptotic bodies were detected (further magnified in the upper right inset red rectangle in figure panel B). Numbers of cCas3-positive apoptotic bodies per colonic crypt were counted manually (C), showing a statistically significant difference. Paired Students t-Test, **p=0.0024 vs. water (data shown as mean±SD, 30 crypts per mouse were analysed, n=3 mice in each group). Images taken from sections scanned using the Hamamatsu Nanozoomer and analysed with the Hamamatsu NDP Viewer software at 10X and 20X magnification (bar at lower left indicates 250µm, bar in red rectangle indicates 100µm).

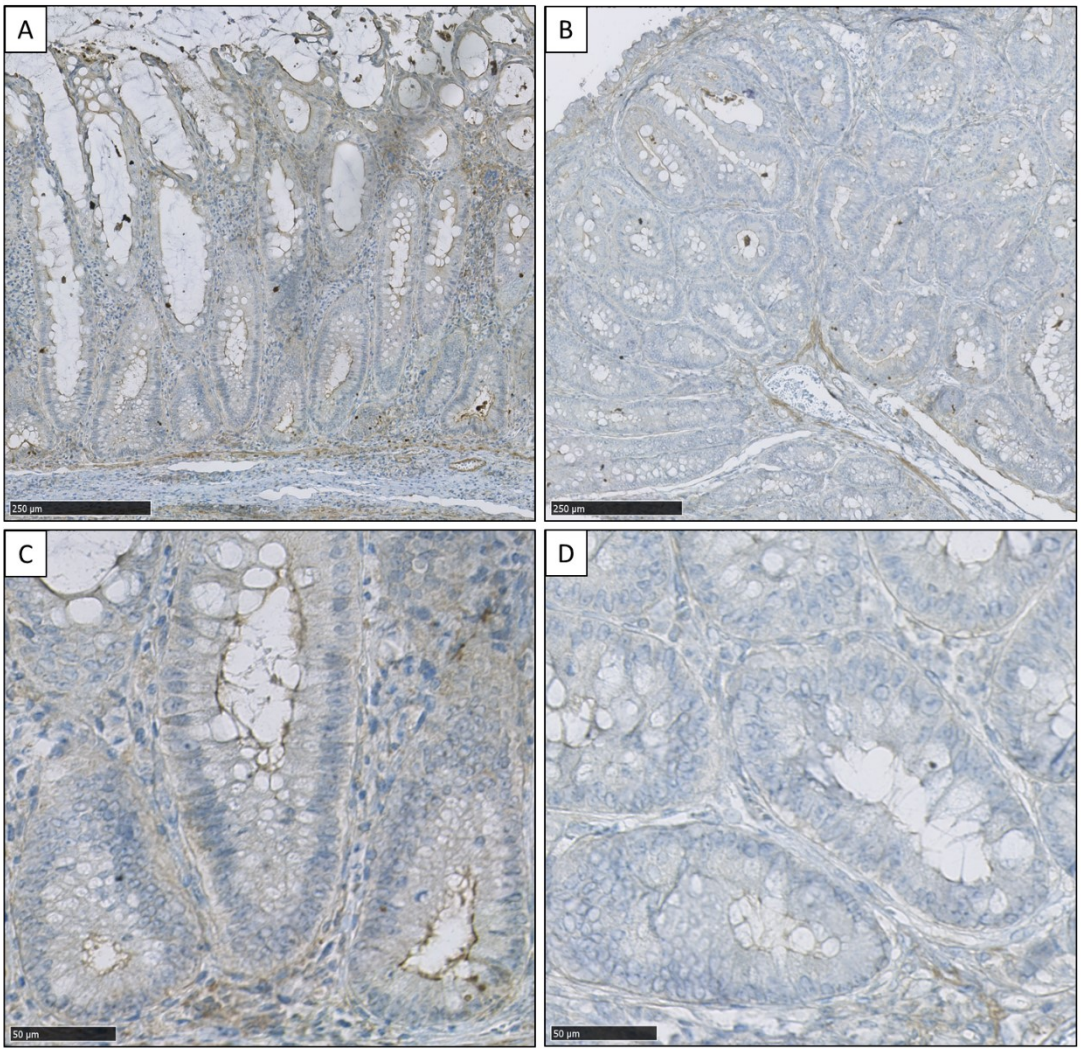

Figure 6.87: Representative images of immunohistochemical analysis of cCas3 in a large intestinal adenoma (A and C) and a caecal adenoma (B and D), from 2 ethanol-treated *Aldh1b1*$^{flox/flox}$*; Msh2*$^{flox/-}$*; Lgr5CreERT2*$^{+/-}$*; mTmG*$^{+/-}$ mice. In both examples, there are almost no apoptotic bodies within the regions of dysplastic cells in the adenomas, indicating rare apoptotic events detectable in dMMR colonic adenomas. Images taken from sections scanned using the Hamamatsu Nanozoomer and analysed with the Hamamatsu NDP Viewer software at 10X (A and B) and 40X (C and D) magnification (bar at lower left indicates 250µm and 50 µm).

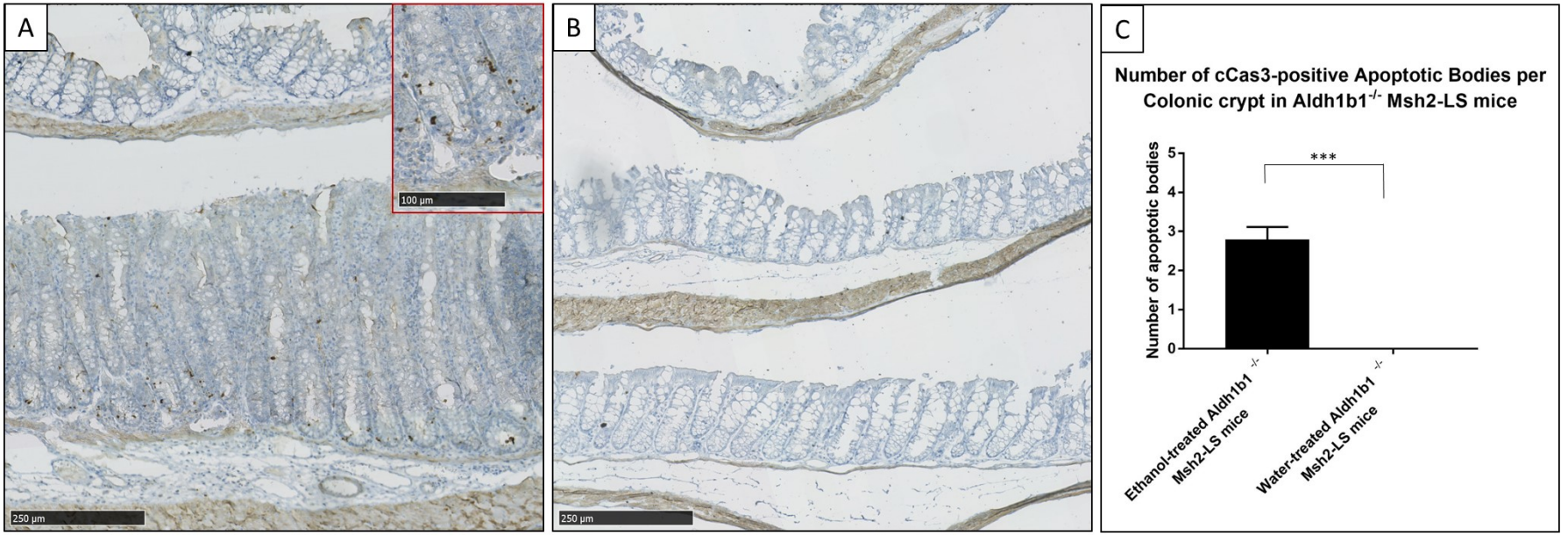

Figure 6.88: Representative images of immunohistochemical analysis of cCas3 in large intestinal mucosal epithelium of induced *Aldh1b1*$^{-/-}$*; Msh2*$^{flox/-}$*; Lgr5CreERT2*$^{+/-}$*; mTmG*$^{+/-}$mice treated with either 20% ethanol in drinking water (A), or normal/standard water (B). The number of apoptotic bodies positive for cCas3 in the hyperproliferative colonic crypts of ethanol-treated *Aldh1b1*$^{-/-}$ Msh2-LS (EtOH_*Aldh1b1*$^{-/-}$_*Msh2*$^{fl\ KO}$) mice (further magnified in the upper right inset red rectangle in figure panel A) was significantly higher compared with the colonic epithelium of water-treated *Aldh1b1*$^{-/-}$ Msh2-LS (H_2O_*Aldh1b1*$^{-/-}$_*Msh2*$^{fl\ KO}$) mice, in which no apoptotic bodies were detected (further magnified in the upper right inset red rectangle in figure panel B). Numbers of cCas3-positive apoptotic bodies per colonic crypt were counted manually (C), showing a statistically significant difference. Paired Students t-Test, ***p=0.0001 vs. water (data shown as mean±SD, 30 crypts per mouse were analysed, n=3 mice in each group). Images taken from sections scanned using the Hamamatsu Nanozoomer and analysed with the Hamamatsu NDP Viewer software at 10X and 20X magnification (bar at lower left indicates 250µm, bar in red rectangle indicates 100µm).

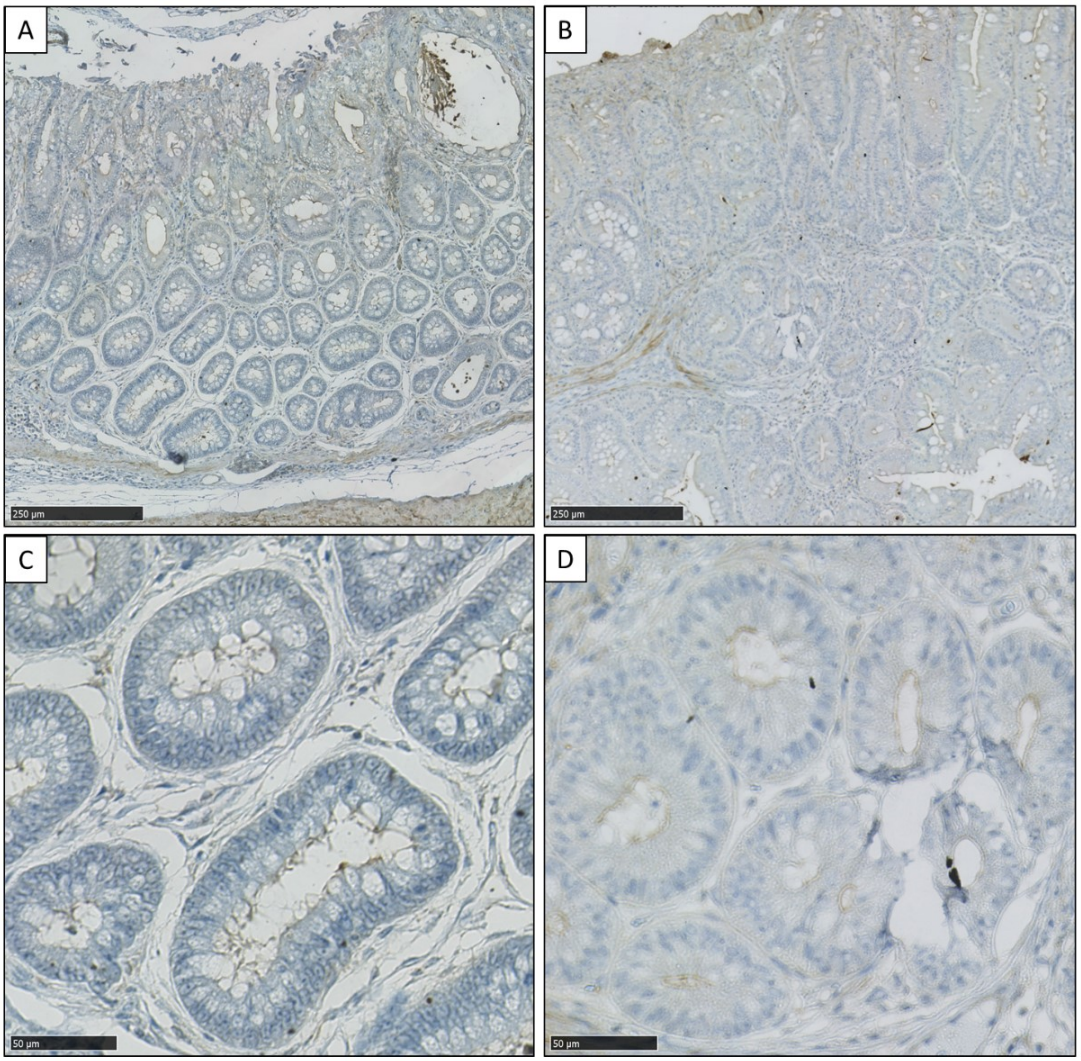

Figure 6.89: Representative images of immunohistochemical analysis of cCas3 in a large intestinal adenoma (A and C) and a caecal adenoma (B and D), from 2 ethanol-treated *Aldh1b1*$^{-/-}$; *Msh2*$^{flox/-}$; *Lgr5CreERT2*$^{+/-}$; *mTmG*$^{+/-}$ mice. In both examples, there are almost no apoptotic bodies within the regions of dysplastic cells in the adenomas, indicating rare apoptotic events detectable in dMMR colonic adenomas. Images taken from sections scanned using the Hamamatsu Nanozoomer and analysed with the Hamamatsu NDP Viewer software at 10X (A and B) and 40X (C and D) magnification (bar at lower left indicates 250µm and 50 µm).

6.6 Plasma acetaldehyde concentrations from the *Aldh1b1* conditional-knockout Msh2-LS and *Aldh1b1* constitutive-knockout Msh2-LS mouse models with and without ethanol treatment

6.6.1 Methods

During the necropsy dissection procedure, blood was taken from the Aldh1b1 conditional-knockout Msh2-LS and Aldh1b1 constitutive-knockout Msh2-LS mice by post-mortem cardiac puncture. Blood was collected in heparinized tubes, which were centrifuged at 3000 X g for 15 min at 4◦C to allow blood fractionation. Acetaldehyde is a highly volatile compound, classified as a VOC (Missia et al., 2010; Sarigiannis et al., 2011). To preserve the acetaldehyde concentration, plasma was collected in cryo-tubes and immediately snap-frozen in liquid nitrogen and stored at −80◦C until analysis. Plasma samples were analysed in a single batch and plasma acetaldehyde concentrations were determined using an enzymatic acetaldehyde assay kit (K-ACHYD; Megazyme), as described in Materials and Methods.

6.6.2 Results

In *Aldh1b1*$^{flox/flox}$ Msh2-LS mice, plasma acetaldehyde levels were analysed comparing samples from EtOH_*Aldh1b1*$^{fl/fl}$_*Msh2*$^{fl\ KO}$ mice and H_2O_*Aldh1b1*$^{fl/fl}$_*Msh2*$^{fl\ KO}$ mice, as well as comparing these with EtOH_*Aldh1b1*$^{fl/fl}$_*Msh2*^{fl} mice and H_2O_*Aldh1b1*$^{fl/fl}$_*Msh2*^{fl} mice, after long-term ethanol or water treatment (experimental mice were treated with ethanol for between 10 and 52 weeks prior to sacrifice).

Plasma acetaldehyde levels were statistically significantly higher in EtOH_*Aldh1b1*$^{fl/fl}$_*Msh2*$^{fl\ KO}$ mice compared with H_2O_*Aldh1b1*$^{fl/fl}$_*Msh2*$^{fl\ KO}$ mice (p=0.0019, Mann-Whitney U-test) (Figure 6.90). The difference in plasma acetaldehyde levels between H_2O_*Aldh1b1*$^{fl/fl}$_*Msh2*^{fl} mice and EtOH_*Aldh1b1*$^{fl/fl}$_*Msh2*^{fl} mice did not show any statistically significant differences. Plasma acetaldehyde levels in the EtOH_*Aldh1b1*$^{fl/fl}$_*Msh2*$^{fl\ KO}$ mice were slightly higher compared with the EtOH_*Aldh1b1*$^{fl/fl}$_*Msh2*^{fl} mice, but this difference was not statistically significant.

In *Aldh1b1*$^{-/-}$ Msh2-LS mice, plasma acetaldehyde levels were analysed comparing samples from EtOH_*Aldh1b1*$^{-/-}$_*Msh2*$^{fl\ KO}$ mice and H_2O_*Aldh1b1*$^{-/-}$_*Msh2*$^{fl\ KO}$ mice, as well as comparing these with EtOH_*Aldh1b1*$^{-/-}$_*Msh2*^{fl} mice and H_2O_*Aldh1b1*$^{-/-}$_*Msh2*^{fl} mice after

long-term ethanol or water treatment (experimental mice were treated with ethanol for between 10 and 52 weeks prior to sacrifice).

Plasma acetaldehyde levels were significantly higher in EtOH_*Aldh1b1*$^{-/-}$_*Msh2*$^{fl\ KO}$ mice compared with H_2O_*Aldh1b1*$^{-/-}$_*Msh2*$^{fl\ KO}$ mice ($p<0.0001$) (Figure 6.91). Plasma acetaldehyde levels in EtOH_*Aldh1b1*$^{-/-}$_*Msh2*^{fl} mice were higher than those in H_2O_*Aldh1b1*$^{-/-}$_*Msh2*^{fl} mice ($p<0.0362$). Plasma acetaldehyde levels in EtOH_*Aldh1b1*$^{-/-}$_*Msh2*$^{fl\ KO}$ mice were significantly higher compared with EtOH_*Aldh1b1*$^{-/-}$_*Msh2*^{fl} mice ($p<0.0001$).

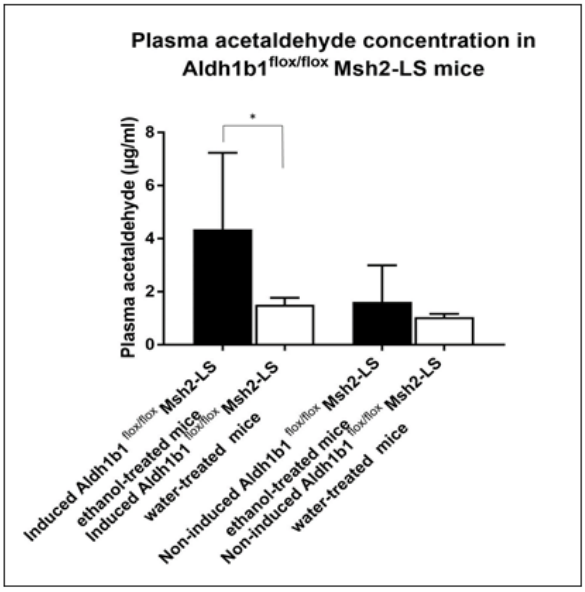

Figure 6.90: Plasma acetaldehyde concentrations in ethanol- and water-treated Tamoxifen-induced *Aldh1b1*$^{flox/flox}$ Msh2-LS (EtOH_*Aldh1b1*$^{fl/fl}$_*Msh2*$^{fl\ KO}$ and H_2O_ *Aldh1b1*$^{fl/fl}$_*Msh2*$^{fl\ KO}$ respectively) mice and ethanol- and water-treated non-induced *Aldh1b1*$^{flox/flox}$ Msh2-LS (EtOH_*Aldh1b1*$^{fl/fl}$_*Msh2*^{fl} and H_2O_*Aldh1b1*$^{fl/fl}$_*Msh2*^{fl} respectively) mice, after long-term ethanol or water treatment. Mann-Whitney U-test was carried out to compare plasma acetaldehyde levels (*$p=0.0159$) (data shown as mean±SD, n=4-6 plasma samples per group).

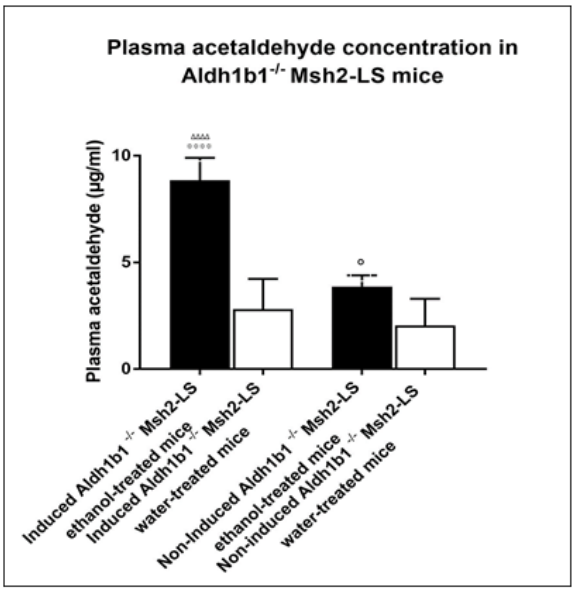

Figure 6.91: Plasma acetaldehyde concentrations in ethanol- and water-treated Tamoxifen-induced *Aldh1b1*$^{-/-}$ Msh2-LS (EtOH_*Aldh1b1*$^{-/-}$_*Msh2*$^{fl\ KO}$ and H_2O_ *Aldh1b1*$^{-/-}$_*Msh2*$^{fl\ KO}$ respectively) mice and ethanol- and water-treated non-induced *Aldh1b1*$^{-/-}$ Msh2-LS (EtOH_*Aldh1b1*$^{-/-}$_*Msh2*^{fl} and H_2O_ *Aldh1b1*$^{-/-}$_*Msh2*^{fl} respectively) mice, after long-term ethanol or water treatment. Mann-Whitney U-test was carried out to compare plasma acetaldehyde concentrations in EtOH_*Aldh1b1*$^{-/-}$_*Msh2*$^{fl\ KO}$ and H_2O_ *Aldh1b1*$^{-/-}$_*Msh2*$^{fl\ KO}$ mice (****p<0.0001), and it was carried out to compare plasma acetaldehyde concentrations in EtOH_*Aldh1b1*$^{-/-}$_*Msh2*$^{fl\ KO}$ mice and EtOH_*Aldh1b1*$^{-/-}$_*Msh2*^{fl} mice ($^{\Delta\Delta\Delta\Delta}$p<0.0001). Mann-Whitney U-test was carried out to compare plasma acetaldehyde concentrations in EtOH_*Aldh1b1*$^{-/-}$_*Msh2*^{fl} and H_2O_ *Aldh1b1*$^{-/-}$_*Msh2*^{fl} mice (°p=0.0362) (data shown as mean±SD, n=4-6 plasma samples per group).

6.7 Discussion

In this chapter, the first aim was to introduce the conditional *Aldh1b1* allele (*Aldh1b1$^{flox/flox}$*) and the constitutive *Aldh1b1* knockout allele (*Aldh1b1$^{-/-}$*) by cross-breeding into the Msh2-LS mouse model, in order to establish an *Msh2$^{flox/-}$; Lgr5CreERT2$^{+/-}$; mTmG$^{+/-}$; Aldh1b1$^{flox/flox}$* colony and an *Msh2$^{flox/-}$; Lgr5CreERT2$^{+/-}$; mTmG$^{+/-}$; Aldh1b1$^{-/-}$* colony. To generate the Aldh1b1 conditional-knockout *(Aldh1b1$^{flox/flox}$*) mice, the *Aldh1b1* tm1a mice were cross-bred with Flpe mice and subsequently, the generated *Msh2$^{+/+}$; Lgr5CreERT2$^{-/-}$; mTmG$^{-/-}$; Aldh1b1$^{flox/flox}$* mice were cross-bred with *Msh2$^{flox/-}$; Lgr5CreERT2$^{+/-}$; mTmG$^{+/+}$; Aldh1b1$^{+/+}$* mice (Msh2-LS model mice) producing: 25% *Msh2$^{flox/+}$; Lgr5CreERT2$^{+/-}$; mTmG$^{+/-}$; Aldh1b1$^{fl/+}$* mice, 25% *Msh2$^{flox/+}$; Lgr5CreERT2$^{-/-}$; mTmG$^{+/-}$; Aldh1b1$^{fl/+}$* mice, 25% *Msh2$^{-/+}$; Lgr5CreERT2$^{+/-}$; mTmG$^{+/-}$; Aldh1b1$^{fl/+}$* mice, and 25% *Msh2$^{-/+}$; Lgr5CreERT2$^{-/-}$; mTmG$^{+/-}$; Aldh1b1$^{fl/+}$* mice. The resulting progeny were used as breeders for the creation of the Aldh1b1 conditional-knockout Msh2-LS experimental subject mice. The mice derived from these matings were predicted to show 1.5% progeny with *Msh2$^{flox/-}$; Lgr5CreERT2$^{+/-}$*; *mTmG$^{+/-}$; Aldh1b1$^{flox/flox}$* genotypes and 0.8% progeny with *Msh2$^{flox/-}$; Lgr5CreERT2$^{+/-}$; mTmG$^{+/+}$; Aldh1b1$^{flox/flox}$* genotypes, and the actual progeny proportions were similar. In *Msh2$^{flox/-}$; Lgr5CreERT2$^{+/-}$; mTmG$^{+/-}$; Aldh1b1$^{flox/flox}$*, loss of Aldh1b1 activity following Cre recombinase activation only occurs in the scattered Lgr5-expressing intestinal epithelial stem cells (that go on to form crypt daughter cells) along with inactivation of the second allele of *Msh2* and conversion to mG expression, by Cre recombinase activity induced following Tamoxifen treatment.

To generate the *Aldh1b1* constitutive-knockout (*Aldh1b1$^{-/-}$*) mice, embryos from the *Aldh1b1* conditional-knockout (*Aldh1b1$^{flox/flox}$*) mice were treated with TAT-Cre *in vitro* and implanted into surrogate mothers using standard techniques. Subsequently, the generated *Msh2$^{+/+}$; Lgr5CreERT2$^{-/-}$; mTmG$^{-/-}$; Aldh1b1$^{-/-}$* mice were cross-bred with *Msh2$^{flox/-}$; Lgr5CreERT2$^{+/-}$; mTmG$^{+/+}$; Aldh1b1$^{+/+}$* mice (Msh2-LS model mice) producing: 25% *Msh2$^{flox/+}$; Lgr5CreERT2$^{+/-}$; mTmG$^{+/-}$; Aldh1b1$^{+/-}$* mice, 25% *Msh2$^{flox/+}$; Lgr5CreERT2$^{-/-}$; mTmG$^{+/-}$; Aldh1b1$^{+/-}$*mice, 25% *Msh2$^{-/+}$; Lgr5CreERT2$^{+/-}$; mTmG$^{+/-}$; Aldh1b1$^{+/-}$* mice, and 25% *Msh2$^{-/+}$; Lgr5CreERT2$^{-/-}$; mTmG$^{+/-}$; Aldh1b1$^{+/-}$* mice. The resulting progeny were used as breeders for the creation of the *Aldh1b1* constitutive-knockout Msh2-LS experimental subject mice. The mice resulting from these matings were predicted to show 1.5% progeny with *Msh2$^{flox/-}$; Lgr5CreERT2$^{+/-}$*; *mTmG$^{+/-}$; Aldh1b1$^{-/-}$* genotypes and 0.8% progeny with *Msh2$^{flox/-}$; Lgr5CreERT2$^{+/-}$; mTmG$^{+/+}$; Aldh1b1$^{-/-}$* genotypes, and the actual progeny proportions were similar. *Msh2$^{flox/-}$; Lgr5CreERT2$^{+/-}$*; *mTmG$^{+/-}$; Aldh1b1$^{-/-}$* mice were shown by immunohistochemistry to have complete loss of

Aldh1b1 in all cells, but only showed loss of Msh2 expression in scattered Lgr5-expressing intestinal stem cells (and crypts populated by their daughter cells) due to Cre recombinase activity induced following Tamoxifen treatment.

The second aim was to study the interaction of defective MMR with either low/moderate or high levels of intestinal acetaldehyde in the model mice when placed on long-term ethanol treatment. In this chapter we investigated whether conditional-knockout and/or constitutive-knockout of *Aldh1b1* resulted in increased plasma levels of acetaldehyde, as a surrogate indicator of increased intraepithelial acetaldehyde in the intestines, previously shown to mediate increased DNA damage (Garaycoechea et al., 2012; Langevin et al., 2011; Müller et al., 2016), that together with defective MMR could influence intestinal tumour formation. Once the *Aldh1b1* conditional-knockout Msh2-LS mouse colony and the *Aldh1b1* constitutive-knockout Msh2-LS mouse colony were established, the long-term ethanol treatment protocol was applied to these two groups of mice for up to one year. It was hypothesised that the conditional-knockout *Aldh1b1*$^{flox/flox}$ mice would result in only scattered stem cells, and subsequently scattered crypts or crypt foci, having inactivated Aldh1b1 enzyme activity, generating mildly to moderately increased plasma levels of acetaldehyde overall, reflecting intestinal intraepithelial levels. In contrast, it was hypothesised that the constitutive-knockout *Aldh1b1*$^{-/-}$ mice would have widespread inactivation of the Aldh1b1 enzyme activity in all cells of the murine body, having the most biologically significant effect in the intestinal epithelium, generating moderately to markedly increased plasma levels of acetaldehyde overall, reflecting intestinal intraepithelial levels.
Ethanol exposure in this experimental design was based on previous experience using *Aldh1b1*-depleted mice and control wildtype mice under long-term (~1 year) treatment with 20% ethanol in drinking water, in which intestinal tumour formation was observed within one year in both groups, indicating that long-term ethanol treatment of mice leads to intestinal tumour development (Müller et al., 2016).
Mice received Tamoxifen treatment by daily i.p. injection for 4 consecutive days, to activate Cre-recombinase in a low proportion of Lgr5-expressing intestinal stem cells, as described in Chapter 3. In both *Aldh1b1* conditional-knockout Msh2-LS mice and *Aldh1b1* constitutive-knockout Msh2-LS mice, body weights of the female and male mice didn't significantly differ during the Tamoxifen treatment, showing successful drug administration and acceptance of the experimental procedure by the mice. *Aldh1b1*$^{flox/flox}$ Msh2-LS mice and *Aldh1b1*$^{-/-}$ Msh2-

LS male mice showed statistically higher mean body weight compared with *Aldh1b1*$^{flox/flox}$ Msh2-LS mice and *Aldh1b1*$^{-/-}$ Msh2-LS female murine mean body weight at the same age (as expected due to normal sexual dimorphism for body weight observed in rodents). On the fifth day after the last Tamoxifen i.p. injection, both *Aldh1b1*$^{flox/flox}$ Msh2-LS mice and *Aldh1b1*$^{-/-}$ Msh2-LS mice received 20% ethanol in drinking water or normal drinking water. EtOH_*Aldh1b1*$^{fl/fl}$_*Msh2*$^{fl\ KO}$ female mice did not show abnormal behaviour or reduced body weight compared with H_2O_*Aldh1b1*$^{fl/fl}$_*Msh2*$^{fl\ KO}$ female mice, indicating good acceptance of the ethanol regime. EtOH_*Aldh1b1*$^{fl/fl}$_*Msh2*$^{fl\ KO}$ and H_2O_*Aldh1b1*$^{fl/fl}$_*Msh2*$^{fl\ KO}$ male mice showed some variation in body weight most likely reflecting the low number of experimental mice in this experimental group. EtOH_*Aldh1b1*$^{-/-}$_*Msh2*$^{fl\ KO}$ female and male mice did not show abnormal behaviour or significantly reduced body weight compared with H_2O_*Aldh1b1*$^{-/-}$_*Msh2*$^{fl\ KO}$ female and male mice, indicating good acceptance of the ethanol regime.

In *Aldh1b1*$^{flox/flox}$ Msh2-LS mice, the liquid consumption per mouse was on average 12.83ml for H_2O_*Aldh1b1*$^{fl/fl}$_*Msh2*$^{fl\ KO}$ male mice, 13.4ml for EtOH_*Aldh1b1*$^{fl/fl}$_*Msh2*$^{fl\ KO}$ male mice, 12.87ml for H_2O_*Aldh1b1*$^{fl/fl}$_*Msh2*$^{fl\ KO}$ female mice, and 9ml for EtOH_*Aldh1b1*$^{fl/fl}$_*Msh2*$^{fl\ KO}$ female mice. In *Aldh1b1*$^{-/-}$ Msh2-LS mice, the liquid consumption per mouse was on average 10.4ml for H_2O_*Aldh1b1*$^{-/-}$_*Msh2*$^{fl\ KO}$ male mice, 10.5ml for EtOH_*Aldh1b1*$^{-/-}$_*Msh2*$^{fl\ KO}$ male mice, 10.2ml for H_2O_*Aldh1b1*$^{-/-}$_*Msh2*$^{fl\ KO}$ female mice, and 11.5ml for EtOH_*Aldh1b1*$^{-/-}$_*Msh2*$^{fl\ KO}$ female mice. In both *Aldh1b1*$^{flox/flox}$ Msh2-LS mice and *Aldh1b1*$^{-/-}$ Msh2-LS mice, no significant differences were observed between any of the liquid consumption comparisons of ethanol-treated versus water-treated males or females.

The cohorts of experimental mice were studied over time for evidence of intestinal (or other) tumour formation. As the study progressed, in both *Aldh1b1*$^{flox/flox}$ Msh2-LS mice and *Aldh1b1*$^{-/-}$ Msh2-LS mice, most of the ethanol-treated Msh2-LS mice displayed either anal prolapse or >20% reduction in body weight as common clinical signs of distress at various times and were culled for necropsy dissection. In *Aldh1b1*$^{flox/flox}$ Msh2-LS mice, 41.7% (5/12 mice) of EtOH_*Aldh1b1*$^{fl/fl}$_*Msh2*$^{fl\ KO}$ mice showed evidence of large intestinal hyperproliferation and adenoma formation (with 1 adenocarcinoma) within an average of 4.5 months of ethanol treatment, compared with no hyperproliferation and no cases of large intestinal adenoma formation in H_2O_*Aldh1b1*$^{fl/fl}$_*Msh2*$^{fl\ KO}$ mice (0%, 0/12 mice) in the same time-period. EtOH_*Aldh1b1*$^{fl/fl}$_*Msh2*$^{fl\ KO}$ mice showed a pattern of tumour distribution of one

or more large intestinal tumours mainly in the proximal colon and mid colon (total 21 neoplasms; 14.3% of neoplasms were found in caecum, 38% in proximal colon, 23.8% in mid-colon, 14.3% in distal colon and 9.6% in the rectum). The overall large intestinal tumour distribution pattern observed in EtOH_*Aldh1b1*$^{fl/fl}$_*Msh2*$^{fl\ KO}$ mice was similar to that observed in EtOH_*Msh2*$^{fl\ KO}$ mice (total 36 neoplasms; 19.5% of neoplasms were found in caecum, 33.4% in proximal colon, 41.7% in mid-colon, 2.7% in distal colon and 2.7% in the rectum). However, in EtOH_*Aldh1b1*$^{fl/fl}$_*Msh2*$^{fl\ KO}$ mice, ethanol-induced colonic adenomas occurred earlier, but not statistically significantly so, than in EtOH_*Msh2*$^{fl\ KO}$ mice (4.5 months on average compared with 6 months). However, EtOH_*Aldh1b1*$^{fl/fl}$_*Msh2*$^{fl\ KO}$ mice showed statistically significantly higher numbers of tumours per mouse compared with EtOH_Msh2$^{fl\ KO}$ mice.

In *Aldh1b1*$^{-/-}$ Msh2-LS mice, 66.7% (8/12 mice) of EtOH_*Aldh1b1*$^{-/-}$_*Msh2*$^{fl\ KO}$ mice showed evidence of large intestinal hyperproliferation and adenoma formation within an average of 6 months of ethanol treatment, compared with no hyperproliferation and no cases of large intestinal adenoma formation in H_2O_*Aldh1b1*$^{-/-}$_*Msh2*$^{fl\ KO}$ mice (0%, 0/12 mice) in the same time-period. EtOH_*Aldh1b1*$^{-/-}$_*Msh2*$^{fl\ KO}$ mice showed a pattern of tumour distribution of one or more large intestinal tumours mainly in the proximal colon and mid colon (total 35 neoplasms; 22.9% of neoplasms were found in caecum, 40% in proximal colon, 22.9% in mid-colon, 0% in distal colon and 14.2% in the rectum). In EtOH_*Aldh1b1*$^{-/-}$_*Msh2*$^{fl\ KO}$ mice, ethanol-induced colonic adenomas occurred at statistically significantly higher numbers per mouse than in EtOH_*Msh2*$^{fl\ KO}$ mice (35 neoplasms in 8/12 EtOH_*Aldh1b1*$^{-/-}$_*Msh2*$^{fl\ KO}$ Msh2-LS mice compared with 36 neoplasms in 15/23 EtOH_*Msh2*$^{fl\ KO}$ mice). As observed in *Aldh1b1*^{wt} Msh2-LS mice, no small intestinal adenomas were seen in either the *Aldh1b1*$^{flox/flox}$ Msh2-LS or *Aldh1b1*$^{-/-}$ Msh2-LS mice, for both ethanol- and water-treated mice. EtOH_*Aldh1b1*$^{-/-}$_*Msh2*$^{fl\ KO}$ mice showed a number of rectal adenomas, but these was not observed in EtOH_*Msh2*$^{fl\ KO}$ mice. Rectal tumours in human LS patients are uncommon, but occur later compared with right-sided neoplasms. Rectal adenomas are observed in LS patients mainly after a procedure on a previously diagnosed right-sided lesion (Lee et al., 2001).

A range of relevant control animal cohorts, including non-induced *Aldh1b1*$^{flox/flox}$ Msh2-LS mice, non-induced *Aldh1b1*$^{-/-}$ Msh2-LS mice and non-induced Msh2-LS mice, were also tested for comparison with tumour formation in these test cohorts, after long-term ethanol- or water-treatment. In the absence of Tamoxifen treatment, the Cre-recombinase is not

activated, preventing the loss of the conditional (floxed) *Msh2* allele and thus, there is no MMR pathway abrogation in all of these non-induced control cohorts, together with no loss of the conditional *Aldh1b1* allele in Lgr5 expressing intestinal epithelial stem cells and their daughter cells of *Aldh1b1*$^{flox/flox}$ Msh2-LS mice.

It was hypothesised that without Cre activation, the Aldh1b1$^{flox/flox}$ Msh2-LS control mice should not present altered or harmful phenotypes, or show an increased intestinal tumour predisposition, or other tumour predisposition, compared with wild-type mice. In the *Aldh1b1*$^{-/-}$ Msh2-LS mouse model, the absence of Tamoxifen treatment prevents the loss of the conditional Msh2 allele in Lgr5-expressing intestinal epithelial stem cells, whereas the loss of Aldh1b1 expression is constitutive in all cells of the mouse. It was hypothesised that without Cre activation, the Aldh1b1$^{-/-}$ Msh2-LS control mice should not show an increased dMMR-driven intestinal tumour predisposition, although it was hypothesised that they may show higher sensitivity to ethanol/acetaldehyde in the whole GI tract due to the constitutive loss of Aldh1b1 expression, compared with wild-type mice. The data shown here provide support for both of these hypotheses. The data related to wild-type control mice have already been discussed in Chapter 4 (4.3).

In both *Aldh1b1* conditional-knockout Msh2-LS mice and *Aldh1b1* constitutive-knockout Msh2-LS mice, body weights of the female and male mice didn't significantly differ during the corn oil treatment, showing successful drug administration and acceptance of the experimental procedures by the mice. EtOH_*Aldh1b1*$^{fl/fl}$_*Msh2*^{fl} and EtOH_*Aldh1b1*$^{-/-}$_*Msh2*^{fl} female and male mice did not show abnormal behaviour or reduced weight compared with H_2O_*Aldh1b1*$^{fl/fl}$_*Msh2*^{fl} and H_2O_*Aldh1b1*$^{-/-}$_*Msh2*^{fl} female and male mice, indicating good acceptance of the ethanol regime. However, the mild variations in the data distributions for the body weight curves for both non-induced *Aldh1b1*$^{flox/flox}$ Msh2-LS mice and non-induced *Aldh1b1*$^{-/-}$ Msh2-LS mice were influenced by the small numbers of mice coming from different litters and starting at different time points.

In non-induced *Aldh1b1*$^{flox/flox}$ Msh2-LS mice, 43% (3/7 mice) of the EtOH_*Aldh1b1*$^{fl/fl}$_*Msh2*^{fl} mice showed zones of colonic crypt epithelial hyperproliferation mainly in the proximal and mid-colon, consistent with this previously described ethanol effect (Müller et al., 2016). However, none of the EtOH_*Aldh1b1*$^{fl/fl}$_*Msh2*^{fl} and H_2O_*Aldh1b1*$^{fl/fl}$_*Msh2*^{fl} mice showed intestinal tumour formation. The tumour incidence in EtOH_*Aldh1b1*$^{fl/fl}$_*Msh2*$^{fl\ KO}$ mice was statistically significantly higher compared with EtOH_*Aldh1b1*$^{fl/fl}$_*Msh2*^{fl} mice ($p=0.0466$).

In non-induced *Aldh1b1*$^{-/-}$ Msh2-LS mice, 33.4% (2/6 mice) of the EtOH_*Aldh1b1*$^{-/-}$_*Msh2*^{fl} mice showed zones of colonic crypt epithelial hyperproliferation mainly in the mid-colon, consistent with this previously described ethanol effect (Müller et al., 2016). However, none of the EtOH_*Aldh1b1*$^{-/-}$_*Msh2*^{fl} and H_2O_ *Aldh1b1*$^{-/-}$_*Msh2*^{fl} mice showed intestinal tumour formation. The tumour incidence in EtOH_*Aldh1b1*$^{-/-}$_*Msh2*$^{fl\ KO}$ mice was statistically significantly higher compared with EtOH_*Aldh1b1*$^{-/-}$_*Msh2*^{fl} mice (p=0.0073).

The tumours and normal tissue samples from *Aldh1b1*$^{flox/flox}$ Msh2-LS mice and *Aldh1b1*$^{-/-}$ Msh2-LS mice were characterised by IHC, comparing samples from ethanol-treated and water-treated mice. IHC was used to investigate the expression of Msh2 in tumours and tissue samples from Tamoxifen-induced *Aldh1b1*$^{flox/flox}$ Msh2-LS mice, Tamoxifen-induced *Aldh1b1*$^{-/-}$ Msh2-LS mice, non-induced *Aldh1b1*$^{flox/flox}$ Msh2-LS mice and non-induced *Aldh1b1*$^{-/-}$ Msh2-LS mice. Tamoxifen treatment induced the loss of Msh2 expression in Lgr5+ expressing crypt epithelial stem cells scattered along the entire SI and LI. The Lgr5+ expressing stem cells, located at the bottom of the crypts, generate daughter cells that can expand to fill the entire crypt-villus epithelium in SI or entire crypt in the colon (Barker et al., 2007; Wojciechowicz et al., 2014). In normal intestinal tissues, Msh2 was strongly expressed in crypt stem cells and transit amplifying cells in the small intestinal crypts, but Msh2 protein expression levels fade in the non-dividing differentiated SI villus cells, and similarly fade in the differentiated cells of the upper third of the colonic crypts (Tomé et al., 2013).
In induced *Aldh1b1*$^{flox/flox}$ Msh2-LS mice, EtOH_*Aldh1b1*$^{fl/fl}$_*Msh2*$^{fl\ KO}$ mice showed 43% Msh2-negative small intestinal crypts and 17% Msh2-negative colonic crypts compared with H_2O_*Aldh1b1*$^{fl/fl}$_*Msh2*$^{fl\ KO}$ mice that showed 24% Msh2-negative small intestinal crypts and 7% Msh2-negative colonic crypts. The percentage of Msh2-negative or dMMR crypts was statistically significantly higher in both SI and colon of EtOH_*Aldh1b1*$^{fl/fl}$_*Msh2*$^{fl\ KO}$ mice (p=0.0056 and p=0.0006 respectively) compared with H_2O_*Aldh1b1*$^{fl/fl}$_*Msh2*$^{fl\ KO}$ mice, consistent with ethanol/acetaldehyde-mediated selection for survival of dMMR cells. The number of Msh2-negative crypts was higher in SI than in the colon in *Aldh1b1*$^{flox/flox}$ Msh2-LS mice, however although tumours were observed in the colon, no tumours formed in the SI.
In induced *Aldh1b1*$^{-/-}$ Msh2-LS mice, EtOH_*Aldh1b1*$^{-/-}$_*Msh2*$^{fl\ KO}$ mice showed 55.7% Msh2-negative small intestinal crypts and 29% Msh2-negative colonic crypts compared with H_2O_*Aldh1b1*$^{-/-}$_*Msh2*$^{fl\ KO}$ mice that showed 28% Msh2-negative small intestinal crypts and 10% Msh2-negative colonic crypts. The percentage of Msh2-negative or dMMR crypts was

statistically significantly higher in both SI and colon of EtOH_*Aldh1b1*$^{-/-}$_*Msh2*$^{fl\ KO}$ mice ($p<0.0001$ for both SI and colon) compared with H_2O_*Aldh1b1*$^{-/-}$_*Msh2*$^{fl\ KO}$ mice, consistent with ethanol/acetaldehyde-mediated selection for survival of dMMR cells. The number of Msh2-negative crypts was higher in SI than in the colon in *Aldh1b1*$^{-/-}$ Msh2-LS mice, however although tumours were observed in the colon, no tumours formed in the small intestine.

In induced Aldh1b*1*$^{flox/flox}$ Msh2-LS mice, the Msh2-negative crypts pattern in SI and colon is similar to the one observed in induced Msh2-LS mice (in EtOH_*Msh2*$^{fl\ KO}$ 43% Msh2-negative small intestinal crypts and 11.2% Msh2-negative colonic crypts compared with H_2O_*Msh2*$^{fl\ KO}$ mice that showed 25.8% Msh2-negative small intestinal crypts and 5% Msh2-negative colonic crypts). By contrast, in induced *Aldh1b1*$^{-/-}$ Msh2-LS mice, the percentage of Msh2-negative crypts is higher in both SI and colon compared with those in both EtOH_*Msh2*$^{fl\ KO}$ and H_2O_*Msh2*$^{fl\ KO}$ mice. Given the significantly higher levels of plasma acetaldehyde in EtOH_*Aldh1b1*$^{-/-}$_*Msh2*$^{fl\ KO}$ mice, this is consistent with the hypothesis that ethanol/acetaldehyde mediates selection, acting significantly via acetaldehyde-induced DNA damage, as shown by the y-H2AX and p53 IHC analyses, bringing about increased survival of dMMR cells in these mice (as explained in Chapter 4, Figure 4.58).

All large intestinal adenomas tested from EtOH_*Aldh1b1*$^{fl/fl}$_*Msh2*$^{fl\ KO}$ mice and EtOH_*Aldh1b1*$^{-/-}$_*Msh2*$^{fl\ KO}$ mice showed Msh2-negative dysplastic glands, often surrounded by or admixed with Msh2-positive crypts showing reactive or hyperproliferative changes. This confirmed colonic adenomas arose from dMMR (Msh2-negative) crypts. This is consistent with observations from human LS patients that the risk of colonic tumour formation correlates with the size of the MMR-deficient crypt clusters that grow over time in affected patients, in line with observations by Wojciechowicz et al, (2014) (Kloor et al., 2012; Shia et al., 2015).

Immunohistochemical analysis of Msh2 expression in the intestinal tissue samples from non-induced *Aldh1b1*$^{flox/flox}$ Msh2-LS control mice and non-induced *Aldh1b1*$^{-/-}$ Msh2-LS treated with either 20% ethanol in drinking water or normal / standard water, showed no Msh2-negative crypts in either small or large intestinal mucosal epithelium, consistent with lack of induction of Cre activity with continued expression of full-length protein from the floxed *Msh2* allele.

IHC was performed to investigate Aldh1b1 murine protein expression. ALDH1B1 is a mitochondrial aldehyde dehydrogenase highly expressed in the intestinal epithelium, especially in the stem cells and transit-amplifying cells of the crypts of both small intestines

and large intestines, and has been proposed to play an important role in acetaldehyde detoxification in the intestines to protect stem and progenitor cells from acetaldehyde-mediated damage (Stagos et al., 2010). In *Aldh1b1*$^{flox/flox}$ Msh2-LS mice, Tamoxifen-treatment induced the loss of Aldh1b1 expression, together with the loss of Msh2, in scattered Lgr5+ expressing intestinal crypt epithelial stem cells and their crypts, shown by IHC. Aldh1b1-negative crypts were observed in the intestinal samples of both EtOH_*Aldh1b1*$^{fl/fl}$_*Msh2*$^{fl\ KO}$ and H_2O_*Aldh1b1*$^{fl/fl}$_*Msh2*$^{fl\ KO}$ mice. Non-induced (no Tamoxifen treatment) *Aldh1b1*$^{flox/flox}$ Msh2-LS model mice treated with either 20% ethanol in drinking water or normal water showed no Aldh1b1-negative crypts in either SI and LI mucosa, consistent with lack of induction of Cre activity with continued expression of protein from the floxed *Aldh1b1* allele. In induced *Aldh1b1*$^{-/-}$ Msh2-LS mice, Aldh1b1 is permanently inactivated in all tissues and cells (Tamoxifen treatment is not required to induce the loss of Aldh1b1 expression) and in both these mice and in non-induced *Aldh1b1*$^{-/-}$ Msh2-LS model mice, treated with either 20% ethanol in drinking water or normal water, IHC showed that all crypts were Aldh1b1-negative in both SI and LI mucosal epithelium, as expected.

IHC was performed to investigate Ki-67 expression in intestinal tissue samples from Tamoxifen-induced *Aldh1b1*$^{flox/flox}$ Msh2-LS mice and *Aldh1b1*$^{-/-}$ Msh2-LS mice to determine proliferative activity. In normal large and small intestinal tissue, Ki-67 is expressed only in the proliferating cells at or near the base of crypts as previously reported (Johnston et al., 1989). In both *Aldh1b1*$^{flox/flox}$ Msh2-LS mice and *Aldh1b1*$^{-/-}$ Msh2-LS mice, the percentage of Ki-67-positive cells per crypt was significantly higher in the colon in EtOH_*Aldh1b1*$^{fl/fl}$_*Msh2*$^{fl\ KO}$ mice and EtOH_*Aldh1b1*$^{-/-}$_*Msh2*$^{fl\ KO}$ mice compared with H_2O_*Aldh1b1*$^{fl/fl}$_*Msh2*$^{fl\ KO}$ mice and H_2O_*Aldh1b1*$^{-/-}$_*Msh2*$^{fl\ KO}$ mice respectively, confirming the presence of large regions of mucosal crypt epithelial hyperproliferation observed in histological sections of ethanol-treated murine colons. The percentage of Ki-67-positive cells per crypt in SI of EtOH_*Aldh1b1*$^{fl/fl}$_*Msh2*$^{fl\ KO}$ mice and EtOH_*Aldh1b1*$^{-/-}$_*Msh2*$^{fl\ KO}$ mice was mildly higher than in the SI of H_2O_*Aldh1b1*$^{fl/fl}$_*Msh2*$^{fl\ KO}$ mice and H_2O_*Aldh1b1*$^{-/-}$_*Msh2*$^{fl\ KO}$ mice respectively. These observations confirm the previously reported association of long-term ethanol treatment of mice and colonic mucosal epithelial hyperproliferation (Müller et al., 2016).

We investigated the expression of β-catenin protein, an intracellular signal transducer in the Wnt signalling pathway (Cong et al., 2003), on tumours and tissue samples from Tamoxifen-induced *Aldh1b1*$^{flox/flox}$ Msh2-LS mice and Tamoxifen-induced *Aldh1b1*$^{-/-}$ Msh2-LS mice. Normal colorectal mucosal crypt epithelium exhibited moderate membranous and weak

cytoplasmic staining for β-catenin, but absent nuclear localisation. In colonic tumours in the EtOH_*Aldh1b1*$^{fl/fl}$_*Msh2*$^{fl\ KO}$ mice and EtOH_*Aldh1b1*$^{-/-}$_*Msh2*$^{fl\ KO}$ mice, immunohistochemical analysis of β-catenin showed a heterogeneous pattern with variable numbers of adenoma cells showing moderately to strongly positive β-catenin nuclear immunostaining due to accumulation and translocation of β-catenin into the nuclei. This pattern has been observed in human MMR-deficient CRC (Lugli et al., 2007).

Ethanol metabolisms plays a major role in intestinal carcinogenesis (Seitz & Stickel, 2007), as described earlier in this chapter. Acetaldehyde is the first product of ethanol metabolism, and aldehydes are very reactive small molecules that can cause a wide range of DNA modifications. In normal conditions, acetaldehyde is oxidized to acetate by ALDHs. ALDH1B1 is the major aldehyde dehydrogenase in the gastrointestinal epithelium (Stagos et al., 2010). In *Aldh1b1* conditional-knockout Msh2-LS mouse model and *Aldh1b1* constitutive-knockout Msh2-LS mice, lack of Aldh1b1 expression leads to increased plasma levels of acetaldehyde and accumulation of acetaldehyde-induced DNA damage. IHC was performed for y-H2AX and p53 to evaluate the DNA damage response in *Aldh1b1* conditional-knockout Msh2-LS mice and *Aldh1b1* constitutive-knockout Msh2-LS mice. Y-H2AX is a key co-ordinator of signalling and activator of DNA damage repair pathways and for this it is considered a specific molecular marker for monitoring DNA damage (Mah et al., 2010). In EtOH_*Aldh1b1*$^{fl/fl}$_*Msh2*$^{fl\ KO}$ mice, a statistically significantly higher percentage of y-H2AX-positive cells in the colon (38.7%) was observed compared with H_2O_*Aldh1b1*$^{fl/fl}$_*Msh2*$^{fl\ KO}$ murine colon (0.5%). In both EtOH_*Aldh1b1*$^{fl/fl}$_*Msh2*$^{fl\ KO}$ and H_2O_*Aldh1b1*$^{fl/fl}$_*Msh2*$^{fl\ KO}$ murine SI, no y-H2AX positive cells were observed.

In EtOH_*Aldh1b1*$^{-/-}$_*Msh2*$^{fl\ KO}$ mice, a statistically significantly higher percentage of y-H2AX-positive cells in murine colon (46%) was observed compared with H_2O_*Aldh1b1*$^{-/-}$_*Msh2*$^{fl\ KO}$ murine colon (0.5%). The percentage of SI y-H2AX-positive cells was higher in EtOH_*Aldh1b1*$^{-/-}$_*Msh2*$^{fl\ KO}$ mice compared with H_2O_*Aldh1b1*$^{-/-}$_*Msh2*$^{fl\ KO}$ mice. In both EtOH_*Aldh1b1*$^{fl/fl}$_*Msh2*$^{fl\ KO}$ mice and in EtOH_*Aldh1b1*$^{-/-}$_*Msh2*$^{fl\ KO}$ mice, colonic and caecal adenomas showed high levels of y-H2AX expression.

The high expression of y-H2AX in EtOH_*Aldh1b1*$^{fl/fl}$_*Msh2*$^{fl\ KO}$ and EtOH_*Aldh1b1*$^{-/-}$_*Msh2*$^{fl\ KO}$ murine colonic mucosal epithelium is consistent with DNA damage induced by acetaldehyde, suggesting that acetaldehyde (more so than ethanol) mediates a significant genotoxic effect, predominantly on dMMR colonic mucosal epithelium rather than on dMMR small intestinal

mucosa, indicating that other protective mechanisms may be operative in the small intestinal epithelium, consistent with the lower incidence of small intestinal cancers compared with colonic cancers in human LS patients. This suggests that Msh2 has a key role in protecting the MMR-proficient colonic epithelial cells against this type of DNA damage, but Msh2 may not be the sole protective mechanism for small intestinal epithelial cells from acetaldehyde-induced DNA damage. By contrast, the presence of y-H2AX-positive cells in EtOH_*Aldh1b1*$^{-/-}$_*Msh2*$^{fl\ KO}$ murine colonic mucosal epithelium confirms the important role of Aldh1b1 in protection of large intestinal epithelial cells from acetaldehyde-induced DNA damage.

Upon DNA damage, increased p53 levels in response can be demonstrated immunohistochemically as a greater proportion of cells containing moderate to high (but variable) nuclear staining of p53 in individual cells (referred as p53 "wildtype pattern") (Köbel et al., 2016; Lakin & Jackson, 1999). In *Aldh1b1*$^{flox/flox}$ Msh2-LS mice, the numbers of cells with either moderate or high levels of p53-positive nuclear staining per colonic crypt was significantly higher in EtOH_*Aldh1b1*$^{fl/fl}$_*Msh2*$^{fl\ KO}$ mice (52.7%) compared with H_2O_*Aldh1b1*$^{fl/fl}$_*Msh2*$^{fl\ KO}$ mice (6.3%), consistent with ethanol/acetaldehyde-induced DNA damage. The percentage of small intestinal p53-positive cells per crypt was higher in EtOH_*Aldh1b1*$^{fl/fl}$_*Msh2*$^{fl\ KO}$ mice (21.7%) compared with H_2O_*Aldh1b1*$^{fl/fl}$_*Msh2*$^{fl\ KO}$ mice (3.3%).

In *Aldh1b1*$^{-/-}$ Msh2-LS mice, the numbers of cells with either moderate or high levels of p53-positive nuclear staining per colonic crypt was significantly higher in EtOH_*Aldh1b1*$^{-/-}$_*Msh2*$^{fl\ KO}$ mice (47.5%) compared with H_2O_*Aldh1b1*$^{-/-}$_*Msh2*$^{fl\ KO}$ mice (3.3%), consistent with ethanol/acetaldehyde-induced DNA damage. The percentage of small intestinal p53-positive cells per crypt was higher in EtOH_*Aldh1b1*$^{-/-}$_*Msh2*$^{fl\ KO}$ mice (20%) compared with H_2O_*Aldh1b1*$^{-/-}$_*Msh2*$^{fl\ KO}$ mice (4%). In both EtOH_*Aldh1b1*$^{fl/fl}$_*Msh2*$^{fl\ KO}$ mice and EtOH_*Aldh1b1*$^{-/-}$_*Msh2*$^{fl\ KO}$ mice, colonic and caecal adenomas showed high percentages of p53-positive cells, with variably moderate to high nuclear p53 positivity and some negative nuclei in a "p53 wildtype" pattern, indicative of widespread response to DNA damage, with no tumours showing either the "overexpression" or "null" patterns associated with *Tp53* mutation.

Caspase-3 (Cas3) is a key executive member of the caspase cascade, with cysteine-aspartic acid protease activity, that acts as one of the key effectors of cell death by apoptosis. It requires proteolytic cleavage into 2 subunits that dimerize to create the active form, cCas3 (Holubec et al., 2005; Talmon et al., 2010). Once activated, cCas3 is responsible for the

cleavage of key target proteins essential in cell proliferation and survival, and cCAS3 is involved in inducing DNA fragmentation, cell shrinkage, chromatin and cytoplasmic condensation and formation of apoptotic cells and bodies. Apoptotic bodies express ligands for phagocytic cell receptors for recognition by phagocytic cells or neighbouring cells (Elmore, 2007). In *Aldh1b1*$^{flox/flox}$ Msh2-LS mice, IHC analysis of cCas3 with quantification of cCas3-positive apoptotic bodies showed significantly higher numbers of cCas3+ apoptotic bodies in EtOH_*Aldh1b1*$^{fl/fl}$_*Msh2*$^{fl\ KO}$ mice compared with very few or no detectable cCas3+ apoptotic bodies in H_2O_*Aldh1b1*$^{fl/fl}$_*Msh2*$^{fl\ KO}$ mice. In *Aldh1b1*$^{-/-}$ Msh2-LS mice, immunohistochemical analysis of cCas3 with quantification of cCas3-positive apoptotic bodies, showed significantly higher numbers of cCas3+ apoptotic bodies in EtOH_*Aldh1b1*$^{-/-}$_*Msh2*$^{fl\ KO}$ mice compared with very few or no detectable cCas3+ apoptotic bodies in H_2O_*Aldh1b1*$^{-/-}$_*Msh2*$^{fl\ KO}$ mice. The detection of cCas3+ apoptotic bodies is consistent with increased apoptosis associated with colonic epithelial exposure to ethanol/acetaldehyde, and it is hypothesised that this is mediated by those colonic epithelial cells with proficient MMR that can recognise severe ethanol/acetaldehyde-induced DNA damage triggering apoptosis. In both EtOH_*Aldh1b1*$^{fl/fl}$_*Msh2*$^{fl\ KO}$ mice and EtOH_*Aldh1b1*$^{-/-}$_*Msh2*$^{fl\ KO}$ mice, colonic and caecal adenomas showed very few or no detectable cCas3+ apoptotic bodies, indicating very few or rare apoptotic events in dMMR colonic tumours, consistent with inactivation of the MMR-mediated process by which ethanol/acetaldehyde-induced DNA damage is recognised leading to apoptosis.

The increased DNA damage observed in EtOH_*Aldh1b1*$^{fl/fl}$_*Msh2*$^{fl\ KO}$ mice and EtOH_*Aldh1b1*$^{-/-}$_*Msh2*$^{fl\ KO}$ mice large intestinal mucosal epithelium is consistent with the high levels of circulating acetaldehyde detected by plasma acetaldehyde assay. Statistically significantly higher plasma acetaldehyde levels were observed in EtOH_*Aldh1b1*$^{fl/fl}$_*Msh2*$^{fl\ KO}$ mice and EtOH_*Aldh1b1*$^{-/-}$_*Msh2*$^{fl\ KO}$ mice compared with H_2O_*Aldh1b1*$^{fl/fl}$_*Msh2*$^{fl\ KO}$ mice and H_2O_*Aldh1b1*$^{-/-}$_*Msh2*$^{fl\ KO}$ mice ($p=0.0019$ and $p<0.0001$, respectively). Furthermore, statistically significantly higher plasma acetaldehyde levels were observed in EtOH_*Aldh1b1*$^{-/-}$_*Msh2*^{fl} mice compared with H_2O_*Aldh1b1*$^{-/-}$_*Msh2*^{fl} mice, consistent with a greater effect due to constitutive loss of Aldh1b1 combined with ethanol exposure.

In conclusion, we successfully introduced both the conditional-knockout *Aldh1b1* allele (*Aldh1b1*$^{flox/flox}$) and the constitutive *Aldh1b1* knockout allele (*Aldh1b1*$^{-/-}$) by cross-breeding into the Msh2-LS mouse model. Ethanol-treatment was shown to cause accumulation of high plasma levels of acetaldehyde in the *Aldh1b1*$^{-/-}$ Msh2-LS mice and lower, more moderate,

levels of plasma acetaldehyde in the *Aldh1b1*$^{flox/flox}$ Msh2-LS mice. Acetaldehyde was shown by immunohistochemical analysis of both y-H2AX and p53 to lead to an increased DNA damage response. Long-term ethanol-treatment was also observed to induce colonic crypt epithelial hyperproliferation, mostly in the proximal and mid colon, and this contributed to intestinal adenoma formation, indicating that ethanol/acetaldehyde can act as tumour promoter in these cells. In both the *Aldh1b1* conditional-knockout Msh2-LS model and *Aldh1b1* constitutive-knockout Msh2-LS model, acetaldehyde-mediated DNA damage and carcinogenic effects appeared to be stronger than in the *Aldh1b1* wild-type Msh2-LS mouse model, as both EtOH_*Aldh1b1*$^{fl/fl}$_*Msh2*$^{fl\,KO}$ mice and EtOH_*Aldh1b1*$^{-/-}$_*Msh2*$^{fl\,KO}$ mice showed increased numbers of precursor colonic crypt foci lesions and large intestinal adenomas (both colonic and caecal adenomas, with occasional progression to adenocarcinoma), compared with EtOH_*Msh2*$^{fl\ KO}$ mice. These results verified the key role of Aldh1b1 in protecting the large intestinal epithelial stem and progenitor cells from acetaldehyde-induced DNA damage.

This study produced strong evidence in support of the hypothesis that there is a gene/environment interaction between dMMR and ethanol/acetaldehyde, demonstrated most notably by the *Aldh1b1* constitutive-knockout Msh2-LS mouse model. In *Aldh1b1*$^{-/-}$ MMR-proficient intestinal epithelial stem cells, acetaldehyde-induced DNA damage is likely to result in activation of the DNA mismatch repair pathway in the case of mild DNA damage or cell death by apoptosis in the case of severe DNA damage (Figure 6.92). By contrast, in *Aldh1b1*$^{-/-}$ MMR-deficient intestinal epithelial stem cells, significant acetaldehyde-induced DNA damage is not recognized by the DNA mismatch repair system, with no activation of either cell cycle arrest, DNA mismatch repair or apoptosis. The DNA-damaged *Aldh1b1*$^{-/-}$ MMR-deficient intestinal epithelial cells show inappropriate survival and subsequent proliferation. This leads to an increase of *Aldh1b1*$^{-/-}$ dMMR intestinal epithelial cells, observed as higher numbers of clusters of *Aldh1b1*$^{-/-}$ dMMR crypt foci, with elevated subsequent tumour formation with both right-sided and left-sided colonic adenomas and occasional adenocarcinomas in these mice (Figure 6.92).

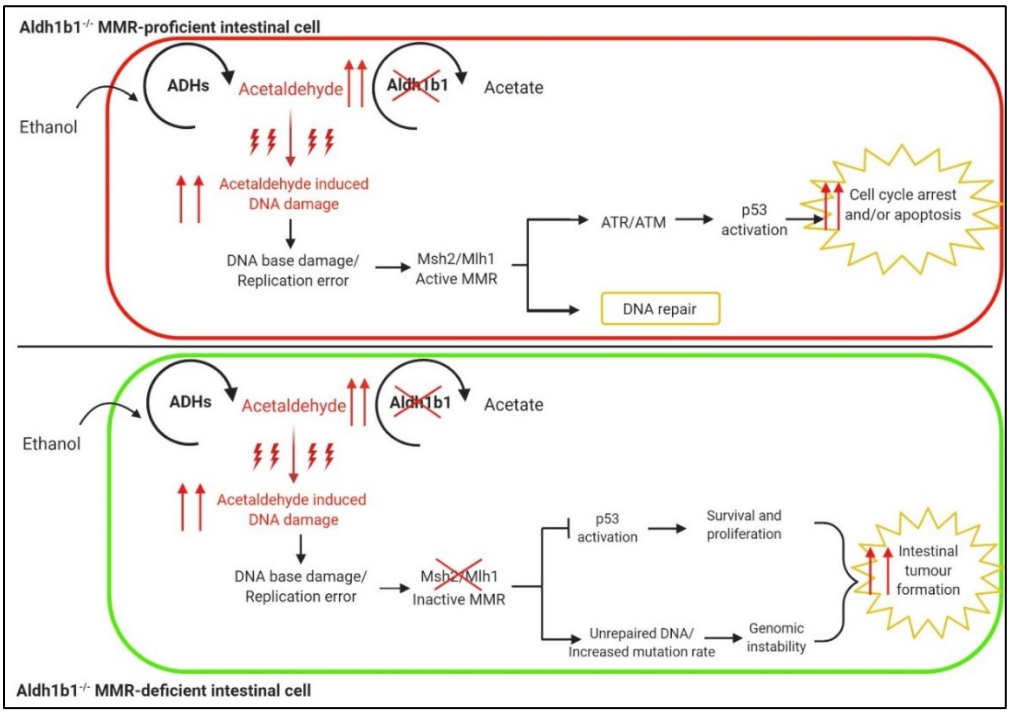

Figure 6.92: Schematic diagram of the proposed model of the MMR/acetaldehyde gene/environment interactions in *Aldh1b1*$^{-/-}$ MMR-proficient and *Aldh1b1*$^{-/-}$ MMR-deficient intestinal epithelial cells. Ethanol is metabolized to highly reactive acetaldehyde by ADHs in intestinal epithelium. Acetaldehyde is further oxidized to acetate by ALDHs, such as ALDH1B1 in intestinal epithelial stem cells and transit-amplifying cells. In some epithelial cells, acetaldehyde can escape the metabolic pathway and induce various forms of DNA base damage, some of which would normally be recognised and repaired by the MMR system, or if unrepaired this base damage may induce replication errors, such as base mismatches or InDels, during S-phase of the cell cycle. In the *Aldh1b1*$^{-/-}$ MMR-proficient intestinal epithelial cell (red cell membrane), ethanol is metabolized to highly reactive acetaldehyde, with reduced oxidation to acetate due to the lack of Aldh1b1, leading to increased levels of highly reactive acetaldehyde that can damage DNA. The *Aldh1b1*$^{-/-}$ MMR-proficient intestinal epithelial cell is able to activate DNA mismatch repair, inducing cell cycle arrest to allow DNA repair. However, high levels of reactive acetaldehyde causing severe acetaldehyde-induced DNA damage may force the *Aldh1b1*$^{-/-}$ MMR-proficient intestinal epithelial cell to activate cell death by apoptosis. By contrast, the *Aldh1b1*$^{-/-}$ MMR-deficient intestinal epithelial cell (green cell membrane) is unable to activate the MMR signalling pathway and so there is neither cell cycle arrest nor apoptosis, following increased acetaldehyde-induced DNA damage, resulting in aberrant survival of DNA-damaged cells and their subsequent proliferation. These proliferating *Aldh1b1*$^{-/-}$ MMR-deficient intestinal epithelial cells populate the crypt and expand further (by crypt fission) to form *Aldh1b1*$^{-/-}$ dMMR crypt foci. Stimulated by ethanol/acetaldehyde to undergo increased proliferation, these cells form hyperproliferative crypts whilst remaining subject to ongoing DNA damage. Thus, these *Aldh1b1*$^{-/-}$ dMMR cells can accumulate mutations reflecting a form of dMMR genomic instability, and are consequently at increased risk of tumour formation, thus explaining the acceleration of colonic adenoma formation and increased probability of evolution to adenocarcinoma. In the *Aldh1b1*$^{flox/flox}$ Msh2-LS model mice, scattered *Aldh1b1*$^{flox/flox}$ *Msh2*$^{flox/-}$ intestinal epithelial stem cells are induced by Tamoxifen-mediated Cre activation to become *Aldh1b1*$^{-/-}$ *Msh2*$^{-/-}$ MMR-deficient intestinal epithelial cells and thus respond to ethanol exposure in a similar way to that described above for the cells with green membranes.

Chapter 7: Investigation of the effects of ethanol/acetaldehyde on defective Mismatch Repair colonic crypt foci precursors in the Msh2-LS models

7.1 Introduction

The *mTmG* reporter transgene was introduced through cross-breeding into the Msh2-LS mouse model, as previously described in Chapter 3. This Cre-mediated reporter construct confers a red fluorescence to cells of all tissues without Cre activation, due to whole body expression of mT. Upon Cre activation, Cre recombines the two LoxP sites surrounding the floxed mT allele and the adjacent polyadenylation site, thus excising this section of DNA, allowing expression of an mG (Chapter 3, Figure 3.3). In the modified version of the *Msh2$^{flox/-}$; Lgr5CreERT2$^{+/-}$; mTmG$^{+/-}$* mouse model (described in Chapter 3), the activation of Cre recombinase by Tamoxifen-treatment generates a *Msh2* knockout allele (*Msh2$^{flox/OFF}$*) and converts the same intestinal stem cells (and their daughter cells) to mG expression, generating dMMR intestinal stem cells that subsequently form dMMR crypts, which are marked by green fluorescent mG expression. In Chapter 3 (3.2.2.3), it was demonstrated that the dMMR crypt foci were positive for mG/GFP by performing IHC analyses of adjacent serial sections using anti-Msh2 antibody and anti-GFP antibody.

In this chapter, the first aim was to use the mTmG transgene reporter system to monitor any changes in the number, size, or distribution of mG+ dMMR crypt foci following ethanol treatment of the mouse models over the time. The second aim was to investigate differences in gene expression patterns between ethanol-treated and water-treated Msh2-LS murine colonic and small intestinal epithelial cells to shed light on why hyperproliferative changes and adenoma formation occur in the colon, but not in the small intestine, in this Msh2-LS model and which signalling pathways are involved.

In Chapter 4 and Chapter 6, evidence was provided that ethanol-treatment can cause tumour formation in the large intestinal mucosal epithelium, but not in the small intestine. This suggested that Msh2 has a key role in protecting the pMMR colonic epithelial cells against some types of ethanol/acetaldehyde-induced DNA damage, but Msh2 may not be the sole protective mechanism for small intestinal epithelium cells from such DNA damage.

The plan was to use FACS to sort mT-expressing red small intestinal and colonic epithelial cells (pMMR) and mG-expressing green small intestinal and colonic epithelial cells (dMMR)

from both ethanol-treated and water-treated murine colon, followed by extraction of RNA and gene expression analysis. However, due to COVID-19-related laboratory restrictions the latter experiment was not fully completed.

7.2 Investigation of ethanol effects on mG-expressing dMMR colonic crypt foci in the Msh2-LS models

7.2.1 Methods

7-9 weeks old *Msh2$^{flox/-}$; Lgr5CreERT2$^{+/-}$; mTmG$^{+/-}$* mice were divided into 4 Groups: A-D (Figure 7.1). Group-A and Group-B mice received i.p. injections of 0.15mg Tamoxifen/g bw on day 1 and 0.1mg Tamoxifen/g bw on day 2, 3 and 4; on day 5 mice were provided with normal drinking water or 20% ethanol in drinking water, respectively. Group-C and Group-D mice received i.p. injections of 0.15mg corn oil/g bw on day 1 and 0.1mg corn oil/g bw on day 2, 3 and 4; on day 5 mice were provided with normal drinking water or 20% ethanol in drinking water, respectively. Group-A to Group-D mice were sacrificed after either 5 days or 15 days of the ethanol or water regime. During the necropsy dissection procedure, small and large intestinal tissues were harvested, inverted on skewer as for preparation of Swiss-rolls, fixed in 10% NBF and kept on ice. The large and small intestines were opened longitudinally and flattened out as whole mount specimens on a transparent petri-dish, until fluorescent microscopic analysis of red mT and green mG fluorescent protein expression (as described in Material and Methods, 2.1.5). Images were acquired and analysed as described in Materials and Methods. The mT and mG protein expression detection was extended so that it was performed in all analyses of the experimental (tumour-watch) *Aldh1b1*-wild-type Msh2-LS mice, *Aldh1b1*-conditional-knockout Msh2-LS mice and *Aldh1b1*-constitutive-knockout Msh2-LS mice, in order to obtain data about changes in the dMMR colonic crypt foci in terms of their size, number and distribution over time. Following image acquisition of small and large intestines, tissues were prepared as Swiss-rolls and fixed in 10% NBF. They were processed using standard tissue processing protocols for paraffin wax embedding.

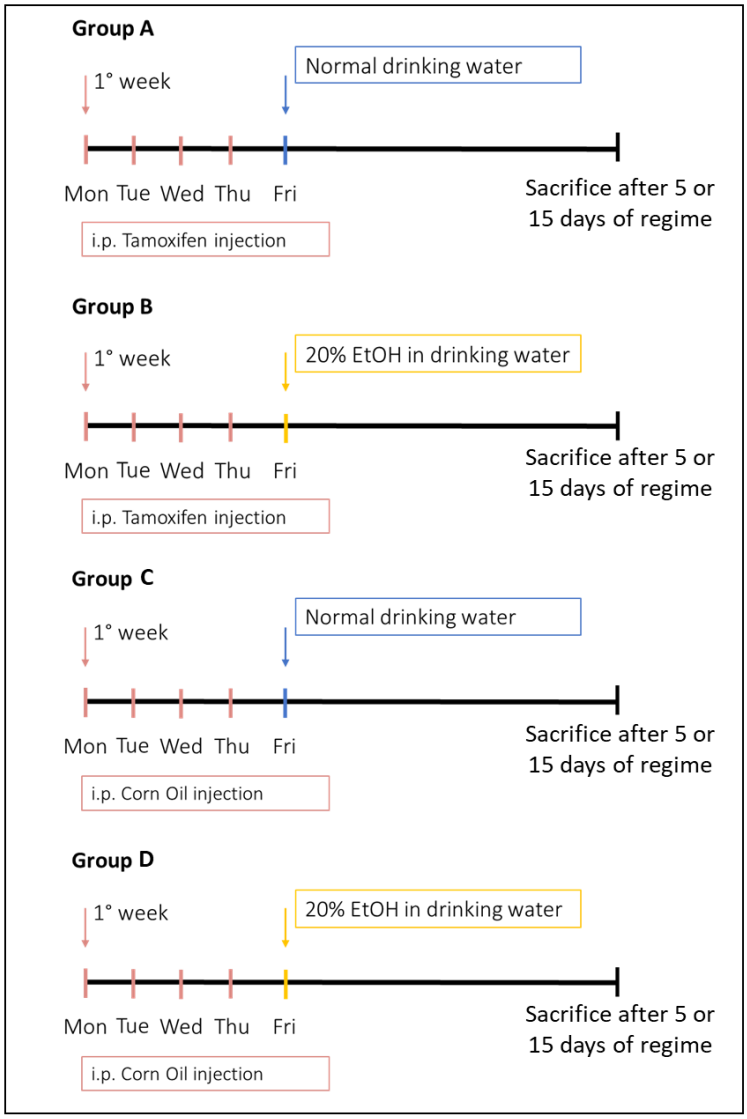

Figure 7.1: Experimental treatment protocols and timelines for Group-A to -D using Msh2-LS mice. Animals in Group-A and Group-B received i.p Tamoxifen injections over 4 days (0.15mg Tamoxifen/g bw on day 1 and 0.1mg Tamoxifen/g bw on day 2, 3 and 4), followed by either standard/normal drinking water (Group-A) or drinking or water containing 20% ethanol (Group-B). Animals in Group-C and Group-D received i.p corn oil injections over 4 days (0.15mg corn oil/g bw on day 1 and 0.1mg corn oil/g bw on day 2, 3 and 4), followed by either standard/normal drinking water (Group-C) or drinking or water containing 20% ethanol (Group-D). (i.p. = intraperitoneal; EtOH= Ethanol).

7.2.2 Results

7.2.2.1 Investigation of ethanol effects on mG-expressing dMMR colonic crypt foci after 5 or 15 days of ethanol or water regimes

The proportional area (as a percentage) of colonic mucosa composed of mG-expressing crypt foci relative to the total area of mG and mT fluorescent protein expression (percentage green area) was quantified in *Msh2$^{flox/-}$; Lgr5CreERT2$^{+/-}$; mTmG$^{+/-}$* (Msh2-LS) mice after 4 i.p. Tamoxifen injections and either 5 days of 20% ethanol in drinking water regime or 5 days of normal drinking water regime (Figure 7.2). There was a statistically significant increase in the percentage green area, combining number and size of crypt foci containing mG-expressing cells, along the large intestinal tract of 5-day ethanol-treated Msh2-LS mice compared with 5-day water-treated Msh2-LS mice (p=0.0003). Moreover, the ethanol-treated Msh2-LS mice showed a statistically significantly higher percentage area of mG-expressing crypt foci in the proximal colon than in the distal colon (p=0.0384) (Figure 7.2). Images of Msh2-LS murine small intestine were acquired after 5 days of either ethanol- or water-treatment regimes (Figure 7.3), but quantification of the mG+ villlus/crypt foci was technically much more difficult due to the extensive and often confluent mG+ villus/crypt foci with some partially mG+ villi, and the complicated folded structure of the small intestinal villi in 3-dimensions, including partially fluorescent green and partially fluorescent red villi that were folded and twisted.

The percentage area of mG+ crypt foci relative to the total area of mT and mG fluorescent protein expression was measured in *Msh2$^{flox/-}$; Lgr5CreERT2$^{+/-}$; mTmG$^{+/-}$* mice after 4 i.p. Tamoxifen injections and either 15 days of 20% ethanol in drinking water or 15 days of normal drinking water (Figure 7.4). There was a larger and statistically significant increase in the percentage area of crypt foci containing mG-expressing cells along the large intestinal tract of 15-day ethanol-treated Msh2-LS mice compared with 15-day water-treated Msh2-LS mice (p<0.0001), more so proximally than distally (p=0.004) (Figure 7.4). Images were acquired of Msh2-LS murine small intestine after 15 days of either ethanol- or water-treatment regimes (Figure 7.5), but the quantitative analysis was technically difficult as previously explained.

Detection of mG+ crypt foci and quantification of the percentage green area was evaluated in the large intestinal tissue samples from non-induced (no Tamoxifen treatment) Msh2-LS model mice after 4 i.p. corn oil injections and either 15 days of 20% ethanol in drinking water, or 15 days of normal drinking water, but these mice showed no mG+ colonic crypt foci (Figure

7.6), consistent with lack of induction of Cre activity with continued expression of mT fluorescent red protein from the *mTmG* construct (presumably together with continued expression of Msh2 protein from the floxed *Msh2* allele) in this tissue.

Higher magnification images were taken during mT and mG protein detection to obtain a better understanding of the cellular localisation of mG expression within intestinal crypts, using the Leica MZ FLIII fluorescence stereomicroscope (Figure 7.7-7.8), showing highly-magnified images of small intestinal mucosa with mG+ cells in strips along the SI villi (Figure 7.8). By contrast, highly-magnified images of Msh2-LS control (no ethanol treatment) murine colon were unable to provide a sufficiently detailed views of the mG+ crypt foci (Figure 7.7). Subsequently, these murine colonic crypts were examined using a confocal microscope to obtain more fine-detailed images of the distribution of mG+ cells within the crypts (Figure 7.9, supplementary CD and Video: https://media.ed.ac.uk/media/1_385a3vwh).

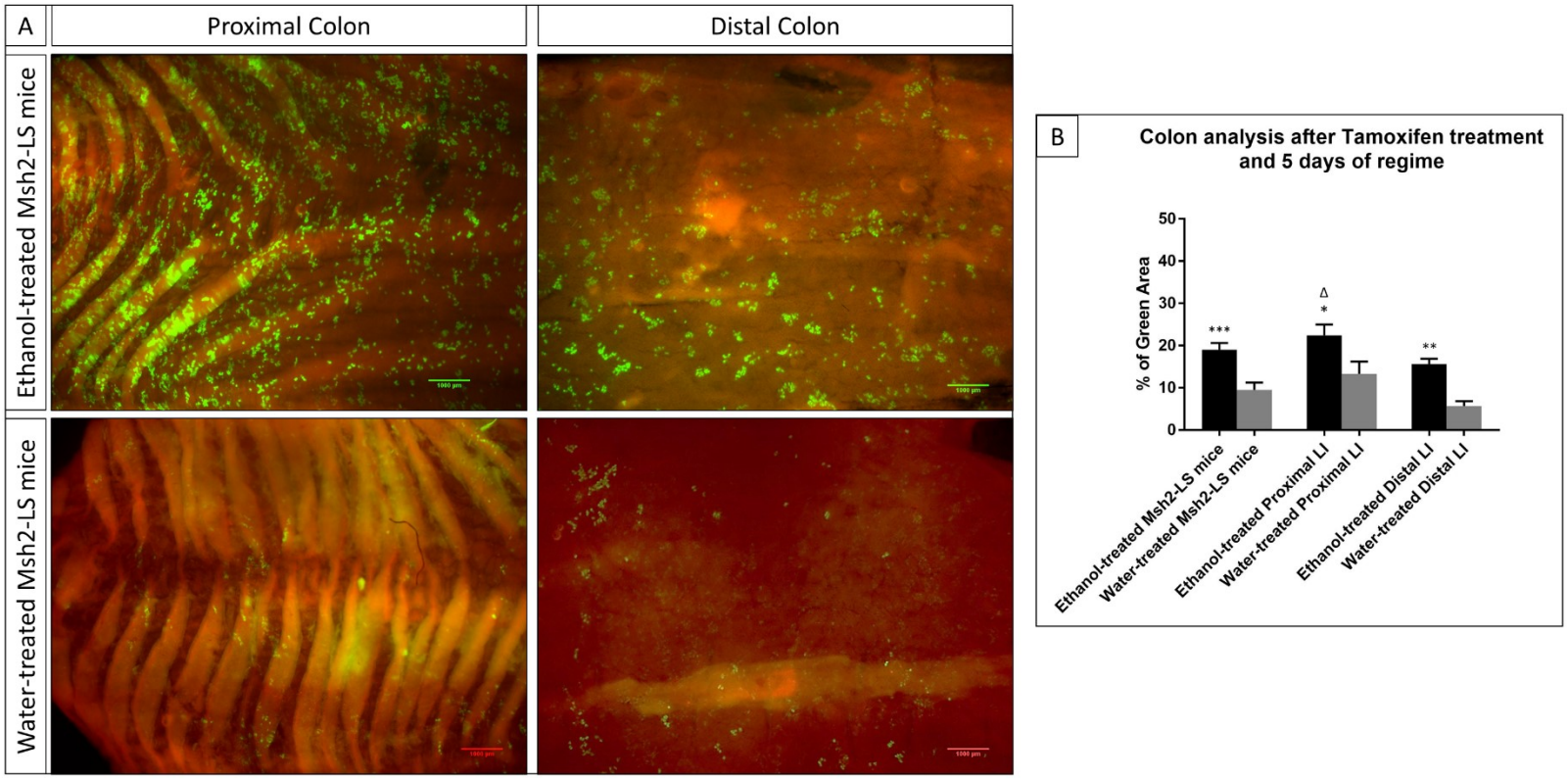

Figure 7.2. A) Fluorescence stereomicroscopic analysis of the mT and mG fluorescent protein expression in whole-mount colonic samples of *Msh2$^{flox/-}$; Lgr5CreERT2$^{+/-}$; mTmG$^{+/-}$* mice after 5 days of either 20% ethanol in drinking water (top row) or 5 days of normal water (row below). Representative fluorescent images of the mT & mG/GFP detection in the proximal colon (left) and distal colon (right). B) The percentage green areas were statistically significantly higher in ethanol-treated Msh2-LS (EtOH_*Msh2$^{fl\ KO}$*) murine whole colon, proximal colon and distal colon compared with water-treated Msh2-LS (H_2O_*Msh2$^{fl\ KO}$*) murine colon equivalents. Students t Test; ***p=0.0003; **p=0.0020; *p=0.0277. The percentage green areas were statistically significantly higher in EtOH_*Msh2$^{fl\ KO}$* murine proximal colon compared with EtOH_*Msh2$^{fl\ KO}$* murine distal colon. Students t Test; $^{\Delta}$p=0.0384. Images taken using the Leica MZ FLIII fluorescence stereomicroscope at 2.5X magnification/1x objective (bar at lower left indicates 1000µm).

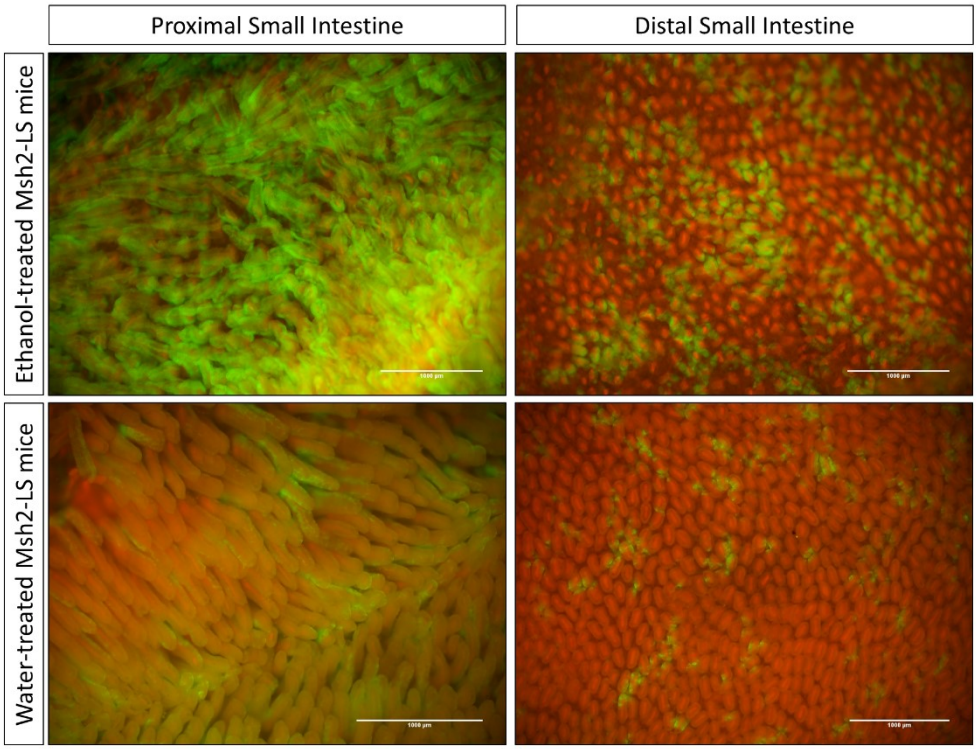

Figure 7.3. Fluorescence stereomicroscopic analysis of the mT and mG fluorescent protein expression in whole-mount small intestinal samples of *Msh2$^{flox/-}$; Lgr5CreERT2$^{+/-}$; mTmG$^{+/-}$*mice after 5 days of either 20% ethanol in drinking water (top row) or 5 days of normal water (row below). Representative fluorescent images of the mT & mG/GFP detection in the proximal small intestine (left) and distal small intestine (right). Images taken using the Leica MZ FLIII fluorescence stereomicroscope at 2.5X and 3.6X magnification/1X objective (bar at lower left indicates 1000µm).

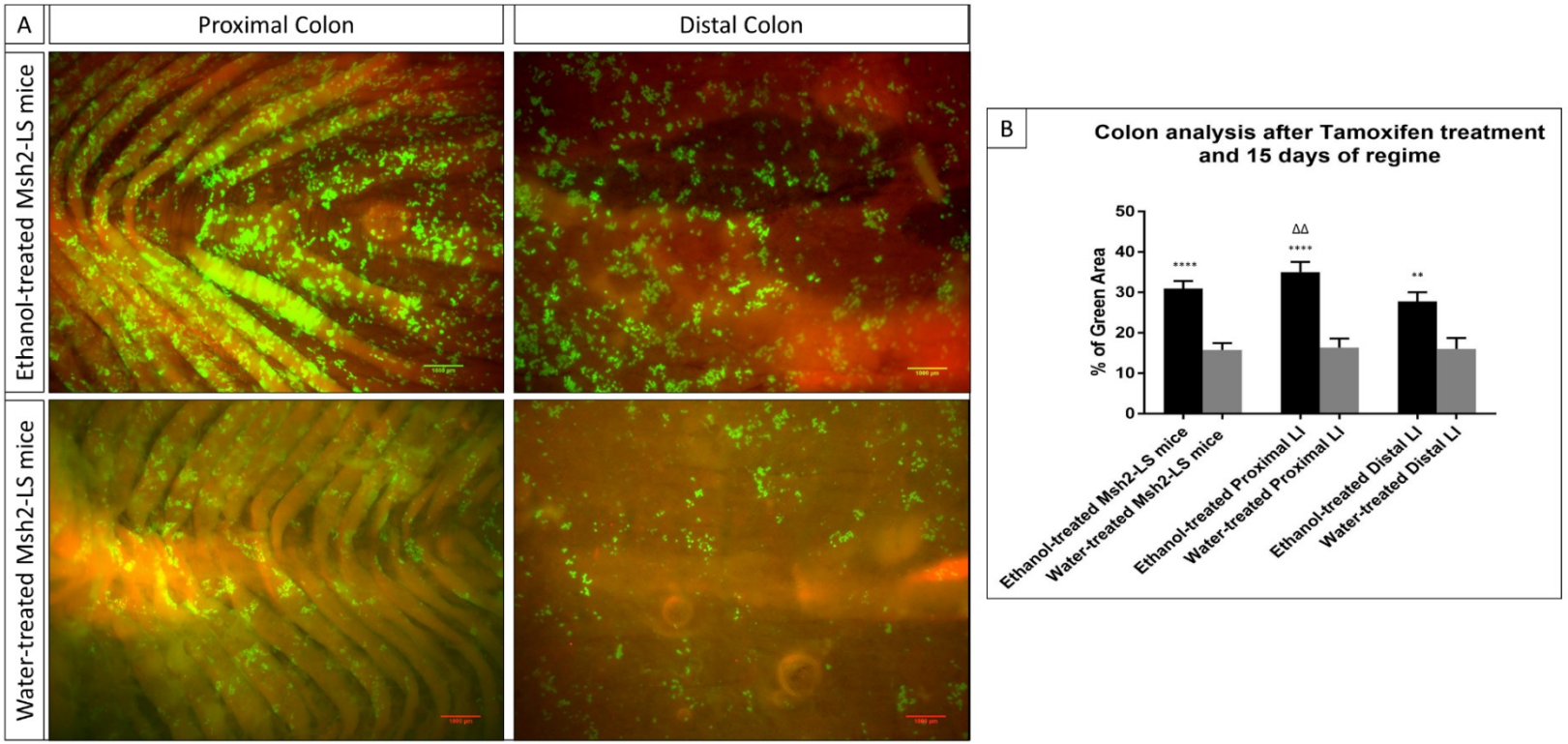

Figure 7.4: A) Fluorescence stereomicroscopic analysis of the mT and mG fluorescent protein expression in whole-mount colonic samples of *Msh2$^{flox/-}$; Lgr5CreERT2$^{+/-}$; mTmG$^{+/-}$* mice after 15 days of either 20% ethanol in drinking water (top row) or 15 days of normal water (row below). Representative fluorescent images of the mT & mG/GFP detection in the proximal colon (left) and distal colon (right). B) The percentage green areas were statistically significantly higher in ethanol-treated Msh2-LS (EtOH_*Msh2$^{fl\ KO}$*) murine whole colon, proximal colon and distal colon compared with water-treated Msh2-LS (H_2O_*Msh2$^{fl\ KO}$*) murine colon equivalents. Students t Test; ****p<0.0001; **p=0.0029. The percentage green areas were statistically significantly higher in EtOH_*Msh2$^{fl\ KO}$* murine proximal colon compared with EtOH_*Msh2$^{fl\ KO}$* murine distal colon. Students t Test; $^{\Delta\Delta}$p=0.0040. Images taken using the Leica MZ FLIII fluorescence stereomicroscope at 2.5X magnification/1X objective (bar at lower left indicates 1000µm).

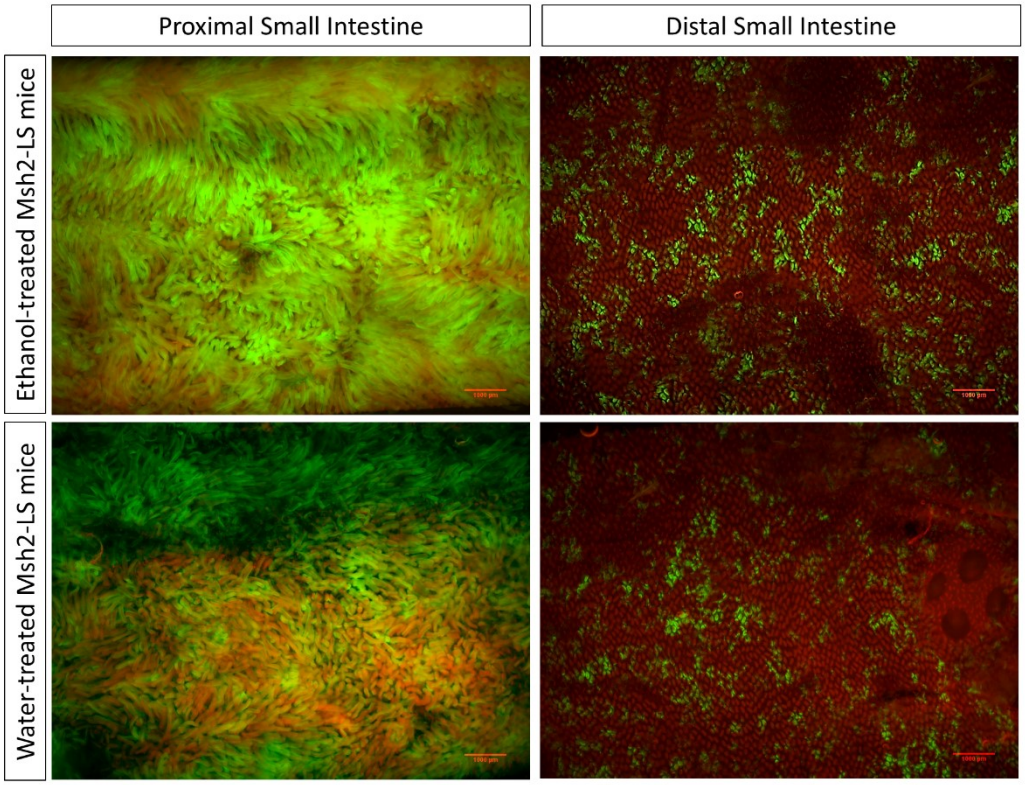

Figure 7.5: Fluorescence stereomicroscopic analysis of the mT and mG fluorescent protein expression in whole-mount small intestinal samples of *Msh2$^{flox/-}$; Lgr5CreERT2$^{+/-}$; mTmG$^{+/-}$*mice after 15 days of either 20% ethanol in drinking water (top row) or 15 days of normal water (row below). Representative fluorescent images of the mT & mG/GFP detection in the proximal small intestine (left) and distal small intestine (right). Images taken using the Leica MZ FLIII fluorescence stereomicroscope at 2.5X magnification/1X objective (bar at lower left indicates 1000µm).

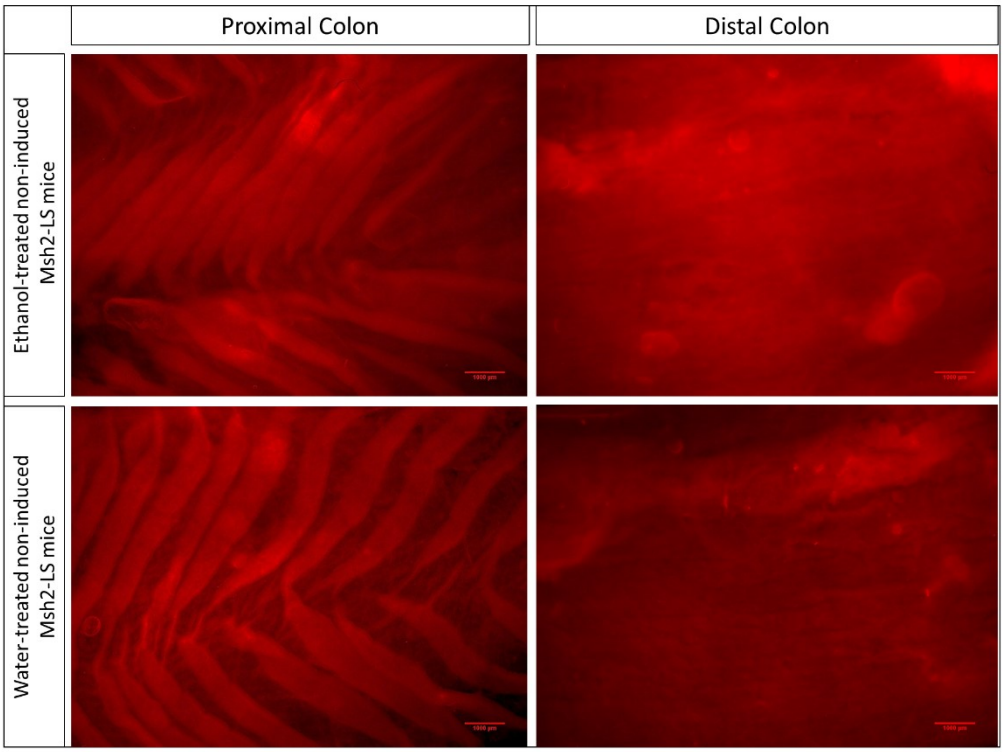

Figure 7.6. Fluorescence stereomicroscopic analysis of the mT and mG fluorescent protein expression in whole-mount colonic samples of non-induced (no Tamoxifen treatment) *Msh2$^{flox/-}$; Lgr5CreERT2$^{+/-}$; mTmG$^{+/-}$* mice after 15 days of either 20% ethanol in drinking water (top row) or 15 days of normal water (row below). Representative fluorescent images show only mT expression (with no mG/GFP detection) in the proximal colon (left) and distal colon (right). Images taken using the Leica MZ FLIII fluorescence stereomicroscope at 2.5X magnification/1X objective (bar at lower left indicates 1000µm).

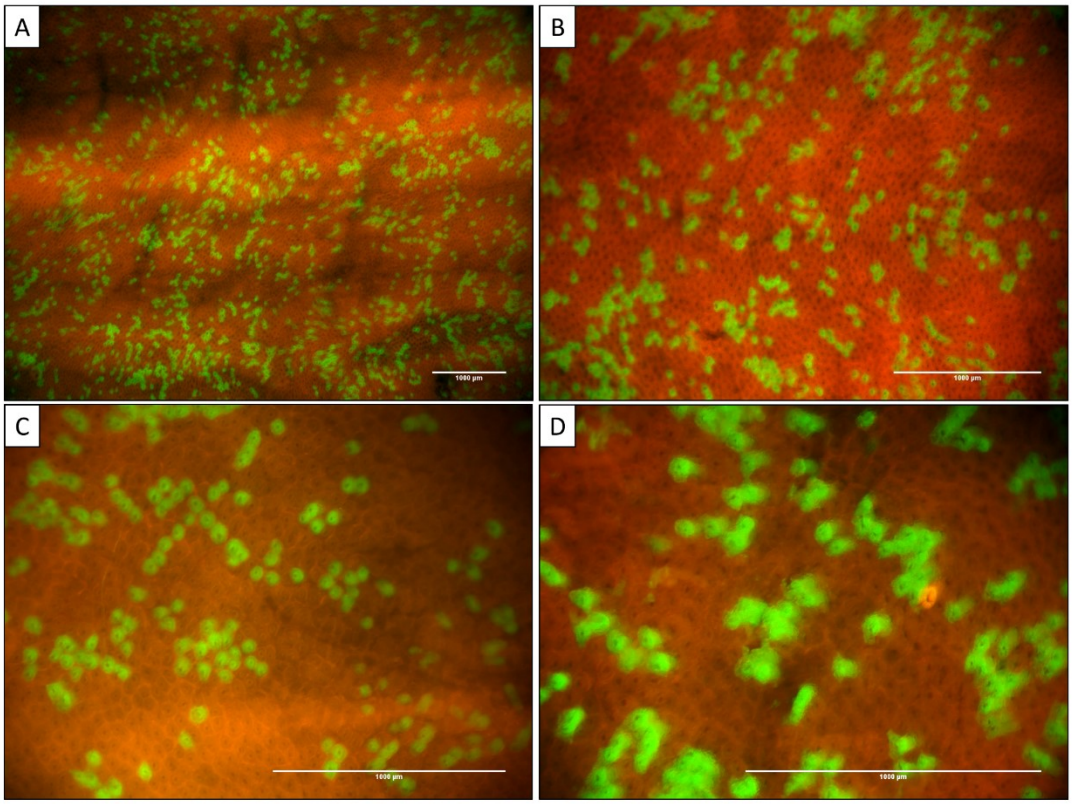

Figure 7.7: Representative images of mT and mG fluorescent protein expression in whole-mount colon samples of *Msh2$^{flox/-}$; Lgr5CreERT2$^{+/-}$; mTmG$^{+/-}$* control (no ethanol treatment) mice. Images taken using the Leica MZ FLIII fluorescence stereomicroscope at 2.5X (A), 4X (B), 6.3X (C) and 8X (D) magnification/1X objective (bar at lower left indicates 1000µm).

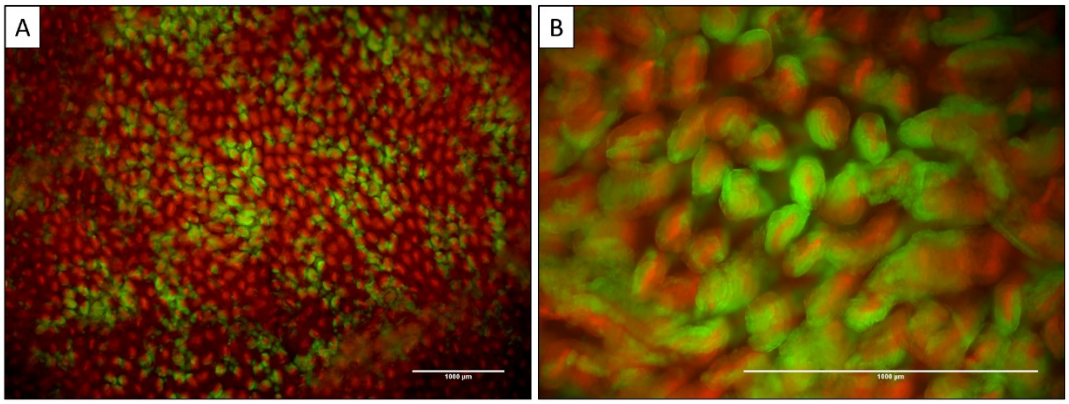

Figure 7.8: Representative images of mT and mG fluorescent protein expression in whole-mount small intestinal samples of *Msh2$^{flox/-}$; Lgr5CreERT2$^{+/-}$; mTmG$^{+/-}$* control (no ethanol treatment) mice, showing green strips of green mG+ epithelium partially lining otherwise red mT+ villi. Images taken using the Leica MZ FLIII fluorescence stereomicroscope at 2.5X (A) and 8X (B) magnification/1X objective (bar at lower left indicates 1000µm).

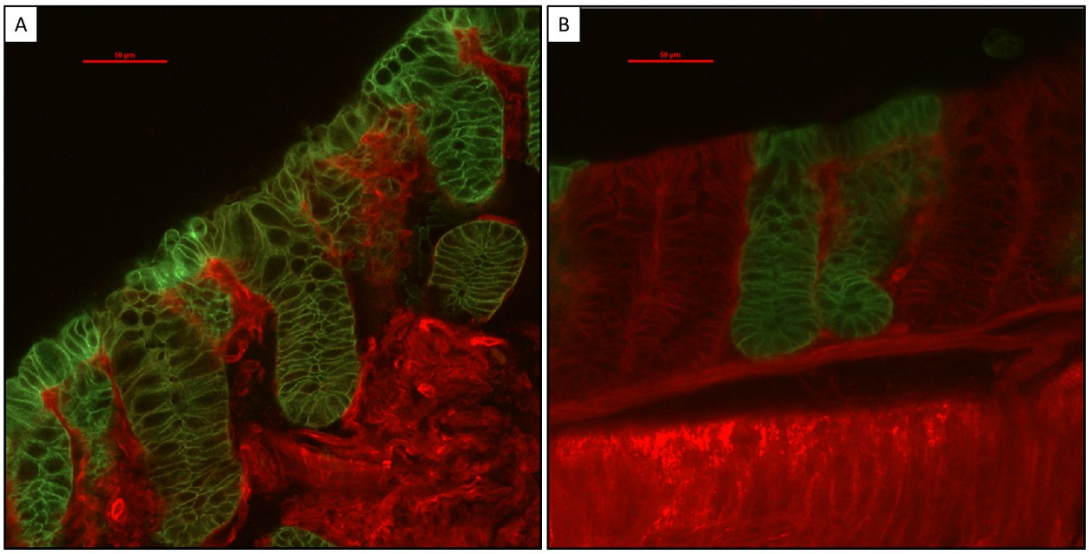

Figure 7.9: Two representative images (A and B) of mT and mG fluorescent protein expression in whole-mount large intestinal mucosa samples of *Msh2$^{flox/-}$; Lgr5CreERT2$^{+/-}$; mTmG$^{+/-}$* mice (no ethanol treatment). The images show the distribution of green mG+ cells in Cre-activated colonic crypts and adjacent surface epithelium of Msh2-LS murine colon (in selected crypts with cells that express mG). In contrast, some of the adjacent crypts, lamina propria cells and smooth muscle cells of the muscularis mucosae express red mT fluorescent protein. Images taken using the Nikon A1R point scanning confocal microscope (bar at lower left indicates 50µm).

7.2.2.1 Investigation of ethanol effects on mG-expressing colonic crypt foci with fluorescence microscopy in *Aldh1b1* wild-type Msh2-LS mice, *Aldh1b1* conditional-knockout Msh2-LS mice and *Aldh1b1* constitutive-knockout Msh2-LS mice.

The combined areas of mT and mG fluorescent protein were detected by fluorescence microscopy and quantified using an ImageJ algorithm in all analyses of the *Aldh1b1*^{wt} Msh2-LS mouse model, *Aldh1b1*$^{flox/flox}$ Msh2-LS mouse model and *Aldh1b1*$^{-/-}$ Msh2-LS mouse model experiments, in order to obtain data about changes in the mG+ colonic crypt foci size and number, measured as percentage green area, as well as their distribution over time under ethanol or water treatment regimes. Small groups (n=3) of mice were used to investigate the changes at 5 days and 15 days, whereas after these times single mice in tumour-watch studies were analysed at longer timepoints. The mG+ crypt foci were quantified in both EtOH_*Msh2*$^{fl\ KO}$ and H_2O_*Msh2*$^{fl\ KO}$ murine colonic samples and there was a peak of percentage green area around the first 15 days of ethanol- or water-treatment (30.9% and 19%, respectively). Subsequently, the percentage of green areas were broadly stable over the following weeks showing a gentle increase over time with some variability towards the end of the experiment, at around 30 to 50 weeks. EtOH_*Msh2*$^{fl\ KO}$ murine colon showed statistically significantly higher percentage green areas than H_2O_*Msh2*$^{fl\ KO}$ murine colon (Figure 7.10). In *Aldh1b1*$^{flox/flox}$ Msh2-LS mice, quantification of the mG+ colonic crypt foci in both EtOH_*Aldh1b1*$^{fl/fl}$_*Msh2*$^{fl\ KO}$ and H_2O_*Aldh1b1*$^{fl/fl}$_*Msh2*$^{fl\ KO}$ mice showed a steady increase in percentage of green area reaching a high peak around 11-12 weeks of ethanol-treatment (39.9%). By contrast, this high peak was not observed in the H_2O_*Aldh1b1*$^{fl/fl}$_*Msh2*$^{fl\ KO}$ murine colon, which showed a pattern very similar to that seen in H_2O_*Msh2*$^{fl\ KO}$ mice. In *Aldh1b1*$^{flox/flox}$ Msh2-LS murine colon, the percentage green areas decreased after 12 weeks to stabilize over the subsequent weeks, with a small increase towards the end of the experiment with some mild variability. EtOH_*Aldh1b1*$^{fl/fl}$_*Msh2*$^{fl\ KO}$ colon showed statistically significantly higher percentage green areas than H_2O_*Aldh1b1*$^{fl/fl}$_*Msh2*$^{fl\ KO}$ murine colon equivalents (Figure 7.11). In EtOH_*Aldh1b1*$^{-/-}$_*Msh2*$^{fl\ KO}$ mice, measurement of the mG+ colonic crypt foci showed a similar trend to that observed in EtOH_*Msh2*$^{fl\ KO}$ mice, in which after the peak seen around 15 days of ethanol-treatment, the percentage green areas settle to a more stable trend with a mild increase over the subsequent weeks towards the end of the experiment. EtOH_*Aldh1b1*$^{-/-}$_*Msh2*$^{fl\ KO}$ murine colon showed statistically significantly higher percentage green areas than H_2O_*Aldh1b1*$^{-/-}$_*Msh2*$^{fl\ KO}$ colon (Figure 7.12).

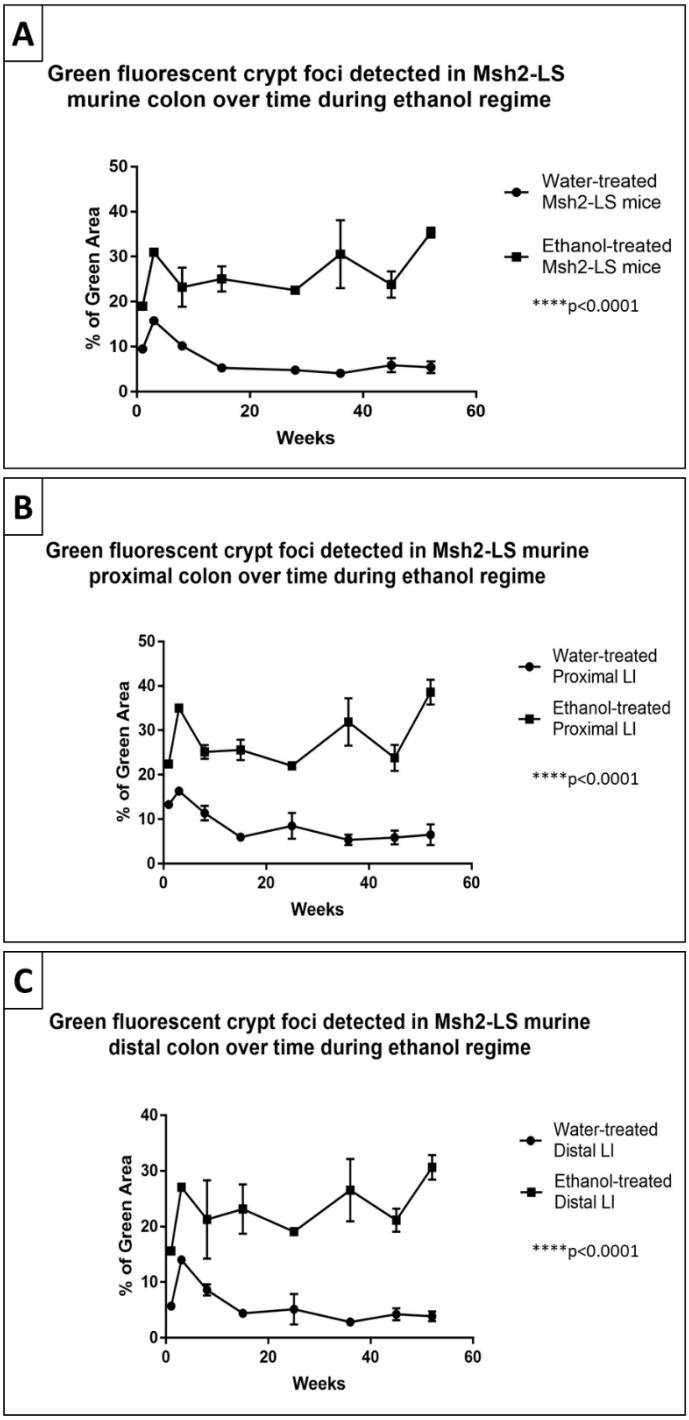

Figure 7.10: Quantification of green fluorescent crypt foci in large intestinal mucosal epithelium of *Aldh1b1*^{wt} Msh2-LS mice treated with either 20% ethanol in drinking water or normal drinking water for various periods of time (x-axis). Percentage green areas were measured in whole-mount specimens of *Aldh1b1*^{wt} Msh2-LS murine whole colonic samples (A), with separate examination of proximal colon (B), and distal colon (C). Ethanol-treated *Aldh1b1*^{wt} Msh2-LS (EtOH_*Msh2*$^{fl\ KO}$) murine colon showed statistically significantly higher percentage green areas than in water-treated *Aldh1b1*^{wt} Msh2-LS (H_2O_*Msh2*$^{fl\ KO}$) murine colon equivalents; 2-way-ANOVA test analysis, ****p<0.0001 vs. water (data shown as mean±SD, n=1-3 mice in each group per time point).

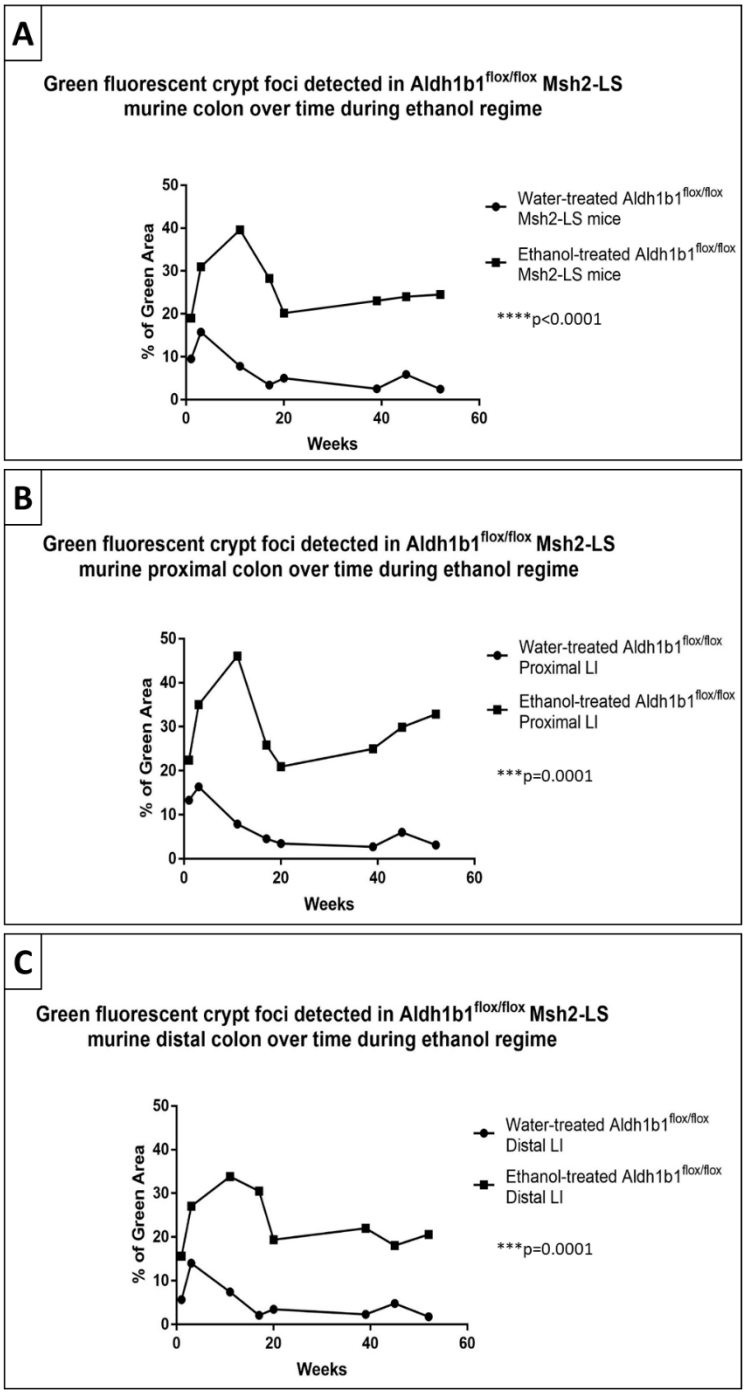

Figure 7.11: Quantification of green fluorescent crypt foci in large intestinal mucosal epithelium of *Aldh1b1*$^{flox/flox}$ Msh2-LS mice treated with either 20% ethanol in drinking water or normal drinking water for various periods of time (x-axis). Percentage green areas were measured in whole-mount specimens of *Aldh1b1*$^{flox/flox}$ Msh2-LS murine whole colonic samples (A), with separate examination of proximal colon (B), and distal colon (C). Ethanol-treated *Aldh1b1*$^{flox/flox}$ Msh2-LS (EtOH_*Aldh1b1*$^{fl/fl}$_*Msh2*$^{fl\ KO}$*)* murine colon showed statistically significantly higher percentage green areas than in water-treated *Aldh1b1*$^{flox/flox}$ Msh2-LS (H_2O_*Aldh1b1*$^{fl/fl}$_*Msh2*$^{fl\ KO}$*)* murine colon equivalents; 2-way-ANOVA test analysis, ****p<0.0001 and ***p=0.0001 vs. water (data shown as mean, n=1-3 mice in each group per time point).

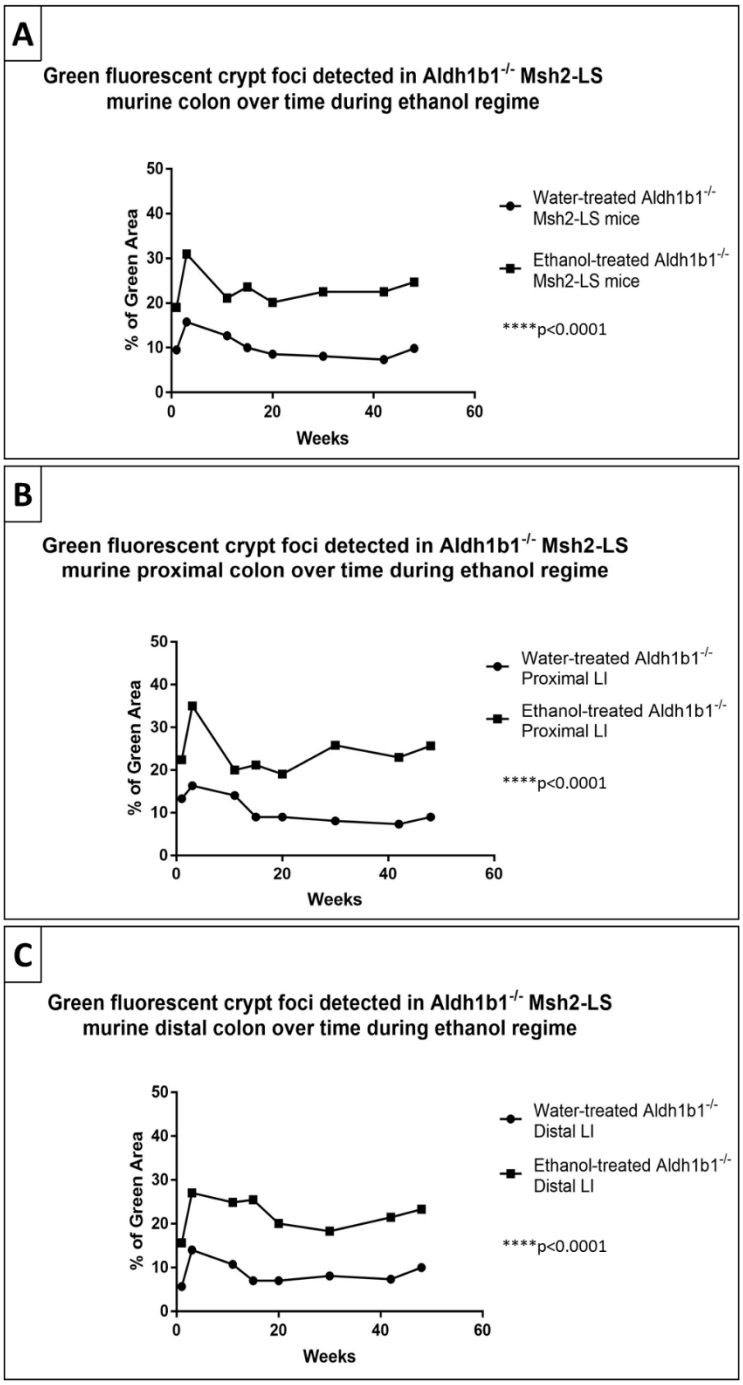

Figure 7.12: Quantification of green fluorescent crypt foci in large intestinal mucosal epithelium of *Aldh1b1*$^{-/-}$ Msh2-LS mice treated with either 20% ethanol in drinking water or normal drinking water, for various periods of time (x-axis). Percentage green areas were measured in whole-mount specimens of *Aldh1b1*$^{-/-}$ Msh2-LS murine colonic samples (A), with separate examination of proximal colon (B), and distal colon (C). Ethanol-treated *Aldh1b1*$^{-/-}$ Msh2-LS (EtOH_*Aldh1b1*$^{-/-}$_*Msh2*$^{fl\ KO}$) murine colon showed statistically significantly higher percentage green areas than in water-treated *Aldh1b1*$^{-/-}$ Msh2-LS (H_2O_*Aldh1b1*$^{-/-}$_*Msh2*$^{fl\ KO}$) murine colon equivalents; 2-way-ANOVA test analysis, ****p<0.0001 vs. water (data shown as mean, n=1-3 mice in each group per time point).

7.2.2.2 Immunohistochemical characterization of mG-expressing intestinal crypt foci in *Aldh1b1* wild-type Msh2-LS mice after long-term ethanol treatment

To test whether the expression of mG/GFP observed by fluorescence microscopic detection, following Cre activation, correlated with the loss of Msh2 expression, IHC analyses were performed using anti-Msh2 antibody and anti-GFP antibody on intestinal tissue serial sections that were almost adjacent to each other. Small intestine, caecum and colon serial (or near serial) sections were cut from Tamoxifen-induced *Msh2$^{flox/-}$; Lgr5CreERT2$^{+/-}$; mTmG$^{+/-}$* mice and immunostained for both mG/GFP and Msh2 proteins.

Small intestinal tissue samples of *Msh2$^{-/-}$* mice were used as Msh2-null controls and GFP-negative expression controls; and SI tissue samples of Tamoxifen-induced *mTmG$^{+/+}$* mice as Msh2-positive and GFP-positive expression controls (Figure 3.9). The lack of DAB-brown staining for both anti-Msh2 and anti-GFP IHC in the *Msh2$^{-/-}$* SI tissues confirmed complete loss of Msh2 expression and lack of mG/GFP expression (Figure 3.9 A-B) in the Msh2-null negative control tissues. The presence of DAB-brown staining in the *mTmG$^{+/+}$* SI tissues confirmed presence of Msh2 expression throughout the SI tissue and GFP expression in some Cre-activated crypts (Figure 3.9 C-D) in the *mTmG$^{+/+}$* positive control tissues.

The IHC analysis of Msh2 in *Msh2$^{flox/-}$; Lgr5CreERT2$^{+/-}$; mTmG$^{+/-}$* murine intestinal tissues showed lack of DAB-brown staining in some crypts scattered along the length of small intestinal mucosa, caecal mucosa and colonic mucosa (Figure 7.13, 7.14, 7.15). The exact same crypts appeared positive for DAB-brown staining after immunohistochemical detection of mG/GFP on the almost adjacent serial sections from the same *Msh2$^{flox/-}$; Lgr5CreERT2$^{+/-}$; mTmG$^{+/-}$* murine intestinal tissue (Figure 7.13, 7.14, 7.15), confirming that the same small intestinal crypts, caecal crypts and colonic crypts had lost Msh2 protein expression and gained mG/GFP expression.

The immunohistochemical detection of Msh2 in large intestinal adenomas (both colonic and caecal) from Msh2-LS mice showed lack of DAB-brown staining (Figure 7.16), however after IHC staining for mG/GFP, the same crypts displayed either weak or no DAB-brown staining in the same adenomatous dysplastic glands (Figure 7.16).

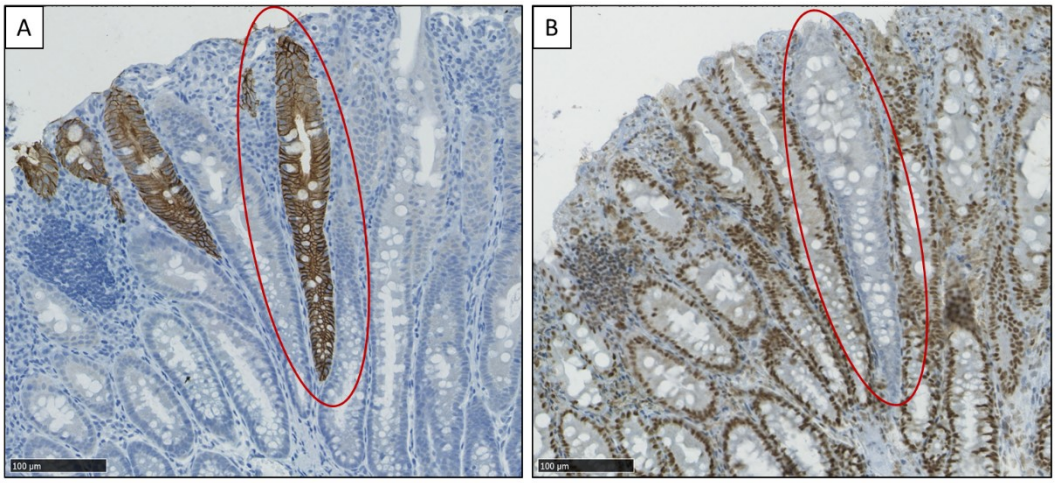

Figure 7.13: Representative images showing the comparison between mG/GFP and Msh2 immunostaining of almost adjacent serial sections of large intestinal mucosal epithelium of *Msh2$^{flox/-}$; Lgr5CreERT2$^{+/-}$; mTmG$^{+/-}$* mice treated with Tamoxifen to activate Cre in scattered Lgr5+ stem cells and their crypts. The same hyperproliferative crypt is positive for mG/GFP (A) and negative for Msh2 (B) (red ovals). Images taken using the Hamamatsu Nanozoomer and analysed with the Hamamatsu NDP Viewer software at 20X magnification (bar at lower left indicates 100um).

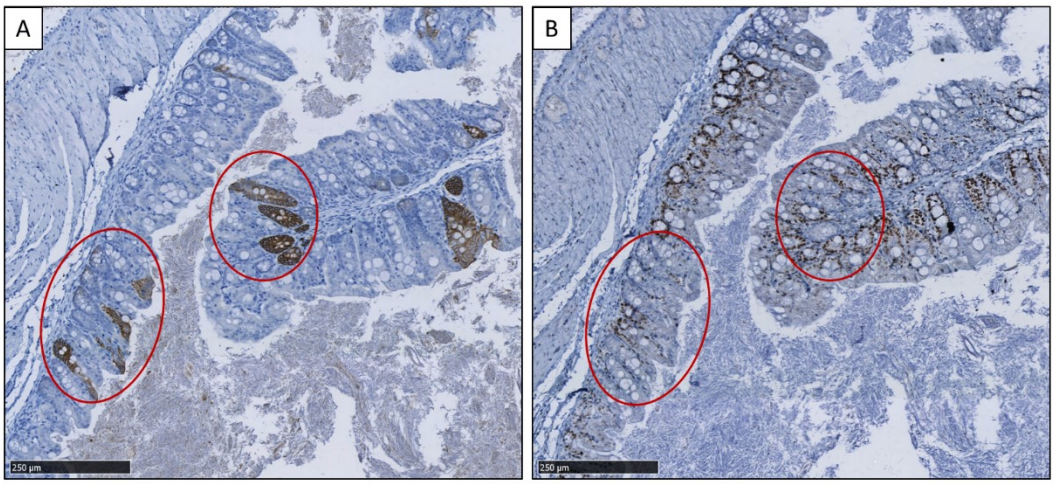

Figure 7.14: Representative images showing the comparison between mG/GFP and Msh2 immunostaining of almost adjacent serial sections of caecal mucosal epithelium of *Msh2$^{flox/-}$; Lgr5CreERT2$^{+/-}$; mTmG$^{+/-}$* mice treated with Tamoxifen to activate Cre in scattered Lgr5+ stem cells and their crypts. The same crypt foci are positive for mG/GFP (A) and negative for Msh2 (B) (red ovals). Images taken using the Hamamatsu Nanozoomer and analysed with the Hamamatsu NDP Viewer software at 10X magnification (bar at lower left indicates 250um).

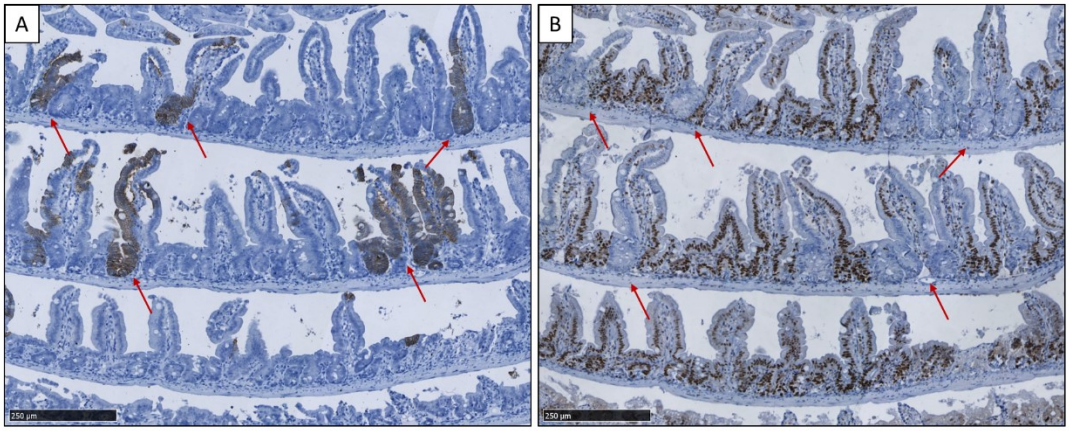

Figure 7.15: Representative comparison between mG/GFP and Msh2 immunostaining of almost adjacent serial sections of small intestinal mucosal epithelium of *Msh2$^{flox/-}$; Lgr5CreERT2$^{+/-}$; mTmG$^{+/-}$* mice treated with Tamoxifen to activate Cre in scattered Lgr5+ stem cells and their crypts. The same crypts, villi and part-villi are positive for mG/GFP (A) and are negative for Msh2 (B) (red arrows). Images taken using the Hamamatsu Nanozoomer and analysed with the Hamamatsu NDP Viewer software at 10X magnification (bar at lower left indicates 250um).

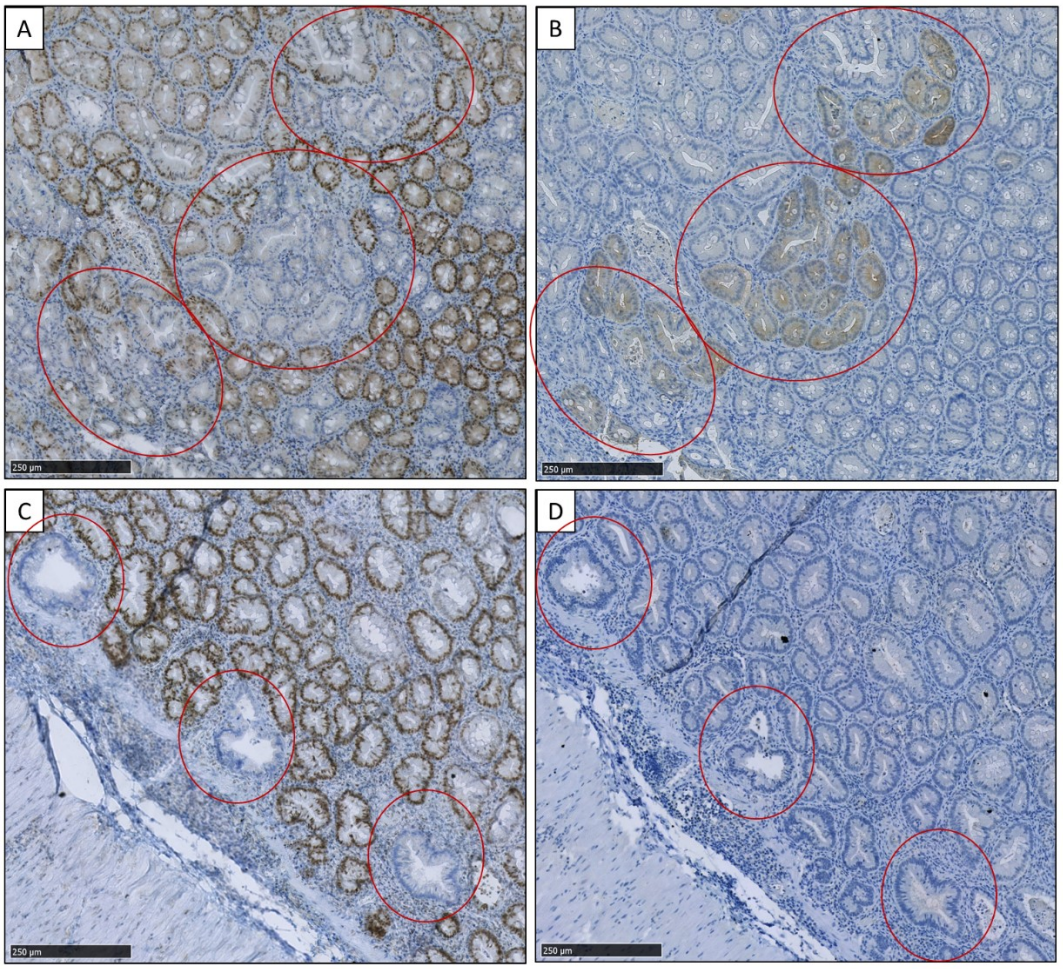

Figure 7.16: Representative adenoma images show the comparison between Msh2 and mG/GFP immunostaining of almost adjacent serial sections of a caecal adenoma (A and B) and a large intestinal adenoma (C and D) from *Msh2$^{flox/-}$; Lgr5CreERT2$^{+/-}$; mTmG$^{+/-}$* mice treated with Tamoxifen to activate Cre in scattered Lgr5+ stem cells and their crypts that may progress to form adenomas. In the caecal adenoma, the same crypt foci are negative for Msh2 (A) and positive for mG/GFP (B) (red ovals), however the GFP staining appears weak in some crypts. In the large intestinal adenoma those dMMR dysplastic crypt foci that are negative for Msh2 (C) are also negative for mG/GFP (D) (red ovals), consistent with GFP mutation resulting in lack of expression (GFP was expressed elsewhere in this section in non-dysplastic crypts). Images taken using the Hamamatsu Nanozoomer and analysed with the Hamamatsu NDP Viewer software at 10X magnification (bar at lower left indicates 250um).

7.3 FACS sorting of mT- and mG-expressing epithelial cells from small and large intestines from the Msh2-LS mouse model

7.3.1 Methods

7-9 weeks old *Msh2$^{flox/-}$; Lgr5CreERT2$^{+/-}$; mTmG$^{+/-}$* mice were divided into two groups. Group-A mice received i.p. injections of 0.15mg Tamoxifen/g bw on day 1 and 0.1mg Tamoxifen/g bw on day 2, 3 and 4; on day 5 mice were provided with normal drinking water for 1.5 months. By contrast, Group-B received i.p. injections of 0.15mg Tamoxifen/g bw on day 1 and 0.1mg Tamoxifen/g bw on day 2, 3 and 4; but on day 5 the Group-B mice were provided with 20% ethanol in drinking water for 1.5 months (Figure 7.17). During the necropsy dissection procedure, morphologically normal-appearing small and large intestinal tissues were harvested, and soaked in cold PBS and kept on ice. Samples of small and large epithelial cells were isolated by FACS from fresh tissue following the protocol described in Materials and Methods, using anti-EpCAM antibody to detect epithelial cells. Disaggregated samples of ethanol-and water-treated Msh2-LS murine small and large intestinal epithelial cells were sorted as EpCAM positive populations in 4 groups: mT-expressing events, mG-expressing events, double-positive mT+mG+ expressing events and double-negative null-mT/null-mG expressing events, using the FACSAria II with BD Accuri C6 analyser (IGMM FACS facility). Resulting data were analysed with FACSDiva 6.3.1 Software.

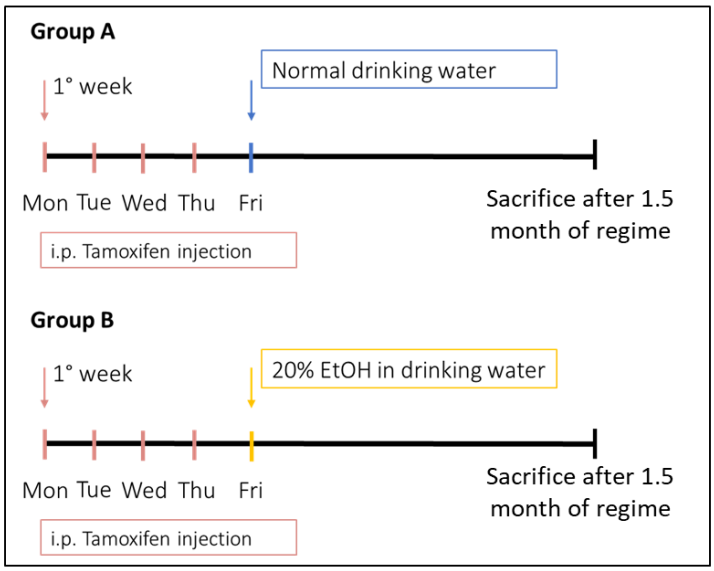

Figure 4.17: Experimental treatment protocols and timelines for Group-A (water-treated) and -B (ethanol-treated) mice, showing 4 days of i.p. injections of Tamoxifen, followed by either standard/normal drinking water (Group-A) or drinking or water containing 20% ethanol (Group-B). (EtOH = Ethanol).

7.3.2 Results

The FACS sorting of the ethanol- and water-treated Msh2-LS large and small intestinal samples did not show any quantitative and qualititative differences between the cell populations, due to loss of cell viability during experimental preparation procedures. EpCAM+ cells were subdivided into 4 groups, mT+/mG- cells, mT-/mG+ cells, double positive mT+/mG+ cells and double-negative mT-/mG- cells. The mT+/mG- cells or mT-/mG+ cells were the result of correct detachment of the intestinal epithelial cells (without or with prior Cre activation, respectively). The number of mT+/mG- cells was higher than the number of mT-/mG+ cells. Some cells that were negative for both mT and mG were detected during the FACS sorting, as a result of loss of both mT and mG expression. Some cells (or cell groups) that were positive for both mT and mG were detected during the FACS sorting, as a result of expression of both mT and mG, most probably due to doublets or larger clusters of mixed cells (Figure 7.18).

All 4 groups of cell samples were collected from each sorted specimen. RNA extraction was performed and resulting RNA samples were stored at -80℃. Due to COVID-19-related laboratory restrictions further analysis of gene expression in these samples was not completed.

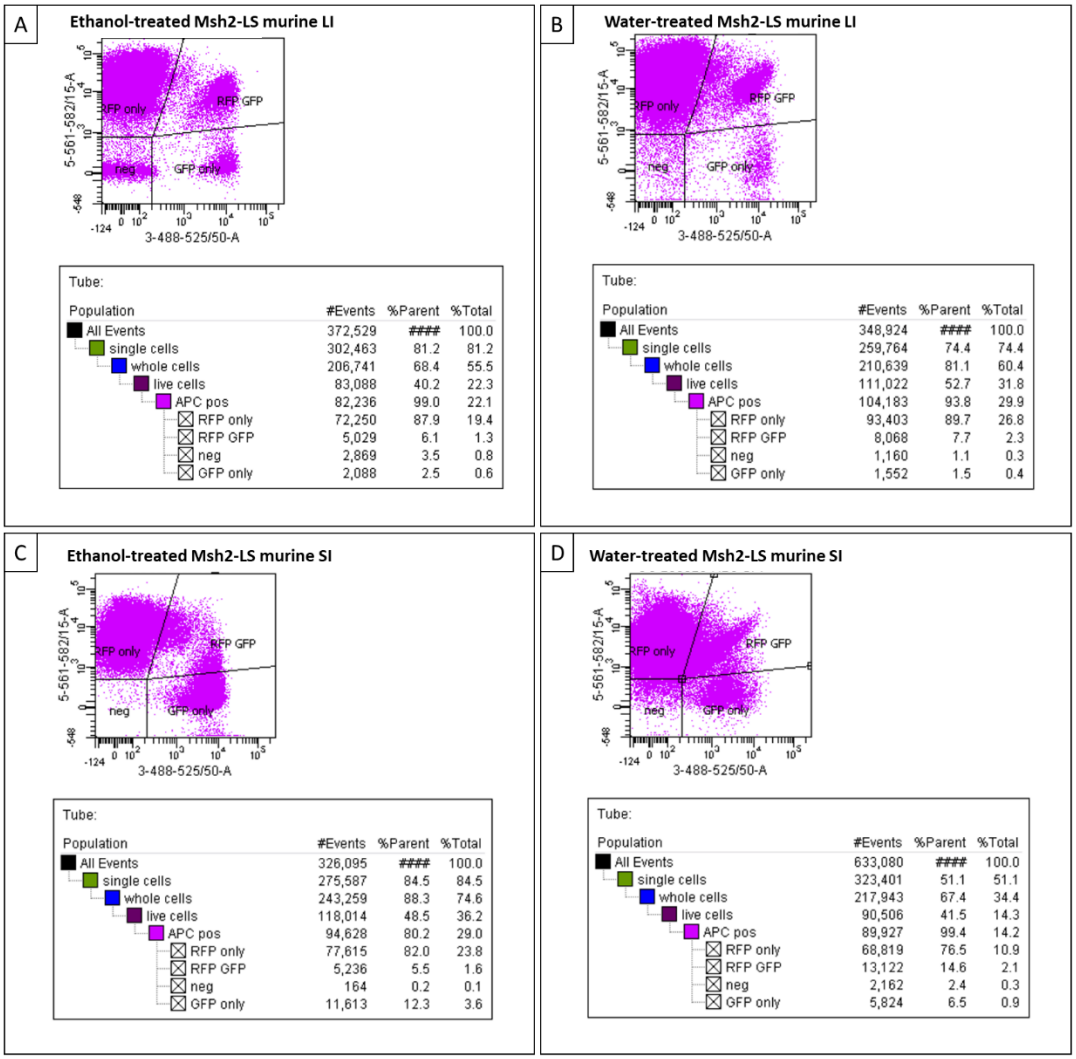

Figure 7.18: Representative graphs of the FACS sorting analysis reports. Ethanol-treated Msh2-LS murine large intestine (A), water-treated Msh2-LS murine large intestine (B), ethanol-treated Msh2-LS murine small intestine (C), and water-treated Msh2-LS murine small intestine were selectively sorted according to their positivity for EpCAM (antigen positive cells=APC pos) in 4 different groups: RFP+ cells (RFP only), cells positive for both RFP and GFP (RFP GFP), cells negative for both RFP and GFP (neg) and GFP+ cells (GFP only). (LI=large intestine, SI=small intestine, RFP= red fluorescent protein [mT], GFP=green fluorescent protein [mG]).

7.4 Discussion

In this chapter, expression of fluorescent green mG or fluorescent red mT proteins from the *mTmG* transgene reporter system was used to monitor any changes in the number, size, or distribution of crypt foci that were dMMR, following ethanol (compared with water) treatment of the mouse models over time. It was previously demonstrated (in Chapter 3) that the same crypts are both negative for Msh2 (confirming that they are dMMR) and positive for mG/GFP immediately following Cre-mediated activation in the Msh2-LS mouse model, and this was confirmed again by the data shown in this chapter for all three of the *Aldh1b1*^{wt} Msh2-LS, *Aldh1b1*$^{flox/flox}$ Msh2-LS and *Aldh1b1*$^{-/-}$ Msh2-LS murine models (data not shown for all cases). Thus, mG expression can be used as a marker to detect and measure percentage green areas of dMMR cells and crypts in these models immediately following Cre activation by Tamoxifen. Long-term studies were also used to follow the natural history of these dMMR crypts as they proliferate to form dMMR crypt foci along with their subsequent potential for evolution to neoplasms over longer periods of time in single mice in the tumour-watch study.

To study the early effects of ethanol/acetaldehyde on dMMR crypts and crypt foci, experimental groups were set up to monitor changes after 5 days or 15 days of either 20% ethanol in drinking water or normal water. Statistically significant increases in the percentage green areas, combining number and size of crypt foci containing mG-expressing cells, were observed along the large intestinal tract for both 5-day and 15-day ethanol-treated Msh2-LS mice compared with 5-day and 15-day water-treated Msh2-LS mice, more so in proximal colon than distal colon, matching the pattern of adenoma distribution. Following the peak around the 15-day timepoint, these percentage green area differences between ethanol- and water-treated Msh2-LS mice stabilised and continued over the longer term, up to 50 weeks, with some variability in the 30-50 week data.

Images of mG+ villi/crypts in the Msh2-LS murine small intestine were acquired after 5 days and 15 days of either ethanol- or water-treatment regimes, but quantification of the mG+ villlus/crypt foci was technically difficult due to the extensive and often confluent mG+ villus/crypt foci and the more complicated folded structure of the small intestinal mucosa in 3-dimensions. However, highly-magnified images of small intestinal mucosa showed the cellular localisation of mG+ cells sometimes in strips along the SI villi and this was corroborated by the anti-GFP IHC stains of Msh2-LS small intestine sections that showed

partial coverage of villi by strips of mG+/GFP+ and Msh2- epithelial cells. The murine colonic crypts were examined using a confocal microscope to obtain more high-powered and fine-detailed images of the distribution of mG+ cells within the colonic crypts. This revealed that the fluorescent green crypt foci observed with the stereomicroscope consisted of whole colonic crypts, either singly or in crypt clusters, that were fully occupied by mG+/GFP+ cells, with mG+/GFP+ cells present on the table surface epithelium of the colon. This was corroborated by the anti-GFP IHC stains of Msh2-LS colon sections that showed mostly whole crypts or groups of crypts containing mG+/GFP+ and Msh2- epithelial cells. These appearances are consistent with scattered colonic crypt Lgr5+ stem cells undergoing Lgr5-driven Cre-mediated concurrent inactivation of the floxed allele of *Msh2* and change from mT to mG expression, with rapid monoclonal conversion of the crypts, such that whole crypts appear positive for mG expression within 5-15 days. Following further exposure to ethanol and its metabolite acetaldehyde, subsequent crypt fission leads to formation of mG+ crypt foci within a few weeks and these continue to expand over time at variable rates.

The detection and quantification of mT and mG fluorescent protein by fluorescence microscopy was extended to all analyses of the *Aldh1b1*^{wt} Msh2-LS, *Aldh1b1*$^{flox/flox}$ Msh2-LS, and *Aldh1b1*$^{-/-}$ Msh2-LS murine model tumour-watch experiments, in order to obtain data about changes in the mG+ dMMR colonic crypts and crypt foci over longer periods of time under long–term ethanol- or water-treatment regimes. In all three mouse models, the ethanol-treated murine colon showed statistically significantly higher percentage green areas than water-treated murine colon. The PGA followed very similar trends in all 3 experimental mouse models, in which after reaching a peak around 15 days (or longer, 11-12 weeks, in the *Aldh1b1*$^{flox/flox}$ Msh2-LS model), the PGA stabilises over the following weeks showing a mild increase over time with some variability towards the end of the study period. In *Aldh1b1*$^{flox/flox}$ Msh2-LS mice, the early peak was higher and this may be consistent with combined inactivation in individual cells of MMR and Aldh1b1 expression with increased levels of intracellular acetaldehyde conferring an increased survival selective advantage upon dMMR cells (relative to MMR-proficient cells that can still undergo cell cycle arrest or apoptosis following DNA damage, as described in Chapter 6, Figure 6.92), with subsequent increased acetaldehyde-driven proliferation resulting in a relatively higher and longer early peak of mG+/dMMR crypt foci.

The PGA of dMMR crypt foci trends over time showed a high early peak that decreased after 15-30 days (11-12 weeks for the *Aldh1b1*$^{flox/flox}$ Msh2-LS model) followed by subsequent stabilisation with a mild increase over time rather than a continually increasing level of PGA over time. Possible explanations for this include a time-related immune response to the early expansion of dMMR/mG+ crypts, with a reduction in dMMR/mG+ crypt foci occurring perhaps due to immune attack against the more immunogenic dMMR crypt cells that may present more frameshift peptides (Seth et al., 2018). This would require future immunological studies to evaluate whether greater numbers of infiltrating T lymphocytes could be found around dMMR crypt foci at the appropriate timepoints. However there is evidence of an immune response with infiltrating CD8+ and other lymphocytes and myeloid cells within and around adenomas shown in Chapter 4, 4.4.2.6. Another explanation might be that dMMR/mG+ crypt cells, including stem cells that populate the whole crypt, may acquire inactivating mutations in the *mG/GFP* gene sequence, resulting in loss of mG expression. Evidence for this was observed in the IHC analyses of adenomas for Msh2 and mG/GFP expression. In addition to confirming the co-localization in the same crypts or crypt foci showing gain of mG expression and loss of Msh2 expression, IHC for Msh2 and mG/GFP showed evidence of a partial or complete lack of GFP expression in some large intestinal adenomas, consistent with acquired mutations in *mG/GFP*.

MMR-deficient cells are characterized by hypermutability (increased mutation rate by 100x – 1000x due to uncorrected mismatches) and microsatellite instability (MSI, variation in length of repetitive or microsatellite sequences, due to uncorrected insertion/deletion loops or InDels), with MSI confirmed in the Msh2-LS murine adenomas described in Chapter 4, 4.6 (Kloor et al., 2012). Analysis of the pCA-mTmG plasmid sequence (used to generate mTmG reporter mice) revealed the presence of several repetitive DNA coding sequences in the membrane-targeted *EGFP* (*mG/GFP*) gene sequence that are highly likely to act as targets for InDel mutations that are not repaired in mismatch repair-deficient cells (Figure 7.19). These are likely to confer susceptibility of the *mG/EGFP* gene to inactivating frameshift mutations, including within dMMR crypt stem cells in the Msh2-LS model, particularly following ethanol/acetaldehyde exposure. Subsequent investigations could include targeted DNA sequencing of the *mG* gene in those colonic adenoma glands (microdissected) that show loss of mG immunostaining to study the proposed acquisition of inactivating InDel mutations in *mG.*

As a result of the induced loss of Msh2 expression with abrogation of MMR in the *Aldh1b1*^{wt} Msh2-LS, *Aldh1b1*$^{flox/flox}$ Msh2-LS and *Aldh1b1*$^{-/-}$ Msh2-LS murine model intestinal epithelial stem cells (and subsequently whole crypts and crypt foci), there will be an increased risk of InDel mutations in repetitive sequences in large numbers of genes that contain exonic repetitive DNA sequences, as well as microsatellite sequences between genes, thus generating expression of InDel mutated proteins or truncated proteins, that are fragmented to frameshift peptides that can be presented as antigenic epitopes on MHC molecules to trigger an immune attack against the dMMR cells. In a previous chapter (Chapter 4) dMMR tumours from the Msh2-LS mouse model were shown to have MSI, functionally confirming this deficiency in mismatch repair. The observation of loss of mG/GFP immunostaining in some adenomas in these models indicate that the *mTmG* transgene reporter can be used effectively for short-term studies (perhaps up to 12-15 weeks, although further studies are required to map these changes more precisely in time) of Cre-mediated DNA recombination in the Msh2-LS models, but in the context of Cre-induced inactivation of the mismatch repair system, the *mTmG* transgene system appears to become a less reliable system to monitor changes in mG+ dMMR crypt foci over longer periods of time due to the proposed time-related acquisition of InDel mutations in the *mG/GFP* gene (Figure 7.20).

In conclusion, a model is proposed (set out in a schematic diagram in Figure 7.20) to show the effects on colonic crypts and crypt foci of the mismatch repair pathway/acetaldehyde gene/environment interactions. These MMR/acetaldehyde interactions are likely to have significant effects on both MMR-proficient and MMR-deficient cells and crypts scattered along the large intestinal mucosa. Following ethanol ingestion and its metabolic conversion to acetaldehyde with acetaldehyde-induced DNA base damage, MMR-proficient intestinal stem cells and crypt daughter cells are able to activate DNA mismatch repair of the (MMR-recognised) base damage, leading to either cell cycle arrest, to allow repair of mild DNA damage, or apoptosis in the case of unrepairable severe DNA damage. However, following loss of the second *Msh2* allele (in the Msh2-LS model), MMR-deficient stem cells and their crypt daughter cells are unable to activate the MMR pathway and so neither cell cycle arrest nor apoptosis can be triggered, resulting in aberrant survival of DNA-damaged cells and their subsequent proliferation (mostly acetaldehyde-induced colonic crypt cell proliferation, as shown in previous chapters). The proliferating dMMR stem cells populate crypts (detected as mG-positive appearing crypts in the Msh2-LS model colon under fluorescent microscopy and shown as green dots on the red background in the schematic diagram), and these crypts

expand further, by crypt fission, to form dMMR crypt foci or clusters. MMR-deficient stem cells and crypts have MSI resulting in accumulation of InDel mutations in microsatellite or repeat sequences, leading to both activation of an increased immune response to frameshift peptides and loss of expression of mG/GFP, as the *mG* gene contains many repetitive sequences. This mutational inactivation of mG generates colonic crypts and crypt foci that lack expression of both mG and mT and would thus be transparent (represented as black dots in the third panel of the schematic diagram). Such transparent crypts and crypt foci would allow red fluorescent light from the underlying mT-expressing tissue (lamina propria, muscularis mucosae, submucosa and muscularis propria) below to shine through and hence should also appear red on fluorescence microscopy, but negative on immunstaining for mG/GFP. This process of dMMR crypt foci expansion would be enhanced by continued exposure over time to acetaldehyde, increasing DNA damage with selective survival and proliferation of dMMR cells and crypts, only partially balanced by some crypt loss from immune attack, with an increasing risk of these precursors forming neoplasms (adenomas) and a risk of further progression to malignancy (adenocarcinomas) in a few cases as mutations accumulate.

>EGFP

GCTCCTCGCCCTTGCTCACGGATCCTACCTTCACGTGGCCATTCTCCTGTCCGTTCGCTTTGGAAGGCGA

CGAGGCCACAGCCGCCTCCCCAGGCCTCTCCGCGGCGGCTTCTCCCTTCGCTGCGGTCTTGGAGAAACAG

CAACCCATCCGCGGTGATGATCCGGAACCCTTAATATAACTTCGTATAATGTATGCTATACGAAGTTATT

AGGTCCCTCGACCTGCAGCCCAAGCTTACTTACCATGTCAGATCCAGACATGATAAGATACATTGATGAG

TTTGGACAAACCACAACTAGAATGCAGTGAAAAAAATGCTTTATTTGTGAAATTTGTGATGCTATTGCTT

TATTTGTAACCATTATAAGCTGCAATAAACAAGTTAACAACAACAATTGCATTCATTTTATGTTTCAGGT

TCAGGGGGAGGTGTGGGAGGTTTTTTAAAGCAAGTAAAACCTCTACAAATGTGGTATGGCTGATTATGAT

CTCTAGTCAAGGCACTATACATCAAATATTCCTTATTAACCCCTTTACAAATTAAAAAGCTAAAGGTACA

CAATTTTTGAGCATAGTTATTAATAGCAGACACTCTATGCCTGTGTGGAGTAAGAAAAAACAGTATGTTA

TGATTATAACTGTTATGCCTACTTATAAAGGTTACAGAATATTTTTCCATAATTTTCTTGTATAGCAGTG

CAGCTTTTTCCTTTGTGGTGTAAATAGCAAAGCAAGCAAGAGTTCTATTACTAAACACAGCATGACTCAA

AAAACTTAGCAATTCTGAAGGAAAGTCCTTGGGGTCTTCTACCTTTCTCTTCTTTTTTGGAGGAGTAGAA

TGNTGAGAGTCAGCAGTAGCCTCATCATCACTAGATGGCATT

Microsatellite Repeats in EGFP		
Position	Repeats	Sequence
309	6	AAAAAA
385	3	AACAACAAC
440	6	TTTTTT
601	3	TGTGTG
614	6	AAAAAA
768	6	AAAAAA
822	6	TTTTTT
861	3	TCATCATCA

Figure 7.19: The *mG/EGFP* gene sequence (from the *mTmG* reporter construct DNA sequence) contains 8 repetitive (microsatellite) sequences (highlighted in yellow), which are summarised in a table of the microsatellite repeats showing their position within the *EGFP* gene, number of repetitions and the repeated sequence. Mononucleotide (e.g. AAAAAA or TTTTTT), dinucleotide (e.g. TGTGTG) and trinucleotide (e.g. AACAACAAC or TCATCATCA) repeats are known to be more susceptible to InDel mutations in MMR-deficient cells in Lynch Syndrome tumours and their precursors, rendering the *mG/EGFP* gene particularly susceptible to mutational inactivation in dMMR crypt stem cells in the Msh2-LS model, particularly following ethanol/acetaldehyde exposure.

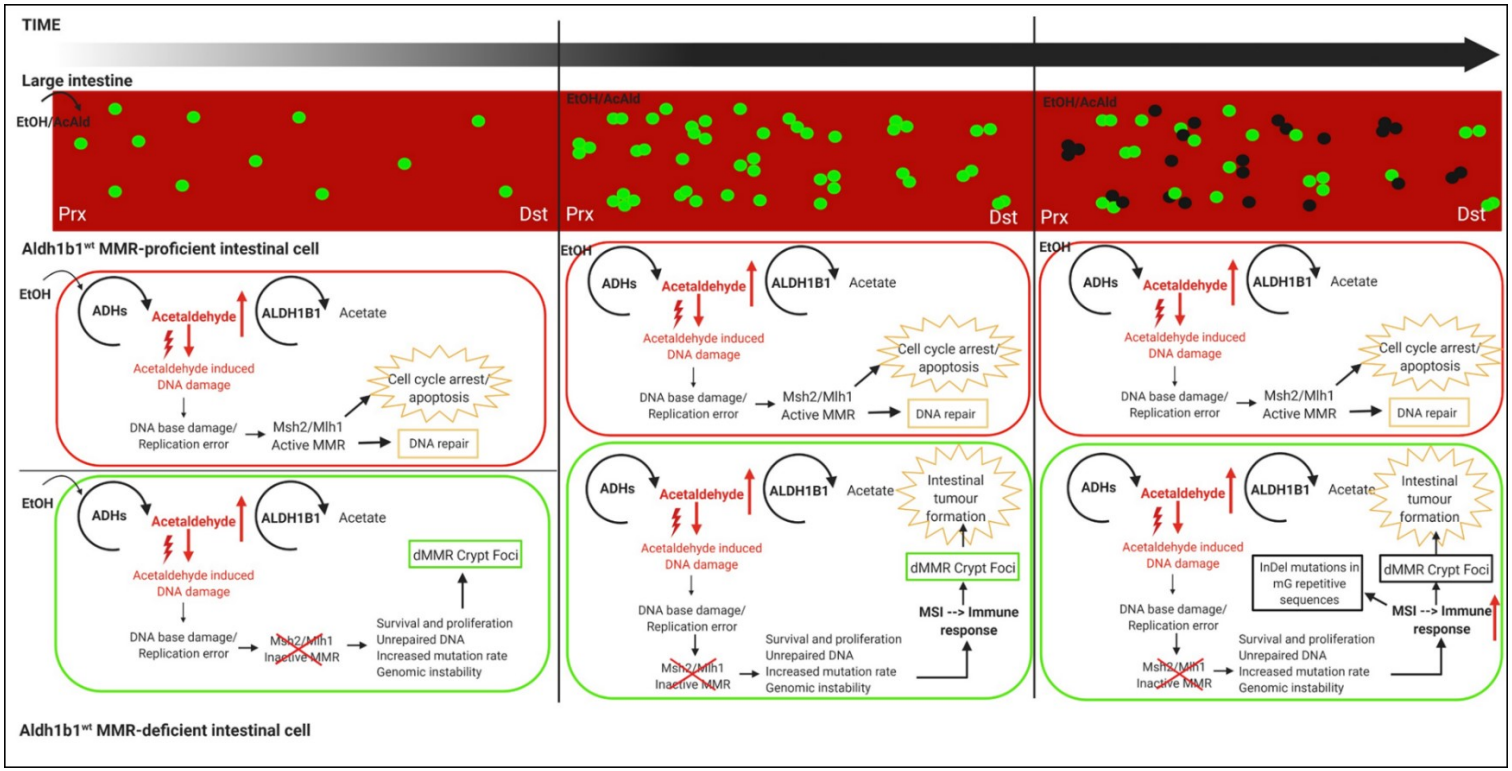

Figure 7.20: Schematic diagram of the proposed model of the effects on crypt foci of MMR/acetaldehyde gene/environment interactions in both MMR-proficient (mG-/mT+ red cells/crypts constituting the red background of the large intestinal mucosa) and MMR-deficient (mG+/mT- green cells/crypts scattered along the large intestinal mucosa, shown as green dots) cells. Upon acetaldehyde (AcAld) exposure (following ethanol (EtOH) ingestion and its metabolism to acetaldehyde), the pMMR intestinal cells (with red cell membranes) are able to activate DNA mismatch repair of the (MMR-recognised) base damage, bringing about either cell cycle arrest (mild DNA damage) or apoptosis (severe DNA damage). By contrast, the dMMR cells (with green cell membranes) are unable to activate the MMR pathway (following Cre-mediated inactivation of *Msh2,* indicated by the red cross through *Msh2*) and so, neither cell cycle arrest nor apoptosis are triggered, resulting in

aberrant survival of DNA-damaged cells and their subsequent proliferation. The proliferating mG+/dMMR stem cells populate crypts (shown as green dots on the red background, first panel), and these crypts expand further (by crypt fission) to form mG+/dMMR crypt foci or clusters (second panel), with more mG+/dMMR crypt foci in the proximal than the distal colon. These mG+/dMMR cells have MSI resulting in accumulation of InDel mutations in microsatellite or repeat sequences, leading to both activation of an increased immune response to frameshift peptides and loss of expression of mG/GFP (as the *mG* gene contains many repetitive sequences) (mG- /mT- crypt foci are represented as black/transparent dots in the third panel). This process is enhanced by continued exposure to acetaldehyde over time increasing DNA damage with selective survival and proliferation of dMMR cells and crypts, only partially balanced by some crypt loss from immune attack, with increasing risk over time of neoplasm formation as mutations accumulate. (Prx=proximal colon; Dst=distal colon).

Chapter 8: Final Discussion, Future Work & Summary

8.1 Ethanol/Acetaldehyde induces colonic neoplasms in a Lynch Syndrome mouse model

In this project the overarching objective was to investigate whether there is a gene/environment interaction between ethanol/acetaldehyde and dMMR, that may cause an acceleration of dMMR-driven intestinal tumour formation. Aims included determining whether ethanol/acetaldehyde can increase the number and size of precursor lesions and colonic adenomas, whether these adenomas can progress to invasive adenocarcinoma, and whether MMR plays a role in protecting intestinal epithelial cells from ethanol/acetaldehyde-induced DNA damage.

The Msh2-LS mouse model, created by Wojciechowicz et al., (2014), was combined with the *mTmG* transgene reporter, generated by Dr. Lou, Stanford University (Muzumdar et al., 2007). This modified version of the Msh2-LS mouse model was successfully generated to establish a colony of *Msh2$^{flox/-}$; Lgr5CreERT2$^{+/-}$; mTmG$^{+/-}$* model mice. In the *Msh2$^{flox/-}$; Lgr5CreERT2$^{+/-}$; mTmG$^{+/-}$* mouse model, the activation of Cre recombinase by Tamoxifen-treatment induced recombination between two inverted *loxP* sites flanking *Msh2* exons 12 and 13 in the floxed *Msh2* allele and also between the *loxP* sites flanking the *mT* sequence in the *mTmG* transgene. This was shown to generate a *Msh2* knockout allele (*Msh2$^{flox/OFF}$*) and convert the same intestinal stem cells to mG expression, forming dMMR intestinal stem cells that subsequently form dMMR crypts, which are marked by green fluorescent mG expression. That these two events occurred in the same cells/crypts was confirmed by IHC for both Msh2 and GFP expression on adjacent serial sections of intestinal tissue, showing colocalization in the same cells/crypts of mG expression and the loss of Msh2 expression.

The *Msh2$^{flox/-}$; Lgr5CreERT2$^{+/-}$; mTmG$^{+/-}$* model mice (Msh2-LS mice) were used to investigate the effects of long-term ethanol treatment on intestinal tumour formation and progression. Long-term ethanol treatment of the Tamoxifen-induced Msh2-LS mice showed evidence of large intestinal hyperproliferation and adenoma formation (with 5 adenocarcinomas) in 65% (15/23 mice) of the EtOH_*Msh2$^{fl\ KO}$* mice, over an average of 6 months of ethanol treatment. This is in stark contrast to the H_2O_*Msh2$^{fl\ KO}$* mice, none of which developed intestinal tumours over the same time period, with only 1 colonic adenoma observed at 15 months (4%, 1/23).

In previous experiments by our group reported by Müller et al., (2016), *Aldh1b1*-depleted mice and WT control mice treated with long-term ethanol showed intestinal tumour formation after 1 year in both groups. In Wojciechowicz et al., (2014), Tamoxifen-induced *Msh2$^{flox/-}$; Lgr5CreERT2$^{+/-}$* mice (without any further treatment) showed intestinal tumour formation within an average of 19 months. Long-term ethanol-treatment of the Tamoxifen-induced Msh2-LS mice provided evidence of ethanol-induced colonic adenoma formation that occurred at higher numbers and at a much earlier time, consistent with ethanol-mediated acceleration of dMMR-driven large intestinal tumour formation.

The EtOH_*Msh2$^{fl\ KO}$* mice showed a pattern of tumour distribution of one or more large intestinal tumours mainly in the proximal colon and mid colon. A similar pattern is observed in human LS patients, in which colonic tumour formation occurs more in the caecum, ascending colon and transverse colon regions (proximal colon), than in the descending colon, sigmoid colon and rectum (distal colon), compared with sporadic colorectal tumours that are predominantly distal in location. Rijcken et al. (2008), described 50% of colonic adenomas in human LS cases were found in the proximal colon, compared with 26% of sporadic adenomas. In addition, proximal LS adenomas progressed to high-grade dysplasia more frequently than distal LS adenomas, and also more showed high-grade dysplasia than larger distal adenomas (Rijcken et al., 2008). Adenomas in LS familial cases were smaller when compared with sporadic adenomas, and proximal LS familial adenomas ≥ 5 mm showed more severe dysplasia than larger proximal sporadic adenomatous polyps (Lynch et al., 2009).

Here, ethanol-treatment of the combined Msh2-LS and *mTmG* mouse model, which was designed to study intestinal tumour formation associated with defective DNA mismatch repair (with Tamoxifen-induced Lgr5-driven Cre activation occurring in small and large intestines, as *Lgr5* is an intestinal stem cell-specific gene) (Barker et al, 2008), has been characterised to show that it represents a good model of human LS in terms of the formation and location of adenomas, with some progressing to adenocarcinomas, only in the colon (not in the small intestine), and these predominantly form in the proximal and mid colon. No small intestinal adenomas were seen in the water- or ethanol-treated Msh2-LS mice, similar to the very low incidence of small intestinal tumours in human LS patients (Schulmann et al., 2005).

8.2 Ethanol/Acetaldehyde increases mismatch repair-deficient crypt foci that act as precursors in the pathogenesis of colonic neoplasms in this Lynch Syndrome mouse model

Msh2 immunohistochemical analysis of Msh2-LS murine intestines showed inducible loss of Msh2 expression in scattered large intestinal crypts and small intestinal crypts and villi. A statistically significantly higher number of dMMR crypt foci were observed in ethanol-treated murine colons compared with water-treated murine colons. However, the number of dMMR crypt/villus foci appeared to be higher in EtOH_*Msh2*$^{fl\ KO}$ murine SI than in colon even though no SI tumours were observed. All large intestinal adenomas from EtOH_*Msh2*$^{fl\ KO}$ mice showed Msh2-negative dysplastic glands, often surrounded by or admixed with Msh2-positive non-dysplastic crypts showing reactive or hyperproliferative changes. This confirmed that colonic adenomas arose from dMMR (Msh2-negative) crypt precursors. This is consistent with observations from human LS patients that the risk of colonic tumour formation correlates with the number and size of the MMR-deficient crypt clusters that expand over time in affected LS patients (Kloor et al., 2012; Shia et al., 2015; Wojciechowicz et al., 2014). The complete abrogation of MMR activity in these crypt foci was confirmed by the presence of Msh6-negative crypts (detected by IHC) scattered along both SI and colon of Tamoxifen-induced Msh2-LS mice in a very similar frequency and pattern as Msh2-negative crypts, as Msh6 is the heterodimeric binding partner of Msh2 and loss of Msh2 is considered to lead to destabilisation and loss of Msh6, but retention of Mlh1 expression, as confirmed in this study (Poulogiannis et al., 2010). Microsatellite instability was also shown in adenomas arising in the Msh2-LS mouse model, validating functional loss of the MMR pathway.

The positive Ki67 immunostaining in elongated large intestine crypts confirmed the presence of extended hyperproliferative zones identified morphologically on routine H&E stains. The proliferation marker Ki67 showed statistically significant higher expression levels in EtOH_*Msh2*$^{fl\ KO}$ murine colon compared with ethanol-treated murine SI and compared with H_2O_*Msh2*$^{fl\ KO}$ murine intestinal tissues (both colon and SI). These observations confirm the previously reported association of long-term ethanol treatment of mice and colonic mucosal epithelial hyperproliferation, likely to act as a tumour promoter in the initiator-promoter model of carcinogenesis (Müller et al., 2016; Scott et al., 1984).

β-catenin is a Wnt signalling pathway intermediate and its nuclear localisation by immunostaining is a useful biomarker of colorectal neoplasms (Cong et al., 2003). Colonic adenomas and adenocarcinomas from EtOH_*Msh2*$^{fl\ KO}$ mice showed a heterogeneous pattern with variable numbers of adenoma cells showing moderately to strongly positive β-catenin nuclear immunostaining, due to accumulation and translocation of β-catenin into the nuclei of dysplastic cells. This pattern supports heterogeneous activation of the Wnt signalling pathway in these tumours and has been observed in human MMR-deficient CRC (Lugli et al., 2007), more often in association with activating mutations in the β-catenin encoding gene *CTNNB1* than *APC* mutations in LS patients (Ahadova et al., 2016; Fukushima et al., 2001; Mirabelli-Primdahl et al., 1999).

Following ethanol treatment, a significant DNA damage response was immunohistochemically detected using antibodies against yH2AX, a DNA damage marker, (Siddiqui, 2015) and p53, which showed the "wild-type pattern" observed previously in response to DNA damage (Köbel et al., 2016). Increased levels of yH2AX and "wild-type pattern" nuclear p53 immunostaining were observed in EtOH_*Msh2*$^{fl\ KO}$ murine large intestine compared with H_2O_*Msh2*$^{fl\ KO}$ murine large intestine, and also compared with almost no to very low expression in ethanol-treated Msh2-LS small intestine. This suggests that Msh2 / MMR plays a key role in protecting the MMR-proficient colonic epithelial cells against this type of DNA damage, but Msh2 appears not to be the sole protective mechanism for small intestinal epithelial cells from ethanol/acetaldehyde-induced DNA damage.

The increased DNA damage observed in EtOH_*Msh2*$^{fl\ KO}$ murine large intestinal mucosal epithelium was consistent with the statistically significantly higher levels of circulating plasma acetaldehyde detected in these mice compared with H_2O_*Msh2*$^{fl\ KO}$ mice by plasma acetaldehyde assay. Acetaldehyde is a highly reactive molecule able to cause a wide range of DNA modifications (Seitz & Stickel, 2007). In the absence of MMR some of these DNA lesions are not recognised and repaired. Loss of MMR pathway function results in dMMR with hypermutability (increased mutation rate by 100x – 1000x due to uncorrected mismatches) and MSI (manifested by variation in length of repetitive microsatellite sequences due to uncorrected insertion/deletion loops). More importantly dMMR results in reduced susceptibility to either cell cycle arrest or apoptosis induced by those types of DNA damage recognised by the MMR system (Poulogiannis et al., 2010; Seth et al., 2018; Toft et al., 1999). Thus, unrepaired acetaldehyde-induced DNA damage in dMMR cells that fail to

arrest or die are likely to result in both an increased mutation rate and aberrant survival with an increased risk of neoplasm formation.

The immunohistochemical analysis of cCAs3, a key effector of cell death by apoptosis (Holubec et al., 2005; Talmon et al., 2010), showed significantly higher numbers of apoptotic bodies in colons from EtOH_*Msh2*$^{fl\ KO}$ mice compared with no detectable cCas3+ apoptotic bodies in colons from H_2O_*Msh2*$^{fl\ KO}$ mice, consistent with increased apoptosis associated with pMMR colonic epithelial cell exposure to ethanol/acetaldehyde (only scattered crypts are defective for MMR in this model, the majority are proficient for MMR as seen by the large area of red fluorescent pMMR crypts compared with the smaller area of green dMMR crypts). The almost complete lack of detection of apoptotic bodies in large intestinal tumours from Msh2-LS mice is consistent with the inability of dMMR cells to activate cell death by apoptosis following DNA damage of MMR-recognisable type. Furthermore, MSI was detected using a panel of microsatellite markers in colonic adenomas from EtOH_*Msh2*$^{fl\ KO}$ mice, functionally confirming abrogation of the mismatch repair system in these adenomas. Detection of infiltrating immune cells (by IHC pilot studies) in the intestinal adenomas of EtOH_*Msh2*$^{fl\ KO}$ mice supports an immune response against dMMR adenoma cells. Defective MMR with MSI causes mutations in protein coding repetitive DNA sequences that are likely to result in production of FSPs (Sæterdal et al., 2001). Such FSPs are novel antigens and elicit both humoral and cellular immune responses, which are seen as TILs around the dMMR crypts in LS patients as well as in dMMR cancers, both sporadic and due to LS (M. Linnebacher et al., 2001; Reuschenbach et al., 2010; Seth et al., 2018a).

The data provide evidence that ethanol and its metabolite acetaldehyde act as tumour promoters causing proliferation of colonic epithelium and can also select for aberrant survival of dMMR cells, via loss of MMR-recognised DNA damage-induced apoptosis. This aberrant survival and proliferation of DNA-damaged dMMR colonic epithelial cells is likely to lead to an increased probability of acquisition and fixation of DNA mutations, including some affecting tumour driver genes, explaining the accelerated colonic adenoma formation. Hence, there is evidence for a selective advantage of the dMMR/ethanol/acetaldehyde interaction, as a gene/environment interaction, that is consistent with accelerated colonic adenoma development and further progression to adenocarcinoma (in some cases) in EtOH_*Msh2*$^{fl\ KO}$ mice. The hyperproliferation process is observed mostly in the proximal colon and mid colon, but not in the small intestine, and is proposed to be a key driver of the

location of tumour formation at these sites in this Msh2-LS model, very similar to the anatomical tumour distribution seen in human Lynch Syndrome patients.

Early in these studies, we attempted to further accelerate dMMR-driven intestinal tumorigenesis in Msh2-LS mice by adding a TMZ treatment (described by Wojciechowicz et al., 2014) to the long-term ethanol treatment. The aim was to accelerate intestinal tumour formation to 2-4 months to reduce the experimental time period, in contrast to the 1 year of ethanol treatment required for intestinal adenoma formation in WT and Aldh1b1-depeleted mice (Müller et al., 2016), and the 1.5 years or longer for intestinal adenoma development in otherwise untreated Msh2-LS model mice (Wojciechowicz et al., 2014). The immunohistochemical analysis of Msh2, Ki67 and β-catenin of tumour and normal intestinal tissue of TMZ- and ethanol-treated Msh2-LS mice confirmed the carcinogenic properties of TMZ, which is known to be a powerful DNA methylating agent and carcinogen. TMZ was shown to confer proliferative advantage upon established dMMR crypt foci with selection for survival and expansion in the Msh2-LS murine intestines that led to intestinal tumour formation (Wojciechowicz et al., 2014). However, the carcinogenic properties of TMZ were too potent in these experiments, inducing early-occurring extra-intestinal tumours (independent of dMMR), predominantly thymic lymphomas, that masked any carcinogenic ethanol effects upon the intestines. The intestinal data obtained were inconclusive as TMZ was too potent a carcinogen to allow exploration of the intestinal tumour-promoting and DNA-damaging effects of ethanol and its major metabolite acetaldehyde, in combination with deficient MMR. For this reason, it was decided to discontinue the experimental use of TMZ in combination with ethanol in the Msh2-LS mouse model and to focus solely on the effects of ethanol without any other carcinogens on the Msh2-LS models.

8.3 Inactivation of *Aldh1b1* allowed exploration of the effects of acetaldehyde on DNA damage and its interaction with deficient mismatch repair during intestinal tumourigenesis in Lynch Syndrome mouse models

Both the conditional-knockout *Aldh1b1* allele (*Aldh1b1^{flox}*) and the constitutive-knockout *Aldh1b1* allele (*Aldh1b1^{-}*) were introduced into the Msh2-LS mouse model to further investigate the gene/environment interaction between acetaldehyde and dMMR, in the context of formation of precursor lesions, adenomas and adenocarcinomas. The *Msh2$^{flox/-}$; Lgr5CreERT2$^{+/-}$; mTmG$^{+/-}$; Aldh1b1$^{flox/flox}$* colony and the *Msh2$^{flox/-}$; Lgr5CreERT2$^{+/-}$; mTmG$^{+/-}$; Aldh1b1$^{-/-}$* colony were established and used in long-term ethanol treatment tumour-watch experiments for up to one year, with the expected changes in Msh2 and Aldh1b1 protein expression confirmed by IHC detection of Msh2 and Aldh1b1. In *Aldh1b1$^{flox/flox}$* Msh2-LS mice, 41.7% (5/12 mice) of EtOH_*Aldh1b1$^{fl/fl}$*_*Msh2$^{fl\ KO}$* mice showed evidence of large intestinal hyperproliferation and adenoma formation (with 1 adenocarcinoma) within an average of 4.5 months of ethanol treatment, compared with no hyperproliferation and no cases of large intestinal adenoma formation in H_2O_*Aldh1b1$^{fl/fl}$*_*Msh2$^{fl\ KO}$* mice (0%, 0/12 mice) over the same time-period. In *Aldh1b1$^{-/-}$* Msh2-LS mice, 66.7% (8/12 mice) of EtOH_*Aldh1b1$^{-/-}$*_*Msh2$^{fl\ KO}$* mice showed evidence of large intestinal hyperproliferation and adenoma formation within an average of 6 months of ethanol treatment, compared with no hyperproliferation and no cases of large intestinal adenoma formation in H_2O_*Aldh1b1$^{-/-}$*_*Msh2$^{fl\ KO}$* mice (0%, 0/12 mice) over the same time-period. As observed in *Aldh1b1^{wt}* Msh2-LS mice, no small intestinal adenomas were seen in either the *Aldh1b1$^{flox/flox}$* Msh2-LS or *Aldh1b1$^{-/-}$* Msh2-LS mice, for both ethanol- and water-treated mice.

The EtOH_*Aldh1b1$^{fl/fl}$*_*Msh2$^{fl\ KO}$* mice showed a pattern of tumour distribution of one or more large intestinal tumours mainly in the proximal colon and mid colon and in some cases in the distal colon, whereas EtOH_*Aldh1b1$^{-/-}$*_*Msh2$^{fl\ KO}$* mice showed one or more tumours in the proximal and mid colon as well as in the rectum (distal colonic or rectal tumours were not observed in EtOH_*Msh2$^{fl\ KO}$* mice). In both EtOH_*Aldh1b1$^{fl/fl}$*_*Msh2$^{fl\ KO}$* mice and EtOH_*Aldh1b1$^{-/-}$*_*Msh2$^{fl\ KO}$* mice, ethanol-induced colonic adenomas occurred at statistically significantly higher numbers of adenomas per mouse than in EtOH_*Msh2$^{fl\ KO}$* mice.

There were high plasma levels of acetaldehyde in the *Aldh1b1*$^{-/-}$ Msh2-LS mice and lower, more moderate levels of plasma acetaldehyde in the *Aldh1b1*$^{flox/flox}$ Msh2-LS mice. Acetaldehyde-induced DNA damage response was detected by immunohistochemical analysis of both yH2AX and p53 (showing the "wild-type pattern"), with high expression of yH2AX and nuclear p53 immunostaining in both EtOH_*Aldh1b1*$^{fl/fl}$_*Msh2*$^{fl\ KO}$ and EtOH_*Aldh1b1*$^{-/-}$_*Msh2*$^{fl\ KO}$ murine large intestine, compared with H_2O_*Aldh1b1*$^{fl/fl}$_*Msh2*$^{fl\ KO}$ and H_2O_*Aldh1b1*$^{-/-}$_*Msh2*$^{fl\ KO}$ murine large intestine. Lower yH2AX and nuclear p53 expression was observed in EtOH_*Aldh1b1*$^{fl/fl}$_*Msh2*$^{fl\ KO}$ and EtOH_*Aldh1b1*$^{-/-}$_*Msh2*$^{fl\ KO}$ murine small intestine. This revealed that acetaldehyde (more so than ethanol) mediated a significant DNA-damaging effect, mainly on dMMR colonic mucosal epithelium rather than on dMMR small intestinal mucosa, indicating that other protective mechanisms appear to be operative in the small intestinal epithelium, consistent with the much lower incidence of small intestinal cancers compared with colonic cancers in human LS patients. This suggests that Msh2 has a key role in protecting the MMR-proficient colonic epithelial cells against this type of DNA damage. Measurement of plasma acetaldehyde showed that the inactivation of *Aldh1b1* led to increased levels of acetaldehyde in the blood, and this likely reflected increased acetaldehyde in intestinal epithelial cells causing more acetaldehyde-mediated DNA damage. Some acetaldehyde-mediated DNA damage, unrecognised in dMMR cells, was associated with increased numbers of intestinal crypt foci in both EtOH_*Aldh1b1*$^{fl/fl}$_*Msh2*$^{fl\ KO}$ and EtOH_*Aldh1b1*$^{-/-}$_*Msh2*$^{fl\ KO}$ mice. The evidence suggests that these increased dMMR crypt foci act as precursors in dMMR-driven intestinal tumour formation, explaining in part the increased numbers of colonic adenomas per mouse in this model. These results verified the key role of Aldh1b1 in protecting the large intestinal epithelial cells, particularly the stem and progenitor cells that have the highest levels of Aldh1b1 expression, from ethanol-derived acetaldehyde-induced DNA damage, consistent with previous observations by our group (Müller et al., 2016).

This study produced strong evidence in support of the hypothesis that there is a gene/environment interaction between dMMR and acetaldehyde, demonstrated most notably by the *Aldh1b1* constitutive-knockout Msh2-LS mouse model. The data provide evidence in support of the proposed models (Figures 8.1 to 8.5) that in *Aldh1b1*$^{-/-}$ MMR-deficient intestinal epithelial stem cells, significant acetaldehyde-induced DNA damage is not recognized by the DNA mismatch repair system, with no activation of either cell cycle arrest or apoptosis. The DNA-damaged *Aldh1b1*$^{-/-}$ MMR-deficient intestinal epithelial cells are

proposed to undergo inappropriate survival and subsequent proliferation, compared with *Aldh1b1*$^{-/-}$ MMR-proficient cells. This is proposed to confer a selective advantage upon the *Aldh1b1*$^{-/-}$ dMMR intestinal epithelial stem cells that leads to more efficient monoclonal crypt conversion (Figure 8.1) and crypt expansion by crypt fission (Figures 8.2-8.3), observed as higher numbers of clusters of *Aldh1b1*$^{-/-}$ dMMR crypt foci. This is further proposed to confer an elevated risk of subsequent tumour formation with both right-sided and left-sided colonic adenomas and occasional adenocarcinomas developing in these mice. In the *Aldh1b1*$^{flox/flox}$ Msh2-LS model mice, scattered *Aldh1b1*$^{flox/flox}$ *Msh2*$^{flox/-}$ intestinal epithelial stem cells are induced by Tamoxifen-mediated Cre activation to become *Aldh1b1*^{KO} MMR-deficient intestinal epithelial stem cells and these respond to ethanol exposure in a similar way to *Aldh1b1*$^{-/-}$ MMR-deficient intestinal epithelial stem cells, with a survival selective advantage over the surrounding *Aldh1b1*^{wt} intestinal epithelial stem cells, including those in the same crypts, thus making monoclonal crypt conversion by these cells more likely (Figure 8.1). The surrounding *Aldh1b1*^{wt} intestinal epithelial crypts and other intestinal cell types (lamina propria and smooth muscle cells) would be able to metabolise more acetaldehyde to acetate leading to relatively lower levels of acetaldehyde in the intestinal tissues compared with constitutive *Aldh1b1* knockout intestines where all cells have lost functional Aldh1b1.

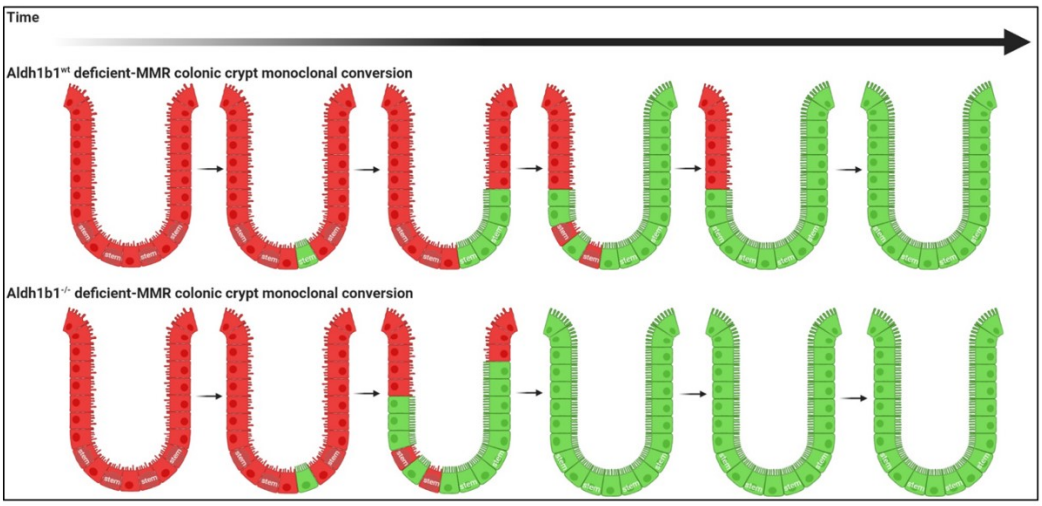

Figure 8.1: Schematic diagram of the proposed model of acetaldehyde-mediated selection for monoclonal conversion by dMMR colonic crypt stem cells following ethanol exposure in the Tamoxifen-induced Cre-activated *Aldh1b1*^{wt} Msh2-LS mouse model (top row) and the Tamoxifen-induced Cre-activated *Aldh1b1*$^{-/-}$ Msh2-LS mouse model (bottom row) over time (shown as a black horizontal arrow). In the Aldh1b1^{wt} Msh2-LS mouse model (top row), Tamoxifen induced Cre-activation in scattered Lgr5+ colonic stem cells converts them to dMMR/mG+ stem cells (green cells, first seen at the crypt base of the second crypt from the left in the top row). Ethanol is metabolised to acetaldehyde (at low intracellular levels in the *Aldh1b1*^{wt} mice), and there is preferential selection for survival of dMMR/mG+ stem cells containing acetaldehyde-induced DNA damage over pMMR/mT+ stem cells (red cells containing the word 'stem") containing acetaldehyde-induced DNA damage. This is because pMMR/mT+ stem cells can recognise acetaldehyde-induced DNA damage (of MMR-recognisable type) and either undergo cell cycle arrest or apoptosis, whereas dMMR/mG+ stems can not do this. This acetaldehyde-driven selective advantage for green dMMR/mG+ stem cells allows them to replace the red pMMR/mT+ stem cells and populate the crypt with their daughter cells over time, gradually leading to monoclonal conversion of the entire crypt with green dMMR/mG+ cells (shown in the sixth crypt). This process is proposed to occur earlier in the *Aldh1b1*$^{-/-}$ Msh2-LS mouse model (complete monoclonal crypt conversion is shown occurring by the fourth crypt in the bottom row), supported by the evidence of more green crypts observable in *Aldh1b1*$^{-/-}$ Msh2-LS mice compared with *Aldh1b1*^{wt} Msh2-LS mice. Under ethanol exposure, the *Aldh1b1*$^{-/-}$ dMMR/mG+ cells are proposed to have an increased selective advantage over the pMMR /mT+ cells due to the higher intracellular levels of acetaldehyde that mediate DNA damage, leading to earlier or faster monoclonal crypt conversion (to be verified by future experiments). In the *Aldh1b1*$^{flox/flox}$ Msh2-LS model mice, scattered *Aldh1b1*$^{flox/flox}$ *Msh2*$^{flox/-}$ intestinal epithelial stem cells are induced by Tamoxifen-mediated Cre-activation to become *Aldh1b1*$^{-/-}$ *Msh2*$^{-/-}$ MMR-deficient intestinal epithelial stem cells and thus the dMMR/mG+ monoclonal crypt conversion occurs in a similar way to that described for the *Aldh1b1*$^{-/-}$ dMMR/mG+ crypts shown in the bottom row.

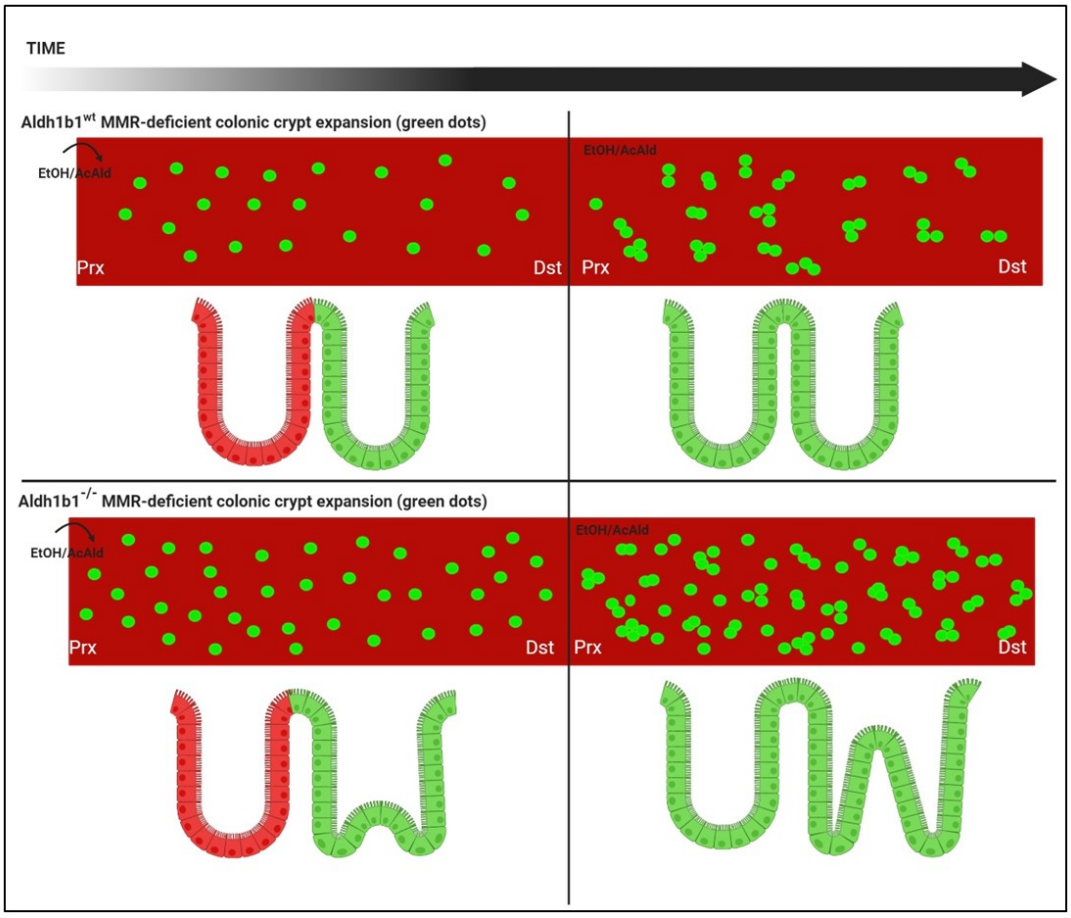

Figure 8.2: Schematic diagram of the proposed model of the selective effects of MMR/acetaldehyde gene/environment interactions on dMMR/mG+ crypts and their expansion to form crypt foci in the *Aldh1b1*^{wt} Msh2-LS mouse model (upper panels) and the *Aldh1b1*$^{-/-}$ Msh2-LS mouse model (lower panels) over time (horizontal black arrow) during ethanol exposure. The dMMR/mG+ crypts (mG+/mT- green crypts scattered along the large intestinal mucosa, shown as green dots on the red background in the left-sided panels) are shown progressing to dMMR/mG+ expanded crypt foci (illustrated as two, three or more clustered green dots in the right-sided panels) over time. The data shows that this process occurs to a greater extent in *Aldh1b1*$^{-/-}$ Msh2-LS (lower panels) compared with the Aldh1b1^{wt} Msh2-LS mice (upper panels). This crypt expansion process is proposed to occur via crypt fission (examples of bifid crypts undergoing crypt fission were observed histologically and this is shown in the lower panels). The more rapid expansion of dMMR/mG+ crypt foci by crypt fission in *Aldh1b1*$^{-/-}$ Msh2-LS mice is proposed to result from higher intracellular acetaldehyde levels conferring a greater selective advantage of acetaldehyde-exposed dMMR/mG+ stem cells for survival and proliferation, that are triggered to initiate the process of crypt fission. The mG-/mT+ red cells/crypts constitute the red background of the large intestinal mucosal epithelial surface. (Prx=proximal colon; Dst=distal colon; EtOH=ethanol; AcAld=Acetaldehyde).

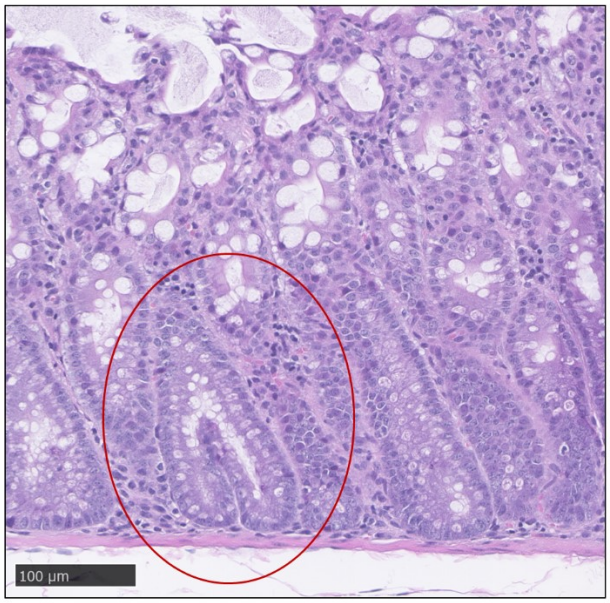

Figure 8.3: Representative image of a colonic crypt undergoing crypt fission (red oval) in a background of colonic epithelial hyperproliferative change in ethanol-treated Msh2-LS mice. Image taken from scanned slide files with the Hamamatsu Nanozoomer NDP Viewer software at 20X magnification (bar at lower left indicates 100µm).

8.4 The *mTmG* transgene reporter system allowed investigation of the effects of ethanol on mG-expressing dMMR crypt foci precursors in the Lynch Syndrome mouse models

The *mTmG* transgene reporter system was used to monitor any changes in the number, size, or distribution of crypt foci that were dMMR, following ethanol (compared with water) treatment of the mouse models over time. The detection of mT and mG fluorescent proteins after 5 days or 15 days of either ethanol or water treatment showed a statistically significant increase in the number and size of mG expressing colonic crypt foci in ethanol-treated mice compared with water-treated mice. Furthermore, the treatment of Msh2-LS mice with ethanol increased the number of mG expressing dMMR crypt foci in a time dependent manner. By contrast, the number of dMMR crypt foci didn't increase under normal drinking water treatment. Ethanol increased mG expressing dMMR crypt foci in the colon, suggesting ethanol/acetaldehyde-mediated selection for expansion of dMMR crypt foci (Figures 8.2-8.3).

The detection and quantification of mT and mG fluorescent protein was extended to all analyses of the *Aldh1b1*^{wt} Msh2-LS, *Aldh1b1*$^{flox/flox}$ Msh2-LS, and *Aldh1b1*$^{-/-}$ Msh2-LS murine model tumour-watch experiments, in order to obtain more data about changes in the mG+ dMMR colonic crypts and crypt foci over longer periods of time under long–term ethanol- or water-treatment regimes. The PGA of dMMR crypt foci showed similar trends over time with a high early peak that decreased after 15-30 days for the Msh2-LS model (11-12 weeks for the *Aldh1b1*$^{flox/flox}$ Msh2-LS model) followed by subsequent stabilisation with a mild increase over time, rather than a continually increasing level of PGA-detected dMMR foci over time. Also the IHC for Msh2 and mG/GFP showed evidence of a partial or complete lack of GFP expression in some large intestinal adenomas, consistent with acquired mutations in repetitive sequences in the *mG/GFP* gene. Analysis of the pCA-mTmG plasmid sequence revealed the presence of several repetitive sequences in the membrane-targeted *EGFP* (*mG/GFP*) gene sequence that are highly likely to act as targets for InDel mutations that are not repaired in mismatch repair-deficient cells. This mutational inactivation of mG would generate colonic crypts and crypt foci that lack expression of both mG and mT (Figures 8.4 and 8.5). The resulting transparent crypts and crypt foci appear red under the fluorescent microscope due to the detection of red fluorescent light from the underlying mT-expressing tissue. However, they were negative on immunostaining for mG/EGFP. Furthermore, there

may be a time-related immune response to the early expansion of dMMR/mG+ crypts, with a reduction in dMMR/mG+ crypt foci occurring perhaps due to immune attack against the more immunogenic dMMR crypt cells that may present more frameshift peptides (Seth et al., 2018). This would require future immunological studies to evaluate whether greater numbers of infiltrating T lymphocytes could be found around dMMR crypt foci at the appropriate time-points.

8.5 Conclusion

In conclusion, a model is proposed (set out in schematic diagrams in Figures 8.4-8.5) to show the effects on colonic crypts and crypt foci of the mismatch repair pathway/acetaldehyde gene/environment interactions. In the *Aldh1b1*^{wt} Msh2-LS mouse model, following ethanol ingestion and its metabolic conversion to acetaldehyde, but before acetaldehyde is fully metabolised to acetate, there is some acetaldehyde-induced DNA base damage. MMR-proficient intestinal stem cells and crypt daughter cells are able to activate DNA mismatch repair of the (MMR-recognised) base damage, leading to either cell cycle arrest, to allow repair of mild DNA damage, or apoptosis in the case of unrepairable severe DNA damage. However, following loss of the second *Msh2* allele, MMR-deficient stem cells and their crypt daughter cells are unable to activate the MMR pathway and so neither cell cycle arrest nor apoptosis can be triggered, resulting in aberrant survival of DNA-damaged cells and their subsequent proliferation (mostly acetaldehyde-induced colonic crypt cell proliferation). The proliferating dMMR stem cells have both a survival advantage (apoptosis blocked by dMMR) and a proliferative advantage (cell cycle arrest inhibited by dMMR) during ethanol/acetaldehyde exposure and thus can rapidly populate crypts by monoclonal crypt conversion (detected as mG-positive cells filling the whole crypt, which appears as a green area/dot (on a red background) on the colonic mucosal surface of the *mTmG* Msh2-LS model colon under fluorescent microscopy, represented as green dots on the red background in the schematic diagram in Figures 8.1 to 8.5). During ongoing ethanol/acetaldehyde exposure, the proliferative advantage allows these green dMMR crypts to expand further, by crypt fission, to form dMMR crypt foci or clusters (Figure 8.2 and 8.3), with more of them observed proximally than distally in the colon, consistent with the acetaldehyde-induced epithelial hyperproliferation occurring more proximally than distally (Figures 8.4 and 8.5).

These dMMR cells/crypts can accumulate mutations from continued exposure to ethanol/acetaldehyde reflecting a form of dMMR genomic instability. MMR-deficient stem cells and crypts have MSI resulting in accumulation of InDel mutations in microsatellites or repeat sequences in coding exons; this is proposed to lead to both activation of an increased immune response to frameshift peptides (presented on major histocompatibility class I molecules on the surface of the affected cells) and loss of expression of mG/GFP green fluorescent protein, as the *mG* gene contains many repetitive sequences. This mutational inactivation of mG generates colonic crypts and crypt foci that lack expression of both mG and mT and should be transparent, but would appear red on fluorescence microscopy due

to transmission of red light from mT-expressing tissues underneath, although they appear negative on immunostaining for mG/EGFP. This process of dMMR crypt foci expansion would be enhanced by continued exposure over time to acetaldehyde, increasing the amounts of DNA damage with selective survival and proliferation of dMMR cells and crypts, only partially balanced by some crypt loss from immune attack, with an increasing risk of neoplasm formation and progression as mutations accumulate.

In the *Aldh1b1*$^{-/-}$ Msh2-LS murine model colon (Figure 8.5), ethanol is metabolized to highly reactive acetaldehyde, with much reduced oxidation to acetate due to the lack of Aldh1b1 enzymic activity. This causes a marked increase in acetaldehyde levels in the colonic stem cells. High levels of reactive acetaldehyde causing severe acetaldehyde-induced DNA damage (of MMR-recognised type) may force the *Aldh1b1*$^{-/-}$ MMR-proficient colonic epithelial cells to activate cell death by apoptosis. This is not the case in *Aldh1b1*$^{-/-}$ MMR-deficient colonic epithelial cells that are unable to activate the MMR signalling pathway and so there is neither cell cycle arrest nor apoptosis, following increased acetaldehyde-induced DNA damage, resulting in aberrant survival of more severely DNA-damaged cells and their subsequent proliferation, also driven by increased levels of acetaldehyde. *Aldh1b1*$^{-/-}$ MMR-deficient colonic epithelial cells proliferate and expand to form higher numbers of *Aldh1b1*$^{-/-}$ dMMR crypt foci, with an elevated risk of accelerated tumour formation, observed as higher numbers of colonic adenomas per mouse, with both right-sided and left-sided colonic adenoma formation. This process of *Aldh1b1*$^{-/-}$ dMMR crypt foci expansion would be enhanced by continued exposure over time to high levels of acetaldehyde, increasing DNA damage with an increasing risk of neoplasm formation and progression to invasive adenocarcinoma as mutations accumulate, particularly if these mutations occur in neoplastic driver genes.

The schematic diagrams in Figures 8.1 to 8.5 are also representative of what occurs in individual colonic stem cells following Tamoxifen-mediated Cre activation in *Aldh1b1*$^{flox/flox}$ Msh2-LS model mice, as this results in inactivation of both copies of *Aldh1b1* and loss of the second *Msh2* allele as well as conversion from mT to mG expression, resulting in mG+ *Aldh1b1*-null, dMMR stem cells that populate crypts to full monoclonal crypt conversion, form crypt foci by crypt fission, and although the circulating levels of acetaldehyde are not as high as in the constitutive knockout *Aldh1b1*$^{-/-}$ Msh2-LS mice, it is proposed that there are increased intracellular levels of acetaldehyde conferring a similarly increased risk of neoplastic progression to adenomas and adenocarcinomas.

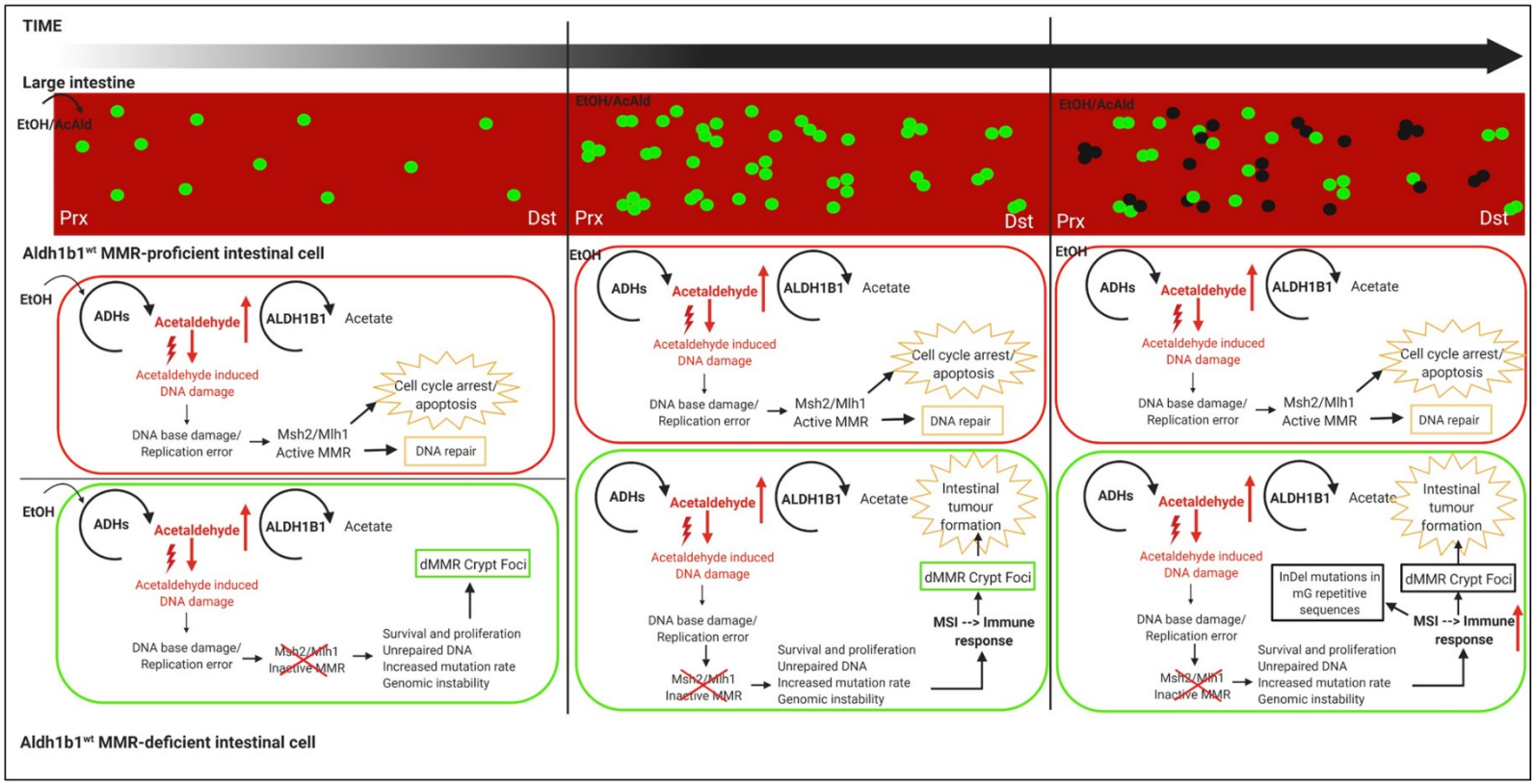

Figure 8.4: Schematic diagram of the proposed model of the effects on cells, crypts and crypt foci of MMR/acetaldehyde gene/environment interactions in both MMR-proficient cells (mG-/mT+ red cells/crypts constituting the red background of the large intestinal mucosa) and MMR-deficient cells (mG+/mT- green cells/crypts scattered along the large intestinal mucosa, shown as green dots) over time (black horizontal arrow) during ethanol exposure. Cells/crypts that lose both mG and mT expression are shown in black (repeat of diagram in Figure 7.20 for comparison with Figure 8.5). (Prx=proximal colon; Dst=distal colon; EtOH=ethanol; AcAld=Acetaldehyde).

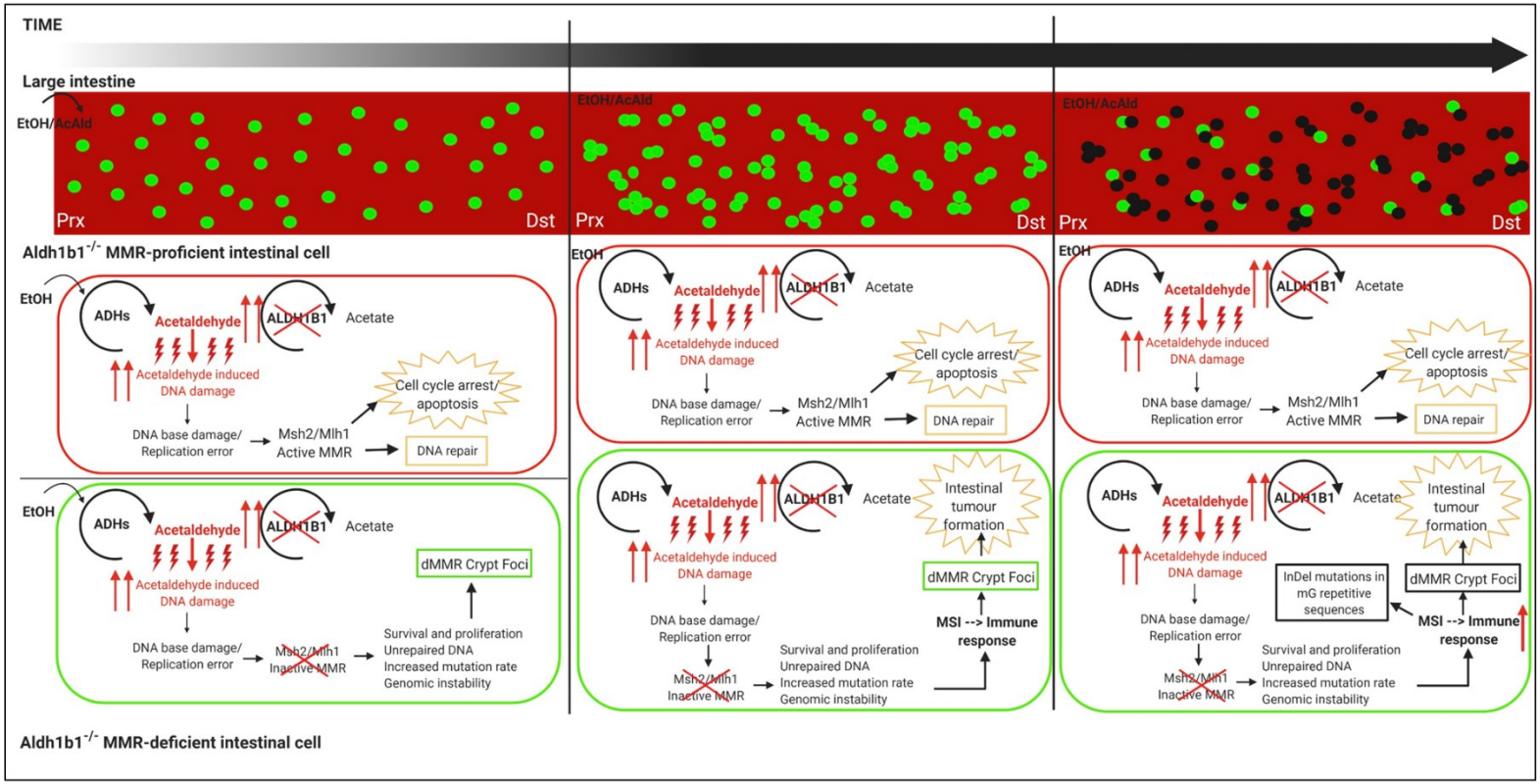

Figure 8.5: Schematic diagram of the proposed model of the effects on cells, crypts and crypt foci of MMR/acetaldehyde gene/environment interactions in both *Aldh1b1*$^{-/-}$ MMR-proficient cells (mG-/mT+ red cells/crypts constituting the red background of the large intestinal mucosa) and *Aldh1b1*$^{-/-}$ MMR-deficient cells (mG+/mT- green cells/crypts scattered along the large intestinal mucosa, shown as green dots) over time (black horizontal arrow) during ethanol exposure. Cells/crypts that lose both mG and mT expression are shown in black. (Prx=proximal colon; Dst=distal colon; EtOH=ethanol; AcAld=Acetaldehyde).

8.6 Future work

This project has characterised the Msh2-LS mouse model and provided evidence for a gene/environment interaction between dMMR and ethanol/acetaldehyde, causing acceleration of dMMR-driven intestinal tumour formation upon ethanol exposure, but there are still many details that need further investigation.

The immune system has an important role in tumour incidence, prognosis and response to immunotherapy in LS patients (Gonzalez et al., 2018). The pilot experiment performed on caecal adenomas of Msh2-LS mice provided evidence of an immune response with infiltrating CD8+ and other lymphocytes and myeloid cells within and around adenomas. Further investigation of the immune response in the Msh2-LS mouse model would give a better understanding of which infiltrating immune cells are present around dMMR crypt foci precursors over the time following expansion of individual dMMR crypts to dMMR crypt foci/ clusters and subsequent evolution to intestinal tumours. This may help to elucidate the nature of the interaction between dMMR intestinal cells and the immune response in the context of the three step process of elimination, equilibrium and escape (Dunn et al., 2004; Seth et al., 2018). This could be performed with a more extensive investigation of the infiltrating immune cells by IHC comparing normal intestinal tissue with early and late dMMR crypt foci and tumours from the Msh2-LS mouse model either treated with 20% ethanol in drinking water or normal water.

Improved knowledge of the gene expression patterns in large intestinal epithelium and small intestinal epithelium of both MMR-proficient cells and MMR-deficient cells, with and without ethanol exposure, would offer improved understanding about why hyperproliferative changes and adenoma formation occur in the colon, but not in the small intestine in this Msh2-LS model and which signalling pathways are involved. This could be done by performing RNA sequencing analysis on the RNA extracted from the mT-expressing red small intestinal and colonic epithelial cells (pMMR cells) for comparison with RNA-seq data from the mG-expressing green small intestinal and colonic epithelial cells (dMMR cells), from both ethanol-treated and water-treated Msh2-LS mice. RNA has already been extracted from these samples following FACS-sorting of the ethanol- and water-treated Msh2-LS large and small intestinal epithelial samples (described in Chapter 7). In addition, adjacent pMMR crypts and early dMMR crypts (identified by IHC staining for Msh2) could be micro-dissected (by laser capture microdissection) and analysed by RNA and DNA extraction for sequencing

to allow comparison to determine signalling pathway changes and mutation changes that occur at the earliest stages of dMMR monoclonal crypt conversion.

Furthermore, generation of an organoid model system from isolated small and large intestinal stem cells of the Msh2-LS mouse model may shed light on the subsequent responses and effects of DNA MMR following ethanol/acetaldehyde-induced DNA damage and other types (e.g. Temozolomide, other aldehydes) of DNA damage induced *in vitro*. Analysis of gene expression in such organoids may reveal the molecular mechanisms and pathways that become activated under ethanol treatment (and other genotoxic agents) in the presence and absence of DNA MMR.

DNA sequencing and RNA sequencing could be performed in both the organoid model and in the Msh2-LS murine colonic crypt foci, adenomas and adenocarcinomas, to investigate the most prevalent driver mutations in tumourigenesis and signalling pathways in this model and to distinguish those gene mutations that occur early in adenomagenesis from those that occur late in this process, which may reveal some actionable gene mutations that may be investigated in human LS patients.

8.7 Summary

In this study, evidence is provided that shows that:

- The Msh2-LS mouse model is a good model of human Lynch Syndrome. Loss of MMR occurs in scattered stem cells, crypts and crypt foci along the small and large intestines. However, with long-term ethanol treatment, tumour formation is only seen in the colon (mainly in the proximal and mid colon, following the locational distribution of ethanol-induced epithelial hyperproliferation) and not seen in the small intestine, closely mirroring human LS intestinal tumour distribution.
- Msh2 has a key role in protecting the MMR-proficient colonic epithelial cells against ethanol/acetaldehyde-induced DNA damage, but there appear to be other protective mechanisms in addition to mismatch repair in small intestinal epithelial cells protecting against acetaldehyde-induced DNA damage.
- Ethanol/acetaldehyde induces regions of hyperproliferation of the large intestinal mucosal epithelium (mostly in the proximal and mid-colon) and this contributes, most likely through the process of tumour promotion, to acceleration of dMMR-driven intestinal adenoma formation compared with water-treated controls.

- Ethanol/acetaldehyde promotes survival and proliferation of aberrant dMMR large intestinal epithelial cells/crypts over the MMR-proficient colonic epithelial cells/crypts. In this way, it increases the number and size of precursor dMMR lesions and elevates the risk of progression to either adenoma or invasive adenocarcinoma.
- Aldh1b1 has a key role of in protecting the large intestinal epithelial stem cells and crypts from acetaldehyde-induced DNA damage, demonstrated in the increased colonic neoplasm formation in both *Aldh1b1*$^{fl/fl}$ Msh1-LS and *Aldh1b1*$^{-/-}$ Msh2-LS models compared with *Aldh1b1*^{wt} Msh2-LS model following ethanol exposure.
- There is strong evidence for a gene/environment interaction between dMMR and acetaldehyde acting via selection for reduced apoptosis, decreased cell cycle arrest, increased DNA damage in addition to dMMR-mediated hypermutation, and colonic epithelial hyperproliferation, collectively contributing to the acceleration of dMMR-driven colonic tumour formation upon ethanol exposure in this Lynch Syndrome model.

Bibliography

Aaltonen, L. A., Peltomäki, P., Mecklin, J. P., Järvinen, H., Jass, J. R., Green, J. S., Lynch, H. T., Watson, P., Tallqvist, G., & Juhola, M. (1994). Replication errors in benign and malignant tumors from hereditary nonpolyposis colorectal cancer patients. Cancer Research, 54(7), 1645–1648.

Aarnio, M., Salovaara, R., Aaltonen, L. A., Mecklin, J. P., & Järvinen, H. J. (1997). Features of gastric cancer in hereditary non-polyposis colorectal cancer syndrome. International Journal of Cancer, 74(5), 551–555. https://doi.org/10.1002/(sici)1097-0215(19971021)74:5<551::aid-ijc13>3.0.co;2-9

Adar, T., Friedman, M., Rodgers, L. H., Shannon, K. M., Zukerberg, L. R., & Chung, D. C. (2019). Gastric cancer in Lynch syndrome is associated with underlying immune gastritis. Journal of Medical Genetics, 56(12), 844–845. https://doi.org/10.1136/jmedgenet-2018-105757

Adar, T., Rodgers, L. H., Shannon, K. M., Yoshida, M., Ma, T., Mattia, A., Lauwers, G. Y., Iafrate, A. J., & Chung, D. C. (2017). A tailored approach to BRAF and MLH1 methylation testing in a universal screening program for Lynch syndrome. Modern Pathology: An Official Journal of the United States and Canadian Academy of Pathology, Inc, 30(3), 440–447. https://doi.org/10.1038/modpathol.2016.211

Agace, W. W., & McCoy, K. D. (2017). Regionalized Development and Maintenance of the Intestinal Adaptive Immune Landscape. Immunity, 46(4), 532–548. https://doi.org/10.1016/j.immuni.2017.04.004

Ager, A., & May, MJ. (2015). Understanding high endothelial venules: Lessons for cancer immunology.

Ahadova, A., Gallon, R., Gebert, J., Ballhausen, A., Endris, V., Kirchner, M., Stenzinger, A., Burn, J., von Knebel Doeberitz, M., Bläker, H., & Kloor, M. (2018). Three molecular pathways model colorectal carcinogenesis in Lynch syndrome: Three pathways of CRC in Lynch syndrome. International Journal of Cancer, 143(1), 139–150. https://doi.org/10.1002/ijc.31300

Ahadova, A., von Knebel Doeberitz, M., Bläker, H., & Kloor, M. (2016). CTNNB1-mutant colorectal carcinomas with immediate invasive growth: A model of interval cancers in Lynch syndrome. Familial Cancer, 15(4), 579–586. https://doi.org/10.1007/s10689-016-9899-z

Ait Ouakrim, D., Dashti, S. G., Chau, R., Buchanan, D. D., Clendenning, M., Rosty, C., Winship, I. M., Young, J. P., Giles, G. G., Leggett, B., Macrae, F. A., Ahnen, D. J., Casey, G., Gallinger, S., Haile, R. W., Le Marchand, L., Thibodeau, S. N., Lindor, N. M., Newcomb, P. A., … Win, A. K. (2015). Aspirin, Ibuprofen, and the Risk of Colorectal Cancer in Lynch Syndrome. Journal of the National Cancer Institute, 107(9). https://doi.org/10.1093/jnci/djv170

Alexander, J., Watanabe, T., Wu, T. T., Rashid, A., Li, S., & Hamilton, S. R. (2001). Histopathological identification of colon cancer with microsatellite instability. The

American Journal of Pathology, 158(2), 527–535. https://doi.org/10.1016/S0002-9440(10)63994-6

Arends, M., Ibrahim, M., Happerfield, L., Frayling, I. M., & Miller, K. (2008). Interpretation of Immunohistochemical Analysis of MisMatch Repair (MMR) Protein Expression in Tissue Sections for Investigation of Suspected Lynch / Hereditary Non-Polyposis Colorectal Cancer (HNPCC) Syndrome. https://www.research.ed.ac.uk/portal/en/publications/interpretation-of-immunohistochemical-analysis-of-mismatch-repair-mmr-protein-expression-in-tissue-sections-for-investigation-of-suspected-lynch--hereditary-nonpolyposis-colorectal-cancer-hnpcc-syndrome(05bf56e2-007d-4353-b0d6-2d85587ceafa)/export.html

Arends, M. J. (2013). Pathways of Colorectal Carcinogenesis. Appl Immunohistochem Mol Morphol, 21(2), 6.

Arnold, M., Sierra, M. S., Laversanne, M., Soerjomataram, I., Jemal, A., & Bray, F. (2017). Global patterns and trends in colorectal cancer incidence and mortality. Gut, 66(4), 683–691. https://doi.org/10.1136/gutjnl-2015-310912

Aune, D., Chan, D. S. M., Vieira, A. R., Navarro Rosenblatt, D. A., Vieira, R., Greenwood, D. C., Kampman, E., & Norat, T. (2013). Red and processed meat intake and risk of colorectal adenomas: A systematic review and meta-analysis of epidemiological studies. Cancer Causes & Control: CCC, 24(4), 611–627. https://doi.org/10.1007/s10552-012-0139-z

Bacher, J. W., Abdel Megid, W. M., Kent-First, M. G., & Halberg, R. B. (2005). Use of mononucleotide repeat markers for detection of microsatellite instability in mouse tumors. Molecular Carcinogenesis, 44(4), 285–292. https://doi.org/10.1002/mc.20146

Bagnardi, V., Rota, M., Botteri, E., Tramacere, I., Islami, F., Fedirko, V., Scotti, L., Jenab, M., Turati, F., Pasquali, E., Pelucchi, C., Galeone, C., Bellocco, R., Negri, E., Corrao, G., Boffetta, P., & La Vecchia, C. (2015). Alcohol consumption and site-specific cancer risk: A comprehensive dose-response meta-analysis. British Journal of Cancer, 112(3), 580–593. https://doi.org/10.1038/bjc.2014.579

Bailey, S. M., & Cunningham, C. C. (2002). Contribution of mitochondria to oxidative stress associated with alcoholic liver disease1 1This article is part of a series of reviews on “Alcohol, Oxidative Stress and Cell Injury”. The full list of papers may be found on the homepage of the journal. Free Radical Biology and Medicine, 32(1), 11–16. https://doi.org/10.1016/S0891-5849(01)00769-9

Baker, S. M., Bronner, C. E., Zhang, L., Plug, A. W., Robatzek, M., Warren, G., Elliott, E. A., Yu, J., Ashley, T., Arnheim, N., Flavell, R. A., & Liskay, R. M. (1995). Male mice defective in the DNA mismatch repair gene PMS2 exhibit abnormal chromosome synapsis in meiosis. Cell, 82(2), 309–319. https://doi.org/10.1016/0092-8674(95)90318-6

Bao, F., Panarelli, N. C., Rennert, H., Sherr, D. L., & Yantiss, R. K. (2010). Neoadjuvant therapy induces loss of MSH6 expression in colorectal carcinoma. The American Journal of Surgical Pathology, 34(12), 1798–1804. https://doi.org/10.1097/PAS.0b013e3181f906cc

Barker, N., van Es, J. H., Jaks, V., Kasper, M., Snippert, H., Toftgård, R., & Clevers, H. (2008). Very long-term self-renewal of small intestine, colon, and hair follicles from cycling Lgr5+ve stem cells. Cold Spring Harbor Symposia on Quantitative Biology, 73, 351–356. https://doi.org/10.1101/sqb.2008.72.003

Barker, Nick, & Clevers, H. (2010). Leucine-rich repeat-containing G-protein-coupled receptors as markers of adult stem cells. Gastroenterology, 138(5), 1681–1696. https://doi.org/10.1053/j.gastro.2010.03.002

Barker, Nick, van Es, J. H., Kuipers, J., Kujala, P., van den Born, M., Cozijnsen, M., Haegebarth, A., Korving, J., Begthel, H., Peters, P. J., & Clevers, H. (2007). Identification of stem cells in small intestine and colon by marker gene Lgr5. Nature, 449(7165), 1003–1007. https://doi.org/10.1038/nature06196

Bartley, A. N., Luthra, R., Saraiya, D. S., Urbauer, D. L., & Broaddus, R. R. (2012). Identification of cancer patients with Lynch syndrome: Clinically significant discordances and problems in tissue-based mismatch repair testing. Cancer Prevention Research (Philadelphia, Pa.), 5(2), 320–327. https://doi.org/10.1158/1940-6207.CAPR-11-0288

Bellizzi, A. M., & Frankel, W. L. (2009). Colorectal Cancer Due to Deficiency in DNA Mismatch Repair Function: A Review. Advances in Anatomic Pathology, 16(6), 405–417. https://doi.org/10.1097/PAP.0b013e3181bb6bdc

Bénard, F., Barkun, A. N., Martel, M., & von Renteln, D. (2018). Systematic review of colorectal cancer screening guidelines for average-risk adults: Summarizing the current global recommendations. World Journal of Gastroenterology, 24(1), 124–138. https://doi.org/10.3748/wjg.v24.i1.124

Bento, D. C., Jones, E., Junaid, S., Tull, J., Williams, G. T., Godkin, A., Ager, A., & Gallimore, A. (2015). High endothelial venules are rare in colorectal cancers but accumulate in extra-tumoral areas with disease progression. OncoImmunology, 4(3), e974374. https://doi.org/10.4161/2162402X.2014.974374

Bicknell, D. C., Kaklamanis, L., Hampson, R., Bodmer, W. F., & Karran, P. (1996). Selection for beta 2-microglobulin mutation in mismatch repair-defective colorectal carcinomas. Current Biology: CB, 6(12), 1695–1697. https://doi.org/10.1016/s0960-9822(02)70795-1

Binder, H., Hopp, L., Schweiger, M. R., Hoffmann, S., Jühling, F., Kerick, M., Timmermann, B., Siebert, S., Grimm, C., Nersisyan, L., Arakelyan, A., Herberg, M., Buske, P., Loeffler-Wirth, H., Rosolowski, M., Engel, C., Przybilla, J., Peifer, M., Friedrichs, N., … Loeffler, M. (2017). Genomic and transcriptomic heterogeneity of colorectal tumours arising in Lynch syndrome. The Journal of Pathology, 243(2), 242–254. https://doi.org/10.1002/path.4948

Bläker, H., Haupt, S., Morak, M., Holinski-Feder, E., Arnold, A., Horst, D., Sieber-Frank, J., Seidler, F., von Winterfeld, M., Alwers, E., Chang-Claude, J., Brenner, H., Roth, W., Engel, C., Löffler, M., Möslein, G., Schackert, H.-K., Weitz, J., Perne, C., … the German Consortium for Familial Intestinal Cancer. (2019). BRAF mutation testing of MSI CRCs in

Lynch syndrome diagnostics: Performance and efficiency according to patient's age [Preprint]. Gastroenterology. https://doi.org/10.1101/19009274

Bodmer, W. F., Browning, M. J., Krausa, P., Rowan, A., Bicknell, D. C., & Bodmer, J. G. (1993). Tumor escape from immune response by variation in HLA expression and other mechanisms. Annals of the New York Academy of Sciences, 690, 42–49. https://doi.org/10.1111/j.1749-6632.1993.tb43994.x

Bouvard, V., Loomis, D., Guyton, K. Z., Grosse, Y., Ghissassi, F. E., Benbrahim-Tallaa, L., Guha, N., Mattock, H., Straif, K., & International Agency for Research on Cancer Monograph Working Group. (2015). Carcinogenicity of consumption of red and processed meat. The Lancet. Oncology, 16(16), 1599–1600. https://doi.org/10.1016/S1470-2045(15)00444-1

Brooks, P. J., & Zakhari, S. (2014). Acetaldehyde and the genome: Beyond nuclear DNA adducts and carcinogenesis: Acetaldehyde and the Genome. Environmental and Molecular Mutagenesis, 55(2), 77–91. https://doi.org/10.1002/em.21824

Brown, K. D., Rathi, A., Kamath, R., Beardsley, D. I., Zhan, Q., Mannino, J. L., & Baskaran, R. (2003). The mismatch repair system is required for S-phase checkpoint activation. Nature Genetics, 33(1), 80–84. https://doi.org/10.1038/ng1052

Brown, K. F., Rumgay, H., Dunlop, C., Ryan, M., Quartly, F., Cox, A., Deas, A., Elliss-Brookes, L., Gavin, A., Hounsome, L., Huws, D., Ormiston-Smith, N., Shelton, J., White, C., & Parkin, D. M. (2018). The fraction of cancer attributable to modifiable risk factors in England, Wales, Scotland, Northern Ireland, and the United Kingdom in 2015. British Journal of Cancer, 118(8), 1130–1141. https://doi.org/10.1038/s41416-018-0029-6

Burkholder, T., Foltz, C., Karlsson, E., Linton, C. G., & Smith, J. M. (2012). Health Evaluation of Experimental Laboratory Mice. Current Protocols in Mouse Biology, 2, 145–165. https://doi.org/10.1002/9780470942390.mo110217

Burn, J., Gerdes, A.-M., Macrae, F., Mecklin, J.-P., Moeslein, G., Olschwang, S., Eccles, D., Evans, D. G., Maher, E. R., Bertario, L., Bisgaard, M.-L., Dunlop, M. G., Ho, J. W., Hodgson, S. V., Lindblom, A., Lubinski, J., Morrison, P. J., Murday, V., Ramesar, R., … Bishop, D. T. (2011). Long-term effect of aspirin on cancer risk in carriers of hereditary colorectal cancer: An analysis from the CAPP2 randomised controlled trial. The Lancet, 378(9809), 2081–2087. https://doi.org/10.1016/S0140-6736(11)61049-0

Burn, J., Mathers, J., & Bishop, D. T. (2012). Lynch syndrome: History, causes, diagnosis, treatment and prevention (CAPP2 trial). Digestive Diseases (Basel, Switzerland), 30 Suppl 2, 39–47. https://doi.org/10.1159/000341892

Cabrita, R., Lauss, M., Sanna, A., Donia, M., Skaarup Larsen, M., Mitra, S., Johansson, I., Phung, B., Harbst, K., Vallon-Christersson, J., van Schoiack, A., Lövgren, K., Warren, S., Jirström, K., Olsson, H., Pietras, K., Ingvar, C., Isaksson, K., Schadendorf, D., … Jönsson, G. (2020). Tertiary lymphoid structures improve immunotherapy and survival in melanoma. Nature, 577(7791), 561–565. https://doi.org/10.1038/s41586-019-1914-8

Calderaro, J., Petitprez, F., Becht, E., Laurent, A., Hirsch, T. Z., Rousseau, B., Luciani, A., Amaddeo, G., Derman, J., Charpy, C., Zucman-Rossi, J., Fridman, W. H., & Sautès-

Fridman, C. (2019). Intra-tumoral tertiary lymphoid structures are associated with a low risk of early recurrence of hepatocellular carcinoma. Journal of Hepatology, 70(1), 58–65. https://doi.org/10.1016/j.jhep.2018.09.003

Canavan, C., Abrams, K. R., & Mayberry, J. (2006). Meta-analysis: Colorectal and small bowel cancer risk in patients with Crohn's disease. Alimentary Pharmacology & Therapeutics, 23(8), 1097–1104. https://doi.org/10.1111/j.1365-2036.2006.02854.x

Cancer Genome Atlas. (2012). Comprehensive molecular characterization of human colon and rectal cancer. Nature, 487(7407), 330–337. https://doi.org/10.1038/nature11252

Cancer Research UK. (2016a). Bowel cancer incidence statistics. https://www.cancerresearchuk.org/health-professional/cancer-statistics/statistics-by-cancer-type/bowel-cancer/incidence

Cancer Research UK. (2016b). Bowel cancer statistics. Cancer Research UK. https://www.cancerresearchuk.org/health-professional/cancer-statistics/statistics-by-cancer-type/bowel-cancer

Cancer Research UK. (2019). Types of bowel cancer | Cancer Research UK. https://www.cancerresearchuk.org/about-cancer/bowel-cancer/stages-types-and-grades/types

Capelle, L. G., Van Grieken, N. C. T., Lingsma, H. F., Steyerberg, E. W., Klokman, W. J., Bruno, M. J., Vasen, H. F. A., & Kuipers, E. J. (2010). Risk and epidemiological time trends of gastric cancer in Lynch syndrome carriers in the Netherlands. Gastroenterology, 138(2), 487–492. https://doi.org/10.1053/j.gastro.2009.10.051

Castaño-Milla, C., Chaparro, M., & Gisbert, J. P. (2014). Systematic review with meta-analysis: The declining risk of colorectal cancer in ulcerative colitis. Alimentary Pharmacology & Therapeutics, 39(7), 645–659. https://doi.org/10.1111/apt.12651

Cerretelli, G., Ager, A., Arends, M. J., & Frayling, I. M. (2020). Molecular pathology of Lynch syndrome. J Pathol, 14.

Chan, D. S. M., Lau, R., Aune, D., Vieira, R., Greenwood, D. C., Kampman, E., & Norat, T. (2011). Red and processed meat and colorectal cancer incidence: Meta-analysis of prospective studies. PloS One, 6(6), e20456. https://doi.org/10.1371/journal.pone.0020456

Chang, C. L., Marra, G., Chauhan, D. P., Ha, H. T., Chang, D. K., Ricciardiello, L., Randolph, A., Carethers, J. M., & Boland, C. R. (2002). Oxidative stress inactivates the human DNA mismatch repair system. American Journal of Physiology. Cell Physiology, 283(1), C148-154. https://doi.org/10.1152/ajpcell.00422.2001

Chau, R., Dashti, S. G., Ait Ouakrim, D., Buchanan, D. D., Clendenning, M., Rosty, C., Winship, I. M., Young, J. P., Giles, G. G., Macrae, F. A., Boussioutas, A., Parry, S., Figueiredo, J. C., Levine, A. J., Ahnen, D. J., Casey, G., Haile, R. W., Gallinger, S., Le Marchand, L., … Win, A. K. (2016). Multivitamin, calcium and folic acid supplements and the risk of colorectal cancer in Lynch syndrome. International Journal of Epidemiology, 45(3), 940–953. https://doi.org/10.1093/ije/dyw036

Chen, Q., Wang, J., Yang, J., Jin, Z., Shi, W., Qin, Y., Yu, F., & He, J. (2015). Association between adult weight gain and colorectal cancer: A dose-response meta-analysis of observational studies. International Journal of Cancer, 136(12), 2880–2889. https://doi.org/10.1002/ijc.29331

Chen, Y., Orlicky, D. J., Matsumoto, A., Singh, S., Thompson, D. C., & Vasiliou, V. (2011). Aldehyde dehydrogenase 1B1 (ALDH1B1) is a potential biomarker for human colon cancer. Biochemical and Biophysical Research Communications, 405(2), 173–179. https://doi.org/10.1016/j.bbrc.2011.01.002

Chen, Z., He, X., Jia, M., Liu, Y., Qu, D., Wu, D., Wu, P., Ni, C., Zhang, Z., Ye, J., Xu, J., & Huang, J. (2013). β-catenin Overexpression in the Nucleus Predicts Progress Disease and Unfavourable Survival in Colorectal Cancer: A Meta-Analysis. PLoS ONE, 8(5), e63854. https://doi.org/10.1371/journal.pone.0063854

Cheng, L., & Lai, M.-D. (2003). Aberrant crypt foci as microscopic precursors of colorectal cancer. World Journal of Gastroenterology : WJG, 9(12), 2642–2649. https://doi.org/10.3748/wjg.v9.i12.2642

Choudhury, S., Pan, J., Amin, S., Chung, F.-L., & Roy, R. (2004). Repair Kinetics of trans-4-Hydroxynonenal-Induced Cyclic 1,N2-Propanodeoxyguanine DNA Adducts by Human Cell Nuclear Extracts. Biochemistry, 43(23), 7514–7521. https://doi.org/10.1021/bi049877r

Claij, N., & te Riele, H. (2004). Msh2 deficiency does not contribute to cisplatin resistance in mouse embryonic stem cells. Oncogene, 23(1), 260–266. https://doi.org/10.1038/sj.onc.1207015

Clendenning, M., Huang, A., Jayasekara, H., Lorans, M., Preston, S., O'Callaghan, N., Pope, B. J., Macrae, F. A., Winship, I. M., Milne, R. L., Giles, G. G., English, D. R., Hopper, J. L., Win, A. K., Jenkins, M. A., Southey, M. C., Rosty, C., Buchanan, D. D., & investigators from the Melbourne Collaborative Cohort Study and the Australasian Colorectal Cancer Family Registry Cohort. (2018). Somatic mutations of the coding microsatellites within the beta-2-microglobulin gene in mismatch repair-deficient colorectal cancers and adenomas. Familial Cancer, 17(1), 91–100. https://doi.org/10.1007/s10689-017-0013-y

Colbeck, E. J., Ager, A., Gallimore, A., & Jones, G. W. (2017). Tertiary Lymphoid Structures in Cancer: Drivers of Antitumor Immunity, Immunosuppression, or Bystander Sentinels in Disease? Frontiers in Immunology, 8, 1830. https://doi.org/10.3389/fimmu.2017.01830

Cong, F., Schweizer, L., Chamorro, M., & Varmus, H. (2003). Requirement for a Nuclear Function of B-Catenin in Wnt Signaling. MOL. CELL. BIOL., 23, 9.

Cook, P. J., Ju, B. G., Telese, F., Wang, X., Glass, C. K., & Rosenfeld, M. G. (2009). Tyrosine dephosphorylation of H2AX modulates apoptosis and survival decisions. Nature, 458(7238), 591–596. https://doi.org/10.1038/nature07849

Copstead-Kirkhorn, L. E. C., & Banasik, J. L. (2014). Pathophysiology—5th Edition. Elsevier Health Sciences.

Crosbie, E. J., Ryan, N. A. J., Arends, M. J., Bosse, T., Burn, J., Cornes, J. M., Crawford, R., Eccles, D., Frayling, I. M., Ghaem-Maghami, S., Hampel, H., Kauff, N. D., Kitchener, H. C., Kitson, S. J., Manchanda, R., McMahon, R. F. T., Monahan, K. J., Menon, U., Møller, P., … Evans, D. G. (2019). The Manchester International Consensus Group recommendations for the management of gynecological cancers in Lynch syndrome. Genetics in Medicine: Official Journal of the American College of Medical Genetics, 21(10), 2390–2400. https://doi.org/10.1038/s41436-019-0489-y

Dai, Z. (2007). Obesity and colorectal cancer risk: A meta-analysis of cohort studies. World Journal of Gastroenterology, 13(31), 4199. https://doi.org/10.3748/wjg.v13.i31.4199

de la Chapelle, A. (2005). The incidence of Lynch syndrome. Familial Cancer, 4(3), 233–237. https://doi.org/10.1007/s10689-004-5811-3

de Rosa, N., Rodriguez-Bigas, M. A., Chang, G. J., Veerapong, J., Borras, E., Krishnan, S., Bednarski, B., Messick, C. A., Skibber, J. M., Feig, B. W., Lynch, P. M., Vilar, E., & You, Y. N. (2016). DNA Mismatch Repair Deficiency in Rectal Cancer: Benchmarking Its Impact on Prognosis, Neoadjuvant Response Prediction, and Clinical Cancer Genetics. Journal of Clinical Oncology: Official Journal of the American Society of Clinical Oncology, 34(25), 3039–3046. https://doi.org/10.1200/JCO.2016.66.6826

de Wind, N., Dekker, M., Berns, A., Radman, M., & te Riele, H. (1995). Inactivation of the mouse Msh2 gene results in mismatch repair deficiency, methylation tolerance, hyperrecombination, and predisposition to cancer. Cell, 82(2), 321–330. https://doi.org/10.1016/0092-8674(95)90319-4

de Wind, N., Dekker, M., Claij, N., Jansen, L., van Klink, Y., Radman, M., Riggins, G., van der Valk, M., van't Wout, K., & te Riele, H. (1999). HNPCC-like cancer predisposition in mice through simultaneous loss of Msh3 and Msh6 mismatch-repair protein functions. Nature Genetics, 23(3), 359–362. https://doi.org/10.1038/15544

Diergaarde, B., Braam, H., Vasen, H. F., Nagengast, F. M., van Muijen, G. N. P., Kok, F. J., & Kampman, E. (2007). Environmental Factors and Colorectal Tumor Risk in Individuals With Hereditary Nonpolyposis Colorectal Cancer. Clinical Gastroenterology and Hepatology, 5(6), 736-742.e1. https://doi.org/10.1016/j.cgh.2007.02.019

Dole, V. P., & Gentry, R. T. (1984). Toward an analogue of alcoholism in mice: Scale factors in the model. Proceedings of the National Academy of Sciences of the United States of America, 81(11), 3543–3546.

Dominguez-Valentin, M. (2020). The Prospective Lynch Syndrome Database (PLSD). European Hereditary Tumour Group (EHTG). https://ehtg.org/collaborative-studies/plsd/

Dominguez-Valentin, M., Sampson, J. R., Seppälä, T. T., ten Broeke, S. W., Plazzer, J.-P., Nakken, S., Engel, C., Aretz, S., Jenkins, M. A., Sunde, L., Bernstein, I., Capella, G., Balaguer, F., Thomas, H., Evans, D. G., Burn, J., Greenblatt, M., Hovig, E., de Vos tot Nederveen Cappel, W. H., … Møller, P. (2020). Cancer risks by gene, age, and gender in 6350 carriers ofpathogenic mismatch repair variants: Findings from the Prospective

Lynch SyndromeDatabase. Genetics in Medicine, 22(1), 15–25. https://doi.org/10.1038/s41436-019-0596-9

Dowty, J. G., Win, A. K., Buchanan, D. D., Lindor, N. M., Macrae, F. A., Clendenning, M., Antill, Y. C., Thibodeau, S. N., Casey, G., Gallinger, S., Marchand, L. L., Newcomb, P. A., Haile, R. W., Young, G. P., James, P. A., Giles, G. G., Gunawardena, S. R., Leggett, B. A., Gattas, M., … Jenkins, M. A. (2013). Cancer risks for MLH1 and MSH2 mutation carriers. Human Mutation, 34(3), 490–497. https://doi.org/10.1002/humu.22262

Drayton, D. L., Liao, S., Mounzer, R. H., & Ruddle, N. H. (2006). Lymphoid organ development: From ontogeny to neogenesis. Nature Immunology, 7(4), 344–353. https://doi.org/10.1038/ni1330

Dukes, C. (1934). Multiple intestinal tumours. The Eugenics Review, 25(4), 241–243.

Dukes, C. (1937). Histological Grading of Rectal Cancer: (Section of Pathology). Proceedings of the Royal Society of Medicine, 30(4), 371–376.

Dukes, C. E. (1956). Pathology of precancerous lesions of the colon and rectum. Gastroenterologia, 86(3), 336–337. https://doi.org/10.1159/000200579

Dukes, C. E., & Bussey, H. J. (1958). The spread of rectal cancer and its effect on prognosis. British Journal of Cancer, 12(3), 309–320. https://doi.org/10.1038/bjc.1958.37

Dukes, Cuthbert. (1926). Simple Tumours of the Large Intestine and their Relation to Cancer. Proceedings of the Royal Society of Medicine, 19(Surg Sect), 8–9.

Dukes, Cuthbert E. (1932). The classification of cancer of the rectum. The Journal of Pathology and Bacteriology, 35(3), 323–332. https://doi.org/10.1002/path.1700350303

Dunn, G. P., Old, L. J., & Schreiber, R. D. (2004). The Three Es of Cancer Immunoediting. Annual Review of Immunology, 22(1), 329–360. https://doi.org/10.1146/annurev.immunol.22.012703.104803

Echterdiek, F., Janikovits, J., Staffa, L., Müller, M., Lahrmann, B., Frühschütz, M., Hartog, B., Nelius, N., Benner, A., Tariverdian, M., Doeberitz, M. von K., Grabe, N., & Kloor, M. (2016). Low density of FOXP3-positive T cells in normal colonic mucosa is related to the presence of beta2-microglobulin mutations in Lynch syndrome-associated colorectal cancer. OncoImmunology, 5(2), e1075692. https://doi.org/10.1080/2162402X.2015.1075692

Edelmann, L., & Edelmann, W. (2004). Loss of DNA mismatch repair function and cancer predisposition in the mouse: Animal models for human hereditary nonpolyposis colorectal cancer. American Journal of Medical Genetics. Part C, Seminars in Medical Genetics, 129C(1), 91–99. https://doi.org/10.1002/ajmg.c.30021

Edelmann, W., Umar, A., Yang, K., Heyer, J., Kucherlapati, M., Lia, M., Kneitz, B., Avdievich, E., Fan, K., Wong, E., Crouse, G., Kunkel, T., Lipkin, M., Kolodner, R. D., & Kucherlapati, R. (2000). The DNA mismatch repair genes Msh3 and Msh6 cooperate in intestinal tumor suppression. Cancer Research, 60(4), 803–807.

Edelmann, W., Yang, K., Kuraguchi, M., Heyer, J., Lia, M., Kneitz, B., Fan, K., Brown, A. M., Lipkin, M., & Kucherlapati, R. (1999). Tumorigenesis in Mlh1 and Mlh1/Apc1638N mutant mice. Cancer Research, 59(6), 1301–1307.

Edelmann, W., Yang, K., Umar, A., Heyer, J., Lau, K., Fan, K., Liedtke, W., Cohen, P. E., Kane, M. F., Lipford, J. R., Yu, N., Crouse, G. F., Pollard, J. W., Kunkel, T., Lipkin, M., Kolodner, R., & Kucherlapati, R. (1997). Mutation in the mismatch repair gene Msh6 causes cancer susceptibility. Cell, 91(4), 467–477. https://doi.org/10.1016/s0092-8674(00)80433-x

Elmore, S. (2007). Apoptosis: A Review of Programmed Cell Death. Toxicologic Pathology, 35(4), 495–516. https://doi.org/10.1080/01926230701320337

Engel, C., Ahadova, A., Seppälä, T. T., Aretz, S., Bigirwamungu-Bargeman, M., Bläker, H., Bucksch, K., Büttner, R., de Vos Tot Nederveen Cappel, W. T., Endris, V., Holinski-Feder, E., Holzapfel, S., Hüneburg, R., Jacobs, M. A. J. M., Koornstra, J. J., Langers, A. M., Lepistö, A., Morak, M., Möslein, G., … Finnish Lynch Syndrome Registry. (2020). Associations of Pathogenic Variants in MLH1, MSH2, and MSH6 With Risk of Colorectal Adenomas and Tumors and With Somatic Mutations in Patients With Lynch Syndrome. Gastroenterology, 158(5), 1326–1333. https://doi.org/10.1053/j.gastro.2019.12.032

Engel, C., Vasen, H. F., Seppälä, T., Aretz, S., Bigirwamungu-Bargeman, M., de Boer, S. Y., Bucksch, K., Büttner, R., Holinski-Feder, E., Holzapfel, S., Hüneburg, R., Jacobs, M. A. J. M., Järvinen, H., Kloor, M., von Knebel Doeberitz, M., Koornstra, J. J., van Kouwen, M., Langers, A. M., van de Meeberg, P. C., … German HNPCC Consortium, the Dutch Lynch Syndrome Collaborative Group, and the Finnish Lynch Syndrome Registry. (2018). No Difference in Colorectal Cancer Incidence or Stage at Detection by Colonoscopy Among 3 Countries With Different Lynch Syndrome Surveillance Policies. Gastroenterology, 155(5), 1400-1409.e2. https://doi.org/10.1053/j.gastro.2018.07.030

Espina, N., Lima, V., Lieber, C. S., & Garro, A. J. (1988). In vitro and in vivo inhibitory effect of ethanol and acetaldehyde on O6-methylguanine transferase. Carcinogenesis, 9(5), 761–766. https://doi.org/10.1093/carcin/9.5.761

Esteller, M., Levine, R., Baylin, S. B., Ellenson, L. H., & Herman, J. G. (1998). MLH1 promoter hypermethylation is associated with the microsatellite instability phenotype in sporadic endometrial carcinomas. Oncogene, 17(18), 2413–2417. https://doi.org/10.1038/sj.onc.1202178

Farres, J., Wang, T. T. Y., Cunningham, S. J., & Weiner, H. (1995). Investigation of the Active Site Cysteine Residue of Rat Liver Mitochondrial Aldehyde Dehydrogenase by Site-Directed Mutagenesis. Biochemistry, 34(8), 2592–2598. https://doi.org/10.1021/bi00008a025

Fearon, E. R., & Vogelstein, B. (1990). A genetic model for colorectal tumorigenesis. Cell, 61(5), 759–767. https://doi.org/10.1016/0092-8674(90)90186-i

Fleming, M., Ravula, S., Tatishchev, S. F., & Wang, H. L. (2012). Colorectal carcinoma: Pathologic aspects. Journal of Gastrointestinal Oncology, 3(3), 153–173. https://doi.org/10.3978/j.issn.2078-6891.2012.030

Foltz, C., & Ullman-Cullere, M. (1998). Guidelines for Assessing the Health and Condition of Mice. Lab Animal, 28.

Frankel, W., Arends, M., Frayling, I. M., & Nagtegaal, I. D. (2019). Lynch Syndrome: Genetic Tumour Syndromes of the Digestive System. In World Health Organization Classification of Tumours of the Digestive System (5th ed.). IARC Press.

Frayling, I., Berry, I., Wallace, A., Payne, S., & Norbury, G. (2016). ACGS best practice guidelines for genetic testing and diagnosis of Lynch syndrome. The Association for Clinical Genomic Science. https://www.acgs.uk.com/media/10774/ls_bpg_approved.pdf

Frayling, I. M. (1999). Microsatellite instability. Gut, 45(1), 1–4. https://doi.org/10.1136/gut.45.1.1

Frayling, Ian M., & Arends, M. J. (2015). How can histopathologists help clinical genetics in the investigation of suspected hereditary gastrointestinal cancer? Diagnostic Histopathology, 21(4), 137–146. https://doi.org/10.1016/j.mpdhp.2015.04.004

Fukushima, H., Yamamoto, H., Itoh, F., Horiuchi, S., Min, Y., Iku, S., & Imai, K. (2001). Frequent alterations of the beta-catenin and TCF-4 genes, but not of the APC gene, in colon cancers with high-frequency microsatellite instability. Journal of Experimental & Clinical Cancer Research: CR, 20(4), 553–559.

Garaycoechea, J. I., Crossan, G. P., Langevin, F., Daly, M., Arends, M. J., & Patel, K. J. (2012). Genotoxic consequences of endogenous aldehydes on mouse haematopoietic stem cell function. Nature, 489(7417), 571–575. https://doi.org/10.1038/nature11368

García-Ruiz, C., Colell, A., París, R., & Fernández-Checa, J. C. (2000). Direct interaction of GD3 ganglioside with mitochondria generates reactive oxygen species followed by mitochondrial permeability transition, cytochrome c release, and caspase activation. The FASEB Journal, 14(7), 847–858. https://doi.org/10.1096/fasebj.14.7.847

Garro, A. J., McBeth, D. L., Lima, V., & Lieber, C. S. (1991). Ethanol Consumption Inhibits Fetal DNA Methylation in Mice: Implications for the Fetal Alcohol Syndrome. Alcoholism: Clinical and Experimental Research, 15(3), 395–398. https://doi.org/10.1111/j.1530-0277.1991.tb00536.x

Gerdes, J., Lemke, H., Baisch, H., Wacker, H. H., Schwab, U., & Stein, H. (1984). Cell cycle analysis of a cell proliferation-associated human nuclear antigen defined by the monoclonal antibody Ki-67. The Journal of Immunology, 133(4), 1710–1715.

Glebov, O. K., Rodriguez, L. M., Nakahara, K., Jenkins, J., Cliatt, J., Humbyrd, C.-J., DeNobile, J., Soballe, P., Simon, R., Wright, G., Lynch, P., Patterson, S., Lynch, H., Gallinger, S., Buchbinder, A., Gordon, G., Hawk, E., & Kirsch, I. R. (2003). Distinguishing Right from Left Colon by the Pattern of Gene Expression. Cancer Epidemiology and Prevention Biomarkers, 12(8), 755–762.

Global Cancer Observatory. (2020). https://gco.iarc.fr/

Gonzalez, H., Hagerling, C., & Werb, Z. (2018). Roles of the immune system in cancer: From tumor initiation to metastatic progression. Genes & Development, 32(19–20), 1267–1284. https://doi.org/10.1101/gad.314617.118

González-Sancho, J. M., Aguilera, O., García, J. M., Pendás-Franco, N., Peña, C., Cal, S., García de Herreros, A., Bonilla, F., & Muñoz, A. (2005). The Wnt antagonist DICKKOPF-1 gene is a downstream target of beta-catenin/TCF and is downregulated in human colon cancer. Oncogene, 24(6), 1098–1103. https://doi.org/10.1038/sj.onc.1208303

Graham, R. P., Kerr, S. E., Butz, M. L., Thibodeau, S. N., Halling, K. C., Smyrk, T. C., Dina, M. A., Waugh, V. M., & Rumilla, K. M. (2015). Heterogenous MSH6 loss is a result of microsatellite instability within MSH6 and occurs in sporadic and hereditary colorectal and endometrial carcinomas. The American Journal of Surgical Pathology, 39(10), 1370–1376. https://doi.org/10.1097/PAS.0000000000000459

Gylling, A., Abdel-Rahman, W. M., Juhola, M., Nuorva, K., Hautala, E., Järvinen, H. J., Mecklin, J., Aarnio, M., & Peltomäki, P. (2007). Is gastric cancer part of the tumour spectrum of hereditary non-polyposis colorectal cancer? A molecular genetic study. Gut, 56(7), 926–933. https://doi.org/10.1136/gut.2006.114876

Hanahan, D., & Weinberg, R. A. (2000). The hallmarks of cancer. Cell, 100(1), 57–70. https://doi.org/10.1016/s0092-8674(00)81683-9

Hanahan, Douglas, & Weinberg, R. A. (2011). Hallmarks of cancer: The next generation. Cell, 144(5), 646–674. https://doi.org/10.1016/j.cell.2011.02.013

Hannan, L. M., Jacobs, E. J., & Thun, M. J. (2009). The Association between Cigarette Smoking and Risk of Colorectal Cancer in a Large Prospective Cohort from the United States. Cancer Epidemiology Biomarkers & Prevention, 18(12), 3362–3367. https://doi.org/10.1158/1055-9965.EPI-09-0661

Hause, R. J., Pritchard, C. C., Shendure, J., & Salipante, S. J. (2016). Classification and characterization of microsatellite instability across 18 cancer types. Nature Medicine, 22(11), 1342–1350. https://doi.org/10.1038/nm.4191

Helmink, B. A., Reddy, S. M., Gao, J., Zhang, S., Basar, R., Thakur, R., Yizhak, K., Sade-Feldman, M., Blando, J., Han, G., Gopalakrishnan, V., Xi, Y., Zhao, H., Amaria, R. N., Tawbi, H. A., Cogdill, A. P., Liu, W., LeBleu, V. S., Kugeratski, F. G., … Wargo, J. A. (2020). B cells and tertiary lymphoid structures promote immunotherapy response. Nature, 577(7791), 549–555. https://doi.org/10.1038/s41586-019-1922-8

Hitchins, & Ward. (2009). Constitutional (germline) MLH1 epimutation as an aetiological mechanism for hereditary non-polyposis colorectal cancer. Journal of Medical Genetics, 46(12), 793–802. https://doi.org/10.1136/jmg.2009.068122

Hitchins, Williams, R., Cheong, K., Halani, N., Lin, V. A. P., Packham, D., Ku, S., Buckle, A., Hawkins, N., Burn, J., Gallinger, S., Goldblatt, J., Kirk, J., Tomlinson, I., Scott, R., Spigelman, A., Suter, C., Martin, D., Suthers, G., & Ward, R. (2005). MLH1 germline epimutations as a factor in hereditary nonpolyposis colorectal cancer. Gastroenterology, 129(5), 1392–1399. https://doi.org/10.1053/j.gastro.2005.09.003

Holmes, & Peter B. Mather and Ujjwal K. Rout. (1986). Biochemical and genetic studies on enzymes of alcohol metabolism: The mouse as a model organism for human studies. Alcohol and Alcoholism. https://doi.org/10.1093/oxfordjournals.alcalc.a044589

Holubec, H., Payne, C. M., Bernstein, H., Dvorakova, K., Bernstein, C., Waltmire, C. N., Warneke, J. A., & Garewal, H. (2005). Assessment of Apoptosis by Immunohistochemical Markers Compared to Cellular Morphology in Ex Vivo-stressed Colonic Mucosa. Journal of Histochemistry & Cytochemistry, 53(2), 229–235. https://doi.org/10.1369/jhc.4A6386.2005

Hsieh, P., & Yamane, K. (2008). DNA mismatch repair: Molecular mechanism, cancer, and ageing. Mechanisms of Ageing and Development, 129(7–8), 391–407. https://doi.org/10.1016/j.mad.2008.02.012

Hsu, L. C., & Chang, W. C. (1991). Cloning and characterization of a new functional human aldehyde dehydrogenase gene. The Journal of Biological Chemistry, 266(19), 12257–12265.

Hsu, Y.-L., Lin, C.-C., Jiang, J.-K., Lin, H.-H., Lan, Y.-T., Wang, H.-S., Yang, S.-H., Chen, W.-S., Lin, T.-C., Lin, J.-K., Lin, P.-C., & Chang, S.-C. (2019). Clinicopathological and molecular differences in colorectal cancer according to location. The International Journal of Biological Markers, 34(1), 47–53. https://doi.org/10.1177/1724600818807164

Hu, W., Feng, Z., Eveleigh, J., Iyer, G., Pan, J., Amin, S., Chung, F.-L., & Tang, M.-S. (2002). The major lipid peroxidation product, trans-4-hydroxy-2-nonenal, preferentially forms DNA adducts at codon 249 of human p53 gene, a unique mutational hotspot in hepatocellular carcinoma. Carcinogenesis, 23(11), 1781–1789. https://doi.org/10.1093/carcin/23.11.1781

Huels, D. J., Bruens, L., Hodder, M. C., Cammareri, P., Campbell, A. D., Ridgway, R. A., Gay, D. M., Solar-Abboud, M., Faller, W. J., Nixon, C., Zeiger, L. B., McLaughlin, M. E., Morrissey, E., Winton, D. J., Snippert, H. J., van Rheenen, J., & Sansom, O. J. (2018). Wnt ligands influence tumour initiation by controlling the number of intestinal stem cells. Nature Communications, 9(1), 1132. https://doi.org/10.1038/s41467-018-03426-2

Husemoen, L. L. N., Fenger, M., Friedrich, N., Tolstrup, J. S., Beenfeldt Fredriksen, S., & Linneberg, A. (2008). The Association of ADH and ALDH Gene Variants With Alcohol Drinking Habits and Cardiovascular Disease Risk Factors. Alcoholism: Clinical and Experimental Research. https://doi.org/10.1111/j.1530-0277.2008.00780.x

IARC. (2010). Alcohol consumption and ethyl carbamate. IARC Monographs on the Evaluation of Carcinogenic Risks to Humans, 96, 3–1383.

InSiGHT. (2020a). Graphs and statistics for the MLH1 gene. https://databases.lovd.nl/shared/genes/MLH1/graphs

InSiGHT. (2020b). Graphs and statistics for the MSH2 gene. https://databases.lovd.nl/shared/genes/MSH2/graphs

InSiGHT. (2020c). Graphs and statistics for the MSH6 gene. https://databases.lovd.nl/shared/genes/MSH6/graphs

InSiGHT. (2020d). Graphs and statistics for the PMS2 gene. https://databases.lovd.nl/shared/genes/PMS2/graphs

InSiGHT. (2020e). MMR gene variant classification. InSiGHT. https://www.insight-group.org/criteria/

Jackson, B. C., Reigan, P., Miller, B., Thompson, D. C., & Vasiliou, V. (2015). Human ALDH1B1 polymorphisms may affect the metabolism of acetaldehyde and all-trans retinaldehyde – in vitro studies and computational modeling. Pharmaceutical Research, 32(5), 1648–1662. https://doi.org/10.1007/s11095-014-1564-3

Jahid, S., & Lipkin, S. (2010). Mouse models of Inherited Cancer Syndromes. Hematology/Oncology Clinics of North America, 24(6), 1205–1228. https://doi.org/10.1016/j.hoc.2010.08.011

Jenkins, M. A., Reece, J. C., & Win, A. K. (2018). The International Mismatch Repair Consortium. In L. Valle, S. B. Gruber, & G. Capellá (Eds.), Hereditary Colorectal Cancer: Genetic Basis and Clinical Implications (pp. 479–495). Springer International Publishing. https://doi.org/10.1007/978-3-319-74259-5_30

Jenkins, M. A., Win, A. K., Templeton, A. S., Angelakos, M. S., Buchanan, D. D., Cotterchio, M., Figueiredo, J. C., Thibodeau, S. N., Baron, J. A., Potter, J. D., Hopper, J. L., Casey, G., Gallinger, S., Le Marchand, L., Lindor, N. M., Newcomb, P. A., & Haile, R. W. (2018). The Colon Cancer Family Registry Cohort (CCFRC). International Journal of Epidemiology, 47(2), 387–388i. https://doi.org/10.1093/ije/dyy006

Jessup, C. J., Redston, M., Tilton, E., & Reimann, J. D. R. (2016). Importance of universal mismatch repair protein immunohistochemistry in patients with sebaceous neoplasia as an initial screening tool for Muir-Torre syndrome. Human Pathology, 49, 1–9. https://doi.org/10.1016/j.humpath.2015.10.005

Jiang, Y., Ben, Q., Shen, H., Lu, W., Zhang, Y., & Zhu, J. (2011). Diabetes mellitus and incidence and mortality of colorectal cancer: A systematic review and meta-analysis of cohort studies. European Journal of Epidemiology, 26(11), 863–876. https://doi.org/10.1007/s10654-011-9617-y

Johnston, P. G., O'Brien, M. J., & Dervan, P. A. (1989). Lmmunohistochemical Analysis of Cell Kinetic Parameters in Colonic Adenocarcinomas, Adenomas, and Normal Mucosa. 20(7), 5.

Ju, J. Y., Mills, A. M., Mahadevan, M. S., Fan, J., Culp, S. H., Thomas, M. H., & Cathro, H. P. (2018). Universal Lynch Syndrome Screening Should be Performed in All Upper Tract Urothelial Carcinomas. The American Journal of Surgical Pathology, 42(11), 1549–1555. https://doi.org/10.1097/PAS.0000000000001141

Jun, S.-Y., Lee, E.-J., Kim, M.-J., Chun, S. M., Bae, Y. K., Hong, S. U., Choi, J., Kim, J. M., Jang, K.-T., Kim, J. Y., Kim, G. I., Jung, S. J., Yoon, G., & Hong, S.-M. (2017). Lynch syndrome-related small intestinal adenocarcinomas. Oncotarget, 8(13), 21483–21500. https://doi.org/10.18632/oncotarget.15277

Kabbarah, O., Ann Mallon, M., Pfeifer, J. D., Edelmann, W., Kucherlapati, R., & Goodfellow, P. J. (2003). A panel of repeat markers for detection of microsatellite instability in murine tumors. Molecular Carcinogenesis, 38(4), 155–159. https://doi.org/10.1002/mc.10157

Karran, P. (2001). Mechanisms of tolerance to DNA damaging therapeutic drugs. Carcinogenesis, 22(12), 1931–1937. https://doi.org/10.1093/carcin/22.12.1931

Kasajima, A., Sers, C., Sasano, H., Jöhrens, K., Stenzinger, A., Noske, A., Buckendahl, A.-C., Darb-Esfahani, S., Müller, B. M., Budczies, J., Lehman, A., Dietel, M., Denkert, C., & Weichert, W. (2010). Down-regulation of the antigen processing machinery is linked to a loss of inflammatory response in colorectal cancer. Human Pathology, 41(12), 1758–1769. https://doi.org/10.1016/j.humpath.2010.05.014

Kastenhuber, E., & Lowe, S. (2017). Putting p53 in context. Cell, 170(6), 1062–1078. https://doi.org/10.1016/j.cell.2017.08.028

Kedrin, D., & Gala, M. K. (2015). Genetics of the serrated pathway to colorectal cancer. Clinical and Translational Gastroenterology, 6, e84. https://doi.org/10.1038/ctg.2015.12

Kempers, M. J., Kuiper, R. P., Ockeloen, C. W., Chappuis, P. O., Hutter, P., Rahner, N., Schackert, H. K., Steinke, V., Holinski-Feder, E., Morak, M., Kloor, M., Büttner, R., Verwiel, E. T., van Krieken, J. H., Nagtegaal, I. D., Goossens, M., van der Post, R. S., Niessen, R. C., Sijmons, R. H., … Ligtenberg, M. J. (2011). HIGH COLORECTAL AND LOW ENDOMETRIAL CANCER RISK IN EPCAM DELETION-POSITIVE LYNCH SYNDROME: A COHORT STUDY. The Lancet Oncology, 12(1), 49–55. https://doi.org/10.1016/S1470-2045(10)70265-5

Kim, H., & D'Andrea, A. D. (2012). Regulation of DNA cross-link repair by the Fanconi anemia/BRCA pathway. Genes & Development, 26(13), 1393–1408. https://doi.org/10.1101/gad.195248.112

Kloor, M., Huth, C., Voigt, A. Y., Benner, A., Schirmacher, P., von Knebel Doeberitz, M., & Bläker, H. (2012). Prevalence of mismatch repair-deficient crypt foci in Lynch syndrome: A pathological study. The Lancet Oncology, 13(6), 598–606. https://doi.org/10.1016/S1470-2045(12)70109-2

Kloor, M., Michel, S., Buckowitz, B., Rüschoff, J., Büttner, R., Holinski-Feder, E., Dippold, W., Wagner, R., Tariverdian, M., Benner, A., Schwitalle, Y., Kuchenbuch, B., & von Knebel Doeberitz, M. (2007). Beta2-microglobulin mutations in microsatellite unstable colorectal tumors. International Journal of Cancer, 121(2), 454–458. https://doi.org/10.1002/ijc.22691

Kloor, M., Michel, S., & von Knebel Doeberitz, M. (2010). Immune evasion of microsatellite unstable colorectal cancers. International Journal of Cancer, 127(5), 1001–1010. https://doi.org/10.1002/ijc.25283

Köbel, M., Piskorz, A. M., Lee, S., Lui, S., LePage, C., Marass, F., Rosenfeld, N., Mes Masson, A.-M., & Brenton, J. D. (2016). Optimized p53 immunohistochemistry is an accurate predictor of TP53 mutation in ovarian carcinoma: P53 immunohistochemistry predicts

TP53 mutation status. The Journal of Pathology: Clinical Research, 2(4), 247–258. https://doi.org/10.1002/cjp2.53

Koelzer, V. H., Baker, K., Kassahn, D., Baumhoer, D., & Zlobec, I. (2012). Prognostic impact of β-2-microglobulin expression in colorectal cancers stratified by mismatch repair status. Journal of Clinical Pathology, 65(11), 996–1002. https://doi.org/10.1136/jclinpath-2012-200742

Kucherlapati, M. H., Lee, K., Nguyen, A. A., Clark, A. B., Hou, H., Rosulek, A., Li, H., Yang, K., Fan, K., Lipkin, M., Bronson, R. T., Jelicks, L., Kunkel, T. A., Kucherlapati, R., & Edelmann, W. (2010). An Msh2 conditional knockout mouse for studying intestinal cancer and testing anticancer agents. Gastroenterology, 138(3), 993-1002.e1. https://doi.org/10.1053/j.gastro.2009.11.009

Kulaylat, M. N., & Dayton, M. T. (2010). Ulcerative colitis and cancer. Journal of Surgical Oncology, 101(8), 706–712. https://doi.org/10.1002/jso.21505

Lakin, N. D., & Jackson, S. P. (1999). Regulation of p53 in response to DNA damage. Oncogene, 18(53), 7644–7655. https://doi.org/10.1038/sj.onc.1203015

Landrum, M. J., & Kattman, B. L. (2018). ClinVar at five years: Delivering on the promise. Human Mutation, 39(11), 1623–1630. https://doi.org/10.1002/humu.23641

Langevin, F., Crossan, G. P., Rosado, I. V., Arends, M. J., & Patel, K. J. (2011). Fancd2 counteracts the toxic effects of naturally produced aldehydes in mice. Nature, 475(7354), 53–58. https://doi.org/10.1038/nature10192

Le, D. T., Uram, J. N., Wang, H., Bartlett, B. R., Kemberling, H., Eyring, A. D., Skora, A. D., Luber, B. S., Azad, N. S., Laheru, D., Biedrzycki, B., Donehower, R. C., Zaheer, A., Fisher, G. A., Crocenzi, T. S., Lee, J. J., Duffy, S. M., Goldberg, R. M., de la Chapelle, A., … Diaz, L. A. (2015). PD-1 Blockade in Tumors with Mismatch-Repair Deficiency. The New England Journal of Medicine, 372(26), 2509–2520. https://doi.org/10.1056/NEJMoa1500596

Lee, J., Nicholas J. Petrelli, & Miguel A. Rodriguez-Bigas. (2001). Rectal cancer in hereditary nonpolyposis colorectal cancer. The American Journal of Surgery, 4.

Lee, P., Forey, B., Coombs, K., Hamling, J., & Thornton, A. (2016). Epidemiological evidence on environmental tobacco smoke and cancers other than lung or breast. https://f1000research.com/articles/7-146

Leufkens, A. M., Van Duijnhoven, F. J. B., Siersema, P. D., Boshuizen, H. C., Vrieling, A., Agudo, A., Gram, I. T., Weiderpass, E., Dahm, C., Overvad, K., Tjønneland, A., Olsen, A., Boutron–Ruault, M., Clavel–Chapelon, F., Morois, S., Palli, D., Grioni, S., Tumino, R., Sacerdote, C., … Bueno–de–Mesquita, H. B. (2011). Cigarette Smoking and Colorectal Cancer Risk in the European Prospective Investigation Into Cancer and Nutrition Study. Clinical Gastroenterology and Hepatology, 9(2), 137–144. https://doi.org/10.1016/j.cgh.2010.10.012

Levine, A. J. (1997). P53, the Cellular Gatekeeper for Growth and Division. Cell, 88(3), 323–331. https://doi.org/10.1016/S0092-8674(00)81871-1

Li, L., McVety, S., Younan, R., Liang, P., Du Sart, D., Gordon, P. H., Hutter, P., Hogervorst, F. B. L., Chong, G., & Foulkes, W. D. (2006). Distinct patterns of germ-line deletions in MLH1 and MSH2: The implication of Alu repetitive element in the genetic etiology of Lynch syndrome (HNPCC). Human Mutation, 27(4), 388. https://doi.org/10.1002/humu.9417

Liang, P. S., Chen, T.-Y., & Giovannucci, E. (2009). Cigarette smoking and colorectal cancer incidence and mortality: Systematic review and meta-analysis. International Journal of Cancer, 124(10), 2406–2415. https://doi.org/10.1002/ijc.24191

Ligtenberg, M. J. L., Kuiper, R. P., Chan, T. L., Goossens, M., Hebeda, K. M., Voorendt, M., Lee, T. Y. H., Bodmer, D., Hoenselaar, E., Hendriks-Cornelissen, S. J. B., Tsui, W. Y., Kong, C. K., Brunner, H. G., van Kessel, A. G., Yuen, S. T., van Krieken, J. H. J. M., Leung, S. Y., & Hoogerbrugge, N. (2009). Heritable somatic methylation and inactivation of MSH2 in families with Lynch syndrome due to deletion of the 3' exons of TACSTD1. Nature Genetics, 41(1), 112–117. https://doi.org/10.1038/ng.283

Liljegren, A., Barker, G., Elliott, F., Bertario, L., Bisgaard, M. L., Eccles, D., Evans, G., Macrae, F., Maher, E., Lindblom, A., Rotstein, S., Nilsson, B., Mecklin, J.-P., Möslein, G., Jass, J., Fodde, R., Mathers, J., Burn, J., & Bishop, D. T. (2008). Prevalence of adenomas and hyperplastic polyps in mismatch repair mutation carriers among CAPP2 participants: Report by the colorectal adenoma/carcinoma prevention programme 2. Journal of Clinical Oncology: Official Journal of the American Society of Clinical Oncology, 26(20), 3434–3439. https://doi.org/10.1200/JCO.2007.13.2795

Linnebacher, M., Gebert, J., Rudy, W., Woerner, S., Yuan, Y. P., Bork, P., & von Knebel Doeberitz, M. (2001). Frameshift peptide-derived T-cell epitopes: A source of novel tumor-specific antigens. International Journal of Cancer, 93(1), 6–11. https://doi.org/10.1002/ijc.1298

Linnebacher, Michael, Gebert, J., Rudy, W., Woerner, S., Yuan, Y. P., Bork, P., & Doeberitz, M. von K. (2001). Frameshift peptide-derived T-cell epitopes: A source of novel tumor-specific antigens. International Journal of Cancer, 93(1), 6–11. https://doi.org/10.1002/ijc.1298

Linneberg, A., Gonzalez-Quintela, A., Vidal, C., Jørgensen, T., Fenger, M., Hansen, T., Pedersen, O., & Husemoen, L. L. N. (2009). Genetic determinants of both ethanol and acetaldehyde metabolism influence alcohol hypersensitivity and drinking behaviour among Scandinavians: Genetics of alcohol sensitivity. Clinical & Experimental Allergy, 40(1), 123–130. https://doi.org/10.1111/j.1365-2222.2009.03398.x

Liu, C., Russell, R. M., Seitz, H. K., & Wang, X.-D. (2001). Ethanol enhances retinoic acid metabolism into polar metabolites in rat liver via induction of cytochrome P4502E1. Gastroenterology, 120(1), 179–189. https://doi.org/10.1053/gast.2001.20877

Llosa, N. J., Cruise, M., Tam, A., Wicks, E. C., Hechenbleikner, E. M., Taube, J. M., Blosser, R. L., Fan, H., Wang, H., Luber, B. S., Zhang, M., Papadopoulos, N., Kinzler, K. W., Vogelstein, B., Sears, C. L., Anders, R. A., Pardoll, D. M., & Housseau, F. (2015). The vigorous immune microenvironment of microsatellite instable colon cancer is balanced by multiple counter-inhibitory checkpoints. Cancer Discovery, 5(1), 43–51. https://doi.org/10.1158/2159-8290.CD-14-0863

Loeffler, M., Birke, A., Winton, D., & Potten, C. (1993). Somatic mutation, monoclonality and stochastic models of stem cell organization in the intestinal crypt. Journal of Theoretical Biology, 160(4), 471–491. https://doi.org/10.1006/jtbi.1993.1031

Loeffler, M., Bratke, T., Paulus, U., Li, Y. Q., & Potten, C. S. (1997). Clonality and life cycles of intestinal crypts explained by a state dependent stochastic model of epithelial stem cell organization. Journal of Theoretical Biology, 186(1), 41–54. https://doi.org/10.1006/jtbi.1996.0340

Lopez-Garcia, C., Klein, A. M., Simons, B. D., & Winton, D. J. (2010). Intestinal stem cell replacement follows a pattern of neutral drift. Science (New York, N.Y.), 330(6005), 822–825. https://doi.org/10.1126/science.1196236

Lorenz, R. G., & Newberry, R. D. (2004). Isolated lymphoid follicles can function as sites for induction of mucosal immune responses. Annals of the New York Academy of Sciences, 1029, 44–57. https://doi.org/10.1196/annals.1309.006

Loughrey, M., Arends, M., Brown, I., Burgart, L., Cunningham, C., Flejou, J., Kakar, S., Kirsch, R., Kojima, M., Lugli, A., Rosty, C., Sheahan, K., West, N., Wilson, R., & Nagtegaal, I. (2020). Colorectal Cancer Histopathology Reporting Guide (ISBN:978-1-922324-01-6). International Collaboration on Cancer Reporting, Sydney, Australia.

Loukola, A., Salovaara, R., Kristo, P., Moisio, A.-L., Kääriäinen, H., Ahtola, H., Eskelinen, M., Härkönen, N., Julkunen, R., Kangas, E., Ojala, S., Tulikoura, J., Valkamo, E., Järvinen, H., Mecklin, J.-P., de la Chapelle, A., & Aaltonen, L. A. (1999). Microsatellite Instability in Adenomas as a Marker for Hereditary Nonpolyposis Colorectal Cancer. The American Journal of Pathology, 155(6), 1849–1853.

Lugli, A., Zlobec, I., Minoo, P., Baker, K., Tornillo, L., Terracciano, L., & Jass, J. R. (2007). Prognostic significance of the wnt signalling pathway molecules APC, ?-catenin and E-cadherin in colorectal cancer?a tissue microarray-based analysis. Histopathology, 50(4), 453–464. https://doi.org/10.1111/j.1365-2559.2007.02620.x

Luo, W., Cao, Y., Liao, C., & Gao, F. (2012). Diabetes mellitus and the incidence and mortality of colorectal cancer: A meta-analysis of 24 cohort studies. Colorectal Disease: The Official Journal of the Association of Coloproctology of Great Britain and Ireland, 14(11), 1307–1312. https://doi.org/10.1111/j.1463-1318.2012.02875.x

Lutgens, M. W. M. D., Vleggaar, F. P., Schipper, M. E. I., Stokkers, P. C. F., van der Woude, C. J., Hommes, D. W., de Jong, D. J., Dijkstra, G., van Bodegraven, A. A., Oldenburg, B., & Samsom, M. (2008). High frequency of early colorectal cancer in inflammatory bowel disease. Gut, 57(9), 1246–1251. https://doi.org/10.1136/gut.2007.143453

Lynch, H., Lynch, P., Lanspa, S., Snyder, C., Lynch, J., & Boland, C. (2009). Review of the Lynch syndrome: History, molecular genetics, screening, differential diagnosis, and medicolegal ramifications. Clinical Genetics, 76(1), 1–18. https://doi.org/10.1111/j.1399-0004.2009.01230.x

Mah, L.-J., El-Osta, A., & Karagiannis, T. C. (2010). γH2AX: A sensitive molecular marker of DNA damage and repair. Leukemia, 24(4), 679–686. https://doi.org/10.1038/leu.2010.6

Marchitti, S. A., Brocker, C., Stagos, D., & Vasiliou, V. (2008). Non-P450 aldehyde oxidizing enzymes: The aldehyde dehydrogenase superfamily. Expert Opinion on Drug Metabolism & Toxicology, 4(6), 697–720. https://doi.org/10.1517/17425250802102627

Marks, K., & West, N. (2020). Molecular assessment of colorectal cancer through Lynch syndrome screening. Diagnostic Histopathology, 26(1), 47–50. https://doi.org/10.1016/j.mpdhp.2019.10.012

Martinez-Useros, J., & Garcia-Foncillas, J. (2016). Obesity and colorectal cancer: Molecular features of adipose tissue. Journal of Translational Medicine, 14. https://doi.org/10.1186/s12967-016-0772-5

Mcilhatton, M. A., Boivin, G. P., & Groden, J. (2016). Manipulation of DNA Repair Proficiency in Mouse Models of Colorectal Cancer. BioMed Research International, 2016, 1–18. https://doi.org/10.1155/2016/1414383

McIntyre, R. E., Buczacki, S. J. A., Arends, M. J., & Adams, D. J. (2015). Mouse models of colorectal cancer as preclinical models. BioEssays: News and Reviews in Molecular, Cellular and Developmental Biology, 37(8), 909–920. https://doi.org/10.1002/bies.201500032

Mensenkamp, A. R., Vogelaar, I. P., van Zelst-Stams, W. A. G., Goossens, M., Ouchene, H., Hendriks-Cornelissen, S. J. B., Kwint, M. P., Hoogerbrugge, N., Nagtegaal, I. D., & Ligtenberg, M. J. L. (2014). Somatic mutations in MLH1 and MSH2 are a frequent cause of mismatch-repair deficiency in Lynch syndrome-like tumors. Gastroenterology, 146(3), 643-646.e8. https://doi.org/10.1053/j.gastro.2013.12.002

Michel, S., Linnebacher, M., Alcaniz, J., Voss, M., Wagner, R., Dippold, W., Becker, C., von Knebel Doeberitz, M., Ferrone, S., & Kloor, M. (2010). Lack of HLA class II antigen expression in microsatellite unstable colorectal carcinomas is caused by mutations in HLA class II regulatory genes. International Journal of Cancer, 127(4), 889–898. https://doi.org/10.1002/ijc.25106

Mihaylova, V. T., Bindra, R. S., Yuan, J., Campisi, D., Narayanan, L., Jensen, R., Giordano, F., Johnson, R. S., Rockwell, S., & Glazer, P. M. (2003). Decreased expression of the DNA mismatch repair gene Mlh1 under hypoxic stress in mammalian cells. Molecular and Cellular Biology, 23(9), 3265–3273. https://doi.org/10.1128/mcb.23.9.3265-3273.2003

Mirabelli-Primdahl, L., Gryfe, R., Kim, H., Millar, A., Luceri, C., Dale, D., Holowaty, E., Bapat, B., Gallinger, S., & Redston, M. (1999). B-Catenin Mutations Are Specific for Colorectal Carcinomas with Microsatellite Instability but Occur in Endometrial Carcinomas Irrespective of Mutator Pathway. 7.

Missia, D. A., Demetriou, E., Michael, N., Tolis, E. I., & Bartzis, J. G. (2010). Indoor exposure from building materials: A field study. Atmospheric Environment, 44(35), 4388–4395. https://doi.org/10.1016/j.atmosenv.2010.07.049

Modrich, P., & Lahue, R. (1996). Mismatch repair in replication fidelity, genetic recombination, and cancer biology. Annual Review of Biochemistry, 65, 101–133. https://doi.org/10.1146/annurev.bi.65.070196.000533

Møller, P., Seppälä, T., Bernstein, I., Holinski-Feder, E., Sala, P., Evans, D. G., Lindblom, A., Macrae, F., Blanco, I., Sijmons, R., Jeffries, J., Vasen, H., Burn, J., Nakken, S., Hovig, E., Rødland, E. A., Tharmaratnam, K., de Vos tot Nederveen Cappel, W. H., Hill, J., … in collaboration with The Mallorca Group (http://mallorca-group.eu). (2017). Cancer incidence and survival in Lynch syndrome patients receiving colonoscopic and gynaecological surveillance: First report from the prospective Lynch syndrome database. Gut, 66(3), 464–472. https://doi.org/10.1136/gutjnl-2015-309675

Møller, P., Seppälä, T. T., Bernstein, I., Holinski-Feder, E., Sala, P., Gareth Evans, D., Lindblom, A., Macrae, F., Blanco, I., Sijmons, R. H., Jeffries, J., Vasen, H. F. A., Burn, J., Nakken, S., Hovig, E., Rødland, E. A., Tharmaratnam, K., de Vos tot Nederveen Cappel, W. H., Hill, J., … Capella, G. (2018). Cancer risk and survival in path_MMR carriers by gene and gender up to 75 years of age: A report from the Prospective Lynch Syndrome Database. Gut, 67(7), 1306–1316. https://doi.org/10.1136/gutjnl-2017-314057

Morak, M., Ibisler, A., Keller, G., Jessen, E., Laner, A., Gonzales-Fassrainer, D., Locher, M., Massdorf, T., Nissen, A. M., Benet-Pagès, A., & Holinski-Feder, E. (2018). Comprehensive analysis of the MLH1 promoter region in 480 patients with colorectal cancer and 1150 controls reveals new variants including one with a heritable constitutional MLH1 epimutation. Journal of Medical Genetics, 55(4), 240–248. https://doi.org/10.1136/jmedgenet-2017-104744

Morin, P. J., Sparks, A. B., Korinek, V., Barker, N., Clevers, H., Vogelstein, B., & Kinzler, K. W. (1997). Activation of β-Catenin-Tcf Signaling in Colon Cancer by Mutations in β-Catenin or APC | Science. https://science.sciencemag.org/content/275/5307/1787.long

Mowat, A. M., & Agace, W. W. (2014). Regional specialization within the intestinal immune system. Nature Reviews. Immunology, 14(10), 667–685. https://doi.org/10.1038/nri3738

Müller, Mike F., Ibrahim, A. E. K., & Arends, M. J. (2016). Molecular pathological classification of colorectal cancer. Virchows Archiv, 469(2), 125–134. https://doi.org/10.1007/s00428-016-1956-3

Müller, Mike F, Zhou, Y., Adams, D. J., & Arends, M. J. (2016). Effects of long-term ethanol consumption and Aldh1b1 depletion on intestinal tumourigenesis in mice: Long-term ethanol consumption and Aldh1b1 depletion in mice. The Journal of Pathology, 241(5), 649–660. https://doi.org/10.1002/path.4869

Müller, Mike Freya, Kendall, T. J., Adams, D. J., Zhou, Y., & Arends, M. J. (2018). The murine hepatic sequelae of long-term ethanol consumption are sex-specific and exacerbated by Aldh1b1 loss. Experimental and Molecular Pathology, 105, 63–70. https://doi.org/10.1016/j.yexmp.2018.05.008

Muzumdar, M. D., Tasic, B., Miyamichi, K., Li, L., & Luo, L. (2007). A global double-fluorescent Cre reporter mouse.

Naguib, A., Mitrou, P. N., Gay, L. J., Cooke, J. C., Luben, R. N., Ball, R. Y., McTaggart, A., Arends, M. J., & Rodwell, S. A. (2010). Dietary, lifestyle and clinicopathological factors associated

with BRAF and K-ras mutations arising in distinct subsets of colorectal cancers in the EPIC Norfolk study. BMC Cancer, 10(1), 99. https://doi.org/10.1186/1471-2407-10-99

Nagy, A. (2000). Cre recombinase: The universal reagent for genome tailoring. Genesis, 26(2), 99–109. https://doi.org/10.1002/(SICI)1526-968X(200002)26:2<99::AID-GENE1>3.0.CO;2-B

Nandan, M. O., Ghaleb, A. M., & Bialkowska, A. B. (2016). Krüppel-like factor 5 is essential for proliferation and survival of mouse intestinal epithelial stem cells. 19.

National Institute for Health and Care Excellence. (2017). Molecular testing strategies for Lynch syndrome in people with colorectal cancer.

Niessen, R. C., Hofstra, R. M. W., Westers, H., Ligtenberg, M. J. L., Kooi, K., Jager, P. O. J., de Groote, M. L., Dijkhuizen, T., Olderode-Berends, M. J. W., Hollema, H., Kleibeuker, J. H., & Sijmons, R. H. (2009). Germline hypermethylation of MLH1 and EPCAM deletions are a frequent cause of Lynch syndrome. Genes, Chromosomes & Cancer, 48(8), 737–744. https://doi.org/10.1002/gcc.20678

Nilbert, M., Planck, M., Fernebro, E., Borg, A., & Johnson, A. (1999). Microsatellite instability is rare in rectal carcinomas and signifies hereditary cancer. European Journal of Cancer (Oxford, England: 1990), 35(6), 942–945. https://doi.org/10.1016/s0959-8049(99)00045-3

Ning, Y., Wang, L., & Giovannucci, E. L. (2010). A quantitative analysis of body mass index and colorectal cancer: Findings from 56 observational studies. Obesity Reviews, 11(1), 19–30. https://doi.org/10.1111/j.1467-789X.2009.00613.x

Noffsinger, A. E. (2009). Serrated polyps and colorectal cancer: New pathway to malignancy. Annual Review of Pathology, 4, 343–364. https://doi.org/10.1146/annurev.pathol.4.110807.092317

Pande, M., Lynch, P. M., Hopper, J. L., Jenkins, M. A., Gallinger, S., Haile, R. W., LeMarchand, L., Lindor, N. M., Campbell, P. T., Newcomb, P. A., Potter, J. D., Baron, J. A., Frazier, M. L., & Amos, C. I. (2010). Smoking and colorectal cancer in Lynch syndrome: Results from the Colon Cancer Family Registry and the University of Texas M.D. Anderson Cancer Center. Clinical Cancer Research: An Official Journal of the American Association for Cancer Research, 16(4), 1331–1339. https://doi.org/10.1158/1078-0432.CCR-09-1877

Petitprez, F., de Reyniès, A., Keung, E. Z., Chen, T. W.-W., Sun, C.-M., Calderaro, J., Jeng, Y.-M., Hsiao, L.-P., Lacroix, L., Bougoüin, A., Moreira, M., Lacroix, G., Natario, I., Adam, J., Lucchesi, C., Laizet, Y. H., Toulmonde, M., Burgess, M. A., Bolejack, V., … Fridman, W. H. (2020). B cells are associated with survival and immunotherapy response in sarcoma. Nature, 577(7791), 556–560. https://doi.org/10.1038/s41586-019-1906-8

Pfuderer, P. L., Ballhausen, A., Seidler, F., Stark, H.-J., Grabe, N., Frayling, I. M., Ager, A., von Knebel Doeberitz, M., Kloor, M., & Ahadova, A. (2019). High endothelial venules are associated with microsatellite instability, hereditary background and immune evasion in colorectal cancer. British Journal of Cancer, 121(5), 395–404. https://doi.org/10.1038/s41416-019-0514-6

Pietrocola, F., Galluzzi, L., Bravo-San Pedro, J. M., Madeo, F., & Kroemer, G. (2015). Acetyl coenzyme A: A central metabolite and second messenger. Cell Metabolism, 21(6), 805–821. https://doi.org/10.1016/j.cmet.2015.05.014

Plon, S. E., Eccles, D. M., Easton, D., Foulkes, W. D., Genuardi, M., Greenblatt, M. S., Hogervorst, F. B. L., Hoogerbrugge, N., Spurdle, A. B., & Tavtigian, S. (2008). Sequence variant classification and reporting: Recommendations for improving the interpretation of cancer susceptibility genetic test results. Human Mutation, 29(11), 1282–1291. https://doi.org/10.1002/humu.20880

Pöschl, G., Stickel, F., Wang, X. D., & Seitz, H. K. (2004). Alcohol and cancer: Genetic and nutritional aspects. Proceedings of the Nutrition Society, 63(1), 65–71. https://doi.org/10.1079/PNS2003323

Poulogiannis, G., Frayling, I. M., & Arends, M. J. (2010). DNA mismatch repair deficiency in sporadic colorectal cancer and Lynch syndrome. Histopathology, 56(2), 167–179. https://doi.org/10.1111/j.1365-2559.2009.03392.x

Poulogiannis, G., Ichimura, K., Hamoudi, R. A., Luo, F., Leung, S. Y., Yuen, S. T., Harrison, D. J., Wyllie, A. H., & Arends, M. J. (2010). Prognostic relevance of DNA copy number changes in colorectal cancer. The Journal of Pathology, 220(3), 338–347. https://doi.org/10.1002/path.2640

Prolla, T. A., Baker, S. M., Harris, A. C., Tsao, J. L., Yao, X., Bronner, C. E., Zheng, B., Gordon, M., Reneker, J., Arnheim, N., Shibata, D., Bradley, A., & Liskay, R. M. (1998). Tumour susceptibility and spontaneous mutation in mice deficient in Mlh1, Pms1 and Pms2 DNA mismatch repair. Nature Genetics, 18(3), 276–279. https://doi.org/10.1038/ng0398-276

Radu, O. M., Nikiforova, M. N., Farkas, L. M., & Krasinskas, A. M. (2011). Challenging cases encountered in colorectal cancer screening for Lynch syndrome reveal novel findings: Nucleolar MSH6 staining and impact of prior chemoradiation therapy. Human Pathology, 42(9), 1247–1258. https://doi.org/10.1016/j.humpath.2010.11.016

Rehm, H. L., Berg, J. S., Brooks, L. D., Bustamante, C. D., Evans, J. P., Landrum, M. J., Ledbetter, D. H., Maglott, D. R., Martin, C. L., Nussbaum, R. L., Plon, S. E., Ramos, E. M., Sherry, S. T., & Watson, M. S. (2015). ClinGen—The Clinical Genome Resource. The New England Journal of Medicine, 372(23), 2235–2242. https://doi.org/10.1056/NEJMsr1406261

Rehm, J., Room, R., Monteiro, M., Gmel, G., Graham, K., Rehn, N., Sempos, C. T., & Jernigan, D. (2003). Alcohol as a Risk Factor for Global Burden of Disease. European Addiction Research, 9(4), 157–164. https://doi.org/10.1159/000072222

Reitmair, A. H., Schmits, R., Ewel, A., Bapat, B., Redston, M., Mitri, A., Waterhouse, P., Mittrücker, H. W., Wakeham, A., & Liu, B. (1995). MSH2 deficient mice are viable and susceptible to lymphoid tumours. Nature Genetics, 11(1), 64–70. https://doi.org/10.1038/ng0995-64

Reizel, Y., Chapal-Ilani, N., Adar, R., Itzkovitz, S., Elbaz, J., Maruvka, Y. E., Segev, E., Shlush, L. I., Dekel, N., & Shapiro, E. (2011). Colon Stem Cell and Crypt Dynamics Exposed by Cell

Lineage Reconstruction. PLOS Genetics, 7(7), e1002192. https://doi.org/10.1371/journal.pgen.1002192

Reuschenbach, M., Kloor, M., Morak, M., Wentzensen, N., Germann, A., Garbe, Y., Tariverdian, M., Findeisen, P., Neumaier, M., Holinski-Feder, E., & Doeberitz, M. von K. (2010). Serum antibodies against frameshift peptides in microsatellite unstable colorectal cancer patients with Lynch syndrome. Familial Cancer, 9(2), 173–179. https://doi.org/10.1007/s10689-009-9307-z

Rijcken, F. E. M., Koornstra, J. J., van der Sluis, T., Boersma-van Ek, W., Kleibeuker, J. H., & Hollema, H. (2008). Early Carcinogenic Events in HNPCC Adenomas: Differences with Sporadic Adenomas. Digestive Diseases and Sciences, 53(6), 1660–1668. https://doi.org/10.1007/s10620-007-0041-9

Ryan, N. A. J., McMahon, R., Tobi, S., Snowsill, T., Esquibel, S., Wallace, A. J., Bunstone, S., Bowers, N., Mosneag, I. E., Kitson, S. J., O'Flynn, H., Ramchander, N. C., Sivalingam, V. N., Frayling, I. M., Bolton, J., McVey, R. J., Evans, D. G., & Crosbie, E. J. (2020). The proportion of endometrial tumours associated with Lynch syndrome (PETALS): A prospective cross-sectional study. PLOS Medicine, 17(9), e1003263. https://doi.org/10.1371/journal.pmed.1003263

Ryder, E., Doe, B., Gleeson, D., Houghton, R., Dalvi, P., Grau, E., Habib, B., Miklejewska, E., Newman, S., Sethi, D., Sinclair, C., Vyas, S., Wardle-Jones, H., Bussell, J., Galli, A., Salisbury, J., & Ramirez-Solis, R. (2014). Rapid conversion of EUCOMM/KOMP-CSD alleles in mouse embryos using a cell-permeable Cre recombinase. Transgenic Res, 9.

Sæterdal, I., Bjørheim, J., Lislerud, K., Gjertsen, M. K., Bukholm, I. K., Olsen, O. C., Nesland, J. M., Eriksen, J. A., Møller, M., Lindblom, A., & Gaudernack, G. (2001). Frameshift-mutation-derived peptides as tumor-specific antigens in inherited and spontaneous colorectal cancer. Proceedings of the National Academy of Sciences, 98(23), 13255–13260. https://doi.org/10.1073/pnas.231326898

Santamaría, E., Muñoz, J., Fernández-Irigoyen, J., Sesma, L., Mora, M. I., Berasain, C., Lu, S. C., Mato, J. M., Prieto, J., Avila, M. A., & Corrales, F. J. (2006). Molecular Profiling of Hepatocellular Carcinoma in Mice with a Chronic Deficiency of Hepatic S -Adenosylmethionine: Relevance in Human Liver Diseases. Journal of Proteome Research, 5(4), 944–953. https://doi.org/10.1021/pr050429v

Sarigiannis, D. A., Karakitsios, S. P., Gotti, A., Liakos, I. L., & Katsoyiannis, A. (2011). Exposure to major volatile organic compounds and carbonyls in European indoor environments and associated health risk. Environment International, 37(4), 743–765. https://doi.org/10.1016/j.envint.2011.01.005

Sautès-Fridman, C., Petitprez, F., Calderaro, J., & Fridman, W. H. (2019). Tertiary lymphoid structures in the era of cancer immunotherapy. Nature Reviews. Cancer, 19(6), 307–325. https://doi.org/10.1038/s41568-019-0144-6

Schatoff, E. M., Leach, B. I., & Dow, L. E. (2017). WNT Signaling and Colorectal Cancer. Current Colorectal Cancer Reports, 13(2), 101–110. https://doi.org/10.1007/s11888-017-0354-9

Schoen, R. E., Weissfeld, J. L., Kuller, L. H., Thaete, F. L., Evans, R. W., Hayes, R. B., & Rosen, C. J. (2005). Insulin-Like Growth Factor-I and Insulin Are Associated With the Presence and Advancement of Adenomatous Polyps. Gastroenterology, 129(2), 464–475. https://doi.org/10.1053/j.gastro.2005.05.051

Schulmann, K., Brasch, F. E., Kunstmann, E., Engel, C., Pagenstecher, C., Vogelsang, H., Krüger, S., Vogel, T., Knaebel, H.-P., Rüschoff, J., Hahn, S. A., Knebel-Doeberitz, M. V., Moeslein, G., Meltzer, S. J., Schackert, H. K., Tympner, C., Mangold, E., & Schmiegel, W. (2005). HNPCC-associated small bowel cancer: Clinical and molecular characteristics. Gastroenterology, 128(3), 590–599. https://doi.org/10.1053/j.gastro.2004.12.051

Schwitalle, Y., Linnebacher, M., Ripberger, E., Gebert, J., & Doeberitz, M. von K. (2004). Immunogenic peptides generated by frameshift mutations in DNA mismatch repair-deficient cancer cells. Cancer Immunity Archive, 4(1). https://cancerimmunolres.aacrjournals.org/content/canimmarch/4/1/14

Scott, R. E., Wille, J. J., & Wier, M. L. (1984). Mechanisms for the Initiation and Promotion of Carcinogenesis: A Review and a New Concept. Mayo Clinic Proceedings, 59(2), 107–117. https://doi.org/10.1016/S0025-6196(12)60244-4

Sears, C. L., & Pardoll, D. M. (2018). The intestinal microbiome influences checkpoint blockade. Nature Medicine, 24(3), 254–255. https://doi.org/10.1038/nm.4511

Seitz, H. K., & Stickel, F. (2007). Molecular mechanisms of alcohol-mediated carcinogenesis. Nature Reviews Cancer, 7(8), 599–612. https://doi.org/10.1038/nrc2191

Seitz, H. K., & Stickel, F. (2010). Acetaldehyde as an underestimated risk factor for cancer development: Role of genetics in ethanol metabolism. Genes & Nutrition, 5(2), 121–128. https://doi.org/10.1007/s12263-009-0154-1

Sekine, S., Ogawa, R., Saito, S., Ushiama, M., Shida, D., Nakajima, T., Taniguchi, H., Hiraoka, N., Yoshida, T., & Sugano, K. (2017). Cytoplasmic MSH2 immunoreactivity in a patient with Lynch syndrome with an EPCAM-MSH2 fusion. Histopathology, 70(4), 664–669. https://doi.org/10.1111/his.13104

Seppälä, T., Pylvänäinen, K., Evans, D. G., Järvinen, H., Renkonen-Sinisalo, L., Bernstein, I., Holinski-Feder, E., Sala, P., Lindblom, A., Macrae, F., Blanco, I., Sijmons, R., Jeffries, J., Vasen, H., Burn, J., Nakken, S., Hovig, E., Rødland, E. A., Tharmaratnam, K., … Mallorca Group. (2017). Colorectal cancer incidence in path_MLH1 carriers subjected to different follow-up protocols: A Prospective Lynch Syndrome Database report. Hereditary Cancer in Clinical Practice, 15, 18. https://doi.org/10.1186/s13053-017-0078-5

Seppälä, T. T., Ahadova, A., Dominguez-Valentin, M., Macrae, F., Evans, D. G., Therkildsen, C., Sampson, J., Scott, R., Burn, J., Möslein, G., Bernstein, I., Holinski-Feder, E., Pylvänäinen, K., Renkonen-Sinisalo, L., Lepistö, A., Lautrup, C. K., Lindblom, A., Plazzer, J.-P., Winship, I., … Møller, P. (2019). Lack of association between screening interval and cancer stage in Lynch syndrome may be accounted for by over-diagnosis; a prospective Lynch syndrome database report. Hereditary Cancer in Clinical Practice, 17(1), 8. https://doi.org/10.1186/s13053-019-0106-8

Seth, S., Ager, A., Arends, M. J., & Frayling, I. M. (2018). Lynch syndrome—Cancer pathways, heterogeneity and immune escape. The Journal of Pathology, 246(2), 129–133. https://doi.org/10.1002/path.5139

Shi, L., & Tu, B. P. (2015). Acetyl-CoA and the regulation of metabolism: Mechanisms and consequences. Current Opinion in Cell Biology, 33, 125–131. https://doi.org/10.1016/j.ceb.2015.02.003

Shia, J., Stadler, Z. K., Weiser, M. R., Vakiani, E., Mendelsohn, R., Markowitz, A. J., Shike, M., Boland, C. R., & Klimstra, D. S. (2015). Mismatch repair deficient-crypts in non-neoplastic colonic mucosa in Lynch syndrome: Insights from an illustrative case. Familial Cancer, 14(1), 61–68. https://doi.org/10.1007/s10689-014-9751-2

Shia, J., Zhang, L., Shike, M., Guo, M., Stadler, Z., Xiong, X., Tang, L. H., Vakiani, E., Katabi, N., Wang, H., Bacares, R., Ruggeri, J., Boland, C. R., Ladanyi, M., & Klimstra, D. S. (2013). Secondary mutation in a coding mononucleotide tract in MSH6 causes loss of immunoexpression of MSH6 in colorectal carcinomas with MLH1/PMS2 deficiency. Modern Pathology : An Official Journal of the United States and Canadian Academy of Pathology, Inc, 26(1), 131–138. https://doi.org/10.1038/modpathol.2012.138

Siddiqui, M. S. (2015). Persistent γH2AX: A promising molecular marker of DNA damage and aging. Mutation Research, 19.

Sie, A. S., Mensenkamp, A. R., Adang, E. M. M., Ligtenberg, M. J. L., & Hoogerbrugge, N. (2014). Fourfold increased detection of Lynch syndrome by raising age limit for tumour genetic testing from 50 to 70 years is cost-effective. Annals of Oncology: Official Journal of the European Society for Medical Oncology, 25(10), 2001–2007. https://doi.org/10.1093/annonc/mdu361

Simpkins, S. B., Bocker, T., Swisher, E. M., Mutch, D. G., Gersell, D. J., Kovatich, A. J., Palazzo, J. P., Fishel, R., & Goodfellow, P. J. (1999). MLH1 promoter methylation and gene silencing is the primary cause of microsatellite instability in sporadic endometrial cancers. Human Molecular Genetics, 8(4), 661–666. https://doi.org/10.1093/hmg/8.4.661

Sinicrope, F. A., & Sargent, D. J. (2009). Clinical implications of microsatellite instability in sporadic colon cancers. Current Opinion in Oncology, 21(4), 369–373. https://doi.org/10.1097/CCO.0b013e32832c94bd

Sipos, F., & Muezes, G. (2011). Isolated lymphoid follicles in colon: Switch points between inflammation and colorectal cancer? World Journal of Gastroenterology, 17(13), 1666–1673. https://doi.org/10.3748/wjg.v17.i13.1666

Skarnes, W. C., Rosen, B., West, A. P., Koutsourakis, M., Bushell, W., Iyer, V., Mujica, A. O., Thomas, M., Harrow, J., Cox, T., Jackson, D., Severin, J., Biggs, P., Fu, J., Nefedov, M., de Jong, P. J., Stewart, A. F., & Bradley, A. (2011). A conditional knockout resource for the genome-wide study of mouse gene function. Nature, 474(7351), 337–342. https://doi.org/10.1038/nature10163

Smith, M. J., Urquhart, J. E., Harkness, E. F., Miles, E. K., Bowers, N. L., Byers, H. J., Bulman, M., Gokhale, C., Wallace, A. J., Newman, W. G., & Evans, D. G. (2016). The Contribution of Whole Gene Deletions and Large Rearrangements to the Mutation Spectrum in Inherited Tumor Predisposing Syndromes: HUMAN MUTATION. Human Mutation, 37(3), 250–256. https://doi.org/10.1002/humu.22938

Smyrk, T. C., Watson, P., Kaul, K., & Lynch, H. T. (2001). Tumor-infiltrating lymphocytes are a marker for microsatellite instability in colorectal carcinoma.

Snippert, H. J., Schepers, A. G., van Es, J. H., Simons, B. D., & Clevers, H. (2014). Biased competition between Lgr5 intestinal stem cells driven by oncogenic mutation induces clonal expansion. EMBO Reports, 15(1), 62–69. https://doi.org/10.1002/embr.201337799

Snippert, H. J., van der Flier, L. G., Sato, T., van Es, J. H., van den Born, M., Kroon-Veenboer, C., Barker, N., Klein, A. M., van Rheenen, J., Simons, B. D., & Clevers, H. (2010). Intestinal crypt homeostasis results from neutral competition between symmetrically dividing Lgr5 stem cells. Cell, 143(1), 134–144. https://doi.org/10.1016/j.cell.2010.09.016

Snowsill, T., Coelho, H., Huxley, N., Jones-Hughes, T., Briscoe, S., Frayling, I. M., & Hyde, C. (2017). Molecular testing for Lynch syndrome in people with colorectal cancer: Systematic reviews and economic evaluation. Health Technology Assessment (Winchester, England), 21(51), 1–238. https://doi.org/10.3310/hta21510

Snowsill, T., Huxley, N., Hoyle, M., Jones-Hughes, T., Coelho, H., Cooper, C., Frayling, I., & Hyde, C. (2014). A systematic review and economic evaluation of diagnostic strategies for Lynch syndrome. Health Technology Assessment (Winchester, England), 18(58), 1–406. https://doi.org/10.3310/hta18580

South, C. D., Hampel, H., Comeras, I., Westman, J. A., Frankel, W. L., & de la Chapelle, A. (2008). The frequency of Muir-Torre syndrome among Lynch syndrome families. Journal of the National Cancer Institute, 100(4), 277–281. https://doi.org/10.1093/jnci/djm291

Staffa, L., Echterdiek, F., Nelius, N., Benner, A., Werft, W., Lahrmann, B., Grabe, N., Schneider, M., Tariverdian, M., von Knebel Doeberitz, M., Bläker, H., & Kloor, M. (2015). Mismatch repair-deficient crypt foci in Lynch syndrome—Molecular alterations and association with clinical parameters. PloS One, 10(3), e0121980. https://doi.org/10.1371/journal.pone.0121980

Stagos, D., Chen, Y., Brocker, C., Donald, E., Jackson, B. C., Orlicky, D. J., Thompson, D. C., & Vasiliou, V. (2010). Aldehyde Dehydrogenase 1B1: Molecular Cloning and Characterization of a Novel Mitochondrial Acetaldehyde-Metabolizing Enzyme. Drug Metabolism and Disposition, 38(10), 1679–1687. https://doi.org/10.1124/dmd.110.034678

Steinert, G., Schölch, S., Niemietz, T., Iwata, N., García, S. A., Behrens, B., Voigt, A., Kloor, M., Benner, A., Bork, U., Rahbari, N. N., Büchler, M. W., Stoecklein, N. H., Weitz, J., & Koch, M. (2014). Immune escape and survival mechanisms in circulating tumor cells of colorectal cancer. Cancer Research, 74(6), 1694–1704. https://doi.org/10.1158/0008-5472.CAN-13-1885

Steinmetz, C. G., Xie, P., Weiner, H., & Hurley, T. D. (1997). Structure of mitochondrial aldehyde dehydrogenase: The genetic component of ethanol aversion. Structure (London, England: 1993), 5(5), 701–711. https://doi.org/10.1016/s0969-2126(97)00224-4

Stojic, L., Mojas, N., Cejka, P., di Pietro, M., Ferrari, S., Marra, G., & Jiricny, J. (2004). Mismatch repair-dependent G2 checkpoint induced by low doses of SN1 type methylating agents requires the ATR kinase. Genes & Development, 18(11), 1331–1344. https://doi.org/10.1101/gad.294404

Stojic, Lovorka, Brun, R., & Jiricny, J. (2004). Mismatch repair and DNA damage signalling. DNA Repair, 3(8–9), 1091–1101. https://doi.org/10.1016/j.dnarep.2004.06.006

Stranford, S., & Ruddle, N. H. (2012). Follicular dendritic cells, conduits, lymphatic vessels, and high endothelial venules in tertiary lymphoid organs: Parallels with lymph node stroma. Frontiers in Immunology, 3, 350. https://doi.org/10.3389/fimmu.2012.00350

Talmon, G. A., Saigh, Q. M., DiMaio, D., Wisecarver, J. L., & Radio, S. J. (2010). Characterization of Epithelial Apoptosis in Biopsies of Small-Bowel Allografts Using Cleaved Caspase 3 Immunostaining. International Journal of Surgical Pathology, 6.

Taylor, A., Brady, A. F., Frayling, I. M., Hanson, H., Tischkowitz, M., Turnbull, C., Side, L., & UK Cancer Genetics Group (UK-CGG). (2018). Consensus for genes to be included on cancer panel tests offered by UK genetics services: Guidelines of the UK Cancer Genetics Group. Journal of Medical Genetics, 55(6), 372–377. https://doi.org/10.1136/jmedgenet-2017-105188

Taylor, C. F., Charlton, R. S., Burn, J., Sheridan, E., & Taylor, G. R. (2003). Genomic deletions in MSH2 or MLH1 are a frequent cause of hereditary non-polyposis colorectal cancer: Identification of novel and recurrent deletions by MLPA. Human Mutation, 22(6), 428–433. https://doi.org/10.1002/humu.10291

Ten Broeke, S. W., van Bavel, T. C., Jansen, A. M. L., Gómez-García, E., Hes, F. J., van Hest, L. P., Letteboer, T. G. W., Olderode-Berends, M. J. W., Ruano, D., Spruijt, L., Suerink, M., Tops, C. M., van Eijk, R., Morreau, H., van Wezel, T., & Nielsen, M. (2018). Molecular Background of Colorectal Tumors From Patients With Lynch Syndrome Associated With Germline Variants in PMS2. Gastroenterology, 155(3), 844–851. https://doi.org/10.1053/j.gastro.2018.05.020

Terasaki, H., Saitoh, T., Shiokawa, K., & Katoh, M. (2002). Frizzled-10, up-regulated in primary colorectal cancer, is a positive regulator of the WNT - beta-catenin—TCF signaling pathway. International Journal of Molecular Medicine, 9(2), 107–112.

Thiel, A., Heinonen, M., Kantonen, J., Gylling, A., Lahtinen, L., Korhonen, M., Kytölä, S., Mecklin, J.-P., Orpana, A., Peltomäki, P., & Ristimäki, A. (2013). BRAF mutation in sporadic colorectal cancer and Lynch syndrome. Virchows Archiv: An International Journal of Pathology, 463(5), 613–621. https://doi.org/10.1007/s00428-013-1470-9

Thomas, A., Tanaka, M., Trepel, J., Reinhold, W. C., Rajapakse, V. N., & Pommier, Y. (2017). Temozolomide in the Era of Precision Medicine. Cancer Research, 77(4), 823–826. https://doi.org/10.1158/0008-5472.CAN-16-2983

Thompson, B. A., Spurdle, A. B., Plazzer, J.-P., Greenblatt, M. S., Akagi, K., Al-Mulla, F., Bapat, B., Bernstein, I., Capellá, G., den Dunnen, J. T., du Sart, D., Fabre, A., Farrell, M. P., Farrington, S. M., Frayling, I. M., Frebourg, T., Goldgar, D. E., Heinen, C. D., Holinski-Feder, E., … Genuardi, M. (2014). Application of a five-tiered scheme for standardized classification of 2,360 unique mismatch repair gene variants lodged on the InSiGHT locus-specific database. Nature Genetics, 46(2), 107–115. https://doi.org/10.1038/ng.2854

Thompson, Martins, A., & Spurdle, A. B. (2015). A review of mismatch repair gene transcripts: Issues for interpretation of mRNA splicing assays. Clinical Genetics, 87(2), 100–108. https://doi.org/10.1111/cge.12450

Thrumurthy, S. G., Thrumurthy, S. S. D., Gilbert, C. E., Ross, P., & Haji, A. (2016). Colorectal adenocarcinoma: Risks, prevention and diagnosis. BMJ (Clinical Research Ed.), 354, i3590. https://doi.org/10.1136/bmj.i3590

Tikidzhieva, A., Benner, A., Michel, S., Formentini, A., Link, K.-H., Dippold, W., von Knebel Doeberitz, M., Kornmann, M., & Kloor, M. (2012). Microsatellite instability and Beta2-Microglobulin mutations as prognostic markers in colon cancer: Results of the FOGT-4 trial. British Journal of Cancer, 106(6), 1239–1245. https://doi.org/10.1038/bjc.2012.53

Toft, N. J., Winton, D. J., Kelly, J., Howard, L. A., Dekker, M., Riele, H. T., Arends, M. J., Wyllie, A. H., Margison, G. P., & Clarke, A. R. (1999). Msh2 status modulates both apoptosis and mutation frequency in the murine small intestine. Proc. Natl. Acad. Sci. USA, 5.

Tomé, S., Simard, J. P., Slean, M. M., Holt, I., Morris, G. E., Wojciechowicz, K., te Riele, H., & Pearson, C. E. (2013). Tissue-specific mismatch repair protein expression: MSH3 is higher than MSH6 in multiple mouse tissues. DNA Repair, 12(1), 46–52. https://doi.org/10.1016/j.dnarep.2012.10.006

Tomlinson, I., & Bodmer, W. (1999). Selection, the mutation rate and cancer: Ensuring that the tail does not wag the dog. Nature Medicine, 5(1), 11–12. https://doi.org/10.1038/4687

Tomlinson, I. P., Novelli, M. R., & Bodmer, W. F. (1996). The mutation rate and cancer. Proceedings of the National Academy of Sciences of the United States of America, 93(25), 14800–14803. https://doi.org/10.1073/pnas.93.25.14800

Treuting, P. M., Arends, M., & Dintzis, S. (2017a). Upper Gastrointestinal Tract. In Comparative Anatomy and Histology: A Mouse, Rat and Human Atlas. Elsevier Science.

Treuting, P. M., Arends, M., & Dintzis, S. M. (2017b). Lower Gastrointestinal Tract. In P. M. Treuting, S. M. Dintzis, & K. S. Montine (Eds.), Comparative Anatomy and Histology: A Mouse, Rat and Human Atlas (pp. 213–228). Elsevier Science.

Truta, B., Chen, Y.-Y., Blanco, A. M., Deng, G., Conrad, P. G., Kim, Y. H., Park, E. T., Kakar, S., Kim, Y. S., Velayos, F., Sleisenger, M. H., & Terdiman, J. P. (2008). Tumor histology helps

to identify Lynch syndrome among colorectal cancer patients. Familial Cancer, 7(3), 267–274. https://doi.org/10.1007/s10689-008-9186-8

van Duijnhoven, F. J. B., Botma, A., Winkels, R., Nagengast, F. M., Vasen, H. F. A., & Kampman, E. (2013). Do lifestyle factors influence colorectal cancer risk in Lynch syndrome? Familial Cancer, 12(2), 285–293. https://doi.org/10.1007/s10689-013-9645-8

van Kruijsdijk, R. C. M., van der Wall, E., & Visseren, F. L. J. (2009). Obesity and cancer: The role of dysfunctional adipose tissue. Cancer Epidemiology, Biomarkers & Prevention: A Publication of the American Association for Cancer Research, Cosponsored by the American Society of Preventive Oncology, 18(10), 2569–2578. https://doi.org/10.1158/1055-9965.EPI-09-0372

van Lier, M. G. F., Leenen, C. H. M., Wagner, A., Ramsoekh, D., Dubbink, H. J., van den Ouweland, A. M. W., Westenend, P. J., de Graaf, E. J. R., Wolters, L. M. M., Vrijland, W. W., Kuipers, E. J., van Leerdam, M. E., Steyerberg, E. W., Dinjens, W. N. M., & LIMO Study Group. (2012). Yield of routine molecular analyses in colorectal cancer patients ≤70 years to detect underlying Lynch syndrome. The Journal of Pathology, 226(5), 764–774. https://doi.org/10.1002/path.3963

Vasen, Blanco, I., Aktan-Collan, K., Gopie, J. P., Alonso, A., Aretz, S., Bernstein, I., Bertario, L., Burn, J., Capella, G., Colas, C., Engel, C., Frayling, I. M., Genuardi, M., Heinimann, K., Hes, F. J., Hodgson, S. V., Karagiannis, J. A., Lalloo, F., … Möslein, G. (2013). Revised guidelines for the clinical management of Lynch syndrome (HNPCC): Recommendations by a group of European experts. Gut, 62(6), 812–823. https://doi.org/10.1136/gutjnl-2012-304356

Vasen, Ghorbanoghli, Z., Bourdeaut, F., Cabaret, O., Caron, O., Duval, A., Entz-Werle, N., Goldberg, Y., Ilencikova, D., Kratz, C. P., Lavoine, N., Loeffen, J., Menko, F. H., Muleris, M., Sebille, G., Colas, C., Burkhardt, B., Brugieres, L., Wimmer, K., & on behalf of the EU-Consortium Care for CMMR-D (C4CMMR-D). (2014). Guidelines for surveillance of individuals with constitutional mismatch repair-deficiency proposed by the European Consortium “Care for CMMR-D” (C4CMMR-D). Journal of Medical Genetics, 51(5), 283–293. https://doi.org/10.1136/jmedgenet-2013-102238

Vasen, H. F., Nagengast, F. M., & Khan, P. M. (1995). Interval cancers in hereditary non-polyposis colorectal cancer (Lynch syndrome). Lancet (London, England), 345(8958), 1183–1184. https://doi.org/10.1016/s0140-6736(95)91016-6

Vasen, Möslein, G., Alonso, A., Aretz, S., Bernstein, I., Bertario, L., Blanco, I., Bülow, S., Burn, J., Capella, G., Colas, C., Engel, C., Frayling, I., Friedl, W., Hes, F. J., Hodgson, S., Järvinen, H., Mecklin, J.-P., Møller, P., … Wijnen, J. (2008). Guidelines for the clinical management of familial adenomatous polyposis (FAP). Gut, 57(5), 704–713. https://doi.org/10.1136/gut.2007.136127

Vasen, Möslein, G., Alonso, A., Aretz, S., Bernstein, I., Bertario, L., Blanco, I., Bulow, S., Burn, J., Capella, G., Colas, C., Engel, C., Frayling, I., Rahner, N., Hes, F. J., Hodgson, S., Mecklin, J.-P., Møller, P., Myrhøj, T., … Müller, H. (2010). Recommendations to improve identification of hereditary and familial colorectal cancer in Europe. Familial Cancer, 9(2), 109–115. https://doi.org/10.1007/s10689-009-9291-3

Vasiliou, V., Zakhari, S., Seitz, H. K., & Hoek, J. B. (2015). Biological Basis of Alcohol-Induced Cancer. Springer International Publishing. https://link.springer.com/book/10.1007/978-3-319-09614-8

Veniaminova, N. A., Hayes, M. M., Varney, J. M., & Merchant, J. L. (2012). Conditional deletion of menin results in antral G cell hyperplasia and hypergastrinemia. American Journal of Physiology-Gastrointestinal and Liver Physiology, 303(6), G752–G764. https://doi.org/10.1152/ajpgi.00109.2012

Vogelstein, B., Fearon, E. R., Hamilton, S. R., Kern, S. E., Preisinger, A. C., Leppert, M., Smits, A. M. M., & Bos, J. L. (2010, January 14). Genetic Alterations during Colorectal-Tumor Development (world) [Research-article]. Http://Dx.Doi.Org/10.1056/NEJM198809013190901; Massachusetts Medical Society. https://doi.org/10.1056/NEJM198809013190901

Wagner, A., van der Klift, H., Franken, P., Wijnen, J., Breukel, C., Bezrookove, V., Smits, R., Kinarsky, Y., Barrows, A., Franklin, B., Lynch, J., Lynch, H., & Fodde, R. (2002). A 10-Mb paracentric inversion of chromosome arm 2p inactivates MSH2 and is responsible for hereditary nonpolyposis colorectal cancer in a North-American kindred. Genes, Chromosomes & Cancer, 35(1), 49–57. https://doi.org/10.1002/gcc.10094

Wang, X.-D., Liu, C., Chung, J., Stickel, F., Seitz, H. K., & Russell, R. M. (1998). Chronic alcohol intake reduces retinoic acid concentration and enhances AP-1 (c-Jun and c-Fos) expression in rat liver. Hepatology, 28(3), 744–750. https://doi.org/10.1002/hep.510280321

Wedden, S., Miller, K., Frayling, I. M., Thomas, T., Chefani, A., Miller, K., Hamblin, A., Taylor, J. C., & D'Arrigo, C. (2019). Colorectal Cancer Stratification in the Routine Clinical Pathway: A District General Hospital Experience. Applied Immunohistochemistry & Molecular Morphology: AIMM, 27(6), e54–e62. https://doi.org/10.1097/PAI.0000000000000631

Weiss, A., & Attisano, L. (2013). The TGFbeta Superfamily Signaling Pathway. WIREs Developmental Biology, 2(1), 47–63. https://doi.org/10.1002/wdev.86

Williams, A. B., & Schumacher, B. (2016). P53 in the DNA-Damage-Repair Process. Cold Spring Harbor Perspectives in Medicine, 6(5). https://doi.org/10.1101/cshperspect.a026070

Win, A. K., Dowty, J. G., English, D. R., Campbell, P. T., Young, J. P., Winship, I., Macrae, F. A., Lipton, L., Parry, S., Young, G. P., Buchanan, D. D., Martínez, M. E., Jacobs, E. T., Ahnen, D. J., Haile, R. W., Casey, G., Baron, J. A., Lindor, N. M., Thibodeau, S. N., … Jenkins, M. A. (2011). Body mass index in early adulthood and colorectal cancer risk for carriers and non-carriers of germline mutations in DNA mismatch repair genes. British Journal of Cancer, 105(1), 162–169. https://doi.org/10.1038/bjc.2011.172

Woerner, S. M., Gebert, J., Yuan, Y. P., Sutter, C., Ridder, R., Bork, P., & von Knebel Doeberitz, M. (2001). Systematic identification of genes with coding microsatellites mutated in DNA mismatch repair-deficient cancer cells. International Journal of Cancer, 93(1), 12–19. https://doi.org/10.1002/ijc.1299

Wojciechowicz, K., Cantelli, E., Van Gerwen, B., Plug, M., Van Der Wal, A., Delzenne-Goette, E., Song, J.-Y., De Vries, S., Dekker, M., & Riele, H. T. (2014). Temozolomide Increases the Number of Mismatch Repair–Deficient Intestinal Crypts and Accelerates Tumorigenesis in a Mouse Model of Lynch Syndrome. Gastroenterology, 147(5), 1064-1072.e5. https://doi.org/10.1053/j.gastro.2014.07.052

World Health Organization (WHO). (2018). Global status report on alcohol and health 2018. https://www.who.int/publications-detail-redirect/9789241565639

Worrall, S., & Thiele, G. M. (2001). Protein modification in ethanol toxicity. Adverse Drug Reactions and Toxicological Reviews, 20(3), 133–159.

Xue, K., Li, F.-F., Chen, Y.-W., Zhou, Y.-H., & He, J. (2017). Body mass index and the risk of cancer in women compared with men: A meta-analysis of prospective cohort studies. European Journal of Cancer Prevention: The Official Journal of the European Cancer Prevention Organisation (ECP), 26(1), 94–105. https://doi.org/10.1097/CEJ.0000000000000231

Yamane, L., Scapulatempo-Neto, C., Reis, R. M., & Guimarães, D. P. (2014). Serrated pathway in colorectal carcinogenesis. World Journal of Gastroenterology, 20(10), 2634–2640. https://doi.org/10.3748/wjg.v20.i10.2634

Yokoyama, A., Muramatsu, T., Ohmori, T., Yokoyama, T., Okuyama, K., Takahashi, H., Hasegawa, Y., Higuchi, S., Maruyama, K., Shirakura, K., & Ishii, H. (1998). Alcohol-related cancers and aldehyde dehydrogenase-2 in Japanese alcoholics. Carcinogenesis, 19(8), 1383–1387. https://doi.org/10.1093/carcin/19.8.1383

Yoshioka, K., Yoshioka, Y., & Hsieh, P. (2006). ATR kinase activation mediated by MutSalpha and MutLalpha in response to cytotoxic O6-methylguanine adducts. Molecular Cell, 22(4), 501–510. https://doi.org/10.1016/j.molcel.2006.04.023

Yu, H.-S., Oyama, T., Isse, T., Kitakawa, K., Ogawa, M., Pham, T.-T.-P., & Kawamoto, T. (2009). Characteristics of aldehyde dehydrogenase 2 (Aldh2) knockout mice. Toxicology Mechanisms and Methods, 19(9), 535–540. https://doi.org/10.3109/15376510903401708

Zhang, H., Richards, B., Wilson, T., Lloyd, M., Cranston, A., Thorburn, A., Fishel, R., & Meuth, M. (1999). Apoptosis Induced by Overexpression of hMSH2 or hMLH1. Cancer Research, 59(13), 3021–3027.

Zhang, J., Stevens, M. F. G., & Bradshaw, T. D. (2012). Temozolomide: Mechanisms of Action, Repair and Resistance.

Zhang, N., Yantiss, Rhonda K., Nam, Hyung-song, Chin, Y., Zhou, X. K., Scherl, E. J., Bosworth, B. P., Subbaramaiah, K., Dannenberg, A. J., & Benezra, R. (2014). ID1 Is a Functional Marker for Intestinal Stem and Progenitor Cells Required for Normal Response to Injury. Stem Cell Reports.

Zhu, X.-D., & Sadowski, P. D. (1995). Cleavage-dependent Ligation by the FLP Recombinase: Characterization of a mutant flp protein with an alteration in a catalytic amino acid.

Journal of Biological Chemistry, 270(39), 23044–23054. https://doi.org/10.1074/jbc.270.39.23044

Zuo, B., Du, X., Zhao, J., Yang, H., Wang, C., Wu, Y., Lu, J., Wang, Y., & Chen, Z. (2012). Analysis of Microsatellite Polymorphism in Inbred Knockout Mice. PLoS ONE, 7(4), e34555. https://doi.org/10.1371/journal.pone.0034555

Appendix 1

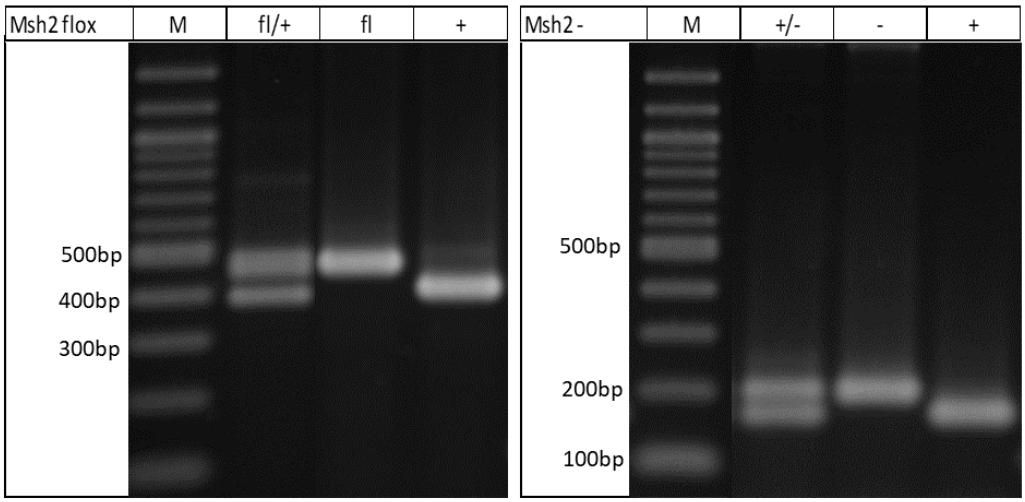

Supplementary Figure 2.1: The left panel shows an electrophoretic gel photograph with representative results for the PCR genotyping assay DNA products for *Msh2*^{wt} *Msh2*- and *Msh2*^{flox} alleles (genotypes shown above the lanes). In this assay, the Msh2^{flox} (Msh2 flox) allele produces a 460bp band (upper single band indicating fl genotype), whereas the *Msh2* wild-type (wt or +) allele produces a 389bp band (lower single band indicating + genotype), whereas the heterozygous state is shown by the presence of both bands (two bands of 460bp and 389bp indicating fl/+ genotype). The right panel shows representative results for the PCR genotyping assay DNA products for the *Msh*^{wt} (+) and *Msh2*$^{-}$ alleles (Msh2- or -). In this assay, the *Msh2*$^{-}$ allele produces a 194bp band (upper single band indicating - genotype) and wt allele produces a 164bp band (lower single band indicating + genotype), whereas the heterozygous state is shown by the presence of both bands (194bp and 164bp indicating +/- genotype) (M=DNA ladder, bp= base pair).

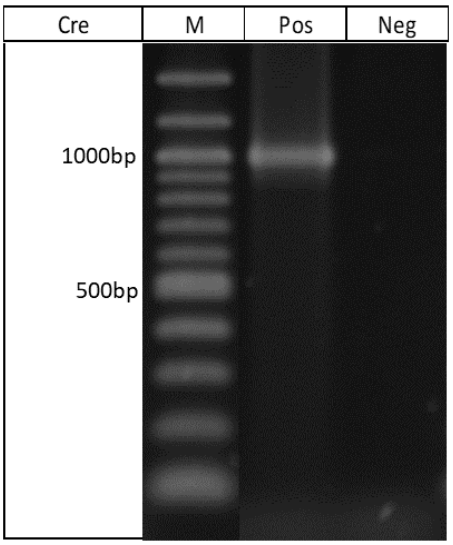

Supplementary Figure 2.2: The electrophoretic gel photograph shows representative results for the PCR genotyping assay for presence of the *Cre* allele. Presence of the Cre allele is shown by a 1000bp band ("Pos", which can be either $Cre^{+/-}$ or $Cre^{+/+}$), whereas the absence of a band indicates that Cre is not present ("Neg" or $Cre^{-/-}$) (M=DNA ladder, bp= base pair).

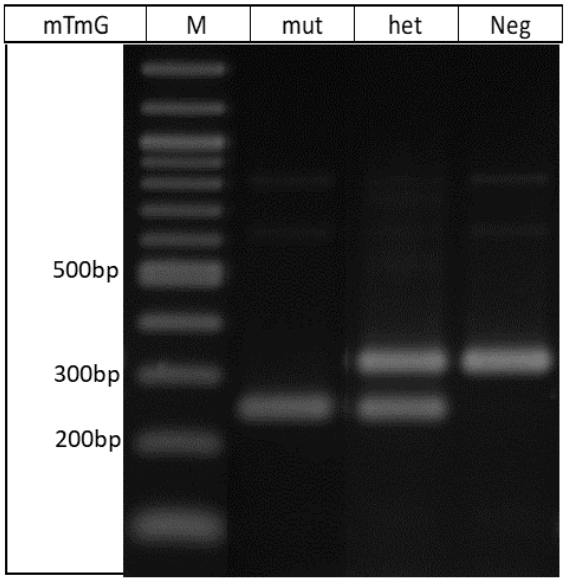

Supplementary Figure 2.3: The electrophoretic gel photograph shows representative results for the PCR genotyping assay for presence of the *mTmG* allele. The *mTmG* allele produces a 250bp band ("mut", $mTmG^{+/+}$), whereas the absence of this allele produces a 330bp band ("Neg", $mTmG^{-/-}$), and the heterozygous state is shown by the presence of both bands ("het", $mTmG^{+/-}$) (M=DNA ladder, bp= base pair).

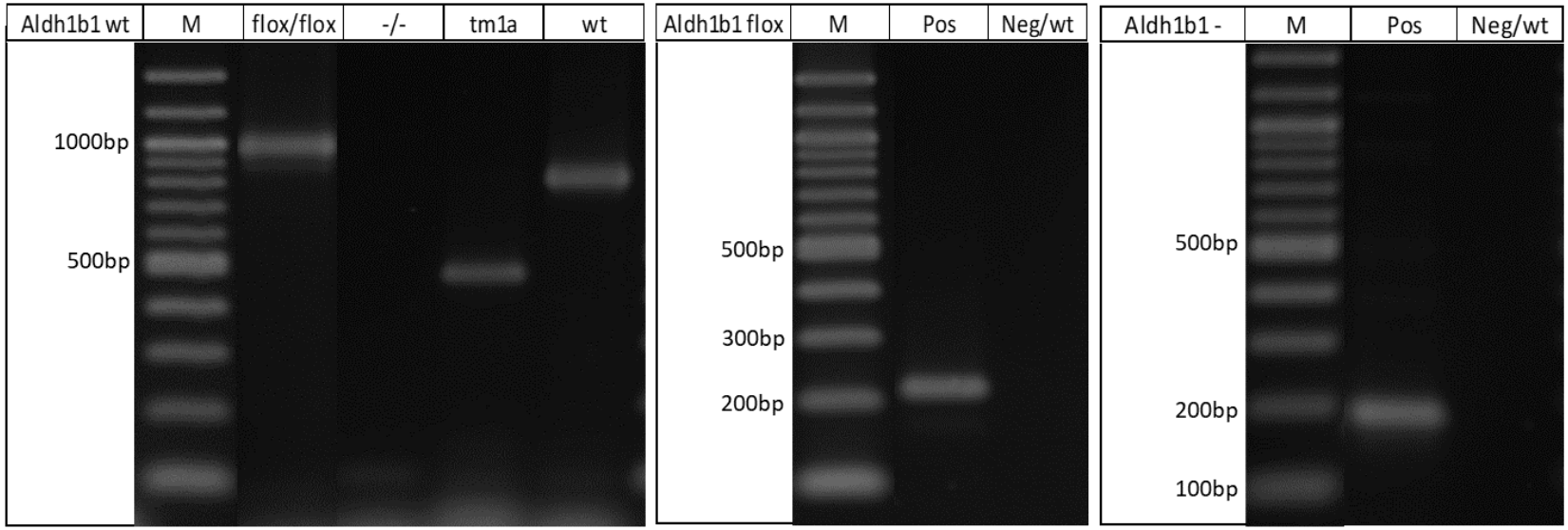

Supplementary Figure 2.4: The 3 electrophoretic gel photographs show representative results for the 3 separate PCR genotyping assays for Aldh1b1wt, Aldh1b1flox and Aldh1b1-alleles. In the first panel (left), the Aldh1b1tm1a allele produces a 445bp band ("tm1a" or "KnockOut Ready" or "KOR", single band indicating tm1a/tm1a genotype), the Aldh1b1flox allele produces a 1000bp band ("flox", single band indicating "flox/flox" genotype), the Aldh1b1- allele is shown by the absence of a band (absent band indicating -/- genotype), and the wild-type Aldh1b1wt allele produces a 775bp band ("wt", single band indicating a Aldh1b1wt/wt genotype). In the second panel (centre), the Aldh1b1flox allele produces a 218bp band ("Pos", single band indicating "flox/flox" genotype) and the Aldh1b1 wild-type allele is shown by the absence of a band ("Neg/wt"). In the third panel (right), the Aldh1b1- allele produces a 177bp band ("Pos", single band indicating a Aldh1b1-/- genotype) and the Aldh1b1 wild-type allele is shown by the absence of a band ("Neg/wt") (M=DNA ladder, bp= base pair).

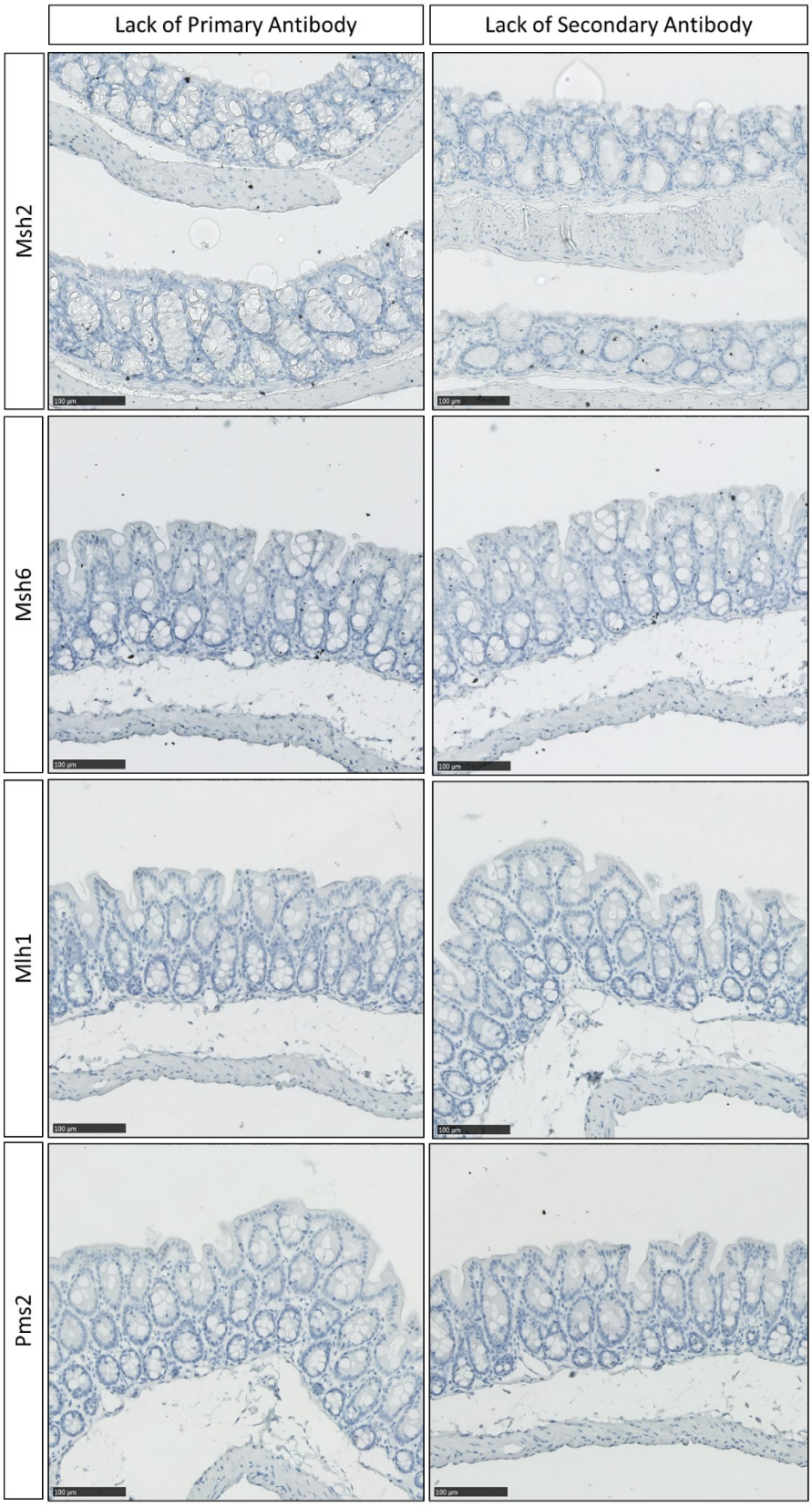
Lack of Primary Antibody
Lack of Secondary Antibody
Msh2
Msh6
Mlh1
Pms2
100 µm

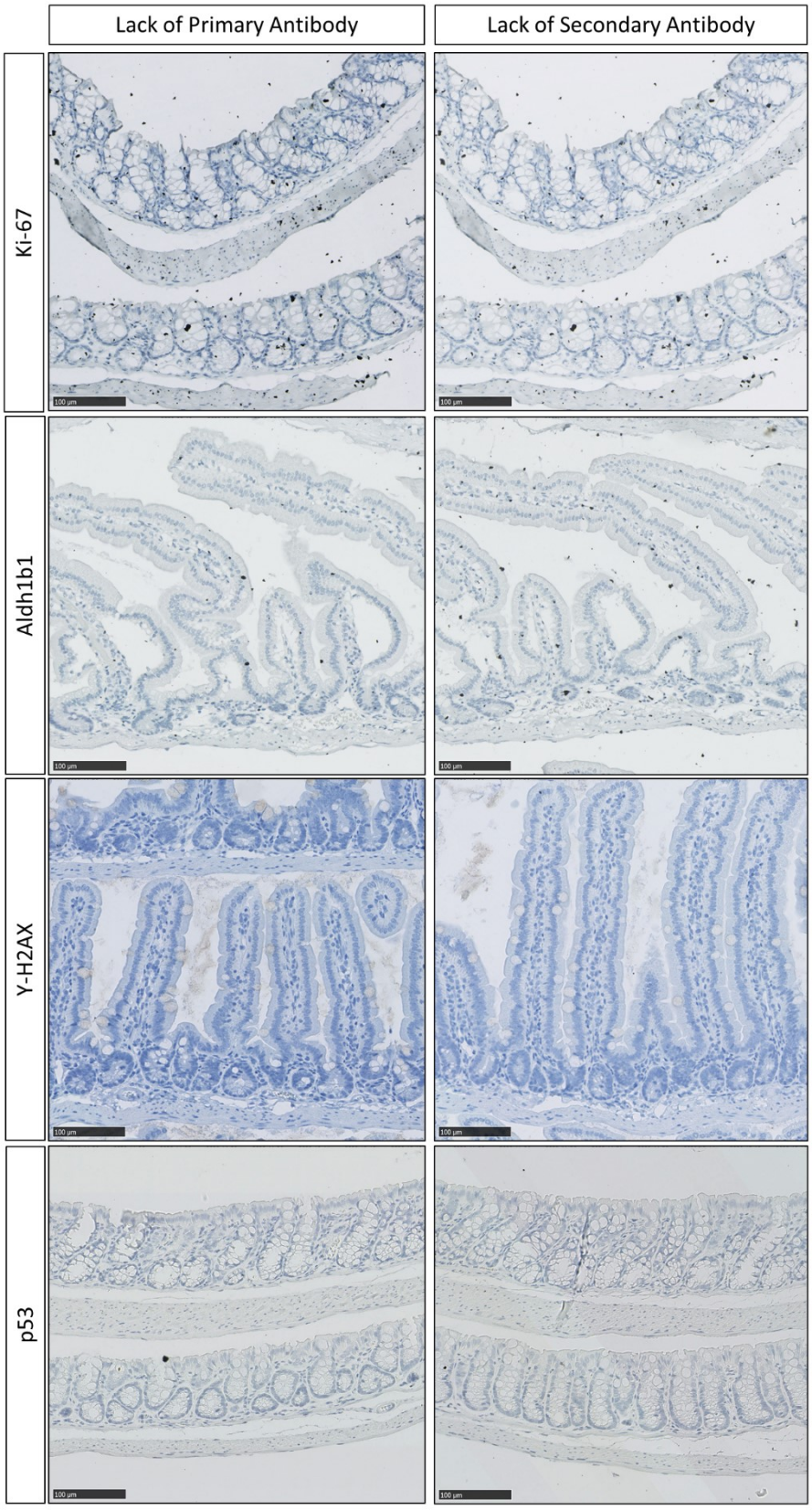
Lack of Primary Antibody
Lack of Secondary Antibody
Ki-67
Aldh1b1
Y-H2AX
p53
100 µm

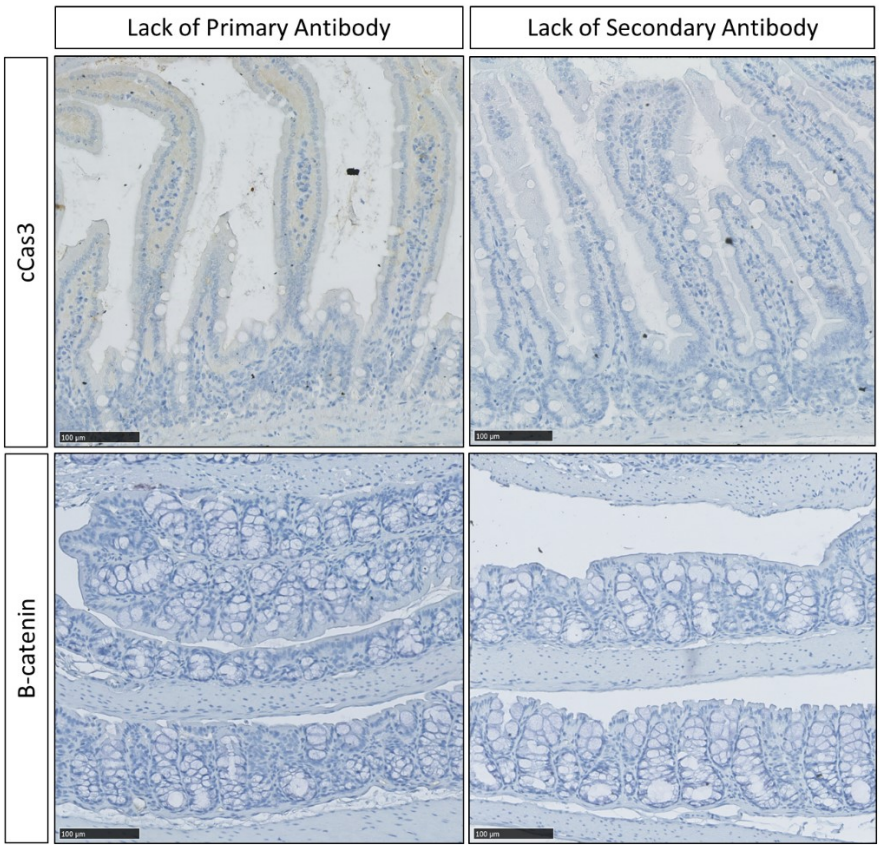

Supplementary Figure 2.5: Photomicrographs illustrating the immunohistochemistry antibody technical controls performed with the absence of the primary (or the secondary) antibody against Msh2, Msh6, Mlh1, Pms2, Ki-67, Aldh1b1, y-H2AX, p53, cCas3 (cleaved Caspase-3) and B-catenin proteins. IHC performed with antibody diluent and no primary antibody (left column) and/or secondary antibody (right column) using either normal small intestine or normal colon murine tissue. Images taken from IHC stained sections scanned using the Hamamatsu Nanozoomer and analysed with the Hamamatsu NDP Viewer software at 20X magnification, showing no evidence of positivity for the target proteins (bar at lower left indicates 100µm).

A	Msh2+ Lgr5Cre+	Msh2+ Lgr5Cre-	Msh2- Lgr5Cre-	Msh2- Lgr5Cre+
Msh2flox Lgr5Cre-	Msh2fl/+ Lgr5Cre+/-	Msh2fl/+ Lgr5Cre-/-	Msh2fl/- Lgr5Cre-/-	Msh2fl/- Lgr5Cre+/-
Msh2flox Lgr5Cre-	Msh2fl/+ Lgr5Cre+/-	Msh2fl/+ Lgr5Cre-/-	Msh2fl/- Lgr5Cre-/-	Msh2fl/- Lgr5Cre+/-
Msh2flox Lgr5Cre-	Msh2fl/+ Lgr5Cre+/-	Msh2fl/+ Lgr5Cre-/-	Msh2fl/- Lgr5Cre-/-	Msh2fl/- Lgr5Cre+/-
Msh2flox Lgr5Cre-	Msh2fl/+ Lgr5Cre+/-	Msh2fl/+ Lgr5Cre-/-	Msh2fl/- Lgr5Cre-/-	Msh2fl/- Lgr5Cre+/-

B	Msh2flox Lgr5Cre-	Msh2- Lgr5Cre-	Msh2flox Lgr5Cre-	Msh2- Lgr5Cre-
Msh2flox Lgr5Cre+	Msh2fl/fl Lgr5Cre+/-	Msh2fl/- Lgr5Cre+/-	Msh2fl/fl Lgr5Cre+/-	Msh2fl/- Lgr5Cre+/-
Msh2- Lgr5Cre-	Msh2fl/- Lgr5Cre-/-	Msh2-/- Lgr5Cre-/-	Msh2fl/- Lgr5Cre-/-	Msh2-/- Lgr5Cre-/-
Msh2flox Lgr5Cre-	Msh2fl/fl Lgr5Cre-/-	Msh2fl/- Lgr5Cre-/-	Msh2fl/fl Lgr5Cre-/-	Msh2fl/- Lgr5Cre-/-
Msh2- Lgr5Cre+	Msh2fl/- Lgr5Cre+/-	Msh2-/- Lgr5Cre+/-	Msh2fl/- Lgr5Cre+/-	Msh2-/- Lgr5Cre+/-

Supplementary Table 3.1: Tabular representation of the inter-cross to generate the Msh2-LS mouse model experimental subjects. A) Inter-cross between *Msh2* $^{flox/flox}$ and the *Msh2*$^{+/-}$*; Lgr5CreERT2* $^{+/-}$ mice. B) Inter-cross between *Msh2*$^{flox/-}$*; Lgr5CreERT2*$^{+/-}$ and *Msh2*$^{flox/-}$*; Lgr5CreERT2*$^{-/-}$ mice.

A	Msh2+ Lgr5Cre- mTmG +	Msh2+ Lgr5Cre- mTmG +	Msh2+ Lgr5Cre- mTmG +	Msh2+ Lgr5Cre- mTmG +	Msh2+ Lgr5Cre- mTmG +	Msh2+ Lgr5Cre- mTmG +	Msh2+ Lgr5Cre- mTmG +	Msh2+ Lgr5Cre- mTmG +
Msh2flox Lgr5Cre+ mTmG-	Msh2 fl/+ Lgr5Cre+/- mTmG +/-	Msh2 fl/+ Lgr5Cre+/- mTmG +/-	Msh2 fl/+ Lgr5Cre+/- mTmG +/-	Msh2 fl/+ Lgr5Cre+/- mTmG +/-	Msh2 fl/+ Lgr5Cre+/- mTmG +/-	Msh2 fl/+ Lgr5Cre+/- mTmG +/-	Msh2 fl/+ Lgr5Cre+/- mTmG +/-	Msh2 fl/+ Lgr5Cre+/- mTmG +/-
Msh2flox Lgr5Cre+ mTmG-	Msh2 fl/+ Lgr5Cre+/- mTmG +/-	Msh2 fl/+ Lgr5Cre+/- mTmG +/-	Msh2 fl/+ Lgr5Cre+/- mTmG +/-	Msh2 fl/+ Lgr5Cre+/- mTmG +/-	Msh2 fl/+ Lgr5Cre+/- mTmG +/-	Msh2 fl/+ Lgr5Cre+/- mTmG +/-	Msh2 fl/+ Lgr5Cre+/- mTmG +/-	Msh2 fl/+ Lgr5Cre+/- mTmG +/-
Msh2flox Lgr5Cre- mTmG-	Msh2 fl/+ Lgr5Cre-/- mTmG +/-	Msh2 fl/+ Lgr5Cre-/- mTmG +/-	Msh2 fl/+ Lgr5Cre-/- mTmG +/-	Msh2 fl/+ Lgr5Cre-/- mTmG +/-	Msh2 fl/+ Lgr5Cre-/- mTmG +/-	Msh2 fl/+ Lgr5Cre-/- mTmG +/-	Msh2 fl/+ Lgr5Cre-/- mTmG +/-	Msh2 fl/+ Lgr5Cre-/- mTmG +/-
Msh2flox Lgr5Cre- mTmG-	Msh2 fl/+ Lgr5Cre-/- mTmG +/-	Msh2 fl/+ Lgr5Cre-/- mTmG +/-	Msh2 fl/+ Lgr5Cre-/- mTmG +/-	Msh2 fl/+ Lgr5Cre-/- mTmG +/-	Msh2 fl/+ Lgr5Cre-/- mTmG +/-	Msh2 fl/+ Lgr5Cre-/- mTmG +/-	Msh2 fl/+ Lgr5Cre-/- mTmG +/-	Msh2 fl/+ Lgr5Cre-/- mTmG +/-
Msh2- Lgr5Cre+ mTmG -	Msh2 -/+ Lgr5Cre+/- mTmG +/-	Msh2 -/+ Lgr5Cre+/- mTmG +/-	Msh2 -/+ Lgr5Cre+/- mTmG +/-	Msh2 -/+ Lgr5Cre+/- mTmG +/-	Msh2 -/+ Lgr5Cre+/- mTmG +/-	Msh2 -/+ Lgr5Cre+/- mTmG +/-	Msh2 -/+ Lgr5Cre+/- mTmG +/-	Msh2 -/+ Lgr5Cre+/- mTmG +/-
Msh2- Lgr5Cre+ mTmG -	Msh2 -/+ Lgr5Cre+/- mTmG +/-	Msh2 -/+ Lgr5Cre+/- mTmG +/-	Msh2 -/+ Lgr5Cre+/- mTmG +/-	Msh2 -/+ Lgr5Cre+/- mTmG +/-	Msh2 -/+ Lgr5Cre+/- mTmG +/-	Msh2 -/+ Lgr5Cre+/- mTmG +/-	Msh2 -/+ Lgr5Cre+/- mTmG +/-	Msh2 -/+ Lgr5Cre+/- mTmG +/-
Msh2- Lgr5Cre- mTmG -	Msh2 -/+ Lgr5Cre-/- mTmG +/-	Msh2 -/+ Lgr5Cre-/- mTmG +/-	Msh2 -/+ Lgr5Cre-/- mTmG +/-	Msh2 -/+ Lgr5Cre-/- mTmG +/-	Msh2 -/+ Lgr5Cre-/- mTmG +/-	Msh2 -/+ Lgr5Cre-/- mTmG +/-	Msh2 -/+ Lgr5Cre-/- mTmG +/-	Msh2 -/+ Lgr5Cre-/- mTmG +/-
Msh2- Lgr5Cre- mTmG -	Msh2 -/+ Lgr5Cre-/- mTmG +/-	Msh2 -/+ Lgr5Cre-/- mTmG +/-	Msh2 -/+ Lgr5Cre-/- mTmG +/-	Msh2 -/+ Lgr5Cre-/- mTmG +/-	Msh2 -/+ Lgr5Cre-/- mTmG +/-	Msh2 -/+ Lgr5Cre-/- mTmG +/-	Msh2 -/+ Lgr5Cre-/- mTmG +/-	Msh2 -/+ Lgr5Cre-/- mTmG +/-

B	Msh2- Lgr5Cre+ mTmG +	Msh2- Lgr5Cre+ mTmG -	Msh2- Lgr5Cre- mTmG +	Msh2- Lgr5Cre- mTmG -	Msh2+ Lgr5Cre+ mTmG +	Msh2+ Lgr5Cre+ mTmG -	Msh2+ Lgr5Cre- mTmG +	Msh2+ Lgr5Cre- mTmG -
Msh2flox Lgr5Cre- mTmG-	Msh2fl/- Lgr5Cre+/- mTmG+/-	Msh2fl/- Lgr5Cre+/- mTmG-/-	Msh2fl/- Lgr5Cre-/- mTmG+/-	Msh2fl/- Lgr5Cre-/- mTmG-/-	Msh2fl/+ Lgr5Cre+/- mTmG+/-	Msh2fl/+ Lgr5Cre+/- mTmG-/-	Msh2fl/+ Lgr5Cre-/- mTmG+/-	Msh2fl/+ Lgr5Cre-/- mTmG-/-
Msh2flox Lgr5Cre- mTmG+	Msh2fl/- Lgr5Cre+/- mTmG+/+	Msh2fl/- Lgr5Cre+/- mTmG+/-	Msh2fl/- Lgr5Cre-/- mTmG+/+	Msh2fl/- Lgr5Cre-/- mTmG+/-	Msh2fl/+ Lgr5Cre+/- mTmG+/+	Msh2fl/+ Lgr5Cre+/- mTmG+/-	Msh2fl/+ Lgr5Cre-/- mTmG+/+	Msh2fl/+ Lgr5Cre-/- mTmG+/-
Msh2flox Lgr5Cre- mTmG-	Msh2fl/- Lgr5Cre+/- mTmG+/-	Msh2fl/- Lgr5Cre+/- mTmG-/-	Msh2fl/- Lgr5Cre-/- mTmG+/-	Msh2fl/- Lgr5Cre-/- mTmG-/-	Msh2fl/+ Lgr5Cre+/- mTmG+/-	Msh2fl/+ Lgr5Cre+/- mTmG-/-	Msh2fl/+ Lgr5Cre-/- mTmG+/-	Msh2fl/+ Lgr5Cre-/- mTmG-/-
Msh2flox Lgr5Cre- mTmG+	Msh2fl/- Lgr5Cre+/- mTmG+/+	Msh2fl/- Lgr5Cre+/- mTmG+/-	Msh2fl/- Lgr5Cre-/- mTmG+/+	Msh2fl/- Lgr5Cre-/- mTmG+/-	Msh2fl/+ Lgr5Cre+/- mTmG+/+	Msh2fl/+ Lgr5Cre+/- mTmG+/-	Msh2fl/+ Lgr5Cre-/- mTmG+/+	Msh2fl/+ Lgr5Cre-/- mTmG+/-
Msh2+ Lgr5Cre+ mTmG -	Msh2+/- Lgr5Cre+/- mTmG+/-	Msh2+/- Lgr5Cre+/- mTmG-/-	Msh2+/- Lgr5Cre-/- mTmG+/-	Msh2+/- Lgr5Cre-/- mTmG-/-	Msh2+/+ Lgr5Cre+/- mTmG+/-	Msh2+/+ Lgr5Cre+/- mTmG-/-	Msh2+/+ Lgr5Cre-/- mTmG+/-	Msh2+/+ Lgr5Cre-/- mTmG-/-
Msh2+ Lgr5Cre- mTmG+	Msh2+/- Lgr5Cre+/- mTmG+/+	Msh2+/- Lgr5Cre+/- mTmG+/-	Msh2+/- Lgr5Cre-/- mTmG+/+	Msh2+/- Lgr5Cre-/- mTmG+/-	Msh2+/+ Lgr5Cre+/- mTmG+/+	Msh2+/+ Lgr5Cre+/- mTmG+/-	Msh2+/+ Lgr5Cre-/- mTmG+/+	Msh2+/+ Lgr5Cre-/- mTmG+/-
Msh2+ Lgr5Cre- mTmG -	Msh2+/- Lgr5Cre+/- mTmG+/-	Msh2+/- Lgr5Cre+/- mTmG-/-	Msh2+/- Lgr5Cre-/- mTmG+/-	Msh2+/- Lgr5Cre-/- mTmG-/-	Msh2+/+ Lgr5Cre+/- mTmG+/-	Msh2+/+ Lgr5Cre+/- mTmG-/-	Msh2+/+ Lgr5Cre-/- mTmG+/-	Msh2+/+ Lgr5Cre-/- mTmG-/-
Msh2+ Lgr5Cre- mTmG +	Msh2+/- Lgr5Cre+/- mTmG+/+	Msh2+/- Lgr5Cre+/- mTmG+/-	Msh2+/- Lgr5Cre-/- mTmG+/+	Msh2+/- Lgr5Cre-/- mTmG+/-	Msh2+/+ Lgr5Cre+/- mTmG+/+	Msh2+/+ Lgr5Cre+/- mTmG+/-	Msh2+/+ Lgr5Cre-/- mTmG+/+	Msh2+/+ Lgr5Cre-/- mTmG+/-

Supplementary Table 3.2: Tabular representation of the inter-cross to introduce the *mTmG* transgene into the Msh2-LS mouse model. A) Cross-breeding between *Msh2$^{flox/-}$; Lgr5CreERT2$^{+/-}$* and *mTmG$^{+/+}$* mice. B) Cross-breeding between *Msh2$^{+/-}$; Lgr5CreERT2$^{+/-}$; mTmG$^{+/-}$* and *Msh2$^{flox/+}$; Lgr5CreERT2$^{+/-}$; mTmG$^{+/-}$* mice.

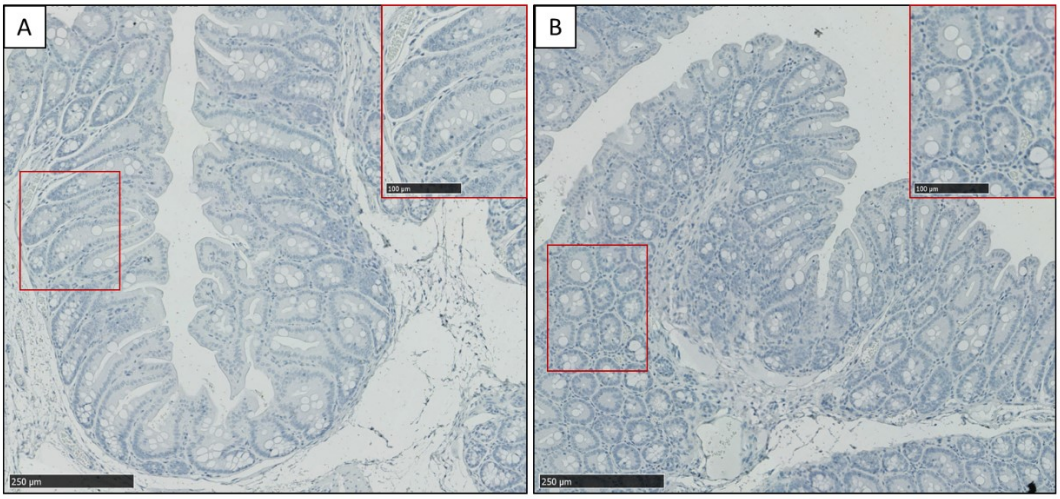

Supplementary Figure 4.1: Immunohistochemical analysis of Pms2 protein expression in caecal mucosal epithelium of Msh2-LS mice treated with either 20% ethanol in drinking water (A) or normal / standard water (B). Images taken from Pms2 IHC stained sections scanned using the Hamamatsu Nanozoomer and analysed with the Hamamatsu NDP Viewer software at 10X and 20X magnification, showing no evidence of nuclear positivity for Pms2 protein (bar at lower left indicates 250µm, bar in red rectangle indicates 100µm).

	Msh2+ Lgr5Cre- mTmG- Aldh1b1flox	Msh2+ Lgr5Cre- mTmG- Aldh1b1flox	Msh2+ Lgr5Cre- mTmG- Aldh1b1flox	Msh2+ Lgr5Cre- mTmG- Aldh1b1flox	Msh2+ Lgr5Cre- mTmG- Aldh1b1flox	Msh2+ Lgr5Cre- mTmG- Aldh1b1flox	Msh2+ Lgr5Cre- mTmG- Aldh1b1flox	Msh2+ Lgr5Cre- mTmG- Aldh1b1flox	Msh2+ Lgr5Cre- mTmG- Aldh1b1flox	Msh2+ Lgr5Cre- mTmG- Aldh1b1flox	Msh2+ Lgr5Cre- mTmG- Aldh1b1flox	Msh2+ Lgr5Cre- mTmG- Aldh1b1flox	Msh2+ Lgr5Cre- mTmG- Aldh1b1flox	Msh2+ Lgr5Cre- mTmG- Aldh1b1flox	Msh2+ Lgr5Cre- mTmG- Aldh1b1flox	Msh2+ Lgr5Cre- mTmG- Aldh1b1flox
Msh2flox Lgr5Cre+ mTmG+ Aldh1b1+	Msh2 fl/+ Lgr5Cre+/- mTmG +/- Aldh1b1fl/+	Msh2 fl/+ Lgr5Cre+/- mTmG +/- Aldh1b1fl/+	Msh2 fl/+ Lgr5Cre+/- mTmG +/- Aldh1b1fl/+	Msh2 fl/+ Lgr5Cre+/- mTmG +/- Aldh1b1fl/+	Msh2 fl/+ Lgr5Cre+/- mTmG +/- Aldh1b1fl/+	Msh2 fl/+ Lgr5Cre+/- mTmG +/- Aldh1b1fl/+	Msh2 fl/+ Lgr5Cre+/- mTmG +/- Aldh1b1fl/+	Msh2 fl/+ Lgr5Cre+/- mTmG +/- Aldh1b1fl/+	Msh2 fl/+ Lgr5Cre+/- mTmG +/- Aldh1b1fl/+	Msh2 fl/+ Lgr5Cre+/- mTmG +/- Aldh1b1fl/+	Msh2 fl/+ Lgr5Cre+/- mTmG +/- Aldh1b1fl/+	Msh2 fl/+ Lgr5Cre+/- mTmG +/- Aldh1b1fl/+	Msh2 fl/+ Lgr5Cre+/- mTmG +/- Aldh1b1fl/+	Msh2 fl/+ Lgr5Cre+/- mTmG +/- Aldh1b1fl/+	Msh2 fl/+ Lgr5Cre+/- mTmG +/- Aldh1b1fl/+	Msh2 fl/+ Lgr5Cre+/- mTmG +/- Aldh1b1fl/+
Msh2flox Lgr5Cre+ mTmG+ Aldh1b1+	Msh2 fl/+ Lgr5Cre+/- mTmG +/- Aldh1b1fl/+	Msh2 fl/+ Lgr5Cre+/- mTmG +/- Aldh1b1fl/+	Msh2 fl/+ Lgr5Cre+/- mTmG +/- Aldh1b1fl/+	Msh2 fl/+ Lgr5Cre+/- mTmG +/- Aldh1b1fl/+	Msh2 fl/+ Lgr5Cre+/- mTmG +/- Aldh1b1fl/+	Msh2 fl/+ Lgr5Cre+/- mTmG +/- Aldh1b1fl/+	Msh2 fl/+ Lgr5Cre+/- mTmG +/- Aldh1b1fl/+	Msh2 fl/+ Lgr5Cre+/- mTmG +/- Aldh1b1fl/+	Msh2 fl/+ Lgr5Cre+/- mTmG +/- Aldh1b1fl/+	Msh2 fl/+ Lgr5Cre+/- mTmG +/- Aldh1b1fl/+	Msh2 fl/+ Lgr5Cre+/- mTmG +/- Aldh1b1fl/+	Msh2 fl/+ Lgr5Cre+/- mTmG +/- Aldh1b1fl/+	Msh2 fl/+ Lgr5Cre+/- mTmG +/- Aldh1b1fl/+	Msh2 fl/+ Lgr5Cre+/- mTmG +/- Aldh1b1fl/+	Msh2 fl/+ Lgr5Cre+/- mTmG +/- Aldh1b1fl/+	Msh2 fl/+ Lgr5Cre+/- mTmG +/- Aldh1b1fl/+
Msh2flox Lgr5Cre+ mTmG+ Aldh1b1+	Msh2 fl/+ Lgr5Cre+/- mTmG +/- Aldh1b1fl/+	Msh2 fl/+ Lgr5Cre+/- mTmG +/- Aldh1b1fl/+	Msh2 fl/+ Lgr5Cre+/- mTmG +/- Aldh1b1fl/+	Msh2 fl/+ Lgr5Cre+/- mTmG +/- Aldh1b1fl/+	Msh2 fl/+ Lgr5Cre+/- mTmG +/- Aldh1b1fl/+	Msh2 fl/+ Lgr5Cre+/- mTmG +/- Aldh1b1fl/+	Msh2 fl/+ Lgr5Cre+/- mTmG +/- Aldh1b1fl/+	Msh2 fl/+ Lgr5Cre+/- mTmG +/- Aldh1b1fl/+	Msh2 fl/+ Lgr5Cre+/- mTmG +/- Aldh1b1fl/+	Msh2 fl/+ Lgr5Cre+/- mTmG +/- Aldh1b1fl/+	Msh2 fl/+ Lgr5Cre+/- mTmG +/- Aldh1b1fl/+	Msh2 fl/+ Lgr5Cre+/- mTmG +/- Aldh1b1fl/+	Msh2 fl/+ Lgr5Cre+/- mTmG +/- Aldh1b1fl/+	Msh2 fl/+ Lgr5Cre+/- mTmG +/- Aldh1b1fl/+	Msh2 fl/+ Lgr5Cre+/- mTmG +/- Aldh1b1fl/+	Msh2 fl/+ Lgr5Cre+/- mTmG +/- Aldh1b1fl/+
Msh2flox Lgr5Cre+ mTmG+ Aldh1b1+	Msh2 fl/+ Lgr5Cre+/- mTmG +/- Aldh1b1fl/+	Msh2 fl/+ Lgr5Cre+/- mTmG +/- Aldh1b1fl/+	Msh2 fl/+ Lgr5Cre+/- mTmG +/- Aldh1b1fl/+	Msh2 fl/+ Lgr5Cre+/- mTmG +/- Aldh1b1fl/+	Msh2 fl/+ Lgr5Cre+/- mTmG +/- Aldh1b1fl/+	Msh2 fl/+ Lgr5Cre+/- mTmG +/- Aldh1b1fl/+	Msh2 fl/+ Lgr5Cre+/- mTmG +/- Aldh1b1fl/+	Msh2 fl/+ Lgr5Cre+/- mTmG +/- Aldh1b1fl/+	Msh2 fl/+ Lgr5Cre+/- mTmG +/- Aldh1b1fl/+	Msh2 fl/+ Lgr5Cre+/- mTmG +/- Aldh1b1fl/+	Msh2 fl/+ Lgr5Cre+/- mTmG +/- Aldh1b1fl/+	Msh2 fl/+ Lgr5Cre+/- mTmG +/- Aldh1b1fl/+	Msh2 fl/+ Lgr5Cre+/- mTmG +/- Aldh1b1fl/+	Msh2 fl/+ Lgr5Cre+/- mTmG +/- Aldh1b1fl/+	Msh2 fl/+ Lgr5Cre+/- mTmG +/- Aldh1b1fl/+	Msh2 fl/+ Lgr5Cre+/- mTmG +/- Aldh1b1fl/+
Msh2flox Lgr5Cre- mTmG+ Aldh1b1+	Msh2fl/+ Lgr5Cre-/- mTmG +/- Aldh1b1fl/+	Msh2fl/+ Lgr5Cre-/- mTmG +/- Aldh1b1fl/+	Msh2fl/+ Lgr5Cre-/- mTmG +/- Aldh1b1fl/+	Msh2fl/+ Lgr5Cre-/- mTmG +/- Aldh1b1fl/+	Msh2fl/+ Lgr5Cre-/- mTmG +/- Aldh1b1fl/+	Msh2fl/+ Lgr5Cre-/- mTmG +/- Aldh1b1fl/+	Msh2fl/+ Lgr5Cre-/- mTmG +/- Aldh1b1fl/+	Msh2fl/+ Lgr5Cre-/- mTmG +/- Aldh1b1fl/+	Msh2fl/+ Lgr5Cre-/- mTmG +/- Aldh1b1fl/+	Msh2fl/+ Lgr5Cre-/- mTmG +/- Aldh1b1fl/+	Msh2fl/+ Lgr5Cre-/- mTmG +/- Aldh1b1fl/+	Msh2fl/+ Lgr5Cre-/- mTmG +/- Aldh1b1fl/+	Msh2fl/+ Lgr5Cre-/- mTmG +/- Aldh1b1fl/+	Msh2fl/+ Lgr5Cre-/- mTmG +/- Aldh1b1fl/+	Msh2fl/+ Lgr5Cre-/- mTmG +/- Aldh1b1fl/+	Msh2fl/+ Lgr5Cre-/- mTmG +/- Aldh1b1fl/+
Msh2flox Lgr5Cre- mTmG+ Aldh1b1+	Msh2fl/+ Lgr5Cre-/- mTmG +/- Aldh1b1fl/+	Msh2fl/+ Lgr5Cre-/- mTmG +/- Aldh1b1fl/+	Msh2fl/+ Lgr5Cre-/- mTmG +/- Aldh1b1fl/+	Msh2fl/+ Lgr5Cre-/- mTmG +/- Aldh1b1fl/+	Msh2fl/+ Lgr5Cre-/- mTmG +/- Aldh1b1fl/+	Msh2fl/+ Lgr5Cre-/- mTmG +/- Aldh1b1fl/+	Msh2fl/+ Lgr5Cre-/- mTmG +/- Aldh1b1fl/+	Msh2fl/+ Lgr5Cre-/- mTmG +/- Aldh1b1fl/+	Msh2fl/+ Lgr5Cre-/- mTmG +/- Aldh1b1fl/+	Msh2fl/+ Lgr5Cre-/- mTmG +/- Aldh1b1fl/+	Msh2fl/+ Lgr5Cre-/- mTmG +/- Aldh1b1fl/+	Msh2fl/+ Lgr5Cre-/- mTmG +/- Aldh1b1fl/+	Msh2fl/+ Lgr5Cre-/- mTmG +/- Aldh1b1fl/+	Msh2fl/+ Lgr5Cre-/- mTmG +/- Aldh1b1fl/+	Msh2fl/+ Lgr5Cre-/- mTmG +/- Aldh1b1fl/+	Msh2fl/+ Lgr5Cre-/- mTmG +/- Aldh1b1fl/+
Msh2flox Lgr5Cre- mTmG+ Aldh1b1+	Msh2fl/+ Lgr5Cre-/- mTmG +/- Aldh1b1fl/+	Msh2fl/+ Lgr5Cre-/- mTmG +/- Aldh1b1fl/+	Msh2fl/+ Lgr5Cre-/- mTmG +/- Aldh1b1fl/+	Msh2fl/+ Lgr5Cre-/- mTmG +/- Aldh1b1fl/+	Msh2fl/+ Lgr5Cre-/- mTmG +/- Aldh1b1fl/+	Msh2fl/+ Lgr5Cre-/- mTmG +/- Aldh1b1fl/+	Msh2fl/+ Lgr5Cre-/- mTmG +/- Aldh1b1fl/+	Msh2fl/+ Lgr5Cre-/- mTmG +/- Aldh1b1fl/+	Msh2fl/+ Lgr5Cre-/- mTmG +/- Aldh1b1fl/+	Msh2fl/+ Lgr5Cre-/- mTmG +/- Aldh1b1fl/+	Msh2fl/+ Lgr5Cre-/- mTmG +/- Aldh1b1fl/+	Msh2fl/+ Lgr5Cre-/- mTmG +/- Aldh1b1fl/+	Msh2fl/+ Lgr5Cre-/- mTmG +/- Aldh1b1fl/+	Msh2fl/+ Lgr5Cre-/- mTmG +/- Aldh1b1fl/+	Msh2fl/+ Lgr5Cre-/- mTmG +/- Aldh1b1fl/+	Msh2fl/+ Lgr5Cre-/- mTmG +/- Aldh1b1fl/+
Msh2flox Lgr5Cre- mTmG+ Aldh1b1+	Msh2fl/+ Lgr5Cre-/- mTmG +/- Aldh1b1fl/+	Msh2fl/+ Lgr5Cre-/- mTmG +/- Aldh1b1fl/+	Msh2fl/+ Lgr5Cre-/- mTmG +/- Aldh1b1fl/+	Msh2fl/+ Lgr5Cre-/- mTmG +/- Aldh1b1fl/+	Msh2fl/+ Lgr5Cre-/- mTmG +/- Aldh1b1fl/+	Msh2fl/+ Lgr5Cre-/- mTmG +/- Aldh1b1fl/+	Msh2fl/+ Lgr5Cre-/- mTmG +/- Aldh1b1fl/+	Msh2fl/+ Lgr5Cre-/- mTmG +/- Aldh1b1fl/+	Msh2fl/+ Lgr5Cre-/- mTmG +/- Aldh1b1fl/+	Msh2fl/+ Lgr5Cre-/- mTmG +/- Aldh1b1fl/+	Msh2fl/+ Lgr5Cre-/- mTmG +/- Aldh1b1fl/+	Msh2fl/+ Lgr5Cre-/- mTmG +/- Aldh1b1fl/+	Msh2fl/+ Lgr5Cre-/- mTmG +/- Aldh1b1fl/+	Msh2fl/+ Lgr5Cre-/- mTmG +/- Aldh1b1fl/+	Msh2fl/+ Lgr5Cre-/- mTmG +/- Aldh1b1fl/+	Msh2fl/+ Lgr5Cre-/- mTmG +/- Aldh1b1fl/+
Msh2- Lgr5Cre+ mTmG+ Aldh1b1+	Msh2+/- Lgr5Cre+/- mTmG +/- Aldh1b1fl/+	Msh2+/- Lgr5Cre+/- mTmG +/- Aldh1b1fl/+	Msh2+/- Lgr5Cre+/- mTmG +/- Aldh1b1fl/+	Msh2+/- Lgr5Cre+/- mTmG +/- Aldh1b1fl/+	Msh2+/- Lgr5Cre+/- mTmG +/- Aldh1b1fl/+	Msh2+/- Lgr5Cre+/- mTmG +/- Aldh1b1fl/+	Msh2+/- Lgr5Cre+/- mTmG +/- Aldh1b1fl/+	Msh2+/- Lgr5Cre+/- mTmG +/- Aldh1b1fl/+	Msh2+/- Lgr5Cre+/- mTmG +/- Aldh1b1fl/+	Msh2+/- Lgr5Cre+/- mTmG +/- Aldh1b1fl/+	Msh2+/- Lgr5Cre+/- mTmG +/- Aldh1b1fl/+	Msh2+/- Lgr5Cre+/- mTmG +/- Aldh1b1fl/+	Msh2+/- Lgr5Cre+/- mTmG +/- Aldh1b1fl/+	Msh2+/- Lgr5Cre+/- mTmG +/- Aldh1b1fl/+	Msh2+/- Lgr5Cre+/- mTmG +/- Aldh1b1fl/+	Msh2+/- Lgr5Cre+/- mTmG +/- Aldh1b1fl/+
Msh2- Lgr5Cre+ mTmG+ Aldh1b1+	Msh2+/- Lgr5Cre+/- mTmG +/- Aldh1b1fl/+	Msh2+/- Lgr5Cre+/- mTmG +/- Aldh1b1fl/+	Msh2+/- Lgr5Cre+/- mTmG +/- Aldh1b1fl/+	Msh2+/- Lgr5Cre+/- mTmG +/- Aldh1b1fl/+	Msh2+/- Lgr5Cre+/- mTmG +/- Aldh1b1fl/+	Msh2+/- Lgr5Cre+/- mTmG +/- Aldh1b1fl/+	Msh2+/- Lgr5Cre+/- mTmG +/- Aldh1b1fl/+	Msh2+/- Lgr5Cre+/- mTmG +/- Aldh1b1fl/+	Msh2+/- Lgr5Cre+/- mTmG +/- Aldh1b1fl/+	Msh2+/- Lgr5Cre+/- mTmG +/- Aldh1b1fl/+	Msh2+/- Lgr5Cre+/- mTmG +/- Aldh1b1fl/+	Msh2+/- Lgr5Cre+/- mTmG +/- Aldh1b1fl/+	Msh2+/- Lgr5Cre+/- mTmG +/- Aldh1b1fl/+	Msh2+/- Lgr5Cre+/- mTmG +/- Aldh1b1fl/+	Msh2+/- Lgr5Cre+/- mTmG +/- Aldh1b1fl/+	Msh2+/- Lgr5Cre+/- mTmG +/- Aldh1b1fl/+
Msh2- Lgr5Cre+ mTmG+ Aldh1b1+	Msh2+/- Lgr5Cre+/- mTmG +/- Aldh1b1fl/+	Msh2+/- Lgr5Cre+/- mTmG +/- Aldh1b1fl/+	Msh2+/- Lgr5Cre+/- mTmG +/- Aldh1b1fl/+	Msh2+/- Lgr5Cre+/- mTmG +/- Aldh1b1fl/+	Msh2+/- Lgr5Cre+/- mTmG +/- Aldh1b1fl/+	Msh2+/- Lgr5Cre+/- mTmG +/- Aldh1b1fl/+	Msh2+/- Lgr5Cre+/- mTmG +/- Aldh1b1fl/+	Msh2+/- Lgr5Cre+/- mTmG +/- Aldh1b1fl/+	Msh2+/- Lgr5Cre+/- mTmG +/- Aldh1b1fl/+	Msh2+/- Lgr5Cre+/- mTmG +/- Aldh1b1fl/+	Msh2+/- Lgr5Cre+/- mTmG +/- Aldh1b1fl/+	Msh2+/- Lgr5Cre+/- mTmG +/- Aldh1b1fl/+	Msh2+/- Lgr5Cre+/- mTmG +/- Aldh1b1fl/+	Msh2+/- Lgr5Cre+/- mTmG +/- Aldh1b1fl/+	Msh2+/- Lgr5Cre+/- mTmG +/- Aldh1b1fl/+	Msh2+/- Lgr5Cre+/- mTmG +/- Aldh1b1fl/+

Msh2- Lgr5Cre+ mTmG+ Aldh1b1+	Msh2+/- Lgr5Cre+/- mTmG +/- Aldh1b1fl/+	Msh2+/- Lgr5Cre+/- mTmG +/- Aldh1b1fl/+	Msh2+/- Lgr5Cre+/- mTmG +/- Aldh1b1fl/+	Msh2+/- Lgr5Cre+/- mTmG +/- Aldh1b1fl/+	Msh2+/- Lgr5Cre+/- mTmG +/- Aldh1b1fl/+	Msh2+/- Lgr5Cre+/- mTmG +/- Aldh1b1fl/+	Msh2+/- Lgr5Cre+/- mTmG +/- Aldh1b1fl/+	Msh2+/- Lgr5Cre+/- mTmG +/- Aldh1b1fl/+	Msh2+/- Lgr5Cre+/- mTmG +/- Aldh1b1fl/+	Msh2+/- Lgr5Cre+/- mTmG +/- Aldh1b1fl/+	Msh2+/- Lgr5Cre+/- mTmG +/- Aldh1b1fl/+	Msh2+/- Lgr5Cre+/- mTmG +/- Aldh1b1fl/+	Msh2+/- Lgr5Cre+/- mTmG +/- Aldh1b1fl/+	Msh2+/- Lgr5Cre+/- mTmG +/- Aldh1b1fl/+	Msh2+/- Lgr5Cre+/- mTmG +/- Aldh1b1fl/+	Msh2+/- Lgr5Cre+/- mTmG +/- Aldh1b1fl/+
Msh2- Lgr5Cre- mTmG+ Aldh1b1+	Msh2+/- Lgr5Cre-/- mTmG +/- Aldh1b1fl/+	Msh2+/- Lgr5Cre-/- mTmG +/- Aldh1b1fl/+	Msh2+/- Lgr5Cre-/- mTmG +/- Aldh1b1fl/+	Msh2+/- Lgr5Cre-/- mTmG +/- Aldh1b1fl/+	Msh2+/- Lgr5Cre-/- mTmG +/- Aldh1b1fl/+	Msh2+/- Lgr5Cre-/- mTmG +/- Aldh1b1fl/+	Msh2+/- Lgr5Cre-/- mTmG +/- Aldh1b1fl/+	Msh2+/- Lgr5Cre-/- mTmG +/- Aldh1b1fl/+	Msh2+/- Lgr5Cre-/- mTmG +/- Aldh1b1fl/+	Msh2+/- Lgr5Cre-/- mTmG +/- Aldh1b1fl/+	Msh2+/- Lgr5Cre-/- mTmG +/- Aldh1b1fl/+	Msh2+/- Lgr5Cre-/- mTmG +/- Aldh1b1fl/+	Msh2+/- Lgr5Cre-/- mTmG +/- Aldh1b1fl/+	Msh2+/- Lgr5Cre-/- mTmG +/- Aldh1b1fl/+	Msh2+/- Lgr5Cre-/- mTmG +/- Aldh1b1fl/+	Msh2+/- Lgr5Cre-/- mTmG +/- Aldh1b1fl/+
Msh2- Lgr5Cre- mTmG+ Aldh1b1+	Msh2+/- Lgr5Cre-/- mTmG +/- Aldh1b1fl/+	Msh2+/- Lgr5Cre-/- mTmG +/- Aldh1b1fl/+	Msh2+/- Lgr5Cre-/- mTmG +/- Aldh1b1fl/+	Msh2+/- Lgr5Cre-/- mTmG +/- Aldh1b1fl/+	Msh2+/- Lgr5Cre-/- mTmG +/- Aldh1b1fl/+	Msh2+/- Lgr5Cre-/- mTmG +/- Aldh1b1fl/+	Msh2+/- Lgr5Cre-/- mTmG +/- Aldh1b1fl/+	Msh2+/- Lgr5Cre-/- mTmG +/- Aldh1b1fl/+	Msh2+/- Lgr5Cre-/- mTmG +/- Aldh1b1fl/+	Msh2+/- Lgr5Cre-/- mTmG +/- Aldh1b1fl/+	Msh2+/- Lgr5Cre-/- mTmG +/- Aldh1b1fl/+	Msh2+/- Lgr5Cre-/- mTmG +/- Aldh1b1fl/+	Msh2+/- Lgr5Cre-/- mTmG +/- Aldh1b1fl/+	Msh2+/- Lgr5Cre-/- mTmG +/- Aldh1b1fl/+	Msh2+/- Lgr5Cre-/- mTmG +/- Aldh1b1fl/+	Msh2+/- Lgr5Cre-/- mTmG +/- Aldh1b1fl/+
Msh2- Lgr5Cre- mTmG+ Aldh1b1+	Msh2+/- Lgr5Cre-/- mTmG +/- Aldh1b1fl/+	Msh2+/- Lgr5Cre-/- mTmG +/- Aldh1b1fl/+	Msh2+/- Lgr5Cre-/- mTmG +/- Aldh1b1fl/+	Msh2+/- Lgr5Cre-/- mTmG +/- Aldh1b1fl/+	Msh2+/- Lgr5Cre-/- mTmG +/- Aldh1b1fl/+	Msh2+/- Lgr5Cre-/- mTmG +/- Aldh1b1fl/+	Msh2+/- Lgr5Cre-/- mTmG +/- Aldh1b1fl/+	Msh2+/- Lgr5Cre-/- mTmG +/- Aldh1b1fl/+	Msh2+/- Lgr5Cre-/- mTmG +/- Aldh1b1fl/+	Msh2+/- Lgr5Cre-/- mTmG +/- Aldh1b1fl/+	Msh2+/- Lgr5Cre-/- mTmG +/- Aldh1b1fl/+	Msh2+/- Lgr5Cre-/- mTmG +/- Aldh1b1fl/+	Msh2+/- Lgr5Cre-/- mTmG +/- Aldh1b1fl/+	Msh2+/- Lgr5Cre-/- mTmG +/- Aldh1b1fl/+	Msh2+/- Lgr5Cre-/- mTmG +/- Aldh1b1fl/+	Msh2+/- Lgr5Cre-/- mTmG +/- Aldh1b1fl/+
Msh2- Lgr5Cre- mTmG+ Aldh1b1+	Msh2+/- Lgr5Cre-/- mTmG +/- Aldh1b1fl/+	Msh2+/- Lgr5Cre-/- mTmG +/- Aldh1b1fl/+	Msh2+/- Lgr5Cre-/- mTmG +/- Aldh1b1fl/+	Msh2+/- Lgr5Cre-/- mTmG +/- Aldh1b1fl/+	Msh2+/- Lgr5Cre-/- mTmG +/- Aldh1b1fl/+	Msh2+/- Lgr5Cre-/- mTmG +/- Aldh1b1fl/+	Msh2+/- Lgr5Cre-/- mTmG +/- Aldh1b1fl/+	Msh2+/- Lgr5Cre-/- mTmG +/- Aldh1b1fl/+	Msh2+/- Lgr5Cre-/- mTmG +/- Aldh1b1fl/+	Msh2+/- Lgr5Cre-/- mTmG +/- Aldh1b1fl/+	Msh2+/- Lgr5Cre-/- mTmG +/- Aldh1b1fl/+	Msh2+/- Lgr5Cre-/- mTmG +/- Aldh1b1fl/+	Msh2+/- Lgr5Cre-/- mTmG +/- Aldh1b1fl/+	Msh2+/- Lgr5Cre-/- mTmG +/- Aldh1b1fl/+	Msh2+/- Lgr5Cre-/- mTmG +/- Aldh1b1fl/+	Msh2+/- Lgr5Cre-/- mTmG +/- Aldh1b1fl/+

Supplementary Table 6.1: Tabular representation of the generation of the *Aldh1b1* conditional-knockout Msh2-LS mouse model experimental subjects. Representation of the breeding between the *Msh2*$^{+/+}$*; Lgr5CreERT2*$^{-/-}$*; mTmG*$^{-/-}$*; Aldh1b1*$^{flox/flox}$ *with Msh2*$^{flox/-}$*; Lgr5CreERT2*$^{+/-}$*; mTmG*$^{+/+}$*; Aldh1b1*$^{+/+}$ mice.

	Msh2+ Lgr5Cre- mTmG- Aldh1b1flox	Msh2+ Lgr5Cre- mTmG- Aldh1b1flox	Msh2+ Lgr5Cre- mTmG- Aldh1b1flox	Msh2+ Lgr5Cre- mTmG- Aldh1b1flox	Msh2+ Lgr5Cre- mTmG- Aldh1b1flox	Msh2+ Lgr5Cre- mTmG- Aldh1b1flox	Msh2+ Lgr5Cre- mTmG- Aldh1b1flox	Msh2+ Lgr5Cre- mTmG- Aldh1b1flox	Msh2+ Lgr5Cre- mTmG- Aldh1b1flox	Msh2+ Lgr5Cre- mTmG- Aldh1b1flox	Msh2+ Lgr5Cre- mTmG- Aldh1b1flox	Msh2+ Lgr5Cre- mTmG- Aldh1b1flox	Msh2+ Lgr5Cre- mTmG- Aldh1b1flox	Msh2+ Lgr5Cre- mTmG- Aldh1b1flox	Msh2+ Lgr5Cre- mTmG- Aldh1b1flox	Msh2+ Lgr5Cre- mTmG- Aldh1b1flox
Msh2flox Lgr5Cre+ mTmG+ Aldh1b1+	Msh2 fl/+ Lgr5Cre+/- mTmG +/- Aldh1b1fl/+	Msh2 fl/+ Lgr5Cre+/- mTmG +/- Aldh1b1fl/+	Msh2 fl/+ Lgr5Cre+/- mTmG +/- Aldh1b1fl/+	Msh2 fl/+ Lgr5Cre+/- mTmG +/- Aldh1b1fl/+	Msh2 fl/+ Lgr5Cre+/- mTmG +/- Aldh1b1fl/+	Msh2 fl/+ Lgr5Cre+/- mTmG +/- Aldh1b1fl/+	Msh2 fl/+ Lgr5Cre+/- mTmG +/- Aldh1b1fl/+	Msh2 fl/+ Lgr5Cre+/- mTmG +/- Aldh1b1fl/+	Msh2 fl/+ Lgr5Cre+/- mTmG +/- Aldh1b1fl/+	Msh2 fl/+ Lgr5Cre+/- mTmG +/- Aldh1b1fl/+	Msh2 fl/+ Lgr5Cre+/- mTmG +/- Aldh1b1fl/+	Msh2 fl/+ Lgr5Cre+/- mTmG +/- Aldh1b1fl/+	Msh2 fl/+ Lgr5Cre+/- mTmG +/- Aldh1b1fl/+	Msh2 fl/+ Lgr5Cre+/- mTmG +/- Aldh1b1fl/+	Msh2 fl/+ Lgr5Cre+/- mTmG +/- Aldh1b1fl/+	Msh2 fl/+ Lgr5Cre+/- mTmG +/- Aldh1b1fl/+
Msh2flox Lgr5Cre+ mTmG+ Aldh1b1+	Msh2 fl/+ Lgr5Cre+/- mTmG +/- Aldh1b1fl/+	Msh2 fl/+ Lgr5Cre+/- mTmG +/- Aldh1b1fl/+	Msh2 fl/+ Lgr5Cre+/- mTmG +/- Aldh1b1fl/+	Msh2 fl/+ Lgr5Cre+/- mTmG +/- Aldh1b1fl/+	Msh2 fl/+ Lgr5Cre+/- mTmG +/- Aldh1b1fl/+	Msh2 fl/+ Lgr5Cre+/- mTmG +/- Aldh1b1fl/+	Msh2 fl/+ Lgr5Cre+/- mTmG +/- Aldh1b1fl/+	Msh2 fl/+ Lgr5Cre+/- mTmG +/- Aldh1b1fl/+	Msh2 fl/+ Lgr5Cre+/- mTmG +/- Aldh1b1fl/+	Msh2 fl/+ Lgr5Cre+/- mTmG +/- Aldh1b1fl/+	Msh2 fl/+ Lgr5Cre+/- mTmG +/- Aldh1b1fl/+	Msh2 fl/+ Lgr5Cre+/- mTmG +/- Aldh1b1fl/+	Msh2 fl/+ Lgr5Cre+/- mTmG +/- Aldh1b1fl/+	Msh2 fl/+ Lgr5Cre+/- mTmG +/- Aldh1b1fl/+	Msh2 fl/+ Lgr5Cre+/- mTmG +/- Aldh1b1fl/+	Msh2 fl/+ Lgr5Cre+/- mTmG +/- Aldh1b1fl/+
Msh2flox Lgr5Cre+ mTmG+ Aldh1b1+	Msh2 fl/+ Lgr5Cre+/- mTmG +/- Aldh1b1fl/+	Msh2 fl/+ Lgr5Cre+/- mTmG +/- Aldh1b1fl/+	Msh2 fl/+ Lgr5Cre+/- mTmG +/- Aldh1b1fl/+	Msh2 fl/+ Lgr5Cre+/- mTmG +/- Aldh1b1fl/+	Msh2 fl/+ Lgr5Cre+/- mTmG +/- Aldh1b1fl/+	Msh2 fl/+ Lgr5Cre+/- mTmG +/- Aldh1b1fl/+	Msh2 fl/+ Lgr5Cre+/- mTmG +/- Aldh1b1fl/+	Msh2 fl/+ Lgr5Cre+/- mTmG +/- Aldh1b1fl/+	Msh2 fl/+ Lgr5Cre+/- mTmG +/- Aldh1b1fl/+	Msh2 fl/+ Lgr5Cre+/- mTmG +/- Aldh1b1fl/+	Msh2 fl/+ Lgr5Cre+/- mTmG +/- Aldh1b1fl/+	Msh2 fl/+ Lgr5Cre+/- mTmG +/- Aldh1b1fl/+	Msh2 fl/+ Lgr5Cre+/- mTmG +/- Aldh1b1fl/+	Msh2 fl/+ Lgr5Cre+/- mTmG +/- Aldh1b1fl/+	Msh2 fl/+ Lgr5Cre+/- mTmG +/- Aldh1b1fl/+	Msh2 fl/+ Lgr5Cre+/- mTmG +/- Aldh1b1fl/+
Msh2flox Lgr5Cre+ mTmG+ Aldh1b1+	Msh2 fl/+ Lgr5Cre+/- mTmG +/- Aldh1b1fl/+	Msh2 fl/+ Lgr5Cre+/- mTmG +/- Aldh1b1fl/+	Msh2 fl/+ Lgr5Cre+/- mTmG +/- Aldh1b1fl/+	Msh2 fl/+ Lgr5Cre+/- mTmG +/- Aldh1b1fl/+	Msh2 fl/+ Lgr5Cre+/- mTmG +/- Aldh1b1fl/+	Msh2 fl/+ Lgr5Cre+/- mTmG +/- Aldh1b1fl/+	Msh2 fl/+ Lgr5Cre+/- mTmG +/- Aldh1b1fl/+	Msh2 fl/+ Lgr5Cre+/- mTmG +/- Aldh1b1fl/+	Msh2 fl/+ Lgr5Cre+/- mTmG +/- Aldh1b1fl/+	Msh2 fl/+ Lgr5Cre+/- mTmG +/- Aldh1b1fl/+	Msh2 fl/+ Lgr5Cre+/- mTmG +/- Aldh1b1fl/+	Msh2 fl/+ Lgr5Cre+/- mTmG +/- Aldh1b1fl/+	Msh2 fl/+ Lgr5Cre+/- mTmG +/- Aldh1b1fl/+	Msh2 fl/+ Lgr5Cre+/- mTmG +/- Aldh1b1fl/+	Msh2 fl/+ Lgr5Cre+/- mTmG +/- Aldh1b1fl/+	Msh2 fl/+ Lgr5Cre+/- mTmG +/- Aldh1b1fl/+
Msh2flox Lgr5Cre- mTmG+ Aldh1b1+	Msh2fl/+ Lgr5Cre-/- mTmG +/- Aldh1b1fl/+	Msh2fl/+ Lgr5Cre-/- mTmG +/- Aldh1b1fl/+	Msh2fl/+ Lgr5Cre-/- mTmG +/- Aldh1b1fl/+	Msh2fl/+ Lgr5Cre-/- mTmG +/- Aldh1b1fl/+	Msh2fl/+ Lgr5Cre-/- mTmG +/- Aldh1b1fl/+	Msh2fl/+ Lgr5Cre-/- mTmG +/- Aldh1b1fl/+	Msh2fl/+ Lgr5Cre-/- mTmG +/- Aldh1b1fl/+	Msh2fl/+ Lgr5Cre-/- mTmG +/- Aldh1b1fl/+	Msh2fl/+ Lgr5Cre-/- mTmG +/- Aldh1b1fl/+	Msh2fl/+ Lgr5Cre-/- mTmG +/- Aldh1b1fl/+	Msh2fl/+ Lgr5Cre-/- mTmG +/- Aldh1b1fl/+	Msh2fl/+ Lgr5Cre-/- mTmG +/- Aldh1b1fl/+	Msh2fl/+ Lgr5Cre-/- mTmG +/- Aldh1b1fl/+	Msh2fl/+ Lgr5Cre-/- mTmG +/- Aldh1b1fl/+	Msh2fl/+ Lgr5Cre-/- mTmG +/- Aldh1b1fl/+	Msh2fl/+ Lgr5Cre-/- mTmG +/- Aldh1b1fl/+
Msh2flox Lgr5Cre- mTmG+ Aldh1b1+	Msh2fl/+ Lgr5Cre-/- mTmG +/- Aldh1b1fl/+	Msh2fl/+ Lgr5Cre-/- mTmG +/- Aldh1b1fl/+	Msh2fl/+ Lgr5Cre-/- mTmG +/- Aldh1b1fl/+	Msh2fl/+ Lgr5Cre-/- mTmG +/- Aldh1b1fl/+	Msh2fl/+ Lgr5Cre-/- mTmG +/- Aldh1b1fl/+	Msh2fl/+ Lgr5Cre-/- mTmG +/- Aldh1b1fl/+	Msh2fl/+ Lgr5Cre-/- mTmG +/- Aldh1b1fl/+	Msh2fl/+ Lgr5Cre-/- mTmG +/- Aldh1b1fl/+	Msh2fl/+ Lgr5Cre-/- mTmG +/- Aldh1b1fl/+	Msh2fl/+ Lgr5Cre-/- mTmG +/- Aldh1b1fl/+	Msh2fl/+ Lgr5Cre-/- mTmG +/- Aldh1b1fl/+	Msh2fl/+ Lgr5Cre-/- mTmG +/- Aldh1b1fl/+	Msh2fl/+ Lgr5Cre-/- mTmG +/- Aldh1b1fl/+	Msh2fl/+ Lgr5Cre-/- mTmG +/- Aldh1b1fl/+	Msh2fl/+ Lgr5Cre-/- mTmG +/- Aldh1b1fl/+	Msh2fl/+ Lgr5Cre-/- mTmG +/- Aldh1b1fl/+
Msh2flox Lgr5Cre- mTmG+ Aldh1b1+	Msh2fl/+ Lgr5Cre-/- mTmG +/- Aldh1b1fl/+	Msh2fl/+ Lgr5Cre-/- mTmG +/- Aldh1b1fl/+	Msh2fl/+ Lgr5Cre-/- mTmG +/- Aldh1b1fl/+	Msh2fl/+ Lgr5Cre-/- mTmG +/- Aldh1b1fl/+	Msh2fl/+ Lgr5Cre-/- mTmG +/- Aldh1b1fl/+	Msh2fl/+ Lgr5Cre-/- mTmG +/- Aldh1b1fl/+	Msh2fl/+ Lgr5Cre-/- mTmG +/- Aldh1b1fl/+	Msh2fl/+ Lgr5Cre-/- mTmG +/- Aldh1b1fl/+	Msh2fl/+ Lgr5Cre-/- mTmG +/- Aldh1b1fl/+	Msh2fl/+ Lgr5Cre-/- mTmG +/- Aldh1b1fl/+	Msh2fl/+ Lgr5Cre-/- mTmG +/- Aldh1b1fl/+	Msh2fl/+ Lgr5Cre-/- mTmG +/- Aldh1b1fl/+	Msh2fl/+ Lgr5Cre-/- mTmG +/- Aldh1b1fl/+	Msh2fl/+ Lgr5Cre-/- mTmG +/- Aldh1b1fl/+	Msh2fl/+ Lgr5Cre-/- mTmG +/- Aldh1b1fl/+	Msh2fl/+ Lgr5Cre-/- mTmG +/- Aldh1b1fl/+
Msh2flox Lgr5Cre- mTmG+ Aldh1b1+	Msh2fl/+ Lgr5Cre-/- mTmG +/- Aldh1b1fl/+	Msh2fl/+ Lgr5Cre-/- mTmG +/- Aldh1b1fl/+	Msh2fl/+ Lgr5Cre-/- mTmG +/- Aldh1b1fl/+	Msh2fl/+ Lgr5Cre-/- mTmG +/- Aldh1b1fl/+	Msh2fl/+ Lgr5Cre-/- mTmG +/- Aldh1b1fl/+	Msh2fl/+ Lgr5Cre-/- mTmG +/- Aldh1b1fl/+	Msh2fl/+ Lgr5Cre-/- mTmG +/- Aldh1b1fl/+	Msh2fl/+ Lgr5Cre-/- mTmG +/- Aldh1b1fl/+	Msh2fl/+ Lgr5Cre-/- mTmG +/- Aldh1b1fl/+	Msh2fl/+ Lgr5Cre-/- mTmG +/- Aldh1b1fl/+	Msh2fl/+ Lgr5Cre-/- mTmG +/- Aldh1b1fl/+	Msh2fl/+ Lgr5Cre-/- mTmG +/- Aldh1b1fl/+	Msh2fl/+ Lgr5Cre-/- mTmG +/- Aldh1b1fl/+	Msh2fl/+ Lgr5Cre-/- mTmG +/- Aldh1b1fl/+	Msh2fl/+ Lgr5Cre-/- mTmG +/- Aldh1b1fl/+	Msh2fl/+ Lgr5Cre-/- mTmG +/- Aldh1b1fl/+
Msh2- Lgr5Cre+ mTmG+ Aldh1b1+	Msh2+/- Lgr5Cre+/- mTmG +/- Aldh1b1fl/+	Msh2+/- Lgr5Cre+/- mTmG +/- Aldh1b1fl/+	Msh2+/- Lgr5Cre+/- mTmG +/- Aldh1b1fl/+	Msh2+/- Lgr5Cre+/- mTmG +/- Aldh1b1fl/+	Msh2+/- Lgr5Cre+/- mTmG +/- Aldh1b1fl/+	Msh2+/- Lgr5Cre+/- mTmG +/- Aldh1b1fl/+	Msh2+/- Lgr5Cre+/- mTmG +/- Aldh1b1fl/+	Msh2+/- Lgr5Cre+/- mTmG +/- Aldh1b1fl/+	Msh2+/- Lgr5Cre+/- mTmG +/- Aldh1b1fl/+	Msh2+/- Lgr5Cre+/- mTmG +/- Aldh1b1fl/+	Msh2+/- Lgr5Cre+/- mTmG +/- Aldh1b1fl/+	Msh2+/- Lgr5Cre+/- mTmG +/- Aldh1b1fl/+	Msh2+/- Lgr5Cre+/- mTmG +/- Aldh1b1fl/+	Msh2+/- Lgr5Cre+/- mTmG +/- Aldh1b1fl/+	Msh2+/- Lgr5Cre+/- mTmG +/- Aldh1b1fl/+	Msh2+/- Lgr5Cre+/- mTmG +/- Aldh1b1fl/+
Msh2- Lgr5Cre+ mTmG+ Aldh1b1+	Msh2+/- Lgr5Cre+/- mTmG +/- Aldh1b1fl/+	Msh2+/- Lgr5Cre+/- mTmG +/- Aldh1b1fl/+	Msh2+/- Lgr5Cre+/- mTmG +/- Aldh1b1fl/+	Msh2+/- Lgr5Cre+/- mTmG +/- Aldh1b1fl/+	Msh2+/- Lgr5Cre+/- mTmG +/- Aldh1b1fl/+	Msh2+/- Lgr5Cre+/- mTmG +/- Aldh1b1fl/+	Msh2+/- Lgr5Cre+/- mTmG +/- Aldh1b1fl/+	Msh2+/- Lgr5Cre+/- mTmG +/- Aldh1b1fl/+	Msh2+/- Lgr5Cre+/- mTmG +/- Aldh1b1fl/+	Msh2+/- Lgr5Cre+/- mTmG +/- Aldh1b1fl/+	Msh2+/- Lgr5Cre+/- mTmG +/- Aldh1b1fl/+	Msh2+/- Lgr5Cre+/- mTmG +/- Aldh1b1fl/+	Msh2+/- Lgr5Cre+/- mTmG +/- Aldh1b1fl/+	Msh2+/- Lgr5Cre+/- mTmG +/- Aldh1b1fl/+	Msh2+/- Lgr5Cre+/- mTmG +/- Aldh1b1fl/+	Msh2+/- Lgr5Cre+/- mTmG +/- Aldh1b1fl/+
Msh2- Lgr5Cre+ mTmG+ Aldh1b1+	Msh2+/- Lgr5Cre+/- mTmG +/- Aldh1b1fl/+	Msh2+/- Lgr5Cre+/- mTmG +/- Aldh1b1fl/+	Msh2+/- Lgr5Cre+/- mTmG +/- Aldh1b1fl/+	Msh2+/- Lgr5Cre+/- mTmG +/- Aldh1b1fl/+	Msh2+/- Lgr5Cre+/- mTmG +/- Aldh1b1fl/+	Msh2+/- Lgr5Cre+/- mTmG +/- Aldh1b1fl/+	Msh2+/- Lgr5Cre+/- mTmG +/- Aldh1b1fl/+	Msh2+/- Lgr5Cre+/- mTmG +/- Aldh1b1fl/+	Msh2+/- Lgr5Cre+/- mTmG +/- Aldh1b1fl/+	Msh2+/- Lgr5Cre+/- mTmG +/- Aldh1b1fl/+	Msh2+/- Lgr5Cre+/- mTmG +/- Aldh1b1fl/+	Msh2+/- Lgr5Cre+/- mTmG +/- Aldh1b1fl/+	Msh2+/- Lgr5Cre+/- mTmG +/- Aldh1b1fl/+	Msh2+/- Lgr5Cre+/- mTmG +/- Aldh1b1fl/+	Msh2+/- Lgr5Cre+/- mTmG +/- Aldh1b1fl/+	Msh2+/- Lgr5Cre+/- mTmG +/- Aldh1b1fl/+

Msh2- Lgr5Cre+ mTmG+ Aldh1b1+	Msh2+/- Lgr5Cre+/- mTmG +/- Aldh1b1fl/+	Msh2+/- Lgr5Cre+/- mTmG +/- Aldh1b1fl/+	Msh2+/- Lgr5Cre+/- mTmG +/- Aldh1b1fl/+	Msh2+/- Lgr5Cre+/- mTmG +/- Aldh1b1fl/+	Msh2+/- Lgr5Cre+/- mTmG +/- Aldh1b1fl/+	Msh2+/- Lgr5Cre+/- mTmG +/- Aldh1b1fl/+	Msh2+/- Lgr5Cre+/- mTmG +/- Aldh1b1fl/+	Msh2+/- Lgr5Cre+/- mTmG +/- Aldh1b1fl/+	Msh2+/- Lgr5Cre+/- mTmG +/- Aldh1b1fl/+	Msh2+/- Lgr5Cre+/- mTmG +/- Aldh1b1fl/+	Msh2+/- Lgr5Cre+/- mTmG +/- Aldh1b1fl/+	Msh2+/- Lgr5Cre+/- mTmG +/- Aldh1b1fl/+	Msh2+/- Lgr5Cre+/- mTmG +/- Aldh1b1fl/+	Msh2+/- Lgr5Cre+/- mTmG +/- Aldh1b1fl/+	Msh2+/- Lgr5Cre+/- mTmG +/- Aldh1b1fl/+	Msh2+/- Lgr5Cre+/- mTmG +/- Aldh1b1fl/+
Msh2- Lgr5Cre- mTmG+ Aldh1b1+	Msh2+/- Lgr5Cre-/- mTmG +/- Aldh1b1fl/+	Msh2+/- Lgr5Cre-/- mTmG +/- Aldh1b1fl/+	Msh2+/- Lgr5Cre-/- mTmG +/- Aldh1b1fl/+	Msh2+/- Lgr5Cre-/- mTmG +/- Aldh1b1fl/+	Msh2+/- Lgr5Cre-/- mTmG +/- Aldh1b1fl/+	Msh2+/- Lgr5Cre-/- mTmG +/- Aldh1b1fl/+	Msh2+/- Lgr5Cre-/- mTmG +/- Aldh1b1fl/+	Msh2+/- Lgr5Cre-/- mTmG +/- Aldh1b1fl/+	Msh2+/- Lgr5Cre-/- mTmG +/- Aldh1b1fl/+	Msh2+/- Lgr5Cre-/- mTmG +/- Aldh1b1fl/+	Msh2+/- Lgr5Cre-/- mTmG +/- Aldh1b1fl/+	Msh2+/- Lgr5Cre-/- mTmG +/- Aldh1b1fl/+	Msh2+/- Lgr5Cre-/- mTmG +/- Aldh1b1fl/+	Msh2+/- Lgr5Cre-/- mTmG +/- Aldh1b1fl/+	Msh2+/- Lgr5Cre-/- mTmG +/- Aldh1b1fl/+	Msh2+/- Lgr5Cre-/- mTmG +/- Aldh1b1fl/+
Msh2- Lgr5Cre- mTmG+ Aldh1b1+	Msh2+/- Lgr5Cre-/- mTmG +/- Aldh1b1fl/+	Msh2+/- Lgr5Cre-/- mTmG +/- Aldh1b1fl/+	Msh2+/- Lgr5Cre-/- mTmG +/- Aldh1b1fl/+	Msh2+/- Lgr5Cre-/- mTmG +/- Aldh1b1fl/+	Msh2+/- Lgr5Cre-/- mTmG +/- Aldh1b1fl/+	Msh2+/- Lgr5Cre-/- mTmG +/- Aldh1b1fl/+	Msh2+/- Lgr5Cre-/- mTmG +/- Aldh1b1fl/+	Msh2+/- Lgr5Cre-/- mTmG +/- Aldh1b1fl/+	Msh2+/- Lgr5Cre-/- mTmG +/- Aldh1b1fl/+	Msh2+/- Lgr5Cre-/- mTmG +/- Aldh1b1fl/+	Msh2+/- Lgr5Cre-/- mTmG +/- Aldh1b1fl/+	Msh2+/- Lgr5Cre-/- mTmG +/- Aldh1b1fl/+	Msh2+/- Lgr5Cre-/- mTmG +/- Aldh1b1fl/+	Msh2+/- Lgr5Cre-/- mTmG +/- Aldh1b1fl/+	Msh2+/- Lgr5Cre-/- mTmG +/- Aldh1b1fl/+	Msh2+/- Lgr5Cre-/- mTmG +/- Aldh1b1fl/+
Msh2- Lgr5Cre- mTmG+ Aldh1b1+	Msh2+/- Lgr5Cre-/- mTmG +/- Aldh1b1fl/+	Msh2+/- Lgr5Cre-/- mTmG +/- Aldh1b1fl/+	Msh2+/- Lgr5Cre-/- mTmG +/- Aldh1b1fl/+	Msh2+/- Lgr5Cre-/- mTmG +/- Aldh1b1fl/+	Msh2+/- Lgr5Cre-/- mTmG +/- Aldh1b1fl/+	Msh2+/- Lgr5Cre-/- mTmG +/- Aldh1b1fl/+	Msh2+/- Lgr5Cre-/- mTmG +/- Aldh1b1fl/+	Msh2+/- Lgr5Cre-/- mTmG +/- Aldh1b1fl/+	Msh2+/- Lgr5Cre-/- mTmG +/- Aldh1b1fl/+	Msh2+/- Lgr5Cre-/- mTmG +/- Aldh1b1fl/+	Msh2+/- Lgr5Cre-/- mTmG +/- Aldh1b1fl/+	Msh2+/- Lgr5Cre-/- mTmG +/- Aldh1b1fl/+	Msh2+/- Lgr5Cre-/- mTmG +/- Aldh1b1fl/+	Msh2+/- Lgr5Cre-/- mTmG +/- Aldh1b1fl/+	Msh2+/- Lgr5Cre-/- mTmG +/- Aldh1b1fl/+	Msh2+/- Lgr5Cre-/- mTmG +/- Aldh1b1fl/+
Msh2- Lgr5Cre- mTmG+ Aldh1b1+	Msh2+/- Lgr5Cre-/- mTmG +/- Aldh1b1fl/+	Msh2+/- Lgr5Cre-/- mTmG +/- Aldh1b1fl/+	Msh2+/- Lgr5Cre-/- mTmG +/- Aldh1b1fl/+	Msh2+/- Lgr5Cre-/- mTmG +/- Aldh1b1fl/+	Msh2+/- Lgr5Cre-/- mTmG +/- Aldh1b1fl/+	Msh2+/- Lgr5Cre-/- mTmG +/- Aldh1b1fl/+	Msh2+/- Lgr5Cre-/- mTmG +/- Aldh1b1fl/+	Msh2+/- Lgr5Cre-/- mTmG +/- Aldh1b1fl/+	Msh2+/- Lgr5Cre-/- mTmG +/- Aldh1b1fl/+	Msh2+/- Lgr5Cre-/- mTmG +/- Aldh1b1fl/+	Msh2+/- Lgr5Cre-/- mTmG +/- Aldh1b1fl/+	Msh2+/- Lgr5Cre-/- mTmG +/- Aldh1b1fl/+	Msh2+/- Lgr5Cre-/- mTmG +/- Aldh1b1fl/+	Msh2+/- Lgr5Cre-/- mTmG +/- Aldh1b1fl/+	Msh2+/- Lgr5Cre-/- mTmG +/- Aldh1b1fl/+	Msh2+/- Lgr5Cre-/- mTmG +/- Aldh1b1fl/+

Supplementary Table 6.2: Tabular representation of the generation of the *Aldh1b1* conditional-knockout Msh2-LS mouse model experimental subjects. Representation of the breeding between the *Msh2*$^{+/-}$*; Lgr5CreERT2*$^{-/-}$*; mTmG*$^{+/-}$*; Aldh1b1*$^{flox/+}$ *with Msh2*$^{flox/+}$*; Lgr5CreERT2*$^{+/-}$*; mTmG*$^{+/-}$*; Aldh1b1*$^{flox/+}$ mice.

	Msh2+ Lgr5Cre- mTmG- Aldh1b1-	Msh2+ Lgr5Cre- mTmG- Aldh1b1-	Msh2+ Lgr5Cre- mTmG- Aldh1b1-	Msh2+ Lgr5Cre- mTmG- Aldh1b1-	Msh2+ Lgr5Cre- mTmG- Aldh1b1-	Msh2+ Lgr5Cre- mTmG- Aldh1b1-	Msh2+ Lgr5Cre- mTmG- Aldh1b1-	Msh2+ Lgr5Cre- mTmG- Aldh1b1-	Msh2+ Lgr5Cre- mTmG- Aldh1b1-	Msh2+ Lgr5Cre- mTmG- Aldh1b1-	Msh2+ Lgr5Cre- mTmG- Aldh1b1-	Msh2+ Lgr5Cre- mTmG- Aldh1b1-	Msh2+ Lgr5Cre- mTmG- Aldh1b1-	Msh2+ Lgr5Cre- mTmG- Aldh1b1-	Msh2+ Lgr5Cre- mTmG- Aldh1b1-	Msh2+ Lgr5Cre- mTmG- Aldh1b1-
Msh2flox Lgr5Cre+ mTmG+ Aldh1b1+	Msh2 fl/+ Lgr5Cre+/- mTmG +/- Aldh1b1+/-	Msh2 fl/+ Lgr5Cre+/- mTmG +/- Aldh1b1+/-	Msh2 fl/+ Lgr5Cre+/- mTmG +/- Aldh1b1+/-	Msh2 fl/+ Lgr5Cre+/- mTmG +/- Aldh1b1+/-	Msh2 fl/+ Lgr5Cre+/- mTmG +/- Aldh1b1+/-	Msh2 fl/+ Lgr5Cre+/- mTmG +/- Aldh1b1+/-	Msh2 fl/+ Lgr5Cre+/- mTmG +/- Aldh1b1+/-	Msh2 fl/+ Lgr5Cre+/- mTmG +/- Aldh1b1+/-	Msh2 fl/+ Lgr5Cre+/- mTmG +/- Aldh1b1+/-	Msh2 fl/+ Lgr5Cre+/- mTmG +/- Aldh1b1+/-	Msh2 fl/+ Lgr5Cre+/- mTmG +/- Aldh1b1+/-	Msh2 fl/+ Lgr5Cre+/- mTmG +/- Aldh1b1+/-	Msh2 fl/+ Lgr5Cre+/- mTmG +/- Aldh1b1+/-	Msh2 fl/+ Lgr5Cre+/- mTmG +/- Aldh1b1+/-	Msh2 fl/+ Lgr5Cre+/- mTmG +/- Aldh1b1+/-	Msh2 fl/+ Lgr5Cre+/- mTmG +/- Aldh1b1+/-
Msh2flox Lgr5Cre+ mTmG+ Aldh1b1+	Msh2 fl/+ Lgr5Cre+/- mTmG +/- Aldh1b1+/-	Msh2 fl/+ Lgr5Cre+/- mTmG +/- Aldh1b1+/-	Msh2 fl/+ Lgr5Cre+/- mTmG +/- Aldh1b1+/-	Msh2 fl/+ Lgr5Cre+/- mTmG +/- Aldh1b1+/-	Msh2 fl/+ Lgr5Cre+/- mTmG +/- Aldh1b1+/-	Msh2 fl/+ Lgr5Cre+/- mTmG +/- Aldh1b1+/-	Msh2 fl/+ Lgr5Cre+/- mTmG +/- Aldh1b1+/-	Msh2 fl/+ Lgr5Cre+/- mTmG +/- Aldh1b1+/-	Msh2 fl/+ Lgr5Cre+/- mTmG +/- Aldh1b1+/-	Msh2 fl/+ Lgr5Cre+/- mTmG +/- Aldh1b1+/-	Msh2 fl/+ Lgr5Cre+/- mTmG +/- Aldh1b1+/-	Msh2 fl/+ Lgr5Cre+/- mTmG +/- Aldh1b1+/-	Msh2 fl/+ Lgr5Cre+/- mTmG +/- Aldh1b1+/-	Msh2 fl/+ Lgr5Cre+/- mTmG +/- Aldh1b1+/-	Msh2 fl/+ Lgr5Cre+/- mTmG +/- Aldh1b1+/-	Msh2 fl/+ Lgr5Cre+/- mTmG +/- Aldh1b1+/-
Msh2flox Lgr5Cre+ mTmG+ Aldh1b1+	Msh2 fl/+ Lgr5Cre+/- mTmG +/- Aldh1b1+/-	Msh2 fl/+ Lgr5Cre+/- mTmG +/- Aldh1b1+/-	Msh2 fl/+ Lgr5Cre+/- mTmG +/- Aldh1b1+/-	Msh2 fl/+ Lgr5Cre+/- mTmG +/- Aldh1b1+/-	Msh2 fl/+ Lgr5Cre+/- mTmG +/- Aldh1b1+/-	Msh2 fl/+ Lgr5Cre+/- mTmG +/- Aldh1b1+/-	Msh2 fl/+ Lgr5Cre+/- mTmG +/- Aldh1b1+/-	Msh2 fl/+ Lgr5Cre+/- mTmG +/- Aldh1b1+/-	Msh2 fl/+ Lgr5Cre+/- mTmG +/- Aldh1b1+/-	Msh2 fl/+ Lgr5Cre+/- mTmG +/- Aldh1b1+/-	Msh2 fl/+ Lgr5Cre+/- mTmG +/- Aldh1b1+/-	Msh2 fl/+ Lgr5Cre+/- mTmG +/- Aldh1b1+/-	Msh2 fl/+ Lgr5Cre+/- mTmG +/- Aldh1b1+/-	Msh2 fl/+ Lgr5Cre+/- mTmG +/- Aldh1b1+/-	Msh2 fl/+ Lgr5Cre+/- mTmG +/- Aldh1b1+/-	Msh2 fl/+ Lgr5Cre+/- mTmG +/- Aldh1b1+/-
Msh2flox Lgr5Cre+ mTmG+ Aldh1b1+	Msh2 fl/+ Lgr5Cre+/- mTmG +/- Aldh1b1+/-	Msh2 fl/+ Lgr5Cre+/- mTmG +/- Aldh1b1+/-	Msh2 fl/+ Lgr5Cre+/- mTmG +/- Aldh1b1+/-	Msh2 fl/+ Lgr5Cre+/- mTmG +/- Aldh1b1+/-	Msh2 fl/+ Lgr5Cre+/- mTmG +/- Aldh1b1+/-	Msh2 fl/+ Lgr5Cre+/- mTmG +/- Aldh1b1+/-	Msh2 fl/+ Lgr5Cre+/- mTmG +/- Aldh1b1+/-	Msh2 fl/+ Lgr5Cre+/- mTmG +/- Aldh1b1+/-	Msh2 fl/+ Lgr5Cre+/- mTmG +/- Aldh1b1+/-	Msh2 fl/+ Lgr5Cre+/- mTmG +/- Aldh1b1+/-	Msh2 fl/+ Lgr5Cre+/- mTmG +/- Aldh1b1+/-	Msh2 fl/+ Lgr5Cre+/- mTmG +/- Aldh1b1+/-	Msh2 fl/+ Lgr5Cre+/- mTmG +/- Aldh1b1+/-	Msh2 fl/+ Lgr5Cre+/- mTmG +/- Aldh1b1+/-	Msh2 fl/+ Lgr5Cre+/- mTmG +/- Aldh1b1+/-	Msh2 fl/+ Lgr5Cre+/- mTmG +/- Aldh1b1+/-
Msh2flox Lgr5Cre- mTmG+ Aldh1b1+	Msh2fl/+ Lgr5Cre-/- mTmG +/- Aldh1b1+/-	Msh2fl/+ Lgr5Cre-/- mTmG +/- Aldh1b1+/-	Msh2fl/+ Lgr5Cre-/- mTmG +/- Aldh1b1+/-	Msh2fl/+ Lgr5Cre-/- mTmG +/- Aldh1b1+/-	Msh2fl/+ Lgr5Cre-/- mTmG +/- Aldh1b1+/-	Msh2fl/+ Lgr5Cre-/- mTmG +/- Aldh1b1+/-	Msh2fl/+ Lgr5Cre-/- mTmG +/- Aldh1b1+/-	Msh2fl/+ Lgr5Cre-/- mTmG +/- Aldh1b1+/-	Msh2fl/+ Lgr5Cre-/- mTmG +/- Aldh1b1+/-	Msh2fl/+ Lgr5Cre-/- mTmG +/- Aldh1b1+/-	Msh2fl/+ Lgr5Cre-/- mTmG +/- Aldh1b1+/-	Msh2fl/+ Lgr5Cre-/- mTmG +/- Aldh1b1+/-	Msh2fl/+ Lgr5Cre-/- mTmG +/- Aldh1b1+/-	Msh2fl/+ Lgr5Cre-/- mTmG +/- Aldh1b1+/-	Msh2fl/+ Lgr5Cre-/- mTmG +/- Aldh1b1+/-	Msh2fl/+ Lgr5Cre-/- mTmG +/- Aldh1b1+/-
Msh2flox Lgr5Cre- mTmG+ Aldh1b1+	Msh2fl/+ Lgr5Cre-/- mTmG +/- Aldh1b1+/-	Msh2fl/+ Lgr5Cre-/- mTmG +/- Aldh1b1+/-	Msh2fl/+ Lgr5Cre-/- mTmG +/- Aldh1b1+/-	Msh2fl/+ Lgr5Cre-/- mTmG +/- Aldh1b1+/-	Msh2fl/+ Lgr5Cre-/- mTmG +/- Aldh1b1+/-	Msh2fl/+ Lgr5Cre-/- mTmG +/- Aldh1b1+/-	Msh2fl/+ Lgr5Cre-/- mTmG +/- Aldh1b1+/-	Msh2fl/+ Lgr5Cre-/- mTmG +/- Aldh1b1+/-	Msh2fl/+ Lgr5Cre-/- mTmG +/- Aldh1b1+/-	Msh2fl/+ Lgr5Cre-/- mTmG +/- Aldh1b1+/-	Msh2fl/+ Lgr5Cre-/- mTmG +/- Aldh1b1+/-	Msh2fl/+ Lgr5Cre-/- mTmG +/- Aldh1b1+/-	Msh2fl/+ Lgr5Cre-/- mTmG +/- Aldh1b1+/-	Msh2fl/+ Lgr5Cre-/- mTmG +/- Aldh1b1+/-	Msh2fl/+ Lgr5Cre-/- mTmG +/- Aldh1b1+/-	Msh2fl/+ Lgr5Cre-/- mTmG +/- Aldh1b1+/-
Msh2flox Lgr5Cre- mTmG+ Aldh1b1+	Msh2fl/+ Lgr5Cre-/- mTmG +/- Aldh1b1+/-	Msh2fl/+ Lgr5Cre-/- mTmG +/- Aldh1b1+/-	Msh2fl/+ Lgr5Cre-/- mTmG +/- Aldh1b1+/-	Msh2fl/+ Lgr5Cre-/- mTmG +/- Aldh1b1+/-	Msh2fl/+ Lgr5Cre-/- mTmG +/- Aldh1b1+/-	Msh2fl/+ Lgr5Cre-/- mTmG +/- Aldh1b1+/-	Msh2fl/+ Lgr5Cre-/- mTmG +/- Aldh1b1+/-	Msh2fl/+ Lgr5Cre-/- mTmG +/- Aldh1b1+/-	Msh2fl/+ Lgr5Cre-/- mTmG +/- Aldh1b1+/-	Msh2fl/+ Lgr5Cre-/- mTmG +/- Aldh1b1+/-	Msh2fl/+ Lgr5Cre-/- mTmG +/- Aldh1b1+/-	Msh2fl/+ Lgr5Cre-/- mTmG +/- Aldh1b1+/-	Msh2fl/+ Lgr5Cre-/- mTmG +/- Aldh1b1+/-	Msh2fl/+ Lgr5Cre-/- mTmG +/- Aldh1b1+/-	Msh2fl/+ Lgr5Cre-/- mTmG +/- Aldh1b1+/-	Msh2fl/+ Lgr5Cre-/- mTmG +/- Aldh1b1+/-
Msh2flox Lgr5Cre- mTmG+ Aldh1b1+	Msh2fl/+ Lgr5Cre-/- mTmG +/- Aldh1b1+/-	Msh2fl/+ Lgr5Cre-/- mTmG +/- Aldh1b1+/-	Msh2fl/+ Lgr5Cre-/- mTmG +/- Aldh1b1+/-	Msh2fl/+ Lgr5Cre-/- mTmG +/- Aldh1b1+/-	Msh2fl/+ Lgr5Cre-/- mTmG +/- Aldh1b1+/-	Msh2fl/+ Lgr5Cre-/- mTmG +/- Aldh1b1+/-	Msh2fl/+ Lgr5Cre-/- mTmG +/- Aldh1b1+/-	Msh2fl/+ Lgr5Cre-/- mTmG +/- Aldh1b1+/-	Msh2fl/+ Lgr5Cre-/- mTmG +/- Aldh1b1+/-	Msh2fl/+ Lgr5Cre-/- mTmG +/- Aldh1b1+/-	Msh2fl/+ Lgr5Cre-/- mTmG +/- Aldh1b1+/-	Msh2fl/+ Lgr5Cre-/- mTmG +/- Aldh1b1+/-	Msh2fl/+ Lgr5Cre-/- mTmG +/- Aldh1b1+/-	Msh2fl/+ Lgr5Cre-/- mTmG +/- Aldh1b1+/-	Msh2fl/+ Lgr5Cre-/- mTmG +/- Aldh1b1+/-	Msh2fl/+ Lgr5Cre-/- mTmG +/- Aldh1b1+/-
Msh2- Lgr5Cre+ mTmG+ Aldh1b1+	Msh2+/- Lgr5Cre+/- mTmG +/- Aldh1b1+/-	Msh2+/- Lgr5Cre+/- mTmG +/- Aldh1b1+/-	Msh2+/- Lgr5Cre+/- mTmG +/- Aldh1b1+/-	Msh2+/- Lgr5Cre+/- mTmG +/- Aldh1b1+/-	Msh2+/- Lgr5Cre+/- mTmG +/- Aldh1b1+/-	Msh2+/- Lgr5Cre+/- mTmG +/- Aldh1b1+/-	Msh2+/- Lgr5Cre+/- mTmG +/- Aldh1b1+/-	Msh2+/- Lgr5Cre+/- mTmG +/- Aldh1b1+/-	Msh2+/- Lgr5Cre+/- mTmG +/- Aldh1b1+/-	Msh2+/- Lgr5Cre+/- mTmG +/- Aldh1b1+/-	Msh2+/- Lgr5Cre+/- mTmG +/- Aldh1b1+/-	Msh2+/- Lgr5Cre+/- mTmG +/- Aldh1b1+/-	Msh2+/- Lgr5Cre+/- mTmG +/- Aldh1b1+/-	Msh2+/- Lgr5Cre+/- mTmG +/- Aldh1b1+/-	Msh2+/- Lgr5Cre+/- mTmG +/- Aldh1b1+/-	Msh2+/- Lgr5Cre+/- mTmG +/- Aldh1b1+/-
Msh2- Lgr5Cre+ mTmG+ Aldh1b1+	Msh2+/- Lgr5Cre+/- mTmG +/- Aldh1b1+/-	Msh2+/- Lgr5Cre+/- mTmG +/- Aldh1b1+/-	Msh2+/- Lgr5Cre+/- mTmG +/- Aldh1b1+/-	Msh2+/- Lgr5Cre+/- mTmG +/- Aldh1b1+/-	Msh2+/- Lgr5Cre+/- mTmG +/- Aldh1b1+/-	Msh2+/- Lgr5Cre+/- mTmG +/- Aldh1b1+/-	Msh2+/- Lgr5Cre+/- mTmG +/- Aldh1b1+/-	Msh2+/- Lgr5Cre+/- mTmG +/- Aldh1b1+/-	Msh2+/- Lgr5Cre+/- mTmG +/- Aldh1b1+/-	Msh2+/- Lgr5Cre+/- mTmG +/- Aldh1b1+/-	Msh2+/- Lgr5Cre+/- mTmG +/- Aldh1b1+/-	Msh2+/- Lgr5Cre+/- mTmG +/- Aldh1b1+/-	Msh2+/- Lgr5Cre+/- mTmG +/- Aldh1b1+/-	Msh2+/- Lgr5Cre+/- mTmG +/- Aldh1b1+/-	Msh2+/- Lgr5Cre+/- mTmG +/- Aldh1b1+/-	Msh2+/- Lgr5Cre+/- mTmG +/- Aldh1b1+/-
Msh2- Lgr5Cre+ mTmG+ Aldh1b1+	Msh2+/- Lgr5Cre+/- mTmG +/- Aldh1b1+/-	Msh2+/- Lgr5Cre+/- mTmG +/- Aldh1b1+/-	Msh2+/- Lgr5Cre+/- mTmG +/- Aldh1b1+/-	Msh2+/- Lgr5Cre+/- mTmG +/- Aldh1b1+/-	Msh2+/- Lgr5Cre+/- mTmG +/- Aldh1b1+/-	Msh2+/- Lgr5Cre+/- mTmG +/- Aldh1b1+/-	Msh2+/- Lgr5Cre+/- mTmG +/- Aldh1b1+/-	Msh2+/- Lgr5Cre+/- mTmG +/- Aldh1b1+/-	Msh2+/- Lgr5Cre+/- mTmG +/- Aldh1b1+/-	Msh2+/- Lgr5Cre+/- mTmG +/- Aldh1b1+/-	Msh2+/- Lgr5Cre+/- mTmG +/- Aldh1b1+/-	Msh2+/- Lgr5Cre+/- mTmG +/- Aldh1b1+/-	Msh2+/- Lgr5Cre+/- mTmG +/- Aldh1b1+/-	Msh2+/- Lgr5Cre+/- mTmG +/- Aldh1b1+/-	Msh2+/- Lgr5Cre+/- mTmG +/- Aldh1b1+/-	Msh2+/- Lgr5Cre+/- mTmG +/- Aldh1b1+/-

Msh2- Lgr5Cre+ mTmG+ Aldh1b1+	Msh2+/- Lgr5Cre+/- mTmG +/- Aldh1b1+/-	Msh2+/- Lgr5Cre+/- mTmG +/- Aldh1b1+/-	Msh2+/- Lgr5Cre+/- mTmG +/- Aldh1b1+/-	Msh2+/- Lgr5Cre+/- mTmG +/- Aldh1b1+/-	Msh2+/- Lgr5Cre+/- mTmG +/- Aldh1b1+/-	Msh2+/- Lgr5Cre+/- mTmG +/- Aldh1b1+/-	Msh2+/- Lgr5Cre+/- mTmG +/- Aldh1b1+/-	Msh2+/- Lgr5Cre+/- mTmG +/- Aldh1b1+/-	Msh2+/- Lgr5Cre+/- mTmG +/- Aldh1b1+/-	Msh2+/- Lgr5Cre+/- mTmG +/- Aldh1b1+/-	Msh2+/- Lgr5Cre+/- mTmG +/- Aldh1b1+/-	Msh2+/- Lgr5Cre+/- mTmG +/- Aldh1b1+/-	Msh2+/- Lgr5Cre+/- mTmG +/- Aldh1b1+/-	Msh2+/- Lgr5Cre+/- mTmG +/- Aldh1b1+/-	Msh2+/- Lgr5Cre+/- mTmG +/- Aldh1b1+/-	Msh2+/- Lgr5Cre+/- mTmG +/- Aldh1b1+/-
Msh2- Lgr5Cre- mTmG+ Aldh1b1+	Msh2+/- Lgr5Cre-/- mTmG +/- Aldh1b1+/-	Msh2+/- Lgr5Cre-/- mTmG +/- Aldh1b1+/-	Msh2+/- Lgr5Cre-/- mTmG +/- Aldh1b1+/-	Msh2+/- Lgr5Cre-/- mTmG +/- Aldh1b1+/-	Msh2+/- Lgr5Cre-/- mTmG +/- Aldh1b1+/-	Msh2+/- Lgr5Cre-/- mTmG +/- Aldh1b1+/-	Msh2+/- Lgr5Cre-/- mTmG +/- Aldh1b1+/-	Msh2+/- Lgr5Cre-/- mTmG +/- Aldh1b1+/-	Msh2+/- Lgr5Cre-/- mTmG +/- Aldh1b1+/-	Msh2+/- Lgr5Cre-/- mTmG +/- Aldh1b1+/-	Msh2+/- Lgr5Cre-/- mTmG +/- Aldh1b1+/-	Msh2+/- Lgr5Cre-/- mTmG +/- Aldh1b1+/-	Msh2+/- Lgr5Cre-/- mTmG +/- Aldh1b1+/-	Msh2+/- Lgr5Cre-/- mTmG +/- Aldh1b1+/-	Msh2+/- Lgr5Cre-/- mTmG +/- Aldh1b1+/-	Msh2+/- Lgr5Cre-/- mTmG +/- Aldh1b1+/-
Msh2- Lgr5Cre- mTmG+ Aldh1b1+	Msh2+/- Lgr5Cre-/- mTmG +/- Aldh1b1+/-	Msh2+/- Lgr5Cre-/- mTmG +/- Aldh1b1+/-	Msh2+/- Lgr5Cre-/- mTmG +/- Aldh1b1+/-	Msh2+/- Lgr5Cre-/- mTmG +/- Aldh1b1+/-	Msh2+/- Lgr5Cre-/- mTmG +/- Aldh1b1+/-	Msh2+/- Lgr5Cre-/- mTmG +/- Aldh1b1+/-	Msh2+/- Lgr5Cre-/- mTmG +/- Aldh1b1+/-	Msh2+/- Lgr5Cre-/- mTmG +/- Aldh1b1+/-	Msh2+/- Lgr5Cre-/- mTmG +/- Aldh1b1+/-	Msh2+/- Lgr5Cre-/- mTmG +/- Aldh1b1+/-	Msh2+/- Lgr5Cre-/- mTmG +/- Aldh1b1+/-	Msh2+/- Lgr5Cre-/- mTmG +/- Aldh1b1+/-	Msh2+/- Lgr5Cre-/- mTmG +/- Aldh1b1+/-	Msh2+/- Lgr5Cre-/- mTmG +/- Aldh1b1+/-	Msh2+/- Lgr5Cre-/- mTmG +/- Aldh1b1+/-	Msh2+/- Lgr5Cre-/- mTmG +/- Aldh1b1+/-
Msh2- Lgr5Cre- mTmG+ Aldh1b1+	Msh2+/- Lgr5Cre-/- mTmG +/- Aldh1b1+/-	Msh2+/- Lgr5Cre-/- mTmG +/- Aldh1b1+/-	Msh2+/- Lgr5Cre-/- mTmG +/- Aldh1b1+/-	Msh2+/- Lgr5Cre-/- mTmG +/- Aldh1b1+/-	Msh2+/- Lgr5Cre-/- mTmG +/- Aldh1b1+/-	Msh2+/- Lgr5Cre-/- mTmG +/- Aldh1b1+/-	Msh2+/- Lgr5Cre-/- mTmG +/- Aldh1b1+/-	Msh2+/- Lgr5Cre-/- mTmG +/- Aldh1b1+/-	Msh2+/- Lgr5Cre-/- mTmG +/- Aldh1b1+/-	Msh2+/- Lgr5Cre-/- mTmG +/- Aldh1b1+/-	Msh2+/- Lgr5Cre-/- mTmG +/- Aldh1b1+/-	Msh2+/- Lgr5Cre-/- mTmG +/- Aldh1b1+/-	Msh2+/- Lgr5Cre-/- mTmG +/- Aldh1b1+/-	Msh2+/- Lgr5Cre-/- mTmG +/- Aldh1b1+/-	Msh2+/- Lgr5Cre-/- mTmG +/- Aldh1b1+/-	Msh2+/- Lgr5Cre-/- mTmG +/- Aldh1b1+/-
Msh2- Lgr5Cre- mTmG+ Aldh1b1+	Msh2+/- Lgr5Cre-/- mTmG +/- Aldh1b1+/-	Msh2+/- Lgr5Cre-/- mTmG +/- Aldh1b1+/-	Msh2+/- Lgr5Cre-/- mTmG +/- Aldh1b1+/-	Msh2+/- Lgr5Cre-/- mTmG +/- Aldh1b1+/-	Msh2+/- Lgr5Cre-/- mTmG +/- Aldh1b1+/-	Msh2+/- Lgr5Cre-/- mTmG +/- Aldh1b1+/-	Msh2+/- Lgr5Cre-/- mTmG +/- Aldh1b1+/-	Msh2+/- Lgr5Cre-/- mTmG +/- Aldh1b1+/-	Msh2+/- Lgr5Cre-/- mTmG +/- Aldh1b1+/-	Msh2+/- Lgr5Cre-/- mTmG +/- Aldh1b1+/-	Msh2+/- Lgr5Cre-/- mTmG +/- Aldh1b1+/-	Msh2+/- Lgr5Cre-/- mTmG +/- Aldh1b1+/-	Msh2+/- Lgr5Cre-/- mTmG +/- Aldh1b1+/-	Msh2+/- Lgr5Cre-/- mTmG +/- Aldh1b1+/-	Msh2+/- Lgr5Cre-/- mTmG +/- Aldh1b1+/-	Msh2+/- Lgr5Cre-/- mTmG +/- Aldh1b1+/-

Supplementary Table 6.3: Tabular representation of the generation of the *Aldh1b1* constitutive-knockout Msh2-LS mouse model experimental subjects. Representation of the breeding between the *Msh2*$^{+/+}$*; Lgr5CreERT2*$^{-/-}$*; mTmG*$^{-/-}$*; Aldh1b1*$^{-/-}$ with *Msh2*$^{flox/-}$*; Lgr5CreERT2*$^{+/-}$*; mTmG*$^{+/+}$*; Aldh1b1*$^{+/+}$ mice.

	Msh2+ Lgr5Cre+ mTmG+ Aldh1b1-	Msh2+ Lgr5Cre+ mTmG+ Aldh1b1+	Msh2+ Lgr5Cre- mTmG+ Aldh1b1-	Msh2+ Lgr5Cre- mTmG+ Aldh1b1+	Msh2+ Lgr5Cre+ mTmG- Aldh1b1-	Msh2+ Lgr5Cre+ mTmG- Aldh1b1+	Msh2+ Lgr5Cre- mTmG- Aldh1b1-	Msh2+ Lgr5Cre- mTmG- Aldh1b1+	Msh2fl Lgr5Cre+ mTmG+ Aldh1b1-	Msh2fl Lgr5Cre+ mTmG+ Aldh1b1+	Msh2fl Lgr5Cre- mTmG+ Aldh1b1-	Msh2fl Lgr5Cre- mTmG+ Aldh1b1+	Msh2fl Lgr5Cre+ mTmG- Aldh1b1-	Msh2fl Lgr5Cre+ mTmG- Aldh1b1+	Msh2fl Lgr5Cre- mTmG- Aldh1b1-	Msh2fl Lgr5Cre- mTmG- Aldh1b1+
Msh2- Lgr5Cre- mTmG+ Aldh1b1-	Msh2+/- Lgr5Cre+/- mTmG+/+ Aldh1b1f-/-	Msh2+/- Lgr5Cre+/- mTmG+/+ Aldh1b1-/+	Msh2+/- Lgr5Cre-/- mTmG+/+ Aldh1b1-/-	Msh2+/- Lgr5Cre-/- mTmG+/+ Aldh1b1-/+	Msh2+/- Lgr5Cre+/- mTmG+/- Aldh1b1-/-	Msh2+/- Lgr5Cre+/- mTmG+/- Aldh1b1-/+	Msh2+/- Lgr5Cre-/- mTmG+/- Aldh1b1-/-	Msh2+/- Lgr5Cre-/- mTmG+/- Aldh1b1-/+	Msh2fl/- Lgr5Cre+/- mTmG+/+ Aldh1b1-/-	Msh2fl/- Lgr5Cre+/- mTmG+/+ Aldh1b1-/+	Msh2fl/- Lgr5Cre-/- mTmG+/+ Aldh1b1-/-	Msh2fl/- Lgr5Cre-/- mTmG+/+ Aldh1b1-/+	Msh2fl/- Lgr5Cre+/- mTmG+/- Aldh1b1-/-	Msh2fl/- Lgr5Cre+/- mTmG+/- Aldh1b1-/+	Msh2fl/- Lgr5Cre-/- mTmG+/- Aldh1b1-/-	Msh2fl/- Lgr5Cre-/- mTmG+/- Aldh1b1-/+
Msh2- Lgr5Cre- mTmG+ Aldh1b1+	Msh2+/- Lgr5Cre+/- mTmG+/+ Aldh1b1-/+	Msh2+/- Lgr5Cre+/- mTmG+/+ Aldh1b1+/+	Msh2+/- Lgr5Cre-/- mTmG+/+ Aldh1b1-/+	Msh2+/- Lgr5Cre-/- mTmG+/+ Aldh1b1+/+	Msh2+/- Lgr5Cre+/- mTmG+/- Aldh1b1-/+	Msh2+/- Lgr5Cre+/- mTmG+/- Aldh1b1+/+	Msh2+/- Lgr5Cre-/- mTmG+/- Aldh1b1-/+	Msh2+/- Lgr5Cre-/- mTmG+/- Aldh1b1+/+	Msh2fl/- Lgr5Cre+/- mTmG+/+ Aldh1b1-/+	Msh2fl/- Lgr5Cre+/- mTmG+/+ Aldh1b1+/+	Msh2fl/- Lgr5Cre-/- mTmG+/+ Aldh1b1-/+	Msh2fl/- Lgr5Cre-/- mTmG+/+ Aldh1b1+/+	Msh2fl/- Lgr5Cre+/- mTmG+/- Aldh1b1-/+	Msh2fl/- Lgr5Cre+/- mTmG+/- Aldh1b1+/+	Msh2fl/- Lgr5Cre-/- mTmG+/- Aldh1b1-/+	Msh2fl/- Lgr5Cre-/- mTmG+/- Aldh1b1+/+
Msh2- Lgr5Cre- mTmG- Aldh1b1-	Msh2+/- Lgr5Cre+/- mTmG+/- Aldh1b1-/-	Msh2+/- Lgr5Cre+/- mTmG+/- Aldh1b1-/+	Msh2+/- Lgr5Cre-/- mTmG+/- Aldh1b1-/-	Msh2+/- Lgr5Cre-/- mTmG+/- Aldh1b1-/+	Msh2+/- Lgr5Cre+/- mTmG-/- Aldh1b1-/-	Msh2+/- Lgr5Cre+/- mTmG-/- Aldh1b1-/+	Msh2+/- Lgr5Cre-/- mTmG-/- Aldh1b1-/-	Msh2+/- Lgr5Cre-/- mTmG-/- Aldh1b1-/+	Msh2fl/- Lgr5Cre+/- mTmG+/- Aldh1b1-/-	Msh2fl/- Lgr5Cre+/- mTmG+/- Aldh1b1-/+	Msh2fl/- Lgr5Cre-/- mTmG+/- Aldh1b1-/-	Msh2fl/- Lgr5Cre-/- mTmG+/- Aldh1b1-/+	Msh2fl/- Lgr5Cre+/- mTmG-/- Aldh1b1-/-	Msh2fl/- Lgr5Cre+/- mTmG-/- Aldh1b1-/+	Msh2fl/- Lgr5Cre-/- mTmG-/- Aldh1b1-/-	Msh2fl/- Lgr5Cre-/- mTmG-/- Aldh1b1-/+
Msh2- Lgr5Cre- mTmG- Aldh1b1+	Msh2+/- Lgr5Cre+/- mTmG+/- Aldh1b1-/+	Msh2+/- Lgr5Cre+/- mTmG+/- Aldh1b1+/+	Msh2+/- Lgr5Cre-/- mTmG+/- Aldh1b1-/+	Msh2+/- Lgr5Cre-/- mTmG+/- Aldh1b1+/+	Msh2+/- Lgr5Cre+/- mTmG+/- Aldh1b1-/+	Msh2+/- Lgr5Cre+/- mTmG+/- Aldh1b1+/+	Msh2+/- Lgr5Cre-/- mTmG-/- Aldh1b1-/+	Msh2+/- Lgr5Cre-/- mTmG-/- Aldh1b1+/+	Msh2fl/- Lgr5Cre+/- mTmG+/- Aldh1b1-/+	Msh2fl/- Lgr5Cre+/- mTmG+/- Aldh1b1+/+	Msh2fl/- Lgr5Cre-/- mTmG+/- Aldh1b1-/+	Msh2fl/- Lgr5Cre-/- mTmG+/- Aldh1b1+/+	Msh2fl/- Lgr5Cre+/- mTmG-/- Aldh1b1-/+	Msh2fl/- Lgr5Cre+/- mTmG-/- Aldh1b1+/+	Msh2fl/- Lgr5Cre-/- mTmG-/- Aldh1b1-/+	Msh2fl/- Lgr5Cre-/- mTmG-/- Aldh1b1+/+
Msh2- Lgr5Cre- mTmG+ Aldh1b1-	Msh2+/- Lgr5Cre+/- mTmG+/+ Aldh1b1-/-	Msh2+/- Lgr5Cre+/- mTmG+/+ Aldh1b1-/+	Msh2+/- Lgr5Cre-/- mTmG+/+ Aldh1b1-/-	Msh2+/- Lgr5Cre-/- mTmG+/+ Aldh1b1-/+	Msh2+/- Lgr5Cre+/- mTmG+/- Aldh1b1-/-	Msh2+/- Lgr5Cre+/- mTmG+/- Aldh1b1-/+	Msh2+/- Lgr5Cre-/- mTmG+/- Aldh1b1-/-	Msh2+/- Lgr5Cre-/- mTmG+/- Aldh1b1-/+	Msh2fl/- Lgr5Cre+/- mTmG+/+ Aldh1b1-/-	Msh2fl/- Lgr5Cre+/- mTmG+/+ Aldh1b1-/+	Msh2fl/- Lgr5Cre-/- mTmG+/+ Aldh1b1-/-	Msh2fl/- Lgr5Cre-/- mTmG+/+ Aldh1b1-/+	Msh2fl/- Lgr5Cre+/- mTmG+/- Aldh1b1-/-	Msh2fl/- Lgr5Cre+/- mTmG+/- Aldh1b1-/+	Msh2fl/- Lgr5Cre-/- mTmG+/- Aldh1b1-/-	Msh2fl/- Lgr5Cre-/- mTmG+/- Aldh1b1-/+
Msh2- Lgr5Cre- mTmG+ Aldh1b1+	Msh2+/- Lgr5Cre+/- mTmG+/+ Aldh1b1-/+	Msh2+/- Lgr5Cre+/- mTmG+/+ Aldh1b1+/+	Msh2+/- Lgr5Cre-/- mTmG+/+ Aldh1b1-/+	Msh2+/- Lgr5Cre-/- mTmG+/+ Aldh1b1+/+	Msh2+/- Lgr5Cre+/- mTmG+/- Aldh1b1-/+	Msh2+/- Lgr5Cre+/- mTmG+/- Aldh1b1+/+	Msh2+/- Lgr5Cre-/- mTmG+/- Aldh1b1-/+	Msh2+/- Lgr5Cre-/- mTmG+/- Aldh1b1+/+	Msh2fl/- Lgr5Cre+/- mTmG+/+ Aldh1b1-/+	Msh2fl/- Lgr5Cre+/- mTmG+/+ Aldh1b1+/+	Msh2fl/- Lgr5Cre-/- mTmG+/+ Aldh1b1-/+	Msh2fl/- Lgr5Cre-/- mTmG+/+ Aldh1b1+/+	Msh2fl/- Lgr5Cre+/- mTmG+/- Aldh1b1-/+	Msh2fl/- Lgr5Cre+/- mTmG+/- Aldh1b1+/+	Msh2fl/- Lgr5Cre-/- mTmG+/- Aldh1b1-/+	Msh2fl/- Lgr5Cre-/- mTmG+/- Aldh1b1+/+
Msh2- Lgr5Cre- mTmG- Aldh1b1flox	Msh2+/- Lgr5Cre+/- mTmG+/- Aldh1b1-/-	Msh2+/- Lgr5Cre+/- mTmG+/- Aldh1b1-/+	Msh2+/- Lgr5Cre-/- mTmG+/- Aldh1b1-/-	Msh2+/- Lgr5Cre-/- mTmG+/- Aldh1b1-/+	Msh2+/- Lgr5Cre+/- mTmG-/- Aldh1b1-/-	Msh2+/- Lgr5Cre+/- mTmG-/- Aldh1b1-/+	Msh2+/- Lgr5Cre-/- mTmG-/- Aldh1b1-/-	Msh2+/- Lgr5Cre-/- mTmG-/- Aldh1b1-/+	Msh2fl/- Lgr5Cre+/- mTmG+/- Aldh1b1-/-	Msh2fl/- Lgr5Cre+/- mTmG+/- Aldh1b1-/+	Msh2fl/- Lgr5Cre-/- mTmG+/- Aldh1b1-/-	Msh2fl/- Lgr5Cre-/- mTmG+/- Aldh1b1-/+	Msh2fl/- Lgr5Cre+/- mTmG-/- Aldh1b1-/-	Msh2fl/- Lgr5Cre+/- mTmG-/- Aldh1b1-/+	Msh2fl/- Lgr5Cre-/- mTmG-/- Aldh1b1-/-	Msh2fl/- Lgr5Cre-/- mTmG-/- Aldh1b1-/+
Msh2- Lgr5Cre- mTmG- Aldh1b1+	Msh2+/- Lgr5Cre+/- mTmG+/- Aldh1b1-/+	Msh2+/- Lgr5Cre+/- mTmG+/- Aldh1b1+/+	Msh2+/- Lgr5Cre-/- mTmG+/- Aldh1b1-/+	Msh2+/- Lgr5Cre-/- mTmG+/- Aldh1b1+/+	Msh2+/- Lgr5Cre+/- mTmG-/- Aldh1b1-/+	Msh2+/- Lgr5Cre+/- mTmG-/- Aldh1b1+/+	Msh2+/- Lgr5Cre-/- mTmG-/- Aldh1b1-/+	Msh2+/- Lgr5Cre-/- mTmG-/- Aldh1b1+/+	Msh2fl/- Lgr5Cre+/- mTmG+/- Aldh1b1-/+	Msh2fl/- Lgr5Cre+/- mTmG+/- Aldh1b1+/+	Msh2fl/- Lgr5Cre-/- mTmG+/- Aldh1b1-/+	Msh2fl/- Lgr5Cre-/- mTmG+/- Aldh1b1+/+	Msh2fl/- Lgr5Cre+/- mTmG-/- Aldh1b1-/+	Msh2fl/- Lgr5Cre+/- mTmG-/- Aldh1b1+/+	Msh2fl/- Lgr5Cre-/- mTmG-/- Aldh1b1-/+	Msh2fl/- Lgr5Cre-/- mTmG-/- Aldh1b1+/+
Msh2+ Lgr5Cre- mTmG+ Aldh1b1flox	Msh2+/+ Lgr5Cre+/- mTmG+/+ Aldh1b1-/-	Msh2+/+ Lgr5Cre+/- mTmG+/+ Aldh1b1-/+	Msh2+/+ Lgr5Cre-/- mTmG+/+ Aldh1b1-/-	Msh2+/+ Lgr5Cre-/- mTmG+/+ Aldh1b1-/+	Msh2+/+ Lgr5Cre+/- mTmG+/- Aldh1b1-/-	Msh2+/+ Lgr5Cre+/- mTmG+/- Aldh1b1-/+	Msh2+/+ Lgr5Cre-/- mTmG+/- Aldh1b1-/-	Msh2+/+ Lgr5Cre-/- mTmG+/- Aldh1b1-/+	Msh2fl/+ Lgr5Cre+/- mTmG+/+ Aldh1b1-/-	Msh2fl/+ Lgr5Cre+/- mTmG+/+ Aldh1b1-/+	Msh2fl/+ Lgr5Cre-/- mTmG+/+ Aldh1b1-/-	Msh2fl/+ Lgr5Cre-/- mTmG+/+ Aldh1b1-/+	Msh2fl/+ Lgr5Cre+/- mTmG+/- Aldh1b1-/-	Msh2fl/+ Lgr5Cre+/- mTmG+/- Aldh1b1-/+	Msh2fl/+ Lgr5Cre-/- mTmG+/- Aldh1b1-/-	Msh2fl/+ Lgr5Cre-/- mTmG+/- Aldh1b1-/+
Msh2+ Lgr5Cre- mTmG+ Aldh1b1+	Msh2+/+ Lgr5Cre+/- mTmG+/+ Aldh1b1-/+	Msh2+/+ Lgr5Cre+/- mTmG+/+ Aldh1b1+/+	Msh2+/+ Lgr5Cre-/- mTmG+/+ Aldh1b1-/+	Msh2+/+ Lgr5Cre-/- mTmG+/+ Aldh1b1+/+	Msh2+/+ Lgr5Cre+/- mTmG+/- Aldh1b1-/+	Msh2+/+ Lgr5Cre+/- mTmG+/- Aldh1b1+/+	Msh2+/+ Lgr5Cre-/- mTmG+/- Aldh1b1-/+	Msh2+/+ Lgr5Cre-/- mTmG+/- Aldh1b1+/+	Msh2fl/+ Lgr5Cre+/- mTmG+/+ Aldh1b1-/+	Msh2fl/+ Lgr5Cre+/- mTmG+/+ Aldh1b1+/+	Msh2fl/+ Lgr5Cre-/- mTmG+/+ Aldh1b1-/+	Msh2fl/+ Lgr5Cre-/- mTmG+/+ Aldh1b1+/+	Msh2fl/+ Lgr5Cre+/- mTmG+/- Aldh1b1-/+	Msh2fl/+ Lgr5Cre+/- mTmG+/- Aldh1b1+/+	Msh2fl/+ Lgr5Cre-/- mTmG+/- Aldh1b1-/+	Msh2fl/+ Lgr5Cre-/- mTmG+/- Aldh1b1+/+
Msh2+ Lgr5Cre- mTmG- Aldh1b1flox	Msh2+/+ Lgr5Cre+/- mTmG+/- Aldh1b1-/-	Msh2+/+ Lgr5Cre+/- mTmG+/- Aldh1b1-/+	Msh2+/+ Lgr5Cre-/- mTmG+/- Aldh1b1-/-	Msh2+/+ Lgr5Cre-/- mTmG+/- Aldh1b1-/+	Msh2+/+ Lgr5Cre+/- mTmG-/- Aldh1b1-/-	Msh2+/+ Lgr5Cre+/- mTmG-/- Aldh1b1-/+	Msh2+/+ Lgr5Cre-/- mTmG-/- Aldh1b1-/-	Msh2+/+ Lgr5Cre-/- mTmG-/- Aldh1b1-/+	Msh2fl/+ Lgr5Cre+/- mTmG+/- Aldh1b1-/-	Msh2fl/+ Lgr5Cre+/- mTmG+/- Aldh1b1-/+	Msh2fl/+ Lgr5Cre-/- mTmG+/- Aldh1b1-/-	Msh2fl/+ Lgr5Cre-/- mTmG+/- Aldh1b1-/+	Msh2fl/+ Lgr5Cre+/- mTmG-/- Aldh1b1-/-	Msh2fl/+ Lgr5Cre+/- mTmG-/- Aldh1b1-/+	Msh2fl/+ Lgr5Cre-/- mTmG-/- Aldh1b1-/-	Msh2fl/+ Lgr5Cre-/- mTmG-/- Aldh1b1-/+
Msh2+ Lgr5Cre- mTmG- Aldh1b1+	Msh2+/+ Lgr5Cre+/- mTmG+/- Aldh1b1-/+	Msh2+/+ Lgr5Cre+/- mTmG+/- Aldh1b1+/+	Msh2+/+ Lgr5Cre-/- mTmG+/- Aldh1b1-/+	Msh2+/+ Lgr5Cre-/- mTmG+/- Aldh1b1+/+	Msh2+/+ Lgr5Cre+/- mTmG-/- Aldh1b1-/+	Msh2+/+ Lgr5Cre+/- mTmG-/- Aldh1b1+/+	Msh2+/+ Lgr5Cre-/- mTmG-/- Aldh1b1-/+	Msh2+/+ Lgr5Cre-/- mTmG-/- Aldh1b1+/+	Msh2fl/+ Lgr5Cre+/- mTmG+/- Aldh1b1-/+	Msh2fl/+ Lgr5Cre+/- mTmG+/- Aldh1b1+/+	Msh2fl/+ Lgr5Cre-/- mTmG+/- Aldh1b1-/+	Msh2fl/+ Lgr5Cre-/- mTmG+/- Aldh1b1+/+	Msh2fl/+ Lgr5Cre+/- mTmG-/- Aldh1b1-/+	Msh2fl/+ Lgr5Cre+/- mTmG-/- Aldh1b1+/+	Msh2fl/+ Lgr5Cre-/- mTmG-/- Aldh1b1-/+	Msh2fl/+ Lgr5Cre-/- mTmG-/- Aldh1b1+/+

Msh2+ Lgr5Cre- mTmG+ Aldh1b1flox	Msh2+/+ Lgr5Cre+/- mTmG+/+ Aldh1b1-/-	Msh2+/+ Lgr5Cre+/- mTmG+/+ Aldh1b1-/+	Msh2+/+ Lgr5Cre-/- mTmG+/+ Aldh1b1-/-	Msh2+/+ Lgr5Cre-/- mTmG+/+ Aldh1b1-/+	Msh2+/+ Lgr5Cre+/- mTmG+/- Aldh1b1-/-	Msh2+/+ Lgr5Cre+/- mTmG+/- Aldh1b1-/+	Msh2+/+ Lgr5Cre-/- mTmG+/- Aldh1b1-/-	Msh2+/+ Lgr5Cre-/- mTmG+/- Aldh1b1-/+	Msh2fl/+ Lgr5Cre+/- mTmG+/+ Aldh1b1-/-	Msh2fl/+ Lgr5Cre+/- mTmG+/+ Aldh1b1-/+	Msh2fl/+ Lgr5Cre-/- mTmG+/+ Aldh1b1-/-	Msh2fl/+ Lgr5Cre-/- mTmG+/+ Aldh1b1-/+	Msh2fl/+ Lgr5Cre+/- mTmG+/- Aldh1b1-/-	Msh2fl/+ Lgr5Cre+/- mTmG+/- Aldh1b1-/+	Msh2fl/+ Lgr5Cre-/- mTmG+/- Aldh1b1-/-	Msh2fl/+ Lgr5Cre-/- mTmG+/- Aldh1b1-/+
Msh2+ Lgr5Cre- mTmG+ Aldh1b1+	Msh2+/+ Lgr5Cre+/- mTmG+/+ Aldh1b1-/+	Msh2+/+ Lgr5Cre+/- mTmG+/+ Aldh1b1+/+	Msh2+/+ Lgr5Cre-/- mTmG+/+ Aldh1b1-/+	Msh2+/+ Lgr5Cre-/- mTmG+/+ Aldh1b1+/+	Msh2+/+ Lgr5Cre+/- mTmG+/- Aldh1b1-/+	Msh2+/+ Lgr5Cre+/- mTmG+/- Aldh1b1+/+	Msh2+/+ Lgr5Cre-/- mTmG+/- Aldh1b1-/+	Msh2+/+ Lgr5Cre-/- mTmG+/- Aldh1b1+/+	Msh2fl/+ Lgr5Cre+/- mTmG+/+ Aldh1b1-/+	Msh2fl/+ Lgr5Cre+/- mTmG+/+ Aldh1b1+/+	Msh2fl/+ Lgr5Cre-/- mTmG+/+ Aldh1b1-/+	Msh2fl/+ Lgr5Cre-/- mTmG+/+ Aldh1b1+/+	Msh2fl/+ Lgr5Cre+/- mTmG+/- Aldh1b1-/+	Msh2fl/+ Lgr5Cre+/- mTmG+/- Aldh1b1+/+	Msh2fl/+ Lgr5Cre-/- mTmG+/- Aldh1b1-/+	Msh2fl/+ Lgr5Cre-/- mTmG+/- Aldh1b1+/+
Msh2+ Lgr5Cre- mTmG- Aldh1b1flox	Msh2+/+ Lgr5Cre+/- mTmG+/- Aldh1b1-/-	Msh2+/+ Lgr5Cre+/- mTmG+/- Aldh1b1-/+	Msh2+/+ Lgr5Cre-/- mTmG+/- Aldh1b1-/-	Msh2+/+ Lgr5Cre-/- mTmG+/- Aldh1b1-/+	Msh2+/+ Lgr5Cre+/- mTmG-/- Aldh1b1-/-	Msh2+/+ Lgr5Cre+/- mTmG-/- Aldh1b1-/+	Msh2+/+ Lgr5Cre-/- mTmG-/- Aldh1b1-/-	Msh2+/+ Lgr5Cre-/- mTmG-/- Aldh1b1-/+	Msh2fl/+ Lgr5Cre+/- mTmG+/- Aldh1b1-/-	Msh2fl/+ Lgr5Cre+/- mTmG+/- Aldh1b1-/+	Msh2fl/+ Lgr5Cre-/- mTmG+/- Aldh1b1-/-	Msh2fl/+ Lgr5Cre-/- mTmG+/- Aldh1b1-/+	Msh2fl/+ Lgr5Cre+/- mTmG-/- Aldh1b1-/-	Msh2fl/+ Lgr5Cre+/- mTmG-/- Aldh1b1-/+	Msh2fl/+ Lgr5Cre-/- mTmG-/- Aldh1b1-/-	Msh2fl/+ Lgr5Cre-/- mTmG-/- Aldh1b1-/+
Msh2+ Lgr5Cre- mTmG- Aldh1b1+	Msh2+/+ Lgr5Cre+/- mTmG+/- Aldh1b1-/+	Msh2+/+ Lgr5Cre+/- mTmG+/- Aldh1b1+/+	Msh2+/+ Lgr5Cre-/- mTmG+/- Aldh1b1-/+	Msh2+/+ Lgr5Cre-/- mTmG+/- Aldh1b1+/+	Msh2+/+ Lgr5Cre+/- mTmG-/- Aldh1b1-/+	Msh2+/+ Lgr5Cre+/- mTmG-/- Aldh1b1+/+	Msh2+/+ Lgr5Cre-/- mTmG-/- Aldh1b1-/+	Msh2+/+ Lgr5Cre-/- mTmG-/- Aldh1b1+/+	Msh2fl/+ Lgr5Cre+/- mTmG+/- Aldh1b1-/+	Msh2fl/+ Lgr5Cre+/- mTmG+/- Aldh1b1+/+	Msh2fl/+ Lgr5Cre-/- mTmG+/- Aldh1b1-/+	Msh2fl/+ Lgr5Cre-/- mTmG+/- Aldh1b1+/+	Msh2fl/+ Lgr5Cre+/- mTmG-/- Aldh1b1-/+	Msh2fl/+ Lgr5Cre+/- mTmG-/- Aldh1b1+/+	Msh2fl/+ Lgr5Cre-/- mTmG-/- Aldh1b1-/+	Msh2fl/+ Lgr5Cre-/- mTmG-/- Aldh1b1+/+

Supplementary Table 6.4: Tabular representation of the generation of the *Aldh1b1* constitutive-knockout Msh2-LS mouse model experimental subjects. Representation of the breeding between the $Msh2^{+/-}$; $Lgr5CreERT2^{-/-}$; $mTmG^{+/-}$; $Aldh1b1^{+/-}$ with $Msh2^{flox/+}$; $Lgr5CreERT2^{+/-}$; $mTmG^{+/-}$; $Aldh1b1^{+/-}$ mice.

Appendix 2

Journal of Pathology
J Pathol 2020; **250:** 518–531
Published online 28 April 2020 in Wiley Online Library (wileyonlinelibrary.com) DOI: 10.1002/path.5422

INVITED REVIEW

Molecular pathology of Lynch syndrome

Guia Cerretelli[1], Ann Ager[2], Mark J Arends[1] and Ian M Frayling[3]*

[1] *Division of Pathology, Cancer Research UK Edinburgh Centre, University of Edinburgh, Edinburgh, UK*
[2] *Division of Infection and Immunity, School of Medicine and Systems Immunity Research Institute, Cardiff University, Cardiff, UK*
[3] *Inherited Tumour Syndromes Research Group, Institute of Cancer & Genetics, School of Medicine, Cardiff University, Cardiff, UK*

**Correspondence to: IM Frayling, Inherited Tumour Syndromes Research Group, Institute of Cancer & Genetics, School of Medicine, Cardiff University, CF14 4XN, UK. E-mail: fraylingim@cardiff.ac.uk*

Abstract

Lynch syndrome (LS) is characterised by predisposition to colorectal, endometrial, and other cancers and is caused by inherited pathogenic variants affecting the DNA mismatch repair (MMR) genes *MLH1*, *MSH2*, *MSH6*, and *PMS2*. It is probably the most common predisposition to cancer, having an estimated prevalence of between 1/100 and 1/180. Resources such as the International Society for Gastrointestinal Hereditary Cancer's MMR gene variant database, the Prospective Lynch Syndrome Database (PLSD), and the Colon Cancer Family Register (CCFR), as well as pathological and immunological studies, are enabling advances in the understanding of LS. These include defined criteria by which to interpret gene variants, the function of MMR in the normal control of apoptosis, definition of the risks of the various cancers, and the mechanisms and pathways by which the colorectal and endometrial tumours develop, including the critical role of the immune system. Colorectal cancers in LS can develop along three pathways, including flat intramucosal lesions, which depend on the underlying affected *MMR* gene. This gives insights into the limitations of colonoscopic surveillance and highlights the need for other forms of anti-cancer prophylaxis in LS. Finally, it shows that the processes of autoimmunisation and immunoediting fundamentally constrain the development of tumours in LS and explain the efficacy of immune checkpoint blockade therapy in MMR-deficient tumours.

Keywords: Lynch syndrome; colorectal cancer; endometrial cancer; DNA mismatch repair; apoptosis; gene database; gene variant interpretation; immunoediting; immunotherapy

Received 9 February 2020; Revised 2 March 2020; Accepted 3 March 2020

No conflicts of interest were declared.

Introduction

Lynch syndrome (LS), previously called hereditary non-polyposis colorectal cancer (HNPCC), is probably the most common major cause of inherited susceptibility to cancer, with an estimated prevalence in the general population of between 1/100 and 1/180 [1]. LS is characterised by predisposition to a range of cancers, involving most frequently the colorectum and endometrium, and also many other organ sites including ovary, stomach, small intestine, hepatobiliary tract, pancreas, urinary tract, prostate, brain, and sebaceous skin tumours [2,3].

LS is caused by constitutional (germline) pathogenic variants affecting one of four genes encoding the DNA Mismatch Repair (MMR) system components: *MLH1*, *MSH2*, *MSH6*, and *PMS2*, and hence the current commonly accepted diagnostic definition of LS is carrying such a variant [1,4–8]. However, although we acknowledge that there is an opinion that LS can only be diagnosed in such individuals once cancer has been diagnosed, this is contrary to the hereditary polyposes, which are characterised by the macroscopic syndromic feature of multiple pre-malignant tumours [9]. Allied to this, a major purpose of diagnosis of a cancer-predisposing condition is to identify those who would benefit from surveillance and prophylactic surgery to prevent cancer [5]. Hence, our view is that it is inconsistent and to a degree cruel to discriminate against LS by expecting such individuals to develop cancer in order to be diagnosed with the condition, especially as cancer does not always occur [2,3,10]. As we discuss later on, the definition of LS could, and perhaps should, therefore, move to one that incorporates recently identified specific microscopic and molecular pre-malignant syndromic features.

DNA MMR recognises and repairs mismatched bases (*e.g.* C opposite T) and insertions or deletions in repetitive sequences. In LS patients, this *MMR* gene constitutional variant, when combined with an acquired second pathogenic variant due to somatic mutation in the wild-type allele of the same *MMR* gene, results in the complete loss of MMR pathway function in the affected cells. Deficiency of MMR (dMMR) leads to hypermutability, resulting in an increase in the mutation rate by 100- to 1000-fold due to uncorrected base mismatches,

and to microsatellite instability (MSI) due to variation in the lengths of repetitive sequences (*e.g.* AAAAAAA… or CACACACA…. or similar, known as microsatellites) due to uncorrected insertion/deletion loops that are prone to occur as DNA replication errors in repetitive sequences [11]. However, crucially, dMMR does not simply fail to repair mismatches, it elicits a reduced susceptibility to apoptosis induced by DNA damage recognised by the MMR pathway [11–14].

The International Society for Gastrointestinal Hereditary Cancer (InSiGHT) was the first expert group to define pathogenicity of gene variants according to an agreed set of criteria based upon Bayesian probability, using the five-tier classification system of Plon *et al* [4,15–17]. In this system, Class 5 variants are pathogenic and Class 4 likely pathogenic, with Class 3 being variants of uncertain significance (VUS), and Classes 2 and 1 being likely benign and benign respectively. InSiGHT maintains the world reference database of variants observed in *MMR* genes, as Leiden Open Variation Databases (LOVDs), which are now linked to ClinVar as part of the ClinVar-ClinGen partnership, and accordingly, 82% of the Class 4 and 5 variants listed affect *MLH1* and *MSH2*, with 13% affecting *MSH6* and 5% *PMS2* [16,18–20]. It should be noted that these pathogenic variants are mostly from cases ascertained by family history. As more cases of LS are ascertained from systematic testing of cancer cases and incidentally from gene panel testing, more patients will be identified with pathogenic variants in *MSH6* and *PMS2*, and thus the proportions due to the different MMR genes will alter [6].

All types of variants are seen as pathogenic: nonsense, frameshift, splice-site, missense, insertion–deletion, and large deletions/rearrangements, the largest so far being a 10 Mb inversion affecting *MSH2* and which is visible cytogenetically [21–23]. Approximately 60% of all putative pathogenic missense mutations causing LS actually disrupt splicing and are thus, in effect, truncating [24]. Up to 3% of LS cases are due to variants involving the 3′ end of the *EPCAM* gene (immediately adjacent to *MSH2*), that result in hypermethylation of the *MSH2* promoter or partial deletion of *MSH2* [25,26]. Another infrequent but important cause of LS is constitutional methylation of the *MLH1* promoter, which occurs in 1–2% of cases [27–29]. This is usually sporadic in nature, so it is neither inherited nor heritable, and relatives are therefore not at risk. However, in a small number of patients, the hypermethylation may be secondary to a large deletion involving *LRRFIP2*, the gene upstream of *MLH1*, and it is the deletion that is the pathogenic variant: The methylation is secondary [29]. Given the risks to relatives it is therefore important to distinguish such cases, and this is achieved by testing both the tumour and constitutional DNA, and finding *MLH1* promoter methylation in both, perhaps in the context of an LS family history. It has to be borne in mind that approximately 15% of sporadic *colon* cancers are also dMMR due to somatic, so acquired, epimutation of both *MLH1* alleles by promoter hypermethylation [30]. This is a function of such tumours arising from right-sided serrated lesions [31]. A similar proportion of sporadic *endometrial* cancers also have biallelic hypermethylation of *MLH1*, and as with colon cancers a small proportion are due to constitutional methylation plus a somatic mutation in the normal *MLH1* allele [27,28,32,33].

Other genetic conditions relating to Lynch syndrome

Muir-Torre syndrome (MTS) is a descriptive diagnosis of an individual in which both skin sebaceous neoplasms (and keratoacanthoma-like lesions) and a 'visceral' carcinoma of any sort has occurred [34,35]. It is a frequently seen combination in LS. Indeed, on close inspection many, perhaps most patients with LS who have had a carcinoma probably have a sebaceous skin lesion and thus MTS [36,37]. However, MTS is also seen in other heritable predispositions, for example, *MUTYH*-associated adenomatous polyposis, or it may be sporadic, so although a marker of possible LS, MTS is not diagnostic [38,39]. Notably, although sebaceous lesions and hyperplasia are often rightly a cause for concern regarding LS and a patient with sebaceous lesions and a visceral cancer warrants testing, it should be noted that in the absence of a family or personal history of LS-associated cancer they are at low risk and do not warrant testing [40,41].

Individuals may inherit pathogenic variants in both copies of a DNA *MMR* gene. When both are in the same gene it causes constitutional mismatch repair deficiency (CMMR-D) syndrome. CMMR-D is a classic recessive DNA repair disorder typically characterised by childhood-onset leukaemia, lymphoma, and colorectal and brain cancers, but also, in contrast to LS, some patients may have multiple colorectal adenomas [42–44]. Signs suggestive of neurofibromatosis type 1 also often occur, such as café-au-lait macules and cutaneous neurofibromata, plus other features such as immune deficiency [45]. In CMMR-D patients, abnormal MMR immunohistochemistry (IHC) is seen in both normal and tumour cells (hence the necessity always to test all four markers) and it is possible to detect constitutional MSI in, for example, blood [46,47]. Patients with CMMR-D due to *MSH6* or *PMS2* variants may show milder disease and later onset [48]. Comprehensive diagnostic criteria and care pathways have been published [7,45].

Patients may also be found who have pathogenic variants in more than one MMR gene, so-called digenic LS. It is not clear if this is more severe than LS due to a pathogenic variant in one gene, but it has clear implications for clinical genetic counselling. However, LS patients can and do co-inherit other forms of predisposition to cancer (or indeed any other genetic condition), and if this is suspected should be pursued [49].

Finally, Turcot syndrome, a combination of colorectal cancer or adenomas and central nervous system tumours, with dominant or recessive inheritance, is another historical descriptive diagnosis that has been related to

LS. However, it is now known that it can be due to CMMR-D, familial adenomatous polyposis (FAP), and probably other conditions, and so as an ambiguous term it should be abandoned [42,44,50].

DNA mismatch repair mechanisms

The MMR pathway is a highly evolutionarily conserved mechanism responsible for the correction of base mismatches (*e.g.* C or G opposite T or A) and insertion/deletion loops (occurring in repetitive sequences such as AAAAAA … or CACACACA … due to insertion or deletion of an extra repeat unit during stalled DNA replication of these repetitive sequences). Such stalling is probably mostly due to replication-associated errors, but is also caused by DNA damage due to oxidative stress, lipid peroxidation, base deamination, methylation, and alkylation [51].

A base mismatch or single nucleotide insertion/deletion error is recognised by the MutSα complex, which is composed of MSH2 and MSH6 proteins. Insertion/deletion loops of 2–8 nucleotides are recognised by the alternative complex MutSβ, composed of MSH2 and MSH3 proteins. MutSα complex activation is characterized by ATPase activity, which is important for the interaction with the mismatched DNA and initiation of repair. The binding of MutSα stimulates ATP hydrolysis, leading to a conformational change that subsequently triggers the recruitment of a second complex MutLα, composed of MLH1 and PMS2 proteins. The tetrameric complex, by sliding on the DNA, searches for the single-strand DNA mismatch on the new strand (daughter strand). This in turn activates proliferating cell nuclear antigen (PCNA) and replication factor C (RFC). MutLα possesses an intrinsic ATP-stimulated endonuclease activity that requires activation by PCNA in order to create an incision in the recently synthesised daughter strand (containing the error). The incision step is followed by the recruitment of exonuclease 1 (EXO1) that removes the newly synthesised DNA strand up to and beyond the mismatch or loop. DNA polymerase δ re-synthesises the DNA, whereas ligase 1 seals the remaining nick [52].

The MMR pathway is involved in a signalling cascade that leads to cell cycle arrest and/or apoptosis, if DNA damage has occurred previously [53]. It has been observed that MMR-deficient cells fail to recruit ataxia-telangiectasia mutated (ATM) and ATM and Rad3-related (ATR); and this prevents p53 phosphorylation in response to DNA damage [12,54]. The underlying mechanisms by which MMR proteins promote DNA damage–induced cell cycle arrest and apoptosis have not been fully elucidated. Two models have been hypothesised: The futile cycling model and the direct damage signalling model. In the futile cycling model, MMR recognises the mismatches triggering the excision of the newly synthesized strand, although the persistent offending damage on the template strand cannot be excised. MMR initiates futile repair cycles, eventually resulting in the formation of DNA double-strand breaks and thus activating the ATM/ATR/p53 signalling pathway to activate cell cycle arrest and/or apoptosis [55]. In the direct damage signalling model, MutSα and MutLα directly recruit ATM/ATR and cause cell cycle arrest and/or apoptosis [56].

A crucial consequence of this is that the low background level of DNA damage in normal cells may stimulate MMR and thus inhibit the cell cycle, or if severe even stimulate apoptosis, and so net cell turnover does not reach its theoretical maximum. However, if MMR deficiency should occur in such cells, there is no such limitation by stalling of the cell cycle or activation of apoptosis and net cell division increases in an uncontrollable fashion, allied to which as a secondary phenomenon the mutation rate increases, which is manifest as MSI and/or abnormal MMR IHC. This is very useful diagnostically, but it is important to appreciate that it is not the increased mutation rate *per se* that is driving the carcinogenic process, and neither does it make adenomas progress any quicker than usual [14]. However, because mutations are strongly biased towards repetitive DNA sequences in dMMR cells, this has profound consequences for the biology of such tumours and patients with LS due to the strong immunological responses this elicits [57,58]. The critical consequences of this are manifest in how LS tumours develop and potentially evade the immune system [59].

Notably, some *MMR* gene variants are associated with abnormal MMR IHC in tumours but not MSI, and *vice versa* [4,15]. In addition, only one of 149 *PMS2* pathogenic variants causative of LS is a missense mutation [18]. However, many other *PMS2* missense variants are seen in CMMR-D (a recessive DNA repair disorder), which is consistent with common, but not complete, overlap between loss of DNA (MMR-recognised) damage repair and apoptotic functions of MMR [18,60,61].

Lynch syndrome databases

In addition to the *MMR* gene variant database maintained by InSiGHT, there are other phenotypic databases aimed at understanding the precise risks that LS patients face. Initial estimates were liable to ascertainment bias and thus tended to overestimate by being necessarily retrospective. The penetrance and expressivity of MMR pathogenic variants differs in LS patients according to the *MMR* gene, age, sex and environmental/lifestyle factors [62]. Several lifestyle factors, such as smoking, alcohol, obesity, are associated with an increased risk of sporadic cancer and have been suggested to have similar effects in LS patients. Therefore, as it is fundamental to quantify accurately the risks of developing cancer for LS patients, in order to provide adequate data for surveillance and care, as well as understand the underlying biology, the PLSD was established in 2012 by the Mallorca Group of InSiGHT [2,63]. The PLSD collects data on LS patients from expert centres and registries worldwide; these patients are thus undergoing colonoscopic surveillance with polypectomy and may also be having therapeutic or prophylactic surgery. It therefore provides

information on the natural history of the disease course and the effects of interventions and lifestyle factors. The PLSD is linked to the InSiGHT MMR LOVD: All patients on the PLSD must have a Class 4 or 5 MMR variant, so pathogenic or likely pathogenic according to the InSiGHT classification [4,15]. The PLSD includes basic information on pathogenic genetic variants, sex, and age, plus information such as cancers or pre-cancers diagnosed, age at diagnoses, age at prophylactic surgical removal of organs, and information on pre-cancers. Every patient is followed as an individual, as the family history is ignored so as not to introduce bias, and the database now has >50 000 patient-years of observations [10]. The PLSD website is public and allows anyone to determine the risks to an individual of an LS-associated cancer in an interactive graphical form according to their affected gene, age, gender, and whether previously affected by cancer [63]. Risks of LS-associated cancers to age 75 are summarised in Table 1; those for *PMS2* affecting both sexes are combined due to the smaller numbers available, and numbers have been rounded throughout for clarity [10].

Important parallel efforts have been made in defining risks in Lynch syndrome by the CCFR and the International Mismatch Repair Consortium (IMRC) [64,65]. The CCFR is an international consortium of six institutes in the United States, Canada, and Australasia formed as a resource to support studies on the aetiology, prevention, and clinical management of colorectal cancer, and utilises a form of modified segregation analysis to minimise retrospective ascertainment bias [65,66]. It currently has data on >42 500 individuals from >15 000 families on its records and has made significant advances in demonstrating how environmental and lifestyle factors affect cancer risks in LS, such as smoking, increased body mass index, and alcohol consumption [67–69]. By contrast, reduced cancer risk is seen with, for example, hormone replacement therapy, vitamin and mineral supplements, nonsteroidal anti-inflammatory drug (NSAID) use, and parity, but there is no change in risk associated with oral contraceptive use [70,71]. The IMRC is a worldwide collaboration of more than 115 investigators from 59 centres, with 20 000 individuals with LS from 8800 families, facilitated by InSiGHT and the Collaborative Group of the Americas on Inherited Gastrointestinal Cancer (CGA-IGC) [64,72].

Finally, is the initiative to determine the effects of aspirin prophylaxis on LS patients, although this is a series of clinical trials rather than a database. Remarkably, the CAPP2 trial has shown that only 2–4 years of treatment with 600 mg/d of aspirin significantly reduces the risk of colorectal cancer up to more than 10 years post treatment, and likely also reduces the risks of other

Table 1 Average risks of Lynch syndrome–associated cancers to age 75 years

Males				
Cancer type	*MLH1*	*MSH2*	*MSH6*	*PMS2*
Any cancer	71% [63–81%]	75% [66–86%]	42% [25–67%]	See below
Colorectal (bowel)	57% [49–68%]	51% [41–65%]	18% [8–43%]	See below
Stomach, small bowel, bile duct, gallbladder, and pancreas	22% [16–30%]	20% [14–28%]	8% [3–30%]	See below
Ureter and kidney	5% [3–10%]	18% [13–25%]	2% [<1–24%]	See below
Urinary bladder	7% [4–13%]	13% [8–21%]	8% [3–30%]	See below
Prostate	14% [9–22%]	24% [17–33%]	9% [3–31%]	5% [<1–68%]
Brain	0.7% [<1–5%]	8% [4–15%]	2% [<1–24%]	See below
Females				
Cancer type	*MLH1*	*MSH2*	*MSH6*	*PMS2*
Any cancer	81% [74–88%]	84% [77–91%]	62% [47–78%]	See below
Colorectal (bowel)	48% [41–57%]	47% [39–55%]	20% [12–41%]	See below
Endometrium	37% [30–47%]	49% [40–61%]	41% [29–62%]	3% [5–50%]
Ovaries	11% [7–20%]	17% [12–31%]	11% [4–39%]	3% [<1–43%]
Stomach, small bowel, bile duct, gallbladder, and pancreas	11% [7–17%]	13% [9–19%]	4% [3–30%]	See below
Ureter and kidney	4% [2–8%]	19% [14–27%]	6% [2–27%]	See below
Urinary bladder	5% [3–11%]	8% [5–14%]	1% [<1–23%]	See below
Brain	2% [<1–5%]	3% [1–8%]	1% [<1–23%]	See below
Both Sexes combined				
Cancer type				*PMS2*
Any cancer				34% [19–60%]
Colorectal (bowel)				10% [3–41%]
Stomach, small bowel, bile duct, gallbladder, and pancreas				4% [1–34%]
Ureter and kidney				4% [<1–34%]
Urinary bladder				<1% [0–31%]
Brain				<1% [0–31%]

Data from the Prospective Lynch Syndrome Database (PLSD) [10,63].
Note that the individuals studied are under colonoscopic surveillance and may have had prophylactic or therapeutic surgery, which is allowed for in the estimates.

LS cancers, although this is less certain. Notably, side-effects possibly attributable to aspirin were at a low rate and actually slightly more common, although non-significantly, in the placebo compared to treatment arm [73–75]. A follow-up randomised double-blind dose non-inferiority trial, CaPP3, is now in progress to determine the optimum dose of aspirin for long-term prophylaxis [76].

Pathology of Lynch syndrome cancers

Typical histological features of LS tumours are best exemplified by colorectal cancer (CRC), which often shows a combination of the presence of prominent tumour-infiltrating lymphocytes, Crohn-like peritumoural lymphoid aggregates, poor differentiation, frequently with areas of mucinous and/or signet-ring cell patterns, sometimes with a medullary growth pattern [77,78]. These characteristics can be seen in both Lynch syndrome CRC and sporadic dMMR bowel cancers but are not sufficiently specific to distinguish them from MMR-proficient (pMMR) cancers.

Fewer data have been published about non-colorectal LS-associated cancers. LS-associated endometrial cancers can be seen more frequently than sporadic cancers in the lower uterine segment, are mostly of the endometrioid type, and are often with poor differentiation, solid or dyscohesive, with prominent tumour-infiltrating lymphocytes and Crohn-like peritumoural lymphoid aggregates [79–84]. LS-associated ovarian cancers are typically of endometrioid or clear cell type, with some tumour-infiltrating lymphocytes [79,80,85,86]. LS-associated gastric carcinomas are mostly of the intestinal-type with fewer diffuse-type, and rarely of mucinous type, and an associated immune gastritis is reported [87–90]. LS-associated small intestinal adenocarcinomas often display mucinous, signet-ring cell, or medullary differentiation, with tumour-infiltrating lymphocytes and Crohn-like reactions, as do ampullary adenocarcinomas [91]. LS-associated pancreatic cancers are mostly acinar cell carcinomas and medullary carcinomas [92].

Testing for Lynch syndrome cancers

Testing of (usually selected) patients with CRC, endometrial cancer, and/or other types of LS-associated cancer is recommended by many guidelines and organisations, generally starting with testing the tumours for either the presence of MSI or the absence (or abnormal expression) of mismatch repair proteins. There is no consensus regarding whether MMR immunohistochemistry or MSI testing is the better first test in *colorectal* cancers as they have similar test performance characteristics in detecting LS: Sensitivity of MSI is 88 ~ 100% and IHC 73 ~ 100%, with specificity of MSI 68 ~ 84% versus IHC 78 ~ 98% [93,94]. They may be used serially, or in combination [93–97]. However, evidence is now emerging that IHC may be the preferred option when testing *endometrial* cancers (systematic testing of which is now under consideration by the UK National Institute for Health and Care Excellence (NICE) as a recent UK study has shown that while MSI and IHC have similar specificity (83.7 versus 81%), MSI has only 56.3% sensitivity compared to 100% for IHC [82,83].

MMR IHC is the better option for small biopsies, cancers with a low tumour cell proportion, or intense inflammatory reaction. Subsequent testing for *MLH1* promoter hypermethylation and somatic (rather than constitutional/germline) mutations can be used to clarify the risk of inherited pathogenic variants in suspected LS patients. *MLH1* promoter hypermethylation testing may be used as an alternative to *BRAF* V600E mutation analysis in colonic cancers [98–100]. The use of larger targeted gene mutation panels (or whole exome/genome sequencing) that includes MMR tumour testing with mutation analyses is becoming more widespread [101].

Immunohistochemical staining for the four major DNA mismatch repair proteins (MLH1, MSH2, MSH6, and PMS2) is probably the most common test to screen CRCs and other tumours for dMMR [93,95,97]. The nuclear expression of all four proteins suggests mismatch repair proficiency with microsatellite stability [102–104]. Loss or abnormality of nuclear staining for any of the proteins indicates dMMR and suggests the most likely *MMR* gene involved [103,104]. Loss of MSH2 alone or loss of both MSH2 and MSH6 suggests that a mutation or abnormality in MSH2 is most likely. Similarly, loss of MLH1 alone or loss of both MLH1 and PMS2 suggests an underlying mutation, abnormality, or promoter methylation in MLH1. Combined loss of both MSH2 and MSH6 (or of both MLH1 and PMS2) reflects the heterodimeric binding of MSH2 with MSH6 (or of MLH1 with PMS2) in the mismatch repair complex MutSα (or of MutLα), such that loss of the first protein partner generates instability and loss of the second [37]. Usually, there is nuclear staining in the nuclei of both tumour cells and adjacent normal epithelial cells, stromal cells, and lymphocytes.

In a dMMR tumour due to *MSH2* mutation, there is loss of nuclear MSH2 and MSH6 and intact staining for MLH1 and PMS2. In a dMMR tumour due to *MLH1* mutation, there is loss of nuclear MLH1 and PMS2 and intact staining for MSH2 and MSH6. This pattern of combined MLH1 and PMS2 loss could be seen either in a sporadic tumour (most commonly due to *MLH1* promoter methylation) or in LS due to constitutional *MLH1* mutation. Correct MMR IHC interpretation requires adequate internal control staining of the adjacent stromal and lymphoid cells to confirm good fixation of the tissue region [102,103]. Patchy intact nuclear staining may occur due to variable fixation, tissue hypoxia, or unequal antibody diffusion [105,106]. Cytoplas-
105,106]. Cytoplasmic staining may occur, but if nuclear staining is lost, this is considered abnormal, indicating dMMR [107]. Weak, patchy nucleolar staining, or sometimes absence of MSH6 has been described in rectal tumours following neoadjuvant treatment without MSI or a mutation confirmed by molecular testing [108,109]. Notably, heterogeneous staining or loss of

MSH6 can be due to a secondary (non-germline) acquired somatic mutation in the *MSH6* coding mononucleotide tract [110,111]. Approximately 3–10% of LS-associated dMMR tumours show no abnormality on IHC testing (presumably because of variants that disrupt normal MMR protein function but nonetheless enable protein detection by IHC) [112].

Testing DNA extracted from tumours for MSI involves investigating the presence of extra alleles (longer or shorter) at a microsatellite locus compared with normal microsatellite length determined from normal tissue or blood from the same individual [113]. Microsatellites vary in their propensity to show instability, and thus the frequency with which the same microsatellite is altered varies in different tumour types. Instability is more likely to be observed at mononucleotide repeats (*e.g.* AAAAA …) than at dinucleotide repeats (*e.g.* CACACA …). Microsatellite loci or markers used in colonic cancer MSI testing are known to have reduced sensitivity at detecting MSI in non-colonic cancers, including endometrial, small intestinal, or gastric cancers; in tumours from LS patients with *MSH6* or *PMS2* mutations; and in colonic adenomas [114]. Therefore, a proportion of LS-associated tumours may not appear to have MSI using the standard test but might be identified by abnormal MMR immunohistochemistry.

The efficacy of MMR IHC and MSI may be significantly enhanced by testing more than one tumour from the same individual or family, particularly if there are tumours that are multiple or rarely seen in LS (*e.g.* colorectal adenomas, small intestinal cancers, hepatobiliary, upper urinary tract, and cutaneous sebaceous tumours) [15,115]. Consistent IHC abnormality of one mismatch repair protein in more than one tumour from an individual or family represents very good evidence for variant pathogenicity [15,116]. Some CRCs due to *MUTYH*-associated polyposis (MAP) or proofreading polymerase-associated polyposis (PPAP) may exhibit MSI and/or abnormal IHC due to somatically acquired *MMR* gene mutations.

Approximately 13–15% of sporadic colonic cancers have dMMR, usually due to epigenetic silencing of both alleles of *MLH1* by promoter hypermethylation. Hence, although overall unselected dMMR colonic cancers have a relatively poor positive predictive value for LS, because the proportion of colonic cancers with MSI due to LS varies with age this can be exploited clinically. In individuals younger than the age of 57, more than half of all dMMR colonic cancers will be due to LS, whereas over this age less than half will be, although even at age 70 approximately 25% dMMR colonic cancers will be due to LS (Figure 1) [8,104,117]. In contrast, pMMR has a good negative predictive value for LS. Further tests (*BRAF* mutation and *MLH1* methylation tests) are required for MLH1-negative cancers to distinguish between LS and sporadic origin [93,94,96]. Another important practice point is that *rectal* cancers are distinct from *colonic* cancers in the diagnosis of LS. Because sporadic colonic cancers with dMMR arise largely from right-sided serrated lesions, sporadic rectal cancers with dMMR are correspondingly rare, if they occur at all, and hence a rectal cancer with dMMR at any age must be considered to be due to LS until proven otherwise [118,119].

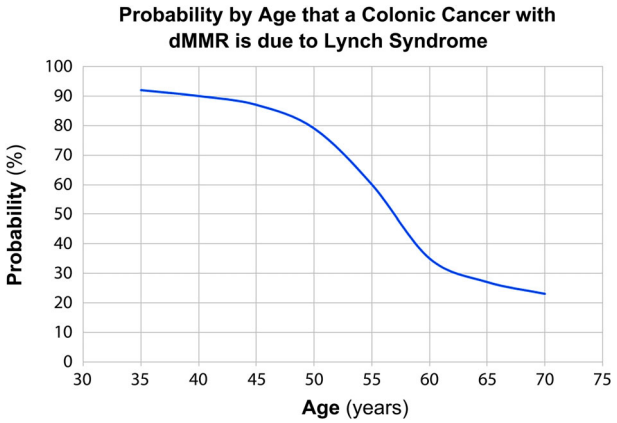

Figure 1. Probability by age that a colonic cancer with dMMR is due to Lynch syndrome. The graph shows the probability by age that a colonic cancer with dMMR is due to Lynch syndrome [8,104,117]. Note that this does not apply to rectal cancers, because right-sided serrated lesions that give rise to sporadic dMMR colonic cancers do not occur in the rectum; hence a rectal cancer with dMMR is due to LS until proven otherwise [118,119].

The activating missense variant *BRAF* p.V600E occurs in sporadic colonic cancers with dMMR, but not in those due to LS; therefore, *BRAF* p.V600E is highly predictive of the tumour being of sporadic origin rather than LS [31,93,94,96,120]. However, sporadic tumours may occasionally occur in patients with LS, so the absence of *BRAF* p.V600E does not definitively diagnose LS but does indicate that LS is more likely. Alternatively, detection of *MLH1* promoter hypermethylation in a colonic cancer provides good, although not unequivocal, evidence that the tumour is sporadic in origin, as occasional sporadic tumours do occur in LS and constitutional *MLH1* promoter methylation can be found in a small proportion of patients with LS [28,29]. *BRAF* p.V600E testing is only of use in distinguishing CRCs; it has no utility in, for example, endometrial cancer.

LS is definitively diagnosed following tumour testing by constitutional/germline MMR gene sequencing to identify a pathogenic constitutional variant [4–6,121]. Patients with digenic LS, who have inherited pathogenic variants in more than one *MMR* gene, are occasionally seen (and more will be as gene panel testing becomes prevalent), but it is unclear if their risks are increased over those patients with a pathogenic variant in one MMR gene. It is often useful to have samples from more than one individual in the family, because case segregation studies may be required to determine pathogenicity or whether an individual is a phenocopy [4,15]. If the family shows evidence of hereditary transmission of LS but no point mutation is found, tests for large-scale mutations, such as deletion of a whole exon (or more), can be performed; 12–40% of pathogenic variants are of this type [21,23,122–127]. LS-related tumour types that are rare in the general population and thus have a high predictive value for LS, such as small intestinal and

hepatobiliary cancer, upper urinary tract and bladder (under age 60) transitional cell carcinoma, or skin sebaceous adenoma/carcinomas, are therefore worth testing [40]. Synchronous or metachronous bowel cancers are also significant, as is the development of any two LS-related tumours (*e.g.* CRC and endometrial cancer), and all such cases warrant testing for LS.

Neoplastic precursors in Lynch syndrome

When LS was being defined in the early 1990s, the only known pathway to CRC was based on the work of Dukes, Bussey, and Morson on FAP. First was Dukes' concept of 'simple tumours and cancer' in 1925 as part of his system for the staging of rectal cancer in FAP, followed by the adenoma to carcinoma pathway in 1958 [128–130]. Naturally, the reasonable assumption was that the same pathway applied in LS and colonoscopic surveillance to remove premalignant adenomas would thus be beneficial in LS. When early data started to come in on the efficacy of surveillance in LS, it became obvious that there was a large number of interval cancers, and, moreover, these occurred despite the interval between colonoscopies being steadily reduced to less than 3 years and sometimes even less than 1 year, because it appeared that LS cancers developed much more rapidly than sporadic ones, assuming they all arose from adenomas [6,131]. Moreover, because of the increased mutation rate (the MSI) observed in LS cancers, allied with the prevailing concept that genomic instability characterised all cancer, it was further assumed that this must be what was driving a faster adenoma-carcinoma progression, although not all parties were convinced [11,14,132]. In addition, although dMMR adenomas could be found in LS patients, further doubts were raised when aspirin treatment failed to reduce the incidence of adenomas (although it later reduced that of CRCs), and results from the PLSD became available [2,73,116,133,134]. LS patients on colonoscopic surveillance at various intervals could finally be compared [133]. Remarkably, within the limits measurable, colonoscopy did not appear to reduce the rate at which colorectal cancers were arising in LS patients, despite it being associated with a significant reduction in mortality and, in addition, stage was not related to the interval since last colonoscopy—completely the opposite of population screening programmes, which are based primarily on adenoma removal [2,133–135]. What was going on? Although LS patient survival is certainly improved by colonoscopic surveillance, enabling earlier diagnosis and a degree of downstaging, together this mass of evidence was leading to the conclusion that a pathway independent of adenomas must be occurring, and moreover, a pathway in which precursors were less obvious on colonoscopy [94].

At about the same time, it was discovered that LS patients harbour an enormous number of dMMR crypts in the colorectum (~1/cm^2 mucosa, so ~10 000 crypts/patient), which are not dysplastic, and yet LS patients only go on to eventually develop between zero and perhaps one, two, or three cancers [136,137]. Could these be leading to cancers, perhaps by an occult route? This was answered shortly afterwards by the finding of flat intramucosal cancers in which the Wnt pathway was activated by mutations not in *APC*, as in classical adenomas, but in beta-catenin; indeed mutations in repetitive coding sequences, exactly as predicted, would result from dMMR [138]. It is intriguing that subsequent work to sequence LS cancers has shown that some 61% of *APC* mutations are predicted to occur after MMR deficiency occurs, as they are found in repetitive sequences, exactly as would be expected in dMMR tumours. Hence, a proportion of these beta-catenin–mutant flat lesions acquire secondary *APC* mutations, thence to become polypoid adenomas and subsequently cancers [139,140]. Thus, it is now understood that there are at least *three* pathways to CRCs in LS, not including sporadic colonic cancer due to a right-sided sessile lesion, which are occasionally observed (Figure 2). The first pathway is *via* sporadic adenomas that acquire secondary dMMR. The second pathway is *via* flat cancers within the mucosa that arise directly from dMMR crypts, and the third pathway is LS-specific adenomas that arise from these flat lesions due to secondary *APC* mutations [139]. Hence, a proportion of LS CRCs arise from flat lesions, which are inherently more difficult to detect, let alone remove on colonoscopy, explaining at least in part the apparent high rate of interval cancers, but also removing the need to invoke a faster progression rate in LS. Building on this, it has been shown that the cancers in patients with LS due to *PMS2* mutations arise largely along pathway 1 (*i.e.* from sporadic adenomas), going further to explain why patients with pathogenic *PMS2* variants have only a small increased risk of CRC [142]. It is interesting that very recently it has been found that pathway 2 predominates over pathway 3 in patients with pathogenic *MLH1* variants, but pathway 3 predominates over pathway 2 in those with *MSH2* pathogenic variants [143]. These fascinating findings have clear implications for future surveillance strategies, which of necessity must now also include modalities such as aspirin prophylaxis and vaccines to address the inherently limited efficacy of colonoscopy and increased risks of cancers in LS at sites other than the large bowel, which are becoming the predominant cause of mortality in LS patients under surveillance [2,3].

It is of note that a number of observers have now found dMMR glands in morphologically normal endometrium from LS patients, which in turn has implications for the understanding of LS carcinogenesis in that organ [146].

Immune escape of Lynch syndrome neoplasms

The early general observations of large local tumours and a lower rate of metastasis, together with a strong immune reaction to LS cancers such as increased tumour infiltrating lymphocytes (TIL) and tertiary lymphoid structures (TLS; also termed Crohn-like peritumoural

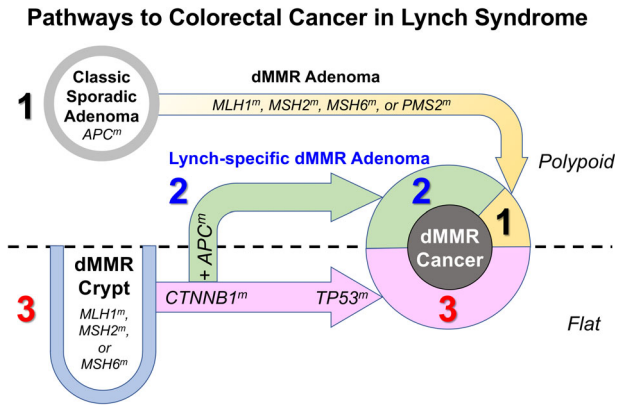

Figure 2. Pathways to colorectal cancer in Lynch syndrome. There are three pathways to dMMR colorectal cancers in LS [138,139]. Pathway 1: Classic sporadic adenomas, initiated by Wnt pathway activation due to mutations in *APC* (*APC*^{m}), acquired dMMR through somatic mutation of the remaining normal *MMR* allele (*MLH1*^{m}, *MSH2*^{m}, *MSH6*^{m}, or *PMS2*^{m}). This can occur at any stage of the adenoma, from early through to adenoma-carcinoma transition. Pathway 3: Crypts that have acquired dMMR due to somatic mutation of the normal *MMR* allele are not dysplastic, but if they undergo somatic mutation of beta-catenin (*CTNNB1*^{m}), which activates the Wnt pathway, they become flat carcinomas that later acquire mutations in *TP53* (*TP53*^{m}), an otherwise rare event in dMMR CRCs [138,141]. Pathway 2: A proportion of Pathway 3 lesions acquire secondary *APC* mutations and thus become polypoid adenomas. Because of this unique combination of somatic events, these Pathway 2 adenomas are, as far as is known, specific to LS (*hence* 'Lynch-specific dMMR adenomas'). Regarding pathways 2 and 3 in their original proposal, Ahadova and colleagues remark: 'For better visibility, pre-malignant lesions that do not develop into cancer are not included in the diagram, because their number greatly exceeds the number of carcinomas' [139]. Pathway 1 predominates in patients with LS due to *PMS2* pathogenic variants, whereas *CTNNB1*-mutant tumours are more likely in *MLH1* patients and *APC*-mutant tumours are more likely in *MSH2* and *MSH6* patients [142,143]. Note that sporadic colonic cancers that arise from serrated lesions with MLH1 deficiency due to somatic biallelic hypermethylation of the *MLH1* promoter can and do occur in LS, albeit perhaps less often due to the enhanced immunity in LS patients against dMMR cells because of chronic autoimmunisation from the novel frameshift peptides generated from dMMR crypts [31,57,59,136,139,144,145].

lymphoid aggregates or follicles), later backed up by gene expression signatures characteristic of immune cell activation, all indicate an important role for the immune system in LS [57,147,148]. However, this needs to be put in the context of the normal immune architecture in the bowel. Gut-associated lymphoid tissue (GALT) comprises both isolated and aggregated lymphoid follicles in both the small and large intestines. Humans have approximately 30 000 isolated lymphoid follicles (ILFs) scattered throughout the large and small intestine, but especially in the colon [149]. ILFs vary in their distribution within the large and small intestines, may be mucosal or sub-mucosal, and at their simplest may consist of a single follicle, with or without some T cells [150,151]. They are considered to be the main source of immune priming in the colon and from where Crohn's disease originates, and they have specialised follicle-associated epithelium (FAE), which overlies a subepithelial dome containing numerous macrophages, dendritic cells, T and B lymphocytes, and special antigen sampling microfold/M/cells [152,153]. The FAE has a crucial role in the initiation of the mucosal and systemic immune responses [154]. However, the relationship between Crohn-like follicles in LS and ILF in normal colon is not completely clear. In LS, the follicles are generally peritumoural and not located inside cancers, and, although they do not have FAE, they do have T cells, B cells, and germinal centres [58,155]. Whether they are induced *de novo*, as in chronic inflammation, or develop from submucosal ILFs remains to be determined [156]. Crohn-like follicles/TLS are found in CRCs apart from LS; however, the frequency/number is highest in LS patients compared to sporadic dMMR and pMMR CRCs, which is not simply related to age [58].

In recent years, there has been a growing interest in TLSs in a variety of cancers including CRC, in particular as prognostic indicators of cancer progression and responses to immunotherapy [153,157]. In hepatocellular carcinoma, intratumoral TLSs correlated with a lower risk of early relapse after surgery [158]. In sarcoma, melanoma, and renal cell carcinoma, both intratumoural location and the presence of B cells (but not T cells), and particularly germinal centres, correlate with improved outcomes to checkpoint blockade immunotherapy [159–161]. Further studies of the location, cellular composition, and presence of germinal centres in TLS in hereditary dMMR may therefore shed light on their role in LS.

In dMMR cells, predictable mutations can and do occur in repetitive protein coding sequences and result in frameshift peptides (FSPs) [162–164]. Such FSPs are novel antigens and elicit both humoral and cellular immune responses, which are seen as TILs around the dMMR crypts in LS patients as well as in dMMR cancers, both sporadic and due to LS [136,144,163,165]. In the face of such responses, how is it possible for tumours, let alone cancers, to develop in LS? The answer lies in the three-step process of elimination, equilibrium, and escape [59,166]. Cells generating FSPs, presented on their surface by MHC-I, are subjected to attack by cytotoxic T lymphocytes (CTLs), resulting in *elimination*. However, cells that randomly acquire activating mutations in PD-L1 before they are eliminated can hold the immune system to a local standstill (activating the PD-1 – PD-L1 immune checkpoint)—the process of *equilibrium*. Subsequently, if before being eliminated these cells manage to acquire inactivating mutations in MHC-I or MHC-II (HLA classes I & II) that abrogate presentation of FSPs on their surface, they are then able to *escape* the immune system, at least locally. Given the huge number of dMMR crypts in an LS patient, but that the average LS patient manifests between zero and one, two, or three CRCs, it is clear that the process of elimination must be highly efficient, giving a different perspective on cancer biology [2,139].

A number of different escape mechanisms have been observed. The most common, seen in approximately 30% of dMMR CRCs, is mutation of beta-2-microglobulin

(*B2M*), which prevents MHC-I presentation of FSPs. This was an early observation, the full significance of which is only now apparent [145,167–170]. The outgrowth of such *B2M* mutant clones is a prime example of cancer immunoediting, which has been further related to variation in host immune function, for example, mucosal density of FOXP3-positive regulatory T cells, indicating that such factors may be additional modifiers of LS [171]. It is notable that *B2M* mutations in dMMR cancers are significantly associated with an almost zero rate of metastasis and thus indicate highly favourable prognosis [172,173]. In addition to mutations in *B2M*, mutations of *CIITA* or *RFX5* are seen in approximately 20% of dMMR CRCs and prevent MHC-II antigen presentation, whereas approximately 10% of dMMR CRCs have mutations of *TAP1* or *TAP2*, which are antigenic peptide transporters responsible for antigen presentation, thus also preventing antigen presentation on the cell surface [174,175]. In such ways, tumour cells escape the attention of the host's immune system, both locally and in the circulation, but are in turn liable to attack with help from immunotherapy, such as anti-PD-1 or PD-L1 immune checkpoint blockade [176,177].

The full variety of mechanisms by which tumours, and dMMR tumours in particular, manage to evade the immune system has yet to be determined. Undoubtedly, the colorectal microbiome plays an important part in the process of CRC development in LS as well as sporadically [178]. Intriguingly, the immune response to dMMR CRCs in the form of the development of high endothelial venules (HEVs) responsible for trafficking lymphocytes into lymphoid follicles/TLS is stronger in LS patients than in sporadic dMMR colonic cancers, and especially high HEV densities in *B2M*-mutant tumours support the concept of immunoediting during tumour evolution [58]. Such higher HEV densities in *B2M*-mutant tumours imply that under strong immunoselective pressure created by immune cells recruited *via* HEVs, tumour cells that have lost MHC class I antigens gain growth advantage due to immunoediting, thus revealing a major role of HEVs in enhancing the immunoselective pressure on highly immunogenic cancers. Taken together with the high numbers of dMMR crypts in LS and the low numbers of CRCs that actually manifest, these findings all point toward a longer process of immunoediting in LS CRCs, possibly due to the pre-existing dMMR crypts immunising LS patients against their own propensity to cancer, and explaining the higher proportion of *B2M* mutations in LS compared to sporadic CRCs [58,136,137]. However, these HEVs generally recruit naïve lymphocytes from the blood into tissues and HEV-containing Crohn-like aggregates are generally seen in a peritumoural location in both pMMR and dMMR cancers, so our understanding of HEV and TLS in LS is as yet incomplete [58,155,179].

Conclusions

The major carcinogenic effect of dMMR is to reduce apoptosis and increase the net cell turnover rate. The raised mutation rate *per se* is of little or no consequence, but the bias to frameshift mutations in repetitive sequences caused by dMMR is of fundamental consequence, first in auto-immunising LS patients to FSPs and second in thus modifying the evolution of dMMR cancers by immunoediting.

That some *MMR* gene variants are associated with abnormal MMR IHC in tumours, but not MSI, and *vice versa*, plus the observation of, for example, certain *PMS2* variants in cases of CMMR-D but not LS, challenges the concept of *in vitro* functional tests in assessing variant pathogenicity [4,15,18,60,61]. Which function should be tested: DNA repair, or apoptosis, or both? [4,180–182]. We would therefore advise caution in the interpretation of such assays until this is clarified.

It is now understood that there are three main pathways to CRC in LS, including *via* sporadic adenomas, but also *via* occult intramucosal dMMR crypts and then beta-catenin-mutant flat cancers, which are directly invasive, some of which acquire secondary *APC* mutations to become polypoid [138,139]. Moreover, the likelihood that tumours follow particular pathways is related to the underlying gene affected by a pathogenic variant, and hence the variation in expression of LS starts to be explained and may lead to surveillance protocols becoming more tailored to genotype [3,10,142,143].

Currently, LS is defined by an individual carrying a pathogenic variant in an *MMR* gene, but interpretation of variants as pathogenic often requires tests on tumours for dMMR [4,6]. As part of the interpretational process, tests of MMR function may be performed *in vitro*, but this too is problematic and interpretation cannot be based solely on such analyses [4,180–182]. However, recent advances in understanding the pathways and responses to cancer in LS bring the possibility of alternative means of diagnosing LS independent of cancer itself, indeed perhaps even an alternative definition involving the immune system. The nature of the intense immune response to cancers in LS, manifest as the stronger HEV response seen in individuals with LS from an early age (16 years) allied to specific T- and B-cell responses to FSPs can be considered syndromic features characteristic of LS [58,163,165]. In addition, the dMMR crypts seen in the normal large bowel mucosa and the dMMR glands seen in normal endometrium can also be considered syndromic features characteristic of LS [136]. So, all taken together we may be approaching a definition of LS in molecular terms, in which the development of cancer, although of great importance clinically, is not necessary to achieve diagnosis. This in turn may enable the classification as pathogenic of many variants in *MMR* genes, and *MSH6* and *PMS2* in particular, which is currently problematic due to their reduced penetrance.

Acknowledgements

We wish to thank William Agace, Allan Mowat, Emma Crosbie, Aysel Ahadova, and Matthias Kloor for their

advice and helpful discussions during preparation of this work.

Author contributions statement

All authors contributed to preparation and review of the manuscript.

Abbreviations

ATM, ataxia-telangiectasia mutated; ATR, ATM and Rad3-related; CCFR, Colon Cancer Family Register; CGA-IGC, Collaborative Group of the Americas on Inherited Gastrointestinal Cancer; CMMR-D, Constitutional mismatch repair deficiency syndrome; dMMR, deficiency of MMR; FAE, follicle-associated epithelium; FAP, familial adenomatous polyposis; FSP, frameshift peptide; GALT, gut-associated lymphoid tissue; HEV, high endothelial venule; HNPCC, hereditary non-polyposis colorectal cancer; IHC, immunohistochemistry; ILF, isolated lymphoid follicle; IMRC, International Mismatch Repair Consortium; InSiGHT, International Society for Gastrointestinal Hereditary Cancer; LOVD, Leiden Open Variation Databases; LS, Lynch syndrome; MAP, *MUTYH*-associated polyposis; MMR, DNA mismatch repair; MSI, microsatellite instability; MTS, Muir-Torre syndrome; PLSD, Prospective Lynch Syndrome Database; pMMR, proficiency of MMR; PPAP, proof-reading polymerase-associated polyposis; TIL, tumour-infiltrating lymphocyte; TLS, tertiary lymphoid structure; VUS, variant of uncertain significance

References

1. Frankel WL, Arends MJ, Frayling IM, *et al*. Lynch syndrome. In *Digestive System Tumours* (5th edn), Arends MJ, Carniero F, Lax SF, *et al*. (eds). International Agency for Research on Cancer: Lyon, 2019; 515–521.
2. Moller P, Seppala T, Bernstein I, *et al*. Cancer incidence and survival in Lynch syndrome patients receiving colonoscopic and gynaecological surveillance: first report from the prospective Lynch syndrome database. *Gut* 2017; **66:** 464–472.
3. Moller P, Seppala TT, Bernstein I, *et al*. Cancer risk and survival in path_MMR carriers by gene and gender up to 75 years of age: a report from the prospective Lynch syndrome database. *Gut* 2018; **67:** 1306–1316.
4. Thompson BA, Spurdle AB, Plazzer JP, *et al*. Application of a 5-tiered scheme for standardized classification of 2,360 unique mismatch repair gene variants in the InSiGHT locus-specific database. *Nat Genet* 2014; **46:** 107–115.
5. Vasen H, Möslein G, Alonso A, *et al*. Recommendations to improve identification of hereditary and familial colorectal cancer in Europe. *Fam Cancer* 2010; **9:** 109–115.
6. Vasen HF, Blanco I, Aktan-Collan K, *et al*. Revised guidelines for the clinical management of Lynch syndrome (HNPCC): recommendations by a group of European experts. *Gut* 2013; **62:** 812–823.
7. Vasen HF, Ghorbanoghli Z, Bourdeaut F, *et al*. Guidelines for surveillance of individuals with constitutional mismatch repair-deficiency proposed by the European consortium "care for CMMR-D" (C4CMMR-D). *J Med Genet* 2014; **51:** 283–293.
8. Frayling I, Berry I, Wallace A, *et al*., ACGS best practice guidelines for genetic testing and diagnosis of Lynch syndrome. Association for Clinical Genomic Science. 2016. Available from: https://www.acgs.uk.com/media/10774/ls_bpg_approved.pdf
9. Vasen HF, Moeslein G, Alonso A, *et al*. Guidelines for the clinical management of familial adenomatous polyposis (FAP). *Gut* 2008; **57:** 704–713.
10. Dominguez-Valentin M, Sampson JR, Seppala TT, *et al*. Cancer risks by gene, age, and gender in 6350 carriers of pathogenic mismatch repair variants: findings from the prospective Lynch syndrome database. *Genet Med* 2020; **22:** 15–25.
11. Poulogiannis G, Frayling IM, Arends MJ. DNA mismatch repair deficiency in sporadic colorectal cancer and Lynch syndrome. *Histopathology* 2010; **56:** 167–179.
12. Toft NJ, Winton DJ, Kelly J, *et al*. Msh2 status modulates both apoptosis and mutation frequency in the murine small intestine. *Proc Natl Acad Sci U S A* 1999; **96:** 3911–3915.
13. Zhang H, Richards B, Wilson T, *et al*. Apoptosis induced by overexpression of hMSH2 or hMLH1. *Cancer Res* 1999; **59:** 3021–3027.
14. Tomlinson I, Bodmer W. Selection, the mutation rate and cancer: ensuring that the tail does not wag the dog. *Nat Med* 1999; **5:** 11–12.
15. (InSiGHT) ISfGHT. MMR gene variant classification. [Accessed 29 February 2020]. Available from: http://www.insight-group.org/criteria/
16. (InSiGHT) ISfGHT. Variant Classification Expert Panel (VCEP). [Accessed 29 February 2020]. Available from: https://www.ncbi.nlm.nih.gov/clinvar/submitters/500189/
17. Plon SE, Eccles DM, Easton D, *et al*. Sequence variant classification and reporting: recommendations for improving the interpretation of cancer susceptibility genetic test results. *Hum Mutat* 2008; **29:** 1282–1291.
18. Plazzer J-P, Dominguez-Valentin M, Thompson BA. MMR Variant LOVD. In: (InSiGHT) ISfGHC, 2011.
19. Landrum MJ, Kattman BL. ClinVar at five years: delivering on the promise. *Hum Mutat* 2018; **39:** 1623–1630.
20. Rehm HL, Berg JS, Brooks LD, *et al*. ClinGen—the clinical genome resource. *N Engl J Med* 2015; **372:** 2235–2242.
21. Wagner A, van der Klift H, Franken P, *et al*. A 10-Mb paracentric inversion of chromosome arm 2p inactivates MSH2 and is responsible for hereditary nonpolyposis colorectal cancer in a north-American kindred. *Genes Chromosomes Cancer* 2002; **35:** 49–57.
22. Li L, McVety S, Younan R, *et al*. Distinct patterns of germ-line deletions in MLH1 and MSH2: the implication of Alu repetitive element in the genetic etiology of Lynch syndrome (HNPCC). *Hum Mutat* 2006; **27:** 388–388.
23. Taylor C, Charlton R, Burn J, *et al*. Genomic deletions in MSH2 or MLH1 are a frequent cause of hereditary non-polyposis colorectal cancer: identification of novel and recurrent deletions by MLPA. *Hum Mutat* 2003; **22:** 428–433.
24. Thompson BA, Martins A, Spurdle AB. A review of mismatch repair gene transcripts: issues for interpretation of mRNA splicing assays. *Clin Genet* 2015; **87:** 100–108.
25. Kempers MJ, Kuiper RP, Ockeloen CW, *et al*. Risk of colorectal and endometrial cancers in EPCAM deletion-positive Lynch syndrome: a cohort study. *Lancet Oncol* 2011; **12:** 49–55.
26. Niessen RC, Hofstra RM, Westers H, *et al*. Germline hypermethylation of MLH1 and EPCAM deletions are a frequent cause of Lynch syndrome. *Genes Chromosomes Cancer* 2009; **48:** 737–744.
27. Hitchins M, Williams R, Cheong K, *et al*. MLH1 germline epimutations as a factor in hereditary nonpolyposis colorectal cancer. *Gastroenterology* 2005; **129:** 1392–1399.

28. Hitchins MP, Ward RL. Constitutional (germline) MLH1 epimutation as an aetiological mechanism for hereditary non-polyposis colorectal cancer. *J Med Genet* 2009; **46:** 793–802.
29. Morak M, Ibisler A, Keller G, *et al*. Comprehensive analysis of the MLH1 promoter region in 480 patients with colorectal cancer and 1150 controls reveals new variants including one with a heritable constitutional MLH1 epimutation. *J Med Genet* 2018; **55:** 240–248.
30. Sinicrope FA, Sargent DJ. Clinical implications of microsatellite instability in sporadic colon cancers. *Curr Opin Oncol* 2009; **21:** 369–373.
31. Noffsinger AE. Serrated polyps and colorectal cancer: new pathway to malignancy. *Annu Rev Pathol* 2009; **4:** 343–364.
32. Esteller M, Levine R, Baylin SB, *et al*. MLH1 promoter hypermethylation is associated with the microsatellite instability phenotype in sporadic endometrial carcinomas. *Oncogene* 1998; **17:** 2413–2417.
33. Simpkins SB, Bocker T, Swisher EM, *et al*. MLH1 promoter methylation and gene silencing is the primary cause of microsatellite instability in sporadic endometrial cancers. *Hum Mol Genet* 1999; **8:** 661–666.
34. Muir EG, Bell AJ, Barlow KA. Multiple primary carcinomata of the colon, duodenum, and larynx associated with kerato-acanthomata of the face. *Br J Surg* 1967; **54:** 191–195.
35. Torre D. Multiple sebaceous tumours. *Arch Dermatol* 1968; **98:** 549.
36. Lynch HT, Fusaro RM, Roberts L, *et al*. Muir-Torre syndrome in several members of a family with a variant of the Cancer family syndrome. *Br J Dermatol* 1985; **113:** 295–301.
37. South CD, Hampel H, Comeras I, *et al*. The frequency of Muir-Torre syndrome among Lynch syndrome families. *J Natl Cancer Inst* 2008; **100:** 277–281.
38. Ponti G, Ponz de Leon M, Maffei S, *et al*. Attenuated familial adenomatous polyposis and Muir-Torre syndrome linked to compound biallelic constitutional MYH gene mutations. *Clin Genet* 2005; **68:** 442–447.
39. Kacerovska D, Drlik L, Slezakova L, *et al*. Cutaneous sebaceous lesions in a patient with MUTYH-associated polyposis mimicking Muir-Torre syndrome. *Am J Dermatopathol* 2016; **38:** 915–923.
40. Jessup CJ, Redston M, Tilton E, *et al*. Importance of universal mismatch repair protein immunohistochemistry in patients with sebaceous neoplasia as an initial screening tool for Muir-Torre syndrome. *Hum Pathol* 2016; **49:** 1–9.
41. Roberts ME, Riegert-Johnson DL, Thomas BC, *et al*. Screening for Muir-Torre syndrome using mismatch repair protein immunohistochemistry of sebaceous neoplasms. *J Genet Couns* 2013; **22:** 393–405.
42. Durno CA, Holter S, Sherman PM, *et al*. The gastrointestinal phenotype of germline biallelic mismatch repair gene mutations. *Am J Gastroenterol* 2010; **105:** 2449–2456.
43. Jeans AF, Frayling I, Jasani B, *et al*. Cerebral primitive neuroectodermal tumor in an adult with a heterozygous MSH2 mutation. *Nat Rev Clin Oncol* 2009; **6:** 295–299.
44. Fernandez-Rozadilla C, Alvarez-Barona M, Schamschula E, *et al*. Early colorectal cancers provide new evidence for a Lynch syndrome-to-CMMRD phenotypic continuum. *Cancers* 2019; **11:** E1081.
45. Wimmer K, Kratz CP, Vasen HF, *et al*. Diagnostic criteria for constitutional mismatch repair deficiency syndrome: suggestions of the European consortium 'care for CMMRD' (C4CMMRD). *J Med Genet* 2014; **51:** 355–365.
46. Gallon R, Muhlegger B, Wenzel SS, *et al*. A sensitive and scalable microsatellite instability assay to diagnose constitutional mismatch repair deficiency by sequencing of peripheral blood leukocytes. *Hum Mutat* 2019; **40:** 649–655.
47. Bodo S, Colas C, Buhard O, *et al*. Diagnosis of constitutional mismatch repair-deficiency syndrome based on microsatellite instability and lymphocyte tolerance to methylating agents. *Gastroenterology* 2015; **149:** 1017–1029 e1013.
48. Li L, Hamel N, Baker K, *et al*. A homozygous PMS2 founder mutation with an attenuated constitutional mismatch repair deficiency phenotype. *J Med Genet* 2015; **52:** 348–352.
49. Whitworth J, Skytte A-B, Sunde L, *et al*. Multilocus inherited neoplasia alleles syndrome: a case series and review. *JAMA Oncol* 2016; **2:** 373–379.
50. Hamilton SR, Liu B, Parsons RE, *et al*. The molecular basis of Turcot's syndrome. *N Engl J Med* 1995; **332:** 839–847.
51. Modrich P, Lahue R. Mismatch repair in replication fidelity, genetic recombination, and cancer biology. *Annu Rev Biochem* 1996; **65:** 101–133.
52. Hsieh P, Yamane K. DNA mismatch repair: molecular mechanism, cancer, and ageing. *Mech Ageing Dev* 2008; **129:** 391–407.
53. Stojic L, Brun R, Jiricny J. Mismatch repair and DNA damage signalling. *DNA Repair (Amst)* 2004; **3:** 1091–1101.
54. Brown KD, Rathi A, Kamath R, *et al*. The mismatch repair system is required for S-phase checkpoint activation. *Nat Genet* 2003; **33:** 80–84.
55. Stojic L, Mojas N, Cejka P, *et al*. Mismatch repair-dependent G2 checkpoint induced by low doses of SN1 type methylating agents requires the ATR kinase. *Genes Dev* 2004; **18:** 1331–1344.
56. Yoshioka K, Yoshioka Y, Hsieh P. ATR kinase activation mediated by MutSalpha and MutLalpha in response to cytotoxic O6-methylguanine adducts. *Mol Cell* 2006; **22:** 501–510.
57. Llosa NJ, Cruise M, Tam A, *et al*. The vigorous immune microenvironment of microsatellite instable colon cancer is balanced by multiple counter-inhibitory checkpoints. *Cancer Discov* 2015; **5:** 43–51.
58. Pfuderer PL, Ballhausen A, Seidler F, *et al*. High endothelial venules are associated with microsatellite instability, hereditary background and immune evasion in colorectal cancer. *Br J Cancer* 2019; **121:** 395–404.
59. Seth S, Ager A, Arends MJ, *et al*. Lynch syndrome - cancer pathways, heterogeneity and immune escape. *J Pathol* 2018; **246:** 129–133.
60. Herkert JC, Niessen RC, Olderode-Berends MJ, *et al*. Paediatric intestinal cancer and polyposis due to bi-allelic PMS2 mutations: case series, review and follow-up guidelines. *Eur J Cancer* 2011; **47:** 965–982.
61. Jackson CC, Holter S, Pollett A, *et al*. Café-au-lait macules and pediatric malignancy caused by biallelic mutations in the DNA mismatch repair (MMR) gene PMS2. *Pediatr Blood Cancer* 2008; **50:** 1268–1270.
62. Diergaarde B, Braam H, Vasen HF, *et al*. Environmental factors and colorectal tumor risk in individuals with hereditary nonpolyposis colorectal cancer. *Clin Gastroenterol Hepatol* 2007; **5:** 736–742.
63. Dominguez-Valentin M. Prospective Lynch Syndrome Database (PLSD). 2020. [Accessed 29 February 2020]. Available from: www.PLSD.eu
64. Jenkins MA, Haile RW, Macrae F, *et al*. International Mismatch Repair Consortium (IMRC). [Accessed 29 February 2020]. Available from: https://sphinx.org.au/imrc
65. Jenkins MA, Figueiredo JC, Gallinger S, *et al*. Colon Cancer Family Register (CCFR). [Accessed 29 February 2020]; Available from: https://coloncfr.org/
66. Dowty JG, Win AK, Buchanan DD, *et al*. Cancer risks for MLH 1 and MSH 2 mutation carriers. *Hum Mutat* 2013; **34:** 490–497.
67. Pande M, Lynch PM, Hopper JL, *et al*. Smoking and colorectal cancer in Lynch syndrome: results from the Colon Cancer family registry and the University of Texas MD Anderson Cancer Center. *Clin Cancer Res* 2010; **16:** 1331–1339.
68. Pande M, Lynch PM, Hopper JL, *et al*. Smoking and colorectal cancer in Lynch syndrome: results from the Colon Cancer family registry and the University of Texas M.D. Anderson Cancer center. *Clin Cancer Res* 2010; **16:** 1331–1339.

69. Win A, Dowty J, English D, *et al*. Body mass index in early adulthood and colorectal cancer risk for carriers and non-carriers of germline mutations in DNA mismatch repair genes. *Br J Cancer* 2011; **105:** 162–169.
70. Ait Ouakrim D, Dashti SG, Chau R, *et al*. Aspirin, ibuprofen, and the risk of colorectal cancer in Lynch syndrome. *J Natl Cancer Inst* 2015; **107:** djv170.
71. Chau R, Dashti SG, Ait Ouakrim D, *et al*. Multivitamin, calcium and folic acid supplements and the risk of colorectal cancer in Lynch syndrome. *Int J Epidemiol* 2016; **45:** 940–953.
72. Cancer CGotAoIG. CGA-IGC. [Accessed 29 February 2020]. Available from: https://www.cgaigc.com/
73. Burn J, Gerdes AM, Macrae F, *et al*. Long-term effect of aspirin on cancer risk in carriers of hereditary colorectal cancer: an analysis from the CAPP2 randomised controlled trial. *Lancet* 2011; **378:** 2081–2087.
74. Burn J, Mathers J, Bishop DT. Lynch syndrome: history, causes, diagnosis, treatment and prevention (CAPP2 trial). *Dig Dis* 2012; **30**(Suppl 2): 39–47.
75. Liljegren A, Barker G, Elliott F, *et al*. Prevalence of adenomas and hyperplastic polyps in mismatch repair mutation carriers among CAPP2 participants: report by the colorectal adenoma/carcinoma prevention programme 2. *J Clin Oncol* 2008; **26:** 3434–3439.
76. Burn J. Cancer Prevention Program 3 (CaPP3). [Accessed 29 February 2020]. Available from: http://www.capp3.org/
77. Alexander J, Watanabe T, Wu TT, *et al*. Histopathological identification of colon cancer with microsatellite instability. *Am J Pathol* 2001; **158:** 527–535.
78. Truta B, Chen YY, Blanco AM, *et al*. Tumor histology helps to identify Lynch syndrome among colorectal cancer patients. *Fam Cancer* 2008; **7:** 267–274.
79. Chui MH, Gilks CB, Cooper K, *et al*. Identifying Lynch syndrome in patients with ovarian carcinoma: the significance of tumor subtype. *Adv Anat Pathol* 2013; **20:** 378–386.
80. Niskakoski A, Pasanen A, Lassus H, *et al*. Molecular changes preceding endometrial and ovarian cancer: a study of consecutive endometrial specimens from Lynch syndrome surveillance. *Mod Pathol* 2018; **31:** 1291–1301.
81. Walsh MD, Cummings MC, Buchanan DD, *et al*. Molecular, pathologic, and clinical features of early-onset endometrial cancer: identifying presumptive Lynch syndrome patients. *Clin Cancer Res* 2008; **14:** 1692–1700.
82. Crosbie EJ. The Proportion of Endometrial Tumours Associated with Lynch Syndrome: a prospective diagnostic test accuracy study of unselected screening of endometrial cancer for Lynch syndrome. 2020.
83. Crosbie EJ, Ryan NA, Arends MJ, *et al*. The Manchester international consensus group recommendations for the management of gynecological cancers in Lynch syndrome. *Genet Med* 2019; **21:** 2390–2400.
84. Broaddus RR, Lynch HT, Chen LM, *et al*. Pathologic features of endometrial carcinoma associated with HNPCC: a comparison with sporadic endometrial carcinoma. *Cancer* 2006; **106:** 87–94.
85. Ryan N, Evans D, Green K, *et al*. Pathological features and clinical behavior of Lynch syndrome-associated ovarian cancer. *Gynecol Oncol* 2017; **144:** 491–495.
86. Woolderink J, De Bock G, de Hullu J, *et al*. Characteristics of Lynch syndrome associated ovarian cancer. *Gynecol Oncol* 2018; **150:** 324–330.
87. Aarnio M, Salovaara R, Aaltonen LA, *et al*. Features of gastric cancer in hereditary non-polyposis colorectal cancer syndrome. *Int J Cancer* 1997; **74:** 551–555.
88. Capelle LG, Van Grieken NC, Lingsma HF, *et al*. Risk and epidemiological time trends of gastric cancer in Lynch syndrome carriers in The Netherlands. *Gastroenterology* 2010; **138:** 487–492.
89. Gylling A, Abdel-Rahman WM, Juhola M, *et al*. Is gastric cancer part of the tumour spectrum of hereditary non-polyposis colorectal cancer? A molecular genetic study. *Gut* 2007; **56:** 926–933.
90. Adar T, Friedman M, Rodgers LH, *et al*. Gastric cancer in Lynch syndrome is associated with underlying immune gastritis. *J Med Genet* 2019; **56:** 844–845.
91. Jun S-Y, Lee E-J, Kim M-J, *et al*. Lynch syndrome-related small intestinal adenocarcinomas. *Oncotarget* 2017; **8:** 21483.
92. Wilentz RE, Goggins M, Redston M, *et al*. Genetic, immunohistochemical, and clinical features of medullary carcinoma of the pancreas: a newly described and characterized entity. *Am J Pathol* 2000; **156:** 1641–1651.
93. Snowsill T, Coelho H, Huxley N, *et al*. Molecular testing for Lynch syndrome in people with colorectal cancer: systematic reviews and economic evaluation. *Health Technol Assess* 2017; **21:** 1–238.
94. Snowsill T, Huxley N, Hoyle M, *et al*. A systematic review and economic evaluation of diagnostic strategies for Lynch syndrome. *Health Technol Assess* 2014; **18:** 1–406.
95. Wedden S, Miller K, Frayling IM, *et al*. Colorectal Cancer stratification in the routine clinical pathway: a district general hospital experience. *Appl Immunohistochem Mol Morphol* 2019; **27:** e54–e62.
96. National Institute for Health and Care Excellence. *Molecular Testing Strategies for Lynch Syndrome in People with Colorectal Cancer: Diagnostics Guidance [DG27]*. [Accessed 24 April 2020]. Available from https://www.nice.org.uk/guidance/dg27.
97. Sie AS, Mensenkamp AR, Adang EM, *et al*. Fourfold increased detection of Lynch syndrome by raising age limit for tumour genetic testing from 50 to 70 years is cost-effective. *Ann Oncol* 2014; **25:** 2001–2007.
98. Adar T, Rodgers LH, Shannon KM, *et al*. A tailored approach to BRAF and MLH1 methylation testing in a universal screening program for Lynch syndrome. *Mod Pathol* 2017; **30:** 440–447.
99. Bläker H, Haupt S, Morak M, *et al*. BRAF mutation testing in Lynch syndrome diagnostics: Performance and efficiency according to patient's age. *medRxiv* 2019. https://doi.org/10.1101/19009274. Not peer reviewed.
100. Marks K, West N. Molecular assessment of colorectal cancer through Lynch syndrome screening. *Diagn Histopathol* 2020; **26:** 47–50.
101. Taylor A, Brady AF, Frayling IM, *et al*. Consensus for genes to be included on cancer panel tests offered by UK genetics services: guidelines of the UK cancer genetics group. *J Med Genet* 2018; **55:** 372–377.
102. Arends M, Ibrahim M, Happerfield L, *et al*. Interpretation of immunohistochemical analysis of mismatch repair (MMR) protein expression in tissue sections for investigation of suspected Lynch/hereditary non-polyposis colorectal Cancer (HNPCC) syndrome. *UK NEQAS ICC & ISH Recommendations* 2008; **1:** 1–2.
103. Frayling IM, Arends MJ. How can histopathologists help clinical genetics in the investigation of suspected hereditary gastrointestinal cancer? *Diagn Histopathol* 2015; **21:** 137–146.
104. Mensenkamp AR, Vogelaar IP, van Zelst-Stams WA, *et al*. Somatic mutations in MLH1 and MSH2 are a frequent cause of mismatch-repair deficiency in Lynch syndrome-like tumors. *Gastroenterology* 2014; **146:** 643–646. e648.
105. Chang CL, Marra G, Chauhan DP, *et al*. Oxidative stress inactivates the human DNA mismatch repair system. *Am J Physiol Cell Physiol* 2002; **283:** C148–C154.
106. Mihaylova VT, Bindra RS, Yuan J, *et al*. Decreased expression of the DNA mismatch repair gene Mlh1 under hypoxic stress in mammalian cells. *Mol Cell Biol* 2003; **23:** 3265–3273.
107. Sekine S, Ogawa R, Saito S, *et al*. Cytoplasmic MSH2 immunoreactivity in a patient with Lynch syndrome with an EPCAM-MSH2 fusion. *Histopathology* 2017; **70:** 664–669.

108. Bao F, Panarelli NC, Rennert H, *et al*. Neoadjuvant therapy induces loss of MSH6 expression in colorectal carcinoma. *Am J Surg Pathol* 2010; **34:** 1798–1804.
109. Radu OM, Nikiforova MN, Farkas LM, *et al*. Challenging cases encountered in colorectal cancer screening for Lynch syndrome reveal novel findings: nucleolar MSH6 staining and impact of prior chemoradiation therapy. *Hum Pathol* 2011; **42:** 1247–1258.
110. Graham RP, Kerr SE, Butz ML, *et al*. Heterogenous MSH6 loss is a result of microsatellite instability within MSH6 and occurs in sporadic and hereditary colorectal and endometrial carcinomas. *Am J Surg Pathol* 2015; **39:** 1370–1376.
111. Shia J, Zhang L, Shike M, *et al*. Secondary mutation in a coding mononucleotide tract in MSH6 causes loss of immunoexpression of MSH6 in colorectal carcinomas with MLH1/PMS2 deficiency. *Mod Pathol* 2013; **26:** 131–138.
112. Bartley AN, Luthra R, Saraiya DS, *et al*. Identification of cancer patients with Lynch syndrome: clinically significant discordances and problems in tissue-based mismatch repair testing. *Cancer Prev Res (Phila)* 2012; **5:** 320–327.
113. Frayling IM. Microsatellite instability. *Gut* 1999; **45:** 1–4.
114. Hause RJ, Pritchard CC, Shendure J, *et al*. Classification and characterization of microsatellite instability across 18 cancer types. *Nat Med* 2016; **22:** 1342–1350.
115. Ju JY, Mills AM, Mahadevan MS, *et al*. Universal Lynch syndrome screening should be performed in all upper tract urothelial carcinomas. *Am J Surg Pathol* 2018; **42:** 1549–1555.
116. Loukola A, Salovaara R, Kristo P, *et al*. Microsatellite instability in adenomas as a marker for hereditary nonpolyposis colorectal cancer. *Am J Pathol* 1999; **155:** 1849–1853.
117. van Lier MG, Leenen CH, Wagner A, *et al*. Yield of routine molecular analyses in colorectal cancer patients≤ 70 years to detect underlying Lynch syndrome. *J Pathol* 2012; **226:** 764–774.
118. De Rosa N, Rodriguez-Bigas MA, Chang GJ, *et al*. DNA mismatch repair deficiency in rectal cancer: benchmarking its impact on prognosis, neoadjuvant response prediction, and clinical cancer genetics. *J Clin Oncol* 2016; **34:** 3039.
119. Nilbert M, Planck M, Fernebro E, *et al*. Microsatellite instability is rare in rectal carcinomas and signifies hereditary cancer. *Eur J Cancer* 1999; **35:** 942–945.
120. Thiel A, Heinonen M, Kantonen J, *et al*. BRAF mutation in sporadic colorectal cancer and Lynch syndrome. *Virchows Arch* 2013; **463:** 613–621.
121. Vasen HF, Möslein G, Alonso A, *et al*. Guidelines for the clinical management of Lynch syndrome (hereditary non-polyposis cancer). *J Med Genet* 2007; **44:** 353–362.
122. Ligtenberg MJ, Kuiper RP, Chan TL, *et al*. Heritable somatic methylation and inactivation of MSH2 in families with Lynch syndrome due to deletion of the 3′ exons of TACSTD1. *Nat Genet* 2009; **41:** 112.
123. Smith MJ, Urquhart JE, Harkness EF, *et al*. The contribution of whole gene deletions and large rearrangements to the mutation spectrum in inherited tumor predisposing syndromes. *Hum Mutat* 2016; **37:** 250–256.
124. InSiGHT. Graphs & statistics on gene MSH2. [Accessed 29 February 2020]. Available from: https://databases.lovd.nl/shared/genes/MSH2/graphs
125. InSiGHT. Graphs & statistics on gene MLH1. [Accessed 29 February 2020]. Available from: https://databases.lovd.nl/shared/genes/MLH1/graphs
126. InSiGHT. Graphs & statistics on gene MSH6. [Accessed 29 February 2020]. Available from: https://databases.lovd.nl/shared/genes/MSH6/graphs
127. InSiGHT. Graphs & statistics on gene PMS2. [Accessed 29 February 2020]. Available from: https://databases.lovd.nl/shared/genes/PMS2/graphs
128. Dukes C. Simple tumours of the large intestine and their relation to cancer. *Proc R Soc Med* 1926; **19:** 8–9.
129. Dukes C, Bussey H. The spread of rectal cancer and its effect on prognosis. *Br J Cancer* 1958; **12:** 309.
130. Dukes CE. The classification of cancer of the rectum. *J Pathol Bacteriol* 1932; **35:** 323–332.
131. Vasen H, Nagengast F, Meera KP. Interval cancers in hereditary non-polyposis colorectal cancer (Lynch syndrome). *Lancet* 1995; **345:** 1183–1184.
132. Tomlinson IP, Novelli M, Bodmer W. The mutation rate and cancer. *Proc Natl Acad Sci U S A* 1996; **93:** 14800–14803.
133. Seppälä T, Pylvänäinen K, Evans DG, *et al*. Colorectal cancer incidence in path_MLH1 carriers subjected to different follow-up protocols: a prospective Lynch syndrome database report. *Hered Cancer Clin Pract* 2017; **15:** 18.
134. Seppälä TT, Ahadova A, Dominguez-Valentin M, *et al*. Lack of association between screening interval and cancer stage in Lynch syndrome may be accounted for by over-diagnosis; a prospective Lynch syndrome database report. *Hered Cancer Clin Pract* 2019; **17:** 8.
135. Engel C, Vasen HF, Seppälä T, *et al*. No difference in colorectal cancer incidence or stage at detection by colonoscopy among 3 countries with different Lynch syndrome surveillance policies. *Gastroenterology* 2018; **155:** 1400–1409.e1402.
136. Kloor M, Huth C, Voigt AY, *et al*. Prevalence of mismatch repair-deficient crypt foci in Lynch syndrome: a pathological study. *Lancet Oncol* 2012; **13:** 598–606.
137. Staffa L, Echterdiek F, Nelius N, *et al*. Mismatch repair-deficient crypt foci in Lynch syndrome–molecular alterations and association with clinical parameters. *PLoS One* 2015; **10:** e0121980.
138. Ahadova A, von Knebel DM, Bläker H, *et al*. CTNNB1-mutant colorectal carcinomas with immediate invasive growth: a model of interval cancers in Lynch syndrome. *Fam Cancer* 2016; **15:** 579–586.
139. Ahadova A, Gallon R, Gebert J, *et al*. Three molecular pathways model colorectal carcinogenesis in Lynch syndrome. *Int J Cancer* 2018; **143:** 139–150.
140. Binder H, Hopp L, Schweiger MR, *et al*. Genomic and transcriptomic heterogeneity of colorectal tumours arising in Lynch syndrome. *J Pathol* 2017; **243:** 242–254.
141. Kloth M, Ruesseler V, Engel C, *et al*. Activating ERBB2/HER2 mutations indicate susceptibility to pan-HER inhibitors in Lynch and Lynch-like colorectal cancer. *Gut* 2016; **65:** 1296–1305.
142. Ten Broeke SW, van Bavel TC, Jansen AM, *et al*. Molecular background of colorectal tumors from patients with Lynch syndrome associated with germline variants in PMS2. *Gastroenterology* 2018; **155:** 844–851.
143. Engel C, Ahadova A, Seppälä TT, *et al*. Associations of pathogenic variants in MLH1, MSH2, and MSH6 with risk of colorectal adenomas and tumors and with somatic mutations in patients with Lynch syndrome. *Gastroenterology* 2020; **158:** 1326–1333.
144. Linnebacher M, Gebert J, Rudy W, *et al*. Frameshift peptide-derived T-cell epitopes: a source of novel tumor-specific antigens. *Int J Cancer* 2001; **93:** 6–11.
145. Kloor M, Michel S, von Knebel Doeberitz M. Immune evasion of microsatellite unstable colorectal cancers. *Int J Cancer* 2010; **127:** 1001–1010.
146. Ryan AJ, Crosbie EJ, Arends MJ, Wilkinson N. Personal communications. 2019.
147. Aaltonen LA, Peltomäki P, Mecklin J-P, *et al*. Replication errors in benign and malignant tumors from hereditary nonpolyposis colorectal cancer patients. *Cancer Res* 1994; **54:** 1645–1648.
148. Smyrk TC, Watson P, Kaul K, *et al*. Tumor-infiltrating lymphocytes are a marker for microsatellite instability in colorectal carcinoma. *Cancer* 2001; **91:** 2417–2422.

149. Sipos F, Műzes G. Isolated lymphoid follicles in colon: switch points between inflammation and colorectal cancer? *World J Gastroenterol* 2011; **17:** 1666–1673.
150. Agace WW, McCoy KD. Regionalized development and maintenance of the intestinal adaptive immune landscape. *Immunity* 2017; **46:** 532–548.
151. Mowat AM, Agace WW. Regional specialization within the intestinal immune system. *Nat Rev Immunol* 2014; **14:** 667–685.
152. Stranford SP, Ruddle NH. Follicular dendritic cells, conduits, lymphatic vessels, and high endothelial venules in tertiary lymphoid organs: parallels with lymph node stroma. *Front Immunol* 2012; **3:** 350.
153. Colbeck EJ, Ager A, Gallimore A, *et al*. Tertiary lymphoid structures in cancer: drivers of antitumor immunity, immunosuppression, or bystander sentinels in disease? *Front Immunol* 2017; **8:** 1830.
154. Lorenz RG, Newberry RD. Isolated lymphoid follicles can function as sites for induction of mucosal immune responses. *Ann N Y Acad Sci* 2004; **1029:** 44–57.
155. Bento DC, Jones E, Junaid S, *et al*. High endothelial venules are rare in colorectal cancers but accumulate in extra-tumoral areas with disease progression. *Onco Targets Ther* 2015; **4:** e974374.
156. Drayton DL, Liao S, Mounzer RH, *et al*. Lymphoid organ development: from ontogeny to neogenesis. *Nat Immunol* 2006; **7:** 344–353.
157. Sautès-Fridman C, Petitprez F, Calderaro J, *et al*. Tertiary lymphoid structures in the era of cancer immunotherapy. *Nat Rev Cancer* 2019; **19:** 307–325.
158. Calderaro J, Petitprez F, Becht E, *et al*. Intra-tumoral tertiary lymphoid structures are associated with a low risk of early recurrence of hepatocellular carcinoma. *J Hepatol* 2019; **70:** 58–65.
159. Cabrita R, Lauss M, Sanna A, *et al*. Tertiary lymphoid structures improve immunotherapy and survival in melanoma. *Nature* 2020; **577:** 561–565.
160. Helmink BA, Reddy SM, Gao J, *et al*. B cells and tertiary lymphoid structures promote immunotherapy response. *Nature* 2020; **577:** 549–555.
161. Petitprez F, de Reyniès A, Keung EZ, *et al*. B cells are associated with survival and immunotherapy response in sarcoma. *Nature* 2020; **577:** 556–560.
162. Sæterdal I, Bjørheim J, Lislerud K, *et al*. Frameshift-mutation-derived peptides as tumor-specific antigens in inherited and spontaneous colorectal cancer. *Proc Natl Acad Sci U S A* 2001; **98:** 13255–13260.
163. Schwitalle Y, Linnebacher M, Ripberger E, *et al*. Immunogenic peptides generated by frameshift mutations in DNA mismatch repair-deficient cancer cells. *Cancer Immun* 2004; **4:** 14.
164. Woerner SM, Gebert J, Yuan YP, *et al*. Systematic identification of genes with coding microsatellites mutated in DNA mismatch repair-deficient cancer cells. *Int J Cancer* 2001; **93:** 12–19.
165. Reuschenbach M, Kloor M, Morak M, *et al*. Serum antibodies against frameshift peptides in microsatellite unstable colorectal cancer patients with Lynch syndrome. *Fam Cancer* 2010; **9:** 173–179.
166. Dunn GP, Old LJ, Schreiber RD. The three Es of cancer immunoediting. *Annu Rev Immunol* 2004; **22:** 329–360.
167. Bicknell DC, Kaklamanis L, Hampson R, *et al*. Selection for β2-microglobulin mutation in mismatch repair-defective colorectal carcinomas. *Curr Biol* 1996; **6:** 1695–1697.
168. Bodmer W, Browning M, Krausa P, *et al*. Tumor escape from immune response by variation in HLA expression and other mechanisms. *Ann N Y Acad Sci* 1993; **690:** 42–49.
169. Clendenning M, Huang A, Jayasekara H, *et al*. Somatic mutations of the coding microsatellites within the beta-2-microglobulin gene in mismatch repair-deficient colorectal cancers and adenomas. *Fam Cancer* 2018; **17:** 91–100.
170. Kloor M, Michel S, Buckowitz B, *et al*. Beta2-microglobulin mutations in microsatellite unstable colorectal tumors. *Int J Cancer* 2007; **121:** 454–458.
171. Echterdiek F, Janikovits J, Staffa L, *et al*. Low density of FOXP3-positive T cells in normal colonic mucosa is related to the presence of beta2-microglobulin mutations in Lynch syndrome-associated colorectal cancer. *Onco Targets Ther* 2016; **5:** e1075692.
172. Koelzer VH, Baker K, Kassahn D, *et al*. Prognostic impact of β-2-microglobulin expression in colorectal cancers stratified by mismatch repair status. *J Clin Pathol* 2012; **65:** 996–1002.
173. Tikidzhieva A, Benner A, Michel S, *et al*. Microsatellite instability and Beta2-microglobulin mutations as prognostic markers in colon cancer: results of the FOGT-4 trial. *Br J Cancer* 2012; **106:** 1239–1245.
174. Kasajima A, Sers C, Sasano H, *et al*. Down-regulation of the antigen processing machinery is linked to a loss of inflammatory response in colorectal cancer. *Hum Pathol* 2010; **41:** 1758–1769.
175. Michel S, Linnebacher M, Alcaniz J, *et al*. Lack of HLA class II antigen expression in microsatellite unstable colorectal carcinomas is caused by mutations in HLA class II regulatory genes. *Int J Cancer* 2010; **127:** 889–898.
176. Steinert G, Schölch S, Niemietz T, *et al*. Immune escape and survival mechanisms in circulating tumor cells of colorectal cancer. *Cancer Res* 2014; **74:** 1694–1704.
177. Le DT, Uram JN, Wang H, *et al*. PD-1 blockade in tumors with mismatch-repair deficiency. *N Engl J Med* 2015; **372:** 2509–2520.
178. Sears CL, Pardoll DM. The intestinal microbiome influences checkpoint blockade. *Nat Med* 2018; **24:** 254–255.
179. Ager A, May MJ. Understanding high endothelial venules: lessons for cancer immunology. *Onco Targets Ther* 2015; **4:** e1008791.
180. Drost M, Zonneveld JB, van Dijk L, *et al*. A cell-free assay for the functional analysis of variants of the mismatch repair protein MLH1. *Hum Mutat* 2010; **31:** 247–253.
181. Heinen CD, Rasmussen LJ. Determining the functional significance of mismatch repair gene missense variants using biochemical and cellular assays. *Hered Cancer Clin Pract* 2012; **10:** 9.
182. Takahashi M, Shimodaira H, Andreutti-Zaugg C, *et al*. Functional analysis of human MLH1 variants using yeast and in vitro mismatch repair assays. *Cancer Res* 2007; **67:** 4595–4604.